# PROCEEDINGS

**EFBP'2000**

# European Forum
# on Ballistics
# of Projectiles

Saint-Louis, France
April 11 - 14, 2000

**20010122 161**

Edited by M. Giraud and V. Fleck

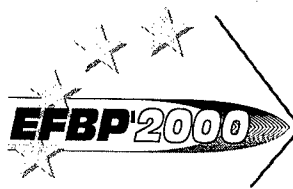ISL, French-German Research Institute of Saint-Louis - France

# REPORT DOCUMENTATION PAGE

Form Approved OMB No. 0704-0188

Public reporting burden for this collection of information is estimated to average 1 hour per response, including the time for reviewing instructions, searching existing data sources, gathering and maintaining the data needed, and completing and reviewing the collection of information. Send comments regarding this burden estimate or any other aspect of this collection of information, including suggestions for reducing this burden to Washington Headquarters Services, Directorate for Information Operations and Reports, 1215 Jefferson Davis Highway, Suite 1204, Arlington, VA 22202-4302, and to the Office of Management and Budget, Paperwork Reduction Project (0704-0188), Washington, DC 20503.

| 1. AGENCY USE ONLY (Leave blank) | 2. REPORT DATE | 3. REPORT TYPE AND DATES COVERED |
|---|---|---|
| | | Conference Proceedings, 11-14 April 2000 |

| 4. TITLE AND SUBTITLE | 5. FUNDING NUMBERS |
|---|---|
| European Forum on Ballistics of Projectiles [EFBP] | F61775-00-WF037 |

**6. AUTHOR(S)**

Edited by: M. Giraud, V. Fleck

| 7. PERFORMING ORGANIZATION NAME(S) AND ADDRESS(ES) | |
|---|---|
| Institut Franco-Allemand de Saint Louis<br>5 Rue du General Cassagnou<br>Saint Louis 68301<br>France | N/A |

| 9. SPONSORING/MONITORING AGENCY NAME(S) AND ADDRESS(ES | 10. SPONSORING/MONITORING AGENCY REPORT NUMBER |
|---|---|
| EOARD<br>PSC 802 Box 14<br>FPO 09499-0200 | CSP 00-5037 |

**11. SUPPLEMENTARY NOTES**

| 12a. DISTRIBUTION/AVAILABILITY STATEMENT | 12b. DISTRIBUTION CODE |
|---|---|
| Approved for public release; distribution is unlimited.. | A |

**ABSTRACT (Maximum 200 words)**

This is an interdisciplinary conference. Topics include: Defence Research Organization; Projectiles; Internal Ballistics/Propulsion; Launch Dynamics; Aeroballistics; Flight Dynamics; Terminal Ballistic Effects and Vulnerability; Sensors and Metrology; and Perspectives towards the 21st Century.

| 14. SUBJECT TERMS | | 15. NUMBER OF PAGES |
|---|---|---|
| EOARD, Projectiles, Aerodynamics, Ballistics Science, Propulsion, Aeroballistics, Flight dynamics, Sensors, Metrology | | |
| | | 16. PRICE CODE |

| 17. SECURITY CLASSIFICATION OF REPORT | 18. SECURITY CLASSIFICATION OF THIS PAGE | 19. SECURITY CLASSIFICATION OF ABSTRACT | 20. LIMITATION OF ABSTRACT |
|---|---|---|---|
| UNCLASSIFIED | UNCLASSIFIED | UNCLASSIFIED | UL |

NSN 7540-01-280-5500

Standard Form 298 (Rev. 2-89)
Prescribed by ANSI Std. 239-18
298-102

PROCEEDINGS

EFBP'2000

# European Forum
# on Ballistics
# of Projectiles

Saint-Louis, France
April 11 - 14, 2000

ISL

Edited by M. Giraud and V. Fleck

Hosted by ISL, French-German Research Institute of Saint-Louis - France

All papers submitted to EFBP'2000 are unclassified. Papers published in the Proceedings may not be reproduced in any media without written permission from ISL and the authors.

All papers have been submitted in their final form by the authors for camera-ready reproduction.

# Sponsors

Celsius
BOFORS TEST CENTER

Celsius
BOFORS WEAPON SYSTEMS

BOFORS (BTC and BWS) (Sweden)

SAINT-LOUIS

City of Saint-Louis (France)

EOARD (UK)

GIAT *industries*

GIAT industries (France)

DRS HADLAND

DRS
TECHNOLOGIES

HADLAND (UK)

ETIENNE
LACROIX

LACROIX (France)

WEIBEL SCIENTIFIC

WEIBEL (Denmark)

# European Forum on Ballistics of Projectiles

Saint-Louis, France, April 11 - 14, 2000 _____ **EFBP'2000**

## Forum Scope and Objectives

Mark the close of the twentieth century with a special occasion to:

* provide a forum for open debates among engineers, scientists and programme managers from academia, laboratories, industry and governments;
* offer an opportunity for meaningful dialogue and exchange of knowledge among distinguished European experts in the ballistics of projectiles;
* identify opportunities for new cooperative or fully collaborative programmes;

and thus:

* define the 2000 state of the art on the ballistics of projectiles with emphasis on comparative studies, research and programme overviews, collaborative research programmes;
* promote and stimulate the corresponding research in Europe.

## Participation

73 contributions have been selected, among which 39 will be presented orally and 34 in poster sessions. Members of governmental agencies, universities and industries of the 15 following countries have participated in the Forum:

| | | |
|---|---|---|
| Austria | Finland | Spain |
| Belgium | France | Sweden |
| Canada | Germany | Switzerland |
| Croatia | Netherlands | United Kingdom |
| Denmark | Norway | USA |

## Major treated topics

Defence Research Organisation
Projectiles
Internal Ballistics and Propulsion
Launch Dynamics
Intermediate Ballistics and Aeroballistics
Terminal Effects and Vulnerability
Sensors and Metrology
Perspectives towards the 21st Century

## Programme Committee

Chairmen: Marc GIRAUD, Volker FLECK, ISL, France - Germany
Members: IGA Christian CANNAVO, DGA/SPART, France
Roxan CAYZAC, GIAT, France
Iris CREWTHER, DPA, Switzerland
BDir Paul GUSE, WTD 91, Germany
Rudi HEISER, EMI, Germany
Rob IJSSELSTEIN, TNO, Netherlands
Bo JANZON, FOA, Sweden
Col. Marc PIRLOT, ERM, Belgium
Vicente SANCHEZ-GALVEZ, UPM, Spain
David SCOTT, DERA, Great Britain


## Organising Committee: ISL

Chairmen: Marc GIRAUD, Volker FLECK
Members: Claude BERNER
Pierre-Yves CHANTERET
Dieter HENSEL
Jean-François LEGENDRE
Hartmuth F. LEHR
Julio SRULIJES

Secretaries: Marie-Louise HENGY, Edith MUSCH
Assistants: Jean-Pierre BOURRÉ, Guy FUCHS, Dorothée LAXER

# Table of contents

# Internal Ballistics and Propulsion

# Launch Dynamics

## Intermediate Ballistics and Aeroballistics

## Terminal Effects and Vulnerability

## Sensors and Metrology

## Perspectives towards the 21st Century

Defence Research Organisation

# OVERVIEW OF THE DEFENCE RESEARCH IN FRANCE

## D. ESTOURNET

Director of R & T,
DSP/SREA, 4bis, rue de la Porte d'Issy, Paris, F-00457 Armées, France

**Abstract :** Within the French MoD organisation for preparing the future, the Prospective Plan deals with the geostrategic, political, technical and operational aspects to consider new armaments to be developed in the future. For the short and mid terms, it aims at ensuring operational and technical coherence of armaments. In addition to technology policy and international co-operation objectives, it gives guidance for the R & T Master Plan. The latter is characterized by annual guidance, annual planning and integrated guidance and evaluation process.

## 1. SUMMARY

Three parts will be reviewed. First, the general organisation of DGA and general considerations about the Defence Studies. Then, the Prospective Plan. Finally, the main topics : the Research and Technology activity, which we call in France "les études amont", literally "the Upstream Studies", what is emphasizes their rôle in the preparation of the Armament Programmes.

## 2. ORGANISATION

Within the French Ministry of Defence (see Figure 1), the "Délégation Générale pour l'Armement" (DGA) is in charge to provide the Armed Forces with the equipment they need, at the proper time and at best cost.
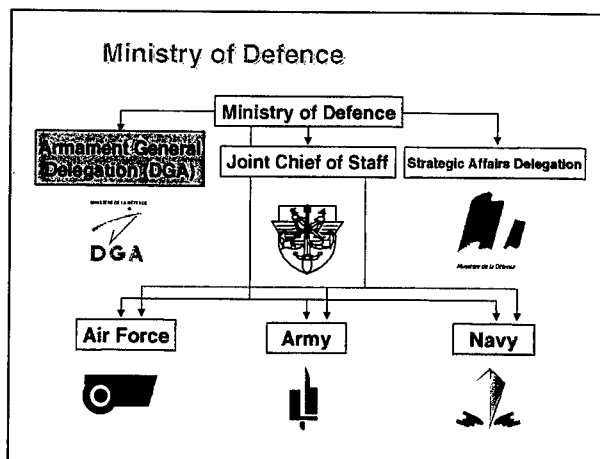


Figure 1 : French MoD

The DGA organisation (see Figure 2) is built on the consolidation of its resources in main bodies, each of them being in charge of homogeneous activities. DRH (Human Resources) and DGO (Management and Organisation) are responsible for internal regulations and support activities. Industrial activity, including maintenance and repair, is the "core's business" of the Directorate for Navy Shipbuilding (DCN) and of the Service for Aircraft Maintenance (SMA). All the tests and expertise that the DGA programme managers and contractors may need, are included in the scope of work and competence of the Directorate for Test and Evaluation Centres (DCE). Preparing - and ensuring co-ordination of - the international activities are the responsibility of the DCI (Directorate for Co-operation and Industrial Strategy) and of the DRI (Directorate for International Relations).

Finally, *last but not least*, the services in charge of managing studies, programmes and other procurement operations for the benefit of the armies belong to the Directorate for Procurement Policy and Quality Control (DPM), Directorate for Weapon Systems (DSA) and **Directorate for Force Systems and Prospective Analysis (DSP)**. The latter is in charge of preparing the future programmes, and, namely, of the drafting of the Prospective Plan (DSP/SASF) and of the supervision of Research and Technology activity (DSP/SREA).
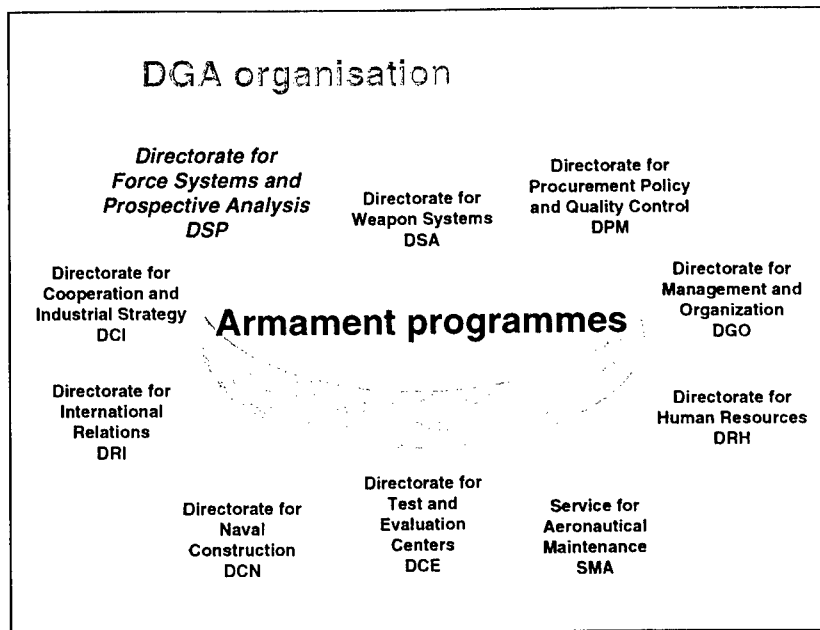


Figure 2 : DGA organisation

At this stage, it is important to note (see Figure 3) that Defence Studies conducted before launching the programmes are not limited to the R & T ones. Social, Economic and Politico-Military Studies on one hand, Operational and Technical/Operational Studies on the other, are separated from the R & T. These three categories have clearly different aims and contents.
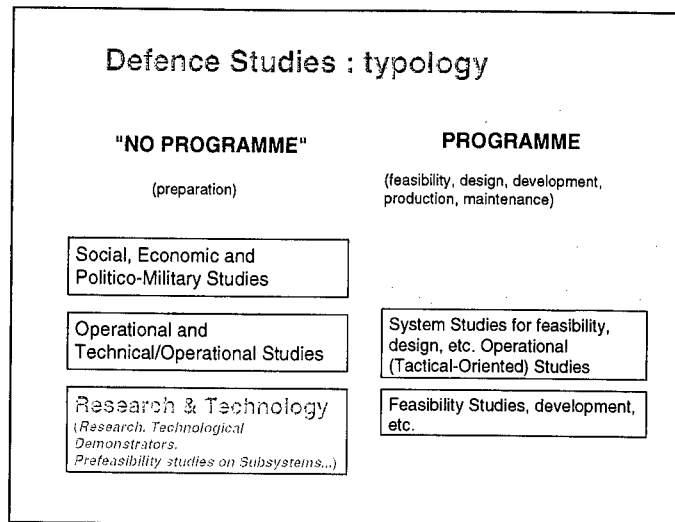
Figure 3 : Defence Studies, typology

This flowchart (see Figure 4), focusing on the early stages of Programme Phases, highlights the specific rôle of R & T besides other activities/studies preparing Armament Programmes.
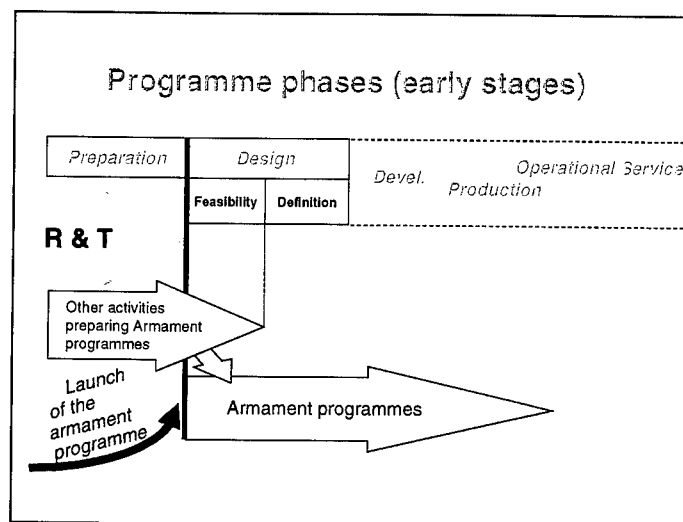


Figure 4 : Programme phases, early stages

## 3. PROSPECTIVE PLAN

The Prospective Plan ("PP30"), drafted jointly by Military Staffs, DGA and DAS, throws light on the future through the results of long term strategic studies (geopolitic prospects, defence policies), assessment of emerging technologies (foreseeable threats, technology breakthroughs) and economic forecasts.

For the long term (up to 30 years), the PP30 deals with the geostrategic, political, technical and operational aspects to consider new armaments to be developed in the future. For the short and mid terms, it aims at ensuring operational and technical coherence of armaments fielded and to be fielded soon. The PP30 is organized along 8 "Force Systems" and drafted by teams of 8 "Force System Architects" (ASF from DGA) and 8 Operational Coherence Officers (OCO from the armies). In addition to industry policy, technology policy and international co-operation objectives, it gives guidance for the R & T Master Plan.

The 8 fields are : Deterrence, Command, control, communications and intelligence, Strategic and tactical mobility, Deep Strike, Air/Land warfare and control, Air/Sea warfare and control, Air/Space warfare and control, Readiness. The involvement of EFBP in different Force Systems has to be underlined.

## 4. RESEARCH AND TECHNOLOGY

The R & T activity consists of two categories. *Research* means aiming at becoming/remaining a competent manufacturer, with scientific, technological or demonstrator contents, covering selected technological sectors, and contract placed with industry plus subcontracting to laboratories, e.g. 120 mm electrothermal-chemical (ETC) gun studies currently in progress by German and French companies and ISL. *Study* means aiming at becoming/remaining a competent "specifier" or buyer, with expertise, knowledge, simulation, test contents, covering all sectors and contract placed with [Near]-state body plus industry, e.g. code to be implemented at DCE for simulation of air-to-ground warhead penetration.

The R & T Master Plan is characterized by annual guidance and annual plan made of 300 to 400 "PEA" (single technical aim programme), 2/3 of them are grouped into "PF" and "PS" (single military aim programme), e.g. "balanced protection of armoured vehicles" in the field of EFBP. International policy is included in guidance part of the Plan and all TAs are included in PEAs.

R & T co-operation is undertaken to save money, and to multiply ideas or cross-check results, to prepare armament programme co-operation, to help European [industry] alliances, and to increase the "Tech Base". By means of exchange of knowledge on organisation, visit of laboratories and facilities, exchange of scientists, exchange of nationally acquired knowledge, setting up common programmes with co-ordinated management - nationally executed -, setting up common programmes with integrated management and execution facilities.

For integrated "guidance and assessment" purposes, a new process has been established. The inputs are prospective analysis, international co-operation, industry policy, economic resources, evaluation from year n - 1, therefore providing with guidance for Research projects proposals. After planning and financing of approved Research projects has been done, monitoring of execution and evaluation of results will provide the next annual cycle with new guidance.

The R & T Master plan is structured with some forty technical areas, among which "weapons, ammunition, pyrotechnics, detonics and terminal ballistics", covering the ballistics areas of this forum.

# THE UK MOD RESEARCH STRUCTURE

## WEATHERLEY D I

Defence Evaluation and Research Agency, Fort Halstead, Sevenoaks, Kent  TN14 7BP United Kingdom

**Abstract:** The structure and modus operandi of the UK MOD research customer organisation has changed recently in response to recommendations in the 1998 Strategic Defence Review. The changes have created a structure that relates research priorities to the likely future capability needs of the UK armed forces. At the same time the nature of the customer-supplier link is being considered, principally by assessing the role and nature of DERA, currently the prime contractor for UK MOD research.

## 1 INTRODUCTION

The recent UK Strategic Defence Review included a detailed and comprehensive policy-driven assessment of the likely future role, structure, modus operandi and capability needs of the UK Armed Forces. It stimulated a number of important developments, for example:

- the integration of martime, ground and air components into coherent UK joint forces under unified command;
- the creation of a single Ministry of Defence (MOD) Capability Management customer organisation responsible for obtaining the Defence capabilities needed by those forces;
- the adoption of a new capability procurement methodology ('Smart Procurement') and the creation of a new supplier organisation.

The MOD spends over £400 million per annum on research to support the procurement and maintenance of the platforms, equipment and infrastructure which constitute UK Defence capabilities. The post-SDR changes in procurement approach have had an impact upon the nature of the research programme and the way in which it is managed. This research programme has two inter-related main elements, one to provide direct support to the development of capability requirement and the other to create and maintain an underlying science and technology base for potential Defence application. Each of these elements is specified, undertaken and delivered in a formal customer/supplier manner for the MOD customers shown in Figure 1.

Figure 1 : Top Level MOD Customer Organisation
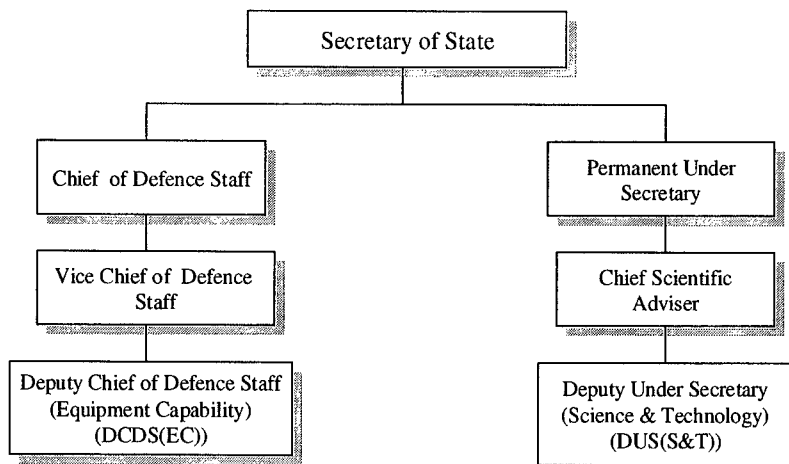
## 2 THE MOD CUSTOMER ORGANISATION

The Capability Management organisation, headed at 3* level by *DCDS (Equipment Capability) (DCDS(EC))*, is responsible for developing a balanced, coherent and affordable Equipment Plan and procurement programme which is based upon the capability needs of the UK Armed Forces. Implicit in this role is the enactment of Balance of Investment (BOI) decisions across the equipment programme in order to deliver the maximum level of military capability achievable within cost targets. This organisation is also responsible for managing the equipment approvals process within MOD, and for oversight of extant capability after equipment has entered Service – the through life capability management approach which is a cornerstone of Smart Procurement. Finally, it is the MOD customer for the *Applied Research Programme (ARP)*, which is the research element supporting the development of capability requirement, and for individual Technology Demonstrator programmes undertaken to reduce technical risk associated with specific procurements.

The organisation is based around 4 joint capability areas, each the responsibility of a 2* Capability Manager, which reflect the changes and priorities identified during the Strategic Defence Review exercise and developed subsequently. These areas are associated with the capabilities required by UK Armed Forces undertaking the various roles required of them:

Strategic Deployment - The capability to deploy joint forces to the theatre of operations, including sustaining and withdrawing those forces. The protection of the deployment lines of communication. The deployment and protection of the national strategic deterrent system.

Strike - The capability to apply effective force throughout the theatre of operations but in particular in those parts of the theatre controlled by an enemy. It includes control of the theatre airspace and the supporting activity needed to enable deep strike operations, but not operations in direct support of a land contact battle.

Manoeuvre - The capability directly to engage enemy land forces, to shape the immediate battle-space, and tactically to manoeuvre land forces.

Information Superiority - The capabilities needed to direct joint operations, including the collection, processing and dissemination of information, the execution of command, and the infrastructure for joint force communications.

Capability strategy, the overall shape of the equipment programme and high level BOI issues are managed via the top-level Joint Capabilities Board.

The longer term strategic element of the MOD research programme, the *Corporate Research Programme (CRP)*, is undertaken for the Central Scientific Staffs which are headed at 3* level by *DUS (Science & Technology) (DUS(S&T))*. This organisation is responsible for ensuring MOD access to the scientific and technical advice necessary to support UK Defence

needs, for developing the technology strategy for MOD (including a strategy for International Research Collaboration (IRC)), and for developing and maintaining MOD access to a relevant science and technology base.

## 3 THE SUPPLIER ORGANISATIONS

The key formal interface between the MOD customer organisation and its suppliers is illustrated in Figure 2. The *Defence Procurement Agency (DPA)* is an Agency of the UK MOD and was created in April 1999. Its role is to procure platforms and systems, to manage major upgrades, and to provide a range of procurement-related services, guidance and standards. It replaces the earlier MOD Procurement Executive, whose structure could be traced back to its roots in the Admiralty, War Office and Air Ministry.

Figure 2 : Top Level MOD Customer-Supplier Interface

**CUSTOMER**



**SUPPLIER**
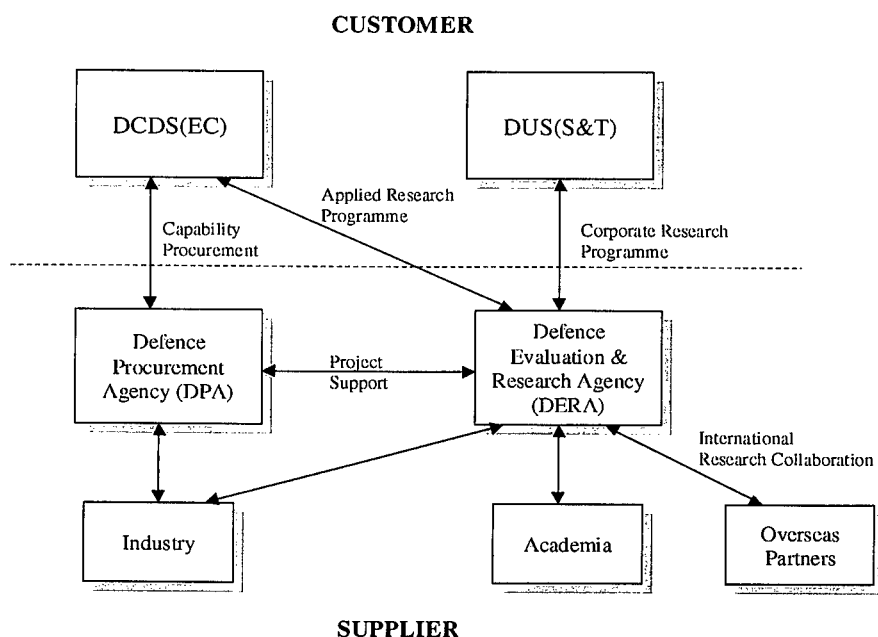
The Defence and Evaluation Research Agency (DERA) was created in April 1995 as an Agency of the MOD. It has its roots in the earlier MOD research establishments (ARE, RAE, RARDE, RSRE, etc), as shown in Figure 3. DERA exists primarily to serve its MOD customers, but exploitation of the wealth-creation potential of programmes of work and facilities required for Defence purposes is pursued where appropriate.

Figure 3 : Evolution of DERA
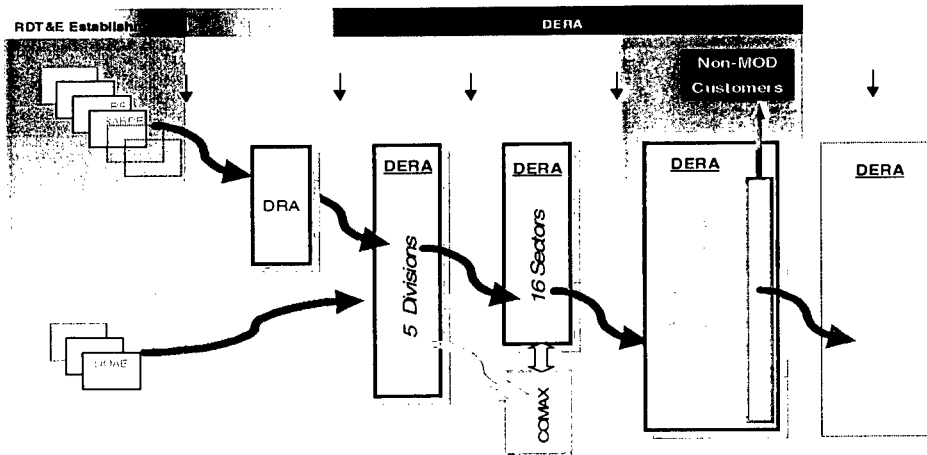


In addition to its key role in procurement, *industry* undertakes research and provides services by sub contract from DERA. This is mainly to contribute to the ARP, although significant input is made to the CRP. In a similar manner, research sponsored *academia* provides an important contribution to the CRP.

*Overseas partners* contribute to the UK MOD research base by means of a range of co-operative and collaborative arrangements undertaken in accordance with extant IRC policy.

## 4 THE MOD RESEARCH PROGRAMMES

### 4.1 Applied Research

The ARP mission is to provide, via research and technology demonstration, technical options at quantified cost and risk to enable the definition of requirements for equipment which will best meet the needs of UK Armed Forces over the next 20 years. Issues of specific current interest include those technologies and systems concepts which offer the highest potential pay-off in terms of performance, cost saving, improvements to precision, survivability, lethality, countermeasure resistance, versatility and adaptability.

Figure 4 : ARP Activities

**Maritime**
Sub-surface reconnaissance & the undersea environment
Naval EW & C3I
Surface ship & submarine characteristics
Underwater, above water and anti-submarine warfare
Operational Analysis

**Land**
Tactical surveillance & countermeasures
Armoured fighting vehicles; combat support vehicles
Anti-armour and personal combat
Indirect fire systems; Short range air defence
Battlefield Engineering & robotic land vehicles
Land tactical CIS
Combat readiness and simulation
Chemical and biological defence
Operational Analysis

**Air**
Tactical air intelligence & reconnaissance
Joint Systems UAVs; Tri-service helicopters
Aircraft flight
Offensive air missions
Air superiority aircraft & anti-air weapons
Air C3I; Air electronic combat
Maritime air systems integration, performance assessment
Air systems training
Supportability and sustainability; Human Factors
Operational Analysis

**ICS**
Tactical, strategic & Joint CIS
Satellite communications & space surveillance
Information assurance

The research programme contents are summarised in Figure 4. The structure has been carried over from the earlier single service approach and is currently being re-brigaded to one suited to the new joint Capability approach. DERA is the prime contractor for the ARP, in which individual packages are managed by a DERA Package Manager (DPM) in concert with the appropriate Capability Management customer. The DPM responsibilities are those of programme formulation and delivery. The annual planning cycle is under review, with a typical earlier form summarised in Figure 5. It is based upon the development and issue of formal documents such as the Form A (Outline requirement), Form B (Proposed Programme) and Form E (Approval to proceed).

Figure 5 : Typical ARP Annual Planning Cycle
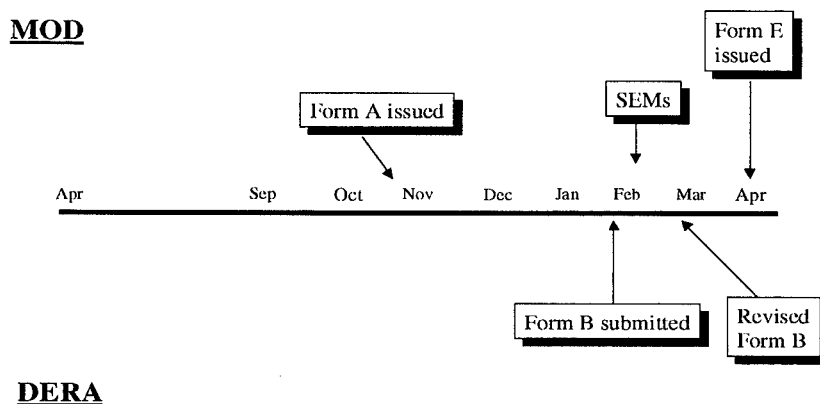


## 4.2 Corporate Research

The purpose of the CRP is to advance, and provide access to, scientific and technical knowledge that has real or potential application to Defence needs, and to maintain and develop the UK science and technology base for Defence purposes. The overall strategy for the CRP is influenced by a number of factors, of which the most significant are the MOD Technology Strategy, the Strategy for Applied Research, and guidance from the Defence Science Advisory Committee (DSAC).

Work within the Corporate programme encompasses 3 complementary categories:

-   'underpinning' research required to maintain and develop the MOD science and technology base;
-   'innovative' research, usually high risk and often speculative, intended to develop new approaches and techniques to the benefit of future Armed Forces capabilities;
-   'targeted' research required to support aspects of the equipment programme.

Figure 6 : CRP Activities

TG0 - Overarching Strategic Studies

TG1 - Acoustics, Magnetics and Hydrodynamics

TG2 - Chemical and Biological Defence

TG3 - Aerodynamics, Propulsion, Guidance and control

TG4 - Materials and Structures

TG5 - Human Sciences and Synthetic Environments

TG6 - Energetic Materials and Terminal Effects

TG7 - Electronic Device Technology

TG8 - Visible and IR Technology

TG9 - Radio Frequency Technology

TG10 - Computing and Information Processing

TG11 - Operational Analysis

TG12 - Ballistic Missile Defence

DERA is the prime contractor for the CRP, which for management purposes is divided into a number of Technology Groups (TGs). Each TG has a MOD customer, within the DUS(S&T) area, and a DERA Technology Group Manager (TGM) who together are responsible for specifying, creating and delivering a research programme which is the best available match to the requirements of the various stakeholders. The range of CRP activities is indicated by the current list of Technology Groups in Figure 6, whilst the formal cycle of programme formulation is summarised in Figure 7.

Figure 7 : CRP Annual Planning Cycle
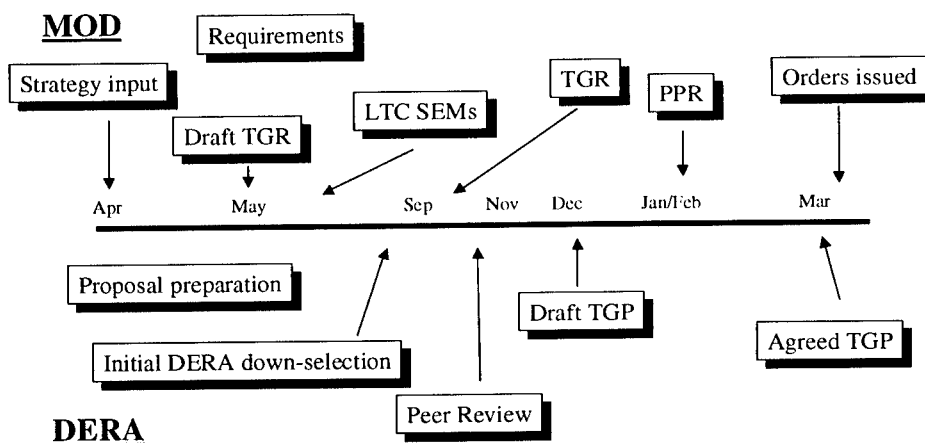
## 5 RECENT AND LIKELY FUTURE CHANGES

The changes within MOD stimulated by the Strategic Defence Review are not yet complete and, although further fundamental change is unlikely in the near term, fine tuning of organisation and procedure will continue for some time. A component of this will be the re-brigading of the ARP activities and refinement of the annual planning cycle. Of more significance are issues relating to the supplier base and the customer-supplier relationship. Of these perhaps of most current significance is that of the role and the nature of DERA.

At present DERA is the prime contractor for the totality of the MOD research programme, sub-contracting a proportion of the work to industry and academia as appropriate. The current Research Competition Pilot is assessing the benefits and risks to MOD of using primary competition within the research programme. This exercise, which could lead to the adoption of primary competition more widely, is a response to the MOD need to ensure efficient access to the best ideas and capabilities in a world where technology is evolving rapidly.

The nature of DERA is currently being devoted, with options for a Public Private Partnership (PPP) being assessed. Discussion of this is outside the scope of this paper, but the outcome could significantly alter the customer-supplier relationship described earlier.

# ON THE DEFENCE RESEARCH ORGANIZATION IN SWEDEN

**Hans Elger**[1], **Allan Linnarson**[1], **Bo Janzon**[2]

(1) FOA Defence Research Establishment , Research Strategy,  SE-172 90 Stockholm, Sweden
(2) FOA Defence Research Establishment , Weapons and Protection Division,
Grindsjön, SE-147 25 Tumba,  Sweden

**Abstract:** The main performers of defence research in Sweden are FOA, FFA and the defence industry. A number of applied projects carried out in co-operation between industry and FOA/FFA. Universities are to a smaller extent engaged in defence research and normally commissioned by FOA/FFA or by industry. The total amount of funding for defence related research and technology development was in 1999 about 250 million Euro. Approximately 25% of this amount is used for strategic research. Important  priorities for defence R&T are:
- Research concerning the overall security situation needed  for parliamentary decisions about directions  for the Swedish future defence.
- Threats against the society of other kinds than military attacks. Vulnerabilities,  crisis management
- Information warfare
- NBC-protection
- Areas of importance for RMA
- Special questions concerning international operations

The funding of research for the military defence is organized in a dialogue process. FOA offers yearly a programme for the defence research. The Supreme Commander accepts the programme and the costs for it after some adjustments.

The government grants FOA the costs for research in the area of NBC and for research regarding the national and international security situation.

FOA is organized in seven Research Divisions. FOA is managed by a staff headed by the Director General. FOA Programme department acts as marketing group and co-operates with the main customers in the research planning process.

## 1. INTRODUCTION

### 1.1 Performers

The main performers of defence research, including technology development, in Sweden are FOA, FFA and the defence industry. FOA and FFA are to a large extent performing research of strategic character whereas industry has its main activities in the field of  advanced technology development.  A number of applied projects are carried out in co-operation between industry and FOA/FFA. Normally these projects are in the area of advanced development. Universities are to a smaller extent engaged in defence research but to a limited degree and normally commissioned by FOA/FFA or by industry.

## 1.2 Funds for defence research

The total amount of funding for defence related research and technology development was in 1999 about 250 million Euro. Approximately 25% of this amount is used for applied research. The rest is used for advanced technology development.

Looking forward the tendency is that activities in this field of will increase considerably. The total amount of funding for R&T is likely to increase slightly during the next five years in order to make this increase possible

## 2. PRIORITIES

Important priorities for defence R&T are
- Research in order to follow development of the overall security situation needed for parliamentary decisions concerning directions for Swedish defence
- Threats against the society of other kinds than military attacks. Vulnerabilities, crisis management
- Information warfare
- NBC-protection
- Areas of importance for RMA
- Special questions concerning international operations

High priority will be given to areas where Sweden cannot rely on defence research in other countries ( e.g. Electronic Warfare ) and to areas where Swedish defence industry has a strong and competitive competence which could be of importance in order to create mutual interdependencies at an industrial level with other countries.

A strategy for research related to military defence was published in 1997. The main priorities expressed in this research are still valid. An excerpt of this strategy is presented in appendix 1.

## 3. OVERVIEW OF THE SYSTEM FOR FUNDING AND TASKING OF DEFENCE RESEARCH

Defence research is today mainly financed in a way where tasks and budgets are knit together at a fairly detailed level. Normally the funding is given to the performers at a project level.

The main funding streams are illustrated in figure1 and the relative size of different customers of FOA is illustrated in figure 2 below.

## 4. THE ORGANIZATION FOR COMMISSIONING OF RESEARCH FOR THE DEFENCE.

### 4.1 Research for the military defence

The funding of research for the military defence is organized in a dialogue process. FOA offers yearly a programme for the defence research. The Supreme Commander normally accepts the programme and the costs for it after some adjustments regarding the items and the volumes of the research.

The dialogue process is based on a hierarchy of documents directing defence research and technology development. This hierarchy includes the following documents:

FMV=Defence
Materiel
Administration
FOA= Defence
Research
Establishment
FFA= The
Aeronautical
Research Institute of
Sweden
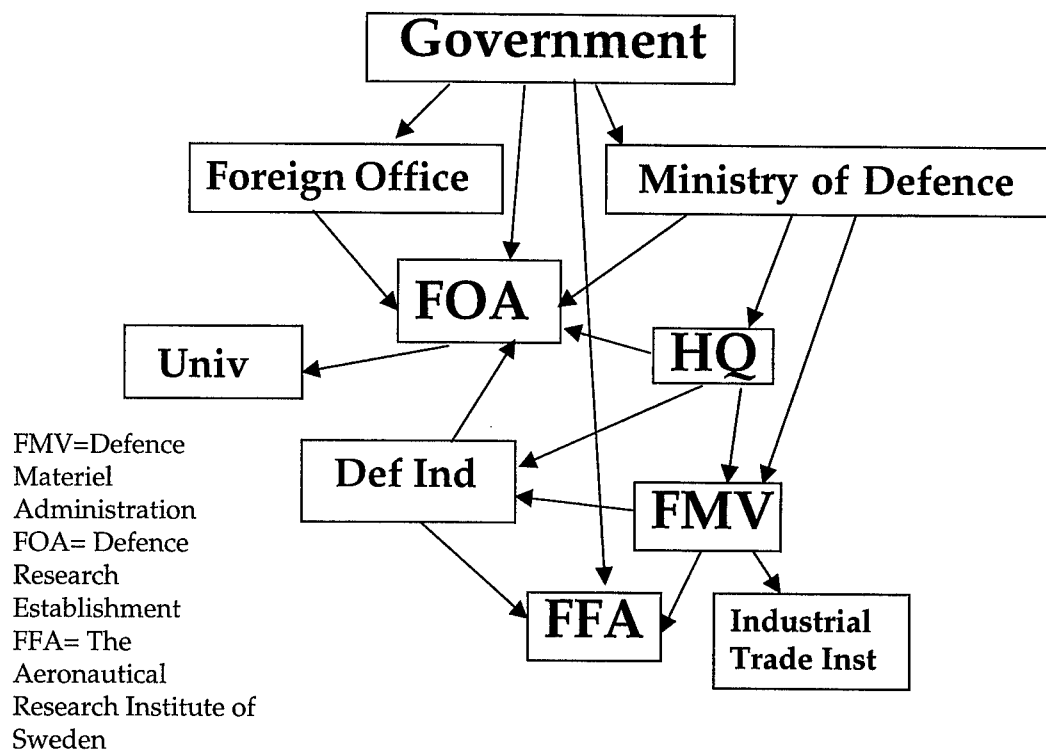
Figure 1: Main Funding Streams
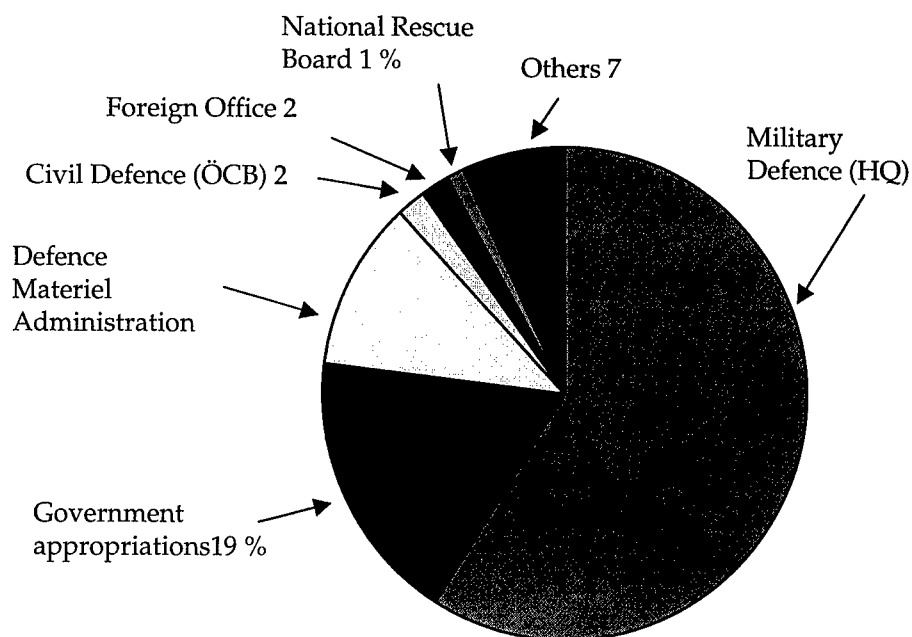


Figure 2: The relative size of the contributions from different customers of FOA

- R&T Strategy (revised when needed and worked out from a long time perspective)
- R&T plans (revised once a year and describing the intended development of research for 3-5 years in around 15 R&T-areas. Appendix 2 )
- R&T tasks (given each year at a procect by project level)

Further the dialogue process is going on in the following organization setting:

- One group for each R&T-area.The group is headed by a representative at the Headquarter. FMV, FFA and FOA are represented in the groups.
- One central group for management of the R&T-process
- One policy group

The final decisions concerning R&T are made by the Supreme Commander.


## 4.2 Research for the government

The government grants FOA the costs for research in the area of NBC and for research regarding the national and international security situation. FOA proposes plans and programmes for these areas. The government frequently requests investigations and research regarding special cases.


## 5. ORGANIZATION OF FOA

FOA is organized in seven Research Divisions and consists of about 1000 persons. Of them about 700 are researchers. The Divisions are:

- Defence Analysis
- Weapons & Protection
- Sensor Technology
- NBC Defence
- Human Sciences
- Guidance & Control and Underwater Sensors
- Command & Control and Warfare Technology

The divisions are supported by an administrative Division.

The Director General, presently Dr. Bengt Anderberg - formerly a Major-General and Head of the Planning Staff of the Supreme Commander's Headquarters - is supported by a staff including a number of functions: FOA's Programme Department, which acts as a marketing group and plans in co-operation with the customers the FOA research overall; the International Section is planning and supervising the many international collaborations FOA is participating in; the Research Strategy group develops long-term strategic directions and follows and discusses research strategy development also with foreign countries.

The FOA Board, headed by Professor Janne Carlsson, former Headmaster of the KTH Royal Institute of Technology, Stockholm, consists of the Director General, members from other Defence Authorities, Industry and Universities and include members of the Swedish Parliament.

# ON THE DEFENCE RESEARCH ORGANISATION
# IN THE NETHERLANDS

## CDRE IR D. VAN DORD

Netherlands Ministry of Defence, DGM/DWOO - POBOX 20701, 2500 ES Den Haag, The Netherlands

**Abstract :** Technology is of major importance to the Netherlands society. The Government has an active research and technology policy and all ministries are involved. The government has submitted a Defence Whitepaper to Parliament. The armed services will become more modular organised. Research and development is also addressed. The aim of Defence research and development is to provide for the required knowledge in an effective and efficient way. The basis for the research and development policy leads to the outlines. The environment for Defence is changing to more uncertainty of future threats. This changing environment has its influence on the knowledge requirements in the different functional areas of interest. The planning recognises three levels of proficiency. In the decision process a number of criteria is applied. Research is tasked by an programmatic approach. Research and development are outsourced as much as possible to amongst others research institutes, universities and industry. The key issue is the direct accessibility of the knowledge base. International cooperation is a conditio sine qua non. This forum is a good example of relevent international cooperation.

## 1. INTRODUCTION

### 1.1 General

As all nations participating in this conference the Netherlands have a society that depends heavily on technology. Technology in all possible manifestations is part of our daily life and its influence will increase by the day. Some technology will seemingly just appear, driven by industrial development normally directed to a segment of the consumer market. Other technological development will be a result of a careful and painstaking government policy.

### 1.2 Government organisation

In the Netherlands, science and technology policy is embedded in all sectors of government care. There is no ministry which has not in one way or another some responsibility for research and development. Two ministries however have an overall responsibility for the establishment and maintenance of the nation wide knowledge infrastructure. The ministry of Education, Culture and Science is responsible for the science part, more in particular the universities and institutions of fundamental and applied research. The ministry of Trade and Industry holds, based on its responsibility for industrial activity, the technology portfolio. Next to these two general policy oriented tasks the vocational ministries have their own requirements for research and development. By definition this is much more application oriented. Examples are ministries of Agriculture and Fisheries, of Transport and Public Works, of Welfare and Health and of course of Defence. The boundaries between all these influence spheres are not sharp. Standing organisations on mutual information exchange and tuning exist. These organisations are led by the ministries of Education, Culture and Science and of Economic Affairs. The organisations ultimately report to the council of ministers thereby embedding science and technology at the highest possible political level.

## 1.3 Defence Whitepaper 2000

In mid 1998 after general elections a new government was formed. In the underlying coalition agreement a new Defence Whitepaper was announced. After publication of an Outline Memorandum in January 1999 this Defence Whitepaper 2000 was sent to Parliament in December 1999. The whitepaper will be subject of hearings and debate between Government and Parliament in the first months of the year 2000. The plans can only be implemented on completion of this process. Research and development is also addressed in the whitepaper. The diversity in tasks, deployment areas and materiel lead to a continuous requirement for scientific knowledge and abilities. The ever increasing complexity requires more and more expertise to decide on procurement, modernization, support and use of weapon systems. Expertise is also required to support the operational, financial-economic and personnel processes. Research and development are the most important tools to support these requirements. The attention will be focussed on control and prioritising of the research and development programmes. More and more is technology useful for both civil and military applications. Defence has to monitor the progress in the civil research and development arena and ensure interaction. International cooperation will be the basic assumption to promote complementarity and to avoid duplication. The support of Defence industry by (co)financing research and development projects remains necessary. Research and development supporting all the main tasks of the armed services will receive priority. The ambition of Defence will be the driving factor for the level of research and development. The research and development will be executed by institutes of the civil knowledge infrastructure albeit under Defence control.

## 2. DEFENCE RESEARCH AND DEVELOPMENT POLICY

### 2.1 General

During the drafting process of the outline memorandum and the whitepaper the policy on research and development was reviewed. This led to the reformulation of the defence research and development policy. The revised policy is founded on the earlier policy and underlying choices, updated in line with both the whitepaper and actual state of affairs in the world of Netherlands defence research and development. Research and development policy is part of the materiel policy and is aimed at activities outside Defence. The activities support all functional areas.

### 2.2 Aim

The aim of research and development is to provide for the required knowledge for Defence in an efficient and effective way through research and development.

### 2.3 Basis

The relevant parts of the basis for the Defence materiel policy for research and development are:
- to provide the means and knowledge to the armed services to enable them to execute their tasks in national and international context. Next to the protection of national and NATO territory, crisismanagement, peace keeping and humanitarian relief operations get special attention.
- to create conditions to fulfill the requirements for exploring and applied research, policy and management support and technology and materiel development.
- the operational requirements give direction to the materiel-logistic process and the require-

ments for research and development. In the final decision budgetary considerations and the possibility of international harmonisation of operational requirements play an important role.
- the policy considerations of other ministries form part of the Defence materiel policy
- to create conditions to involve Netherlands' industry and research institutes in Defence contracts
- to contribute to the maintanance of the required scientific and industrial base in the Netherlands and in the alliance in particular in Europe.
- to implement the policy systematically by the use of control mechanisms, in particular the Integral Defence Planning Process, the Defence Materiel Selection Process and the Budgeting Process

## 2.4 Outlines

The parts of the aim and basis relevant to research and development lead to the following outlines for the research and development policy:
- the determination of the requirements for knowledge and the therefore necessary research and development
- the establishment and maintenance of a for Defence accessible knowledge infrastructure and the encouragement to utilise this infrastructure
- the encouragement of cooperation inside Defence in operational requirements and execution of research and development
- the encouragement of international cooperation in research and development
- the encouragement of the transfer of knowledge between research institutes and industry
- the encouragement of the tuning of military and civil research and development and where possible stimulate the cooperation between both.

## 3 THE ENVIRONMENT

The changes in the environment of Defence occur at an ever higher rate. Defence does not only have to follow these changes, but has also to anticipate new challenges and tasks. Defence research and development have to provide the tools. The present and future situation is characterised by uncertainty on future security threats. The armed services have to perform different tasks in different scenarios and in different coalitions. Flexibility and multiple availability are leading arguments. The heavier combat tasks shape the armed services but with adaptations these armed services will also be available for lighter tasks. The armed services are of modular design. The modules can become part of larger military international entities. The modules have to fit in NATO, WEU, UN, (EU) and ad hoc coalition forces. The flexibility is underlined in the NATO strategic concept. Further improvement of flexibility, readiness, mobility, fighting power, sustainability, safety, interoperability and quality are guidelines. The Netherlands have always supported international cooperation in both European and transatlantic context but also in bi- and multilateral groupings. Research and development complies to this policy. The selection process in materiel projects will have an important influence on research and development. International harmonisation of operational requirements will enhance the chances for cooperation also in the area of research and development. The civil and military knowledge in the world increases rapidly. An increasing part of the knowledge is usable for both civil and military application. Civil technology development can move fast and could have a large impact on military activities. Defence has to follow these developments continuously, consider the relevance for Defence and anticipate if necessary. ICT developments accelerate the transfer of knowledge and enables the formation of "virtual research units", leading to more cooperation possibilities. Cooperation is not only of importance within disciplines but also in multidisciplinary settings, as breakthroughs often occur at

the boundaries and interfaces of disciplines. Furthermore the research questions are often multidisciplinary in nature. The difference in rate of technology development in the US and in the allied nations raises some concern, the so called technology gap. This seems to relate more to the application of technology in weapon systems than to the level of knowledge in the nations. It is more a capability or interoperability gap. The US becomes more and more reluctant to support an unbalanced information exchange.This necessitates a higher research and development effort and more extensive international cooperation, in particular in the West European nations. Because of the limited defence industry activity at the weapon system level the role of the Netherlands in Europe is limited. However, international cooperation is a conditio sine qua non to meet the Netherlands' ambition to provide the armed services with the knowledge they need whereby the own activity has to be interesting enough to attract partners.

## 4. TRENDS IN THE KNOWLEDGE REQUIREMENT

### 4.1 General

The knowledge requirements cover a broad spectrum. In the research and development policy only the trends are adressed.

### 4.2 Operational

In the operational area of interest the trend is towards the modular design of the armed services. The inclusion of these modules in larger international entities requires both joint and combined operations both with other armed services and non governmental organisations. The flexibility, readiness, mobility, fighting power, sustainability, safety, interoperability and quality outline the research and development contours. These lead to the definition of six themes in the operational area of interest. To support the interoperability research and development will be directed to operational and contingency planning, command and control and information. The protection, both active and passive, against weapons of mass destruction is the second theme. It goes without saying that observation is a success factor. The third theme covers observation systems leading to real time situational awareness in a digitised battlefield. The fourth theme adresses the threat by the possibilities of ICT, in short the information operations both offensive and defensive. The non lethal weapons become more and more important and relevant research is covered by the fifth theme. The sixth theme provides for the increasing requirement for scientific support of strategic policy development.

### 4.3 Personnel

In the personnel area of interest the availability of sufficient, qualified and well motivated personnel is the key factor. The research and development requirements are linked to the personnel logistic process, operational readiness, care and protection. Important subjects are training and education and the development and validation of medical examination and selection methods. The support of the labor safety activities need more research and development. During deployment of units the medical care cannot always be the same as in the home country. Research and development will be required to provide the best possible care by improving information and communication methods, better equipment, workmethods, protocols and training. Last but not least the improvement of medical aspects of countering the effects of B and C weapons and the prevention and containment of epidemic infectious diseases. Another area of research and development is the possibility to decrease the physical and mental stress of personnel.

## 4.4 Materiel

The materiel area of interest is dominated by the materiel acquisition processes. Research and development could decrease the risks. The complexity of the tasks and the new technological developments places great demands on the knowledge required to be able to carefully consider what materiel meets the Netherlands' requirements and possibilities best. Research and development have to support the materiel logistic process (operational requirements, acquisition, exploitation, maintenance and disposal). The integral approach becomes more and more important like an improved insight in life cycle costing and life cycle management. The environmental effects of military activities is an important factor. Solutions to minimise these effects are subjects of research and development. Examples are simulations, noise reduction and noise contours. Research and development is also required to support full participation in international projects.

## 4.5 Financial - economic

The subjects in the financial - economic area of interest are partly covered in the previous paragraphs. Support is needed in harmonizing the formulated tasks of the armed services and the financial tasking in the coalition agreement and the Defence Whitepaper. More insight is required in the goals and the therefore required funding. A second field of interest is improved transparancy of the main processes. Finally the development and implementation of a quality-model for the processes in the Defence organisation will require supporting research and development.

## 5. PLANNING, PROGRAMMING AND FINANCING

### 5.1 General

Given the limited financial resources careful choices will have to be made in the investments in the knowledge infrastructure. The tasks of the armed services and the therefore required means are primarily determining the priorities and posteriorities.

### 5.2 Planning

For a good control of the research and development process a direct link to the Integral Defence Planning Process is required. In this process the future knowledge requirement is each year systematically described in a framework of functions and technologies. The ambition level and the investments required to reach that level are stated. Defence recognises 3 ambition levels, the basic, functional expert and designer/developer level. These ambition levels are applicable to both Defence and her supporting knowledge infrastructure. Defence itself will at least need the knowledge to understand the results of research and development and to implement them. The ambition levels in research and development are directly related to higher order, Defence wide, ambitions. In the decision process on research and development a number of criteria is applied:
- task related criteria aimed at the contribution to the performance of the main tasks and processes
- efficiency related criteria aimed at the price/performance ratio
- financial feasibility related criteria aimed at availability of funding
- quality related criteria aimed at feasibility, project risks, expected timeliness and usefulness of results
- knowledge infrastructure related criteria aimed at the ensurance of continuity and policy on

decrease or increase in broadness or depth of the knowledge base

Next to these criteria, care has to be taken of political decisions on or related to research and development.

## 5.3 Programming

In programming and control of research and development distinction is made between the investment in knowledge and the utilisation of it. The investment concerns the creation and maintenance of the knowledge base. The control is systematic and programmatic. The utilisation of the knowledge base concerns process support whereby no new knowledge is generated. This utilisation is more ad hoc and difficult to programme on the long run. For the utilisation the project structure is chosen. In the planning only estimates are included. In the programmatic approach the research and development requirements are clustered to substantial, coherent programmes. In the clustering process the goal is to maximise the coherence within the programmes and to maximise the independence between programmes. Programmes have a concrete scope, are limited in time and budget and have programme plans. Programmes have a programme leader on the research institute side and a programme controller on the Defence side. Requirements, coordination, prioritising, execution, progress control and evaluation of knowledge investment are dealt with at the programme level. For management purposes the programmes are subdivided in projects but these play no role in the formal contacts between the research institutes and Defence. The programmatic approach enables a better tuning and prioritisation of the research and development requirements of the armed services and the central organisation.

## 5.4 Financing

The investment in the knowledge base is in principle financed through central, corporate level, budgets. The ulitisation of the knowledge base is financed through the decentral (armed services) budgets. In the planning documents both central and decentral funding is described.

## 6. KNOWLEDGE INFRASTRUCTURE

## 6.1 General

Defence outsources nearly all research and development to research institutes and industry. The research institutes are part of the civil research organizations. A good synergy between civil and millitary research and development is thereby facilitated. The knowledge infrastructure is composed of components of the:
- Netherlands Organization for Applied Scientific Research (TNO) in particular the group Defence Research
- Large Technological Institutes (GTI), in particular the National Aerospace Laboratory (NLR) and the Maritime Research Institute (MARIN)
- Universities, research schools, academic hospitals and other institutes i.e. Aeromedical Institute
- Industry and engineering agencies
- Entities in the armed services i.e. Ammunition Depot

## 6.2 Accessibility

The policy is aimed at a direct access to the esssential parts of the knowledge infrastructure which can fulfill research and development requirements with priority. Defence accepts no

dependence on an uncertain market mechanism. Furthermore a good deal of the required knowledge is not freely available on the market. The links between Defence and the knowledge infrastructure varies, caused by difference in strategic importance and missions of the different partners.

## 6.3 Ambition

The ambition of Defence is a measure for the willlingness of Defence to invest in the knowledge base. A permanent tuning between Defence and the components of the knowledge infrastructure is necessary.

## 6.4. Cooperation

The policy is aimed at increasing the cooperation between the components of the knowledge infrastructure and by stimulating the use of knowledge that is elsewhere available, both in national and international context.

## 6.5 Independence

As indicated Defence uses external research and development organisations as much as possible. Defence attaches great value to the objectivity and independence of these organisations. Although contract research will be based on clear agreements on deliverables, Defence will respect the scientific integrity of these organisations and their personnel.

## 7. INTERNATIONAL COOPERATION

### 7.1. General

The Netherlands can nationally only provide for part of the requirements of knowledge. Through international cooperation access is gained to the international research and development community and the net effect of the national activities is enhanced (multiplier effect). Cooperation also enables the influencing of the research and development efforts in international groupings. Furthermore a network of good relations is formed. The policy is aimed at maximising the net effect of the own activity by exchange of information and by cooperation projects whereby in some form complementary research and development activities are defined and executed. The policy is further aimed at possibilities of more progressive forms of cooperation. This may lead to narrower tasking of the national research and development organisations to optimise complementarity and minimise duplication. Finally in some cases this might lead to mutual interdependence. Needless to say that this will only be reached after a careful process based on mutual trust.

### 7.2 Defence Technology and Industrial Base (DTIB)

Inernational cooperation also opens possibilities to the Netherlands industry to strengthen their position. Defence facilitates and stimulates synergy between the research and development organisations and the Defence related industry.

### 7.3 Instruments

For the international cooperation the mechanisms are used as developed under NATO and WEAG and under bi- and other multilateral agreements. Examples are the NATO/RTO expert

level activities (formerly known as level 3) and the EUCLID/EUROFINDER and THALES agreements. In all fora a thrust towards more cooperation is experienced, dictated by higher knowledge requirements and lower budgets.

## 8. ORGANISATIONAL ASPECTS

The research and development community has to provide for the required knowledge base, Each manager responsible for specific tasks or processes is also responsible for the definiton of the supporting requirements of research and development. The ultimate responsibility for the requirements of research and development for the armed services lies with the commanders in chief supported by their heads of research. In the central organisation the Director General Materiel staff has an head of research. He is embedded in the Directorate for Research and Development. This directorate is responsible for the Defence wide research and development policy and the tuning of the research and development requirements between the armed services and the central organisation. Furthermore the directorate takes care of the interdepartemental consultation and external management affairs. The heads of research are responsible for the actual implementation of the policy and the actual execution of the research and development plans.

## 9. RELEVANCE TO THIS FORUM

This forum is dedicated to ballistics of projectiles. The Netherlands have a strong activity in this area of interest. In this oral presentation a number of anchor points for your forum was given, more specific: higher weaponeffects, less collateral damage, better protection, and active defence against weapons of mass destruction. Furthermore the necessity for international cooperation was underlined and this forum is just a good example of that desired cooperation. So, in short, this forum is relevant for the Netherlands and is of great use to the Netherlands and I assume for the other participating nations as well. It is very well in line with our national policy on research and development.

# ORGANISATION OF THE DEFENCE RESEARCH IN GERMANY AND OVERVIEW OF FUTURE ORIENTATION

## BDir U. TIEDEMANN

BMVg, Federal Republic of Germany

The first part of this presentation gives a short overview of the various steps of the planning process and the decisions to generate the annual "Research and Technology Program" and to reach program execution.

The second part describes the internal structure "Research and Technology Concept" based on:

> 7 areas of competence
> 45 Technology areas and 14 advanced system technologies
> 99 Technologies and Specific Concepts

It covers:

> Basic Research
> Advanced Technical Demonstration
> System Technology

An outlook on future changes and modifications will be given.

| | Planning Process and Decisions | BMVg Rü I 4 |
|---|---|---|

Part 1

**BWB**

```
┌─────────────────────┐
│    Annual Report    │                    01 /2000
│         and         │
│   Recommandation    │
└─────────────────────┘
```

│ MoD
▼

```
   ╭─────────────────────╮
   │     Submission      │              03 /2000
   │    Annual Report    │
   ╰─────────────────────╯
```

**MoD**

```
┌─────────────────────┐
│     Evaluation      │
│         of          │
│    Annual Report    │
└─────────────────────┘
```

**MoD**

```
        ◇ Annual Directives ◇           07 /2000
```

│ BWB
▼

**BWB**

```
┌─────────────────────┐
│        Total        │
│  Program Proposal   │
└─────────────────────┘
```

│ MoD
▼

**BWB**

```
   ╭─────────────────────╮
   │     Submission      │              09 /2000
   │ Total Program  Proposal │
   ╰─────────────────────╯
```

▼

**MoD**

```
   ╭─────────────────────╮
   │  Program  Approval  │              10 /2000
   ╰─────────────────────╯
```

│ MoF
▼

| 6. LOI  R&T SG FIN | German Planning & Approval Process for  R&T | 01.02.00 |
|---|---|---|

Part 2

MoF — **Budget Request** — 03 /2001

Parliament

Parliament — **Budget Negotiations** — 09-10 /2001

Parliament — **Budget Approval** — 11 /2001

Program Adjustments

President — 01.01.2002

MOD — *Budget Execution Order* — 01 /2002

**Program Execution**

# Areas of Competence

(BWB - Technical Directorates)

**BMVg**
Rü I 4

| | | |
|---|---|---|
| 1 | Reconnaissance, Communication, Navigation, Simulation | FE |
| 2 | Information Technology | IT |
| 3 | „Land"-Systems | KG |
| 4 | „Air"-Systems | LG |
| 5 | „Sea"-Systems | SG |
| 6 | Weapons, Terminal Ballistic, Effectiveness of Fire, Armor Protection | WF |
| 7 | General F&T - Topics | AT |
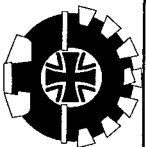
Overview Areas of Competence;

## Technology Fields and Advanced System Technology

**1** # Reconnaissance, Communication, Navigation, Simulation

Basic Research & Advanced Technology Demosntration:

System Technology for:

➔ **Materiel and Technologies for Semi-Conductors**

➔ **Communication Systems**

➔ **Sensors (Collection of  Position-, Geographic- and Target -Data )
incl. Sensordata Analysis for Fuse Systems, Terminal Guidance
Systems; Electronic Countermeasures/ Sensors; Geophysics and
Geographics**

➔ **Electronic Warfare**

➔ **Reconnaissance Systems**
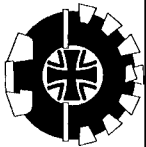
➔ **Communication Technology and Networks**

➔ **General Technologies for Navigation**

➔ **Identification and Coding Systems**

➔ **Indirect Protection(Camouflage, Detection Reduction)**

➔ **Satellite Technology (Sensors) incl. Ground Stations
(Systemtechnology)**

➔ **Simulation Technology,Training Aids; Test Equipment**

➔ **Robotics**

Overview Areas of Competence;
Technology Areas and Advanced System Technology

## 2  Information Processing

Basic Research & Advanced Technology Demosntration:

➔ **Software Technology, Interoperability, Standardisation**

➔ **Information Protection, Information Warfare**

➔ **Information Systems**

➔ **IT - Simulation**

➔ **New IT-Technologies**

System Technology for:

➔ **Information Systems**
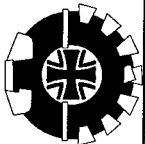
Overview ==>Areas of Competence;
Technology Areas and Advanced System Technology

## 3  „Land" Systems

Basic Research & Advanced Technology Demosntration:

➔ **System Technology for Armored Vehicles; general aspects**

➔ **Engineer Equipment and Special Equipment**

➔ **Vehicle Command, Control,Vehicle Electronics, Fire Control**

System Technology for:

➔ **Combat Vehicles, Transportation Vehicles**

➔ **Equipment to hamper or enhance Troop Movement and Mobility, NBC - Protection**
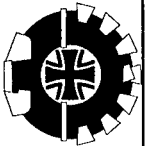
Overview ==>Areas of Competence;

**Technology Areas and Advanced System Technology**

| 4 | „**Air" Systems**

Basic Research & Advanced Technology Demosntration:

→ **General Aspects**

→ **System Technology for Aircrafts**

→ **System Technology for Helicopters**

→ **UAV**

→ **Avionics, Fire Control, Flight Control**

→ **Propulsion Systems**

System Technology for:

→ **Aircrafts**

→ **Helicopters**

→ **UAVs**
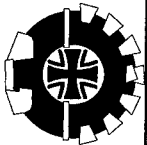
Overview ==>Areas of Competence;
**Technology Areas and Advanced System Technology**

| 5 | „Sea" Systems

Basic Research & Advanced Technology Demosntration:

➔ **General Technology for Surfaceships and -boats; general Aspects**

➔ **General Technology for Submarines; General Aspects**

➔ **Command Control, Fire Control**

➔ **Under Water Weapons**

➔ **Sonar Technology, Navy specific Sensor Systems; Sea Environment**

➔ **Signatures**

System Technology for:

➔ **Surfaceships and -boats**

➔ **Submarines**

➔ **Special Naval Weapons**

Overview ==>Areas of Competence;

**Technology Areas and Advanced System Technology**

**6** **Weapons,Terminal Ballistic, Effectiveness of Fire, Armor Protection**

Basic Research & Advanced Technology Demosntration:

↑ **Effectiveness of Fire, Armor Protection**

↑ **Guns**

↑ **Missiles, Rockets, Air delivered Weapons**

↑ **Beam Weapons and Protection**

↑ **Extended Air Defense**

↑ **Smart Terminal Guidance**

System Technology for:

↑ **Missiles**

↑ **Guns, Artillery Rockets**

Overview ==>Areas of Competence;
Technology Areas and Advanced System Technology

## General F&T - Topics

| 7 |

Basic Research & Advanced Technology Demosntration:

System Technology for:

↑ Evaluation- and Decision Tools,Cost Management & Planning Tools

↑ Scientific Trend Analysis;
New Defense Technologies (Basic Research)

↑ Scientific Friction Technology, Fuel and Lubricants

↑ Materials

↑ NBC - Protection;  Fire Protection

↑ EME - Protection

↑ Human Factors

↑ Foreign Systems

↑ Environmental Protection

↑ Personal Soldier Equipment
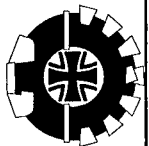
# Area of Competence;
## Technology Areas and Advanced System Technology

**Example:** | **3** | „**Land Systems**

Basic Research & Advanced Technology Demosntration:

➔ **General aspects for armored combat vehicles**
**General Aspects**

- ⇧ **General Aspects**
- ⇧ **Design- & Engineering Principles, Structural Strength**
- ⇧ **Vehicle Dynamics**
- ⇧ **Propulsion Technology**
- ⇧ **Passive Armor Protection**
- ⇧ **Active Armor Protection**

➔ **Engineer Equipment and Special Equipment**

- ⇧ **Design- & Engineering Principles, Structural Strength**

➔ **Vehicle Command, Control,Vehicle Electronics, Fire Control**

- ⇧ **Vehicle Command, Control, Navigation**

# Projectiles

# TRENDS OF PRECISION GUIDED PROJECTILES

TROSKY B.

Diehl Munitionssysteme GmbH & Co. KG

Abstract:    The main requirements of a modern army are maximum precision and
enhancement of maximum range. Different solutions for different requirements will be
shown. The Correction Fuze is a retrofit for existing 155 mm projectiles, using GPS for
range correction only. The Precision Guided Projectile is a new development with range
enhancement and maximum possible accuracy, using a GPS based strap down system.
The primary role of 76 mm naval munitions is anti missile and anti aircraft defense and it
uses on board radar systems for correction commands. The shown 105 mm tank ammunition
is a laser beam rider that combines range enhancement with a superior first hit capability.
The Precision Guided Mortar Munition is a man in the loop system that uses a laser
designator.

## 1. INTRODUCTION

The conventional artillery is firing to area targets up to 30 km range (and beyond 30 km, when
using base bleed) with a resulting accuracy which is strongly range dependent. This situation
makes the know requirements much more important:

Minimisation of the error budget with the resulting benefits:
- Less collateral damage
- Reduced cost per mission
- Less logistic efforts

Range enhancement with the resulting benefits:
- More flexibility
- Less systems needed per mission
- Reduced vulnerability

The requirements for naval, tank and infantry systems are very similar for which some
relevant possible solutions will be discussed here.

## 2. 155 MM ARTILLERY PROJECTILES

The recent artillery systems with conventional unguided projectiles are producing
unacceptable large errors at ranges of 30 km and beyond. At least for this purpose a correction
or guidance is necessary. Also collateral damage is high and the flexibility low, extended
range would give the desired higher flexibility.
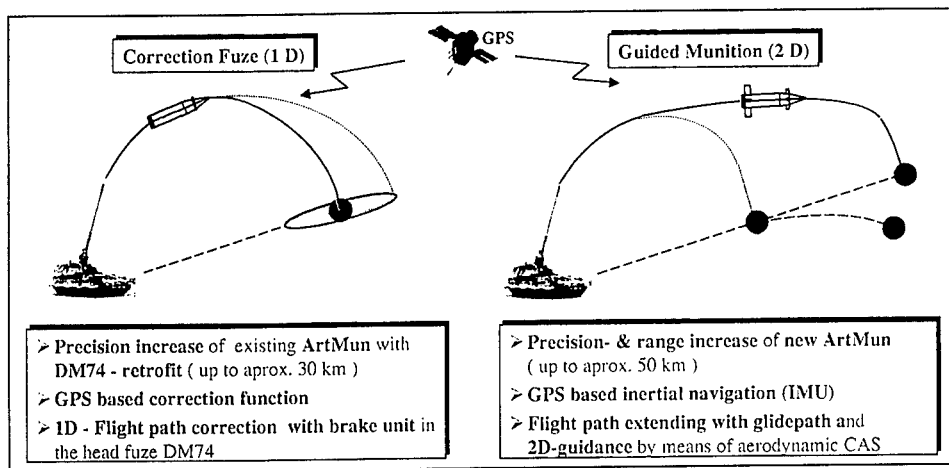
Figure 1 : 1 D and 2 D Concept Comparison

## 2.1 Correction Fuze

The Correction Fuze contains a single correction device that will decrease down range errors significantly and maintain the cross range error which is much lower.

The main benefits of this solution are:

- Retrofit solution, only the fuze has to be changed
- No change to the projectile and no significant change to the firing procedure

Therefore the projectile will be fired with a higher elevation, calculated to hit a virtual target point beyond the real target position, to have a plus/minus two sigma area for correction. A drag break will be opened to increase the total drag of the projectile, at a time that is dependent on the difference between actual and nominal trajectory. After predicting the actual trajectory, using the position data from the GPS and calculating the difference between nominal and forecasted impact, the opening time can be taken from a look up table. The look up tables for different trajectories have been calculated in advance and are loaded into the projectile before launch.

The correction fuze will be a low cost solution easy in handling, because all additional components will be integrated inside the fuze. The main components are:

- GPS receiver with antenna
- Drag device
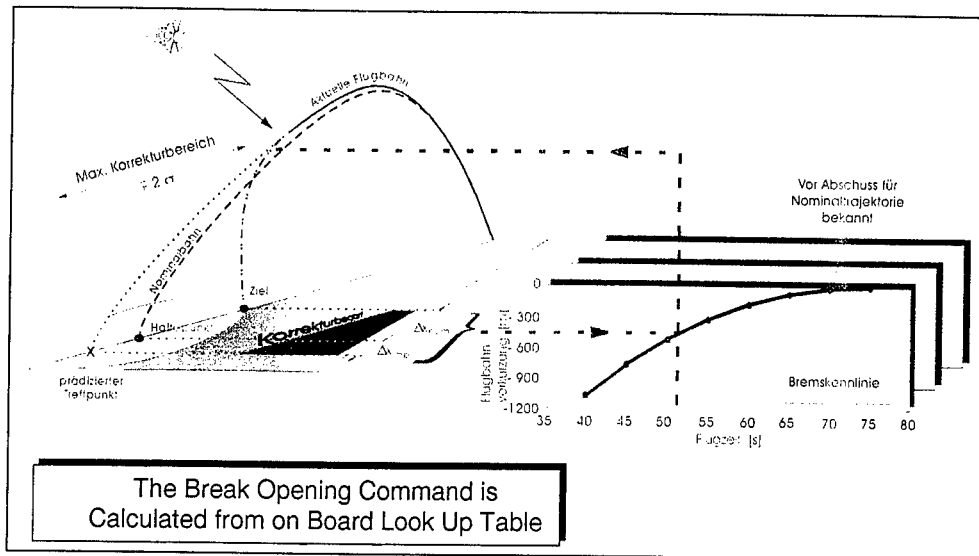
Figure 2 : Correction Fuze Opening Algorithm

## 2.2. Precision Guided Projectile

The Precision Guided Projectile is a totally new ammunition with better accuracy than the Correction Fuze. The resulting accuracy is independent of range. In an ongoing study different concepts for this kind of projectiles are in consideration. One of the concepts will be discussed here.

This concept is shown in Fig. 3 and can be characterised by:

- High modularity
- 4 Canards, 2 axis control actuation system
- Fin stabilised rolling airframe
- Slipping obturator

The projectile will have a slipping obturator and start with a low roll rate. The fins will open immediately after launch and the projectile will fly fin stabilised all the time.
The navigation system consist of a strap down system with Internal Measurement Unit and GPS. The IMU has to be initialised after launch. While the initialisation of the position can be done by using GPS data, the attitude in pitch, yaw and roll must by initialised using estimation algorithms.
After apogee the canards will be deployed and the projectile starts to glide and navigate to the target.
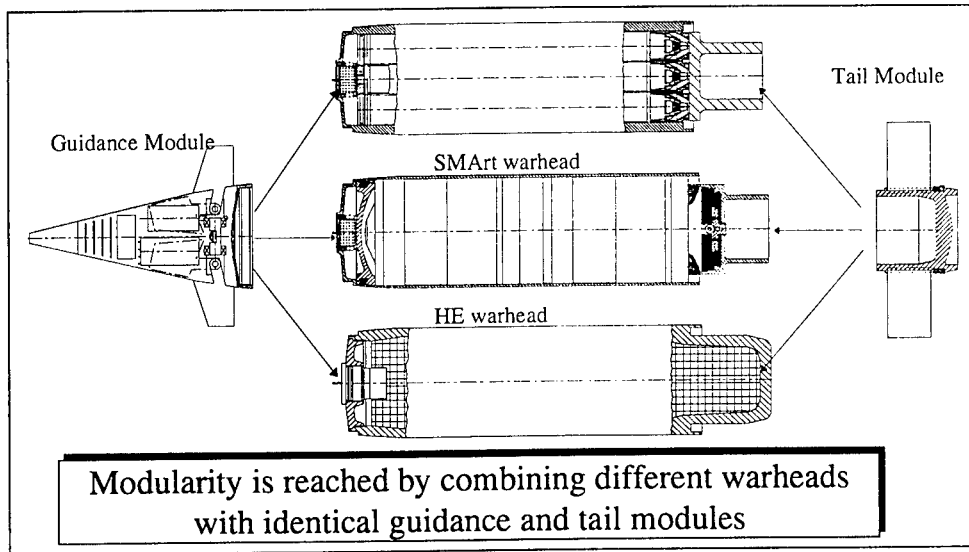
Figure 3 : Modules of the Precision Guided Projectile

## 2.3 Effectiveness Comparison

Effectiveness analysis have been made, comparing conventional artillery projectiles with guided projectiles. One example is given in Fig.4. This diagram shows the number of rounds necessary to defeat single targets, meeting the given criteria and assuming a target location error of 50 m CEP. The target area contains 5 light armoured vehicles and the attacking rounds are 155mm cargo projectiles with standard bomblets. A single target reconnaissance has been assumed. Because of increasing error budget the necessary number of rounds is increasing significantly beyond 25 km range. The error budget for Precision Guided Projectiles using GPS (2-D Correction) is independent of range. The Correction Fuze (1-D Correction) has decreasing range errors only and because of increasing deflection errors the total error budget is not independent of range. From this example it is obvious, that for extended range munition beyond 30 km some kind of correction or guidance is necessary.
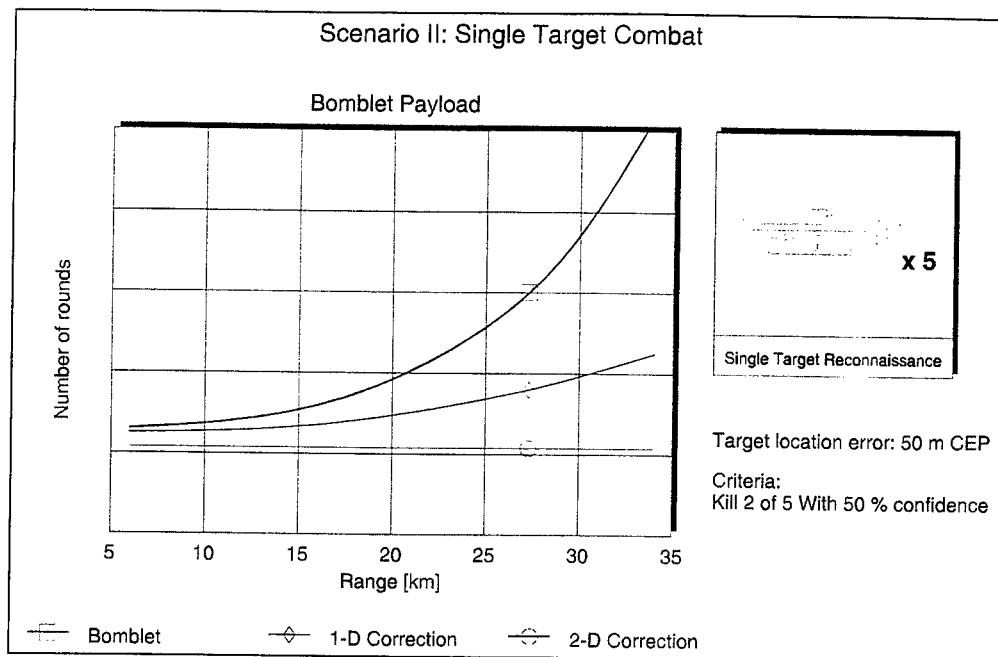
Figure 4 : Effectiveness against Light Armoured Vehicles

## 3. 76 MM NAVAL MUNITION

With the project name DAVIDE/DART the company OTOBREDA is contracted by the Italian Navy to develope a new 76 mm naval munition. The primary role of this projectiles is anti missile and anti aircraft defense.
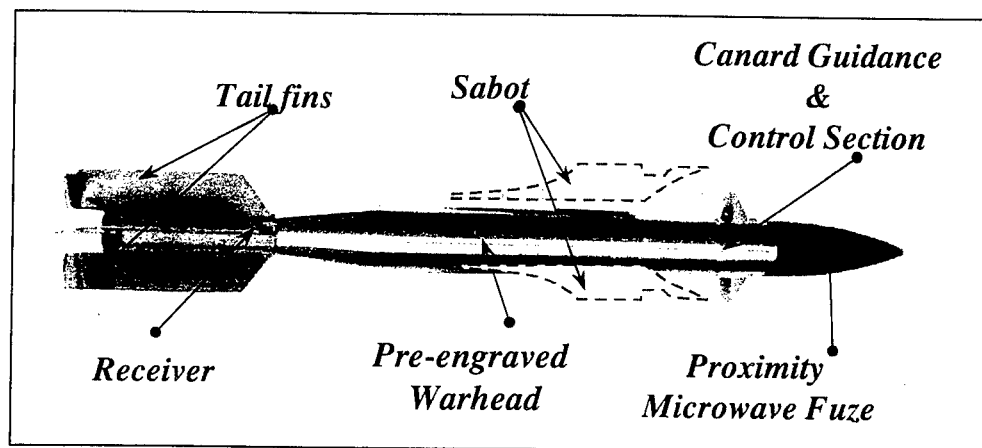


Figure 5 : 76 mm Naval Munition (DAVIDE/DART)

The subcaliber projectiles are fin stabilised with 2 canards 2 axis control system. The rolling airframe has a decoupled roll stabilised control section and two internal electrical motors are

controlling the round. One motor is responsible for roll control and the other is controlling the canard deflections.

The high muzzle velocity of the subcaliber projectile results in a short time of flight to the target and a high manoeuvrability. This was a determined need to hit the modern anti ship missiles with its manoeuvring capability. To minimise the costs, mainly ship-board systems are used to track and control the rounds.

A radar beam rider guidance is used to control the shell in flight.

## 4. SPEAR

SPEAR is a tank gun launched laser precision guided ammunition. The 105 mm projectile is a laser beam rider and the round is rocket assisted. The project is a joint development of KBP (Russia), Krauss- Maffai Wegmann and Diehl Munitionssysteme.

The rolling airframe is controlled by a pneumatic canard actuation system. The guidance section with gyro and optronical receiver is integrated in the back of the projectile.

The main benefits of this system are the extended range of up to 5.5 km , what is much more than the range of conventional rounds and the superior first hit probability.

The SPEAR round is fully compatible in handling, loading and logistics with the existing conventional rounds and the concept is a upgrade package as retrofit kid for NATO tanks.
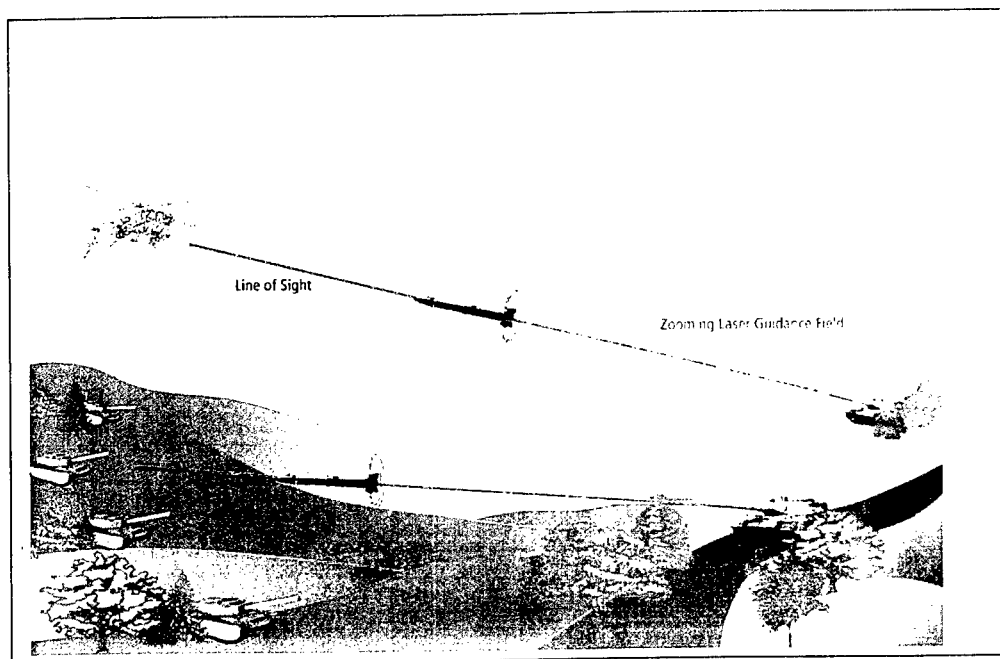


Figure 6 : 105 mm Tank Gun Launched Munition

## 5. PGMM

The Precision Guided Mortar Munition is a 120 mm projectile with a seeker for terminal guidance. It is a man in the loop concept with laser designation of the target.

The fins deploy immediately and the rolling airframe flies fin stabilised. Before apogee the roll reference is calculated by an estimation algorithm using the measurement of the three gyros. After strap down initialisation the wings deploy at apogee and in this configuration a glide to a range of more than 12 km is possible.

During glide phase in-flight corrections are made to guide to a predetermined in-air basket. At this point the seeker starts to scan for laser designator energy on target. After target acquisition PGMM can manoeuvre to attack.
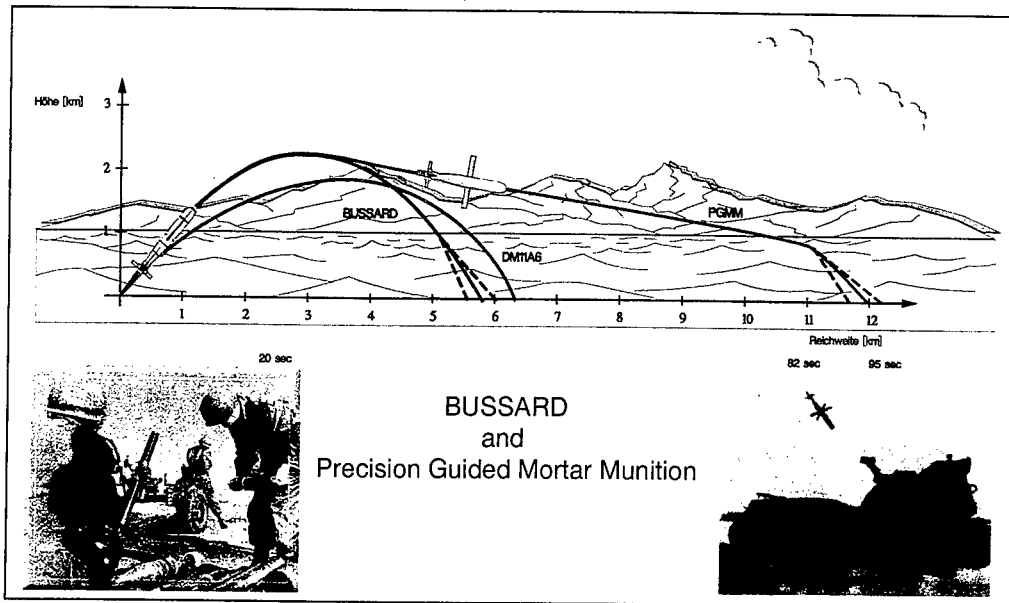


Figure 7 : Precision Guided Mortar Munition Operational Concept

# SMART AMMUNITION ASSESSMENT :
# DCE WORKS IN 155 GAM FEASIBILITY STUDY

DEREGNAUCOURT D.

Etablissement technique de Bourges, 18015 Bourges, France

**Abstract :** The Guided Artillery Munition (GAM) is a feasibility study to develop a smart guided artillery 155 mm ammunition. France, Germany and The Netherlands are co-operating in this project, both on government and industry level. The purpose of this paper is to describe DCE works in this 155 GAM feasibility study :
-   participation as expert in detection area (CELAR), inertial sensors (LRBA), flight mechanic (ETBS) to evaluate which risk areas have been surmounted and which risk areas to be overcome during a future development ;
-   realization of all the gun firing tests to demonstrate the Transition Phase at ETBS.

## 1. INTRODUCTION

The Guided Artillery Munition (GAM) project is a feasibility study for the development of 155 mm smart artillery ammunition, carried out within the framework of a co-operation agreement, at both governmental and industrial level, between France, Germany and The Netherlands. The Ministers of Defence of the three nations concerned signed a Memorandum of Understanding (MOU) on April 23rd, 1992.

GAM operation can be outlined as follows :
A 155 mm cargo-projectile is fired from a standard 155 mm howitzer. Once the cargo-projectile has left the barrel, a time fuse initiates the expulsion of a canister. Velocity and spin rate are reduced and a submunition is released from the canister, deploying eight wings and four fins.
The submunition seeks and finds the horizontal plane and performs a pull-up in order to continue a stable horizontal flight. During the non-powered flight phase, the submunition seeker search for targets. Once a target is found, the seeker locks on the target. Next, the autopilot sends commands to the fins in order to steer the submunition to the target (Figure 1).

In compliance with the operational principle described above and within the framework of the GAM feasibility, three main independent tests were identified :
1.  The **Captive Flight Test** (CFT), in which the submunition seeker was carried under an aircraft and flown over different target configuration. This test was performed to investigate seeker detection and tracking abilities.
2.  The **Open Loop Drop Test** (OLDT), in which the submunition (without seeker) was dropped from an aircraft and has to execute a pre-programmed flight to prove submunition ability to perform a pull-up and to continue a stable horizontal flight.
3.  The **Transition Phase Demonstration** (TPD) to demonstrate that after the firing of a cargo-projectile 155 mm GAM, the complete canister/sub munition expulsion sequence functions correctly.
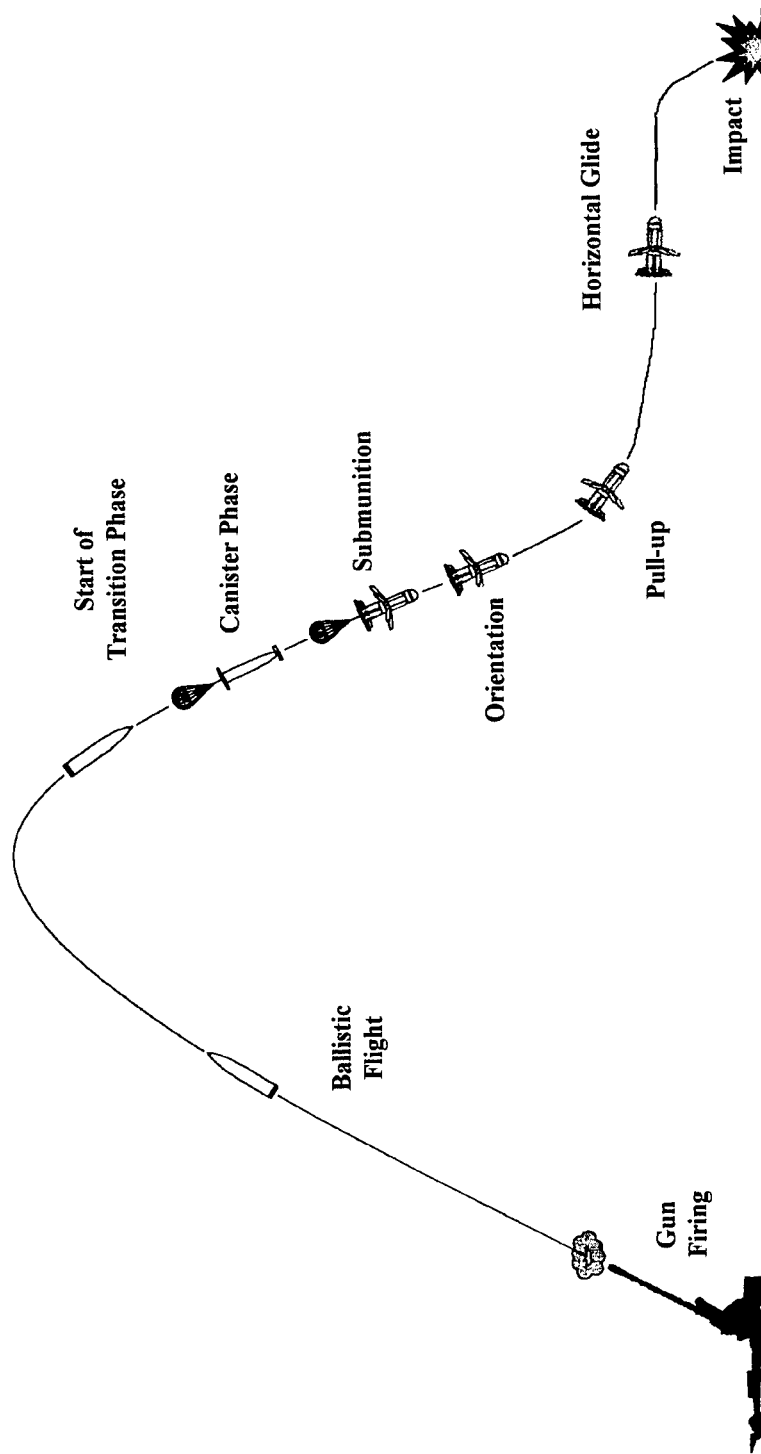
Figure 1 : 155 GAM – Description of different phases

During a Management Comittee (MC), it was decided to establish three trilateral state evaluation workgroups in accordance with the three main work packages :
- Captive Flight Test – Evaluation Subgroup (CFT-ESG) ;
- Open Loop Drop Test - Evaluation Subgroup (OLDT-ESG) ;
- Transition Phase Demonstration - Evaluation Subgroup (TPD-ESG).

Each subgroup was supported by experts from industries involved in the program.

## 2. CELAR PARTICIPATION IN 155 GAM FEASIBILITY STUDY

### 2.1 Captive Flight Test – Evaluation Subgroup (CFT-ESG)

The objective of the CFT-ESG was to evaluate and to analyse the measured CFT – data of the seeker head. Furthermore, the evaluation subgroup might ascertain the capabilities of the seeker head, including Electronic Counter-Countermeasures (ECCM) aspects.

This subgroup was chaired by Germany. The national representatives came from :
- CELAR (DGA/DCE) - France
- WTD 81 – Germany
- TNO-PML – The Netherlands

The CELAR was in this subgroup as expert in weapon systems and in electronic countermeasures in the area of millimetric waves.

The main tasks performed by the CFT-ESG were the following :
- seeker performance in different scenarios :
  - stationary target indication (probability of detection, reduced false alarm rate, signature analysis)
  - moving target indication (probability of detection, reduced false alarm rate, signature analysis)
  - terminal track
  - countermeasures
    active (CELAR and FGAN jammer)
    passive (camouflage, decoys)
- risc calculation for future development

### 2.2 CELAR participation in the CFT

During captive flight tests in which the submunition seeker was carried under an aircraft and flown over different target configuration, CELAR used its active countermeasures in the area of millimetric waves (figure 2).



Figure 2 : 155 GAM – CELAR's jammer

## 3. LRBA PARTICIPATION IN 155 GAM FEASIBILITY STUDY

### 3.1 Open Loop Drop Test – Evaluation Subgroup (OLDT-ESG)

The objective of the OLDT-ESG was to analyse and evaluate the measured data from the flight data recorder and the telemetry data.

This subgroup was chaired by The Netherlands. The national representatives came from :
- LRBA (DGA/DCE) - France
- BWB – Germany
- TNO-PML and DMKL – The Netherlands

The tasks performed by the OLDT-ESG were the following :
- flight performance evaluation,
- subsystem performance evaluation :
  - functioning of the IMU (Inertial Measurement Unit),
  - functioning of inertial navigation,
  - functioning of autopilot algorithms,
  - functioning of FAS (Fins Actuating System),
  - functioning of dataprocessor,
  - subsystem interference,
  - functioning of deployment and locking mechanism of the wings.

### 3.2 Test in laboratory

It was also scheduled that LRBA controlled in laboratory an IMU (Inertial Measurement Unit) before and after a gun hardening test at 8000 g.

## 4. ETBS PARTICIPATION IN 155 GAM FEASIBILITY STUDY

### 4.1 Transition Phase Demonstration – Evaluation Subgroup (TPD-ESG)

The objective of the TPD-ESG was :
- to evaluate GAM performances at system and component levels,
- to determine the limits of the various validations undertaken by the contractors,
- to identify risks to be overcome during a future development.

This subgroup was chaired by France. The national representatives came from :
- ETBS (DGA/DCE) - France
- BWB – Germany
- TNO-PML and DMKL – The Netherlands

The tasks performed by the TPD-ESG were the following :
- cargo shell : to verify gun launch resistance and ballistic behaviour,
- canister phase: to verify the first step of the transition sequence, i. e. canister ejection so as to reduce translation velocity and spin rate,
- fins : to verify fin deployment through wind tunnel tests and gun firings,
- components : gun hardening qualification of submunition (FAS, FAS servo electronics, wirings, deployment electronics, power supply, IMU, ...)
- uncontrolled submunition : demonstration test in which the whole sequence of canister expulsion and uncontrolled submunition ejection is validated. The submunition is equipped with a data gathering device,
- controlled submunition : final demonstration to validate the whole sequence.

## 4.2 Gun firing tests during Transition Phase Demonstration

All gun firing tests to validate the transition phase were made at ETBS ; the main tests were the following :
- horizontal gun firing tests,
- vertical gun firing tests,
- ballistic gun firing tests.

### 4.2.1 Horizontal gun firing tests

The aim of this test was to visualise the primary expulsion phase :
- canister expulsion from cargo shell,
- shell base/canister separation,
- parachute opening and efficiency,
- efficiency of spin brakes in spin deceleration,
- canister/parachute stability.

Test configuration is presented in figures 3 and 4.
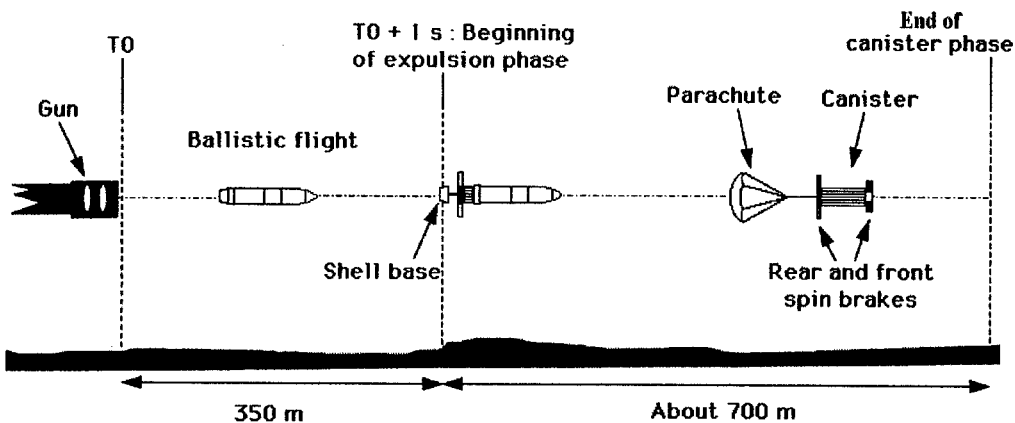


Figure 3 : Horizontal gun firing tests
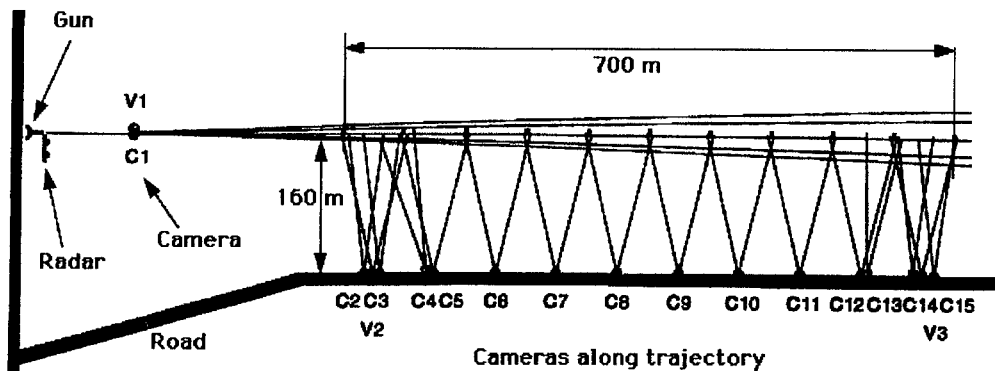


Figure 4 : Test configuration

Nominal kinetic conditions on primary expulsion were not obtainable with only one gun ; two types of tests were carried out :

- with a classic gun (155 TRF1) in order to obtain the nominal linear velocity at first expulsion,
- with a specifically rifled 39 calibre gun in order to obtain the nominal spin rate at first expulsion.

The following measurements were made during these tests :

- initial velocity and velocity on trajectory by Doppler radar,
- pressure in gun chamber,
- visualisation device : video cameras and high speed cameras.

Figure 5 is a Doppler radar curve representing linear velocity/time :
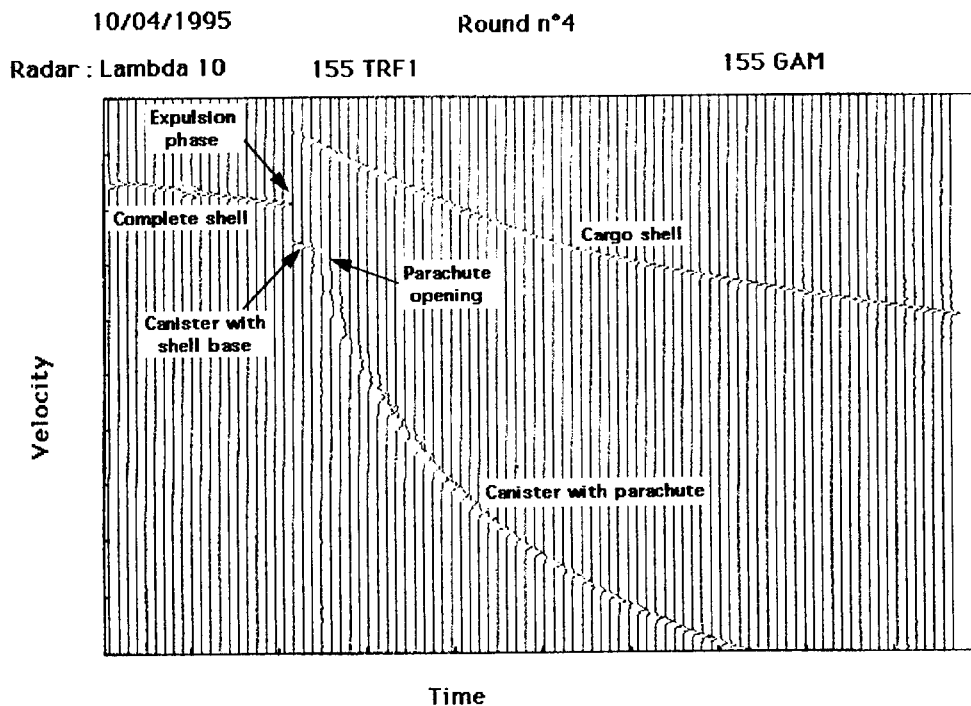


Figure 5 : Doppler radar curve

## 4.2.2 Vertical gun firing tests

The aim of these vertical gun firing tests was to verify the behaviour of submunition mechanical and electronic parts at high G level (in a gun environment) : linear acceleration is in the same direction at the beginning (figure 6) and at the end of the trajectory ; the shell falls onto the base shell (figure 7).

A nominal vertical gun firing test trajectory features may be :

|  |  |
|---|---|
| Gun : | TRF1 |
| Elevation : | $\approx$ 1540 mil. |
| Muzzle velocity : | $\approx$ 770 m/s |
| Max. altitude : | $\approx$ 8000 m |
| Range : | $\approx$ 1200 m |
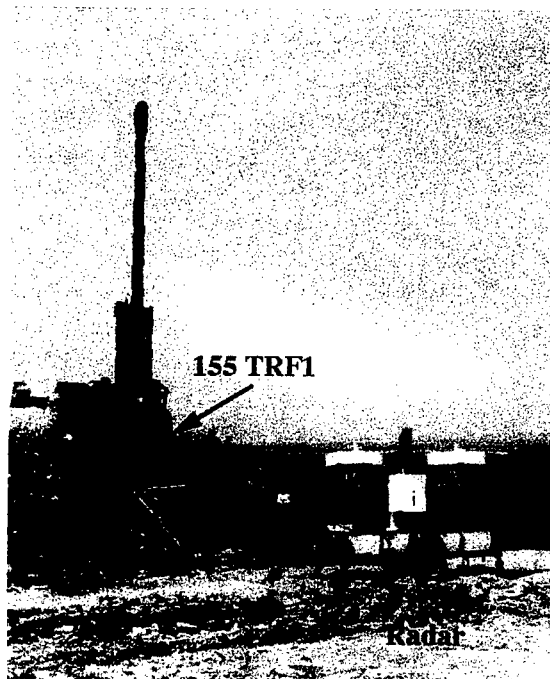
Figure 6 : Gun in firing position
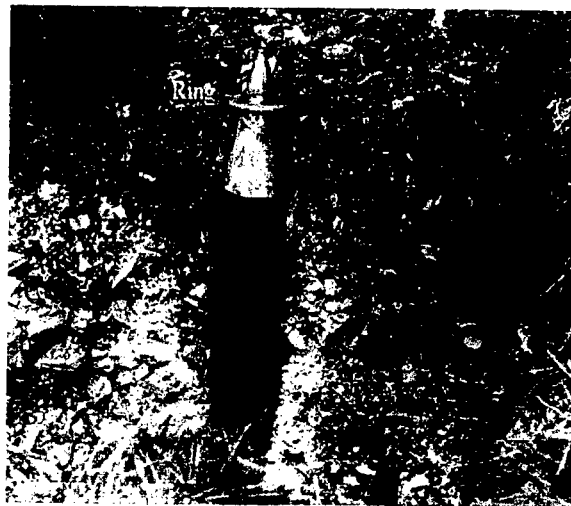


Figure 7 : Shell after firing in the ground

### 4.2.3 Ballistic gun firing tests

These gun firing tests were carried out to validate the functional sequence from cargo shell gun launch through to submunition free flight :
- expulsion of canister from cargo shell, ignited by time fuse,
- separation between shell base and canister base,
- opening and efficiency of parachute,
- spin brake efficiency in spin deceleration,

- stability of canister with parachute,
- expulsion of submunition from canister,
- wings and fins deployment,
- separation between parachute and submunition,
- submunition free flight.

A new ETBS data recording facility was used for these tests : two optical tracking systems (figures 8) :
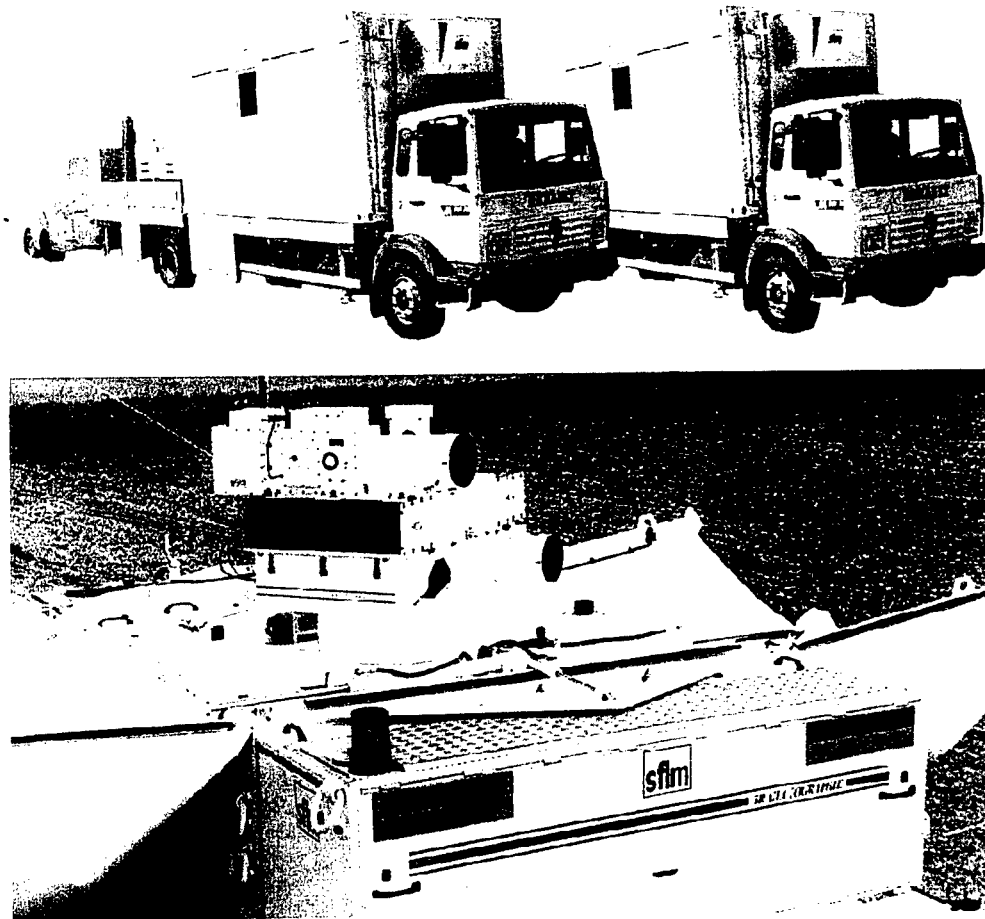


Figure 8 : Optical Tracking System

The Optical tracking system allows different things :
- to see if the complete transition phase from the cargo shell to the submunition is correct,
- to date the different events (ejection of canister, opening of parachute, ejection of submunition, separation between parachute and submunition...),
- to know canister spin rate during the canister phase,
- to know the position and the attitudes of canister and submunition during their flight
- ...

Two exemples are provided in figures 9 and 10.
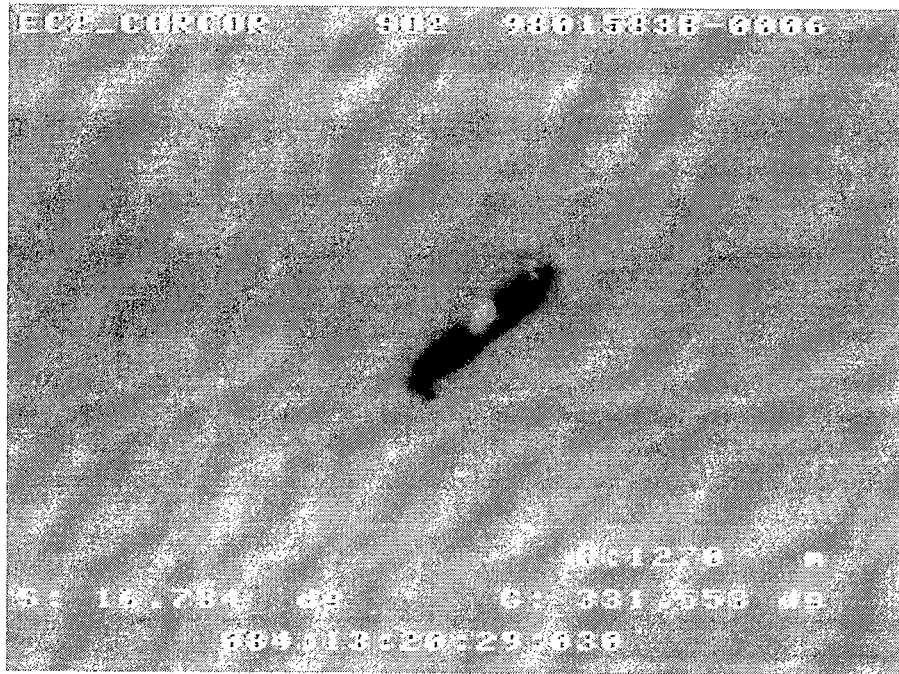
Figure 9 : Canister just before and during second expulsion
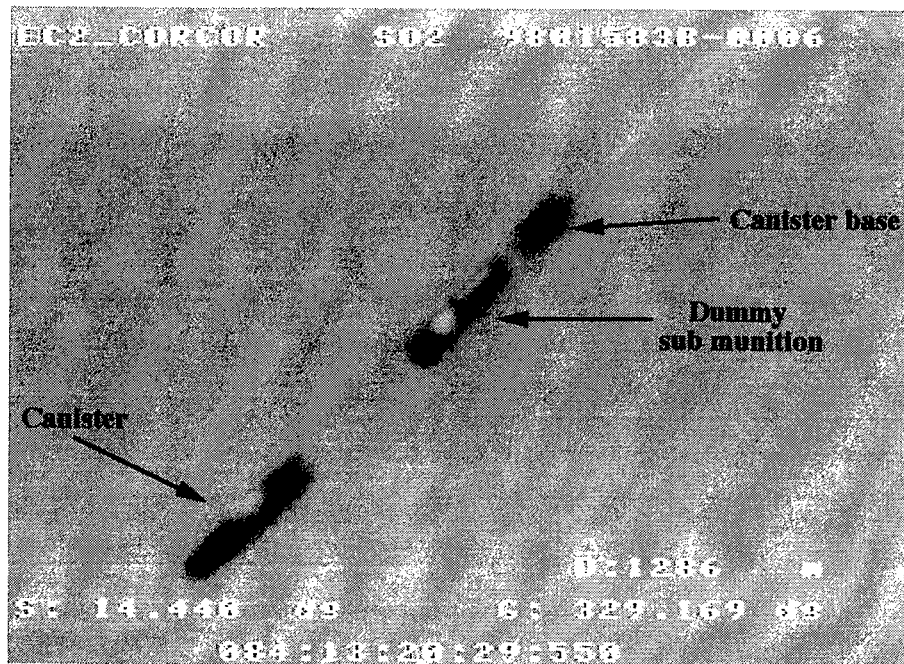
**Picture 1 : Flight of canister**
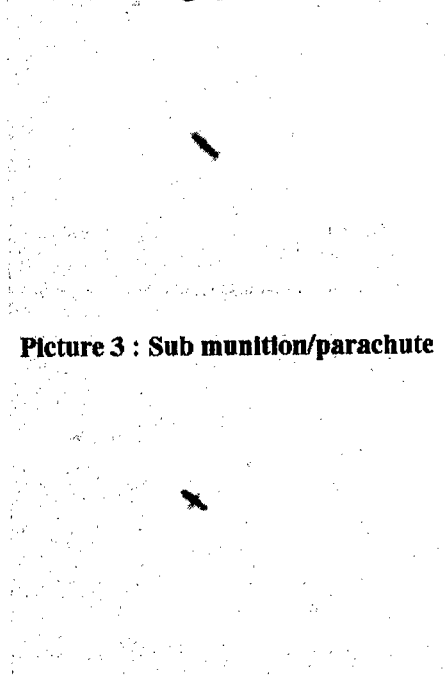
**Picture 2 : Second expulsion**
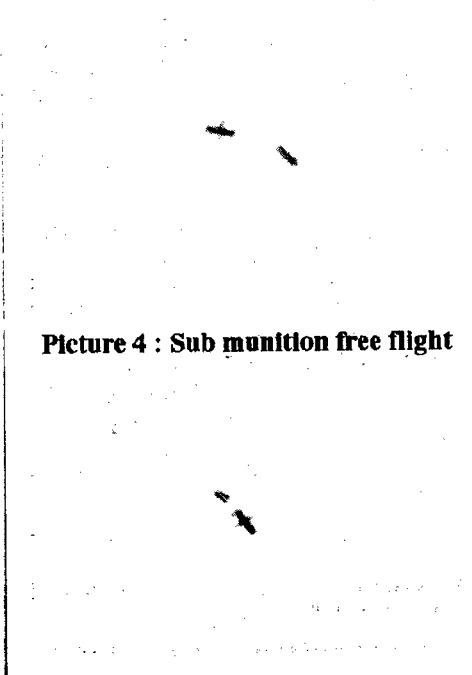
**Picture 3 : Sub munition/parachute**
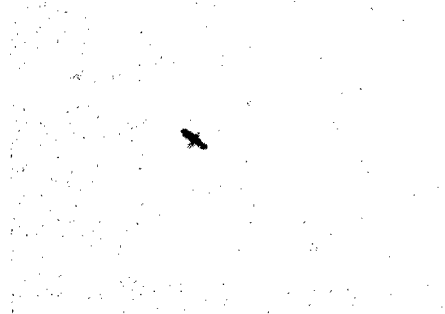
**Picture 4 : Sub munition free flight**
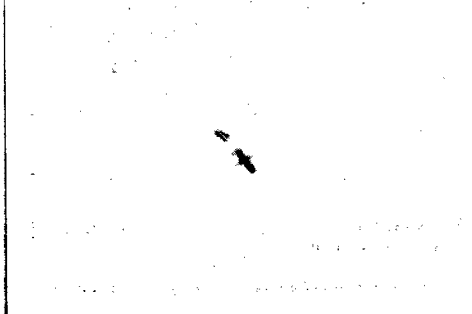
**Sub munition free flight**
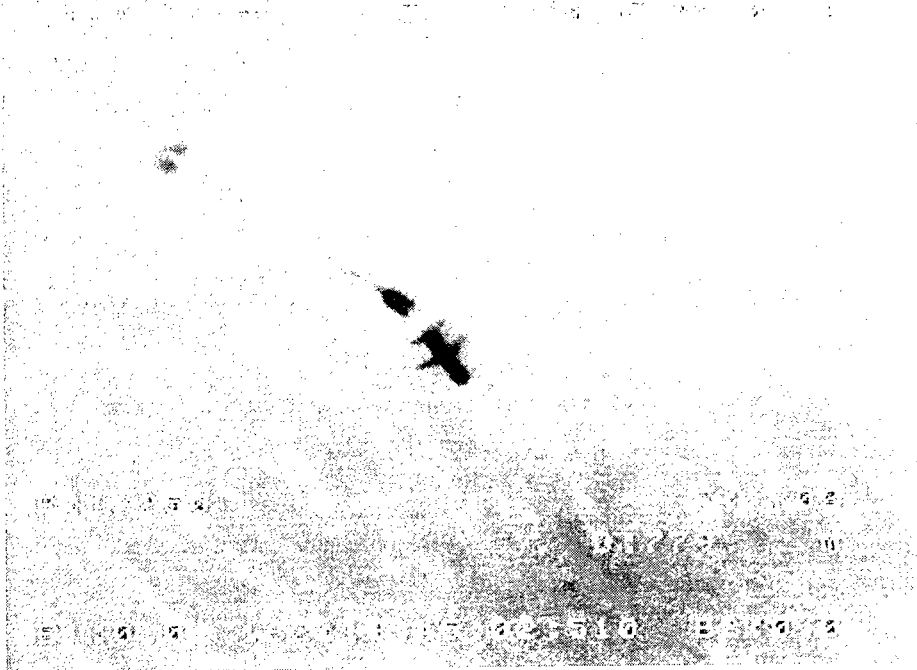
Figure 10 : Views from Optical Tracking System

- 58 -

## 5. CONCLUSION

At request from program services, three centers of DCE performed works during the 155 GAM feasibility study in two domains :

- participation as expert in :
  - detection area (CELAR)
  - inertial sensors (LRBA)
  - flight mechanics (ETBS)

- participation as test center (laboratory or ground) especially ETBS concerning transition phase demonstration tests.

By performing these tasks, the centers of DCE have realized a complete prestation for the Artillery Program Office (DSA/SPART).

# DEVELOPMENT OF AN APFSDS-T MEDIUM CALIBRE AMMUNITION WITH OPTIMIZED PERFORMANCE & STABILITY

## M.Sc JAN G.HASSLID, M.Sc JARL EIRIK STRAUME

Nammo Raufoss AS, P.O. Box 162, N-2831 Raufoss, Norway
Tel. +47-611-52348, Fax. +47-611-52250

**Abstract:** This presentation covers recent analysis and qualification of a sub-calibre system designated for use with modern Infantry Fighting Vehicles, IFV's, equipped with a medium calibre gun. The ammunition concept is based on a low-weight, high strength pusher sabot system, whereas the long rod tungsten projectile is being accelerated to maximum kinetic energy without excessive energy loss due to the parasitic components mass.

The optimization process of a modern sabot design, utilizes state-of-the art simulation tools that allows for in-bore analysis of the penetrator-sabot dynamics. In the separation and exterior ballistics phase, a new approach utilizing Computer Fluid Dynamics, CFD, simulation tools enabled reduction of drag and increased downrange stability.
In the terminal ballistics phase, finally, a 3-D Finite Element, FEM, simulation clearified and calculated state-of-the art penetration capability.
In this work an extensive use of simulation tools are beeing presented. The software is based on commercially available programs with modifications and updates that has been validated in earlier design work within the field of medium calibre ammunition showing excellent match between simulation and the results of verificational test.

## 1. INTRODUCTION

The precision and dispersion for a kinetic energy projectile is controlled by many factors. When isolating the analysis to the projectile solely, we reduce the problem into four dominant areas:

- Interior ballistics
- Intermediate ballistics
- Exterior ballistics
- Terminal ballistics

Since the kinetic energy projectile transitions from a full caliber modus into a subcaliber, long rod with fin stabilization, the importance of understanding the intermediate/transformation ballistics becomes the most dominant area.
This presentation also covers the importance of defining the different verificational test methods and also the critical coupling of understanding the productional aspects of the projectile sub-components. During this work we also realized the importance of having a solid understanding of material dynamics and characterization.

## 2. FUNCTIONAL PRINCIPLE

In the transition from the full caliber modus to the sub-caliber long-rod free flight at the muzzle, we want to strip off the sabot petals as soon as possible. In order to accelerate this separation, the nose-cap is introduced, acting as a booster for the symmetric lift-off of the three sabot petals. The nose-cap is also introduced for handling and gun interface with different feeder mechanisms. The nose-cap material needs to be of a high strength type to survive the launch accelerations, but must also be weak enough to open up by the ram pressure and the spin forces given initial low spin of the projectile.
There is also a requirement for the ammunition to operate within a wide temperature range, and therefore a limited amount of materials can be found to fulfill all theese requirements.

## 3. ANALYSIS

### 3.1 Interior ballistics

As a result from simulation of the structural response inside the barrel due to pressure-time distribution, it was possible to study the dynamics of the penetrator inside the barrel, thus avoiding exaggerated off-set of penetrator mass from the line of symmetry, that would cause increased barrel wear and excessive initial yaw and pitch of the penetrator.
By understanding the dynamics of the barrel-projectile interaction, it was made possible to reduce disturbances in the separation phase, thus reducing the dispersion significantly.

### 3.2 Intermediate ballistics

A parametric CFD model was built up to enable studies of the ram pressure and the flow distribution around the nose-cap at Mach 4,3. This model was a 2D-axisymmetric Euler model.
An analytical study, [1], was carried out to ensure that the nose-cap was intact in its shape as it entered the muzzle zone, otherwise we could not calculate on a symmetric pressure distribution at the tip of the nose.
The analysis considered the nose-cap as a shell conoid, with weak zones introduced at 120 degree inclination. The weak zones were introduced to trigger of the perturbation process for the opening of the nose-cap segments.
The critical loading conditions are described in table 1.

| BOUNDARY CONDITION | CONSTRAINT | LEVEL NOT TO EXCEED |
|---|---|---|
| Elastic stability | Pmuzzle | 55 Mpa |
| Elastic segment stability | Nose radius | 0,8 cm |
| Launch accelerations | Pmax | 460 Mpa |
| Rotational acceleration | Barrel twist+rel.rotation | 1500 Hz |
| Stagnation pressure | Initial velocity | 1490m/s |
| Stagnation pressure | Nose radius | 0,8 cm |
| Stagnation pressure | Weak zone thickness | 0,02 cm |

table 1. critical loading conditions

### 3.2.1 Nose-cap materials

A variety of plastic materials were studied by [2], ending up with candidates in three different categories:
- Thermoplastic elastomere, TEEE
- Polyethylene,PE
- Polyamide,PA
- Reinforced PA-spherulites

The analysis showed that the PE-materials all were too weak in elastic stiffness, and a verificational test with the reinforced PA was turned down with the material to brittle. The focus was held on the polyamide,PA, material.

In addition to the material properties shown in table 2, the production method and the handling of the material is critical [3]. Lessons learned comprises:

- Storage and humidity control
- Flow inlets in the mould
- Temperature of tools and the plastic during casting process
- Recrystallization and voids

| PROPERTY | TEEE,HYTREL | PA #3 | PA #4 | PA # 5 |
|---|---|---|---|---|
| Density, kg/m$^3$ | 1,25 | 1,01 | 1,01 | 1,01 |
| E-modulus, Mpa | 570 | 310 | 900 | 1100 |
| Tensile stress, Mpa | 45,8 | 35 | 40 | 45 |
| Impact stress,kJ/m$^2$ | 6 | 3 | 4 | 5 |

table 2. selected material properties

### 3.3 Exterior ballistics

The projectile is statically stabilized by a set of fin-blades in the fin assembly. This solution demonstrates som critical features for an optimized projectile/penetrator:

- Optimized stabilizer cross-sectional area
- Optimized fin blade area for pitch-yaw motion damping
- Termodynamic buckling avoided
- Induced spin torque
- Tracer cavity for in travel propulsion
- Minimized projectile drag

As a result the projectile features a minimized velocity drop during flight at a very small angle of attack.

This optimization work has been based on CFD-analysis.

## 3.4 Terminal ballistics

With the optimized exterior ballistics the penetrator strikes the target surface at virtually zero pitch and yaw in the desired target range from 300 to 4000 meters. The penetrator kinetic energy is then focused on the target with the novel shaped nose concept:

- Point sharp nose
- High density tungsten alloy
- High strengt & ductility material
- Translational acceleration trap
- Conoid shape of penetrator nose-part

This optimization work was based on DYNA3D analysis with excellent match between simulation predictions and test results. The penetration performance is larger then 115 millimeter RHA(0' NATO) at 1000 meter firing distance.

## 4. RESULTS

The CFD-analysis was used to determine the correct shape of the non-deformed nose-cap. This was done with a parametric model, whereas the nose radius, length and shape of the ramp was modified. The reference model featured a double cone shape, and the modified one was determined to give the best break-up of the nose-cap [4].

The problem that originally caused instability of the projectile during free flight, was traced to the nose-cap not breaking up at all. This caused the nose-cap to move rearwards, eventually striking the fin blade, thus deforming one or two fin-blades. The reference version of the nose-cap turned during the CFD analysis out to delay the break-up of the nose-cap, and a shock-wave at the ramp of the second cone, forced the cap to slide rearwards against the fin.

The modified version of the nose-cap features a distinct and sharp corner at the nose to control the origin of the shock front. I does not have the second ramp like the reference version, and it has a wider opening in the front to allow for pressure build up inside the cap. The result is a faster and more symmetric break-up.

Yaw-cards were used to study the residual spin rate and evidence of pitch/yaw. The results in terms of linear horisontal and vertical dispersion are presented in table 3. In each group five rounds were fired at ambient temperature. Initial velocity v0=1430m/s.

| NOSE-CAP/MATERIAL | HORISONTAL , mils | VERTICAL , mils |
|---|---|---|
| Reference/ Hytrel | 1,38 | 0,86 |
| Modified/ PA #3 | 0,32 | 0,30 |
| Modified/ PA #4 | 0,44 | 0,17 |
| Modified/ PA #5 | 0,09 | 0,16 |

Table 3. result of dispersion test at 100meter

## 5. CONCLUSIONS

The result of the analysis was a dramatic reduction of both the horizontal and vertical dispersion. The improvement is consistent at all temperatures, but of course, with the reference version there was obviously a high risk of deforming the fin blade. It is shown also that it is extremely important to keep trace of the initial and residual spin of the projectile. With the new approach to designing nose-caps a better knowledge of the dynamic behaviour of plastic material was reached that also significantly affected the repetitiveness of the nose-cap break-up.
New design methods have been implemented in the development process and represents a new way of optimization in the interior, intermediate, exterior and terminal ballistics phase with the characteristics of a specific gun and projectile design aimed at safe, reproducable and, not the least, optimized performance [6].

## 6. REFERENCES

1.  Raymond J. Roark, Warren C. Young. 1986. "Formulas for Stress and Strain". McGraw-Hill International Editions, pp. 505-550.
2.  Knut Mathiessen.1998. "Private communications". Technological Institute,Oslo.
3.  Carl Klason, Josef Kuba't. 1997. "Plastics, 4th edition". Sveriges Verkstadsindustrier.
4.  PhD Ivar Oye. 1998. "Aerodynamic Stability of a Long Rod". CFD Norway.
5.  Lars A. Hagen.1998. "Test report 30.11.98". Nammo Raufoss AS.
6.  Jan Hasslid, Jarl-Eirik Straume. 1998. " Development of an APFSDS-T". Raufoss AS,Norway.

# BATTLE DAMAGE ASSESSMENT FROM A 155MM SHELL: THE D²C PROJECT AT THE ISL

F. CHRISTNACHER, J.-P. DUPÉROUX, V. FLECK, P. GNEMMI, E, JUNOD,
A. KÖNEKE, J. KREITZ, J.-F. LEGENDRE, A. LENTZ, A. MATWYSCHUK, PH.
RATEAU, P. RAYMOND, A. SCHNEIDER, E. SOMMER, PH. WERNERT

ISL, French-German Research Institute, BP 34, F.68301 Saint Louis, FRANCE

## 1. ABSTRACT

For a number of years the ISL has worked on a video-sensor equipped artillery shell. We present the scientific areas involved in the development of a technology demonstrator, the principal results obtained in these areas as well as some spin-offs. And we show first results from firings on the German army proving ground in Meppen.

## 2. INTRODUCTION:

In case of armed conflicts precise and rapid information becomes paramount. Especially the avoidance of collateral damage makes rapid target verification a necessity. Immediate Battle Damage Assessment (BDA) can lead to significant savings in logistics and ammunition and can speed up the decision process in action. If satellite imagery, reconnaissance aircraft or drones can give satisfactory results, the time to get the information and thus the decision loop can be very long. Besides, these system tend to be fairly expensive and require quite a bit of logistics.

In order to give the artillery units a certain independence the ISL is working on a novel reconnaissance concept, the observation projectile, internally known as 'D²C' (Detection, Designation, Confirmation). The idea is to equip an artillery shell with a imaging sensor and to enable it to transmit to the ground station images of the target area. In order to demonstrate the feasibility of this concept, many different research areas of the ISL were solicited. In this paper we will concentrate on the technological aspects of our work, though we will also mention the underlying scientific research.

### 2.1.History of the project:

Since the early 1990s, the ISL was looking for research themes that would allow it to take advantage of the vast panoply of research areas and competencies available within the institute. In long discussions with the French authorities, especially with the 'Centre d'Analyse de la Défense' (CAD), a number of different ideas were born, among them the concept of an ammunition able to transmit images from it's flight path back to the ground. Starting from this basic idea, two possible missions for such a shell were defined:

1. Battle Damage Assessment, the shell being fired at the end of a round of howitzer grenades
2. Confirmation of target co-ordinates just before effective fire.

From (2.) it follows that we were thinking of fairly stationary targets, command posts, depots of ammunition or fuel and the like, rather than of armored vehicles or other fast moving targets.

From (1.) we can follow that our shell would have to have the same ballistics as the standard 155 mm round, so that it would be possible to fire it within the rounds of grenades aimed to hit the target without altering the aim, and that it would follow the same path to the target area. So we will have to preserve the mass, mass distribution and moments of inertia, the external geometry and the spin rate of the standard 155 mm shell.

In the course of this work it became apparent that there could be another way to employ the video shell. As we can start observing right from the apogee on, the camera will basically scan the area before it from the horizon on down. Given good visibility (no cloud cover below) we can then build up a triangle-shaped map of the terrain behind the target, the extend and resolution of which will depend on the parameters of the employed optics.

## 2.2.Initial definition of the technological problems:

Besides the high-g environment of about 16,000 g at launch, and a spin rate of about 300/s the 155 mm shell is faced with a number of additional severe conditions. The fuse-tip faces
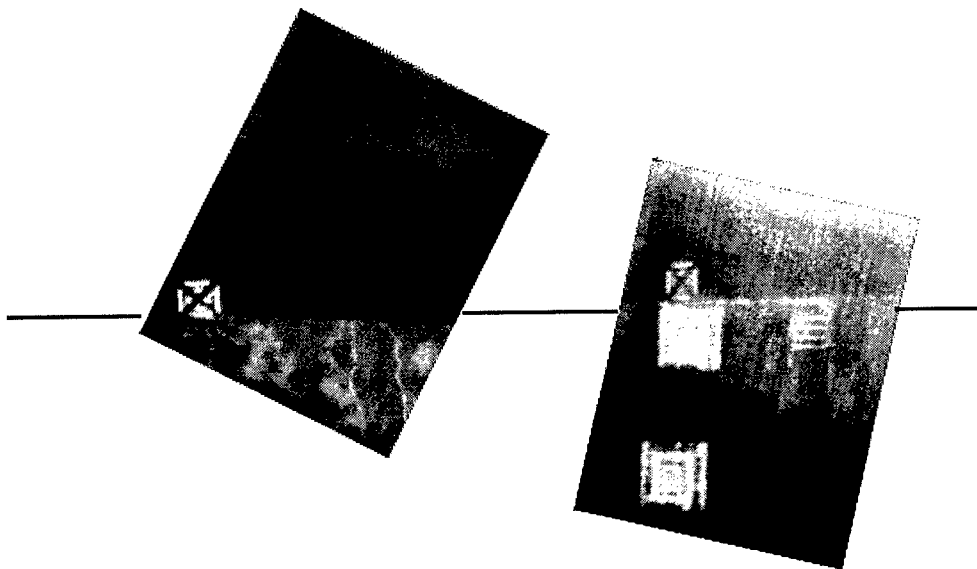


Fig. 1. In-flight images from a 90 mm demonstrator fired at ISL-proving ground [1]

aerodynamic conditions that will lead to a heat up that can reach about 200° above environmental temperature at V0 of 945 m/s. So while glass optics seemed a problem for the acceleration phase, plastic lenses might simply melt or soften and deform during the first phase of the flight.

The spin rate of about 150/s to 200/s at the end of the flight path in the target area forces us to either de-rotate the incoming image in respect to the image sensor or to have a very sensitive CCD-device capable of extremely short exposure times. Otherwise we would end up with motion blur in the outer areas of our pictures. The 'picture explosion' due to the approach of

the target area is a minor problem on this time scale.

Even in the case of a technology demonstrator, our video signal will still have to be transmitted over a distance of about 20 km, typically over a telemetry link on the proving ground.

The first objective of our project is to prove the feasibility of a 155mm howitzer shell with the same aerodynamic and ballistic properties as a standard shell, transmitting the target images to the ground station. In the second phase the transmission over distances of up to 40 or even 60 km will be done using a transponder, deployed by an auxiliary round and suspended at the apogee of the ballistic flight path. In order to respect the ballistic parameters of the shell, the outside geometry will not be modified by the integrated instrumentation. The BDA shell will be fired within a round of standard 155mm shells from a 52 caliber length howitzer.

In the future we hope to be able to integrate important image processing capabilities into the shell so as to implement target recognition on board. This might then give ammunitions the 'intelligence' to autonomously guide themselves to the target.

## 3. AREAS OF RESEARCH INVOLVED:

The $D^2C$ project regroups contributions from a number of research groups working at the ISL. Among these activities we find the areas of Ballistics, Aerodynamics, Mechanics, High-g resistance, Electronics and Optronics. We propose to give a short overview of the main contributions from some of these areas, before presenting the results obtained so far.

### 3.1. Sensors

#### 3.1.1.  Magnetic sensors for in-flight attitude measurement [2]

In order to obtain information about the attitude of the projectile and the instantaneous roll angle, some sort of precise sensor is needed. In our application we need to determine the exact moment to trigger the CCD camera so as to always have the same orientation of the image referred to some outside reference direction. Clearly a type of sensor that does not depend on outside signals, natural (like sunlight), or artificial (like outside emitters), is desirable here. Such a sensor will also be needed if one wants to deploy means of trajectory correction on a spinning projectile.

Among a certain number of possible sensors that we have experimented with, magneto-resistive ones used to detect the direction of the earth's magnetic field are the most promising, since they are fairly simple to use, robust and independent of outside conditions (weather, outside sources ...).

An analysis of the signal from a magnetic sensor on board of a projectile on a ballistic flight path shows the influence of the inclination of the earth's magnetic field, the direction and the azimuth and the curvature of the flight path on the precision of the measured roll angle. The known parameters can be pre-programmed and then used by an on-board calculator to achieve the required measurement precision. (See Poster session VI: *"Determination of the Angular Motion and of the Aerodynamic Coefficients from 3D Magnetic Sensor Signals"*)

#### 3.1.2.  CCD-camera for very short exposure times

The images from the projectile are to be transmitted to the ground station for observation by a human observer. So we need to synchronize the image acquisition with a given roll angle of the shell in order to have the same image orientation at all times. We therefore need an image sensor with an external trigger. Because of the high spin rate we also need very short

exposure times (see Fig. 5.), and we want all pixels to be illuminated synchronously. On the basis of a commercial CCD-chip we developed a camera who's exposure time can be as short as 0.7 µs if the lighting level permits, and that can be triggered by an outside signal. The resolution of the chip is 640x480 pixels. Due to internal buffering, the output represents a valid video signal (NTSC standard, 30 frames per second) at all times, independent of the input trigger frequency. This allows us to use standard video recording equipment to store the images received. In the future we will probably need to replace this design by a numerical format, and we might include some preliminary image processing routines into the camera module. It might be interesting to compress the images before transmission in order to limit the necessary bandwidth, but work is still going on here, since available compression algorithms tend to suppress most of the high-frequency components of the images, and since most object recognition algorithms used to date tend to rely especially on those components.
Some experiments have also been carried out on the use of linear CCD-sensors, that could profit from the shells rotation to scan the image in a circular fashion. The use of magnetic sensors to determine the precise instantaneous roll angle becomes mandatory in this case, since the image restoration algorithm needs this information to reconstruct the image. Our experiments showed that in the case of circular scans the pendular movement of the projectile poses certain problems for image reconstruction. On the other hand, linear CCDs and circular scan can be used to investigate the movements of the shell in flight by determining the movement of the optical axis from the reconstructed images.

## 3.2. Aerodynamics and Ballistics

### 3.2.1. Influence of the tip Geometry on the range of the projectile [3],[5],[10]

to carry out observations from an artillery shell, we clearly need to put our sensors and the related optics somewhere. The obvious spot would be in the fuse-tip, but for optical reasons we need a bigger opening than provided by standard tip geometry. So we will have to modify the outer form of the shell, which would have consequences on the aerodynamic properties
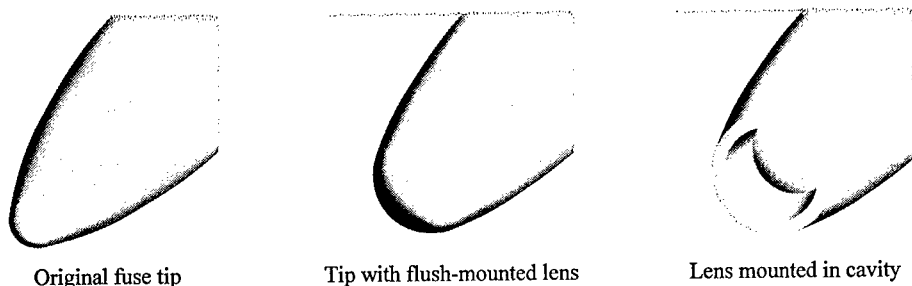


Original fuse tip        Tip with flush-mounted lens        Lens mounted in cavity
Fig. 2. Different tip geometries for the D2C shell

and hence, the ballistics. This is contradictory to the constraints mentioned earlier, i. e., preservation of the ballistics of the original ammunition.
In order to evaluate the influence of different fuse tip geometries, numerical simulations have been carried out on the flow around modified 155 mm shells. This allowed to determine their aerodynamic coefficients. Their ballistic properties are then calculated by means of a numerical code based on a model with 6 degrees of freedom. So we now have the necessary data to choose the optimum tip form for our optical arrangement, given the thermal constraints mentioned below.

### 3.2.2. In-flight measurements of the fuse temperature and aero-thermal simulations of the tip-heating process [6], [7], [13]

One of the problems we are faced with is the temperature rise in the fuse tip due to aerodynamic friction. Since we did not find anything in literature that could give us the necessary information as to whether our optics would withstand the aerodynamic heating, we set out on a combined effort to couple numerical aerodynamic codes with the theory of heat transfer to come up with a method of predicting the temperature of different components in the tips, depending on the parameters of the flight path and the material used. To experimentally verify the simulations, temperature measurements were carried out on board 155mm shells at V0=700 m/s, using tip materials with different thermal conductivity. Fig. 3. shows an example of the comparison between simulation and experimental results.
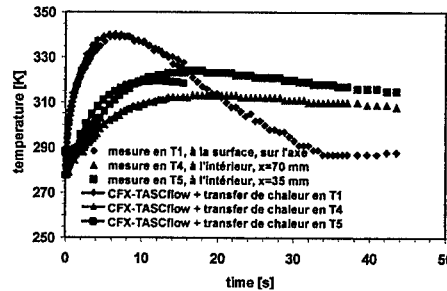


Fig. 3. Comparison of numerical and experimental results of aerodynamic tip heatup

There are different possibilities to overcome any danger to the optics. One of them might be to put the lenses into a recess in the tip as shown in Fig. 2.(c). This has the effect of modifying the flow about the tip region, so that less heat is transferred into the optics. Another possibility would be to protect the optics by means of an ejectable cover that reproduces the outer form of the original fuse tip. Work is going on in this direction too, with experiments on a spinning bench that allows us spin rates of up to 250/s.

### 3.2.3. Erosion by impacting aerosol particles [8], [9]

Besides aerodynamic heating, our optics will also be affected by impacting particles suspended in the air. These can range from sub-micron dust particles up to raindrops or even hail (see Fig. 4.). One way to protect against damage from particle impact might be the cavity mount of the optics as depicted in Fig. 2.(c). There is a compromise here to be sought between the influence on the ballistics of the projectile, the effectiveness of protection of the optics, and the simplicity of the design. One other possibility is the use of a protective cover over the optics, which will be discarded when the observation phase begins. As mentioned, work is going on here on a purely mechanical or electro-mechanical solution
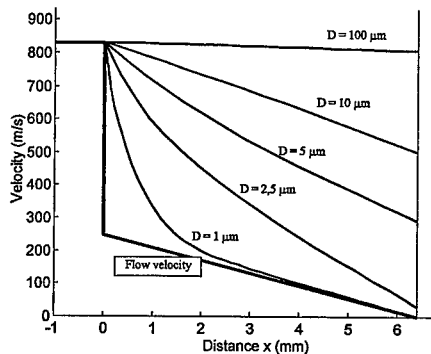


Fig. 4. Influence of particle diameter on impact velocity at Ma=2.5

### 3.3. The imaging system

#### 3.3.1. Influence of the flow field around the tip on image quality

Besides the thermal and mechanical threats to the optical hardware, we have to deal with the

influence of thermally induced differences in density and hence refractive index of the air in front of our lenses. Due to aero-thermal heating, lens-like structures will form ahead of the tip, that might influence the resolution of the optical system. Work is under way to quantify the impact of the thermal lens on the quality of the images. It seems however, that the motion blur and the rotation blur on the outside of the imaged area are by far stronger effects, and that the thermal lens effects can be neglected, especially in the velocity region (about 300 m/s) during the actual observation. Nevertheless we now have a tool permitting to predict image degradation at much higher velocities, as for example in the case of hypervelocity anti-tank ammunitions.

### 3.3.2. Influence of projectile motion on the image quality

The first thing to worry about here is the spin of about 150-200 Hz during the observation phase. As can be seen from Fig. 5., the spin imposes very short exposure times on the camera, implying very high sensitivity. One way to avoid this



a) 0°, 10μs        b) 3.6°, 50μs        c) 7.2°, 100μs
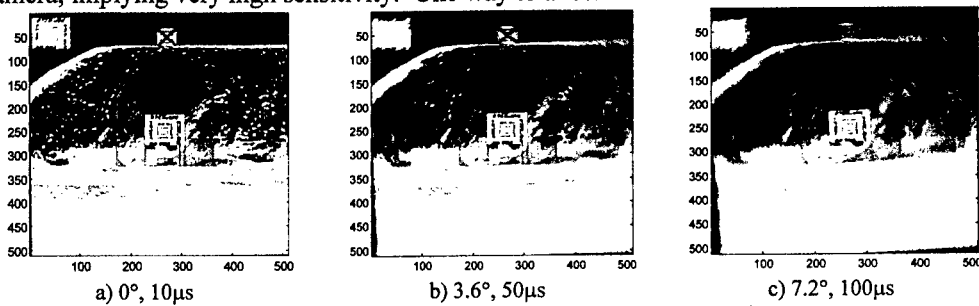
Fig. 5. Rotational blur for different exposure times at 200 Hz spin rate

problem would be to counter-rotate the image on the sensor, another might be the use of image-intensifiers; we are testing their resistance to high accelerations at this time. Another advantage of this solution would be that we gain the night vision for the observation shell.

### 3.3.3. Image-forming optics and high-g resistance [14], [15]. [16], [20], [21]. [22]. [23]

Apart from the thermal stress and the impact of aerosol particles the main solicitation of the optical lenses comes from the acceleration and the vibration of the projectile tip right after leaving the muzzle. We have investigated two possible solutions here. One is to use plastic materials for the lenses, and as a matter of fact the first working projectiles were equipped with PMMA/SMMA doublets. The other approach is to investigate the behavior of different glass materials used for optical lenses under high-g loads.
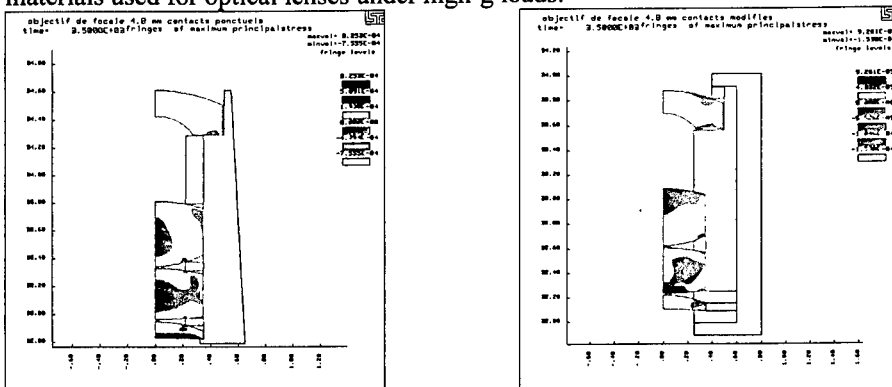


Fig. 6. Comparison of maximum stresses for stock mounts (left) and modified mounts (right)

Tests in the SIBREF recovery facility on parallel-face plates of both glasses and plastics have permitted to understand the different modes and levels of fracture. Specifically we found that for glasses traction stresses are much more critical (with a limit in the order of 15 MPa) than compression, where the rupture limit is in the order of 100 MPa. The tests led us to develop a numerical simulation based on finite element methods to calculate maximum stresses for different geometries of lenses and lens supports. We are now able to predict stresses as a function of material, geometry and acceleration, and the simulation allows us to modify existing lens mounts to minimize the stress load on the optical components (see Fig. 6.)

## 4. DATA TRANSMISSION

### 4.4. S-Band Telemetry [17], [18]

For the transmission of the video images as well as for some of the temperature measurements we used an emitter for the S-Band, developed in-house. The main characteristics are as follows: crystal-controlled PLL programmable in steps of 125 kHz between 2200 and 2300 MHz. Especially in combination with the broadband microstrip antennas developed at the ISL this gives a very flexible system that can easily be adapted to the needs of different proving grounds. The modulation bandwidth of the emitter is about 4 MHz. The output power is switchable between a few mW in standby mode and 0.5 W at full power. The standby mode can be controlled from outside electronics, for example for security reasons during the loading of the shell, so as not to output 500 mW into the gunpowder in the chamber. The diameter of the emitter is 30 mm, its height is 35 mm, and it has been tested successfully at accelerations up to 35,000 g (in a 90 mm shell).



Fig. 7. 500 mW S-Band telemetry emitter

Reception on the ground was done with commercial S-Band receivers.

### 4.5. Data recording aboard the projectile

In some cases such as slowly varying signals, direct transmission to the ground might not be necessary. One example would be the temperature history of the tip due to aerodynamic heating. In these cases we use digital data recorders for ballistics developed at the ISL. Their capacity goes up to 32 kB at a maximum sample rate of 500 kHz, and they offer all the trigger modes that transient recorders have. (see poster session VII: *"Instrumentation for Ballistic Metrology at ISL"*) The advantage here is that we do not need the telemetry but can read out the data from the non-volatile memory after recovery of the projectile.

One other application of these recorders is as a so called 'black box' to monitor a certain number of system parameters during the flight of the projectile. One can often trace the reason for a system failure to specific components after the experiment just by looking at the recorded time history. This of course implies the recovery of the projectile after the firing.

## 5. RESULTS

In September 1999 three shells equipped with video cameras were fired at the German Army proving ground in Meppen over a distance of 16 km. All three cameras worked throughout the flight and even after recovery of the shells. Since this was the first full scale test, the exposure time was fixed to 80 µs, and diaphragms were used to adapt to the lighting level. The lenses used had a focal length of 80 mm, giving a field of view of ±3°. The target area was a grassy plain with a row of trees just before the impact area. The contrast of the original images was very poor, so some enhancement had to be used. Since in these shots the cameras —were free-running, there was no synchronization with the shell's roll angle. Therefor all images had to be rotated into the same angular position afterwards.

Recording of the received images was done using two reception stations, one located near the gun, using a parabolic antenna (±5° opening), the other one about 4.3 km from the target area with an antenna with a wide opening. Both were equipped with VCRs and PCs with framegrabber card. We obtained about nine seconds of useful image data, where the reception near the gun only misses the last three images. (At 30 images/second that gives 1/10 of a second or about 31 m of flight). During the conference we will show the video of the last nine seconds before impact, showing two trees and ending with the images of the leaves of one of the branches that the projectile traversed just before impact on the ground.
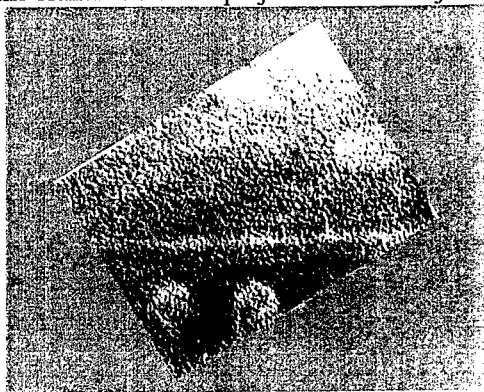


a)   Image no 160, 2.7 seconds to impact
Distance about 840 m, Field 90 x 66 m
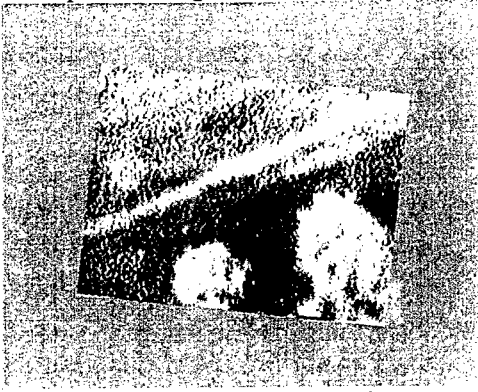
b)   Image no 190, 1.7 seconds to impact
Distance about 535 m, Field 55 x 40 m
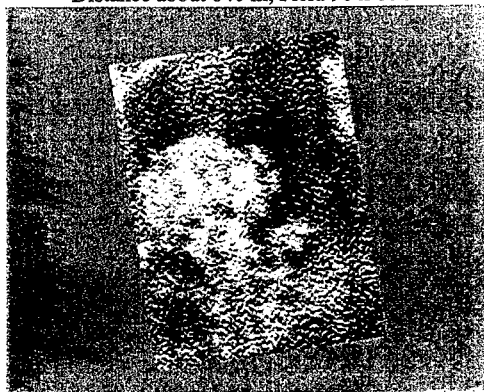
c)   Image no 210, 1.03 seconds
Distance about 325 m, Field 34 x 25 m
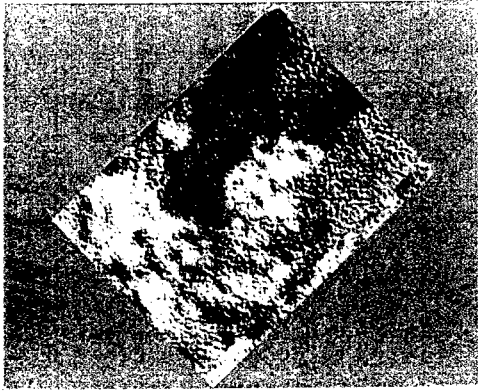
d)   Image no 230, 0.37 seconds
Distance about 115 m, Field 12 x 9 m

Fig. 8.  Images from the video sequence obtained in shot 3, September 15, 1999

Since the original protective window on the CCD-chips had to be replaced in the hardening process, the usual high-pass optical filter was not in place. We therefor have an enlarged

spectral band for the sensor, going up to about 1.4 μm. In the near infrared region vegetation shows a very high emissivity, which explains why the leafs show up very light in the pictures. The images in Fig. 8. are from the same sequence and show the approach of the target area. The light lines in the upper two images are from strips of grass on the field behind the two trees. Their light color is explained above.

As mentioned, the images were post-processed in order to enhance the contrast and to rotate them into the same reference system. Still one can see that the transmission over the distance of 16 km induced quite some noise in the video signal.
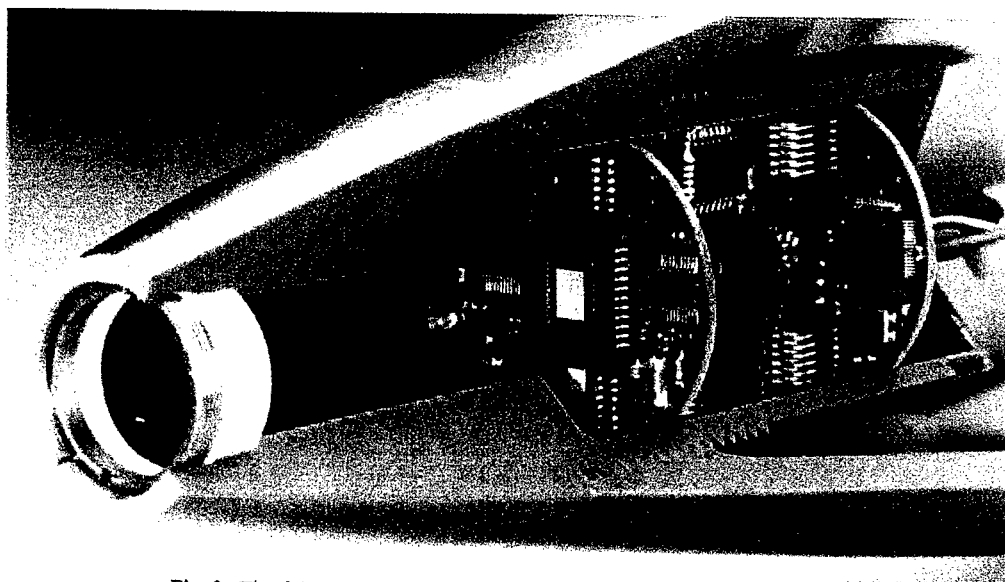


Fig. 9. The CCD-camera and the optics in the nose tip of the 155 mm shell

## 6. OUTLOOK

Now that we have proven the feasibility of using CCD-cameras on artillery shells, the next steps will be to synchronize the camera with the roll angle of the projectile, to improve the optics, to adapt the field of view to the task at hand (damage assessment in the target area or reconnaissance in the area behind the target), and to use digital transmission with the necessary pre-processing in order to get noise-free transmission and the possibility to recover from short signal drop-outs.

## 7. REFERENCES

[1] Rateau Ph., Raymond P., Christnacher F., "Formation et transmission temps réel d'images à bord d'un projectile soumis à de fortes accélérations" Rapport ISL RT501/98
[2] Ph. Rateau, Ph. Wernert, E. Junod - Détermination de la position en roulis d'un projectile en tir tendu ou courbe - Rapport ISL RT    /00 (à paraître)
[3] P. Gnemmi, "Aérobalistique du projectile d'observation : étude théorique de solutions d'intégration du dispositif optique dans la pointe", Rapport ISL R 121/99
[4] V. Fleck, "Cours de balistique extérieure", ENSIETA Brest, Edition décembre 1994
[5] W.B. Sturek, "Application of CFD to the Aerodynamics of Spinning Shell", AIAA-84 0323, 22nd Aerospace Sciences Meeting, Reno, Nevada, USA, January 9-12, 1984
[6] P. Gnemmi, E. Sommer, Etude aérothermique de la pointe du projectile d'observation : validation d'une approche numérique Rapport ISL en cours

[7]  P. Gnemmi, E. Sommer, K.W. Naumann, V. Fleck, Aerothermal Study of a Projectile in Flight: Experiment-Computation Comparison, 18th International Symposium & Exhibition on Ballistics, San Antonio/ TX, USA, November 15-19, 1999, Rapport ISL PU

[8]  Wernert P., Meyer E., "Calcul de la vitesse d'impact de particules atmosphériques sur l'optique au nez du projectile D2C", Rapport ISL R 111/99, 1999.

[9]  Wernert P., Meyer E., "Calcul de la trajectoire de particules en suspension dans l'atmosphère autour du projectile D2C", Rapport ISL en préparation, 2000.

[10] P. Gnemmi, "Aérobalistique du projectile d'observation : étude théorique de solutions d'intégration du dispositif optique dans la pointe", Rapport ISL R 121/99, 1999.

[11] Wernert P., Bichon K., "Etude théorique de l'ouverture d'une coiffe de protection largable pour projectile D2C", Rapport ISL en préparation, 2000.

[12] Optische Strömungsmesstechnik, Oertel Herbert, Oertel Herbert Jr, Editions Braun Karlsruhe, 1989.

[13] P. Gnemmi « Aérobalistique du projectile d'observation : étude théoriques de solutions d'intégration du dispositif optique dans la pointe » Rapport ISL R121/99

[14] Handbook of Optomechanical Engineering, CRC Press, Boca Raton, FL, 1997

[15] P. R. Yoder, "Design and Mounting of Prisms and Small Mirrors in Optical Instruments", Tutorial Texts in Optical Engineering, Vol. TT32, SPIE Optical Engineering Press

[16] B.H. Walker, "Select optical glasses", The Photonics Design and Applications Handbook, Lauren Publishing Co., Pittsfield, MA, H-356, 1993

[17] J. Kreitz, "S-Band Telemetriesender für die ballistische Meßtechnik", ISL-Report geplant in 2000

[18] Ph. Rateau,  P. Hirzlin, "Antennes microrubans á large bande passante pour télémesure balistique en bande L ou S", ISL-Report RT-516/1995, Saint Louis, France, (1995)

[19] F. Christnacher, L. Borne, Ph. Rateau, "Etude de la tenue à l'accélération du remplissage des projectiles 155 mm" Rapport ISL 113/99

[20] Paul Germain, "Mécanique des milieux continus", Masson, Paris (1962)

[21] Legendre, Giraud. "Dual-Purpose Launcher for Ballistic Research - RAMAC and SIBREF-", publié par W. Reinecke (ed.) dans "Proceedings of the 18th International Symposium on Ballistics, November 15-19 1999, San-Antonio, TX, USA", vol. 1, pp. 347-354, Technomic Pub. Co, USA,  ISL # PU 351/99

[22] Legendre, Bauer, Giraud. "Ramac90 : detonation initiation of insensitive dense methane-based mixtures by normal shock waves " publié par K. Takayama and A. Sasoh (eds) dans "Ram-Accelerators, Proceedings of the 3rd Int. Symp. on Ram-Accelerators held in Sendai, Japan, 16-18 July 1997", pp. 223-231, Springer Verlag, Germany, ISL # PU 310/98

[23] Legendre, Giraud, Sommer. "RAMAC 90 facility used as projectile recovery system", 49th meeting of the Aeroballistic Range Association, October 5-9 1998, The Hague, The Netherlands, ISL # PU 376/98

# ON THE PENETRATION EFFICIENCY OF LONG RODS AT CONSTANT STRESS AND ENERGY

LEHR H. F., WOLLMANN E.

ISL, French-German Research Institute of Saint-Louis, France

mailing address in Germany: Deutsch-Französisches Forschungsinstitut Saint-Louis (ISL)
Postfach 1260
D-79574 Weil am Rhein, Germany

*Paper not Available at the Time of Editing*

## ABSTRACT

Throughout the last years perforation power of long rods was steadily increasing thereby creating penetrators of high lengths and aspect ratios.

As a protection against this threat quite a number of targets are being discussed which show moving elements in order to destroy the penetrator. Indeed this is a very effective method as it is well known that slender rods quite often demonstrate failure because of severe structural integrity and stability problems during acceleration and flight phase and of course even more during penetration if strained by lateral forces.

In this situation it is necessary to design a penetrator in such a manner that the long rod will be capable to withstand the acting lateral accelerations exerted by the special protection mechanism.

The paper deals with some considerations on the design of such a penetrator and its optimal layout as far as penetration efficiency is concerned. In a first step a method is described to design long rod penetrators in such a manner that well defined values of bending stress and deflection are met if the rods are subjected to lateral forces. If constant lateral accelerations are assumed this results in cylinders with various dimensions the aspect ratio remarkably not remaining constant. Then considering rods of equal energy these penetrators are examined for maximum penetration efficiency. For the case studied this procedure results in an optimum velocity of 2700 m/s.

In comparison to the reference penetrator (L/D=34, v=1800 m/s) the optimum penetrator has of course reduced mass, but also reduced length and diameter showing an aspect ratio of 40. The perforation power could be increased by nearly 20%.

It could be shown that the optimization procedure of the energy-efficient penetration leads to optimal velocities well above 2500 m/s. The penetration depth could also be increased. Thus it seems evident that the gain in penetration power is due to the special design of the penetrators with constant stress level thereby demonstrating an advantageous tool for optimization of long rod penetrators.

# PERSPECTIVES OF NAVAL ARTILLERY IN SHORE FIRE SUPPORT

**Capitaine de Frégate** (ENSER) **Alain CARRIERE**
Institut Franco-Allemand de Saint Louis, ISL, BP 34, F 68301 Saint Louis

**Abstract:** We report about the future needs for naval artillery (powder guns) to shell shore zones and how to meet such tactical and technical requirements. After a review of some alternative techniques (among them the electromagnetic acceleration) we suggest two possible solutions (in calibre 155 mm):
- with present techniques (for instance "base bleed" used by land forces) after "navalisation" for ranges up to 40 km within a few years (2005?),
- with new techniques (such as "fly-out" projectiles) to reach ranges up to 60 km by 2010-2020.
For such long ranges, trajectory corrections are necessary to reduce dispersions.

## INTRODUCTION

Captain BENNET (Retired) published 1998 [1] a paper about naval artillery, its actual stand and its next future for its AA, surface and shore fire support missions.

Here we report on specific tactical (from the French Navy point of view [2]) and technical needs for shore fire support in mean and longer term and how to meet this requirements.

After a review of some alternative techniques (among them the 3 aspects of electromagnetic acceleration) we suggest two possible (technically realist) solutions (for instance in caliber 155 mm) in the mid or longer term:

-with present techniques (such as the land used "base-bleed" after navalisation) for ranges up to 40 km, within a few years (2005?),

-with new emerging techniques (such as "fly-out" projectiles) for range of 60 km (and perhaps more) after a longer term (2010-2020).

For such long ranges, trajectory correction (at reasonable cost!) are necessary to reduce dispersions (in range and cross direction) in order to meet the tactical requirements.

## 1. Today stand and future needs

**1.1-** Classic naval ordnance (guns) has a serious challenge:
- with sea to sea or sea to air missiles (for precision hits, because their availibility is reduced by their cost and the limited possibility to carry them on board ships and aircrafts {planes and/or helicopters}), their use could be extended to sea-shore and shore-sea missions,
- new emerging (today not yet operational indeed) technologies such as electromagnetic acceleration.

Within a 15 year term, powder gun will remain the most used projection technique, the least expansive (not really cheap!) and the easiest to use (and maintain) to shell shore zones as fire support. Further more, this all weather machine hurls ECM insensitive projectiles which cost is really cheaper than missiles.

**1.2-** As reported Captain BENNET, most navies no longer use "big guns" (former 15" or 381 mm, today >127mm) because for long ranges (today>15 km) sea-sea and sea-shore missiles replace them, for closer ranges shore fire support the main general purpose gun (100 mm in France and Germany) was considered as sufficient.

This tactical concept (since the 1950) is no longer pertinent:

-a more severe air threat (*with modern jets*),

-a permanent sea ("surface") threat,

-*(the submarine threat is not met by longe range guns!, but zonal protection against torpedoes could be treated by medium or intermediate range guns using super caviting projectiles in development),*

-shore fire threat is more sensitive than former with missiles such as Exocet,

to meet such new challenge how to figth these threats to longer ranges with reducing greater dispersions to operational values.

**1.3-** Using 100 mm guns allowed lighter ships but limits pratical range to 15 km (theorical range 17km); this was satisfactory in former decades (with light shore fire threat such as Africa) but today no longer sound in future possible theaters (Middle East, North Africa,...).

If our Staff wish a significant shore fire support policy, it's necessary to use larger caliber guns (155 mm or more) with range up to 40 km (and later to 60km), they can shell wider (deeper) zones (10 to 20 km) when the ships remain out of range of medium or intermediate shore guns (or older missile of 1st generation).

According to Jane's IDR (7-1995) [3] US Navy will significantly increase the range of the guns for shore fire support with 155/L70.

## 2. Possible solutions to improve Artillery with current techniques (1995)

Among usual techniques there are several potentialities we may quote:

-increment of the range by increment of muzzle velocity $Vo$ and/or of the caliber,

-using of "base-bleed" techniques,

-using of post acceleration by Rocket Assisted Projectiles "RAP".

**2.1-** To increase the range $X$ we must increase the muzzle velocity $Vo$ and/or the caliber of the projectile (and the gun!) avoiding the "*come back of big guns*" [2], for instance the 381mm of the former "*JEAN BART*" (French Navy, 1940) quoted by BENNET [1], p.22) and in all cases we must reduce the air drag.

-*In table 1 of the 1rst Appendix, my parametric computations (1998) with THW (variant of CAFOBI [4], and IBN [7]) show that it's very difficult to increase Vo with longer shot travel (or longer barrel) and/or higher maximum pressure Pmx, generating more severe wear of the tube.*

-*In table 2 of the 1rst Appendix, the reader can see that the range X is slightly linear with respect to muzzle velocity Vo, in the domain of conventional velocities (<1200m/s); for higher Vo the range values increase slightly with the square of Vo.*

*For obvious reasons, it's not possible to increase to much the caliber in sofar the weight of the barrel and turret increases as (caliber)³, for instance: 10 t for 100mm and 600 t for 381!, this leads to heavier ships if we use bigger guns over 152 or 155 mm.*

*It's not pertinent to use high velocity guns such as anti-tank guns on board ships (120 mm at 1600 m/s) because their payload is not convenient for shore fire support.*

Actually, this way is strongly limited: 30km in 155mm with Vo#900 m/s!

*Furthermore, firing at maximum range leads to greater dispersions than those at smaller ranges, but "intelligent projectiles" (with fly corrections) could reduce a part of this large dispersion .*

By means of one (of several) correction(s), it would be possible to reduce the great dispersions of these long ranges to conventional values of dispersion of current weapons.

*It's necessary to reduce dispersions of 200..400m to 50...100m; with pyrotechnic actuator, such projectiles would cost #20 kEuros, i.e. 10 times more expansive than the basic existing projectile (2...3kE for 155mm, 1kE for 100mm).*

**2.2-** We may think to the naval use of the "Base Bleed" which allows a range increment of 10km (from 30 to 40km) with the same 155mm gun, and therefore better conditions for shore fire support.

*The "Base Bleed" process, used in several countries (among them France and Sweden), aims an increase of the base pressure by burning powder, this implies a reduction of the base drag and of course of the total drag, therefore, in fine, increases the range.*

**2.3-** An other way has been investigated: the **"post-acceleration"** or "RAP" gave discutable results (outside mortars) but recent progresses have been reported.

*After muzzle ejection und a given path in air, a rocket motor gives a new accelertion to the shell by reduction (or compensation) of the effect of air drag and therefore the range is increased (but also the unwished dispersion which must be reducted by flight corrections).*

After great hopes during 1970-80, the liquid propellant process seems no longer an interesting alternative solution.

*A controlled velocity was expected by controling the mass (or the volume) of liquid propellant introducted in the chamber of the gun. This could avoid the "zones" used in howitzers.*

**3.Possible solutions by using new emerging techniques (after 2010?).**
Several emerging techniques (already quoted by Captain BENNET, [1],p.21) are investigated and could give interesting results (within 10years?), for instance:
**3.1-**Electrical acceleration in its 3 variants: rail, induction and electro-thermal guns,
*It's very difficult to give an accurate forecast of these alternative solutions:*
*\*we may think that the "rail gun" would be the best candidate within 10 years, provided a good solution of wear problem (erosion of the barrel) and mastering the compacity of the electronic compulsator,*
*\*we may quote a US project of 1985: a 203 mm projectile (#100kg) launched at 2500m/s by a rail gun at ranges up to 500km.*
*\* pro memoriam, we quote the hybrid gun "powder+rail" In this assembly, we have a conventional powder gun, but with a rail gun in the 2nd part of the barrel (where gas pressure is severely reducted by expansion). First simulations (1998) show an increment of 200m/s for Vo in the current MN 100mm). Indeed, such assembly can launch only fin stabilised projectiles and seems to complicated for a next operational use on board ships.*
*\* induction (coil gun) do'nt seem to be the best concept within 10 years due to synchronisation problems of impulsions and warming of the projectile unless the use of supra conducting materials at ambient temperature having a good behaviour under intensive magnetic fields,*
*\* electro-thermal gun has scaling problems, the useful reduction effect of the maximum of pressure is better in small calibers (20mm).*
*\*the "Electro-Thermo-Chemical" gun with plasma lighting looks as promising.*

**3.2-**the "gliding" projectile or "fly out" (V. FLECK in ISL [5]).
*The other alternative aeroballistic solutions aimed the reduction of the air drag, here the "fly-out" process uses the air lift to reduce gravity effects and therefore increases the range but even more the dispersion! Simulations by FLECK show these potentialities: 65km in 155mm with Vo=900m/s and yet 40 km with 450m/s (see in Appendix 2), but today no "demonstrator" can confirm the real efficiency of the process. Indeed the technical realisation is really difficult!*

*Very sensitive to aerological perturbations, this process induces very large dispersions. It's necessary to get good corrections of these dispersions, that implies a global cost of 10 to 15 times the cost of the "basic" projectile, with these partial costs:*
*-for electronics: 20 to 30 kE according to the expected quality of the corrections,*
*-for mechanics : 2 to 6 kE.*

**Conclusions.**
To improve the operational ability of ships for shore fire support, we must:
> -increase the muzzle velocity of powder guns,
> -increase the caliber and improve the aerodynamics of their projectiles,
> -reduce significantly the dispersion by one or several flight corrections to get

reasonable values meeting tactical requirements with a "low cost" (10 times the cost of a basic projectile),
> -dispensate sub-munitions to increase terminal effects.

To achieve these requirements, it's possible to forecast:
> -the "navalisation" of the available "base bleed" (used in 155 mm by land forces) to get

ranges up to 40 km by 2005,
> -the use of "fly-out" projectiles to get longer ranges up to 60 km, by 2010-2020, perhaps

the RAP could be an other alternative.
An affirmative evaluation of electrical acceleration (rail,coil, ETC the best?) seems difficult.

**REFERENCES**
[1]   G. BENNET   L'Artillerie navale, son état actuel, son avenir à moyen terme,
              MARINE, No 180, pp. 17-22, juillet 1998
[2]   A. CARRIERE  Perspectives pour l'Artillerie Navale dans son usage contre la terre,
              MARINE, No 184, juillet 1999, pp 29&30   et   ISL PU 339/99
[3]   D. MILLER   Shore Bombardment, Guns back in vogue? IDR, Vol 28,7,pp.26-33, 1995
[4]   H. POURCHER, H SIRET, Application du calcul formel à la Balistique Intérieure "CAFOBI",
              Rapport Ecole navale 1997 & ISL RT 510/97
[5]   V. FLECK, C. BERNER , Increase of Range for an Artillery Projectile by using the Lift Force,
              ISL PU 355/96
[6]   A. CARRIERE  Réseaux de Balistique Extérieure "ABN"   ISL R 122/75
[7]   A. CARRIERE  Réseaux de Balistique Intérieure "IBN"   ISL RT 515/85
[8]   A. CARRIERE  Diverses définitions du coefficient balistique, Mém. Art. Franç. 1983, 57,pp. 583,624

# Appendix 1: Some ballistic data

## 1-Interior Ballistics of powder guns (according to IBN94 and THW97)

IBN: Ballistic Network computed with "KL96" (*Krauth 1974*) revisited by Carrière 1981-94 [7].
THW: WINTER's variant 1997 of analytic model of THORNHILL 1966 [4]

### 1.1-muzzle velocity Vo as function of shot travel L/K for the MN 100mm with Pmx=3 kbars:

| L/K [-] | 30 | 40 | 50 | 60 | 80 | 100 | 150 | remarks |
|---|---|---|---|---|---|---|---|---|
| Vo (m/s) | 778 | 832 | 870 | 892 | 927 | 951 | 987 | IBN ; L/K= shot travel/caliber |
| Vo (THW) | 770 | 826 | 867 | 897 | 940 | 970 | 1020 | THornhill-Winter 1997 |

### 1.2-maximal Pressures Pmx & Pmp as function of muzzle velocity (for L/K=48):

| | | | | | | | values |
|---|---|---|---|---|---|---|---|
| Vo (m/s) | 738 | 860 | 890 | 925 | 948 | 967 | muzzle velocity (IBN) |
| **Pmx (kb)** | **2.2** | **3.3** | **4** | **5** | **6** | **8** | **Breech maximum pressure** |
| Pmp (kb) | 1.9 | 3.0 | 3.7 | 4.7 | 6. | 7.7 | shot base max. pressure (kbars) |
| **Vo (THW)** | 720 | 853 | 895 | 940 | 965 | 990 | muzzle velocity (THW) |

## 2-Exterior Ballistics of conventional projectiles (*near maximum ranges* with ABN74 [6])

Computations with "point mass model" with "*loi B*" by DUPUIS 1922 & Aerology "*CIRA 1972*" [6].

### *2.1-usual guns (100 and 155 mm) with current muzzle velocity values

| **Vo (m/s)** | **500** | **700** | **850** | **1000** | **1200** | **muzzle velocity** |
|---|---|---|---|---|---|---|

**(100 mm)** "ballistic Coefficient " cDupuis= 390.e-6 [8]

| | | | | | | |
|---|---|---|---|---|---|---|
| X (km) | 10.8 | 14.2 | 17 | 20 | 26 | range |
| T (s) | 48 | 57 | 64 | 72 | 83 | time of flight |
| $V_f$ (m/s) | 260 | 280 | 300 | 290 | 300 | final velocity |
| $\sigma_X$ (m) | 61 | 90 | 100 | 130 | 200 | range dispersion |

**(155mm)** bal. Coeff. cDupuis= 250.e-6

| | | | | | | |
|---|---|---|---|---|---|---|
| X (km) | 13. | 18 | 24 | 30 | 43 | |
| T (s) | 56 | 70 | 81 | 93 | 110 | |
| $V_f$ (m/s) | 300 | 320 | 330 | 350 | 380 | |
| $\sigma_X$ (m) | 60 | 100 | 150 | 250 | 400 | |

**Remarks:**

a) the range of 30km with Vo#900m/s is expected with an "improved" projectile: CB=2.e-4
b) the 40km "Base Bleed" range is given by a *fictive* Ball. Coeff. cDupuis=150.e-6.

### *2.2-extrapolation of a 203mm gun or anti-tank arrow projectile

Coeff. Bal. cDupuis= 200.e-6

| **Vo (m/s)** | **500** | **1000** | **1500** | **2000** | **2500** | |
|---|---|---|---|---|---|---|
| X (km) | 14 | 37 | 103 | 200 | 310 | |
| T (s) | 63 | 110 | 170 | 225 | 280 | |
| $V_f$ (m/s) | 320 | 410 | 650 | 1000 | 1200 | |
| $\sigma_X$ (m) | 60 | 300 | 1000 | 1500 | 2400 | |

**Remark:** this affirmation (in §2.1) « *the range X increases linearily with Vo* » is no longer true, because during a great part of the long trajectories the projectiles fly in a rarefied atmosphere (almost vacuum), then ranges become very great in so far Vo>1000 m/s.

**Appendix 2: Some features of modern and new projectiles** (from FLECK [5])



155-mm with
high Lift (155P,B1)

155-mm with
'base bleed' (155BB)
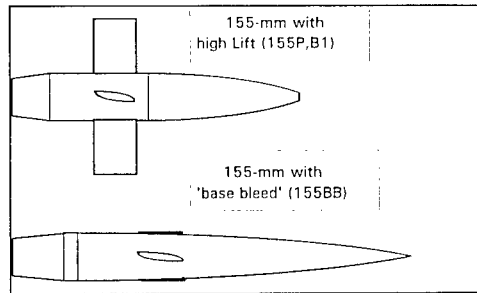
Design of "fly-out" and "BB" projectiles



Y [m]   Trajectory X-Y

15000

10000

5000

0

155BB

Vo =930m/s

Vo =800m/s   155B1

155P

Vo =450m/s

0   10000 20000 30000 40000

X [m]

V [m/s]  Velocity and time of flight

1000

750

500

250

0

155BB

155B1

155P

0   100   200   300

t [s]
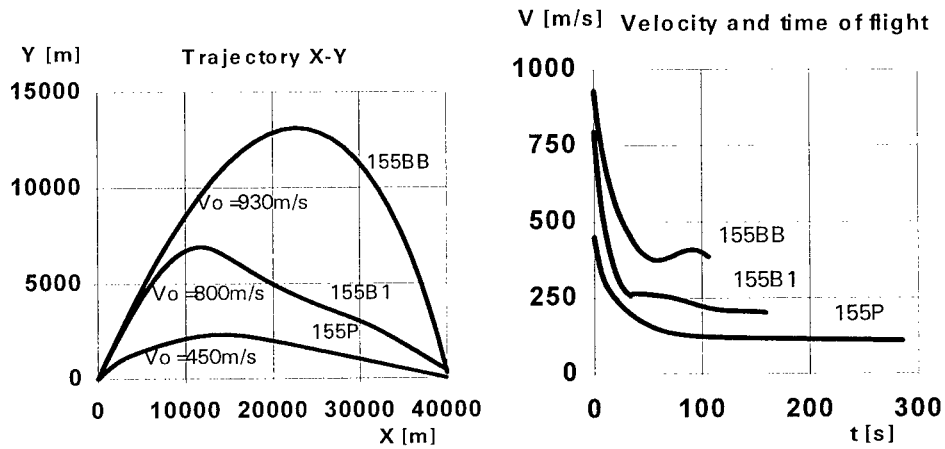
Trajectories of the "BB" ,"B1" & "P" projectiles



**Trajectory X-Y**

12000
10000
8000
6000
4000
2000
0

y/m

0   10000  20000  30000  40000  50000  60000  70000  80000

x/m

Vo=960m/s
Vo=840m/s
Vo=720m/s
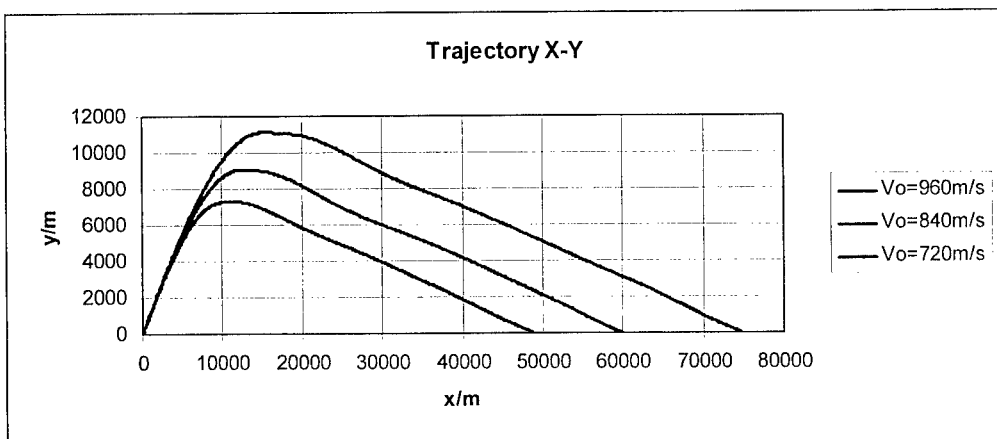
Trajectories of future "fly-out" projectiles

Internal Ballistics and Propulsion

# COLLABORATION BETWEEN THE UNITED KINGDOM AND FRANCE ON THE ASSESSMENT OF NEW HIGH ENERGY GUN PROPELLANTS

CHRIS LEACH[(1)], DAVID DEBENHAM[(2)],
JEAN-YVES KERMARREC[(3)], CHRISTOPHE TORMO[(4)]

(1)(2) DERA Fort Halstead, Sevenoaks, Kent. TN 14 7 BP
' (3)DGA DSA/SPNuc 26 bld Victor 00450 PARIS ARMEES
(4)DGA ETBS. EXT/MBI route de Guerry, 18021 Bourges

**Abstract :** So-called "LOVA" propellants are being investigated by a number of nations in order to meet future systems performance needs and Insensitive Munitions or MURAT requirements. These materials promise high energy and low vulnerability coupled to low flame temperatures and predicted low barrel wear. However, as with all new materials it is essential that the appropriate testing methodology is developed in order to fully understand and exploit the material properties. Both France and the United Kingdom have had a strong interest in these new materials and the associated assessment methodology and for many years the governments have collaborated bi-laterally in the general area of defence research under the Anglo French Defence Research Group (AFDRG). In particular. the vulnerability and ballistic assessment of gun propellants has been conducted under two AFDRG joint programmes (or Technical Arrangements — TAs). These programmes have been highly successful and beneficial to both nations, achieving a greater understanding of these new materials than could have been achieved by totally independent research.

## 1.INTRODUCTION

Weapon designers are faced with the task of defeating ever more challenging armoured targets with high velocity kinetic energy projectiles. As a consequence, higher performance gun propellant charges are required to attain the desired projectile velocities. However, at the same time there is also a growing need to meet NATO Insensitive Munitions, or MURÂT, requirements to avoid increasing the vulnerability of our own fighting vehicles or the logistical chain. Thus, the propellant formulator and charge designer need to design and utilise propellants which exhibit both high performance and reduced vulnerability. Invariably, increasing the energy of conventional propellants, based on the nitro-glycerine/ nitro-cellulose matrix, results in an increase in vulnerability. This as prompted a world-wide interest in the alternative technology of so called "LOVA" propellants - composite materials based on high levels of nitramine fillers bound in either an inert or an energetic polymer matrix. These materials promise high energy and low vulnerability coupled to low flame temperatures and predicted low barrel wear. However, as with all new materials it is essential that the appropriate testing methodology is developed in order to fully understand and exploit the material properties. Both France and the United Kingdom have had a strong interest in these

new materials and the associated assessment methodology and for many years the governments have collaborated bi-laterally in the general area of defence research under the Anglo French Defence Research Group (AFDRG). In particular. the vulnerability and ballistic assessment of gun propellants has been conducted under two AFDRG joint programmes (or Technical Arrangements — TAs).

## 2. RESULTS

The first of these TAs, concentrated on the vulnerability assessment of 'LOVA" candidates. Both nations supplied one baseline and one " LOVA " candidate each. The second one concentrated on ballistic assessment of the previous samples and on vulnerability and ballistic assessment of high energy LOVA propellants.
The UK samples were a LOVA 4 and a LOVA 10. which are a poly/NIMMO binder based composite. The Fr samples were a YH01012 which is an HTPB binder based composite and a XH01501 which is a GAP binder based composite.

| Exchanged propellant | LOVA 4 | YH01012 | LOVA 10 | XH01501 |
|---|---|---|---|---|
| Impetus (kJ/kg) | 1205 | 1170 | 1250 | 1300 |
| Flame Temperature (K) | 3000 | 2900 | 3200 | 3400 |

Table 1 : Exchanged propellant

### 2.1 Vulnerability results

The propellants were tested in the web size and physical form (UK slotted tube and Fr multi-tubular) appropriate to that required for the gun system used for the ballistic assessment, (UK -120 mm, Fr - 105 mm).
The UK vulnerability test results are shown in table 2 below.

| | LOVA 4 | YH01012 | LOVA 10 | XH01501 |
|---|---|---|---|---|
| Shaped Charge Attack (mass ratio) | 0.19 | 0.02 | 0.13 | 0.21 |
| Fragment Attack 1783 m/s 1976 m/s 1919 m/s | | | Zero %TNT | 1.2 %TNT 0.4 %TNT |
| Shock (ELSGT) Go/No go (mm) | 31 | 71 | 30 | 68 |

Table 2 : UK vulnerability test results

The FR vulnerability test results are shown in table 3,4 and 5 below.

| | LOVA 4 | YH01012 | LOVA 10 | XH01501 |
|---|---|---|---|---|
| Velocity (m/s) Reaction | | | 581 No reaction | 584 No reaction |
| Velocity (m/s) Reaction | 833 No reaction | 843 No reaction | 856 No reaction | 880 No reaction |
| Velocity (m/s) Reaction | | | 983 No reaction | 987 No reaction |

Table 3 : FR 12,7 mm bullet attack results

|  |  | LOVA 4 | YH01012 | LOVA 10 | XH01501 |
|---|---|---|---|---|---|
| Velocity (m/s) |  |  |  | 1020 | 1020 |
|  | Reaction |  |  | No reaction | Combustion |
| Velocity (m/s) |  |  |  | 1513 | 1530 |
|  | Reaction |  |  | Combustion | Combustion |
| Velocity (m/s) |  | 2200 | 2197 | 1950 | 1975 |
|  | Reaction | Combustion | Combustion | Combustion | Combustion |

Table 4 : FR fragment impact results

|  |  | LOVA 4 | YH01012 | LOVA 10 | XH01501 |
|---|---|---|---|---|---|
| Attenuator (mm) |  | 0 | 0 |  |  |
|  | Reaction | Deflagration | Deflagration |  |  |
| Attenuator (mm) |  | 20 | 20 | 20 | 20 |
|  | Reaction | Combustion | Combustion | Combustion | Combustion |
| Attenuator (mm) |  | 40 | 40 | 40 | 40 |
|  | Reaction | Combustion | Combustion | Combustion | Combustion |

Table 5 : FR shaped charge attack results

Although test methods were not identical, the results were comparable and the test results obtained by each nation reinforced those of the other. Both "LOVA" candidates were found to be less vulnerable than their lower energy baseline counterparts. All the candidates are less shock sensitive in the form tested than TNT (Go / No go transition - 100mm). It was also possible to conclude that it is feasible to formulate high energy "LOVA" propellants with force constant of 1250 kJ/kg and above, which exhibit low vulnerability to a range of stimuli.

## 2.2 Ballistic results

Ballistic assessment for the LOVA 4 and YH01012 was carried out by firings in medium calibre gun systems – a 40 mm high pressure gun designed for reseach purposes in the UK and a 30 mm gun of the type used on the RAFALE fighter in France. It was concluded that the ballistic behaviour of LOVA gun propellant candidates was different to that for more conventional gun propellants. Although the UK propellant was tested as slotted tube and the French propellant was tested in multi tubular form, the experience gained by both nations was remarkably similar and join conclusions could be drawn. The firings indicated that the pressure exponent was a function of loading density, decreasing with increasing loading density. Another observation is the very low burn rates at low pressures, which may reduce the efficincy of the propellant in the early stages of the ballistic cycle. One observation made in the French firings was that the barrel erosion found in the YH01012 firings seemed to be greater than with conventional propellant. The performance in a gun is less than predicted on the basis of clossed vessel firings and by theoretical calculations based on the impetus of the propellant. The precises causes of this lower than expected performance are more difficult to establish. However, a combined assessment points to the influence of mechanical properties, slow gas generation in the earlier stage of the ballistic cycle just after ignition, and irregular burning of the heterogeneous binder/filler matrix are potential reasons for a decrease in the efficiency of the ballistic cycle.

Ballistic assessment for the LOVA 10 and XH01501 was carried out by firings in large calibre

gun systems – a 120 mm gun in the UK and a 105 mm gun in France. The firings have been conducted recently and the analysis of data is still ongoing. The results are encouraging, with no ignition delay problems and smooth pressure time curves attained. Although the muzzle velocities were higher than that expected with conventional propellants (multi base propellants) the velocity attained was lower than might be expected from propellants with a 1250 kJ/kg and above force constant.

## 3. CONCLUSION

Both nation were able to learn from the collaboration :

Vulnerability testing methodologies were compared and found to give similar results – future programmes will benefit from the ability to read accross results between the two nations.
Two different "LOVA" formulation approaches were contrasted – something that would have proved prohibitively expensive if undertaken by one nation only.
It is feasible to formulate high energy "LOVA" propellants with force constants of 1250 kJ/kg and above, which exhibit low vulnerability to a range of stimuli.

This collaboration confirmed that the ballistic behaviour of "LOVA" propellants is more complex than conventional propellants based on a notro cellulose matrix. System performance is not only influenced by propellant energy but by burn rate profiles, mechanical properties and gas dynamics. Such properties need to be fully understood for "LOVA" gun propellants before system performance can be maximised. This collaboration between France and the UK has laid the foundations for this understanding in both nations.

# Bipartite Solid-Propellant Charge with Consecutive Ignition

G. Zimmermann and E. Gütlin

Fraunhofer-Institut für Kuzzeitdynamik, Ernst-Mach-Institut
Institutsteil Efringen/Kirchen, Am Klingelberg 1, D-79588 Efringen-Kirchen, Germany

## Abstract

Present research interest is centered on increasing gun effectiveness by using complex solid-propellant charges whose combustion results in projectile muzzle velocities of 2000 m/s or more. A novel concept is being pursued at the Ernst-Mach-Institut. In this concept, a bipartite solid-propellant charge with consecutive ignition is investigated consisting of an inner granular propellant fill that is encased by a consolidated propellant. The bipartite charge is fired in a caliber 45-mm test fixture gun. Consecutive ignition of the two different charges, if timed properly, can lead to a significant increase in gun performance. The higher loading density of the bipartite charge, as opposed to the lower fill density given by a conventional single-component solid-propellant charge, results in a much higher projectile launch velocity, if the potential of the bipartite charge assembly is fully exploited. The novel concept is described in detail and sample results of adequate experiments are presented.

## Introduction

In general, the goal of propulsion research is to increase overall system effectiveness. Within a given gun system and constraints for a given projectile mass the most efficacious method of accomplishing this goal is to increase the launch velocity and thus the muzzle energy of the projectile. Higher muzzle velocity increases the range of indirect fire systems and hit probability, enhances terminal effects, and improves weapon lethality. On the other hand, the elastic strength profile or maximum pressure permitted within the gun chamber and along the barrel provides a limit on pressure and, hence, on gun performance. The gun recoil system also imposes constraints on maximum pressure and projectile muzzle velocity. Furthermore, muzzle signature also increases with projectile velocity and projectile stability and drag may be affected.

Guns convert either chemical or electrical energy or, in a hybrid system, a combination of both propulsion means into projectile kinetic energy. However, all techniques to increase the transfer of available energy to the projectile have to account for losses. For example, if solid propellant is added to the gun charge to boost the energy, the additional gas molecules must also be accelerated, with an increase in gas kinetic energy. If high propellant charge to projectile mass ratios, very high peak pressures, or elongated gun barrels are used, then existing chemical propulsion systems are capable of propelling projectiles into very high velocities of $v_0 > 2.5$ km/s, but at conditions that are too extreme for practical military applications. Therefore, research is directed at increasing the chemical energy per unit mass of propellant while maintaining acceptable military characteristics.

In addressing this goal, the Ernst-Mach-Institut (EMI) began to investigate the propulsion in a conventional gun system of caliber 45 mm, see Fig. 1. It made use of the chemical energy released during combustion by a conventional solid-propellant charge consisting of 600 g Q5560. The caliber 45-mm gun has a variable chamber

volume and an elongated gun barrel of 3.535 m corresponding to approximately 80 caliber. Firing the 600 g propellant Q 5560 accelerated a 200 g projectile to a muzzle velocity of more than 2000 m/s.

A further increase of projectile velocity just by the enlarging the charge weight is not possible because it would already cause gun failure exceeding the material stress limit. Therefore, a novel propulsion concept has been proposed. This concept includes a bipartite or two-component charge with consecutive ignition in which the center is made of a conventional granular propellant encased by a consolidated charge. The consecutive ignition is achieved by using two different electrical igniter systems. This concept is described in greater detail and some results of caliber 45-mm gun firings are presented.

## Novel Propulsion (ETC) Concept

### Basic Concept

The basic idea of the propulsion concept is illustrated in Fig. 2. The left drawing in Fig, 2 shows two pressure-vs.-time curves with (1) representing a curve that stays within the safe maximum gun pressure as it is generated by the combustion of a conventional solid-propellant charge, and (2) a curve of much higher pressure that exceeds the safety limit as the weight or loading density of the solid-propellant charge is increased ($p_2 > p_1$) thus releasing much higher energy than admissible, but increasing the projectile velocity (($v_2 > v_1$).

At the right of Fig. 2 also two pressure-vs.-time curves are superimposed. The curve that stays within the safe maximum pressure limit exhibits a steeper rise than curve (1) thus adding a certain amount of kinetic energy for driving the projectile (blue marked zone). The curve that exceeds the safe maximum pressure corresponds to curve (2) at the left of Fig.2 Its overshoot (green marking) would also provide more energy, but for safety reasons it is undesired. However, if both curves could be superimposed so that a broader pressure vs. time curve with increased half-width but limited maximum pressure would result, and both the blue and red marked zones would at least account for the green marked area of curve 2 (Fig. 2, left), if not for more, then such a pressure curve would stay within the safe maximum pressure limit but could transfer much more energy to the projectile, because the energy characterized by the amount of the pressure-time integral is greater than in the cases of curve (1) od (2).

However, the generation of the broader pressure curve is not easy to achieve. Only if it becomes possible to govern the ignition and combustion of a bipartite or multiplex charge so that the ideal case of the broader pressure-time curve is approached, then higher projectile velocity is achievable without exceeding the safe the maximum pressure limit. An adequate design of the propellant charge assembly and the consecutive setoff of the different charge constituents might solve this problem. In a first attempt, here the use of a bipartite charge equipped with special designed igniter trains is investigated.

*Requirements For the Propellant*

The requirements for the combustible materials used in the novel propulsion concept which, in the present first attempt is realized with the bipartite charge, are listed as follows:

1. It is necessary to find or design gun propellants or combustible materials that have high efficiency.
2. Suitable propellants should have high burning rates, but differ from each other to generate the broad pressure curve of Fig. 2 (right).
3. The material of the propellant should have adequate properties to permit the design of consolidated structures having high density.
4. The consolidated portion of the charge should consist of compact propellant layers or plates with defined breaking points so that fragmentation can be induced by the discharge of the electrical igniter and/or by the pressure increase in the gun chamber.
5. The propellant material should permit ignition by locally distributed igniter systems that are triggered consecutively at given times to allow setoff of the charge at different ignition sites.

6.    Different combustible materials should be designed so as to avoid temporary limited undesired crossing of combustion to neighbored charge components.

*Requirements For the Igniter*

For the igniter assemblies the following properties are desired:

1.    an electrical plasma discharge, because it generates high temperature and radiation. Radiation at high temperature causes excavation or spall in the irradiated material, and its transport into deeper layers supports the formation of cavities and acceleration of local burning rates,
2.    consecutive triggering of the igniter sources, located at different sites to generate controlled combustion,
3.    the energy released by the electrical igniter assembly should guarantee defined fragmentation of the combustible component forming the consolidated charge.

## Bipartite Charge

The two-stage or bipartite charge concept is schematically depicted in Fig. 3. In the cross-sectional cut through the bipartite charge assembly, put into the cylindrical steel mantle representing the gun chamber, the projectile base with the fins is recognizable in the center of Fig. 3. Also, the inner igniter is centered and positioned near the projectile's back to initiate the inner charge assembly. The concentric propellant layers include the inner more porous granular propellant fill that is encased by the outer propellant charge. The outer charge consists of pre-fragmented propellant sections or plates of high density that are indicated in Fig. 3 as framed layers. Conductors lead to the two outer igniter systems located between the inner steel and outer charge mantles. The powder layer encasing the outer charge functions as a booster charge. An insulator or insulating plastic jacket separates the steel from the overall charge configuration.

## Experimental

### Caliber 45-mm Gun

The basic design of the caliber 45-mm gun is depicted in Fig. 1. Starting from the setup with a conventional charge of 600 g Q5560, the ETC-oriented tests needed adaptation when using the bipartite charge. In particular, it was necessary to assemble both the charge setup and ignition train. The transfer of electrical energy to the charge led to changes in the breech area.

Figure 4 shows the assembled 45-mm gun chamber setup, closed by the breech block and equipped with a chambrage insert and barrel that are screwed into the gun chamber. The center igniter protrudes into the granular charge which is encased by the consolidated charge to form the bipartite load. At the outside-mantle of the consolidated charge there are two ladder-bridged igniter systems, arranged at the periphery on two opposite sides of the outer consolidated-charge mantle thus covering part of the peripheral area. The electrical energy is transferred to the igniter systems using brass connectors fixed in epoxy (HV-bushings). Measurement ports for mounting pressure gages are drilled into the gun chamber wall. In direction of the chambrage, formed by an additional conical metal insert, a further port serves for measuring the projectile base pressure prior to its acceleration and chamber pressure decay. The 3.535 m barrel is screwed into the gun chamber via a differential thread. The gun chamber volume is varied from 630 to 1260 cm³ by using adequate breech inserts.

### Igniter Systems

The center igniter design is depicted in Fig. 5. It consists of the outer steel casing equipped with a spark gap. The high-voltage (HV) bushing carries the center electrode. The spark gap is connected to an igniter cord (ITLX-cord) protruding approximately 85 mm into the centered granular propellant charge. Gap breakdown is associated with

the formation of a strong shock wave which, in turn, initiates the igniter cord. Then the igniter cord ignites quickly the center charge formed by the inner granular propellant bed

The design of the two peripheric. ladder-bridged outer igniters is shown in Fig. 6. A flexible support made of plastics (polyimid) carries the ladder-bridged copper igniter system 'printed' onto the support. Several connecting ladders exist between the two main bars. They permit electrical breakdown and, therefore, defined coincident generation of arcs along the system thus enabling plasma-based ignition of the consolidated charge. Coincident arcs assure a nearly homogeneous, approximately surface-based initiation of the outer consolidated charge and its fragmentation into more or less defined pieces. These processes commence at the various ignition sites of both ladder-bridged igniters. A thin layer of nitrocellulose (Nc) powder of type N320 between the igniter plastics foils and the consolidated charge boosts this charge initiation.

The time at which the outer ladder-bridged igniter systems are put into action by discharging a capacitor battery is important for the desired ignition and fragmentation behavior of the outer consolidated charge. Since the energy released additionally by the outer charge should overlap the initial pressure curve so that it broadens providing higher energy to the projectile base without crossing the maximum pressure limit, see Fig. 2, the outer igniters should be initiated after the inner granular propellant charge is burnt. Initiation and fragmentation are supported by the high pressure developing from the outer chamber wall towards the center.

## Charge Designs

The inner granular propellant charge consists of the powder Q5560, a well-known propellant usually used in 27-mm cannons. This propellant has been selected, because it suited the present investigations, although it is not optimized for caliber 45-mm firings.

The outer consolidated charge was made of JA2 powder. Again, it was the preferred propellant, because it was available and had an adequate material density of about 1.583 g/cm$^3$. Plates of approximately 3 mm x100 mm x 300 mm were purchased to produce strips and, in a further step, the consolidated charge assembly consisting of strips put in several layers onto the support. This is indicated in Fig. 7 which shows in a photograph how the actual system was prepared.

## High-Voltage Power Supply

In the experiments, the central granular charge was ignited by activating the central igniter. Gap breakdown was initiated by the electrical discharge of a capacitor of 20 µF charged at a voltage of 5 kV. To account also for the ignition of the outer, consolidated charge three special HV power supply modules have been developed and built at EMI. They are shown in the photograph of Fig.8. Each module can store an electrical energy of 13 kiloJoule in a capacitor bank of 260 µF, charged to 10 kV. The electrical circuit is depicted in Figure 9. Each module includes a triggered spark gap (vacuum switch). A variable inductance of max. 1250 µH can be used as pulse-forming network (PFN).

## Fundamental Investigation

### Testing of a Probe

The plasma–based ignition and fragmentation of consolidated charge probes was investigated using a simplified experimental setup and a high-speed camera as shown in the schematic drawing of Figure 10. The intention was to generate data and study conditions needed for optimizing the energy transfer to the propellant charge system.

A probe was stapled onto a plastic support that contains the ladder-bridged igniter system. A thin layer of nitrocellulose (Nc) powder of type N320 was put onto this system and then covered by several layers of consolidated charge segments made from strips of JA2 propellant. A glass plate covered and confined the probe-setup. To record ignition and combustion, a pressure gage was mounted into the bottom of the support.

The igniter system was initiated discharging the storage capacitor across the spark gap.. Plasma-based ignition and fragmentation of the probe was visualized through the glass plate by the high speed camera using the 90°-deflecting mirror. Data recorded additionally included pressure at the bottom plate, electrical current in the discharge circuit, and voltage decrease across the plasma arc. The resistance or impedance during plasma arc discharge was derived from calculation and related to the pressure recorded in the ignition area.

## Sample Results

Figure 11 shows a sequence of 8 consecutive high speed camera recordings taken during the probe testing at times t = 20, 80, 160, 210, 320, 400, 480, and 550 µs. In addition, two photographs were enlarged (Fig. 11, bottom) for times t = 80 and 560 µs after ignition, respectively. The photographs visualize the arc formation; that is, the light passing through the covering propellant layers. Also, it shows how the propellant layers widen up and deform in a step-wise manner.

Figure 12, top presents in two graphs the current vs. time, recorded in test 20 in which the ladder-bridged igniter was not covered by propellant layers and in test 22 where such layers were present. Less damping is encountered in test 20 indicating that the possible transfer of energy transfer is reduced when compared to the case of test 22.

Figure 12. bottom shows in three graphs how the voltage, current, and pressure vs. time varied during the test. Interestingly, the pressure rise starts after a rather short time delay, i.e. at about t = 70 µs after ignition.

## Discussion

After testing various ladder-bridged igniter arrangements and using a variety of propellant assemblies, a system emerged that is presently under investigation.

# Caliber 45-mm Gun Firings

### Firings with a Full-Charge of Propellant Q 5560

As mentioned previously, a number of tests were carried out firing the full load of propellant Q5560 in the caliber 45-mm gun with the elongated barrel. These tests controlled the performance of the gun system. Attempted was an increase in projectile launch or muzzle velocity exceeding 2000 m/s.

For example, with a full charge of 600 g Q5560 a maximum chamber pressure of 510 MPa was measured. The attained maximum projectile muzzle velocity was $v_0$ = 2235 m/s [1,2]. The result of these experiments supported future investigation planned for 2000.

### Future Experiments

Ongoing efforts planned for the year 2000 include a stepwise procedure in which the following conditions shall be investigated:

> 1. *Q 5560 as Center Load and Inert Casing (Fig. 13).*
> 2. *Q 5560 as Center Load with 1/3 Consolidated Charge JA2.*
>    *and 2/3 Inert Casing (Fig. 14).*
> 3. *Q5560 as Center Load encased by 2/3 Consolidated Charge JA2*
>    *and filled with 1/3 Inert Material (Fig. 15).*
> 4. *Final charge assembly.*

The full-charge tests are completed by using only the inner or center load with Q5560 as granular propellant fill. Such a test can provide information on the behavior of the center load. To limit the chamber volume, the granular fill is encased in an inert cartridge (Fig. 13).

In a second step, the center load is encased by 1/3 with the consolidated charge assembly consisting of the JA2 strips. The rest volume is filled by inert material. In this charge assembly we approach stepwise the desired final setup (Fig. 14).

The third step approaches the desired final charge assembly even more. The center load is covered by 2/3 of the Ja2 strips and the rest volume filled with inert material (Fig. 15).

In a final step the desired charge consisting of the center granular part and the outer consolidated propellant charge shall be developed and tested proposing a significant increase in gun performance.

# References

[1]   E. Gütlin and G. Zimmermann
      "Treibladungskonfigurationen für Hochgeschwindigkeits-Pulverkanonen"
      Fraunhofer-EMI Report E 50/99, August 1999.

[2]   E. Gütlin
      "Arbeiten zur Innenballistik von Kanonen mit zeitlich und räumlich verteilter Anzündung"
      Proceedings of the German Military Symposium on Interior Ballistics, Mannheim, May 1999..
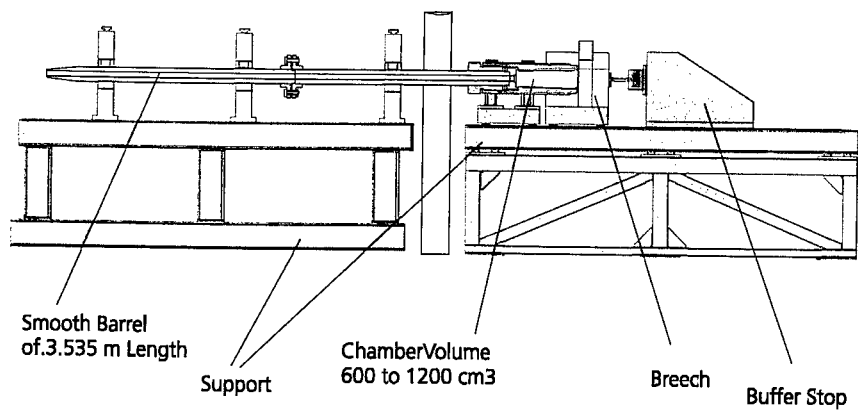
**Figure 1.** Caliber 45-mm test fixture gun

Smooth Barrel
of.3.535 m Length

Support

ChamberVolume
600 to 1200 cm3

Breech

Buffer Stop
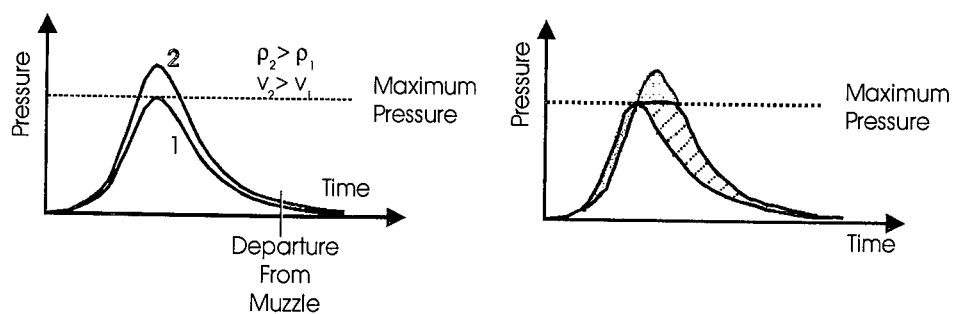


**Figure 2.** Pressure vs. time (Bipartite Charge)
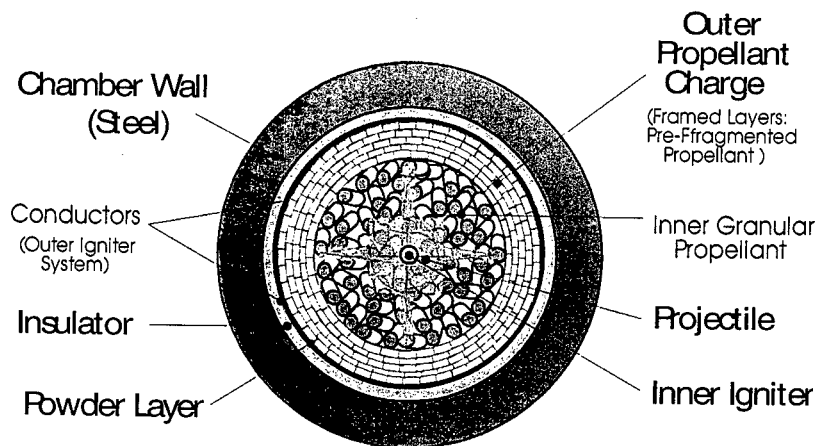


**Figure 3.** Bipartite charge (cross-sectional view)
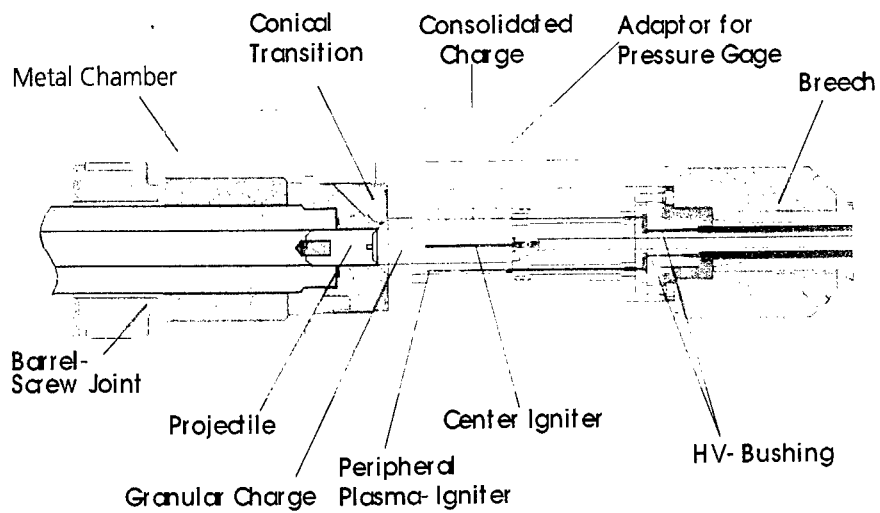
Figure 4.    Assembled 45-mm gun setup
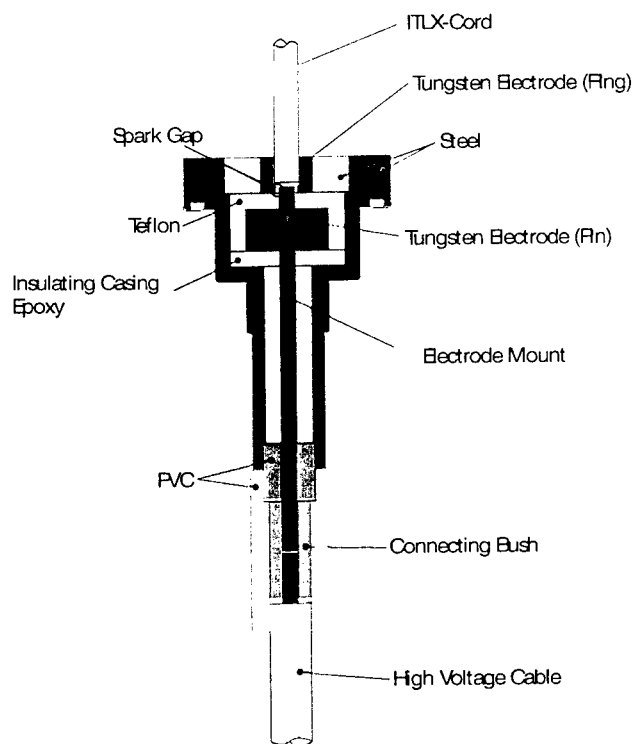


Figure 5.    Center igniter
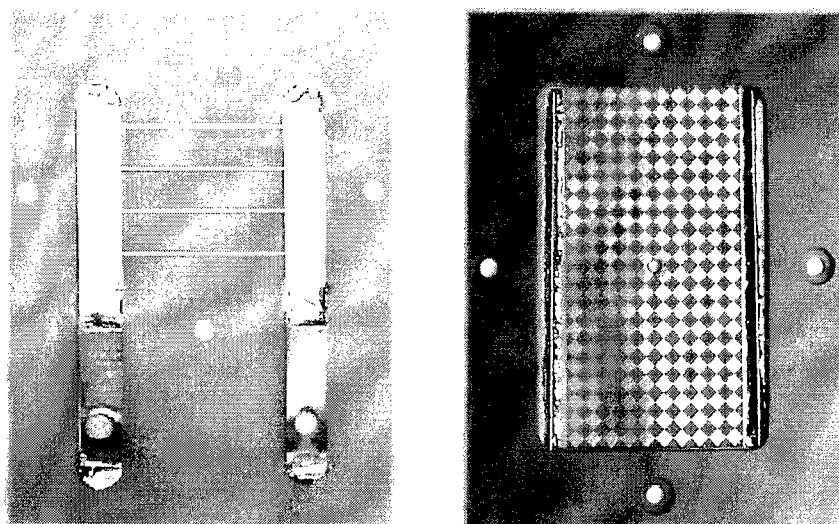
**Figure 6.** Outer ladder-bridged igniter
(Left: earlier version; right: novel version)
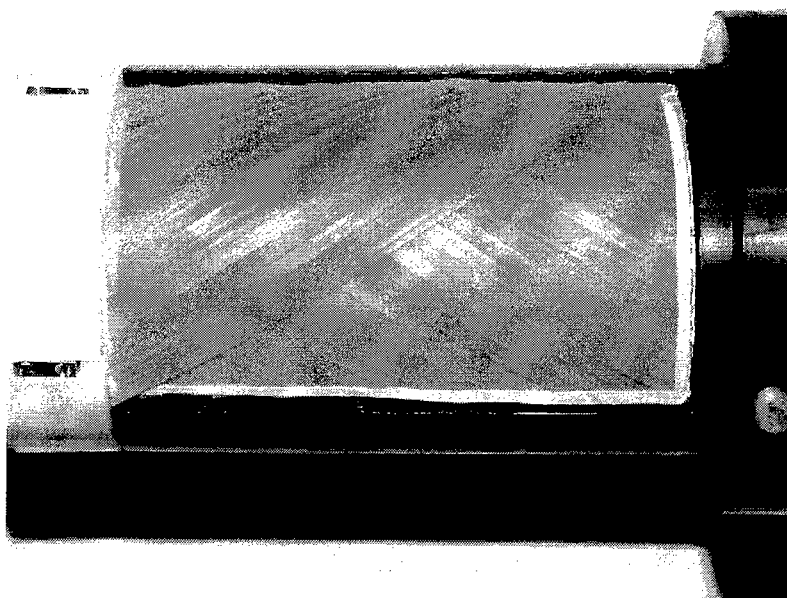


**Figure 7.** Preparation of consolidated charge
(Intermediate stage)
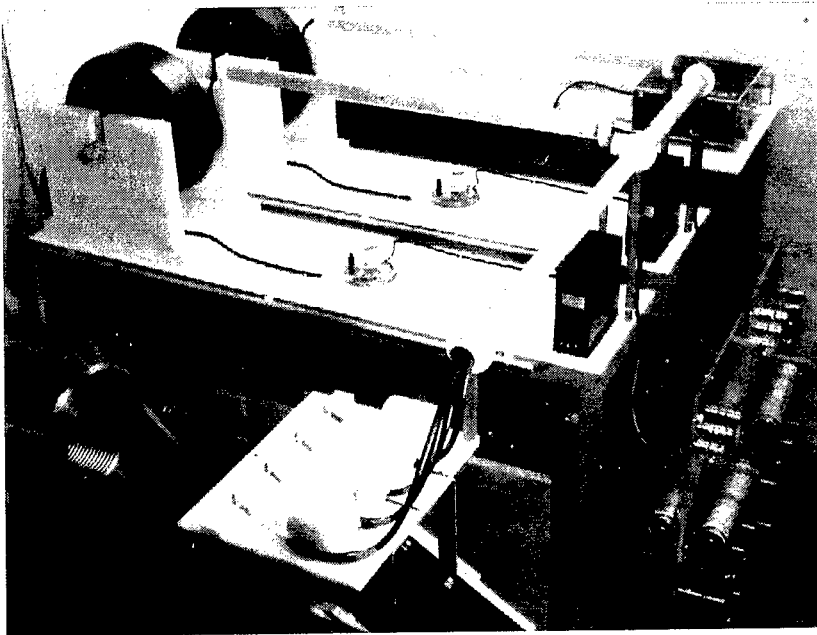
Figure 8.    Pulsed power supply
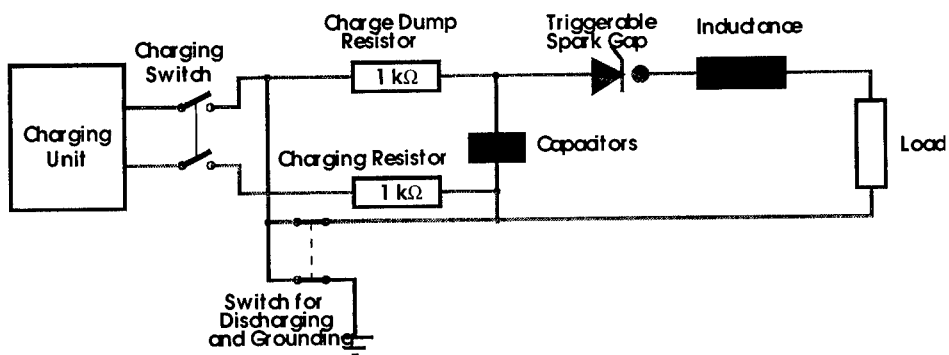


Figure 9.    Electrical Circuit of pulsed power supply
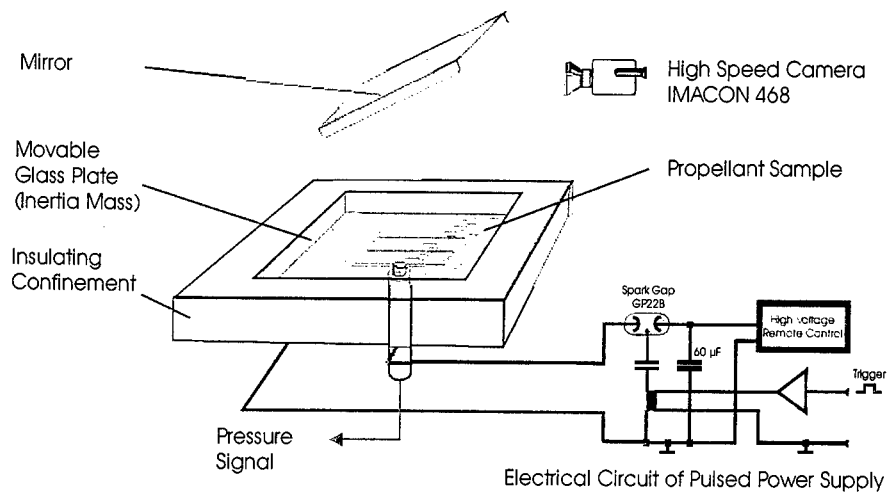
**Figure 10.** Setup for fundamental investigations
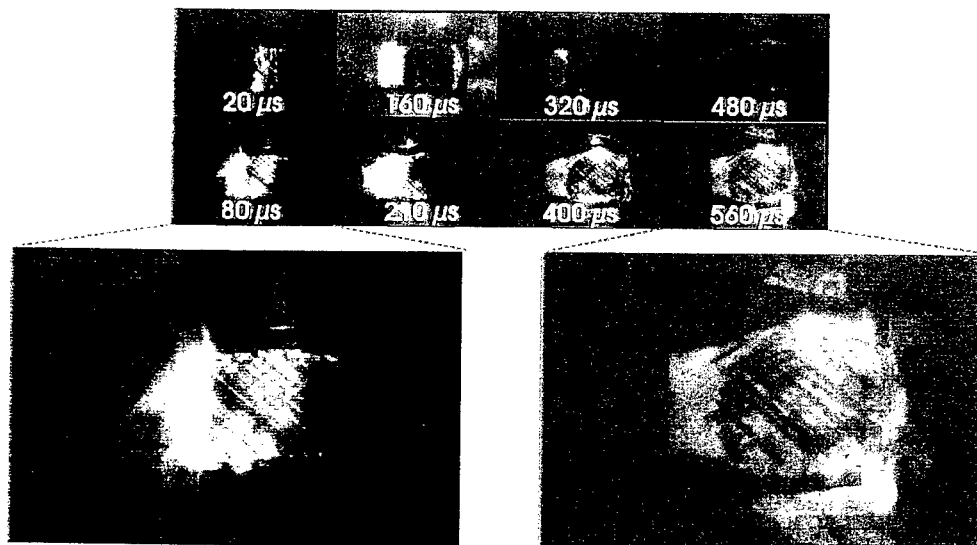


Two enlarged  photographs selected attimes t = 80 and 560 µs.

**Figure 11.** High speed camera recordings during probe testing
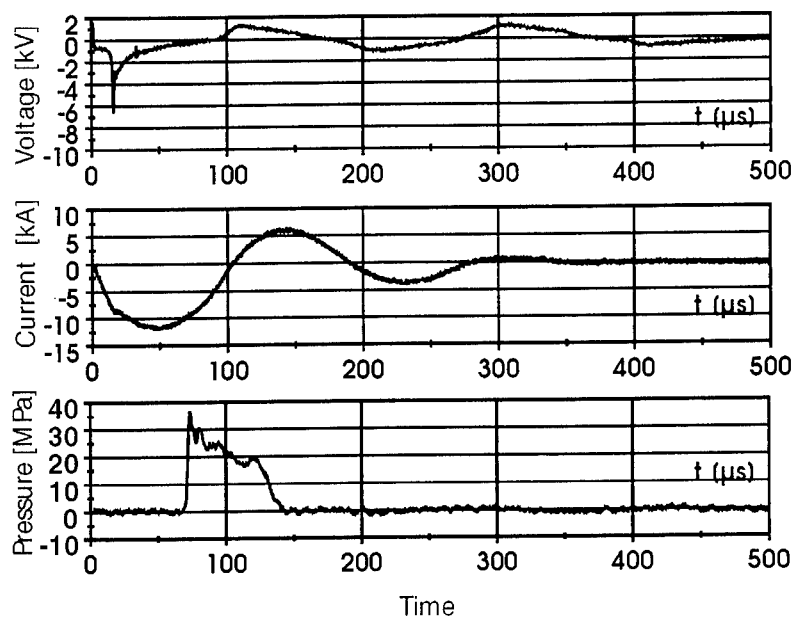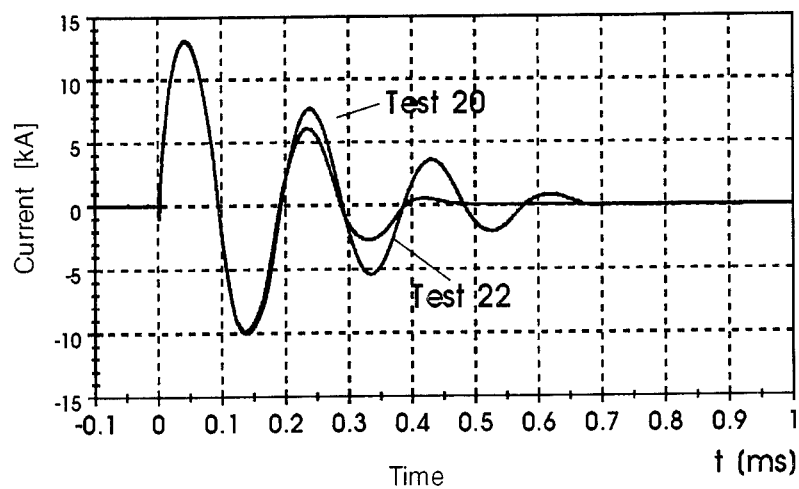
Figure 12.    Top:    current vs. time, test 20 an 22
              Bottom:    voltage, current and pressure vs.time
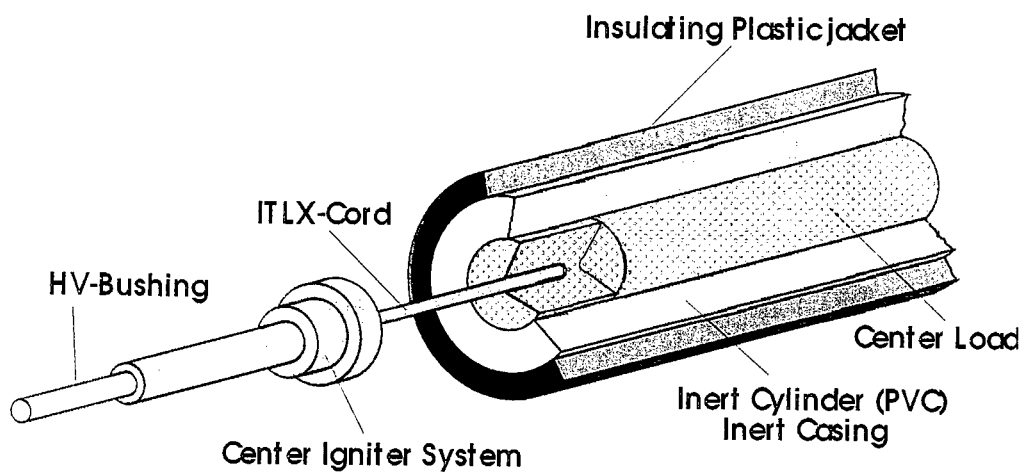
Figure 13.    Full charge test with center load and inert casing
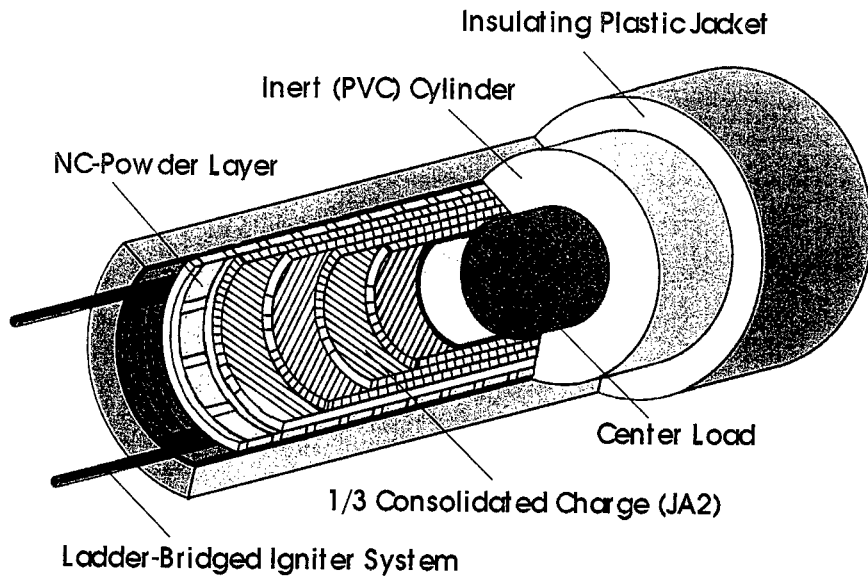


Figure 14.    Full charge test with center load and 1/3 consolidated charge
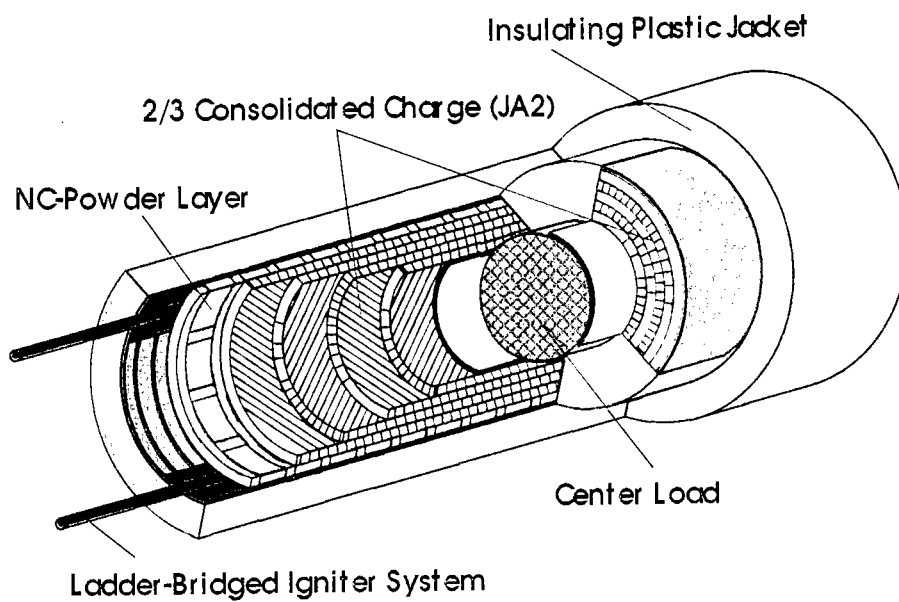
**Figure 15.** Full charge test with center load and 2/3 consolidated charge

# THE CLOSED VESSEL, STILL AN ESSENTIAL EXPERIMENTAL DEVICE FOR INTERIOR BALLISTICS IN THE FUTURE?

BASCHUNG B., GRUNE D.

ISL, French-German Research Institute, BP 34, F-68301 Saint-Louis, France

**Abstract :** In this report a short survey of the historical development and the importance of the closed vessel technique is presented. It is shown that in the past and up to now the closed vessel has provided important data in the field of application of interior ballistics. The applications are very widespread: measurements of the ignition and combustion behaviors of solid propellants (ignition energy, burning rate), optical observations of ignition (sapphire closed vessel), burning interruption at pressures up to 1 GPa to investigate irregular burning behavior at high loading densities, determination of the virial coefficients of an equation of state (combustion gases), and ignition investigations at loading densities similar to those of large-caliber guns. The different closed vessel methods are discussed with regard to their future applications. A new application of the closed vessel with plasma ignition is also shown. Finally this paper discusses the future development of a possible closed vessel technique with microwave ignition of solid propellants.

## 1. INTRODUCTION

Usually ballisticians nowadays do not think about the historical development and the importance of the propellant grain geometry for different caliber guns when talking about solid propellants for arms. It is well-known that the combustion front is perpendicular to the propellant grain surface. That is the reason why the quickness of the burning gas formation is a function of the grain geometry. The basic investigations carried out one hundred years ago by VIEILLE on propellants with special forms led to the empirical burning law:

$$r = \beta \cdot p^{\alpha} \qquad (1)$$

He defined that law from pressure measurements made during burning experiments in closed vessels although the pressure measurement technology was insufficient at the time. The so-called burning rate $r$ is the progress of the flame front on the propellant grain perpendicular to its surface. This law has been used up to now with good results in the field of interior ballistics applications. Even now, for all new created solid propellants, *VIEILLE's burning law* is determined by closed vessel burning experiments. Therefore, the closed vessel still remains an essential experimental device for interior ballistics. But this paper does not deal with this question. Our purpose is to draw attention to the progress made in the closed vessel technique. In particular, the methods now used to study the burning behavior and burning phenomena are presented together with future prospects.

## 2. CLOSED VESSEL APPLICATIONS
### 2.1 General remarks

The main work carried out with a closed vessel consists in pressure measurements during the combustion of a propellant, i.e. the pressure history and the pressure maximum. These

measurements at different loading densities allow to calculate the thermodynamic properties of the combustion gases (co-volume and force), the dynamic vivacity (for quality control) and the burning rate at different ambient temperatures (for applications in interior ballistics) of the propellant. The general instructions for these measurements and calculations are regulated by national or international rules: the NATO regulations STANAG 4115, for example [1]. In general, the burning experiments are carried out at maximal loading densities of 0.3 g/cm$^3$. At this loading density the maximum pressure reaches 500 MPa.

Fig. 1 shows the cross-sectional view of a modern closed vessel [2]. Whereas conventional closed vessels are designed for a working pressure up to 500 MPa, this device allows pressures up to 1 GPa.
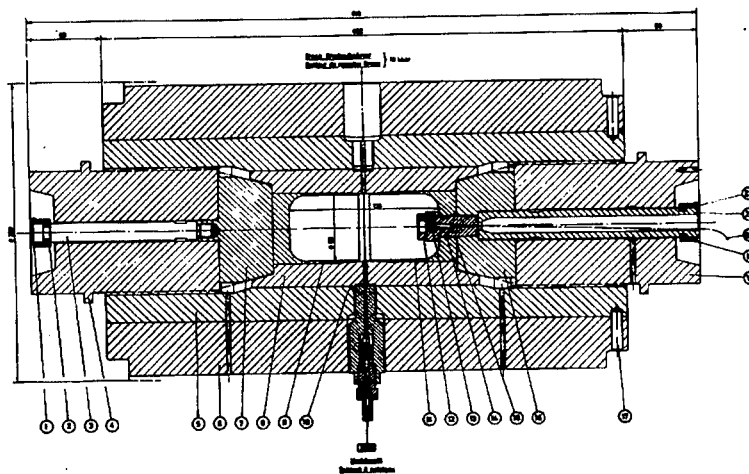


Figure 1 : cross-sectional view of a high-pressure closed vessel up to 1 GPa

The main body (5, 6, 8) consists of three parts which have been assembled by shrink-fitting the parts together. The cylindrical combustion chamber is made gastight by two steel inserts (9, 11). After the maximum pressure has been reached during a burning experiment, a blow-off nozzle (12) opens automatically and rapidly releases nearly all the energy. The propellant is ignited by means of a primer located in the blow-off nozzle. If required the ignition can be enhanced by adding reactive materials or gases. The steel insert (7) opposite the blow-off nozzle can be modified and used for a variety of special tests or measurements. This arrangement and the resistance to high pressures represent an important progress in the applications of the closed vessel technique at present.

## 2.2 Burning behavior at high pressure and high loading density

The theorists in interior ballistics always reproach the experimenters for using loading densities in closed vessels which are too low to predict a true burning law allowing to simulate the true ballistic cycle with computer models. Indeed, a maximum pressure of 500 MPa in the arm is reached with a loading density of about 1.0 g/cm$^3$, whereas a loading density of only 0.3 g/cm$^3$ yields the same maximum pressure in the closed vessel. On the other hand, it is a basic fact that, at maximum pressure in the arm, the actual loading density drops

remarkably. Nevertheless, it is possible that at high loading densities an interaction between different unknown parts of the propellant grains bed takes place in such a manner that the burning rate increases. This behavior is explicable if propellant grains come into contact during the burning. On the contact surface the energy exchange is intensified and therefore, the decomposition of the propellant is faster than VIEILLE's burning law indicates.

The investigation of this irregular burning behavior at high loading densities is made possible by means of combustion experiments in a high-pressure closed vessel. Fig. 2 shows the results of such investigations [3]. It represents the burning rates of three solid propellants as a function of pressure: a double-base propellant (flakes) and two single-base propellants (tubes and 19-holes in geometry). The dashed lines are calculations from the experiment at a high loading density of 0.56 g/cm$^3$ and the solid lines are extrapolations from experiments at low loading densities. The applied loading density leads to a maximum pressure of about 1 GPa in the closed vessel.
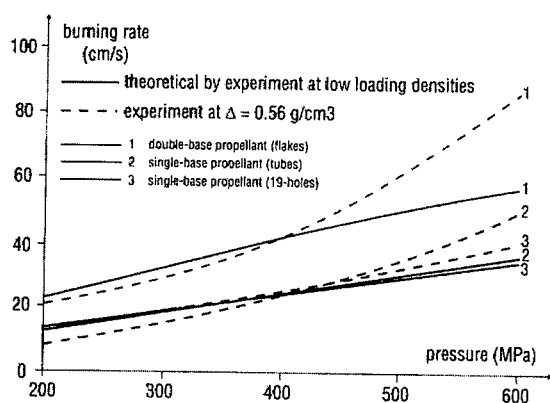


Figure 2 : burning rates of solid propellants at high loading densities

This plot clearly shows that at a loading density of 0.56 g/cm$^3$ and above, the burning rate deviates from VIEILLE's burning law. It seems – that was the assumption – that these deviations increase with the size of the surface of the propellant grains probably coming into contact. For instance, the two single-base propellants have a nearly identical burning rate at low loading densities. But at high loading density, deviations can be calculated. The deviation of the 19-hole perforated propellant is less important than that of the tubular propellant. Also the ratio of outer surface to total surface of the multi-perforated propellant is smaller than that of the tubular propellant. The greatest deviation of the burning rate from VIEILLE's burning law is measured with the double-base propellant in the form of flakes. Indeed, this geometry has the greatest ratio of outer surface to total surface.

This example demonstrates the necessity of combustion experiments at high loading densities in closed vessels to explain deviations of the ballistic cycle between the real shot and simulations using VIEILLE's burning law. The importance of these combustion experiments will increase in future, if the trend towards the development of guns with loading densities higher than 1.0 g/cm$^3$ and towards new ignition technologies (e.g. plasma ignition) remains constant. In this case, different burning phenomena occurring at the same moment have to be investigated in separate closed vessels in order to understand the burning.

## 2.3 Irregular burning behavior of solid propellants due to mechanical defects [4]

Mechanical defects in solid propellants often lead to a devastating destruction in a gun. Therefore, it is of great importance to determine such effects before the propellant is used in a gun. These investigations are carried out by burning interruption during the combustion in closed vessels, followed by a visual estimation. A lot of different methods are in use, but most of them in a low pressure range of 10 to 200 MPa. Investigations in the past showed, that essential defects are observed only at high pressures. Fig. 3 presents a helpful experimental device used at ISL.
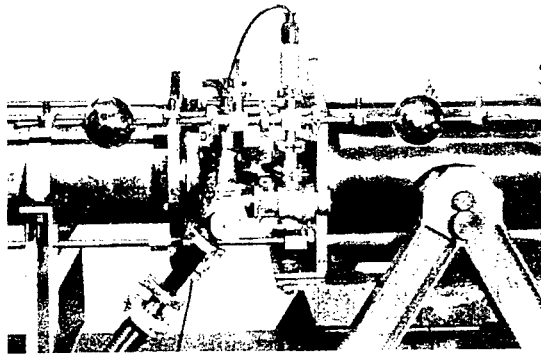
Figure 3 : burning interruption: experimental device

A closed vessel on the right-hand side of the figure, is coupled with a vacuum tank on the left-hand side. The sectional view in fig. 4 allows to describe how it works in particular. The combustion chamber (2) of the closed vessel is reduced so that its section is larger than its length. The vessel is closed on the right with a membrane (3). The whole expansion system (vacuum tank (5) and connecting tube (4)) up to the membrane is evacuated. The membrane thickness controls the opening pressure of the closed vessel and thereby also the burning interruption. A dilution wave produced by the burst of the membrane causes the sudden interruption of the burning.

High pressure bomb (type ISL, 1000 MPa) with membrane and vacuum chamber
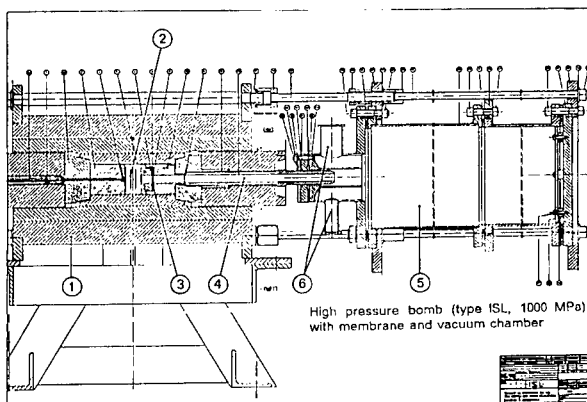
Figure 4 : burning interruption: sectional view of the experimental device

Two examples are given to explain the method allowing to determine an irregular burning behavior by mechanical effects. A first general indication is the comparison between theoretical and measured pressure rise curves $dp/dt = f(p)$. In fig. 5, curve 1 shows the theoretical behavior of cylindrical propellant grains and curve 2 the measured behavior under high pressure. An irregular burning is established. The next step is a further burning test under conditions similar to those used for weapons (high loading density: maximum pressure in the vessel between 1 and 1.5 GPa), but with a membrane placed in the closed vessel instead of the blow-off nozzle to interrupt the burning at 50% of the burnt mass.
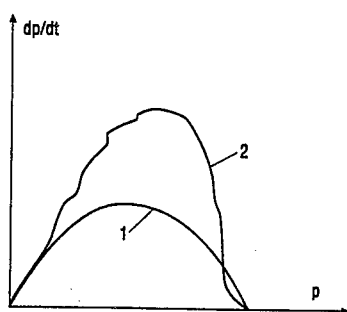


Figure 5 : dp/dt as a function of p for a cylindrical triple-base propellant
curve 1 = theoretical run,  curve 2 = experimental result

The result is shown in fig. 6. After burning has been interrupted, the propellant grains make it clear that the irregular burning is only based on a mechanical defect. The picture in fig. 6 indicates cavity formation (so-called by the authors); in this case it is caused by straightened TAGN needles.



Figure 6 : example of solid propellant combustion with cavity formation

These phenomena take place on several heterogeneous propellants. The criterion to build up a cavity burning is that one component of the propellant has a very high decomposition rate in addition to a critical length. As a further characteristic necessary to build up a cavity burning, it was found that the higher the pressure, the lower the difference may be between the decomposition rate of one component of the propellant and the burning rate of the propellant. Of course, during the extruding process the TAGN needles are straightened in a dangerous axial position. The warning is: "keep off energetic materials which are able to build up

crystals like needles". This is also valid for spherical TAGN, as is shown in the photograph of fig. 7.
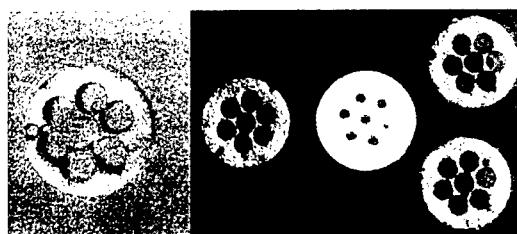


Figure 7 : burning interruption of a 7-hole propellant with
"spherical" TAGN at 440 MPa

These two examples demonstrate the necessity to perform combustion experiments with an interruption process at high pressures in closed vessels if multi-heterogeneous propellants are used. Now and in future, heterogeneous propellants as well as compacted loadings are more and more put into operation. Therefore, it will be important that the manufacturer should be able to test the burning behavior of his own new products with an interruption facility under high pressure.

## 2.4 Burning behavior with new ignition methods
### 2.4.1 Closed vessels facilities

In the past, a lot of special closed vessels were developed to characterize different igniters and igniter materials. Only a small selection of those are mentioned here by name. There is a mini-closed bomb in operation at ARL to study the influence of the propellant loading density on the computed burning rate [5]. The Nexplo Bofors company (Sweden) developed the 10 cm$^3$ EMBLA closed vessel to measure burning rates under real ignition conditions. This installation was tested by WIWEB (Germany) [6]. A further mini-closed vessel was developed by the Dynamit Nobel company in Fürth (Germany) to study the interaction between igniter material and propellant. This submini-bomb was a helpful instrument for the German working group "BAL 21" when studying the ignition behavior on solid propellants during the period 1977 to 1988 [7].

In the same period at ISL the "Two-Stage closed vessel" was developed [8]. This closed vessel allows both to measure the influence of different igniter materials on the propellant ignition and to quantify the ignition energy. All these mini- and submini-closed vessels are only designed to be helpful instruments in special investigations for a short period. Because of the special qualities of these vessels it becomes possible also to measure other physical quantities beside the pressure history, e.g. heat flux, velocity of the ignition front and gas temperature by spectroscopic analysis. High-speed photography can also be performed to make combustion processes visible. A good example presented in fig. 8 is the ISL optic transparent closed vessel made of a monocrystal sapphire. This facility allows both to measure gas temperature by spectroscopic analysis and to use high-speed photography during the combustion process. Ignition can be done by energetic gases, electric igniter, hot wire, or exploding wire. Beside pressure measurements, it is also possible to take samples for gas analysis.
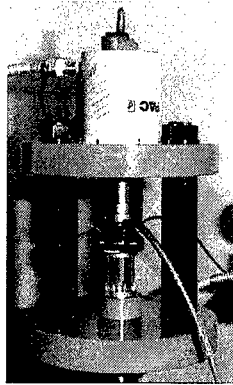
Figure 8 : optic transparent closed vessel up to 60 MPa
(sapphire monocrystal)

As was mentioned previously, all the mini-closed vessels were designed to be helpful in special investigations for a short period only; in future, it is almost certain that such facilities will be used now and then. But one new closed vessel type - used at present - is likely to become a device which will be used for a period of many years. It is the so-called "plasma closed vessel" and serves to study the burning behavior of solid propellants under plasma ignition conditions.

Fig. 9 shows the cross-sectional view of such a multifunction plasma closed vessel for both "plasma jet" and "current injection" configurations [9]. This view represents the plasma jet configuration: in this case, the plasma is generated in the plasma generator (on the left-hand side) and expands through a nozzle into the combustion chamber where the propellant is located. In the "current injection" configuration the plasma is directly generated in the propellant bed of the combustion chamber.
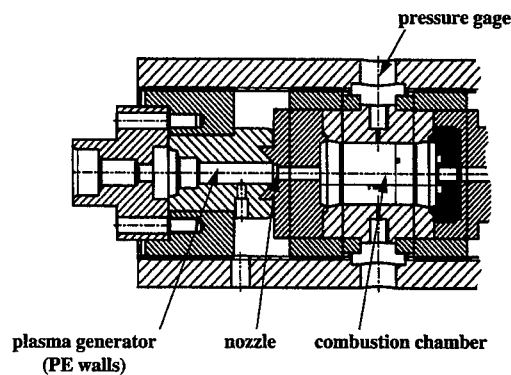


Figure 9 : plasma closed vessel (460 cm$^3$ – 400 MPa)

The propellant is ignited with a hot plasma in order to study the combustion behavior of solid propellants under the influence of a very high temperature. The principle of the plasma generation used in the plasma closed vessel is shown in fig. 10. The working method of the „plasma-capillary" (with a polyethylene cannula) is well-known [10]. Therefore, only the essential points will be explained. First, the plasma generation is initiated by wire explosion

through high voltage (HT) and secondly, sustained by further discharge of a high-voltage capacitor bank. The plasma thus created flows at a high velocity through a nozzle (fig. 9) into an expansion chamber (the combustion chamber) of the closed vessel and ignites the solid propellant. Under these conditions the burning behavior changes remarkably and will be explained with two examples [11].
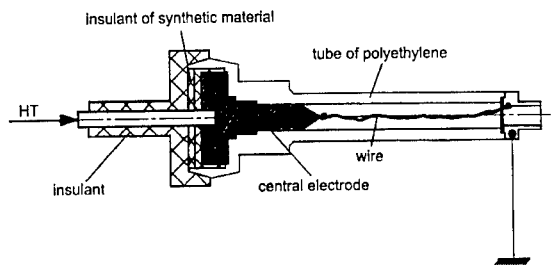


Figure 10 : principle of the plasma generation used in the plasma closed vessel

In fig. 11 the pressure rise curves are shown for a double-base propellant at the same loading density but at different plasma energies. With the conventional closed vessel ignition (curve 1) a progressive but soft pressure rise is noticed. This behavior changes with plasma ignition. The burning of the propellant starts very fast (short ignition delay time) but the gas production seems similar to that of a degressive ball powder during the burning, although the grains are small tubes. By increasing the plasma energy (shown in the order 2, 3 and 4 on the pressure rise curves), the ignition delay times decrease and the degressive burning behaviors increase. The first assumption that the propellant grains could be fractured by the plasma jet was proved to be incorrect as experiments with burning interruption showed that the grains remained undamaged. This behavior could probably be explained not only by the high temperature but also by the components of this type of propellant. It is an optic transparent propellant and contains 50% nitroglycerine.
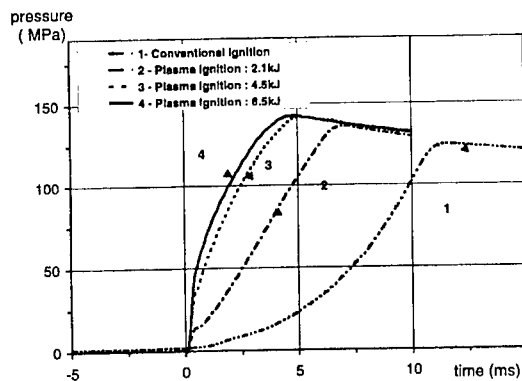


Figure 11 : pressure history of a double-base propellant
with conventional and plasma ignition

The second example is given for a "Low Sensitive Propellant" (LSP). LSP propellants are usually difficult to ignite. As shown on the graph in fig. 12, hot plasma also acts as an excellent igniter for an LSP propellant. The burning duration is reduced from about 35 ms with conventional closed vessel ignition to about 16 to 20 ms with plasma ignition. The different slopes caused by plasma ignition with different plasma energies very clearly indicate a dependence of the burning rate on the supplied electrical energy, which means a dependence on the plasma temperature. These experimental results suggest the need for a new burning law as a function of both pressure and temperature.
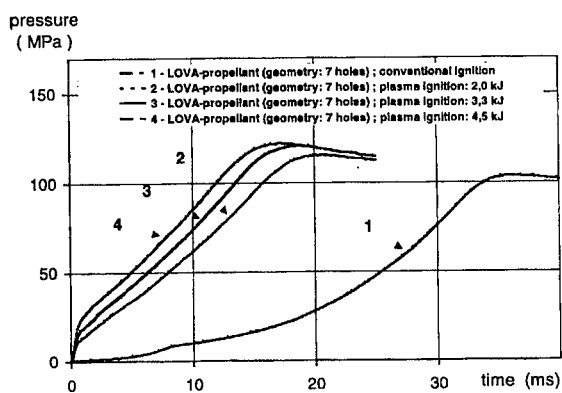


Figure 12 : pressure history of an HTPB-bonded LSP propellant
with conventional and plasma ignition

## 2.4.2 Burning law of an LSP propellant influenced by hot plasma

As is explained in the introduction, the closed vessel technique allows to test the burning behavior as well as to calculate the burning rates of solid propellants as a function of pressure only. This burning rate as a function of pressure is summarized in VIEILLE's burning law which is necessary to calculate the interior ballistic cycle. This method is only verified for the constant explosion temperature of the propellant. However, under plasma conditions the gas temperature is higher than the explosion temperature. Up to now, it has not been possible to measure a temperature profile in the closed vessel during the pressure rise, for instance influenced by hot plasma. Therefore, the pressure rise has to be simulated with a computer program to calculate the temperature as a function of time. The procedure is written in [11]. Here, only the result of such a calculation and a simulation is of interest. In the special case of a supplied plasma energy of 3.3 kJ (curve 3, fig. 12) the results of the experimental pressure history (solid line) and the calculated curve using VIEILLE's burning law (dotted line) are shown in fig. 13.

It can be noted that in the case of plasma ignition there is a distinct difference between the calculation and the experiment. It is not possible to reproduce the experimental results with the assumption that VIEILLE's burning law is valid. This behavior can be explained by the history of the gas temperature: during the whole burning period under plasma ignition conditions the gas temperature is always higher than the explosion temperature ($T_{ex}$) of the propellant with conventional ignition.
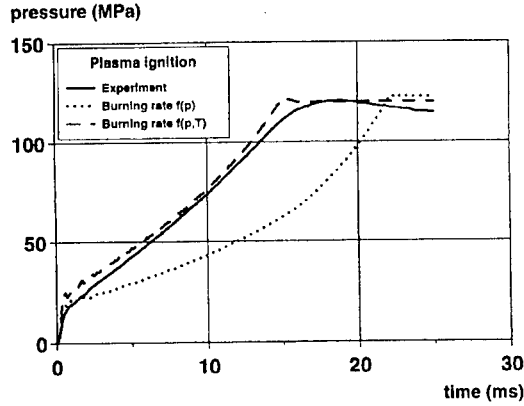
Figure 13 : comparison of the pressure history between experiment and calculations of
the HTPB-bonded LSP propellant with plasma ignition

Thus a dependence of the burning rate is established not only on pressure, but also on temperature $T$. The burning rate is described by Hensel by the following equation:

$$r = \beta \cdot e^{\frac{T - T_{ex}}{T_{ex}}} \cdot p^{\alpha} \qquad T \geq T_{ex} \qquad (2)$$

Equation 2 is valid for a gas temperature higher than $T_{ex}$. This equation shows an improved agreement with the experiment (dashed line in fig. 13).
This example distinctly demonstrates the necessity to perform closed vessel tests for each propellant which will be used in an ETC gun in future.

## 3. CONCLUSION

To answer the question asked in the title of this paper, the closed vessel tests have to be divided into 2 categories: standard applications and new investigations.
The standard applications are regulated by national or international rules, and propellant manufacturers have to take them into account now and in the future. These standard burning tests enclose the determination of thermodynamic properties, quality control (dynamic vivacity), and the calculation of the burning rate for each propellant used in conventional arms. It will be interesting to extend the previous standard applications for high pressures and high loading densities adapted to modern high-performance weapons. This is one point of the progress in the closed vessel technique.
New ignition technologies developed for the plasma ignition used in ETC guns require a new approach in burning tests. At present these types of burning tests are performed in research laboratories. However, if an ETC gun is used in the future then the propellant manufacturer will have to test his propellant under plasma ignition conditions. In particular, it is necessary to verify if the "dynamic vivacity" quality test has to be replaced by another characteristic quantity because VIEILLE's burning law is no longer valid.
Finally, in all the ignition methods mentioned before, the propellant ignition is performed by a mass flow. But, in fact, it would be desirable to ignite the propellant without a mass flow. Microwaves would fulfill this qualification. Each propellant grain would have its own integrated igniter. Moreover, a temperature independence of the burning rate would be

reached by adding small quantities of microwave energy absorbing material. By following this point of view, new types of propellants would have to be synthesized and an advanced closed vessel technology using ignition under microwave conditions would have to be developed in the future.

## 4. REFERENCES

[1]  Stanag 4115 (Edition 2): "Definition and determination of ballistic properties of gun propellants", (1995)
[2]  D. Grune, A. Carrière, "Abbranduntersuchungen von Festtreibstoffen in der manometrischen Bombe bei hohen Drücken", ISL Report RT 508/86, Saint Louis, France, (1986)
[3]  D. Grune, D. Hensel, "Burning behavior of high energy solid propellants in closed vessels at high loading densities", in Proceedings of the *14th International Symposium on Ballistics, Québec, Canada*, pp. 223-229, (1993)
[4]  B. Baschung, D. Grune, "About combustion phenomena of solid propellants under conventional- and plasma-ignition conditions", ISL Report PU 314/99, Saint Louis, France, (1999)
[5]  S. Richardson, W. Oberle, "Influence of propellant loading density on computed burn rate in a mini-closed bomb", ARL Report ARL-MD-404, Aberdeen Proving Ground, MD, USA, (1998)
[6]  K. Kupzik, "Brenngeschwindigkeitsbestimmung von TLP mittels EMBLA", in Proceedings of the *23. Wehrtechnisches Symposium Innenballistik der Rohrwaffen, Mannheim, Germany*, Report No. 14, (1999)
[7]  Final Report BAL21, Dynamit Nobel, Fürth, Germany, (1979)
[8]  D. Grune, "Ignition studies in a two-stage closed vessel using various igniter materials", ISL Report CO 231/86, Saint Louis, France, (1986)
[9]  B. Baschung, D. Grune, "Abbrandverhalten von Treibladungspulvern bei Plasmaanzündung", ISL Report PU 326/99, Saint Louis, France, (1999)
[10] B. Baschung, "Etude phénoménologique des fluides moteurs utilisés dans un générateur de plasma d'un lanceur électrothermique", Thesis, ISL Report R 103/97, Saint Louis, France, (1997)
[11] D. Grune, D. Hensel, "Combustion behavior of LOVA-solid-propellant by ignition with hot plasma gases and its influence on the interior ballistic cycle", in the Proceedings of the *17th International Symposium on Ballistics, Midrand, South Africa*, pp. 1/359-366, (1998)

# BURNING RATE MODELS OF GUN PROPELLANTS

**Eisenreich N., Fischer T., Langer G.**

Fraunhofer-Institut für Chemische Technologie, Joseph-von-Fraunhofer Straße 7,
D-76327 Pfinztal

**Abstract:** The linear burning rate of gun propellants governs the design of charges by interior ballistic simulations. Vieille's law and minor modifications of it provided a sufficient description in the past. Recent efforts to increase performance led to new gun concepts and innovative propellants. The later comprise porous and foamed charges and formulations exhibiting a temperature independent burning. Vieille's law cannot fully fit experiments in these cases. In this proceedings a summary of burning rate models is presented. They have the ability to describe the experimental determined burning behaviour at least in a simplified form and take into account actual progress in reaction kinetics of heterogeneous combustion.

## 1. INTRODUCTION

The linear burning rate is one major input to the simulation of the interior ballistic behavior of gun propellants obtained by closed vessel experiments or gun firings [1].
These simulations use Vieille's (1) law which was derived by analysing experimental pressure records according to the simplified relation (2).

$$r(P) = aP^n \tag{1}$$

$$\frac{dP}{dt} \propto A(P)r(P) \tag{2}$$

Vieille's law describes the dependence of the burning rate on pressure for a broad variety of solid propellant types with sufficient accuracy even if minor modifications are introduced. Recent developments of new classes of propellants concern temperature insensitive propellants, radiation absorbing formulations or compact charges with porous structures. The burning behaviour of these new propellants cannot be described correctly with the existing theories so that an improvement of Vieille's law or completely new approaches have to be taken into account. In the case of solid rocket propellants the modelling of the burning rate of composites [2,3] and modified double base formulations [4-6] resulted also in new descriptions.
This paper reports some modifications to Vieille's law to account for the temperature dependence of the burning rate or the combustion in porous propellants by a simplified analysis of the heat flow in the solid phase. In addition, results of applying more detailed reaction models, heat flow and diffusion in the gaseous phase are briefly outlined.

## 2. TEMPERATURE DEPENDENCE OF THE BURNING RATE

The transition of the condensed phase to the gaseous phase dominates the combustion of solid energetic materials. This means the cold solid is heated up to the temperature of the burning surface caused by energy transfer from the flame. It possibly undergoes phase transitions e.g. to a liquid. The conversion to the gaseous phase can occur by endothermic evaporation, exothermic pyrolysis or heterogeneous reactions induced by some unspecified energy source (Q(x,t) from the flame) in the gaseous phase. These effects can be included in the heat flow equation (3) whereas diffusion of species can be neglected (the following outline is described in more detail in [6,7]).

$$\frac{\partial T}{\partial t} - \frac{\partial^2 T}{\partial x^2} = Q[x,t] + \sum_i q_i \frac{\partial c_i}{\partial t} \tag{3}$$

$$\frac{\partial c_i}{\partial t} = -\sum Z_{i,j} e^{-\frac{E_{i,j}}{RT}} f[c_i, c_j] \tag{4}$$

For an inert solid without phase transition energy the heat flow equation can be solved by use of the Greens function of the heat flow equation [8]:

$$G_U[x,x',t,t'] = \frac{e^{\frac{(x-x')^2}{4(t-t')}}}{\sqrt{4\pi(t-t')}} \tag{5}$$

which enables the construction of any solution for an inert solid (dc/dt=0) for an arbitrary Q(x,t).

A simplified formula for the ignition delay is derived when calculating the time needed to increase the temperature of the propellant to a unspecified pyrolysis temperature $T_p$ by a external heat transfer $Q_R$.

$$T[0,t] = 2Q_R \sqrt{\frac{t}{\pi}} \tag{6}$$

$$t_{ign} \approx \frac{\pi T_p^2}{4Q_R^2} \tag{7}$$

Formula (7) indicates that the ignition delay depends on the square of the pyrolysis temperature and on the inverse of the square of the transferred energy flux. Provided that a stable combustion has developed, equation (3) can be transferred to the coordinate frame of the moving flame front where chemical reactions are taken into account.

$$\frac{\partial T}{\partial t} - r\frac{\partial T}{\partial x} - \frac{\partial^2 T}{\partial x^2} = Q[x,t] + \sum_i \left( q_i \frac{\partial c_i}{\partial t} - rq_i \frac{\partial c_i}{\partial x} \right) \tag{8}$$

After cancelling time dependent terms and substituting of Q and q:

$$r\rho c[T]\frac{dT}{dx} + \lambda \frac{d^2 T}{dx^2} = -Q^*[x] + r\sum_i q_i^* \frac{dc_i}{dx} \tag{9}$$

This equation can be integrated. A phase transition is described by a singular point in the specific heat:

$$c(T) = c + L\delta[T-T_L];\qquad\qquad(10)$$

heating by radiation:

$$Q^*[x] = bIe^{-bx};$$

and using the boundary conditions:

$T[\infty] = T_\infty;\qquad\qquad T[0] = T_s;$

$\lambda dT/dx = -Q_0$, (heat conduction from the flame) at $x = 0$ and

$\lambda dT/dx = 0$ at $x \rightarrow \infty$

$c_i[0] = 1$ and $c_i[\infty] = 0$; (complete conversion)

$$r = \frac{Q_o + I}{\rho\left(c\cdot(T_s - T_\infty) + L - \sum_i q_i{}^*\right)}\qquad\qquad(11)$$

(Note the sign convention: endotherm phase transition $L > 0$ (equ. (10)), exotherm chemical reaction $q > 0$). They show that conductive and radiative heat transfer influence the burning rate in the same way and that endothermic phase transitions decrease and exothermic chemical reactions increase it. Formulas like (11) were derived for ablating surfaces when exposed to heat transfer [9, 10] and discussed by Glick [11], Ewing and Osborn [12] for rocket propellants to describe the dependence on initial temperature. Crow and Grimshow proposed a similar law for gun propellants [13] although the parameters are assigned different.

Formulas (7) and (11) enable to analyse the effects of physical and chemical parameters of solid propellants on ignition delay and linear burning rate. E.g. the higher pyrolysis temperature and the additional melting of HMX or RDX which requires a latent heat L causes the strongly increased ignition delays and the low burning rates of nitramine propellants when compared to doublebase propellants (L=0) at low pressures.

In general the temperature sensitivity $\pi$ is given by $d\ln r/dT_\infty$:

$$\pi = \frac{dr/dT_\infty}{r(T_\infty)} = \frac{1}{T_\infty + L/c - \sum_i \frac{q_i{}^*}{c}}\qquad\qquad(12)$$

Ignoring phase transition energies and chemical reactions, equation (13) allows to obtain the unknown $Q_0$ (I=0) and $T_s$ when fitting it to r-values measured at various $T_\infty$ [6].

$$r = \frac{Q_o + I}{\rho c\cdot(T_s - T_\infty)}\qquad\qquad(13)$$

It was found that (13) represents the temperature dependence of the linear burning rate of many solid propellants very well. The fit parameter $T_s$ is systematically higher than the pyrolysis temperature obtained in thermal analytical experiments (e.g. TG or DSC). $Q_0$ turns out to correspond to the pressure dependence of the burning rate reproducing the pressure

exponent n [6, 14]. Equation (13) can therefore be reformulated to modify Vieille's law for taking into account radiative heat transfer and the dependence on initial temperature:

$$r = \frac{a^* P^n + I}{\rho c \cdot (T_s - T_\infty)}$$  (14)

Fig. 1 shows the least square fit of (13) to the burning rates of the gun propellant JA2 at one temperature (see details [15]).
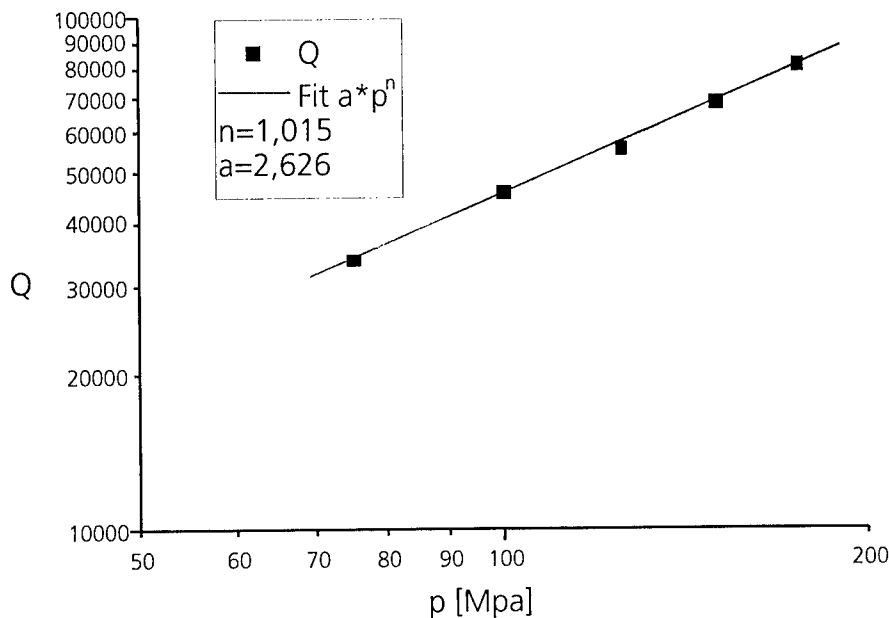


Figure 1: least square fit of Q versus p curve; Q derived from analysing JA2 closed vessel test results using equation (13)

The temperature dependence of the burning rate is influenced by phase transitions and chemical reactions in the condensed phase as obvious from equation (11). Investigations using the various phases of HMX confirmed the influence of latent heat of a structural phase transition on the burning rate [16] at low pressures, especially when testing phase δ.

## 3. REACTIONS IN THE CONDENSED PHASE

If the chemical reactions are uncompleted in the condensed phase $\Sigma q_i^*$ is unknown and a numerical solution has to be found for the burning rate.
A limiting situation is encountered if the energy transfer from the gaseous phase can be neglected. Then, the temperature gradient is small in the zone where the chemical reactions take place which corresponds also to those at highest temperature. The burning rate does not depend on the heat release of the reaction but on chemical kinetics [6, 11, 12]. For a 0th order reaction the Zeldovich formula can be derived (details also for nth order reactions see [6]) if dT/dx=0 is assumed:

$$r = \sqrt{\dfrac{2\lambda Z \displaystyle\int_{T_0}^{T_s} e^{-\frac{E}{RT}}\,dT}{c\rho\left(T_s - T_0 + \dfrac{L}{c}\right)}} \qquad (15)$$

The dependence on $T_0$ of the integral in (15) can normally be ignored so the temperature sensitivity is given:

$$\pi = \dfrac{1}{2(T_s + L/c)} \qquad (16)$$

Such a behaviour was first found for modified double base rocket propellants at low pressures in the super rate burning regime.

Some modified doublebase propellants even exhibit a mesa effect which means that the burning rate decreases with increasing pressure for some pressure range. Within this pressure interval the temperature sensitivity is low due to a change of the mechanisms from reactions in the condensed phase to inert evaporation. In the mesa range the burning rate is given by a combination of (11) and (15) [6]:

$$r = \dfrac{Q_o + I}{\rho\left(c\cdot\left(T_s - T_\infty\right) + L\right)} + \dfrac{\lambda Z \displaystyle\int_{T_0}^{T_s} e^{-\frac{E}{RT}}\,dT}{Q_o + I} \qquad (17)$$

r depending on $Q_0+I$ exhibits a minimum which is given by (15).


## 4. POROUS PROPELLANTS

The burning behaviour of porous and foamed propellants deviates also from Vieille's law. Current predictions of interior ballistics simulations fail when based on a straight forward use of it. The mass conversion rates lie essentially above those obtained by the linear burning of compact materials. Some theoretical approaches assume hot gases of the flame to penetrate the porous solid according to Darcy's law, the velocity of them is proportional to the pressure gradient and the permeability of the material [17-19].

$$\Delta P = -k_d v_{hg} \qquad (18)$$

The gases generate hot spots in the propellant pores which evolve to (quasi) spherical burning zones. This leads to increased burning surfaces and therefore in consequence to a higher burning rate. Also the effect of stand-off distances of the flame which depend on pressure (see e.g. [20, 21]) has to be taken into account.

$$\dfrac{dP}{dt} \propto \dfrac{dm}{dt} = 4\pi\rho\sum_{i,j,k} x_{i,jk}^2(t)r \qquad (19)$$

The implementation of these effects to interior ballistic calculations at ICT is obtained by two different models: A phenomenological model using the concept of cellular automates and a hot spot model using a simplified model of the heat flow equation.

The phenomenological model (details see [22]) enables to apply the linear burning rate to the enlarging pores of burning energetic materials. 2 dimensional form functions are obtained by a formal procedure. In addition on the basis of the Nobel-Abel-equation the adiabatic pressure rise in a closed vessel is simulated. Closed vessel tests with non-porous and porous propellants were used to modify the model parameters.

Explicit consideration of the internal structure of the porous charges enables the qualitative description of the burning phenomena found in experiments [23, 24]. These comprise changes of density, formulation, pore size and pore distribution but also influences of changed experimental parameters like loading density.

Fig. 2 presents the calculated influence of internal structure changes on pressure rise in a closed vessel. In this example the total pore volume respectively the overall density of the porous energetic material was constant (60 % of the theoretical density). The propellants had cube geometry with 1 cm$^3$ volume and the porosity was generated by pores with identical diameters. The calculations were made for three different pore sizes and a non-porous charge all with loading density 0.2 g/cm$^3$.
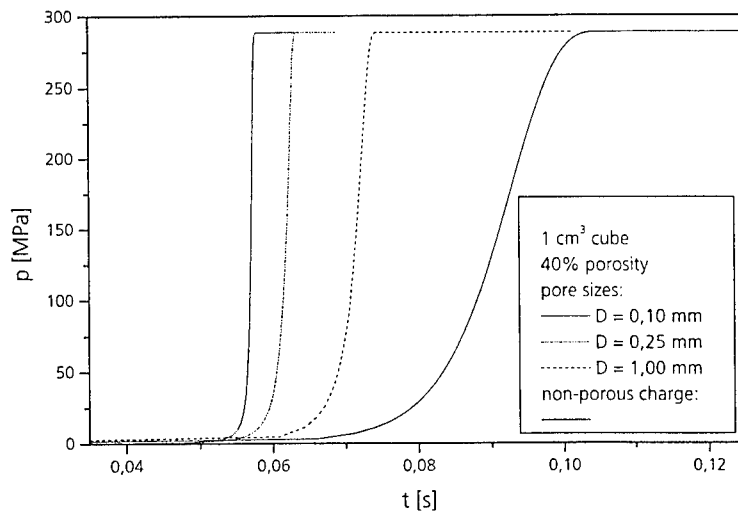


Figure 2: influence of pore size (D = diameter) on pressure rise

In figure 3 the theoretical calculations of the linear burning rate are presented in dependence on loading density for porous and non-porous charges. In experiments the same behaviour is found.
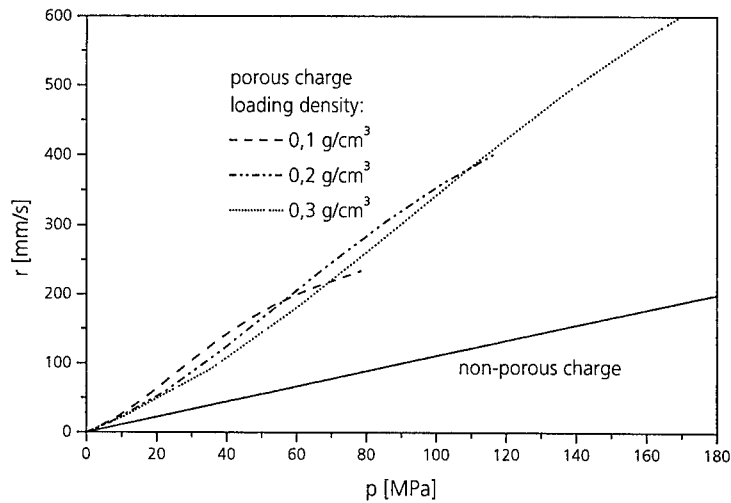
Figure 3: influence of loading density on linear burning rate

A factor that makes quantitative predictions complicate is the strong influence of penetration depth of interaction on the pressure rise (see fig 4).
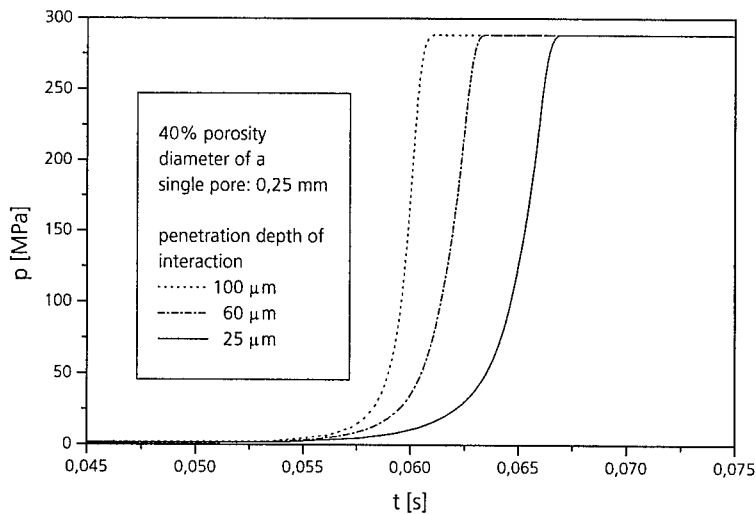


Figure 4: influence of interaction penetration depth on pressure rise

Another approach to describe porous systems use a simplified model of the heat flow equation. A 3-dimensional calculation describes the conversion of the solid based on overall chemical kinetics and heat of reaction [25-28].

The hot spots are approximated by a sum of Gaussian curves; the temperature development is given by

$$T_{hs}(\vec{x},t) = \sum_{i,j,k=1}^{I,J,K} \frac{Q_{i,j,k}e^{-\frac{(\vec{x}-\vec{x}_{i,j,k})^2}{4(t-t_{i,j,k})}}}{\left(4\pi(t-t_{i,j,k})\right)^{3/2}} \quad t_{i,j,k} > t \qquad (20)$$

A propagating hot gas flow with speed $v_{hs}$ initiates hot spots at time $t_{n,j,k}$ possibly including a response time $t_R$ (= 0, here):

$$t_{n,j,k} = t_{n-1,j,k} \frac{x_{n,j,k} - x_{n-1,j,k}}{v_{hS}} + t_R \qquad (21)$$

Chemical reactions of Arrhenius type lead to non-linear behaviour of the heat flow equation which can no longer be solved analytically. An initial temperature distribution is converted to an instantaneous heat source that would provide this temperature distribution. Chemical reactions take place which, in addition, contribute to instantaneous heat sources. An example using nitrocellulose decomposition kinetics is described in [28].

Both methods result in the increased mass conversion rates found experimentally.

## 5. CALCULATION OF BURNING RATES FROM PHYSICAL AND CHEMICAL DATA

Various approaches are made to simplify the complete set of equations to describe the combustion of solid propellants. Meanwhile numerical methods and physical/chemical data are available to calculate a priori burning rates of energetic materials based upon detailed reaction schemes and physical and chemical kinetic data. It was shown for nitromethane that the results correlate to experimental measurements [29,30].

These investigations proceed from the transport equations for the various phases and elementary reaction schemes for a gas phase consisting of $NO_x$, $O_2$, $N_2$ and $CH_x$. They are described in detail by Miller and Bowman [31]. The most important radicals of such flames are CN, NH, NO and OH. They were experimentally investigated for $CH_4/NO_2/O_2$ flames [32-34] and nitromethane [29,35] and nitramine propellants [36-39]. The results are in good agreement with fundamental mechanisms. The CHEMKIN II code enabled the calculation of detailed profiles of species and temperatures on adiabatic conditions which correlate to measured profiles [30].

An application to models of heterogeneous gun propellant combustion requires the reduction of the numerous reaction steps in elementary reaction schemes to some representative steps of simplified mechanisms. In principle, the reduced mechanism should reproduce the dominating features: conversion, time and temperature scales of the original one. As an example the reduction for liquid propellant nitromethane assumed a reaction of two consecutive steps of 1st order: A => B => P, the differential equation of which can be solved analytically.

To compare the measured burning rates with calculations the method of Zarko and Rychkov [40,41] was applied. Zarko et al. developed a 1-dimensional computer code CTEM (Combustion Transients of Energetic Materials) which simulates the transient burning of heterogeneous energetic materials [40,41]. The calculations confirm the difficult ignition of nitromethane and the low pressure burning rate of 0.02 to 0.03 cm/s [42,43]. In figure 5 an ignition to a static burning rate is plotted.
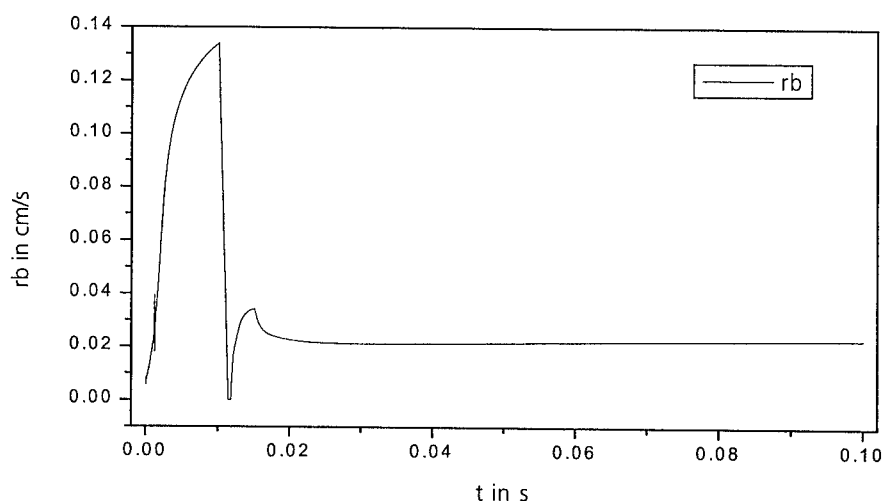


Fig. 5: Transient burning rates (rb) after ignition

## 6. CONCLUSIONS

Vieille's burning rate law is of a surprising simplicity and describes experiments with good agreement in the range of 3 orders of magnitudes of pressures. It uses two parameters where the pressure exponent is of predominant importance.

The temperature dependence of burning rate r is derived by analysing the heat flow in the solid and can be considered as a modification of Vieille's law:
Radiation $Q_R$ can strongly influence the burning rate of solid gun propellants and acts in addition to the heat conduction to the solid.

Burning behaviour of porous and foamed propellants deviates also from current predictions of interior ballistics simulations when based on a straight forward use of Vieille's law. Hot gases of the flame penetrate the porous solid according to Darcy's law and produce an enlarged conversion zone with strongly increased mass conversions.

Recent progress of fundamental research concerning elementary reactions in the gas phase, their availability in computer codes and in fluid dynamics enable development of burning rate models based upon physical and chemical parameters.

## 7. NOMENCLATURE

| | |
|---|---|
| T | temperature |
| E | activation energy |

| Z | pre-exponential |
|---|---|
| r | linear burning rate |
| $\pi$ | temperature sensitivity |
| p | pressure, |
| a | factor, |
| n | pressure exponent |
| I | radiation intensity |
| b | absorbance |
| L | heat of phase transition |
| $T_L$ | temperature of phase transition |
| $Q(x,t)$ | heat flux from an external source |
| $Q_0$ | heat flux at burning surface |
| $Q_R$ | radiative heat flux |
| $\overset{\bullet}{q_i}$ | heat from conversion of species $c_i$ |
| $\lambda$ | heat conductivity |
| $\rho$ | density |
| c | specific heat |
| $c_i$ | concentration of species |
| $v_{hs}$ | velocity of hot gases in a porous solid |
| $k_d$ | Drag of the porous solid to gas penetration |

$$t = \frac{\lambda}{c\rho} t *, \qquad Q = Q*/\lambda, \qquad q_i = \overset{\bullet}{q_i} * /\lambda$$

## 8. LITERATURE

[1]     H. Krier, S.A. Shimpi, "Predicting Uniform Gun Interior Ballistics Part I: An Analysis Of Closed Bomb Testing", Aeronautical and Astronautical Engineering Department University of Illinois at Urbana-Champaign, Technical Report AAE 74-5, (1974)

[2]     M. Summerfield, G. Sutherland, M. Webb, H. Taback, K. Hall, *Techn. Rept. PR-87-P*, Princeton University, New Jersey, (1958)

[3]     M. W. Beckstead, R. L. Derr, C. F. Price, "A Model of Composite Solid Propellant Combustion Based on Multiple Flames", *AIAA Journal*, Vol. 8, pp. 2200-2207, (December 1970)

[4]     Y. B. Zeldovich, *J.Phys. Chem.*, U.S.S.R, 22 (1948) 27

[5]     R.G. Parr, B.L Crawford, *J. Coll. Phys. Chem.*, 54 (1950) 929

[6]     N.Eisenreich, "Vergleich theoretischer und experimenteller Untersuchungen über die Anfangstemperaturabhängigkeit von Festtreibstoffen", *Bericht 8/77*, ICT (1977) Pfinztal

[7]     W. Eckl, S. Kelzenberg, V. Weiser, N. Eisenreich, "Einfache Modelle deer Anzündung von Festreibstoffen", *29th International Annual Conference of ICT*, Karlsruhe, Federal Republic of Germany, P154, (1998)

[8]     H.S. Carslaw, J.C. Jaeger, *Conduction of Heat in Solids, 2. Edition*, Oxford University Press, London, (1973)

[9]     H.G. Landau, *Quart. Appl. Math.*, 8 (1950) 81

[10]    J.I. Masters, *J. Appl. Phys,*. 27 (1956) 477

[11]    R. L. Glick, *AIAA J.*, 5 (1967) 586

[12]    D.L. Ewing, J. R. Osborn, *J. Spacecraft Rockets*, 8 (1971) 290

[13]    A.D. Crow, W.E. Grimshaw, *Roy. Soc. Trans.*, 230 A (1932) 387

[14]    N.Eisenreich et al., ISL, (March 1999)

[15]    V. Weiser, S. Kelzenberg, T. Fischer, A. Baier, G. Langer, N. Eisenreich, W. Eckl, "Burning Phenomena of the Doublebase Gun Propellant JA2", to be published

[16]    M. Herrmann, W.Engel, N. Eisenreich, "Thermal Expansion, Transitions, Sensitivities and Burning Rates of HMX", *Propellants, Explosives, Pyrotechnics*, 17 (1992) 190-195

[17]    B.N. Kondrikov, "Theory of Hydrodynamic Burning Instability of Granular Porous Energetic Materials", *28th Annual Int. Conf. of ICT*, June 24 -27 (1997)

[18]    D.A. Schult, B.J. Matkowsky, V.A, Volpert, A. C. Fernandez-Pello, "Forced Forward Smolder Combustion", *Comb. Flame*, 104 (1996) 2

[19]    N. Ishchenko, Yu. P.Khomenko, "Effect of Force Interphase Interaction on the Characteristics of Convective Combustion of Porous Media", *Combustion, Explosion and Shockwaves*, 93 (1997) 448

[20]    N. Eisenreich, "A Photographic Study of the Combustion Zones of Burning Double Base Propellant Strands", *Propellants and Explosives*, 3 (1978)141-146

[21]    N. Kubota, T.J. Ohlemiller, L.H. Caveny, M. Summerfield, *AIAA J.*, 12 (1974) 1709

[22]    T. S. Fischer , W. Koppenhöfer, G. Langer, M. Weindel, "Modellierung von Abbrandphänomenen bei porösen Ladungen ", *30th International Annual Conference of ICT*, Karlsruhe, Federal Republic of Germany, P98, (1999)

[23]    A. Meßmer, T. S. Fischer, ISL, (March 1999)

[24]    T.S. Fischer, A. Meßmer, G. Langer, "Geschäumte polymergebundene Treibladungen", *23. Wehrtechnisches Symposium – Innenballistik der Rohrwaffen,*Bundesakademie für Wehrverwaltung und Wehrtechnik, Mannheim, (25.05.- 27.05.1999)

[25]    N. Eisenreich, A. Pfeil, "Pyrolysis Craters Produced by Laser Pulse Irradiation on Propellant Solids", *Appl. Phys.,* 15 (1978) 47

[26]    N. Eisenreich, "Successively Initiated Arrays of Hot Spot in a Reactive Medium"in: *BMVg-FBWT 98-1*, FIZBw, Bonn,(1998)
        *Proceedings: Physics of Explosives*, Berchtesgaden, (29 October 1997)

[27]    G. Langer, N. Eisenreich, "Entwicklung von Hotspots in energetischen Materialien", *29th International Annual Conference of ICT, Karlsruhe*, Federal Republic of Germany, P157, (1998)

[28]    G. Langer, N. Eisenreich, "Hot Spots in Energetic Materials", *Propellants. Explosives, Pyrotechnics*, 24 (1999) 113

[29]    W.Eckl, V.Weiser, M.Weindel, N. Eisenreich, "Spectroscopic Investigation of Nitromethane Flames", *Propellants, Explosives, Pyrotechnics* , 22 (1997) 180-183

[30]    S. Kelzenberg, N. Eisenreich, W. Eckl, V. Weiser, *"*Modelling Nitromethane Combustion*", Propellants, Explosives, Pyrotechnics* , 24 (1999) 189-194

[31]    Miller, C. T. Bowman, "Mechanism and Modeling of Nitrogen Chemistry in Combustion", *Progress in Energy and Combustion Sciences*, Vol. 15, Pergamon Press, (1989) pp. 287-338

[32]    M. E. Branch, A. Sadeqi, Alfarayedhi, P. J. Van Tiggelen,"Measurements of the Structrure of Laminar, Premixed Flames of $CH_4/NO_2/O_2$ and $CH_2O/NO_2/O_2$ Mixtures", *Combustion and Flames*, 83, 228-239 (1991)

[33]    L.N. Quang, M. Vanpee, "A Spectroscopic Investigation of the premixed Acetylen-Nitric Oxide Flame", *Proceedings 19th International Symposium on Combustion*, pp. 293-301, (1982)

[34]    Guillaume, P. J. Van Tiggelen, "Spectroscopic Investigation of Acetylene-Nitrous Oxide Flames", *Proceedings 20th International Symposium on Combustion*, pp. 751-760 (1984)

[35]    Weiser, W. Eckl, N. Eisenreich, A. Hoffmann, M. Weindel, "Spectral Characterisation of the Radiative Heat Flux from Dynamic Flame Structures in Pool Fires", *The 9th International Symposium on Transport Phenomena in Thermal-Fluids Engineering (ISTP-9),* Singapore, pp. 274-279 (June 25-28 1996)

[36]    A. Pfeil, N. Eisenreich, H. Krause, "Analysis of Intermediate and Final Products of an Explosive Reaction", *Journal de Physique C4 No. 9*, pp. 209 - 221 (Sept. 1987).

[37]    H. H. Krause, N. Eisenreich, and A. Pfeil, "High Rate Decomposition of Cyclotrimethylenetrinitramine (RDX)", *Propellants, Explosives, Pyrotechnics*, 17 (1992) 179 - 181.

[38]    W.Eckl, N. Eisenreich, "Determination of the Temperature in a Solid Propellant Flame by Analysis of Emission Spectra", *Propellants, Explosives, Pyrotechnics*, 17  (1992) 202 - 206

[39]    W. Eckl, V. Weiser, G. Langer, N. Eisenreich, "Burning Behaviour of Nitramine Model Formulations", *Propellants, Explosives, Pyrotechnics*, 22, 148-151 (1997)

[40]    V.E. Zarko, L.K. Gusachenko, A.D.Rychkov, "Simulation of Combustion of Melting Energetic Materials", *Defence Science Journal*, 46 (1996) 425-433

[41]    L.K. Gusachenko, V.E. Zarko, A.D.Rychkov, "Instability of a Combustion Model with Evaporation on a Surface and Overheat in the Condensed Phase", *Combustion, Explosion and Shock Waves*, 33 (1997) 320

[42]    V.M.Raikova. "Limit Conditions of Combustion and Detonation of Nitroesters and Mixtures on their Base". *Ph.D. Thesis.,* Mendeleev Institute of Chemical Technology, Moscow, (1977)

[43]    B.N.Kondrikov, V.M.Raikova, E.M.Sviridov, T.T.Sidorova, *Data of Combustion Laboratory of Mendeleev*, University of Chemical Technology, Moscow

# STUDY OF THE GAS DISCHARGE AND THE HEAT EXCHANGES OCCURING IN A GUN BARREL AFTER THE PROJECTILE LEAVES THE BARREL - VALIDATION FOR TWO FIRING SCENARII OF THE 30MM GUN

BOISSON D., CAYZAC R., LEGERET G.

Giat Industries, Division des Systèmes d'Armes et de Munitions,Département Balistique Intérieure et Aérobalistique - 7, Route de Guerry, 18023 Bourges Cédex, France

**Abstract** : The MECCAD code is developed in Giat Industries within the prediction of the heating and the cooling of a gun barrel during a burst. The cooling phase is resolved here with enough accuracy to respect the physics of the phenomena, in particular during the gas discharge. After the projectile exit, the discharge of the propellant gas in the barrel is modeled. The main difficulty is to predict the inner flow when the muzzle conditions are subsonic. The results allowed to determine expansion laws which are used as the inputs of the cooling convective and radiative heat exchange laws. Thus, it is possible to calculate the initial barrel temperature just before a new firing. 30mm gun simulations with MECCAD code are carried out for two scenarii of firing (20 shots at a rate of fire of 40 rounds per second and 10 shots at a rate of fire of 0,58 rounds per second). The comparison with experimental results shows a good agreement.

## 1. INTRODUCTION

During the last few years, with gun barrel wear problems, much attention has been focused on the heat exchanges occuring during a shot in a gun barrel (heating phase). Most of the previous investigations were shared with the calculation of the convective [1] and radiative [2] parietal heat fluxes, during this phase.

This paper deals with the calculation of the heat exchanges occuring during the cooling phase i.e. when the projectile leaves the barrel.

The cooling in the bore after the projectile leaves the barrel is a very complex phenomena (very short expension cooling).

Some existing tools such as THETA code [3], NOVA code [4], ..., resolve this cooling in a way which is not satisfying, because in particular the laws used in order to describe the discharge of a propellant, do not respect with enough accuracy the physics of the phenomena.

The heat exchanges laws and the gas discharge laws [8], during the cooling phase, are presented in this paper. They are programmed in a new code named MECCAD.

Then results of the 30mm gun simulations with MECCAD code for two scenarii of firing are compared with experimental results.

## 2. HEAT EXCHANGES OCCURING DURING THE COOLING PHASE

Here, we are looking after the cooling heat exchanges which are used in THETA code [3]. The gas discharge will be treated in the next paragraph. This code calculates (one or two-dimensionally) the temperature everywhere in the barrel, at any time of its heating and of its

cooling, during a burst. The calculation is based on a heat fluxes balances method using 1D and 2D heat balances realized on each elementary mesh of the barrel. The numerical integration used the Gear schemes, and an iterative method for the 2D case.

During the shot, the barrel inner wall receives the total thermal flux resulting from the combustion of the propelling charge and from the friction of the projectile. The convective flux is determined by using MIGAPPAC code [1] which computes the boundary layer at the gas/wall interface ; this code is connected to the internal two-phase flow and adiabatic MOBIDIC code, during the shot [5].

After the projectile exit, during the cooling phase, we used Hottel's law [6] for the estimation of the radiation heat flux and Nusselt's correlation equation for the convective one [7]. This global approach is necessary if we want reasonable calculation times. These laws, which are presented here after, are not validated for gun barrels.

## 2.1 Nusselt's correlation equation [7]

Four correlation equations are used to take into account the different flow rates. In the literature we don't find laws for an sloped cylinder tube with any sort of internal parietal fluxes and temperatures. So we used Nusselt's equations. Moreover we consider here that the breech is not open after the shot.

MIXED AND FORCED CONVECTION

When $Re(x) \geq 10000$

$$h = \frac{\lambda}{Di} 0,036. Re(x)^{0.8}. Pr^{0.33}. (\frac{Di}{L})^{0.055} \tag{1}$$

with
h : inner wall convective exchange coefficient     $(W/m^2.°C)$
$\lambda$ : conductivity coefficient at Tfilm     $(W/m.°C)$
Tfilm : film temperature = (Tgas+Tinnerwall)/2     (°C)
Di : internal diameter     (m)
Re(x) : Reynolds number = $Vgas.Di/\nu_{(Tfilm)}$
$\nu_{(Tfilm)}$ : kinematic viscosity at Tfilm     $(m^2/s)$
Pr : Prandlt number = $\nu_{(Tfilm)}/a_{(Tfilm)}$
$a_{(Tfilm)}$ : diffusivity at Tfilm     $(m^2/s)$
L : tube length     (m)

When $10000 > Re(x) > 2300$

$$h = \left[ \frac{((h2 - h1). Re(x))}{500} + 5h1 - 4h2 \right] \tag{2}$$

$$h1 = 26,46. \frac{\lambda}{Di}. \left( \frac{Pr.Di}{L} \right)^{0.33} \quad and \quad h2 = 18,82. \frac{\lambda}{Di}. Pr^{0.33}. (\frac{Di}{L})^{0.055}$$

When $2300 \geq Re(x) > 8$

$$h = 2,10. \frac{\lambda}{Di}. \left( Re(x). Pr. \frac{Di}{L} \right)^{0.033} \tag{3}$$

## FREE CONVECTION

When $8 \geq Re(x)$ $\qquad\qquad\qquad$ h=8 $\qquad\qquad\qquad\qquad$ (4)

### 2.2 Hottel and Sarofim's law [6]

We consider the radiative heat exchanges between the gas and the inner wall. The gas is supposed to be opaque to the radiation and is at each time an isothermal gray scattering medium. The isothermal gray scattering inner wall surface is supposed to surround all the gas volume. This is an approximation which is realistic for each axial cross section of the tube (issued from the axial discretisation step) since the inner surface temperature of each ones is constant at each time. The radiative model is based on Hottel and Sarofim's equation.

$$\varnothing i = \frac{1}{\dfrac{1}{\varepsilon gas} + \dfrac{1}{\varepsilon iw} - 1} . \sigma . Si . \left( Tgas^4 - Tinnerwall^4 \right) \qquad (5)$$

with : $\varepsilon$ = inner wall and gas emissivity
$\qquad$ $\sigma$ = Stephan-Boltzmann constant $\qquad$ (W/m$^2$.K$^4$)
$\qquad$ Si = surface considered $\qquad\qquad$ (m$^2$)
Here, we don't consider the wall to wall radiation heat exchanges for time calculation reasons (because of the shape factors calculation).

### 3. THE GAS DISCHARGE

The mathematical modelling of the firing process includes the precursor flow discharge and the presence of the projectile. The boundary conditions, after the projectile exit, at and in the barrel muzzle were computed using a 1D unsteady numerical code, based on the characteristics method, according to a pull piston analogy (KAMONO code, [8]). The boundary conditions, before the projectile exit, at and in the barrel muzzle were obtained with the resolution of the 1D Euler equations according to a push piston analogy (DIMONO code, [8]). The numerical strategy is based on the Harten's second order total variation diminishing scheme. When the flow becomes subsonic at the muzzle, the perturbations can move downstream to upstream. The description of the flow discharge in the barrel depends of the intermediate ballistics flow.
The intermediate ballistic flow is modeled as an axisymmetric or 2D plan inviscid flow of a calorically perfect gas and is computed with Harten's second order total variation diminishing scheme (FREIN code, [8]). The complex geometry, evolving in time because of the displacement of the projectile, is taken into account, within the framework of a non adapted uniform cartesian mesh, by means of a special treatment of the boundary conditions based on a generalized reflexion principle.
The gas behaves as a calorically perfect gas, the ratio of specific heats and the perfect gas constant R of the equation of state $p = \rho RT$ were obtained using thermodynamic computations. Moreover, the ambiant atmosphere was not be distinguished from the propellant gas.
The main difficulties concerning the grid system are firstly, the rather complex geometry (in particular the multi-elements muzzle brake case) and secondly, the fact that the computational domain is evolving in time according to the displacement of the projectile.

## 4. CONNECTION OF MIGAPPAC CODE WITH THETA CODE : THE MECCAD CODE

From the 30mm results of KAMONO code [8] (Tgas and Vgas versus time, after the projectile exit), we determine two expansion laws, one for Tgas (exponential law as a function of the time), the other for Vgas (linear law as a function of the time and the axial abscissa). These laws are used as the inputs of the cooling heat exchanges laws and they are easily programmed in THETA code. Figure 1 shows Tgas versus the time.

Then THETA code used as boundary condition during the 1st shot, the convective flux calculated par MIGAPPAC code [1] (before we have to ensure that the gas pressures calculation with MOBIDIC code are in a good agreement with experimental pressures measured along the 30mm barrel). At the end of the 1st shot cooling, just before the 2nd firing, THETA code has calculated a new initial barrel temperature which enables us to calculate the 2nd shot convective flux (with MIGAPPAC) and so on ... until the end of the burst.

## 5. TEMPERATURE MEASUREMENTS IN A 30MM CALIBRE GUN [9]

Internal temperatures were measured using steel/constantan sensors : BRL type.

### 5.1 Sensors location

The gun barrel involves twelve seatings, distributed in four sections along its length. The axial locations are respectively 95mm (section 1), 225mm (section 2) 557mm (section 3) and 1620mm (section 4) from the beginning of the tube.

Due to the very steep temperature gradients existing near the inner surface of the gun barrel, the measuring holes are drilled as to set the sensors at the shortest distance from his surface. The closest distance that could be practically located without destruction due to internal pressure is about 360μm. Others thermocouples are located at 660μm from the inner barrel wall. For each cross section we need two thermocouples located at two depths (for inverse conduction calculation method). This thickness is realized with an total accuracy of +/- 35μm. The gun barrel being rifled, the temperature sensors are spaced so as to be located in the centre of a grove.

The thermoelectric sensors are constituted by 0,25mm diameter constantan wires welded at the bottom of a 1,65mm diameter tapered hole. A precision teflon guide is used to ensure that the measuring wires are located exactly in the centre of the drilled holes. The steel/constantan junction is obtained by using a capacitor discharge technique. The steel wire is welded at the outer surface of the tube.

These sensors are calibrated before the tests.

### 5.2 Data acquisition system

The sampling frequency of the Nicolet data acquisition system used ranges between 5 to 20 KHz. It enables the recording of all the firing scenario and of one part of the cooling phase.

### 5.3 Tests conditions

The tests were carried out on a 30mm calibre rifled gun barrel. The tube length is about 1,70m. The inner surface of this tube is protected by a chromium coating. Three scenarii of firing were realized :
- 20 and 40 shots at a rate of fire of 40 rounds per second,
- and 10 rounds during 20 seconds (at a rate of fire of 0,58 rounds per second) ,

with an inert ammunition of 91gr. We used a 7 holes simple base propellant charge. Mean velocity during the tests appears to be about 1020m/s.

During the tests we saw :

- breakings of some BRL sensors located in section 1 caused by vibrations, hot gases outer flow,
- breakings or melting of some BRL sensors located in section 4 caused by the muzzle break blow,
- thermocouples signals pertubated by the 50Hz local supply circuit frequencies ...

Figures 2 and 3 show the filtered temperatures measured in section 2 for the upstream and downstream thermocouples during :

- a 40 round burst at a rate of fire of 40 rounds/second,
- a 10 round burst during 20 seconds (including about 4 secondes of cooling).

We can see that the upstream temperature value is about 900°C for the 40th shot. We are above the steel/constantan sensor linear area.

## 6. COMPARISON WITH EXPERIMENTAL RESULTS

The comparison was realized with success for the 20 round burst, see [10] and Figure 4.

In this paper, we are looking after the 10 round burst (at a rate of fire of 0,58 rounds/s) ; Figure 5 shows the results obtained with the MECCAD code and with the upstream BRL sensors measurements. The thermocouple is located at 325$\mu$m from the inner wall, in section 2 : we took into account an error of - 35$\mu$m on this BRL location.

We can notice for the first shot that the heating and cooling calculations are equal to the measurements with a difference lower than 10% (without readjusting calculation).

In this type of approach, there always are uncertainties inherent to the measurement (thermocouple layout and response) combined with a rarely accurate knowledge of characteristics $\lambda, \rho$, Cp of chromium.

Moreover, during a shot, experimental temperatures consider the total heat transfers (convective and radiative ones due to powder combustion, and mechanical flux due to friction of the projectile band on the inner wall) while MECCAD code calculates the heating of the barrel only with the convective heat exchanges, see MIGAPPAC code [1].

Regarding to the other shots, the calculated temperature is often upper the measured one. Actually, the burst rate is not exactly the same between measurements and calculation. Sometimes, the experimental cooling phase duration is longer than the calculated one. Nevertheless we can see a good agreement between calculation and measurements for the last shot cooling phase, which duration is about 4 secondes.

Considering this and [10], the comparison compels us to conclude favorably concerning the validation of MECCAD in the case of the 30mm calibre gun.

### 6.1 The others sections

The results of the others comparisons lead to the same conclusion as section 2. But the difference between calculations and experiments decreases when we find near the forcing cone (section 1). On the contrary, this difference increases when we remove from the forcing cone : 2D effect in section 3?

### 6.2 Numerical parametric study

The sensitivity of the barrel heating and cooling to the temperature profile inside the boundary layer was carried out.

First law is Kutateladze and Leontiev's one [1], the other is Crocco's law [1]. We observe a difference of 20° between the two laws at this depth. We used Kutateladze and Leontiev's law for the burst temperature calculation because it gave higher temperature.

Regarding to the sensitivity to the upstream BRL location, see Figure 6. Its influence upon the temperature is not negligible. We took into account in our previous calculation an error of -35µm on the upstream BRL location (because BRL's sensors repairs after breakings involve new machinings of the holes and thus the tapered hole is bring nearer the inner wall).

## 7. CONCLUSION

During the cooling phase, i.e. when the projectile leaves the barrel, we have seen in the literature that the heat exchanges and the discharge of a propellant were not described in a way which was satisfying.

Here, we used Hottel's law for the estimation of the radiative heat flux and Nusselt's correlation equation for the convective flux. The gas discharge in the barrel is modeled with a CFD approach.

The new code named MECCAD enables us to compute the heating and the cooling of a 30mm gun barrel during a 40 round burst at a rate of fire of 40 rounds/s and during a 10 round burst at a rate of fire of 0,58 rounds/s. The results are compared successfully with experimental temperature measurements ; BRL's sensors were located in four sections along the barrel and between 300 and 700 micrometers from the inner barrel wall. It is now possible to predict with MECCAD code the heating and the cooling of medium calibre guns.

Next step of our work will concern the validation of the MECCAD code for the 120mm gun barrel.

Then overheating predictions will be carried out, for example for the 155mm calibre gun, where burst fires can induce wear and / or security problems (self ignition of the modular charges).

## 8. REFERENCES

[1]     D. Boisson, H. Sadat, F. Rigollet, G. Arnaud, C. Grignon. « Computation of Boundary Layers and Calculation of Parietal Heat Flux During a Shot in a Gun Barrel ». 15th Int. Symp. On Ballistics, Jerusalem, Israel, 21-24 may, 1995.

[2]     D. Boisson, F. Rigollet, G. Légeret. « Radiative Heat Transfer in a Gun Barrel ». 17th Int. Symp. On Ballistics, Midrand, South Africa, 23-27 march, 1998.

[3]     D. Boisson, C. Grignon, M. Roux, P. Gillard. « 1D and 2D Thermal Modelling of the Heating and the Cooling of a Gun Barrel During a Burst ». 14th Int. Symp. On Ballistics, Québec, Canada, 26-29 sept, 1993.

[4]     A.W. Horst, G.E. Keller, P.J. Conroy, T.P. Coffee. « The Influence of Propulsion Technique and Firing Rate on Thermal Management Problems in Large Calibre Guns ». 13th Int. Symp. On Ballistics, Stockholm, Sweden, June, 1992.

[5]     R. Briand. « Internal Ballistic MOBIDIC1D code », SNPE Rpt, 1996.

[6]     H.C. Hottel, A.F. Sarofim. « Radiative Transfer ». Mc. Graw Hill, 1967.

[7]     M.N. Ozisik. « Heat Transfer -A Basic Approach ». Mc. Graw Hill, 1985.

[8]     R. Cayzac, E. Carette. « Intermediate Ballistic Computations and Validations ». 17th Int. Symp. On Ballistics, Midrand, South Africa, 23-27 march, 1998.

[9]     Y. Guilmard, D. Boisson . «Parietal Temperatures Measurements in a 30mm Caliber    Gun ».Giat Industries Rpt, March 1996.

[10]    D. Boisson, R. Cayzac, G. Légeret. « Study of the gas discharge and the heat exchanges occuring in a gun barrel after the projectile leaves the barrel - validation the 30mm gun ». 18th Int. Symp. On Ballistics, San Antonio, USA, 15-19 nov, 1999.
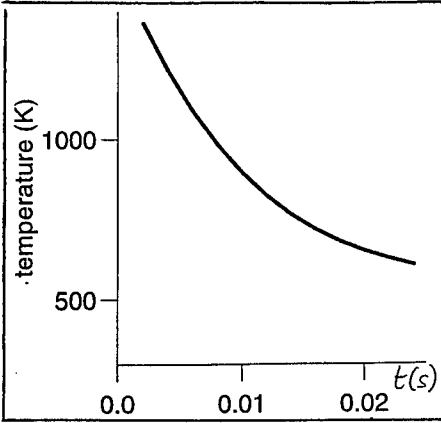
Figure 1.Tgas after the projectile exit
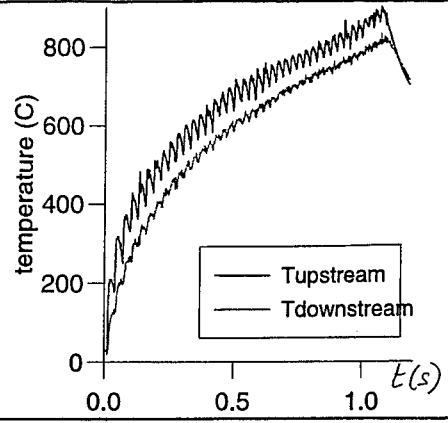


Figure 2.Tmeasured (40 round burst)
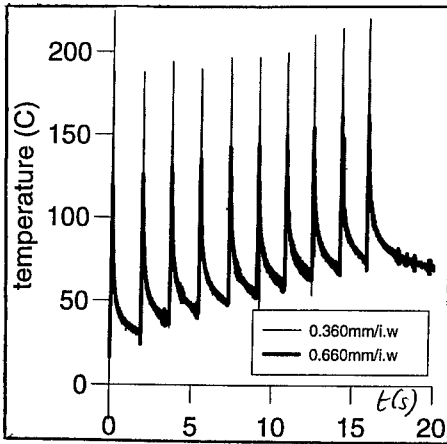


Figure 3.Tmeasured (shot/shot burst)
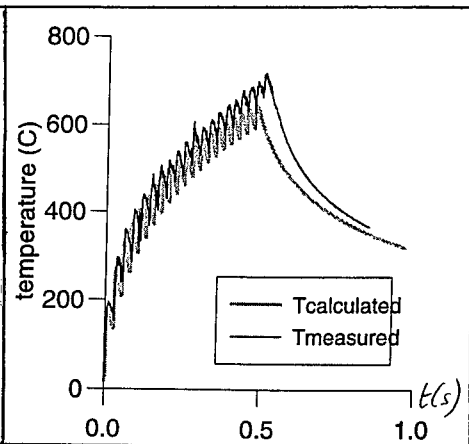


Figure 4.Comparison Tcalculated/Tmeasured
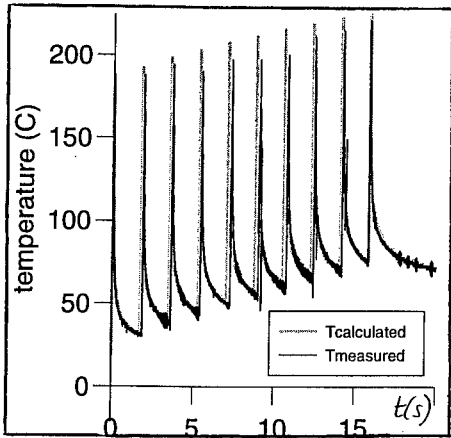


Figure 5.Comparison Tcalculated/Tmeasured
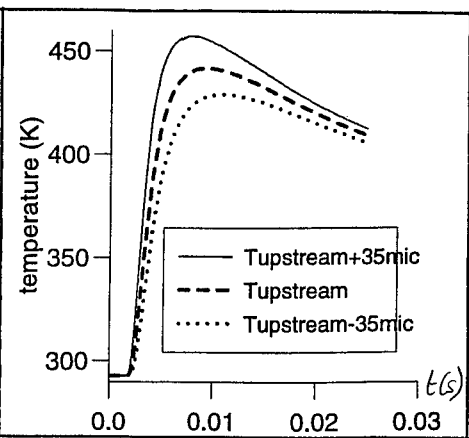


Figure6.Sensitivity to upstream BRL location

- 135 -

# NUMERICAL INVESTIGATIONS FOR MODELING

# INTERIOR BALLISTICS TWO-PHASE FLOW

DELLA PIETA P. , REYNAUD C.

SNPE-CRB, B.P. n$^0$2, 91710 Vert Le Petit, France

**Abstract** : A two-phase model based upon principles of continuum mixture theory
is numerically solved to predict the evolution of combustion in a granulated reactive
material or to analyse interior ballistics events in a solid propellant gun. The unsteady
model equations which constitute a hyperbolic system are solved using a modern high
resolution method. Some applications are given.

## 1. INTRODUCTION

Increasing the part of numerical modeling in the conception of modern types of interior ballistics
propulsion systems is only way to reduce development costs and to better understand the bal-
listics behavior. The numerical tool must include all the physics of the system (flamespreading,
mechanical behavior ...) we want to describe and must be fully validated. For example, the main
characteristics of ammunitions with consolidated charge are an important part of the propellant
charge located around the projectile and the presence of ullage between the charge and the
projectile. Many experimental observations have showed that ignition phase of a consolidated
charge is significantly different from the one of a granular charge. Consequently, the entire
ballistics cycle is different. These remarks are also valid for systems with solid propellant
packaged in several rigid moveable modules.

SNPE develops a next generation code based on a two-phase flow which must be able to
treat all the configurations of gun cartridges. This flow solver must be developed with the
following requirements. First, it must treat geometrical complexities associated with chamber
and projectile boattail. Second, shock or discontinuity capturing is desirable. The ability to
remain stable in the presence of strong porosity gradients is necessary. Third, this flow solver
must be developed with the view that the code will be applied in near future to agglomerate
loads and later to artillery ammunitions for which increment containers are present. Therefore,
its structure must be modular.

This paper addresses the two first requirements. A modeling of a two-phase flow well posed is
presented. Then, the numerical method and the algorithm to treat the previous requirements are
exposed. Some results are shown.

## 2. MODEL OF TWO-PHASE FLOW

The processes that occur in a gun can be viewed as involving the flow of a heterogeneous mixture of two phases, solid propellant and its products of combustion. A microscopic theory of interior ballistic phenomena is computationally intractable. We model only the macroscopic aspects of the flow, that is to say, we use average techniques to get governing equations. To do that, it is necessary to introduce an essentially new macroscopic variable, the solid volume fraction defined as the fraction of a unit macroscopic volume occupied by the solid phase.

An important consideration is the treatment of the solid phase material itself. Gough's mixture theory which is quite successful in simulating interior ballistics assumes an incompressible solid phase. This assumption is reasonable as long as the magnitude of stress waves remains restrained. Such model has been already introduced in MOBIDIC code [1] many years ago. Quasi-static compaction experiments typically monitor stresses as a function of a changing mixture volume. If solid phase is assumed incompressible, then porosity values are determined directly by the observed volume change. For many propellants, the incompressibility assumption can lead to a contradiction for pressure in the range of 100 MPa [2].

Several two-phase models have been developed to study deflagration-to-detonation transition (DDT) problem in granular solid propellant. The multiphase Baer-Nunziato model [3] has been chosen. This one is a continuum mixture theory model. It consists of partial differential equations of conservation applied to each phase. The two phases are compressible and in thermodynamic non-equilibrium. All materials are compressible, even if at moderated pressures, compressibility effects are negligible. The problem of closure is resolved by an equation for the evolution of the solid volume fraction. Considering each phase as compressible yields to a well posed problem and hyperbolic system. The interaction between the phases enters the theory via source terms that are added to the single phase conservation laws. An important part of this model deals with the thermodynamics of the two-phase reactive flow. The second law of thermodynamics, stated as the entropy inequality, imposes restrictions on the response of the mixture.

Conservation of mass :

$$(\rho_a)_t + div\{\rho_a \vec{V}_a\} = c_a^+ \tag{1}$$

Conservation of momentum :

$$(\rho_a \vec{V}_a)_t + div\{\rho_a \vec{V}_a \otimes \vec{V}_a + \phi_a p_a[I]\} = \vec{m}_a^+ \tag{2}$$

Conservation of energy :

$$(\rho_a E_a)_t + div\{(\rho_a E_a + \phi_a p_a)\vec{V}_a\} = e_a^+ \tag{3}$$

The entropy inequality gives a relationship which permits to take into account for both the compressibility of each phase and the compaction by treating the solid volume fraction as an independent variable. The evolution of the solid volume fraction is given as :

$$(\phi_s)_t + \vec{V}_s \cdot \vec{\nabla}\phi_s = F_m + \frac{c_s^+}{\gamma_s} \tag{4}$$

Equation (4) with (1) can also be rewritten in the following conservation form :

$$(\gamma_s)_t + div\{\gamma_s \vec{V}_s\} = -\frac{\gamma_s}{\phi_s} F_m \tag{5}$$

The mixture is saturated $\phi_g + \phi_s = 1$ and interaction terms satisfy :

$$c_g^+ + c_s^+ = 0 \qquad \vec{m}_g^+ + \vec{m}_s^+ = 0 \qquad e_g^+ + e_s^+ = 0 \tag{6}$$

The mass, momentum and energy interactions between the phases are defined by :

$$
\begin{aligned}
c_s^+ &= -\phi_s \gamma_s \frac{\mathcal{S}}{\vartheta} r \\[1mm]
\vec{m}_s^+ &= p_g \vec{\nabla} \phi_s - \vec{D} + c_s^+ \vec{V}_s \\[1mm]
e_s^+ &= [p_g \vec{\nabla} \phi_s - \vec{D}].\vec{V}_s - W_m + c_s^+ E_s + Q
\end{aligned}
\tag{7}
$$

The stress tensors are described as a pressure (deviator components are ignored). In this model, the interfacial velocity is taken equal to the velocity of the less compressible phase and interfacial pressure is modeled by gas pressure. The rate equation of compaction law is given as :

$$F_m = \frac{\phi_s \phi_g}{\mu_c}(p_s - p_g - \beta_s) \tag{8}$$

It expresses the fact that changes in the solid volume fraction are related to pressure differences existing between the two phases and the configuration pressure $\beta_s$. The passage of a compression wave over the solid/gas mixture tends to pressurize the solid in preference to the gas and a pressure relaxation process is going to develop. This state of mechanical desequilibrium is driven by the compaction law. $\mu_c$ expresses the velocity at which pressure equilibrium is reached. The state of mechanical equilibrium is given by $p_s = p_g + \beta_s$. In our situation, it is reasonable to assume pressure equilibrium instantaneously ($\mu_c$ null). To do that, we reuse the basic idea of Saurel [4] : we force the gas and the solid pressure to be in pressure equilibrium by using a relaxation technique : the source term becomes relaxation term. The intergranular pressure $\beta_s$ is a function of the solid volume fraction and reflects the contact between grains. It mesures the level of stress required to produce a given compaction of the granular bed. Quasi-static compaction data are used for the determination of $\beta_s$.

The entropy inequality used by Baer and Nunziato to construct the interphase interaction terms does not give unique expression for $F_m$ and energy exchange term $W_m$. Both forms for $W_m$ given by $(p_s - \beta_s)F_m$ or $p_g F_m$ are compatible with the entropy inequality. Simulations about quasi-static compaction shows that the last formulation $p_g F_m$ leads to right gas temperature evolution and seems more reasonable [5].

Some constitutive relations or equations are necessary to close the system, for example, an equation of state for each phase. The conservation equation on the number density of grains must be also added to determine the burning grain surface. Heating of the solid is done via compression, compaction and convective heat tranfer processes. We assume that compression and compaction heatings (mechanical processes) are uniformly distributed in the solid and give the bulk temperature. Convective heat transfer is deposited at the grain surface. Ignition of the solid phase is based on a simple surface temperature criterion. The grain surface temperature is determined using a relationship which approximates the heat conduction within particles subjected to convective heat transfer from the hot reaction product gases. We deduce surface temperature according to an approximate cubic profile solution. A unit step function is included in the combustion model to prevent combustion from beging predicted until an ignition temperature is reached.

## 3. NUMERICAL METHOD

The main directions of the development of today's two-phase flow models are improvement of the physical models (better closure models, mechanical aspect...) and improvement of the numerical methods. The numerical solver had to be robust and a high precision method is most suitable. Methods based on the resolution of the Riemann problem provide the desired precision. Our system of partial differential equations cannot be written in conservative form and leads to theoretical and practical difficulties to define the weak solutions of the Riemann problem. Important contributions in the field of modern numerical methods for two-phase flow can be found in [4,6].

The numerical method is based on a decomposition of the system that allows us to apply advanced numerical techniques developed and applied to single flows. First, we solve hydro-dynamical system using finite volume with approximate Riemann solver and we include non-conservative terms. Second, we take into account for source terms : combustion, velocity and pressure equilibrium or non-equilibrium effects. Time advance is done by Runge-Kutta method.

### 3.1 Finite volume method

The model equations may be written as :

$$q_t + div \vec{F}(q) = s(q) \tag{9}$$

where $q = (\rho_g, \rho_g \vec{V}_g, \rho_g E_g, \rho_s, \rho_s \vec{V}_s, \rho_s E_s, \gamma_s, n_s)^t$ is the conserved physical vector, $\vec{F}(q)$ is the flux vector and $s(q)$ is the terme source in which non-conservative terms are taken. On integrating (9) over an arbitrary element $\xi$ and using the divergence theorem, we have :

$$\int_\xi q_t \, d\xi = - \int_{\partial \xi} \vec{F}(q).\vec{n} dl + \int_\xi s(q) \, d\xi \tag{10}$$

in which $\vec{n}$ is a unit outward vector normal to the element boundary. On discretizing (10), we get :

$$|\xi| \frac{d\bar{q}}{dt} = - \sum_j F_n^j(q) \, |\partial \xi^j| + |\xi| \, s(q) \tag{11}$$

in which $\bar{q}$ is an average value, $|\xi|$ and $|\partial \xi^j|$ are respectively area of an element and length of one of its sides $j$. $F_n(q)$ is the normal flux. Its evaluation and the treatment of the non-conservative terms are the main numerical difficulties of the two-phase flow case. Based on the rotational invariance property, the normal flux calculation problem can be dealt with as a series of local one-dimensional Riemann problem in the normal direction to the element interface.

### 3.2 Approximate Riemann solver

The AUSM (Advection Upstream Splitting Method) solver has been developed for Euler equations for perfect gas. Its advantages are easy generalization to other conservation laws with complex equations of state and its low cost to compute. AUSM+ version [7] is chosen for its improvement in accuracy and its simplicity over its predecessor AUSM versions.

The interface flux is based on a decomposition of the flux vector into left and right travel-ling waves. The contribution of each wave is determined by the local flow conditions in

accordance with the eigenvalues of the system. The flux fonction consists of convective and pressure terms. Convective terms are quantities convected with a suitably velocity at the cell interface and pressure terms are governed by the acoustic wave speeds.

In one-dimensional, the flux fonction $F_a$ for each phase may be written as a sum of convective and pressure terms pondered by its own volume fraction :

$$F_a = \phi_a \begin{vmatrix} \gamma_a u_a \\ \gamma_a u_a^2 + p_a \\ (\gamma_a E_a + p_a) u_a \end{vmatrix} = \phi_a \left\{ M_a\, c_a \begin{vmatrix} \gamma_a \\ \gamma_a u_a \\ \gamma_a H_a \end{vmatrix} + \begin{vmatrix} 0 \\ p_a \\ 0 \end{vmatrix} \right\} = \phi_a \left\{ M_a\, c_a\, Z_a + P_a \right\} \quad (12)$$

in which $Z_a$ and $P_a$ denote respectively $(\gamma_a, \gamma_a u_a, \gamma_a H_a)^t$ and $(0, p_a, 0)^t$ vectors. The numerical flux at the interface $\tilde{\imath}$ separating the $ith$ and (i+1)$th$ cells expresses as :

$$Z_a^{\tilde{\imath}} = \phi_a^{\tilde{\imath}} \left[ M_a^{\tilde{\imath}}\, c_a^{\tilde{\imath}}\, Z_a^{\tilde{\imath}} + P_a^{\tilde{\imath}} \right] \quad (13)$$

where :

$$Z_a^{\tilde{\imath}} = \begin{cases} Z_a^i & \text{if } M_a^{\tilde{\imath}} \geq 0 \\[2mm] Z_a^{i+1} & \text{if } M_a^{\tilde{\imath}} \leq 0 \end{cases} \quad (14)$$

$M_a^{\tilde{\imath}}$ is a sum of two components associated with left and right travelling waves :

$$M_a^{\tilde{\imath}} = \Re_a^+(M_a^i) + \Re_a^-(M_a^{i+1}) \text{ with } \Re_a^\pm(M_a) = \begin{cases} \pm\frac{1}{4}(M_a \pm 1)^2 \pm \frac{1}{8}(M_a^2 - 1)^2 & \text{if } |M_a| \leq 1 \\[2mm] \frac{1}{2}(M_a \pm |M_a|) & \text{if } |M_a| \geq 1 \end{cases} \quad (15)$$

The interface pressure $p_a^{\tilde{\imath}}$ that figures in $P_a^{\tilde{\imath}}$ is given by :

$$p_a^{\tilde{\imath}} = \Im_a^+(M_a^i) p_a^i + \Im_a^-(M_a^{i+1}) p_a^{i+1} \quad (16)$$

with :

$$\Im_a^\pm(M_a) = \begin{cases} \frac{1}{4}(M_a \pm 1)^2 (2 \mp M_a) \pm \frac{3}{16} M_a (M_a^2 - 1)^2 & \text{if } |M_a| \leq 1 \\[2mm] \dfrac{(M_a \pm |M_a|)}{2 M_a} & \text{if } |M_a| \geq 1 \end{cases} \quad (17)$$

A judicious choice of the common speed of sound $c_a^{\tilde{\imath}}$ may allow, in one-dimensional stationary flow, the exact capturing of a shock wave. Here, the following formula is used (AUSM formulation) :

$$c_a^{\tilde{\imath}} = \begin{cases} c_a^i & \text{if } M_a^{\tilde{\imath}} \geq 0 \\[2mm] c_a^{i+1} & \text{if } M_a^{\tilde{\imath}} \leq 0 \end{cases} \quad (18)$$

Some different choices are the algebric or geometric mean value of $c_a^i$ and $c_a^{i+1}$. Since the solid volume fraction is convected, we take :

$$\phi_s^{\tilde{\imath}} = \begin{cases} \phi_s^i & \text{if } M_s^{\tilde{\imath}} \geq 0 \\[2mm] \phi_s^{i+1} & \text{if } M_s^{\tilde{\imath}} \leq 0 \end{cases} \quad \text{and} \quad \phi_g^{\tilde{\imath}} = 1 - \phi_s^{\tilde{\imath}} \quad (19)$$

To introduce the volume fraction in $Z_a$ and $P_a$ expressions is not adopted for use in AUSM+ because it seems to give bad numerical results.

High order accuracy is achieved by using MUSCL approach of Van Leer. In order to obtain monotonicity, various procedures for slope limitation exist. We use the Minmod limiter. The slope calculations use some variables and several choices are possible. It seems that slope calculations with the variables $(\gamma_g, \vec{V}_g, p_g, \gamma_s, \vec{V}_s, p_s, \phi_s, \vartheta)$ yield better behavior than other choice, but it is not proved. High order accuracy arrounding the sliding line is under study.

### 3.3 Treatment of non-conservative terms

One difficulty for the resolution is the presence of non-conservative terms (proportional to $\vec{\nabla}\phi_s$) in the momentum and energy equations. Robust and accurate discretisation of these terms is required to treat correctly strong porosity gradients.

Contact discontinuities are special simple wave solutions of the system and are obtained by solving the generalized Riemann invariants (only algebric source terms are ignored) associated with linearly degenerate fields. Non-conservative terms are discretized to keep contact discontinuity associated to the eingenvalue $V_s$. The generalized Riemann invariants associated with the double eingenvalue $V_s$ are :

$$V_s \quad S_g \quad \phi_g\gamma_g(V_s - V_g) \quad \phi_s p_s + \phi_g p_g + \phi_g\gamma_g(V_s - V_g)^2 \quad e_g + \frac{p_g}{\gamma_g} + \frac{1}{2}(V_s - V_g)^2 \quad (20)$$

These Riemann invariants show that a uniform two-phase flow with velocity and pressure equilibriums and porosity jump is a simple wave solution of the differential system. Consequently, the discretization of the non-conservative terms must balance the numerical flux for such flow. Thus, discretization of the non-conservative terms depends on the choice of the flux fonction.

### 3.4 Ale formulation

Because our numerical algorithm will use moving cells, an Arbitrary Lagrangian Eulerian version of the AUSM+ solver is necessary. On integrating (9) over a moving element $\xi(t)$ and using the divergence theorem and Leibniz's rule, we have :

$$\frac{\partial}{\partial t}\int_{\xi(t)} q\, d\xi = \int_{\partial\xi(t)}[-\vec{F}(q) + q\vec{\omega}].\vec{n}\, dl + \int_{\xi(t)} s(q)\, d\xi \qquad (21)$$

in which $\vec{\omega}$ is the contol surface velocity vector. According to the use in convective flux formulation of total energy or total enthalpy, the pressure in the work flux is pondered by the fluid velocity or by the interface velocity. The choice makes use of convective flux with total enthalpy. In that case, the pressure flux is independent of the fluid velocity and the resultant numerical formulation reduces exactly to the fixed M-split scheme AUSM+ in the absence of grid motion. Minor modifications are introduced in the fixed AUSM+ solver : the fluid velocity is changed in the fluid velocity relative to the interface velocity ($\vec{V}_a - \vec{\omega}$) and the pressure splitting contains an additional term (relative to the energy flux) which vanishes in fixed grid.

### 3.5 Treatment of source terms

Once hyperbolic system is resolved, we apply numerical method to the following ordinary

differential system where only algebric source terms are present :

$$
\begin{aligned}
(\rho_s)_t &= -\rho_s \mathcal{S}/\vartheta r \, I_1 \\
\rho_s(\vec{V}_s)_t &= -\delta(\vec{V}_s - \vec{V}_g) \, I_2 \\
\rho_s(e_s)_t &= Q \, I_1 - p_g \, F_m \, I_3 \\
(\gamma_s)_t &= -\gamma_s/\phi_s \, F_m \, I_3 \\
(n_s)_t &= 0 \\
(\rho_g + \rho_s)_t &= 0 \\
(\rho_g \vec{V}_g + \rho_s \vec{V}_s)_t &= \vec{0} \\
(\rho_g E_g + \rho_s E_s)_t &= 0
\end{aligned}
\tag{22}
$$

To clarify, the full source operator is split in different partial source terms associated with mass and heat transfers $(I_1 = 1, I_2 = 0, I_3 = 0)$, velocity effect $(I_1 = 0, I_2 = 1, I_3 = 0)$ and pressure effect $(I_1 = 0, I_2 = 0, I_3 = 1)$. For each partial source operator, initial state is given by previous source operator final state. If pressure equilibrium is assumed, operator $I_3$ can be written as :

$$
\begin{aligned}
(e_s)_t &= -p_g \left( \frac{1}{\gamma_s} \right)_t \\[2mm]
p_s &= p_g + \beta_s
\end{aligned}
\tag{23}
$$

These relations lead to a non-linear equation solved by an iterative method [4].

## 4. NUMERICAL ALGORITHM

To solve conservation laws in changing computational domain is not easy when a body is moving inside and then will stretch the computational domain. One idea is to repeat the grid-generation construction at small time increments as the projectile moves, adjusting the conservation laws scheme to account for the grid motion (by so-called Arbitrary Euler Lagrange formulation [8]). The disadvantage of this grid method is that it needs a significant amout of user intervention and encouters difficulties in preserving boundaries and reducing grid skewness. In our case, such geometric difficulties arise when the projectile associated with a complex shape is moving inside the tube.

Other idea is to use a cartesian cut cell mesh approach [9]. A background cartesian mesh is generated on the computational domain and complex afterbody geometry is represented by different types of cut cell. This method may be delicate and long to develop when the moving boundary has a complicated shape. However, it is a solution.

We present a new alternative approach. The method is based on a moving unstructured grid employing volume finite method and does not at any stage involve any remeshing process as the projectile moves. Problems such as mesh distorsion, body motion restriction which may occur when using other mesh approaches are completely avoided. The main ideas are the following.

Because geometrical shape of the boundaries can be complex, we use unstructured mesh method which can cope with any geometries. The initial solution domain is subdivided to a number of quadrangular elements. In order to track the moving boundary (projectile), a new algorithm is employed by which elements are inserted and part of the mesh is fixed to the projectile and follows its movement. To do that, we have developed an ALE non conform treatment for solving the sliding between a fixed and a moving mesh, as illustrated in figure 1.
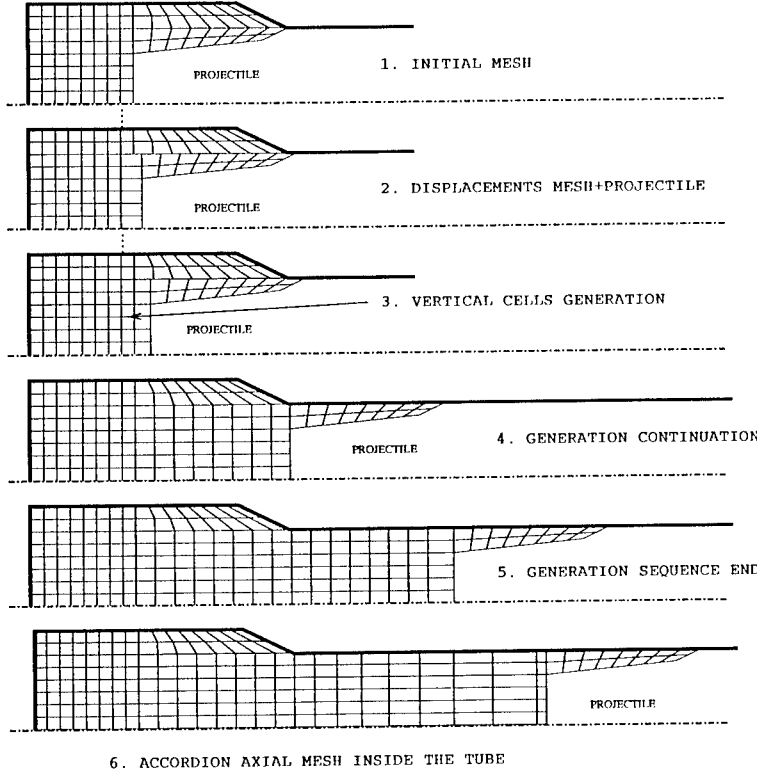
Figure 1 : Two dimensional algorithm

As was stated, solution domain is unstructurally discretized to a number of elements. In such a volume finite element approach, there are no limitations on the type of elements and number of them surrounding an element. This is an excellent feature when solving sliding between cells. Because a part of the mesh is moving, we use Arbitrary Euler Lagrange formulation. In our problem, a part of mesh is moving with the same velocity and therefore elements remain non-deformed except those who are attached to the fixed cells. To avoid distortion of these cells and to keep a good discretization in space, cell generation occurs. This stretch of elements continues until a defined criteria is met. This criteria is that if distance between upper nodes of the upper stretched cell gets larger than a defined value (length of upper fixed cell plus half length of the following), then two new elements are created. The new left element will remain fixed with the same size as the upper fixed cell and the new right element will move. Element insertion process occurs until the end of the afterbody is enough inside the tube. At this stage, accordion or quadratic axial mesh takes place from the forcing cone to the end of the afterbody. It is worths to mention that movement of sliding cells will affect the boundaries as soon as the projectile is moving. Therefore, insertion of new boundaries or alteration must be controlled. Moreover, to remove numerical errors due to grid movement, special care is given to the geometric conservation law (GCL). This law is based on the fact that grid movement should not affect uniform flow field. It is obtained by applying continuity equation to a uniform flow field with zero velocity, i.e.,

$$\frac{\partial |\xi|}{\partial t} - \oint_{\partial \xi} \vec{w}.\vec{d\xi} = 0 \qquad (24)$$

To satisfy GCL, normal velocity of a face may be evaluated [8].

## 5. SOME RESULTS

A brief demonstration of the MOBIDIC-NG code is provided in order to show the advantages of the numerical solver and algorithm.

### 5.1 Interface transport

The objective of this problem is to check the capability and the stability of both model and numerical solution method to describe flow conditions with strong porosity gradients which are typical of many situations where phase separation phenomena are dominating (ullage, propellant arrangements). In particular, we wish to treat the most difficult case where one of the phases disappears or does not exist at initial time.

The test consists of a tube center-filled with moving homogeneous two-phase mixture (velocity is 100 m/s). Monophase zone is described with a solid volume fraction taken equal to 1.E-7. Figure 2 below shows in the space-time plane the predicted value for the solid volume fraction.
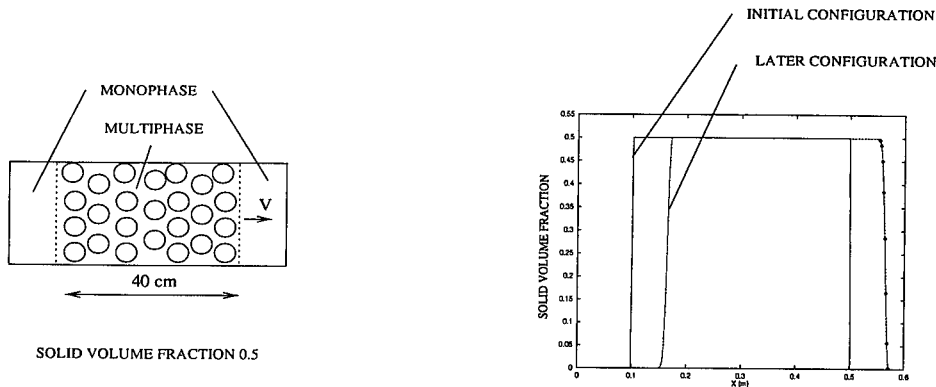


Figure 2 : Interface transport

This figure clearly indicates that the numerical solution is close to the expected analytical solution (initial solution translated). The diffusive character of the numerical method is also tested since a discontinuity in the solid volume fraction is propagated through the solution space.

### 5.2 Hypothetical test

The demonstration is postulated on a charge configuration that has been invented solely for this purpose. The configuration is axisymmetric. Figure 3 shows a schematic of the gun chamber filled with granular propellant. The porosity of the propellant bed is 0.6 and the projectile mass is 0.6 Kg. The charge is ignited at the breech end, near the chamber centerline over a region 2 cm of length and 1 cm in radius during 2 ms of time. Physical characteristics are available from the authors.
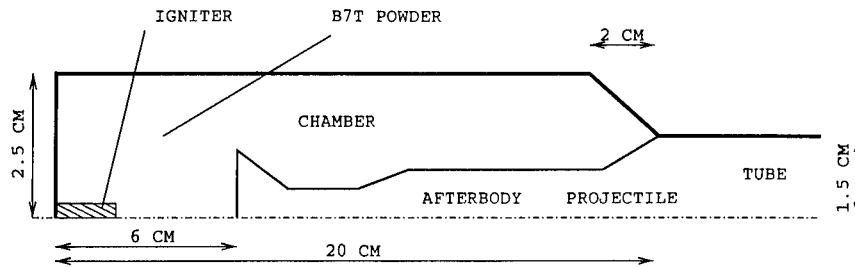
Figure 3 : Schematic of gun configuration

Figure 4 displays the results plotted in pairs - solid volume fraction and gas pressure - at some times.
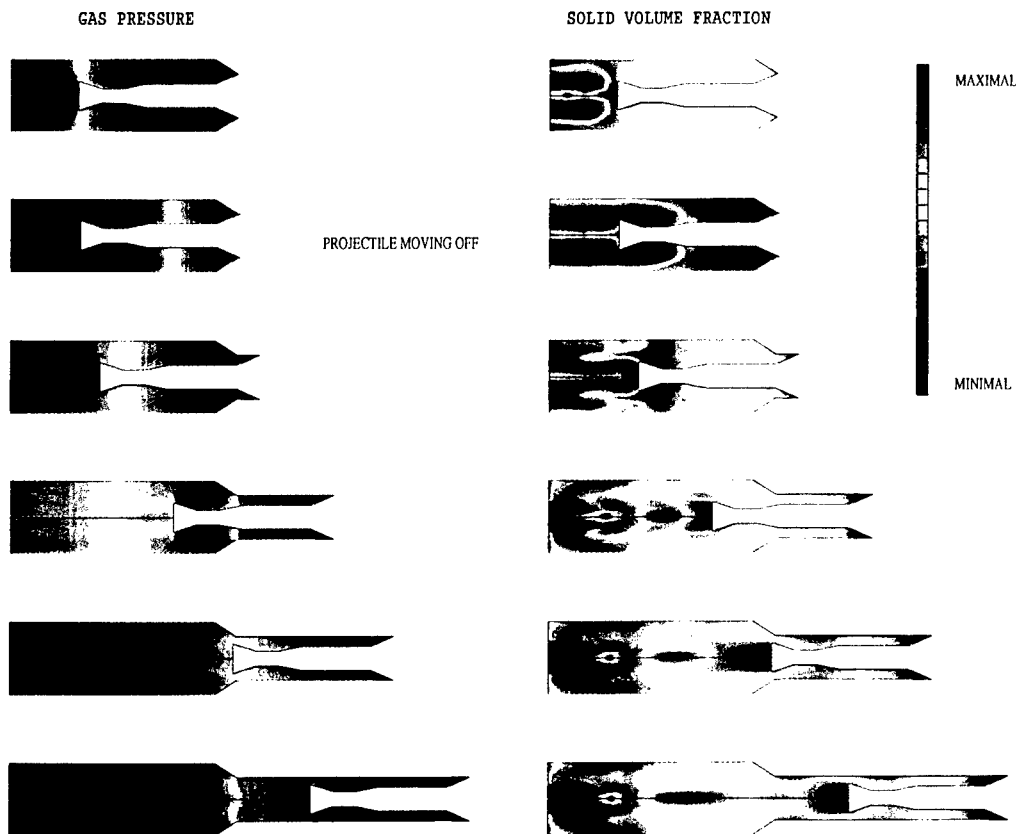


Figure 4 : Computed results

The breech-end igniter starts an ignition wave or flame that begins as a two-dimensional structure and becomes nearly one-dimensional. The projectile starts to move, reducing the projectile base pressure. The entire propellant bed is not of uniform radial porosity although pressure wave structure is one-dimensional. Remarkable fact of this simulation is the monophase zone creating behind the radial shapes of the projectile when this one is accelerating. Propellant grains driving by gases (momentum exchange) is not sufficiently to follow the projectile. Internal boundaries

- 146 -

(multiphase/monophase interface) are automatically captured by the numerical solver avoiding explicit treatment. This possibility offered by the solver is of a great interest.

### 5.3 Opened combustion

Other advantage of this two-phase model is to predict the evolution of a combustion in a granulated reactive material. Thus, MOBIDIC-NG can be utilized for safety problems (DDT problem). In that case, large range of pressure poses theoretical problems for the building of judicious equations of state and JWL equation is often used for the gases.

The following simulation deals with combustion behavior of spherical propellant grains (15 $\mu$m in radius) inside a cylindrical structure half-filled and open on the upper side. Initial ignition occurs on the surface (burning begins inside some cells at atmospheric pressure). Initial solid volume fraction is 0.3. Figure 5 shows the results plotted in pairs - solid volume fraction and gas velocity vector - at certain times.
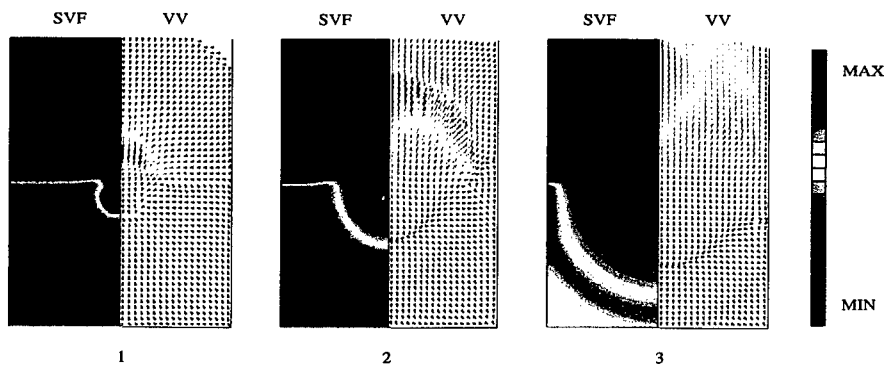


Figure 5 : Computed results (SVF : solid volume fraction VV : velocity vector)

The main difficulty of the problem is to simulate combustion conditions with strong porosity gradients and low-pressure ignition. Numerical results obtained give satisfaction. Compaction wave driven by a spherical flamespreading occurs until it reaches lateral walls. The presence of multiphase/monophase interface implies velocity acceleration of gases toward upper opening. While the results obtained from this simulation are believed to be dependent of input values, the important fact is that these results confirm the potential performances of such code.

### 6. CONCLUSIONS

The development of a next generation interior ballistics code which incorporates multi-phase equations has been described. It can be applied for both interior ballistics and safety problems. Some numerical results presented previously show its performances. Its statement is new and we expect from several experiment/simulation correlations its validation. A part of this validation can be done by the MOBIDIC-NG club users since this code has been delivered to ETBS and next to GIAT Industries.
Objectives as complex geometrical boundaries, stability in presence of strong porosity gradients or discontinuity capturing are reached. Few numerical aspects are under study. The main directions of the development of today's are improvement of the physical models (mechanical behavior, multicomponent mixture ..). As example, agglomerate loads modeling has begun.

### 7. REFERENCES

[1] C. Cuche, M. Derveaux, M. Nicolas, B. Zeller
MOBIDIC : A french Interior Ballistics code based on a two-phase flow model
6 *th* International Symposium on Ballistics - Orlando, October 1981

[2] P.J. Conroy, D.E. Kooker
Implications of propellant rheology
BRL, MD 21005-5066 (approved for public release)

[3] M.R. Baer, J.W. Nunziato
A two-phase mixture theory for the deflagration-to-detonation transition in reactive granular materials
Int. J. Mult. Flow, Vol. 12, N 6, pp. 861-889, 1986

[4] R. Saurel, R. Abgrall
A multiphase Godunov method for compressible multifluid and multiphase flows
J.C.P., N 150, 1999

[5] P. Della Pieta
Comportement mécanique d'un lit de poudre
SNPE report N 21/96/CRB/DFP/TRE/DR 11 Décembre 1996

[6] I. Toumi, A. Kumbaro
An approximate linearized Riemann solver for a two-fluid model
J.C.P., N 124, 1996

[7] M.S. Liou
A Sequel to AUSM : AUSM+
J.C.P. N 129, 1996

[8] P. Della Pieta, B. Briquet, F. Godfroy, J.F. Guery
Couplage fluide/structure et instabilités de fonctionnement
$3^{eme}$ colloque 'Ecoulements internes en propulsion solide', 25-27 Mars 1998, Poitiers

[9] J. Falcovitz, G. Alfandary, G. Hanoch
A two-dimensional conservation laws scheme for compressible flows with moving boundaries
J.C.P. N 138, 1997

## 8. NOMENCLATURE

| | |
|---|---|
| $a$ | subscript, a=g gas, a=s solid |
| $\gamma_a$ | real density of a-phase |
| $\rho_a$ | apparent density ($\rho_a = \phi_a \gamma_a$) |
| $\phi_a$ | volume fraction of a-phase |
| $p_a$ | pressure $p_a = p_a(\gamma_a, e_a)$ |
| $\vec{V}_a$ | velocity |
| $c_a$ | speed of sound of a-phase |
| $M_a$ | Mach number of a-phase |
| $T_a$ | temperature of a-phase |
| $e_a$ | internal energy of a-phase |
| $E_a$ | total energy : $E_a = e_a + \vec{V}_a^2/2$ |
| $H_a$ | total enthalpy : $H_a = E_a + p_a/\gamma_a$ |
| $S_a$ | specific entropy of a-phase |
| $\delta$ | drag coefficient |
| $\vec{D}$ | drag force $\vec{D} = \delta(\vec{V}_s - \vec{V}_g)$ |
| $Q$ | convective energy transfer |
| $\beta_s$ | intergranular pressure |
| $\mu_c$ | compaction viscosity |
| $\mathcal{S}$ | surface grain |
| $\vartheta$ | volume grain |
| $r$ | burn rate |
| $n_s$ | number density |

# Erosion Study in Small Calibre Gun Barrels

SPATZ P., KARAMETAXAS G., HUG C.

Swiss Ammunition Enterprise Corp., Allmendstrasse 74, CH-3602 Thun, SWITZERLAND

**Abstract :** For small calibre ammunition, the use of non-toxic primers, i.e. without heavy metals like barium, lead and mercury, causes serious deposition of common projectile jacket material CuZn10 on the gun barrel. The deposition is observed in a narrow region of few centimetres width, roughly at half length of the barrel. The CuZn10-deposition can be removed only by extended and unusual cleaning procedures.

This study investigated the pronounced local character of the deposition zone in the small calibre gun barrel. We found that there is a strong correlation between the region of the obstinate CuZn10 deposition and the local erosion behaviour. By means of microscope analysis, a length dependent erosion profile for the small gun barrel could be determined. Cross sections of the barrel at different positions were analysed to quantify and qualify radial tears and material outbreaks. The resulting barrel-length dependent density of damages represents the erosion profile. Its maximum corresponds clearly with the region of obstinate deposition. Nevertheless, the erosion profile seems to be independent from the involved ammunition components (primer, propellant, projectile), but it is strongly dependent from the round number applied to the barrel.

## 1. Introduction

To reduce the toxicity of small calibre ammunition we are developing primers without contents of heavy metal components like barium, lead, antimony, etc. The present investigation concernes the swiss ordnance ammunition GP90 (5.6mm or .223) with CuZn10 projectile jacket material. The test barrels are made from stainless steel of the type 14NiCr14. Ammunition consisting a non-toxic primer, conventional propellant and CuZn10 projectile jacket material often showed serious CuZn10 deposition with increasing number of rounds. After a few hundred rounds, the deposited material could not be removed sufficiently with normal cleaning procedure, i.e. less than 0.5 double-strokes per round; it exceeded 1 double-stroke per round. The initial calibre of the tested barrels is 5.56mm and localy diminished

about 20μm after 1500 rounds. The CuZn10 deposition is observed in a relatively narrow region of few centimetres width, roughly at half length of the barrel, whereas with standard ammunition we do not observe an appriciable diminution of the calibre even after applying 7500 rounds.

This study investigates the above described local characteristics of the deposition zone in the small calibre barrel (see figure 1). It is assumed that the local behaviour of the mentioned deposition is related to local erosion phenomena at the inner wall of the gun barrel. The interaction of some elemental components of the non-toxic primer at the eroded surface of 14NiCr14-steel can influence the adhesive behaviour of CuZn10. The erosion results from ambient temperature and pressure conditions as well as from mechanical stresses due to barrel oscillation during the ammunition firing. The erosion features are assigned by radial tears and material outbreaks (see figure 3).

To get a better unterstanding of the correlation between the erosion and the deposition phenomena in the small calibre gun barrel, the following experiments have been carried out: 1) Applying different ammunition components (primers and projectile jacket material) in separate barrels while going up to a fixed number of rounds. Such a proceeding gives us information about the correlation between ammunition components, erosion and deposition of jacket material. 2) Influence of round number by applying the same ammunition configuration to get information about erosion, deposition and the number of rounds. 3) Effects on shooting in the presence of obstinate jacket material deposition when going to high number of rounds. The aim of this third part is to find out, if there are consequences on the accuracy performance and safety aspects. A overview of the experimental set ups are listed in table 1.

Tabel 1:  Overview of the experimental set ups. The standard primer contents heavy metals like barium, lead, antimony, etc.

| Exp.-Nr | Primer | Procectile Jacket | Round Number | Description |
|---|---|---|---|---|
| V01 | Standard (SM) | CuZn10 | 1500 | Influence of primer and projectile jacket material on the development of obstinate deposition by applying a constant number of rounds |
| V02 | Non-toxic Var A | CuZn10 | 1500 | |
| V03 | Non-toxic Var B | CuZn10 | 1500 | |
| V04 | Non-toxic Var B | Sn-covered | 1500 | |
| V05 | | | 0 | Influence of round number on the development of obstinate deposition by applying the same primer and projectile jacket material |
| V06 | Standard (SM) | CuZn10 | 750 | |
| V07 | Standard (SM) | CuZn10 | 1500 | |
| V08 | Standard (SM) | CuZn10 | 3000 | |
| V09 | Non-toxic Var B | CuZn10 | 7500 | Influence of obstinate deposition on accuracy and safty |

Figure 1:   Scematic representation of the local calibre diminution for different experimental setups



V01, 1500 rounds, Standard

V02, 1500 rounds, Non-toxic, Var A

V03, 1500 rounds, Non-toxic, Var B

V04, 1500 rounds, Non-toxic, Var B

V09, 7500 rounds, Non-toxic, Var B

Calibre < 5.535mm
( minimum 5 $\mu$ m)
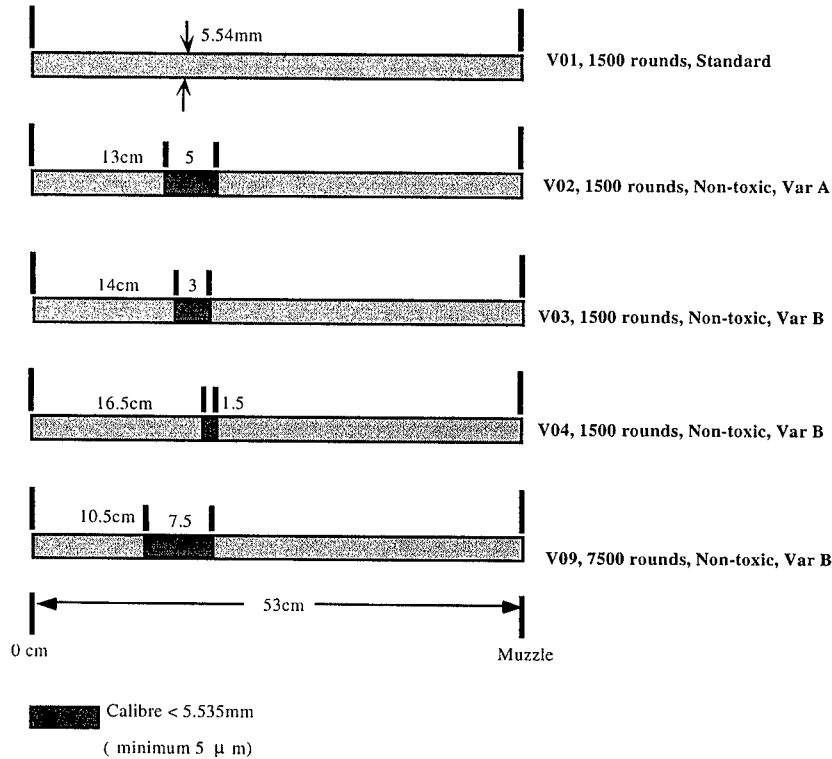
## 2. Experimental

For each experimental configuration (see table 1) we use a new gun barrel of 14NiCr14-steel, which is hardened (nitrated) at the surface. All barrels are issued from the same manufacturing lot.

With each barrel, the number of rounds is continously increased with the ammunition configuration described above. After steps of 100 rounds we apply a soft inside-cleaning of the barrel to remove the burned propellant particles and the slight fouling but not the deposited projectile jacket material. After having reached the final round number (see table 1), the calibre is determined over the barrel length by using special measuring tools. Now, the barrels are cleaned properly to determine the number of double-strokes for reaching calibre values larger than 5.535mm.

For qualitative and quantitative characterisation of the erosion behaviour, the gun barrels are divided into two parts allong the barrel axes. One of the barrel half is radially cutted into several parts of 2cm length (see figure 2). For the following metallographical investigation, the individual parts has been polished with SiC-paper and diamond-paste and afterwards embeded into epoxy resin.

Figur 2:   Cross section of a polished barrel part of 2cm.
Further analysis are done only on the lands of the barrel

Cross section of 2cm barrel parts



Spin direction of the projectile
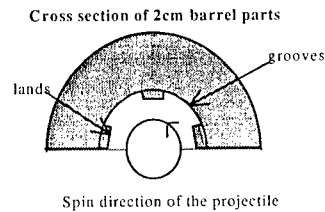
The microscope analysis has been done with a Nikkon microscope (magnification of 400) equiped with a CCD-camera. An image processing has been performed with the software LUCIA M from Laboratory Imaging Ltd. The erosion characterised by radial tears and material outbrakes (see figure 3) can be measured by means of binary image processing. We restrict our erosion analysis to the barrel lands. As resulting values we get the number of tears/barrel land and the damaged area/barrel land for each 2cm-part. This procedure results in a representative curve of erosion behaviour over the barrel length. The measured points at every 2cm are fitted with a polynomial function to get a continous curve.

Figure 3:  Distinction between a) tears and b) material outbreaks
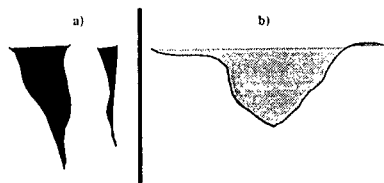
Figur 5: Example for image processing analysis. White areas represent the detected erosion damages like tears and material outbreakes. The number of damages and its area is quantified by the binary image processing.
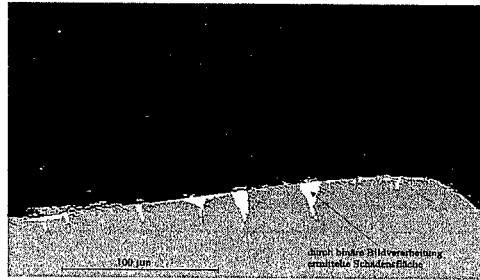


## 3. Results

The experimantal configurations V01-V04 with different ammunition components (primers and projectile jacket material) result in very similar erosion profiles (see figure 6). Near the burning chamber, there is a first maximum of damages follwed by a second one in the zone of 15 cm. This is exactly the same region where the obstinate deposition of CuZn10 is observed. In the case of applying Sn-covered projectiles, the corresponding maximum in the erosion profile is shifted about 5 cm towards the muzzle. Nevertheless, the erosion behaviour seems to be similar for all configurations. From this results, the following conclusion can be made: the length dependent erosion profile is not directely influenced by the applied ammunition configuration (this conclusion must be restricted to the investigated samples).

Figure 6: Erosion profiles for various ammunition configurations by applying a constant number of rounds
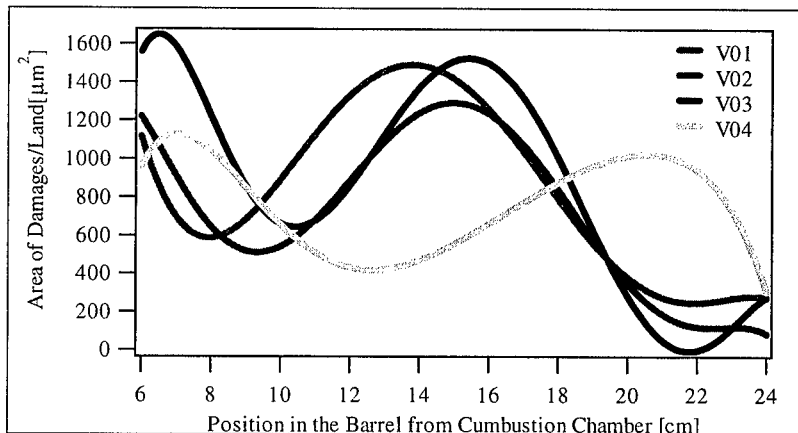
The results from the experimental setups V05-V08 show clearly, that the erosion profile is strongly dependent from the number of rounds applied to the barrel. The comparison of results shown in figure 6 and figure 7 indicates only a weak dependence of the erosion behaviour and the involved ammunition components. However, the observed zone of obstinate deposition of CuZn10 by using a non-toxic primer coincides localy with a maximum peak in the erosion profile (see also figure 1).

Figur 7: Erosion profiles for a given ammunition configuration by applying increasing numbers of rounds
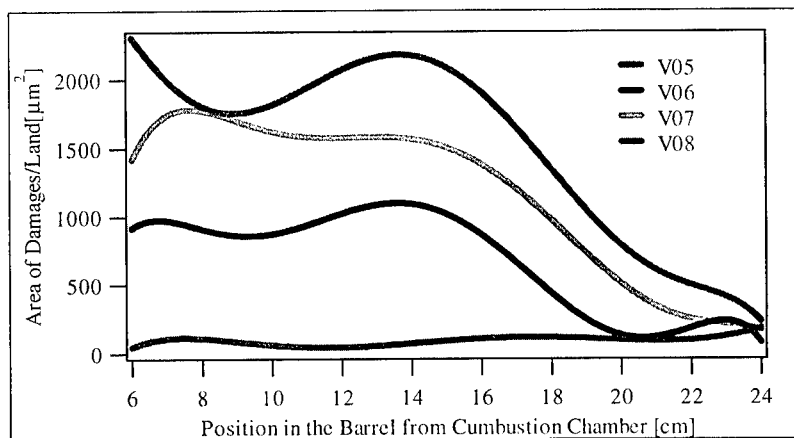


Figur 8 shows the correlation between the total damaged area per barrel land and the number of individual damages (tears and material outbreakes) per lands. Up to a critical point, the damaged area increases linearly with the density of damages. After the critical point, the creation of new damages is reduced. But, existing tears and outbreakes are progressively enlarged.

The $CuZn_{10}$-deposition of projectile jacket material on the gun barrel results in a succesive local diminution of the calibre. Nevertheless, this diminution does not have consequences on the accuracy performance, even at high numbers of rounds. In addition, barrel safty has been checked and proven as to be ensured despite the calibre diminution.

Figur 8: Representation of the erosion mechanisme in the small calibre gun barrel
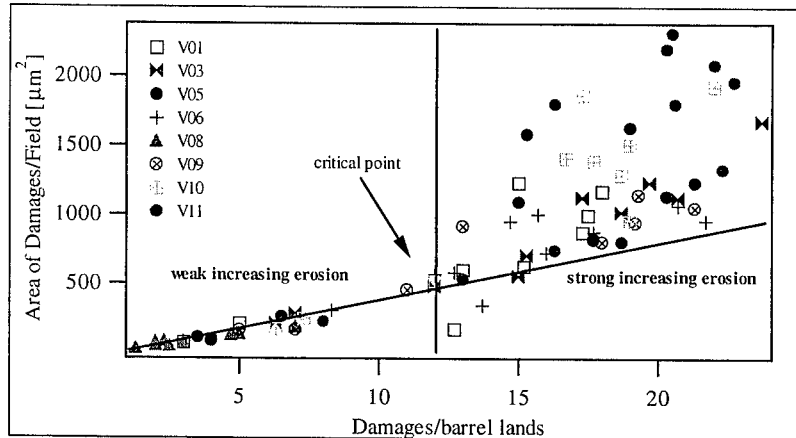


## 4. Conclusion

It seems that the erosion mechanisme is not strongly influenced through the involved ammunition configurations (primer components and projectile jacket material). On the other hand, the obstinate deposition of CuZn10 is only observed when using non-toxic primers and is localized in the same region, where erosion profile has its maximum. Consequently, some elemental parts in non-toxic primers react or interact with the eroded barrel material (14NiCr14- steel) in a manner, that CuZn10 has a high adhesive capacity or build a surface alloy with the steel ground material.

# AN INVESTIGATION OF INACCURACIES IN GRAIN SHAPE ON THE DERIVATION OF PROPELLANT BURN RATE DATA FROM CLOSED VESSEL TESTS.

## POCOCK M D, GUYOTT, C C.

Frazer-Nash Consultancy Ltd, Stonebridge House, Dorking Business Park, Dorking, Surrey, RH4 1HJ, UK.     info@fnc.co.uk     www.fnc.co.uk

**Abstract**: Potential sources of error in internal ballistics modelling are investigated. Specifically the errors investigated arise from an inadequate modelling of the variation in propellant grain surface area as the propellant burns. It is shown that for grain geometries where 'slivering' takes place, simple form functions cannot accurately represent the variation in surface area. This can lead to inaccuracies in the determination of burn law coefficients, and is compared to the use of accurate surface area algorithms, such as those encoded within the FNGUN software. Realistic propellant grains will exhibit discrepancies from the designed geometry. Careful modelling of these slight discrepancies is shown to provide more realistic results from an internal ballistics simulation of a gun system than the usual assumption of "perfect" grains.

## 1   INTRODUCTION

Standard methods for the experimental determination of ballistics properties of propellants have been developed over a number of years [1, 2, 3]. When determining ballistic properties, and indeed when modelling any internal ballistics, an accurate knowledge of the actual propellant grain geometry is as important as knowledge of its chemical properties. In particular, the relationship between depth of propellant burnt (regression distance, $e$) and the surface area ($S$) is fundamental in setting up internal ballistics models. This paper describes two potential sources of error in internal ballistics modelling that are due to the propellant geometry. These are:

- The use of simple form functions in estimating the surface-regression curves of complex grain geometries, especially those which exhibit slivering
- The use of idealised, "perfect" grain geometries instead of more realistic geometries, which exhibit slight discrepancies from the designed dimensions

Both of these sources of error can potentially affect the determination of the burn rate parameters from a closed vessel test, and directly affect the modelling of a gun system.

This paper describes the errors introduced into the determination of the burn rate parameters through the inappropriate use of simple form functions, and demonstrates the direct affect of non-ideal grain geometry on the modelling of a 155mm gun system.

## 2 FORM FUNCTION APPROXIMATION OF THE GRAIN GEOMETRY

This section illustrates potential problems arising from use of a form function for grains that exhibit complex surface-regression curves. The specific example used is a seven-hole multi-tube propellant referred to as 'RDBS', for which the experimental closed vessel data has been obtained from BAe Royal Ordnance, UK [4].

Form functions are often used within internal ballistics calculations to approximate the variation in surface area as the grain burns. The form function relates the mass fraction burnt, $z$, to the fraction, $f$, of the ballistic size remaining:

(1) $$z = (1 - f)(1 + \theta f)$$

The ballistic size, $D$, is taken here are twice the regression distance to all burnt, $\hat{e}$. $D$ is equal to the web thickness for most grain geometries, such as slotted tube and stick. For seven-hole multi-tube the ballistic size is usually taken to be 1.15 times the web thickness to account for the effects of slivering [6].

The form function constant, $\theta$, will be positive for a grain whose surface area decreases with burning and negative when the surface area increases. The actual value can be determined from the grain geometry. For a seven-hole multi-tube, $\theta = -0.17$ [6].

Using (1) and the appropriate constants, the form function representation of the surface area to regression distance curve can be determined. This is plotted in Figure 1, along with an accurate determination of the grain surface area. The accurate determination of surface area is calculated precisely from the grain geometry, and fully accounts for the effects of slivering. Such accurate algorithms are coded within the FNGUN software [5], and it is one of those that is plotted in Figure 1.
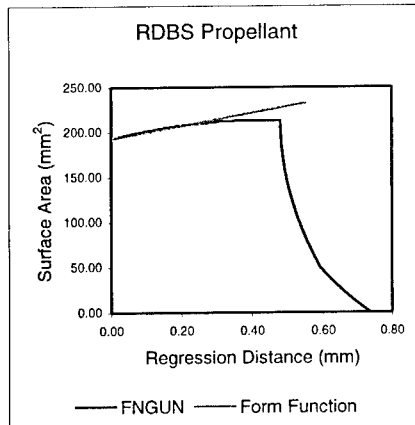


Figure 1.    Surface area calculated by two methods plotted against regression distance, for a 7 hole multi-tube

Figure 1 demonstrates that the form function only provides a good representation of surface area only for the first half of the regression distance. After this, and certainly after the onset of slivering, the form function representation is significantly in error.

## 2.1 Effect of form function approximations on the calculation of burn law coefficients

The burn rate of a propellant, r, is the rate of reduction in size of the propellant with time. This burn rate varies with pressure, p, and this variation is usually approximated by the burn law:

(2)
$$r = \beta p^{\alpha}$$

In [7] a method for the calculation of the coefficients, $\alpha$ and $\beta$, of the burn law is fully described. In essence, the burn rate is written as the product of three derivatives, Equation (3), each of which can be determined from either numerical algorithms or experimental data obtained from closed vessel testing.

(3)
$$r = \frac{de}{dt} = \frac{de}{dz} \bullet \frac{dz}{dp} \bullet \frac{dp}{dt}$$

Here the burn rate is defined as *de/dt*: the change in the thickness of the layer of burnt propellant (regression distance), e, with time, t. The fraction of propellant burnt (by mass) is represented by z.

The second and third terms of (3) are obtained from the Nobel-Able equation and from closed vessel testing respectively. Of interest here is the first term (*de/dz*), which represents the change in regression distance with fraction burnt.

Often, the term (*de/dz*) is calculated using form functions. This provides adequate results for simple grains, such as spheres, cylinders and tubes, but as indicated in the previous section, form functions can not adequately model complex grain geometries.

Once all three terms of (3) are calculated or measured the burn rate can be calculated over a range of pressures, p. Equation (2) can be curve-fitted to this data and the coefficients $\alpha$ and $\beta$ determined: if the values of log(r) are plotted against log(p), the gradient of the best-fit straight line will give $\alpha$ and antilog($\beta$) will be the intercept point.

| RDBS Propellant | FNGUN | Form Function |
|---|---|---|
| $\alpha$ (–) | 0.67 | 0.61 |
| $\beta$ (mm s$^{-1}$ MPa$^{-\alpha}$) | 3.64 | 4.86 |

Table 1: Calculated $\alpha$ and $\beta$ using both a form function and FNGUN to determine (*de/dz*)

Table 1 shows the values of $\alpha$ and $\beta$ calculated for the 7-hole multi-tube RDBS propellant [4] using a form function and an accurate algorithm to calculate the (*de/dz*) term. It can be seen that there are significant differences between the two sets of coefficients.

In order to assess the accuracy of the FNGUN derived prediction of $\alpha$ and $\beta$ values, a model of the closed vessel experiment [4] was made. The pressure-time curve obtained from the model (using the FNGUN predicted $\alpha$ and $\beta$ values) can be compared with the actual closed vessel experimental measurements. Figure 2 shows that excellent agreement is achieved between the experimental pressure time curves and those calculated with FNGUN.

To demonstrate the effects on predicted gun performance of the variations in $\alpha$ and $\beta$ shown in Table 1, a model of a typical 120mm gun system was used. Two calculations were made, the only difference being the values of $\alpha$ and $\beta$ used for the main (7-hole multi-tube)

propellant. The pressure-time curves obtained are shown in Figure 3. It can be seen that the FNGUN and form-function derived $\alpha$ and $\beta$ values give rise to graphs of different shape, with a 4% difference in peak pressure.
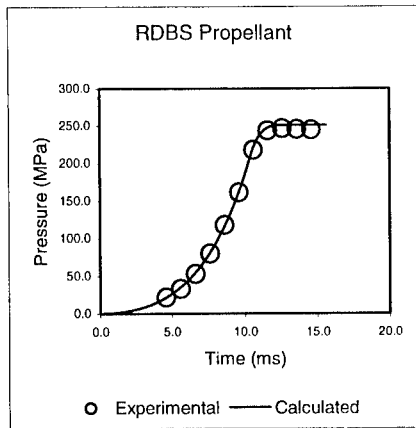


Figure 2.    Closed vessel pressure-time curves - experiment and FNGUN
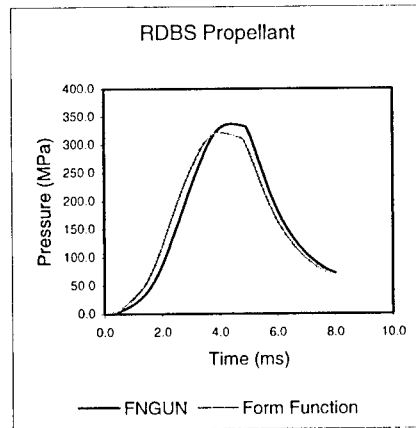
Figure 3.    Calculated pressure-time curves of a typical gun system using values of $\alpha$ and $\beta$ from Table 1

## 3    NON-IDEAL PROPELLANT GRAINS

Real propellant grains will be subject to manufacturing tolerances, and therefore tend not to have the assumed or ideal designed geometry. Some possible imperfections which may occur in actual grains are as follows:

- spherical grains may not be truly spherical
- tubular grains may not have cylindrical holes or a cylindrical outer surface, the hole may be offset, and slots may be tapered, and intersect non-symmetrically with the hole
- cross propellants may have tapered fins, and these may be of different thicknesses

It should be noted that the above discrepancies from ideal geometry may change throughout the length of a propellant grain.

Any of the above discrepancies will affect the relation between surface area and regression distance. An ideal cross or tube propellant will have constant surface area until the grain is completely burn out. Whilst a non-ideal tubular grain may initially have a constant surface area as the regression distance increases the surface area will tend to reduce gradually thus giving a more gradual burn out. Figure 6 illustrates the differences in rate of change of surface area for ideal and non-ideal tubular grains.

The following section determines the surface-regression curve for a grain where the inner hole is offset, but in other respects the grain is perfect. In section 3.2, the ideal and eccentric surface-regression curves are used within an internal ballistics model of a 155mm gun system, and the pressure time curves compared.

## 3.1 Tube with eccentric hole

This section considers a long tubular grain with an eccentric hole. These are typical of the imperfections found in practice, and illustrate the difference in regression distance and the surface area characteristics that are obtained with slight geometrical errors. Such a grain is shown on the left in Figure 4. This grain geometry can be characterised by inner and outer radii ($R_I$ and $R_O$), and an eccentricity ($C$).

During the initial phase of burning, this grain will perform a like an ideal grain, with the surface area remaining constant. Eventually, the inner and outer surfaces will coincide at one point, as is shown in the centre of Figure 4. This is referred to as 'burn-through', and it will occur when $2e = R_O - R_I - C$, ($e$ being the regression distance).

After burn-through the cross-sectional area of the grain will take on a crescent shape, as is shown in the right of Figure 4. The surface area will decrease, and reach zero at 'all-burnt', when $2e = R_O - R_I + C$.
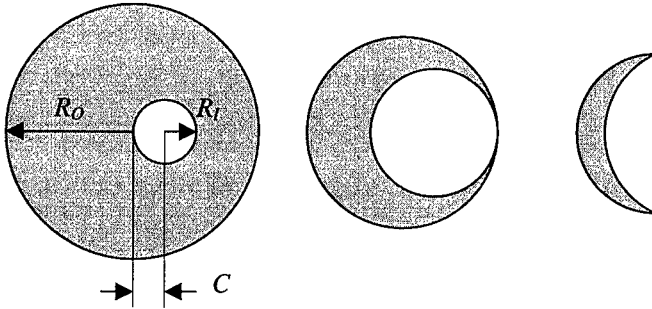


Figure 4.    From left to right: grain shape before igition; at burn-through; after burn-through
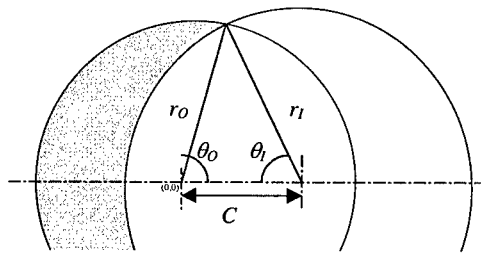


Figure 5.    Calculation of eccentric grain surface area

The surface area of the grain after burn-through can be calculated from the cylindrical area and the end area. Figure 5 shows the geometry used to calculate these areas. The cylindrical area (i.e. when excluding the ends) is obtained from the instantaneous length ($l = L - 2e$) and the perimeter of the cross-section, $p$

$$(4) \qquad p = 2r_o \left[ \pi - \cos^{-1}\left( \frac{C^2 + r_o^2 - r_I^2}{2Cr_o} \right) \right] + 2r_I \cos^{-1}\left( \frac{C^2 + r_I^2 - r_o^2}{2Cr_I} \right)$$

Here $r_O$ and $r_I$ are the instantaneous values of outer and inner radii as shown in Figure 5, and $L$ is the initial grain length. The end area of the grain can be calculated from the integral

- 161 -

$$(5) \qquad a_E = \int\limits_{x=-r_o}^{x=C-r_I} \sqrt{r_o^2 - x^2}\,dx + \int\limits_{x=C-r_I}^{x=r_o\cos\theta_0} \sqrt{r_o^2 - x^2} - \sqrt{r_I^2 - (x-C)^2}\,dx$$

The FNGUN software incorporates algorithms that calculate the end area of a grain from a given variation in perimeter with regression distance.

In Figure 6, three surface regression curves are shown. These are for an ideal concentric grain (i.e. $C = 0$); for a 6% eccentric grain, with the end effects ignored (i.e. using only equation 1); and for the FNGUN representation of the 6% eccentric grain (taking account of cylindrical and end surface areas). The actual parameters and a true representation of the grain cross-sectional area are shown in Table 2.

The variation of the surface regression curve with eccentricity is shown in Figure 7, using 6%, 12% and 25% eccentric grains (note that end effects are ignored for clarity). A 25% eccentricity corresponds to an offset of approximately 1mm for the grain geometry shown in Table 2.

| | |
|---|---|
| $R_O$ | 4.15 mm |
| $R_I$ | 1.75 mm |
| $C$ | 0.25 mm |
| $L$ | 823.0 mm |
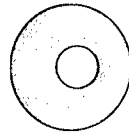
Table 2: Grain parameters and the true proportions of a 6% eccentric grain.
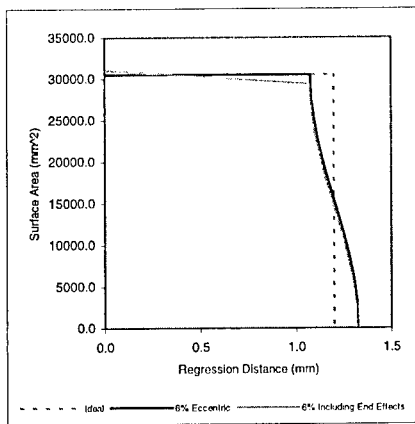


Figure 6. Regression-surface curves for the eccentric grain geometry of Table 2
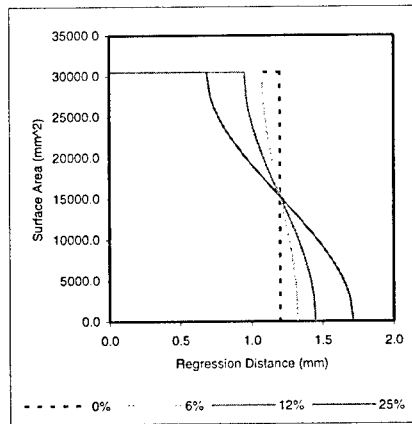
Figure 7. Regression-surface curves for three eccentric grain geometries

## 3.2 Effect of eccentricity on internal ballistics predictions

The eccentric grain geometry described above in Figure 6, has been used within an internal ballistics simulation of a 155mm gun system, and compared with the ideal grain geometry. Figure 8 show the pressure time curves (at the breech) for simulations using the ideal and eccentric grain geometry.

In the case of a perfect (concentric) grain geometry it can be seen that there is a noticeable change in slope of the pressure time curve at the point of all-burnt (at approximately 16ms). This is due to the sudden halt in gas generation that occurs with tubular grain geometries. Figure 8 also shows that this anomalous kink in the pressure time curve is visibly reduced if it is assumed that the hole is offset by 6%. This is due to the gradual burn-out of the eccentric grain, as shown in Figure 6.
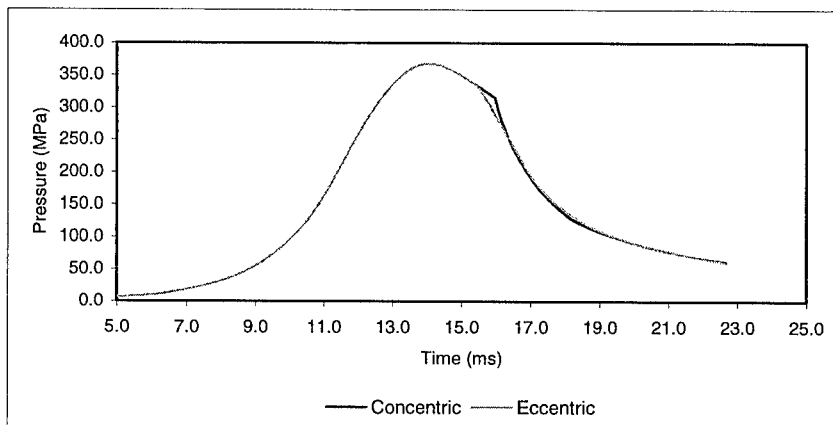


Figure 8.    Pressure-time curves for 155mm gun system using eccentric and concentric grain geometries

## 4    CONCLUSION

The variation in propellant grain geometry as the grain burns is known to be an important factor in internal ballistics modelling, however significant differences between actual and assumed variation in surface area with regression distance have been shown in this paper. These differences in the modelling of the surface regression relationship can affect both the calculation of burn law coefficients and the modelling of entire internal ballistics systems.

It has been shown here that while form functions may adequately describe the variation in surface area with fraction burnt for simple grain geometries, these functions are unable to accurately model complex geometries such as multi-tube. Such a discrepancy between actual and assumed variation in propellant grain geometry was then used to demonstrate the possible errors in deriving burn rate coefficients.

The variation in surface area with regression distance of slightly imperfect grains has been shown to be different to that of ideal grains. In this paper the effect of an offset hole on the surface area variation, regression distance relationship of a tubular propellant has been investigated. By employing a model of more realistic grain geometry, the pressure-time curves obtained have more closely resembled experimentally measured results. Thus the ability to model non-ideal grains, and indeed grains of arbitrary shape, has been shown to be beneficial.

## 5    ACKNOWLEDGEMENTS

# 6 REFERENCES

1. 'Definition and Determination of Ballistic Properties of Gun Propellants', STANAG No. 4115 Edition 2, June 1997.

2. 'Closed Vessel Ballistic Assessment of Gun Propellant', Def Stan 13-191/1, December 1996.

3. 'Application of Closed Vessel Techniques for the Evaluation of Burning Rates of Propellants at Low Pressures', Defence Science Journal, April 1977.

4. 'Closed Vessel Information for FNGUN Paper', private communication between C. Mackenzie, BAe Royal Ordnance and M. Pocock, Frazer-Nash Consultancy Ltd, 21 December 1998.

5. 'FNGUN User Manual', Frazer-Nash Consultancy Ltd, Dorking, UK, 1996.

6. 'Textbook of Ballistics and Gunnery', Volume 1, HMSO, 1987.

7. M. Pocock, C. Guyott, 'An Alternative Method For The Derivation Of Propellant Burn Rate Data From Closed Vessel Tests', in Proceedings of the 18th International Symposium and Exhibition on Ballistics, San Antonio, Texas, p270-276 (1999).

Launch Dynamics

# ISL STUDIES ON ELECTROMAGNETIC RAILGUNS

## P. LEHMANN, H. PETER

French-German Research Institute of Saint-Louis
5 rue du Général Cassagnou
F68301 SAINT LOUIS

**Abstract** : The French-German Research Institute of Saint-Louis (ISL) is involved in research on electromagnetic (EM) propulsion for high-velocity applications.

Railguns are well-known for their capability to reach very high velocities ($v_0 > 2000$ m/s) with overall efficiencies ($E_{kinetic}/E_{electric}$) over 30%. Therefore, they are adequate for anti-armor applications in which impact velocities ranging between 2300 m/s for RHA targets and 3400 m/s for reactive targets are required.

The research efforts have been concentrated on the phenomena occurring in the rails-projectile sliding contact. The work in progress deals with the study of projectiles equipped with metallic fiber-brush armatures allowing a good electrical contact without arcing up to velocities of 2000 m/s with a peak current of about 700 kA.

A novel 10 MJ DES railgun with 12 stages and a 50-mm round bore has been built at ISL. The power supply consists of 200 PFN-LCR units of 50 kJ each, equipped with semiconductor switches. The 6-m-long launcher tube is made of both wound glass-fiber- and wound carbon-fiber-reinforced plastic. The launcher has proved to have an overall efficiency of about 30%. Velocities of 2300 m/s have been achieved with projectile masses ranging from 350 g to 650 g.

## 1. INTRODUCTION

ISL has been studying rail launcher technology since 1987. The principle of the railgun is well-known (Figure 1): between two rails, made of e.g. copper, the projectile, equipped with a conducting armature, is accelerated by the Lorentz force F resulting from the interaction between the current I and the magnetic field B:

$$F = \tfrac{1}{2}L'I^2$$

where L' represents the inductance per unit of length of the rails.
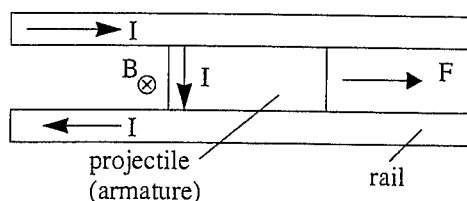


Figure 1: Principle of the railgun

For anti-armor applications, ISL has demonstrated the optimal impact velocity. A given depth of penetration can be reached with a minimum kinetic energy for all the targets (homogeneous, composite, structured or reactive) [1]. This optimal impact velocity is always greater than 2300 m/s for a heavy-alloy penetrator with L/D = 30. For these velocities the electromagnetic rail launchers may have overall efficiencies (kinetic energy/stored electrical energy) over 35% whereas classical powder guns have efficiencies about 20%. Several MA are necessary to accelerate projectiles with a mass of a few kg up to 2500 m/s after 6 m [2].

For the anti-air mission with unguided projectiles, ISL has demonstrated in former studies [3] the high hit probability of bursts of small heavy-alloy long-rod penetrators fired at hypervelocities (v $\cong$ 3000 m/s) at helicopters, aircraft or missiles flying at distances ranging from 1000 m to 3000 m. We have shown [4, 5] that it is more efficient to fire these small penetrators in a single cargo-projectile containing 50 long-rod penetrators. As for the anti-tank application, several MA are necessary to accelerate the cargo-projectile up to 3000 m/s after 4 m.

The main issues of the railguns are the following ones:
- the sliding electrical contact, between rails and armature, is submitted to high current (MA) and high velocity (> 2000 m/s);
- the barrels containing the rails have to sustain the forces separating the rails;
- the energy storage must be small (high electrical energy densities).

To study these issues, ISL mainly uses two railgun facilities:
- EMA3 with an electric storage of 500 kJ to 1 MJ and a 15x15 mm square bore. This facility allows to study the different rail and armature materials and to accelerate projectiles with a mass of about 50 g up to 2000 m/s;
- PEGASUS with an electric storage up to 10 MJ supplying a medium-caliber (30 to 50 mm) round or square bore launcher. The facility has been built to accelerate projectiles of 1 kg up to 2600 m/s or projectiles of 500 g up to 3400 m/s.

## 2. PULSE FORMING NETWORK FOR ELECTRIC RAILGUNS

For military applications, the electrical energy to be stored for one shot reaches 9 MJ to 45 MJ, assuming an overall efficiency of 33%. The power to be delivered to the railgun increases from 2 GW to 10 GW or more for a mean travel duration of the projectile in the barrel of about 5 ms.

Today only a few storage component types are able to deliver simultaneously the aforementioned required energy and pulsed power:
- fast discharge capacitors which need to be connected to a closing switch and a pulse forming inductance, in order to obtain the appropriate pulse shape,
- coils working at normal temperature, connected to the charge by means of an opening switch.

Among these possibilities, ISL has decided to use capacitor banks and has developed a modular Pulse Forming Network (PFN) for the electric railguns which consists of 200 LCR-Pulse Forming Units (PFU) characterized by an energy of 50 kJ each.

One Pulse Forming Unit (PFU) (Figure 2) consists of a 50-kJ capacitor (energy density 600 J/l), a thyristor (ISL/ABB CSF 672-11000) used as main switch, a semiconducting crowbar diode (ISL/ABB DSA 1508-12000), a pulse forming inductor (L = 28 μH) and a flexible coaxial cable which connects the PFU to the railgun. The 11 to 12 kV blocking voltage semiconductor switch-

es have been developed by ISL in cooperation with the ABB Semiconductor Company [6]. Each PFU is equipped with its own safety circuit and can be triggered separately from the other units.
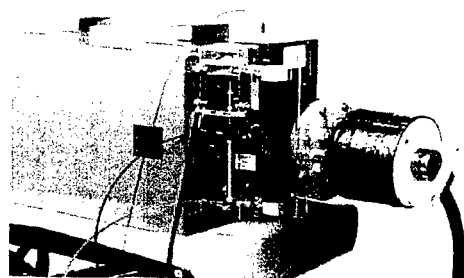


Figure 2: PFU of 50 kJ and switching devices of the energy storage system for railguns

After the main switch S1 has been closed (Figure 3), the capacitor begins to discharge into the coil and the load consisting of the railgun and the projectile. When the voltage across the capacitor becomes negative, the current flows through the diode: the capacitor is nearly short-circuited and the electrostatic energy has been transferred mainly to the coil. The equivalent electric circuit and the resulting current waveform flowing through the projectile are shown in Figure 3.
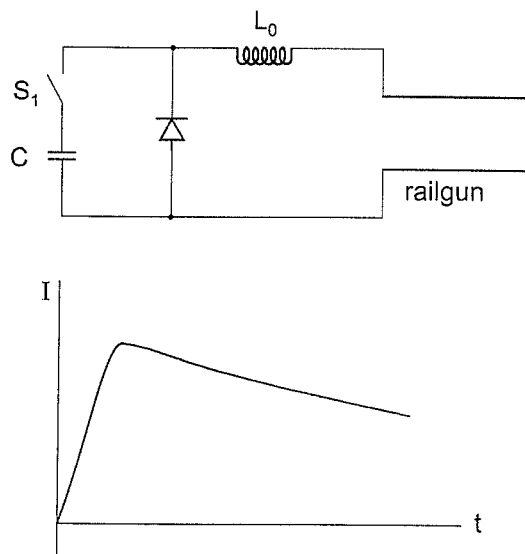


Figure 3: Capacitive pulse forming unit connected to a railgun and typical current waveform feeding the gun

The main advantages of a modular energy supply are:
• a high security standard: each PFU is disconnected from the other,
• a good reliability,
• a high flexibility: an arbitrary total current pulse can be formed by choosing the triggering instant for each PFU,
• an enhanced overall efficiency of the railgun,
• the possibility of using semiconductor switches as the current for each module is limited to 50 kA (this avoids the parallel connecting of thyristors).
Each PFU has a charging voltage of 10.75 kV and can deliver a peak current of about 50 kA.

During the motion of the projectile between the rails, the volume between the breech end and

the rear side of the projectile is growing and has to be filled up with magnetic energy. To enhance the efficiency of the railgun system it is better to use the DES (Distribution Energy Storage), which consists in the distribution of the energy along the rails, such as in the PEGASUS facility. Typical current waveforms calculated with the lumped parameter code ISLAM developed at ISL [7] for a DES feeding a railgun are shown in Figure 4.
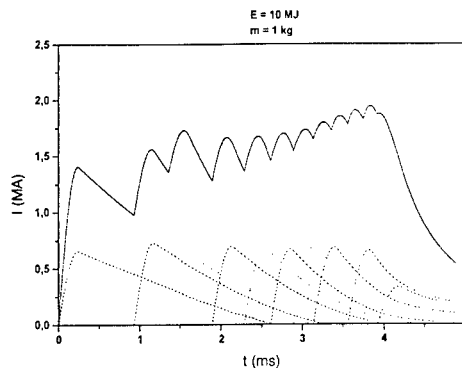


Figure 4: Variation of the calculated total current (solid line) resulting from the sum of the single calculated currents (dashed and dotted lines) as a function of time for a DES railgun

## 3. ELECTRICAL SLIDING CONTACTS IN RAILGUNS

The moving electrical contact between rails and projectile has to bear a current of hundreds of kA to several MA during a few ms. The projectiles used in the ISL railguns are equipped with metallic fiber brushes made e.g. of thin Cu-Cd fibers (diameter = 40 $\mu$m). Figure 5 shows a typical projectile equipped with fiber brushes used in the EMA3 facility. The body is made of Glass-fiber-Reinforced Plastic (GRP) which is an insulating material.



Figure 5: Photograph of a GRP projectile equipped with copper brushes and a penetrator

This kind of projectile can be accelerated with currents reaching 700 kA up to 2000 m/s without any arcing at the rails-projectile interface [8]. Above these current and velocity values, plasma arcs occur.

A flash radiograph of the projectile at the muzzle of the EMA3 railgun (Figure 6) shows the behaviour of the copper brushes. After the fusion and vaporization of the part of the rear brush in contact with the rails, the current goes forward to the next brush. During the acceleration of the projectile, the brushes are straightened and pushed against the rails by the Lorentz (EM) force. This phenomenon improves the electrical contact.
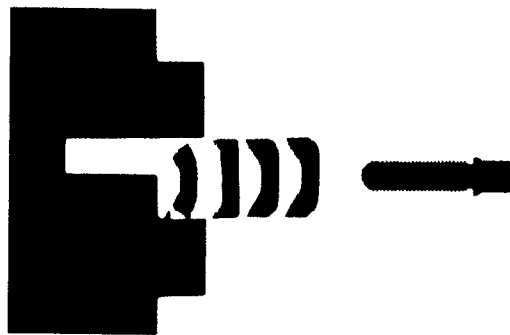
Figure 6: Flash radiograph of a projectile at the muzzle of the EMA3 railgun; the brushes at the rear side are no longer in contact with the rails; the current has moved to the next row of brushes (this is evidenced by the straightening of the brushes by the Lorentz force)

The experimental work (in particular the surface treatment of the rails [9]) associated with the numerical simulation (Figure 7) will allow to find out how to prolong the duration of the metal-metal contact.
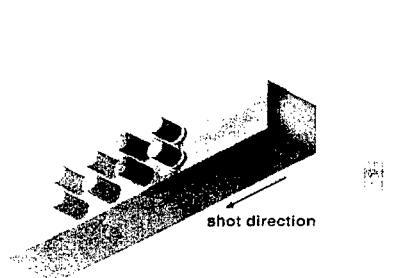


Figure 7: 3D numerical simulation (MEGA code) of the behaviour of the brush armatures (current density, $A/m^2$)

## 4. PEGASUS FACILITY

The PEGASUS (Program of an Electric Gun Arrangement to Study the Utilization in Systems) railgun facility was built in 1998 at ISL [10]. It is a DES railgun supplied by a 10-MJ-capacitor bank made of 200 modules of 50 kJ each (Figure 8).

This facility will be used to accelerate projectiles with a mass of 1 kg up to velocities greater than 2000 m/s in the medium-caliber range (30-50 mm).

The studies undertaken with the PEGASUS facility are:
- projectile and railgun technologies at both high velocities and currents up to 2 MA,
- behaviour of the components, in particular the semiconductor switches, used in this first modular 10 MJ pulsed power supply,
- measuring and synchronization techniques developed for the DES use,
- pulse forming, registration of the electrical values, current pulse shape choice.

The first tests with the PEGASUS facility have been carried out with a 6-m-long and 50-mm round caliber launcher tube. The insulators between the Cu-Cr alloy rails consist of glass fiber reinforced plastic (GRP). The housing is made of both wound glass-fiber- and wound carbon-

fiber-reinforced plastic (Figure 9).
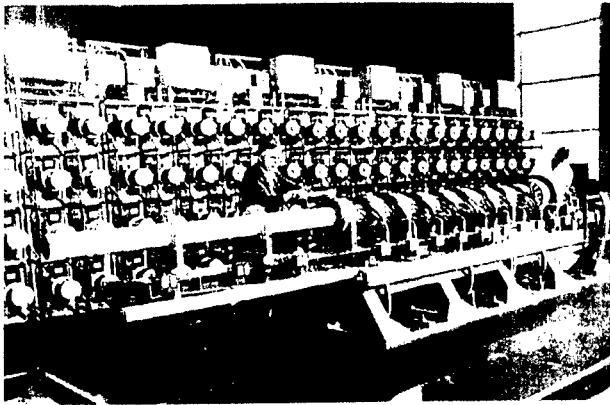


Figure 8: The PEGASUS railgun



(a)
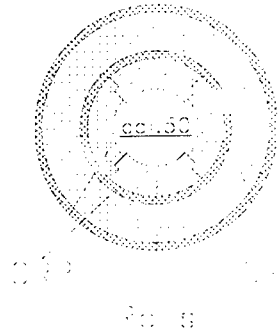


(b)

Figure 9: Cross-section of the railgun. (a) photograph. (b) sketch

The 200 PFU are connected at 13 different locations along the tube. Each connection is supplied by up to 16 coaxial cables, i.e. 16 PFU.

To obtain a good electrical sliding contact between rails and projectile, brush armatures made of copper wires (Figure 10) have been incorporated into the GRP insulating body of the projectile.
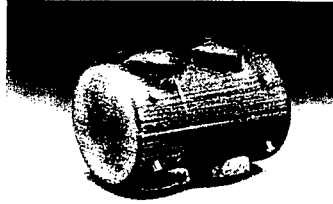
Figure 10: Photograph of a GRP projectile equipped with brush armatures

Figure 11 shows the measured total current versus time profile for the shot with E = 1.34 MJ. The maximum value of the current is 800 kA. The first current pulse (550 kA) causes an acceleration of 4 x $10^6$ m/s$^2$. The muzzle velocity reaches 1250 m/s for this shot.
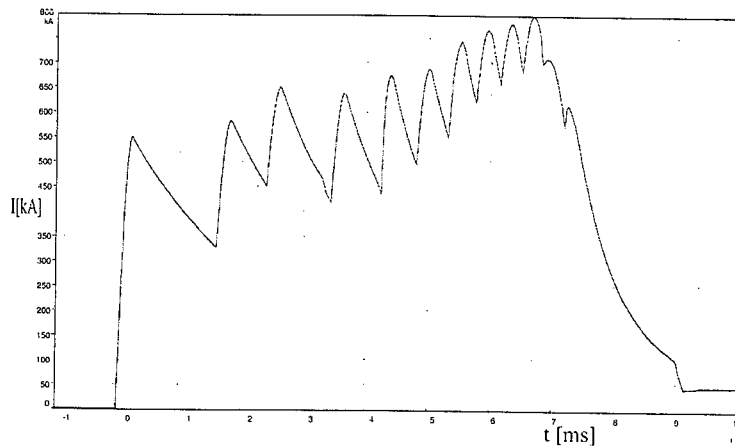


Figure 11: Total current versus time for the GRP projectile (E$_{stored}$ = 1.34 MJ)

The measured muzzle voltage as a function of time, for a shot with a stored energy E = 1.34 MJ, is shown in Figure 12. The first 8 current injections cause the formation of small spikes of about 20 V. After the 8th injection at 5.4 ms and at 1.5 m from the breech, the muzzle voltage is always greater than 100 V, indicating the formation of a plasma arc between the brushes and the rails. The erosion at the ends of the brushes due to the plasma arc can be seen on the flash-radiograph (Figure 13) of the projectile in free flight. The radiograph also shows that the projectile is undamaged and that the two rows of brushes have conducted the current. The current has "jumped" from the rear brushes, after plasma creation, to the front brushes. As can be seen on the flash-radiograph, the current has flowed mainly through the rear brushes (they are straightened by the EM force). The main results obtained with the GRP projectile are given in the following table.

| projectile mass (g) | stored electric energy (MJ) | muzzle velocity (m/s) | overall efficiency (%) |
|---|---|---|---|
| 357.0 | 1.34 | 1250 | 20.8 |
| 356.8 | 3.0 | 2240 | 29.9 |
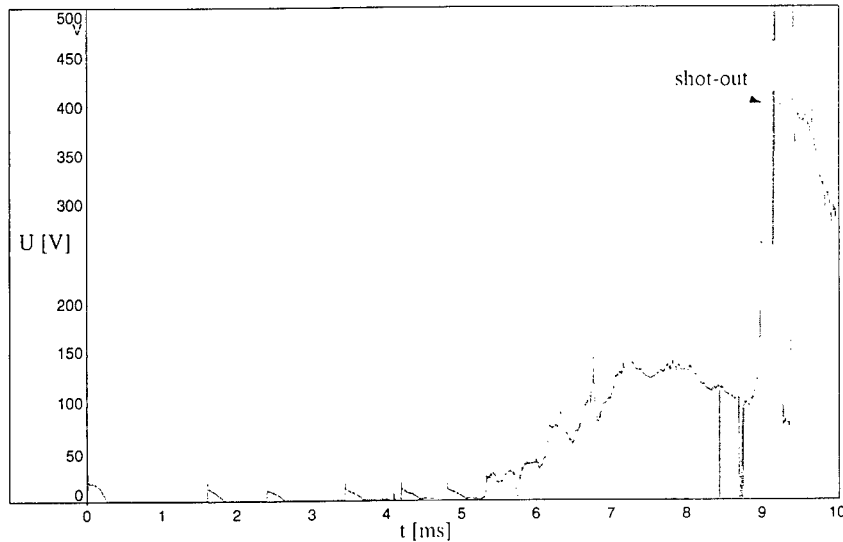
Figure 12: Muzzle voltage versus time for the GRP projectile shown in Figure 8 ($E_{stored}$ = 1.34 MJ)
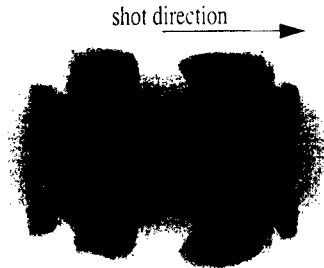


Figure 13: Flash-radiograph of the GRP projectile in flight showing the main current flow through the rear brush

After 8 shots the caliber of the gun has grown more than 1.6 mm in the range between 1 m and 5 m from the breech. For the first and last meters of the railgun the initial caliber of 50 mm remains unchanged. This caliber enlarging along the central part of the launcher after a few shots has led to the need of studying a new type of housing able to sustain the repulsive forces without plastic deformation.

The PEGASUS rail launcher has proved the excellent working order of the 13-stages DES system. The modular power supply in which the energy can be varied up to 10 MJ and the triggering instants can be chosen, allows to obtain a well-adapted current versus time profile. The use of the semiconductor switches for the 200 modules is very efficient.
The first tests with the PEGASUS facility show that the railgun has an overall efficiency in the order of 30%.
The brush armatures provide a good electrical contact without arcing along an acceleration length up to 1.5 m.
Future work will concentrate on the extension of the non-arcing length, on the one hand, and on

- 174 -

the improvement in the stiffness of the launcher tube, on the other hand.

## 5. CONCLUSIONS

The objectives of the ISL activities in the field of ElectroMagnetic railguns are to reach velocities over 2000 m/s with barrels not longer than 6 m to 8 m. This means acceleration levels ranging from $5 \cdot 10^5$ m/s$^2$ to $2 \cdot 10^6$ m/s$^2$ and peak currents from 1 MA to 5 MA, depending on the mass of the projectile (1 to 10 kg).

The physical phenomena involved in these extreme conditions require the development of various research activities, e.g.:

- sliding contacts submitted to both high velocity (2000 m/s) and high current (MA): friction, coating of rails, plasma arcs;
- barrels containing the rails: use of glass-fiber-reinforced epoxy to avoid eddy currents, but stiff enough to sustain the forces separating the rails;
- electrical connecting parts between the power supply and the rails submitted to high-level forces and torques;
- high-power pulsed technology and pulse forming networks giving the appropriate current pulse shape for breech-fed or DES supplies;
- numerical simulation taking into account the velocity skin effects.

## 6. REFERENCES

[1] F. Jamet, E. Wollmann, V. Wegner, P. Lehmann, ISL Report S-RT 909/92, Saint-Louis, France, (1992)

[2] P. Lehmann, V. Schirm, H. Peter, J. Wey, "Rail Launchers to Reach Hypervelocity", *Int. J. Impact Engng*, 17, pp. 509-515,(1995)

[3] F. Jamet, V. Wegner, E. Mayer, V. Fleck, "Intérêt des lanceurs électromagnétiques dans la lutte anti-aéronefs", ISL Report S-RT 908/90, Saint-Louis, France, (1990)

[4] F. Jamet, P. Lehmann, V. Wegner, "Power Conditioning Requirements for Electric Guns", *Proceedings of the 1st International Conference on All Electric Combat Vehicle (AECV)*, Haifa, Israel, May 14-17, 1995

[5] P. Lehmann, "Lanceurs électriques à rails appliqués à la défense anti-aérienne", ISL Report R 115/98, Saint-Louis, France, 1998

[6] E. Spahn, M. Lichtenberger, F. Hatterer, "Pulse Forming Network for the 10 MJ-Railgun PEGASUS", *Proceedings of the 5th European Symposium on Electromagnetic Launch Technology*, Toulouse, France, 10-13 April, 1995

[7] K. Darée, "Modellierung von DES-Railguns mit Hilfe eines iterativen Runge-Kutta-Nystroem-Verfahrens", ISL Report N 606/88

[8] R. Charon et al., ISL Report S-RT 903/97

[9] W. Silberzahn, H. Peter, "Beschichtungen für Elektromagnetische Beschleuniger", *Proceedings of the Wehrtechnisches Symposium*, WIWEB, Erding, Germany, November 10-12, 1998

[10] P. Lehmann, H. Peter, J. Wey, "First Experimental Results with the ISL 10 MJ DES Railgun PEGASUS", to be published in Proceedings of the 10th EML Symposium, San Francisco, California, April 25-28, 2000

# THE UK ETC GUN PROGRAMME FOR THE MILLENNIUM

FIRTH M., WOODLEY C., TAYLOR M., FULLER S., SAVELL G.

Defence Evaluation and Research Agency, Fort Halstead, Sevenoaks, Kent TN14 7BP, United Kingdom

**Abstract :** 'Electric gun' research has been undertaken at the UK Defence Evaluation and Research Agency (DERA), and its predecessors, for many years. One branch of electric gun technology that has been actively pursued over recent years is the electrothermal-chemical (ETC) gun. ETC gun technology shows promise for enhancing aspects of conventional ordnance performance within the constraints imposed by mobile weapon platforms. Potential applications exist for both indirect fire and direct fire weapon systems. The aim of the DERA ETC gun research programme is to attain a level of understanding of ETC gun technology from which to be able to assess its utility as either an upgrade to existing systems or as part of a new weapon system. In recent years, good progress has been made towards the goal of a more complete understanding of plasma generators, the plasmas they produce and the interaction of plasma with propellant. The ability to evaluate ETC gun concepts and demonstrate ETC gun capabilities has been enhanced recently by the commissioning and development of a 155mm experimental ETC gun. Smaller scale experiments continue to be used also. This paper reviews the current state of ETC gun research at DERA and outlines our plans for the future.

## 1. INTRODUCTION

This overview summarises research over the last few years at the UK Defence Evaluation and Research Agency (DERA) in the field of electrothermal-chemical (ETC) guns.

The motivation for research into ETC gun technology in the UK continues to be the improvement of indirect fire gun systems such as artillery and naval fire support [1]. More recently, improvements to direct fire gun systems such as battle tank main armaments have begun to be explored also. Such improvements are considered both for upgrades to existing equipment and as a part of new weapon systems.

The assessment of ETC technology for improving gun system performance is achieved by exploiting the ETC knowledge base. In the UK this resides mainly with DERA. The knowledge base has been grown in recent years through experimentation and the development of simulation capabilities. The knowledge base covers the 'generic' ETC gun technology areas of plasma generators, plasma properties and plasma-propellant interactions. Recent efforts have concentrated on the development of capabilities in ETC gun firings, at both 30 mm and 155 mm calibre, for experimental evaluation of concepts and computer model development and validation.

## 2. PLASMA GENERATORS

A wide variety of ETC plasma generator concepts exist. The UK has concentrated on the capillary plasma generator (CPG). The cornerstone of DERA knowledge on CPGs is the EDENET computer model being developed by Fluid Gravity Engineering Ltd [2]. Version 3

of this model has been used to simulate 155 mm ETC gun firings that employed a breech mounted CPG [3]. Figure 1 compares EDENET version 3 simulations with experimental data of current and voltage from 155 mm ETC gun firings.
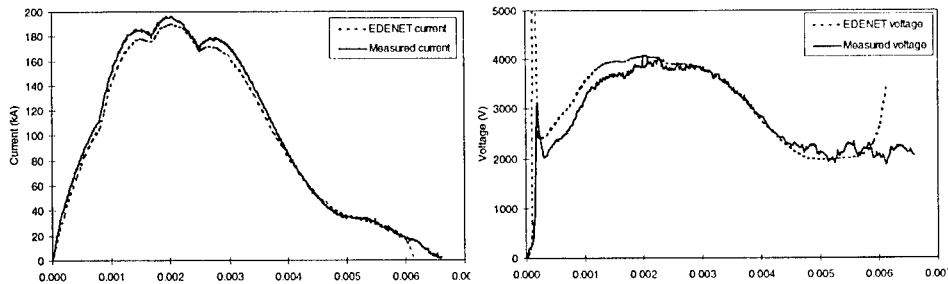


Figure 1: comparison of measured and predicted current (left) and voltage (right) from a 155 mm ETC gun employing a breech mounted capillary plasma generator.

Development and validation of EDENET has been supported by specially designed experiments. For example, X-radiography was used to study the operation of the fuse wire in general and the uniformity of wire break-up and early plasma formation in particular. Figure 2a illustrates a typical result for a vertically oriented unconstrained fuse wire and figure 2b is a similar fuse wire in a plasma generator capillary. Also, a test rig was designed and manufactured that had a current return path approximately co-axial with the capillary to minimise magnetic perturbations of the capillary plasma. This apparatus also had the ability to measure capillary pressure. Figure 3 is a photograph of the test rig, which was used to generate high quality data for model validation.
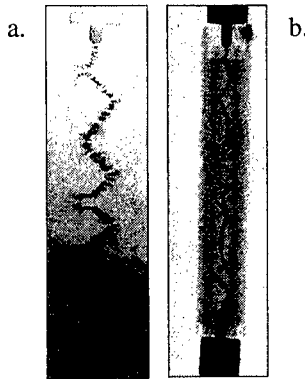


Figure 2: X-ray photographs of an electrically exploded CPG fuse wire
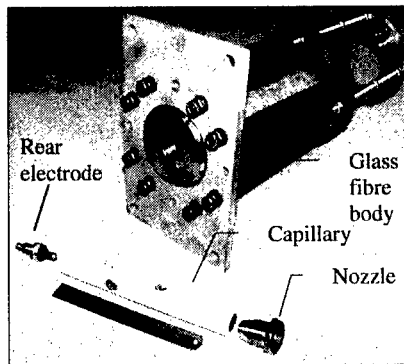
Figure 3: Photograph of CPG test rig

Further development of the EDENET CPG model is planned.

## 3. PLASMA PROPERTIES

For optimal design of plasma generator, and thus for minimisation of electrical power supply requirements, a good knowledge of the plasmas being produced is required. As a starting point towards a knowledge of ETC plasmas in the combustion chambers of guns,

instrumentation techniques have been developed that allow the characterisation of a freely expanding jet of plasma from a CPG operating in atmospheric pressure air. These techniques are centred on fast framing photography and time resolved spectroscopy. Time-resolved spectra of the plasma plume were recorded by use of a masked CCD detector fitted to a monochromator. For each test, 251 spectra were recorded from the far ultra violet to the near infrared. Light from the plume was collected by a 400 μm diameter quartz fibre-optic via a collimating mirror. Figure 4 shows spectra typical of those recorded. Each spectrum was captured with the detection system focussed on a small area of the plume approximately 100 mm from the nozzle of the CPG. The three spectra (figures 4a-c) were recorded at times of 0.25 ms, 0.75 ms and 1.05 ms respectively. The timing of the first two spectra in relation to the CPG current pulse is illustrated in figure 4d. The spectrum in figure 4c corresponds to a time after the CPG current pulse has ended. The value of $T_b$ and the smooth curves in figures 4a-c are the temperature and spectrum of a blackbody emitter that would emit the same radiant flux as the plasma over the spectrometer wavelength interval.
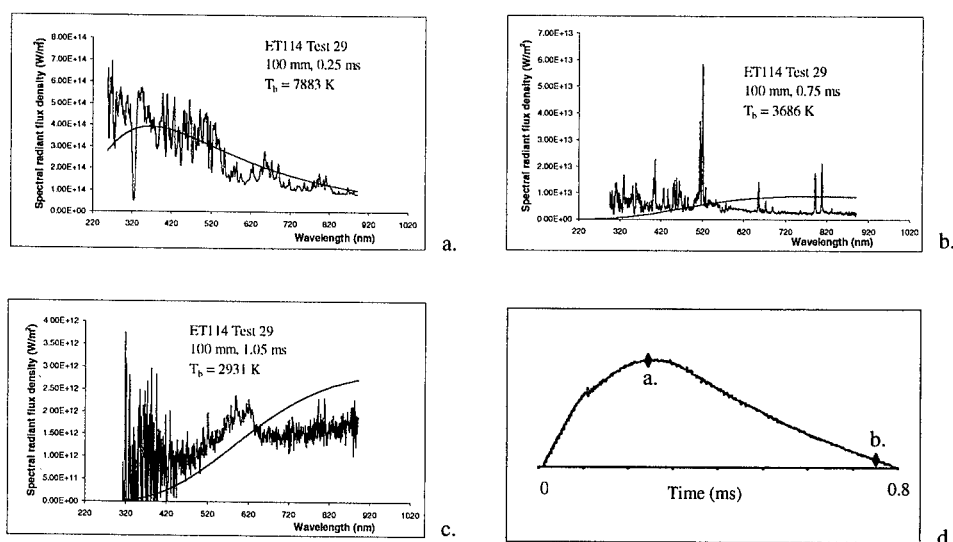


Figure 4: Plasma spectra and CPG current pulse

$T_b$ is used to estimate the total flux density from the plasma over all wavelengths. One of the aims of the work on plasma properties is to be able to determine the partitioning of energy in a CPG firing.

## 4. PLASMA PROPELLANT INTERACTIONS

Plasma can be employed to interact with propellant throughout the internal ballistic cycle. For example, it can be used as an ignition stimulus as well as to affect the propellant gasification rate. The latter effect has been studied extensively at DERA, both theoretically and experimentally [3][4]. Chemical kinetics studies have been undertaken in an attempt to identify key rate determining reactions that could be affected by plasma. Data from pressure vessel firings and ETC gun firings have aided the generation of a modified empirical propellant burn rate law. In equation (1), r is the propellant burn rate, β is the burn rate

coefficient of the solid propellant, P is the gas pressure, $\alpha$ is known as the burn rate pressure index, EP is the electrical power (in MW) and $\Psi$ is called the EGGR coefficient (in $MW^{-1}$).

$$r = \beta P^{\alpha} (1+EP*\Psi) \qquad (1)$$

Equation (1) was used very successfully in the simulation of a wide range of different 155mm ETC gun firing conditions.

Various experiments have been performed to reduce the number of possible mechanisms for the gas generation rate enhancement, such as the variation of CPG fuse wire and electrode material, with mixed success. It is planned to continue research in this area and to increase efforts into understanding plasma ignition of solid propellants.

## 5. 30 MM ETC GUN EXPERIMENTS

Extensive use has been made of the ability to undertake 30 mm calibre ETC gun firings at DERA Fort Halstead in recent years. A relatively large series of firings was undertaken in 1999 to investigate key aspects of the 'smart gun' concept [5][6]. This concept employs an electrothermally induced pressure gradient to increase the velocity of a projectile as it travels along the bore of the gun barrel. The experiments confirmed that, at 30 mm calibre, it is possible to alter the projectile's velocity 'in-bore' in a controlled and prescribed manner. Figure 5 is a photograph of the 30 mm ETC gun. Figure 6 shows typical data obtained during a 30 mm ETC 'smart gun' firing.
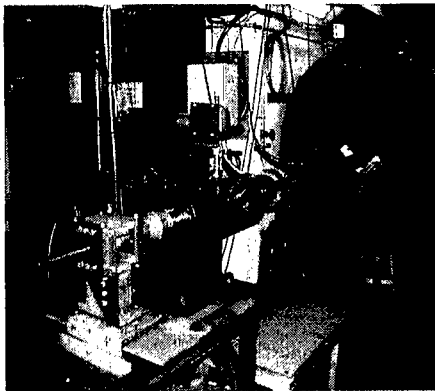


Figure 5: 30 mm ETC gun prepared and ready for firing
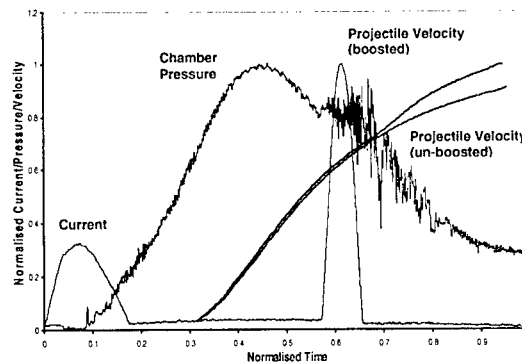


Figure 6: Typical data from 30 mm 'smart gun firing

## 6. 155 MM ETC GUN EXPERIMENTS

A major activity of the DERA ETC programme over the last few years has been the development of a capability to fire 155 mm ETC guns. A 155 mm, 52 calibre ETC gun was commissioned in June 1998. The gun employed a simple screw type of breech mechanism with elastomeric pad obturation. A CPG was integrated into the breech mechanism via a modified vent bolt assembly. Figure 7 shows the gun on a 'range stand', in storage, adjacent to the capacitor bank at the DERA Kirkcudbright facility. Between June 1998 and October 1999 the gun had successfully fired over 50 shots and provided valuable data for computer model validation and ETC concept evaluation.
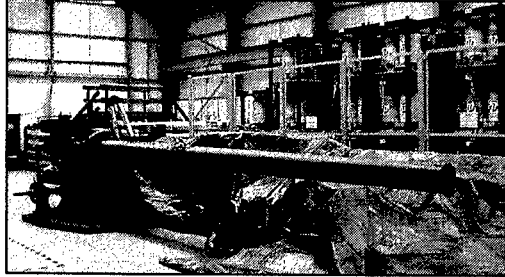
Figure 7: 155 mm, 52 calibre ETC gun

In 1999 the capacitor bank at Kirkcudbright was modified such that it better suited the requirements of an ETC gun [7]. The main components of the modification were the ability to operate some of the capacitor bank modules as a 'Marxed pair', doubling the operating voltage to 22 kV, along with the addition of extra pulse shaping inductors.

A further enhancement to the Kirkcudbright facility was the installation of a 'muffler' to reduce the noise and blast from ETC gun firings. Figure 8 is a photograph of the muffler in place at the end of the Kirkcudbright ballistic tunnel. The inset in figure 8 shows an ETC gun firing using the muffler where the projectile is just discernible towards the top left hand corner.
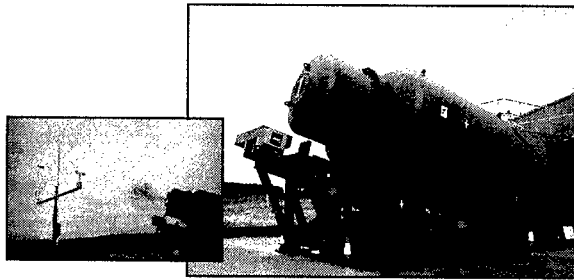


Figure 8: ETC 'muffler' and ETC 155 mm gun firing (inset)

The work described here has resulted in a flexible facility for evaluation of ETC gun technology at large calibre. Along with the ability to fire 155 mm ETC guns, a full range of instrumentation is used such as in-bore microwave Doppler radar and fibre-optic strain gauges to monitor projectile travel. Fast response thermometry is used close to the gun's commencement of rifling to evaluate gun wear, which is an area of concern for ETC gun systems.

## 7. SUMMARY

The UK knowledge base on ETC gun technology is being developed through a combination of experimentation and simulation with a key component being ETC gun firings at 30 mm and 155 mm calibre. This knowledge base is being used to evaluate ETC technology for use in improving both indirect fire and direct fire gun systems.

## 8. REFERENCES

[1]   Haugh D C and Firth M A, 'The UK Electric Gun Programme in 1998', IEEE Transactions on Magnetics, Vol. 35, No 1, January 1999.

[2] Swift D C, *'Hydrocode modelling of plasma capillaries'*, APS Plasma Physics Meeting, New Orleans, 1998.

[3] Woodley C R & Savell G F, *'Modelling Enhanced Gas Generation Rates in a 155mm ETC Gun'*, 18th International Symposium on Ballistics, San Antonio, November 1999.

[4] Woodley C R & Fuller S, *'The effect of plasmas on the combustion rates of solid propellants'*, The International Autumn Seminar on Propellants, Explosives and Pyrotechnics, Shenzen, China, 8-11 October 1997.

[5] Fuller S R, Gilbert S, Mills R, Edwards D, *'Means for Controlling the Muzzle Velocity of a Projectile (Smart Gun)'*, UK Patent application Number 9622615.4, October 1996.

[6] Fuller S R & Firth M, *'Smart gun development'*, Proceedings of the VI European Indirect Fire Symposium, Shrivenham, UK, May 1999.

[7] Hammon J, Hitchcock S, Hopwood D, Lam S K, Gilbert S, Chapman P, Hainsworth G and Wardle H, *'Modifications of the Kirkcudbright Capacitor Bank System for ETC Operations'*, Presented at the 12th IEEE International Pulsed Power Conference, California, June 1999.

# Status and Results of the German R&D Program
# on ETC Technologies

Thomas H.G.G. Weise, Holger Wisken
TZN Forschungs- und Entwicklungszentrum Unterlüß GmbH
Neuensothriether Str. 20, D-29345 Unterlüß
Federal Republic of Germany

**Abstract:** Due to its limited electrical energy requirements the technology of ETC guns has been investigated during the last years with high priority. It is the goal to provide a future main battle tank gun with increased firepower for integration into the next generation of combat fighting vehicles. Current R&D programmes result in a demonstration of the interior ballistic performance of the different ETC concepts. 120mm ETC demonstrators are used to perform this demonstration. The paper gives an overview on the latest ETC technology approaches in the framework of the German R&D program. Basic investigations led to the definition of different ETC concepts for the realization of electrothermal plasma ignition methods and electrothermal combustion control of ETC tailored propellants and charge designs. The most promising concepts were validated in a 105mm ETC gun set-up. Theoretical simulations of the interior ballistic performance of these concepts are performed. Based on the results of the 105mm firings and of the interior ballistic simulations a 120mm ETC cartridge was designed and investigated experimentally. The paper concludes in giving an outlook on the perspectives of the performance of ETC technologies and its power supply technologies in order to provide the access to increased firepower and survivability of existing and succeeding main battle tank systems without leaving the currently introduced boundary conditions of the large calibre weapons.

## 1. INTRODUCTION

Improved protection technologies by active and reactive armor as well as by increased hardeness of armor plating technologies define the requirements of the performance of future tank guns. For the existing conventional tank guns a high level of lethality has to be provided which can be obtained i.e. from improved temperature insensitive propellants. Future tank guns have to provide a significantly higher lethality which can be obtained from advanced propulsion and gun technologies.

In order to met the requirements of future tank guns and close the gap between gun performance and armor plating technologies electric guns with their potential of realizing very high muzzle velocities were investigated within several R&D programmes in the past. In the US these programmes concentrated on the rail gun technology. Laboratory systems were set-up demonstrating muzzle velocities with 2kg projectiles of to up to 3.000 m/s in calibre 90mm [1]. In Germany electrothermal gun technologies were investigated. In 1995 105mm shots were demonstrated firing 2kg projectiles to up to 2.400 m/s [2]. Due to the missing perspective of realising high energy density pulsed power supply technologies for integration into a combat fighting vehicle in the short and mid term time frame several nations including the USA and Germany decided to proceed the investigations with the Electrothermal-Chemical Gun Technology (ETC).

ETC technologies opens the opportunity to reconsider the limited success of past conventional investigations under aspects of

- perfect ignition properties
- electrothermal enhancement of propellant conversion
- access to new high energetic propellant formulations
- access to charge designs with increased loading densities.

From these properties a significant improvement of the interior ballistc gun performance can be obtained at limited and realistic electric energy requirements.

## 2. GOAL OF THE R&D PROGRAM

It was the goal of the German R&D program phase 1 on ETC guns to demonstrate a muzzle energy of at least 14 MJ out of a 120mm Gun within the boundary conditions of the conventional set-up in terms of maximum breech pressure (670 MPa), volume of the charge chamber (10l), projectile travel length (6m), muzzle pressure (<100MPa) and mass of projectile (8,4 kg). The demonstration of this muzzle energy shall be performed by using ETC technologies with available propellants. In addition the results of basic investigations shall predict the performance potential of new propellant formulations and charge designs with ETC technology. An evaluation of the results obtained from the investigations on the gun performance and on the pulsed power supply technology shall result in the short and medium term availability of ETC technologies within the boundary conditions of existing and future large calibre combat fighting vehicle systems.

## 3. BASIC CONSIDERATIONS

The electrothermal energy conversion via approximately massless and volumeless high power plasmas which are arranged in the propellant set-up of the cartridge with a high degree of geometrical flexibility can be used efficiently without time delay for the ignition of the propellant as well as for its combustion control.

### 3.1 Electrothermal Plasma Ignition Methods

The large variety of the properties of the plasma ignition processes which are not given from conventional pyrotechnics enable the development of charge designs with increased performance as well as of new high performance powder formulations based on Nitramin and RDX chemicals. Further advantages are gained from the ETC technologies by the possibility of adjusting the ignition performance directly before or during the development of the shot as well as controlling the combustion during the burning phase of the propellant. These properties can be applied i.e. for a temperature compensation of the propellant.

Fig. 1 gives three different plasma ignition methods schematically. The Plasma Jet Ignition is characterized by a so called plasmaburner which is located in the breech of the charge chamber. Supplying this plasmaburner with electrical energy a high temperature plasmajet is generated and directed into the propellant set-up in the charge chamber. The form and the length as well as the ignition power of the plasmajet can be adjusted by the geometry of the plasmaburner and by the pulsehape of the electric energy supply. The plasmajet interacts with the propellant and results in ignition and combustion enhance-ment during the pressure generation phase. A proper design of the plasmaburner and a good matching of the electrical power pulse can lead to large lengths of the plasmajet. The properties of this method are of interest for solving the ignition of modular charges for artillery guns. The application for large calibre tank gun charges has been investigated with minor success.

The Plasma Surface Ignition realises a plasma coating around the propellant set-up. By this the propellant is ignited from the inner surface of the combustible cartridge case to the inside of the charge set-up over the total lenght of the charge without any time delay in the axial direction.
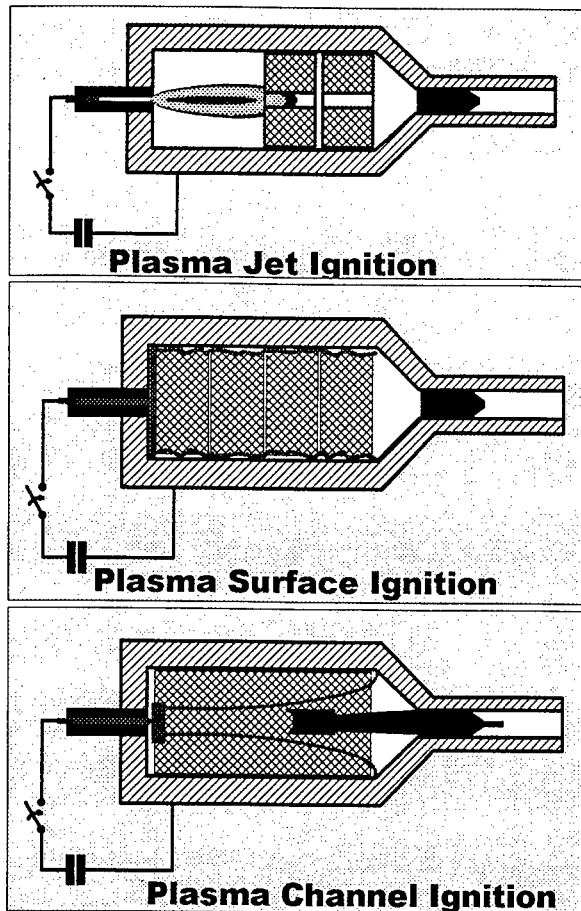
Figure 1: Plasma Ignition Methods (schematically)

This method opens the access to very compact charge designs i.e. coated propellant discs with very high loading densities.

The last method is given by the Plasma Channel Ignition system. Several plasma channels are initiated in the charge set-up by the explosion of thin wires which are located within thin walled propellant tubes. The interaction of these plasma channels leads to the ignition of the propellant. By the electrical energy supply the ignition power is adjusted and in addition, a combustion enhancement can be realized over the entire time period of propellant burning.

The application of the plasma ignition methods for improving the interior ballistic performance requires detailled knowledge of the interaction processes between the plasma and the propellant. The energy transfer mechanism from the plasma to the propellant is provided mainly via radiation processes. Therefore the energy is transmitted into a large volume without any significant time delay. Plasmas are of low mass and of low volume requirements.

In particular the plasma channel ignition method is characterized by its high degree of geometrical flexibility. By the electrical energy supply ignition power can be adjusted. Furtheron the propellant combustion can be enhanced during the burning period. The application of these properties is the basis for the assessment of charge designs with increased interior ballistic performance due to increased loading density or new propellant formulations or a combination of both.

## 3.2 ETC Concepts

Compared to electric guns ETC technologies are characterized by their significantly lower electric energy requirements. The energy for acceleration is provided chemically from the propellant. The electric energy of several percent of the chemical energy is applied just for supplying the plasma ignition and combustion enhancement systems which are arranged within the cartridge.

Currently three different conceptional ETC approaches are under investigation in the German R&D program. By the ETC ignition of new propellants a controlled release of increased chemical energy is performed. ETC controlled ignition and combustion of charge set-ups with

increased loading densities provide the availability of optimized pressure profiles and more efficient acceleration with increased energy. The increase of the propellant surface by ETC controlled fragmentation of compact charges is an alternative approach to access increased loading densities for acceleration.

For the large calibre firings two prime concepts are selected and investigated as being shown in fig. 2.
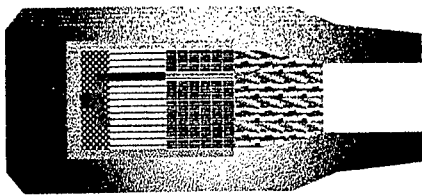


Fig. 2a: Stacked Charge Set-Up          Fig. 2b.: Granular Charge Set-Up
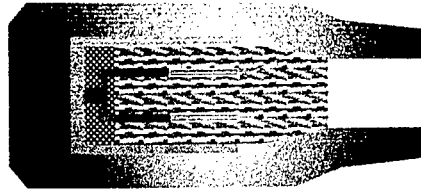
Fig. 2: Large Calibre Prime Concepts

A stacked charge set-up (fig. 2a) consisting of three different types and geometries of propellants is equipped with a three channel plasma ignition system. The combustions of the three charges are ignited and controlled by the electrothermally released energy. Charge 1, located in the rear section of the chamber, consists of stacked transparent propellant grains with a geometric which leads to a low combustion rate given by a large web size and no perforation. Charge 2, located in the middle section, consists also of stacked grains but with a geometry and a perforation adapted to the interior ballistic cycle once being ignited. Charge 3, located in the front section, consits of granular propellant also being adapted to the conventional interior ballistic cycle. All three charges are ignited by the plasma ignition process. After the maximum pressure is achieved a second electric pulse is released into the plasma channels in order to increase the combustion rate of charge 1 and adapt it to the interior ballistic cycle and flat top the pressure pulseshape in the charge chamber.



A grain charge set-up (fig. 2b) consisting of a new propellant formulation (NENA) with LOVA characteristics is ignited by a three channel plasma ignition system. The NENA Propellant is characterized by its increased acceleration force (impetus) and its lower gas temperature. Due to its increased activation energy levels the pyrotechnical ignitibility is not sufficient by increased ignition delays and ignition jitters. Electrothermal plasma ignition is supposed to overcome this ignition problems in order access the good interior ballistic performance of this propellant for a gun application.

Fig. 3: ETC-Sensitivity of optical transparent Propellants

Basic investigations on the interaction of solid propellants with electrically driven high power plasmas show that energy transmission from the plasma to the propellant is performed by

radiation processes [3]. With optical transparent propellants the plasma radiation can be applied to change the surface structure within the volume of the propellant resulting in a significant change of the burn rate after ignition. Fig. 3 gives some results of basic investigations performed on this process in closed vessel experiments. This process can be used to get access to large propellant geometries increasing the loading density of a charge set-up.

## 3.3 Theoretical Investigations on the ETC Combustion Control Concept



Fig. 4: Results of Interior Ballistic Simulations
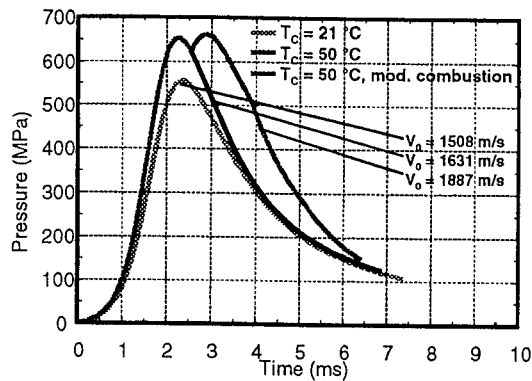
Modeling and simulation is performed to understand the ETC processes. Existing IBHVG2 codes are modified in order to generate first performance estimations of different conceptional approaches. Modified gas dynamic codes are applied for the detailed evaluation of firing results. An ETC model IBECA is under development for the detailed description of all physical and interior ballistic processes [3].

First performance predictions for 120mm ETC concept were calculated by the existing codes. Both IBHVG2 simulations as well as gasdynamic simulations show the performance increase of ETC combustion controlled charge set-ups with higher loading densities. Fig. 4 gives an example of the results of such simulations performed for a 120mm ETC cartridge with a charge set-up due to fig. 2a (stacked charge with three propellant types). It is assumed in the code that the combustion rate of charge 1 is increased by a factor of 4 during the release of the second electric energy pulse. The simulation shows the development of a second pressure maximum generated by the electrothermal controlled combustion of charge 1 after the first pressure maximum. Both the IBHVG2 simulation and the gas dynamic simulation indicate a significant increase of muzzle velocity obtained from this process.

## 4. SET-UP OF THE PLASMA CHANNEL IGNITION SYSTEM

Fig. 4 shows the set-up of a three channel plasma ignition system within a large calibre gun



cartridge schematically. The plasma ignition system is installed within a conventional cartridge with combustible cartridge case. The stub case is modified by a high voltage feed through with a current distributing conductor. Exploding wires which are located within thin walled propellant tubes are igniting the plasmas in several channels.

Fig. 4: Large Calibre Cartridge Set-Up with Plasma Channel Ignition (schematically)

By the interaction of these plasma channels with the propellant ignition and combustion enhancement are performed.


## 5. EXPERIMENTAL RESULTS OBTAINED FROM 105MM ETC FIRINGS

### 5.1 Experimental Set.Up

A first validation of the large calibre ETC concepts was performed with a 105mm ETC gun. Fig. 5 gives a view on the gun and on the ETC cartridge set-up with their main parameters.

The gun is characterized by a charge chamber volume of 6.44 l and a projectile travel length of 6.24 m. The maximum operation pressure is 500 MPa. ETC cartridges made from inert plastic material were used in this gun. Several pressure gages are located in the charge chamber and along the barrel.



| Charge Chamber Volume: | 6.44 l |
|---|---|
| Projectile Travel Length: | 6.24 m |
| Max. Operating Pressure: | 500 MPa |
| $x_p$ Position $p_1$: | 450 mm |
| $x_p$ Position $p_2$: | 715 mm |
| $x_p$ Position $p_3$: | 3414 mm |
| $x_p$ Position $p_4$: | 6064 mm |
| $x_p$ Position $p_5$: | 6714 mm |
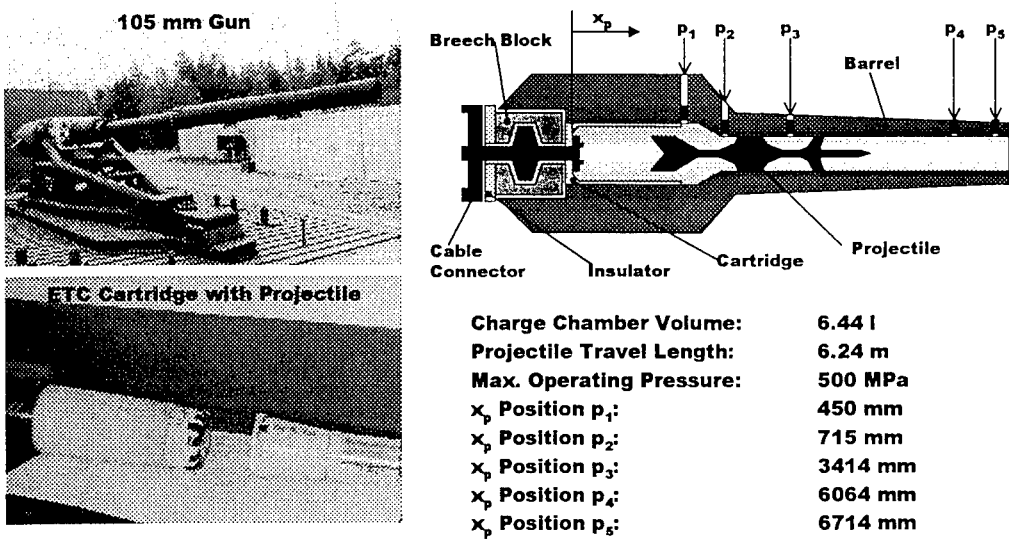
Fig. 5.: Set-Up of the 105mm ETC Gun


### 5.2 105mm Firing Results

A variety of test firings were performed in the 105mm gun. Tests with stacked propellant and double pulse plasma combustion enhancement indicate the function of the interior ballistic processes. Fig. 6 shows the results of two characteristic experiments with these concepts as well as a summary of the results.

## Fig. 6 data

**Shot data (top)**

| Projectile Mass: | 4.2 kg |
|---|---|
| Mass of Propellant: | 5.65 kg |
| el. Energy Input: | 1070 kJ |
| Muzzle Velocity: | 1706 $^m/_s$ |
| Muzzle Energy: | 6.12 MJ |
| Overall efficiency: | 20.2 % |

**Summary of results**

Test Results 105 mm OETC
Mp=4.2 kg, Vb=6.44 ltr., Max. 4 Propellant types

**Shot data (bottom)**

| Projectile Mass: | 4.2 kg |
|---|---|
| Mass of Propellant: | 5.79 kg |
| el. Energy Input: | 1880 kJ |
| Muzzle Velocity: | 1794 $^m/_s$ |
| Muzzle Energy: | 6.76 MJ |
| Overall efficiency: | 22.0 % |

Fig. 6: Characteristic Results of 105mm Test Firings with stacked Propellant and double Pulse Plasma Combustion Control

Projectiles of 4.2kg are accelerated to muzzle velocities of 1.800 m/s. The amount of electric energy which is necessary to realize this concept is high. Up to 2.5MJ were applied during the investigations.

Further tests with granular propellant made from NENA formulations show the excellent interior ballistic performance of this propellant due to its high impetus. Fig. 7 gives the results of two characteristic experiments conducted with two different web sizes of the propellant grains as well as a summary of all test performed with this concept.

## Fig. 7 data

**Shot data (top)**

| Projectile Mass: | 4.2 kg |
|---|---|
| Mass of Propellant: | 5.76 kg |
| Web Size: | 1.3 mm |
| el. Energy Input: | 391 kJ |
| Muzzle Velocity: | 1896 $^m/_s$ |
| Muzzle Energy: | 7.55 MJ |
| Overall efficiency: | 28.6 % |

**Summary of results**

Test Results 105 mm OETC
Mp=4.2 kg, Vb=6.44 ltr., NENA-TLP

**Shot data (bottom)**

| Projectile Mass: | 4.2 kg |
|---|---|
| Mass of Propellant: | 5.76 kg |
| Web Size: | 1.5 mm |
| el. Energy Input: | 347 kJ |
| Muzzle Velocity: | 1716 $^m/_s$ |
| Muzzle Energy: | 6.18 MJ |
| Overall efficiency: | 23.4 % |

| Standard Deviation $t_z$: | 37.3 µs |
|---|---|
| Standard Deviation $p_{max}$: | 3.6 MPa |

Fig. 7: Characteristic Results of 105mm Test Firings with granular NENA Propellant and single Pulse Plasma Channel Ignition

4.2kg projectiles were accelerated to up to 1.900m/s. A one pulse Plasma Channel Ignition was applied with an electrical energy input of about 400kJ only at a propellant temperature of approximately 21°C. A standard deviation of the ignition delay times of only 37.3µs as well as a standard deviation of 3.6 MPa of the maximum pressure values show the excellant performance

of the plasma ignition method even with LOVA type propellants.


## 6. EXPERIMENTAL REULTS OBTAINED FROM 120MM ETC FIRINGS

### 6.1 Experimental Set.Up

The 120mm ETC gun being used for the performance demonstration is shown in fig. 8. The gun platform equals those which has already been used for the 105mm firings. A 120mm L55 barrel is assembled in the breech block. The breech block system consists of a bajonet joint. The electrical connection to the pulsed power supply system is realized by coaxial cables. Projectiles of approximately 8.4 kg are accelerated in the 6m long barrel. The volume of the charge chamber is approximately 10 l. The maximum operation pressure of this test gun is 700 MPa and the design presure is 800 MPa.

**System View**     **Breech Block System**



| Technical Data | |
|---|---|
| Calibre Length: | L55 |
| Projectile Travel: | 6 m |
| Volume Charge Chamber: | 10 l |
| max. Operation Pressure: | 700 MPa |
| Design Pressure: | 800 MPa |
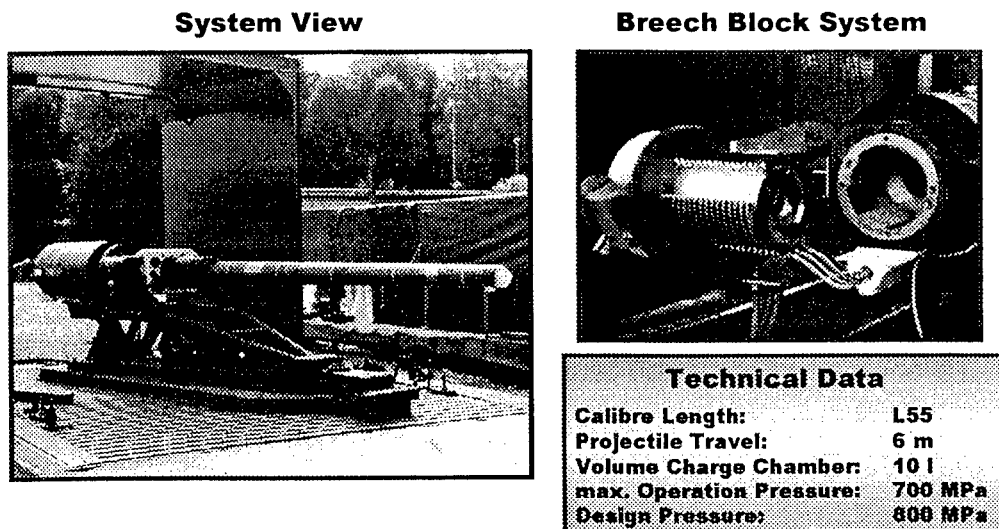
Fig. 8:  Set-Up of the 120mm ETC Gun


### 6.2 120mm Firing Results

Up to now a variety of firings have been performed with a granular NENA propellant charge at two different propellant temperatures. Fig. 9 gives the measured signals of a characteristic shot in which the 8.4 kg projectile was accelerated to a muzzle energy of 14 MJ at a propellant temperature of 50°C.

Discharge current, plasma voltage, breech pressure and energy absorbing power are plotted versus time. The duration of the electric pulse igniting the propellant is 1.2 ms. The maximum discharge current is 12.5 kA. 0.3 ms after igniting the electric discharge the voltage signal shows the characteristic peak due to the explosion of the fuze wires.In the following time period the plasma voltage increases from about 4 kV to a maximum of about 16 kV at the end of the electric discharge pulse. The breech pressure starts rising at about 1.8 ms and reaches its maximum of 670 MPa at t = 3.8 ms. The average power of the energy absorption is about 50 MW. For igniting the charge an electric energy of only 39 kJ is released into the plasma channels.

Fig 9: Measurements of a characteristic NENA Firing

Table 1 gives an overview on the main results of the NENA firings obtained at two different propellant temperatures in comparision to the performance of the LKEII cartridge which provides the current maximum performance level of conventional 120mm ammunition.

With the NENA1 propellant muzzle energies of 14 MJ are demonstrated at propellant temperatures of 21°C and 50°C.

The temperature compensation is performed by an increase of the electrically released energy to 110 kJ. The firings with the NENA2 propellant which differs by its larger web size from the NENA1 propellant are performed at 50°C up to now.

A further increase of the muzzle velocity to 1.839 m/s is obtained with a slightly increased amount of electrically released energy of 101 kJ.

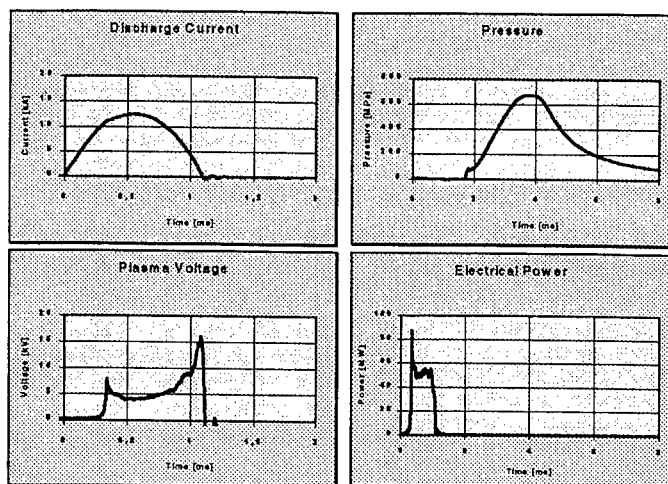By a proper design of the Plasma Channel Ignition and the adjustment of the electric ignition pulseshape the requirements of electric energy for igniting the NENA charge set-up are significantly reduced in the 120mm cartridge. It is expected that energies of only several 100 kJs are sufficient for a fully temperature compensated performance of NENA charge set-ups in a 120mm cartridge providing gun applicable ballistics with high firepower due to the properties of the electrothermal plasma ignition method.

| Charge | Vo [m/s] | | Wo [MJ] | | El. Energy [kJ] | |
|---|---|---|---|---|---|---|
| | 21°C | 50°C | 21°C | 50°C | 21°C | 50°C |
| LKE II | 1,750 | 1,830 | 12.8 | 14.0 | | |
| ETC NENA1 | 1,822 | 1,831 | 13.9 | 14.0 | 110 | 39 |
| ETC NENA2 | | 1,839 | | 14.1 | | 101 |

Table 1:      Results of 120mm NENA Firings

## 7. SUMMARY AND CONCLUSION

The results of the basic investigations, the theoretical simulations and the experimental firings in the large calibre guns show the important properties of the ETC ignition technology in terms of:

- ignition system with low mass, high geometric flexibility, low volume requirements and short energy transfer times at high interaction temperatures
- adjustable ignition power influencing the whole ignition process
- temperature compensation properties
- combustion control properties

- access to high loading densities by volume effect of plasma radiation

By applying these properties the currently existing performance of conventional 120mm gun technologies could be achieved and slightly improved already during the first phase of the German ETC program. Further increase of the loading density in combination with the application of high energetic propellants, i.e. NENA, will lead to a further improvement of the interior ballistic performance in the 120mm gun. Muzzle energies of more than 15 MJ at muzzle volocities of more than 1.900 m/s can be expected during the following phase of the German ETC program.

The limited requirements of electric energy of only several 100 kJ per shot lead to feasible solutions for the realisation of the power supply technology based on the progress obtained from the R&D programmes performed on the energy density improvement [4,5]. The bandwidth of ETC technologies and its electric energy requirements opens the access to increased firepower and survivability of existing and succeeding main battle tank systems without leaving the currently introduced boundary conditions of the large calibre weapons.

## Acknowledges

## References

[1]   McNab, I.R. et.al.   Experiments with the Green Farm Electric Gun Facility, IEEE Transaction on Magnetics, Vol. 31, pp. 338-343, 1995

[2]   Weise, Th. et.al.   Setup and Performance of a 105mm Electrothermal Gun, IEEE Transactions on Magnetics, Volume 33, Pages 345-349, 1997

[3]   Kappen, K. et.al.   Calculation of Plasma Radiation Transport for Description of Propellant Ignition and Simulation of Interior Ballistics in ETC Guns, 10th EML-Symposium, San Francisco, 2000 (to be published)

[4]   Wisken, H. et.al.   High Energy Density Capacitors for ETC Gun Applications, 10th EML-Symposium, San Francisco, 2000 (to be published)

[5]   Wisken, H. et al.   Light activated Semiconductors for ETC Pulsed Power Applications, 10th EML-Symposium, San Francisco, 2000 (to be published)

# 20-MILLIMETRE ETC GUN EXPERIMENTS AT ISL

KAY A., RAUPP J., LICHT H.-H., HENSEL D., PETER H., ZIMMERMANN K.

ISL, French-German Research Institute of Saint-Louis, BP 34, F-68301 Saint-Louis, France

**Abstract:** Electrothermal-chemical (ETC) propulsion experiments were carried out with a modified 20-mm gun, using exploding wire plasma ignition initiated by a capacitor bank (initial voltage 35 kV). The loading density of consolidated propellants, made of surface coated grains with progressive burn rate, was raised up to 1.3 g/cm$^3$. After optimizing the propellant-wire configuration, a very small amount of plasma energy (only 2 kJ) sufficed to reliably create complete combustion. So far, the best results with a projectile of mass 90 g and a loading density of 1.2 g/cm$^3$ yielded kinetic energies of about 60 kJ, though the maximum gas pressure remained below the acceptable value of 500 MPa. This means an increase approaching 30% as compared with an optimal conventional grain charge. Tests with conventional ignition failed to produce regular combustion of consolidated propellants.

## 1. INTRODUCTION

The various electrothermal-chemical (ETC) concepts, which have been proposed recently to improve the performance of conventional large-calibre guns, actually correspond with their essential aspects. This fact is not surprising, since all new ideas must consider the constraints of limited combustion chamber volume, restricted barrel length, prespecified acceptable maximum gas pressure, critical erosion at higher gas temperatures, and low-density storage of electrical energy.

In a 20-mm powder gun with a modified breech, plasma ignition of solid propellants was studied. Thus, the effort and cost could be kept low. The first ETC experiments with this small-calibre gun at ISL, reported by Zimmermann et al. [1], were initiated in 1996, using a plasma jet to ignite several types of grain charges. As these prospective trials proved the "indirect" injection method to be less satisfying with higher loading densities, "direct" plasma ignition by means of exploding wires, mounted inside the combustion chamber, has been preferentially applied to consolidated propellants in the following years, with relatively small amounts of plasma energy as compared with the explosion energy of the charge. We expect that some of the results, which have been achieved with the 20-mm gun under diverse experimental conditions, will be useful for the application to guns of larger calibres.

## 2. EXPERIMENTAL ARRANGEMENT

Most technical details of the set-up correspond to those described in [1], except for the charge configurations in chapter 2.2.

## 2.1 20-mm ETC gun

The combustion chamber of the gun is depicted schematically in Figure 1, and the substantial data are listed below.
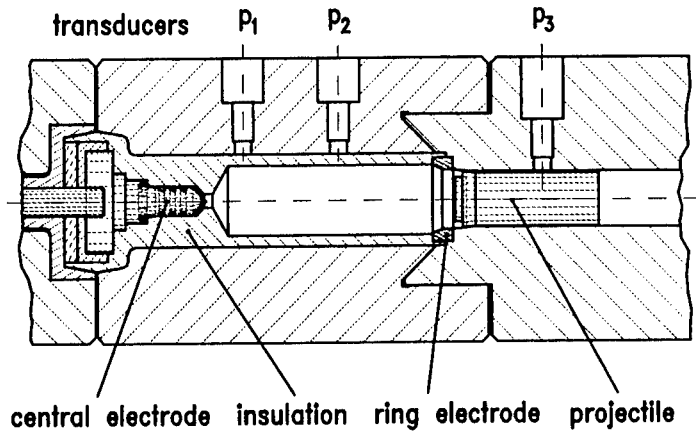


Figure 1: Sketch of the combustion chamber

| calibre | 20 | mm | electrode distance | 83 | mm |
|---|---|---|---|---|---|
| barrel length | 2.43 | m | wire diameter | 0.125 | mm |
| chamber volume | 38 or 40 | cm³ | wire material | | constantan |
| pressure limit | 500 | MPa | insulation material | | polyethylene |
| projectile mass | 90 | g | | | |

The actual volume of the combustion chamber depends on the charge configuration. Two wires are usually mounted between the central electrode which is insulated against the chamber wall by a tubular lining of polyethylene (PE), and the ring electrode which is connected to the chamber wall.

During each firing the pressure histories $p_1(t)$ and $p_2(t)$ at two positions inside the chamber are recorded by Kistler quartz transducers and a third sensor measures the pressure $p_3(t)$ at the initial site of the projectile (see Figure 1). The signal transmission to transient recorders in a protected room is realized by fibre-optic links. The muzzle velocity $v_0$ is determined by means of two light barriers; its regular values range from 950 to 1250 m/s.

### 2.2 Propellant charge and configurations

All results reported in this paper have been achieved with the propellant B19T98 of French origin, equivalent to the German powder A505 (properties: single base, nitrocellulose; grain diameter 2.8 mm, length 3.9 mm; 19 holes of diameter 0.13 mm; standard heat of explosion $Q_{ex} = 4.1$ MJ/kg). In order to reduce the initial burn rate, the grains are coated in a mixture of softening and stabilizing agents (dibutyl phthalate and centralite; mass fraction 5%), before the grains are consolidated into cylindrical bodies with a mean density of 1.5 g/cm³. By this process, the heat of explosion diminishes to $Q_{ex} = 3.5$ MJ/kg, but a favourable progressive burn rate behaviour can be obtained.

Two geometrically different configurations of consolidated cylindrical charges and exploding wires are used. Generally, for technical reasons of production, the charge is composed of three parts.

- 194 -

Configuration (1): In approximately one third of the charge facing the ring electrode the two wires are integrated, whereas they are placed on the outside of the other two parts, as shown in Figure 2a.

Configuration (2): The three parts of the charge are prepared with central bores (inner diameter $\phi_i$ = 7.5 mm, unless otherwise mentioned) and the two wires are laid through this channel (see Figure 2b).
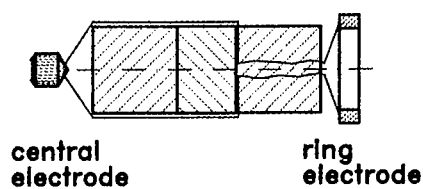


Figure 2a: Charge configuration (1)          Figure 2b: Charge configuration (2)
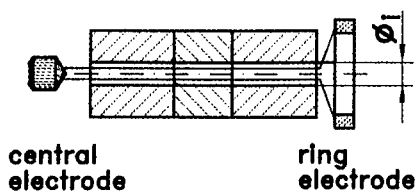
## 2.3 Pulse forming network

The pulse forming network has been well-tried for many years, when it was used with electro-thermal plasma propulsion studies. The electrical circuit is outlined in Figure 3, and its relevant data are listed below.
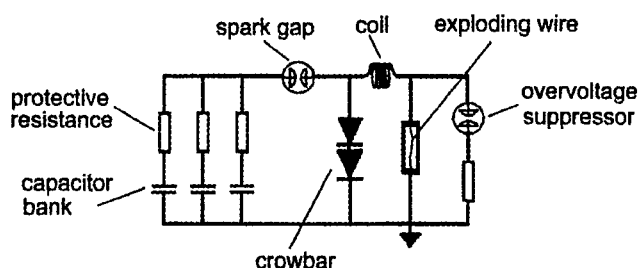


Figure 3: Electrical circuit

| number of capacitors | 1 to 5 | initial voltage | 35 kV |
| capacitance | 5.2 to 26 µF | line inductance | 43 µH |
| stored energy | 3.2 to 16 kJ | coil inductance | 45 µH |
| | | protective resistance | 4.7 Ω |

The discharge of the capacitor bank is initiated by a pressurized spark gap. During the plasma generating discharge, the injected current $I_p(t)$ is measured by a Rogowski coil combined with an integrating circuit, and the variation of the voltage $U_p(t)$ across the electrodes is recorded as well. From these signals, the plasma resistance $R_p(t)$, the injected power $W_p(t)$, and the injected total plasma energy $E_p$ are evaluated after each firing. The efficiency of the injected plasma energy as compared with the stored electrical energy in the capacitor bank normally ranges from 50% to 70%.

## 3. RESULTS AND DISCUSSION

After a decisive modification of the projectile, several systematic test series of plasma ignition were carried out with variations of the loading density, injected plasma energy, charge configuration, and type of propellant; finally, a comparison with conventional ignition was realized.

### 3.1 Influence of the obturating band material

The first firings were performed using projectiles equipped with obturating bands of steel (diameter 20.5 mm). Plasma energies $E_p$ of the lowest level were applied to the charge configuration (1). As soon as the loading density of the consolidated propellant B19T98 was superior to the value of 1.0 g/cm$^3$, even by only a small amount, the pressure in the combustion chamber rapidly rose to maxima augmented considerably by 70%, exceeding the predefined limit of 500 MPa, and significant pressure waves appeared on its rising slope. This effect is clearly demonstrated by the measured pressure histories in Figure 4.
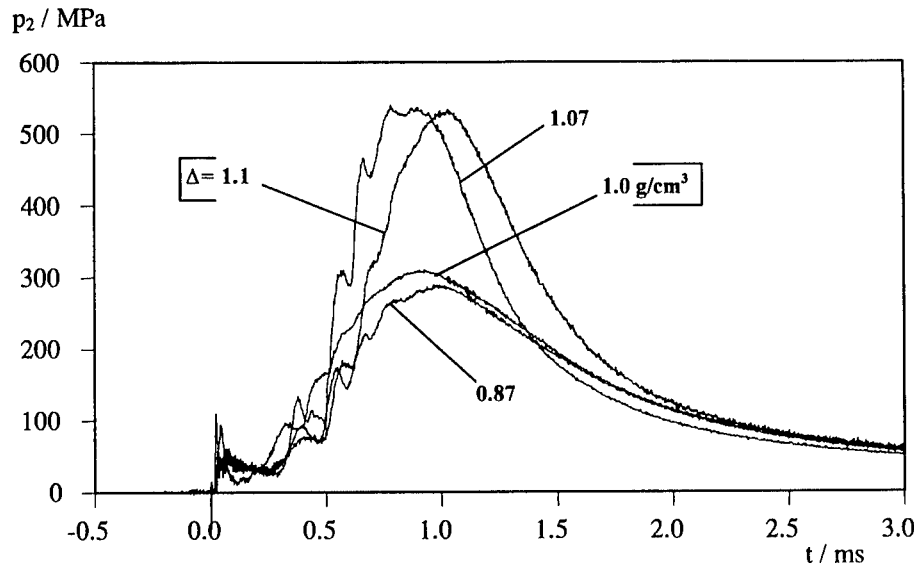


Figure 4: Four pressure histories $p_2(t)$ for loading densities $\Delta$ of about 1.0 g/cm$^3$
(steel obturating band; charge configuration (1); $E_p \approx 2$ kJ)

The problem could be surmounted by replacing the steel obturating band. The projectiles were equipped with soft bands made of polyethylene (PE; diameter 21.0 mm), thus reducing the force of extrusion into the bore. All results reported in the following were achieved with projectiles of this kind.

### 3.2 Performance with higher loading densities

The firings were continued with the modified projectiles, gradually increasing the loading density $\Delta$ up to 1.3 g/cm$^3$. Six typical pressure histories $p_1(t)$ are illustrated in Figure 5a, measured with charge configuration (1) after ignition at the lowest plasma energy level of $E_p \approx 2$ kJ.

Figure 5a: Pressure histories $p_1(t)$ for six loading densities $\Delta$ with $E_p \approx 2$ kJ
(PE obturating band; charge configuration (1))

The comparison with the two pressure curves in Figure 4, corresponding to loading densities of $\Delta = 1.07$ and 1.1 g/cm$^3$, makes the mitigating effect of the polyethylene (PE) band evident. Though the pressure maxima exceed the acceptable limit of 500 MPa for the two highest loading densities $\Delta = 1.25$ and 1.3 g/cm$^3$, the general burning behaviour appears to remain under control, as may be concluded from the "continuous" variation of the shapes with increasing $\Delta$, and from the lack of sudden peaks on the relatively smooth curves.
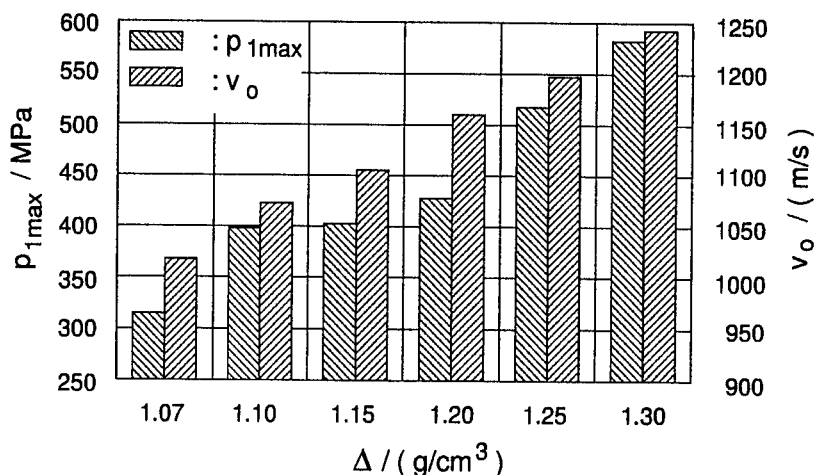


Figure 5b: Peak pressures $p_{1max}$ and muzzle velocities $v_0$ versus $\Delta$

The bar chart in Figure 5b represents the six peak pressures $p_{1max}$ of Figure 5a, together with the corresponding muzzle velocities $v_0$, versus the loading density $\Delta$. The dependence $v_0(\Delta)$ turns out to be approximately linear over the whole range shown, whereas there is a definite increase of the gradient in $p_{1max}(\Delta)$ for values above 1.2 g/cm$^3$.

The data mentioned so far are listed in Table 1. Additionally, the measured values of $p_{2max}$ are noted, which differ considerably from those of $p_{1max}$ in some cases, most probably as a consequence of pressure waves inside the combustion chamber. Also indicated are the calculated values of the initial kinetic energy $E_{kin}$ of the projectile and the total efficiency $\varepsilon$, defined as the ratio of $E_{kin}$ and the total energy available (heat of explosion plus injected plasma energy). The efficiency $\varepsilon$ is found to generally increase with the loading density $\Delta$ and, consequently, with the maximum pressure $p_{max}$.
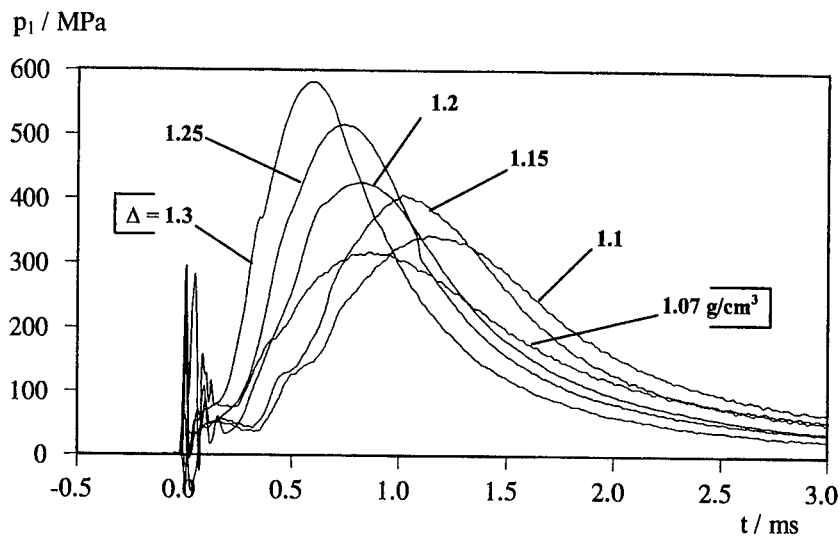
Table 1: Firing results for six loading densities $\Delta$ with $E_p \approx 2$ kJ
(PE obturating band; charge configuration (1))

| $\Delta$ | 1.07 | 1.10 | 1.15 | 1.20 | 1.25 | 1.30 | g/cm$^3$ |
|---|---|---|---|---|---|---|---|
| $p_{1max}$ | 316 | 345 | 404 | 427 | 518 | 583 | MPa |
| $p_{2max}$ | 305 | 329 | 397 | 481 | 540 | 710 | MPa |
| $v_0$ | 1018 | 1072 | 1106 | 1161 | 1197 | 1244 | m/s |
| $E_{kin}$ | 46.6 | 51.7 | 55.1 | 60.7 | 64.5 | 69.6 | kJ |
| $\varepsilon$ | 32.0 | 34.5 | 35.1 | 37.3 | 37.8 | 39.0 | % |

As the best firing performance achieved so far, we would nominate the shot with loading density $\Delta = 1.2$ g/cm$^3$ (see Table 1), which respects the limit for the maximum pressure ($p_{1max}$, $p_{2max} < 500$ MPa). Nevertheless, the efficiency $\varepsilon = 37.3\%$ is comparatively high, and the muzzle kinetic energy $E_{kin} = 60.7$ kJ corresponds to an increase approaching 30% as compared with an optimal grain propellant at its maximum possible loading density of 0.85 g/cm$^3$ (e.g. French propellant GB Sp82, double base, spherical grains; $Q_{ex} = 3.4$ MJ/kg; $p_{max} = 350$ MPa, $v_0 = 1025$ m/s, $E_{kin} = 47.3$ kJ, $\varepsilon = 39.2\%$).

### 3.3 Dependence on the injected plasma energy

The following firing series deals with a variation of the injected plasma energy $E_p$, affecting the combustion process and thus the firing performance. The tests were performed with the charge configuration (2) and a constant loading density $\Delta = 1.1$ g/cm$^3$, connecting between one and five capacitors to the electrical circuit. The presentation of the results follows the same sequence of graphs and tables as in the previous chapter, i.e. pressure histories in Figure 6a, bar chart of $p_{1max}$ and $v_0$ versus $E_p$ in Figure 5b, and the enumerated values in Table 2.

Obviously, with charge configuration (2) the smallest plasma energy $E_p = 2$ kJ does not suffice to create complete combustion, as can be seen from the extremely flat pressure curve in Figure 6a and from the data in Table 2 (e.g. failing efficiency of only 15.2%). Even the amount of $E_p = 3.9$ kJ is not quite sufficient to cause optimal performance, since the efficiency $\varepsilon = 28.5\%$ is still too low. Only from values $E_p \geq 6$ kJ do the shape of the pressure histories and the listed data, like the efficiency, indicate the initiation of regular combustion processes.

Finally, an interesting aspect should be mentioned. From the last two columns in Table 2 one may easily estimate that the lower loading density $\Delta = 1.1$ g/cm$^3$ could be compensated by a higher injected plasma energy $E_p$ between 8 and 10 kJ, in order to yield approximately the same performance as the "best" shot listed in Table 1 with $\Delta = 1.2$ g/cm$^3$ and $E_p \approx 2$ kJ.

Figure 6a: Pressure histories $p_1(t)$ for five plasma energies $E_p$ with $\Delta = 1.1$ g/cm$^3$
(PE obturating band; charge configuration (2))
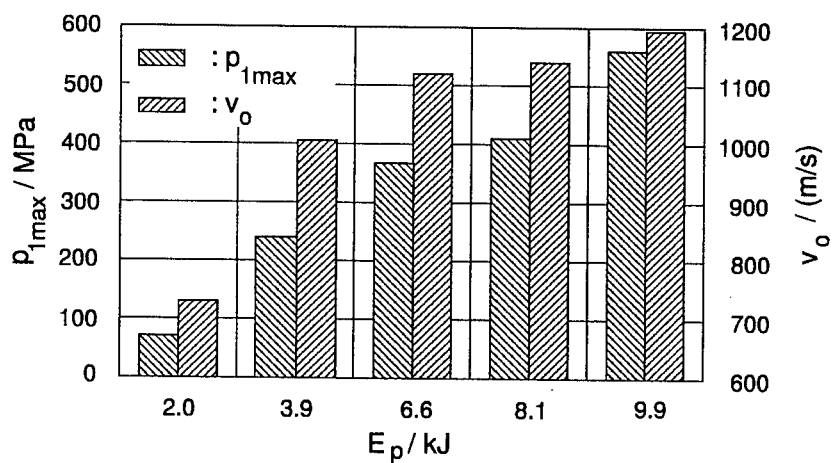


Figure 6b: Peak pressures $p_{1max}$ and muzzle velocities $v_0$ versus $E_p$

Table 2: Firing results for five plasma energies $E_p$ with $\Delta = 1.1$ g/cm$^3$
(PE obturating band; charge configuration (2))

| $E_p$ | 2.0 | 3.9 | 6.6 | 8.1 | 9.9 | kJ |
|---|---|---|---|---|---|---|
| $p_{1max}$ | 70.3 | 239 | 374 | 408 | 562 | MPa |
| $p_{2max}$ | 62.3 | 224 | 389 | 432 | 474 | MPa |
| $v_0$ | 728 | 1006 | 1120 | 1142 | 1193 | m/s |
| $E_{kin}$ | 23.9 | 45.5 | 56.5 | 58.7 | 64.0 | kJ |
| $\varepsilon$ | 15.2 | 28.5 | 34.8 | 35.8 | 38.5 | % |

## 3.4 Miscellaneous exploratory experiments

The findings obtained with the different charge configurations, particularly the poor performance of configuration (2) at lower plasma energy levels, led to tests with a reduced inner diameter $\phi_i$ of the charge (see Figure 2b). Firings with a diameter $\phi_i = 2.5$ mm and the same loading density $\Delta = 1.1$ g/cm³ as before, yielded considerably improved results as compared with $\phi_i = 7.5$ mm. Injecting the plasma energy $E_p \approx 2$ kJ, the efficiency $\epsilon$ increased from 15.2% to 34.8%, and with $E_p \approx 4$ kJ it showed an enhancement from 28.5% to 38.3%. The contrast between the corresponding pressure histories is clearly demonstrated in Figure 7.
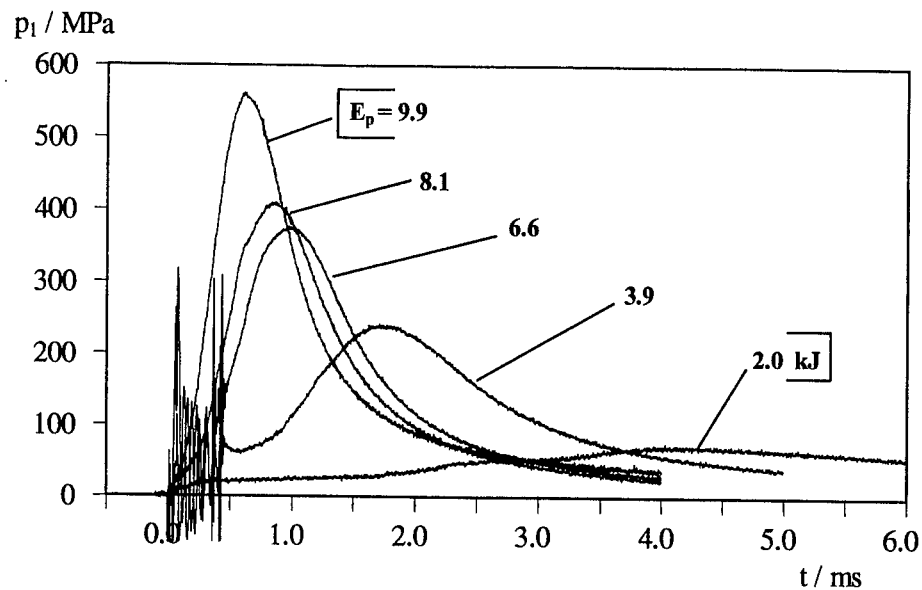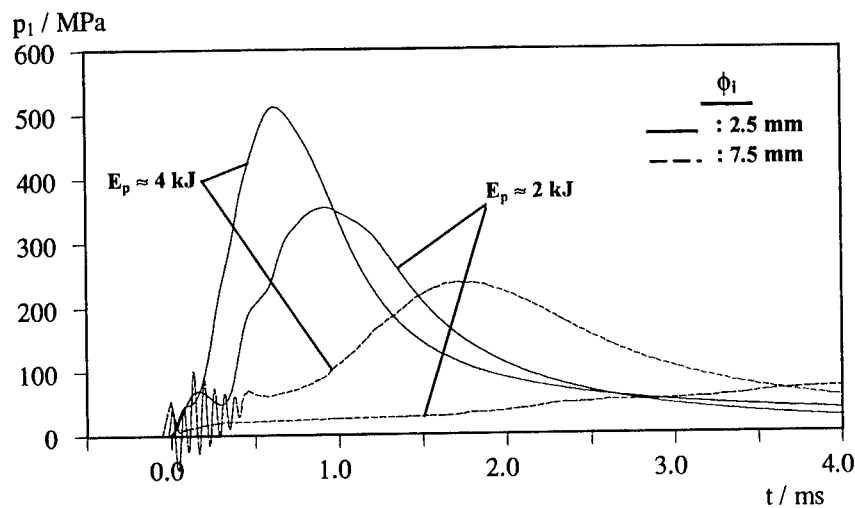


Figure 7: Pressure histories $p_1(t)$ for two plasma energies $E_p$ with $\Delta = 1.1$ g/cm³
(PE obturating band; charge configuration (2) with different $\phi_i$)

Finally, additional experiments were carried out by testing the conventional ignition of consolidated propellants. For this purpose, the charge configuration (2) was used in order to simulate the ignition by exploding wires along the central axis. The channel of diameter $\phi_i = 7.5$ mm was filled with 3 g of black powder, providing the comparatively high amount of about 9 kJ as ignition energy. However, the muzzle velocity never exceeded 1000 m/s with loading densities $\Delta = 1.1$ and 1.2 g/cm³ and the efficiency remained inadequately low at $\epsilon \leq 27\%$.

Besides the above-mentioned propellant B19T98, two other gun powders were tested in the consolidated form after coating their grains.
 – GB Sp82 (its properties are noted at the end of chapter 3.2)
 – B Tu85 (French production, single base, nitrocellulose, tubular grains; $Q_{ex} = 3.55$ MJ/kg)
However, the findings with plasma ignition proved to be disappointing; the combustion remained insufficient and even fragments of unburned propellant were found.

## 4. CONCLUSIONS

The reported investigations with a 20-mm gun have confirmed that the plasma ignition of appropriate consolidated propellants may improve the firing performance to levels of the muzzle kinetic energy which cannot be attained by conventional ignition of grain gun powders; nevertheless, the efficiency is kept relatively high. Experiments with different charge configurations

suggest that the initiation of the combustion develops more efficiently if the contact between the exploding wires and the propellant charge is as close as possible. We intend to apply these results to ETC guns of higher calibre; test launches with plasma ignition in a 60-mm gun have already been initiated.

## 5. REFERENCES

[1]   Zimmermann K., Raupp J., Mura D., Steinbach C., "Experimentelle Untersuchungen zur Anzündung von Festtreibstoffen mit Plasma" (Translation: "Experimental investigations into plasma ignition of solid propellants"), ISL Report RT 508/98, Saint-Louis, France, (1998)

## 6. ACKNOWLEDGEMENTS

# INTERIOR BALLISTICS CODE APPLIED TO ETC CONCEPT

## LEGERET G., BOISSON D.

Giat Industries, Division des Systèmes d'Armes et de Munitions,
Département Balistique Intérieure et Aérobalistique
7 Route de Guerry, 18023 Bourges Cédex, France.

**Abstract :** Propellant ignition thanks to plasma injection is able to increase the ratio [projectile velocity/maximum pressure] for a large calibre gun. Moreover, plasma is expected to ignite more efficiently high density charges.

This paper presents a study about the modification of energy equation and propellant thermodynamic characteristics in a 1D CFD interior ballistics code [1].

Experimental tests made with plasma torches and thermodynamic numerical simulations managed by Giat Industries permitted to determine polynomials giving the evolution of thermodynamic properties (number of mole/kg, force, gamma, flame temperature, enthalpy of formation) versus the composition of the mixture [propellant/working fluid] in atg/kg of C,H,N and O.

These polynomials are specific to an electrical energy. The energy used for the following computations, for grain propellant, is 100 MJ/kg. For other energies, new polynomials have to be determined.

Parametric calculations showed that 1g of plasma working fluid is able to ignite classical propellant charge without rising performances.

Further calculations will be realised adding heat transfers in the 1D and 2D CFD interior ballistics codes, adapted to high density charges.

## 1. INTRODUCTION

Propellant ignition thanks to plasma ignition is able to increase the ratio [projectile velocity/maximum pressure] for a large caliber gun. Moreover, plasma is expected to ignite more efficiently high density charges.

First of all, we list parameters modified by plasma ignition and the method to calculate thermodynamic characteristics. Next, we present different steps occuring during the combustion of grains and new input data corresponding to the plasma action. At last, some parametric calculations illustrate the results giving by this 1D CFD interior ballitics code named MOBI_ETC_1D.

The energy used for these calculations is 100 MJ/kg.

## 2. PARAMETERS MODIFIED BY PLASMA IGNITION

In comparison with usual ignition systems (such as primer tube), plasma modified some parameters such as :

- thermodynamic characteristics,
- burn rate coefficient of propellant grains [2] [3],
- energy equation,
- heat transfers (convective and radiative) between propellant grains, gases and the wall.

## 2.1 Thermodynamic characteristics

Plasma ignition modifies thermodynamic properties of gases :
- N : number of mole/kg,
- Tf : flame temperature (K),
- $F = N.R.Tf$ : force (kJ/kg),
- Cp, Cv : calorific capacities (J/K/kg),
- $\gamma = Cp/Cv$,
- enthalpy of formation (J/kg).

The variation of these parameters is a fonction of the plasma energy.
Experimental tests made with plasma torches coupling with thermodynamic codes applied to plasma injection were carried out by Giat Industries. Thanks to these results,we determined polynomials (for an energy equal to 100 MJ/kg) [4] giving the evolution of thermodynamic properties versus the composition of the mixture [propellant/working fluid] in atg/kg of C, H, O and N.
We can notice that Giat Industries thermodynamics codes applied to plasma injection are able to calculate polynomials for any energies.

## 2.2 Burn rate coefficient

Burn laws ( $= A . P^n$ ) of propellant are different during the plasma ignition [2][3]. They can also be modified after the ignition. In fact, experimental studies show that above all the coefficient A is influenced.
These new laws are in progress. Waiting for them, we plan the possibility to modify A during and after the plasma ignition.

## 2.3 Energy equation

Energy equation is modified adding energy coming from plasma ( = 100 MJ/kg x mass of working fluid).

## 2.4 Heat transfers

Heat transfer laws determination are also in progress. Indeed, like burn rate coefficient, we need to have an important number of experimental results. The end of this task is expected at the end of December 2000.

## 3. CALCULATION PROGRESS

To organize calculation progress, we distinguish three steps occuring during the beginning of the shot.

### 3.1 Step 1 : plasma injection

The first step consists in calculating the working fluid mass injected by the torch. Input data allow to determine the gas flow igniter in the chamber (in kg/m/s). This calculation is stopped as soon as the igniter delivers the mass of plasma figuring in input file.

### 3.2 Step 2 : interaction between working fluid and propellant grains

First of all, we calculate the working fluid characteristics thanks to polynomials. This gas begins to ignite propellant grains. Then, at each time step, MOBI_ETC_1D calculates the composition (in atg/kg of C, H, O and N) of the mixture made of working fluid and grains combustion gas. We use polynomials as long as electrical energy is not transmitted to combustion gas.
As soon as we have the following equality :

Plasma energy x mass of working fluid = total gas mass x Cv x Tf

we stop the polynomials action.

### 3.3 Step 3 : Classical combustion of propellant grains

When electrical energy is transmitted to combustion gas (the plasma influence upon thermodynamic properties is completed), we calculate thermodynamic properties of the mixture made of gas coming from step 2 and new combustion gas.

## 4. INPUT DATA CORRESPONDING TO PLASMA INJECTION

In order to realise calcultations dealing with plasma ignition, we add specific input data corresponding to plasma injection.
These data consist of :
- minimum and maximum abscissae delimiting ignition zone,
- mass of working fluid,
- plasma injection duration,
- factor coefficient affecting A ($AP^n$)  during plasma ignition,
- factor coefficient affecting A after plasma ignition,
- composition in atg/kg (C, H, O, N) and enthalpy of formation of working fluid,
- composition in atg/kg (C, H, O, N) and enthalpy of formation of propellant grains,
- polynomials coefficients (for 100 MJ/kg for the present case).

## 5. PARAMETRIC CALCULATIONS

### 5.1 Presentation

We choose to study the influence of plasma ignition for a 120 mm gun.
The working fluid used is polyethylene and its action length is above : L = 15 cm.
We present hereafter a comparison between a classical primer tube and plasma. We also study the influence of working fluid mass and action length of plasma ignition upon projectile velocity, maximum pressure and pressure waves.

## 5.2 Results

We study variations in relation to the reference (120 mm ignited by primer tube).
Results are collected in the following table :

| Type of igniter | Projectile velocity (m/s) | Breech pressure (MPa) | Pressure waves (MPa) | Gas temp. (K) |
|---|---|---|---|---|
| primer tube | 1773 | 527 | +6;-6;+32 | 3587 |
| plasma, 1g, L=15cm | 1765 | 522 | +12;-5;+30 | 6686 |
| plasma, 0.5g, L=15cm | 1768 | 523 | +10;-5;+30 | 6633 |
| plasma, 1.5g, L=15cm | 1761 | 514 | +12;-7;+30 | 6734 |
| plasma, 2g, L=15cm | 1756 | 512 | +15;-10;+30 | 6753 |
| plasma, 2.5g, L=15cm | 1755 | 505 | +18;-12;+30 | 6776 |
| plasma, 3g, L=15cm | 1752 | 504 | +18;-15;+28 | 6800 |
| plasma, 1g, L=7.5cm | 1765 | 522 | +12;-5;+30 | 6686 |
| plasma, 1g, L=2.5g | 1764 | 518 | +11;-4;+29 | 6738 |

Table 1 : parametric calculations results

Regarding to the pressure waves, there are 3 peaks (1 positive, 1 negative and 1 positive).
We present hereafter figures showing pressure curves (at the breech and at the forcing cone)
calculated for a primer tube igniter and for a plasma made of 1g of polyethylene.

## 6. CONCLUSION

MOBI_ETC_1D allows to test plasma ignition. Indeed, we can choose the mass and the type
(polyethylene, polyoxymethylene, methane ...) of working fluid, minimum and maximum
abscissae delimiting ignition zone. We can calculate the interaction between a type of working
fluid and a type of propellant (single or multi-base with or without solvent, LOVA...).
Results obtained show that plasma ignition doesn't change a lot performances for coventional
charges. We can notice the low value of electrical energy injected (above 100 kJ). Moreover,
we don't take into account burn laws and heat transfers corresponding to plasma. Then, we
plan different further works in order to have a more accuracy code, validated thanks to
experimental tests.

## 7. FURTHER INVESTIGATION

This first version of the 1D-code is not fully validated. We expected interesting experimental
results in June 2000.
We have to intoduce burn laws and heat transfers laws in MOBI_ETC_1D.
We are developping two versions of 2D-CFD-codes. The first will be able to take into
account the same input data that MOBI_ETC_1D, plus the minimum and the maximum
diameters delimiting ignition zone (ex : annular concept of igniter). A second version will be
able to calculate the interaction between a plasma and a high density propellant.

## 8. ACKNOLEDGEMENTS

## 9. REFERENCES

[1]     'User's manual of MOBIDIC 1D code version n°3'
        17 October, 1996
        SNPE Rpt _ Centre de Recherches du Bouchet _ France
        Autor : R. BRIAND

[2]     'Modeling flame spread in plasma ignited gun charges'
        17-23 September, 1996
        16th International Symposium on Ballistics _ San Francisco _ CA _ USA
        Autors : A. WILDEGGER-GAISSMAIER, G.P. WREN, A. HOSANGADI

[3]     'Modelling enhanced gas generation rates in a 155mm ETC gun'
        15-19 November, 1999
        18th International Symposium on Ballistics - San Antonio _ TX _ USA
        Autors : C.R. WOODLEY and G.F. SAVELL

[4]     'Determination of polynomials Force, Number of  moles, Flame temperature versus the values of C,
        H, O and N atg/kg and of enthalpy of formation'
        November 1999
        Note N° 2660/EME/99 _ Giat Industries _ France
        Autor : L. BRUNET
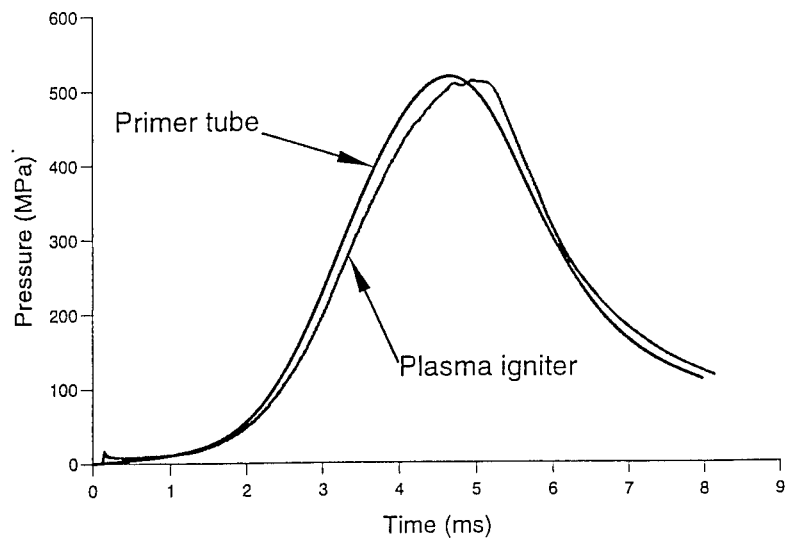
Figure 1 : Breech pressure calculated for a primer tube igniter and for a plasma ignition
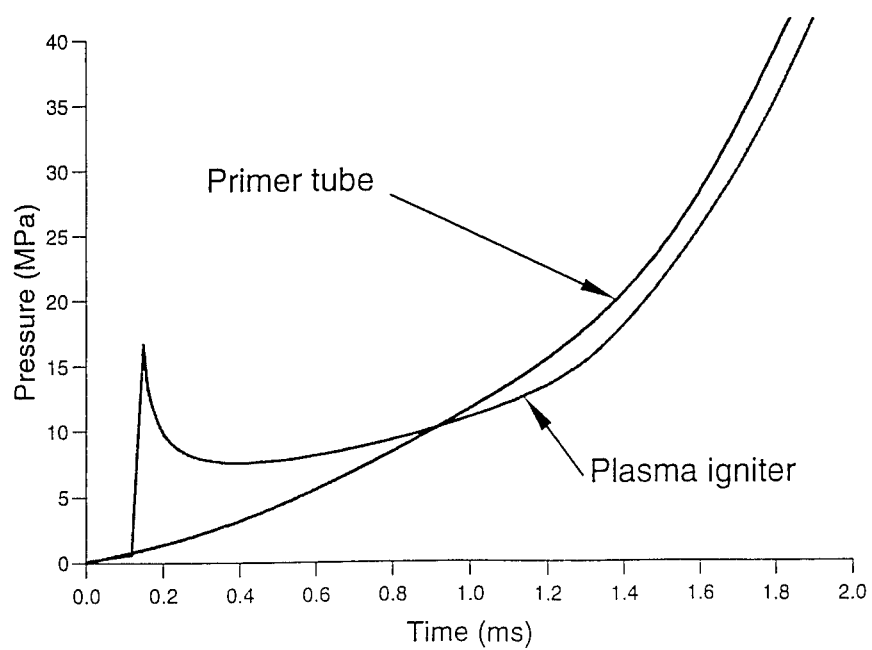


Figure 2 : Breech pressure calculated for a primer tube igniter and for a plasma ignition (ZOOM)
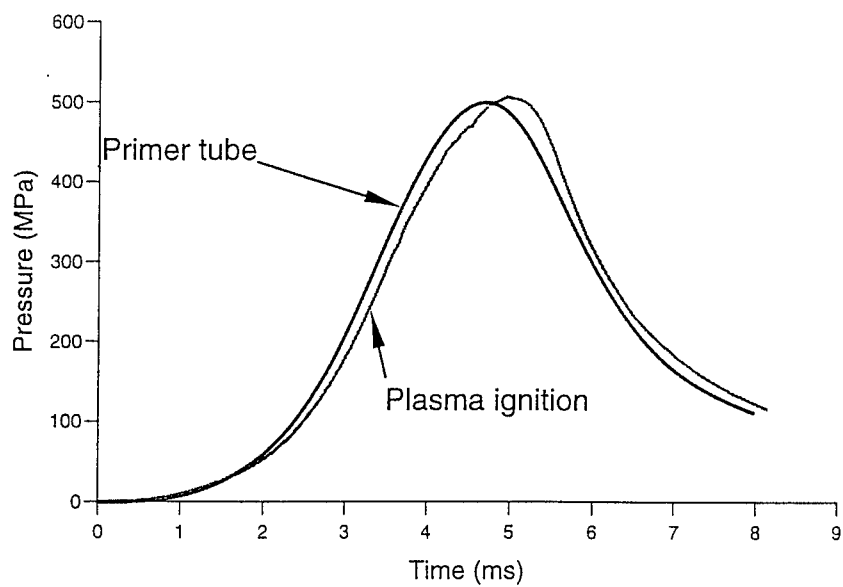
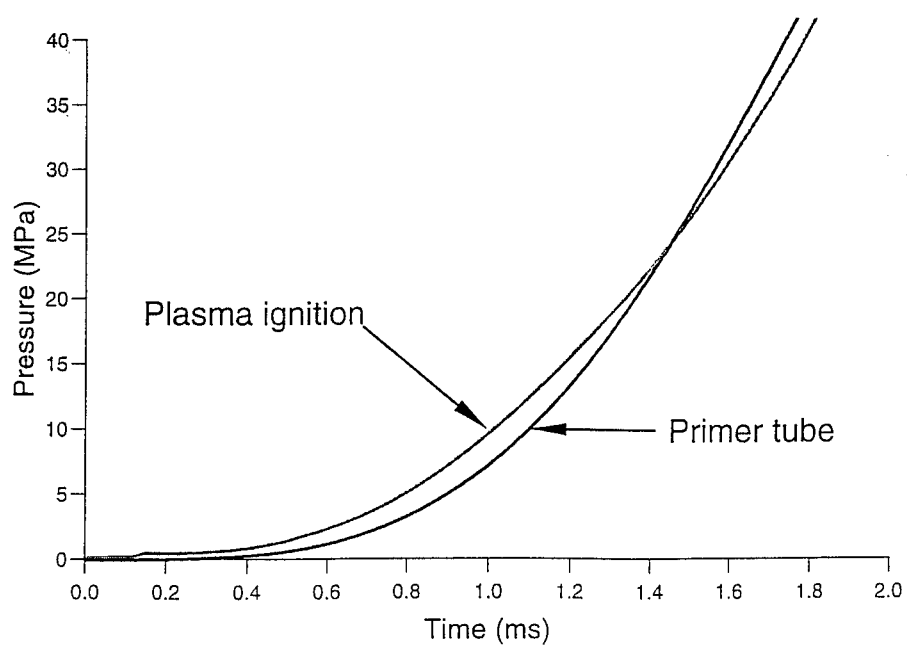Figure 3: Forcing cone pressure calculated for a primer tube igniter and for a plasma ignition



Figure 4: Forcing cone pressure calculated for a primer tube igniter and for a plasma ignition (ZOOM)

# ARTYFIRE - A BELGIAN FIELD ARTILLERY FIRE CONTROL COMPUTER PROGRAM

## DYCKMANS G. [(1)], GOOR R. [(2)], VANCRAEYNEST K. [(3)]

(1) KMS-ABAL, Royal Military Academy, Department of Ballistics & Weapon Systems, Belgium
(2) Artillery School – 6A, Office of Research and Artillery Studies, Belgium
(3) GST-DTT, Army Staff, Belgium

**Abstract :** Artyfire is the name of a computer program that is used since July 1996 by the Belgian field artillery battalions and batteries for fire control processing. The software has been entirely developed within the Belgian Army. This paper presents the background for developing Artyfire, it describes in a general way the main algorithms that are used in the software, and it discusses the on-going activities in this area.

## 1. FIRING ELEMENTS

It is clear that a fire control computer program must be able to compute firing elements i.e. quadrant elevation, azimuth of fire and fuze setting. This can be achieved in several ways. For many years, calculations were based upon the numerical and graphical firing tables, and the so-called manual gunnery techniques were applied. With the advent of electronic pocket calculators and the first computer systems, people started to approximate the contents of the numerical firing table by a series of polynomial functions, the coefficients of which were stored in the calculating device, and the well known correction theory was programmed. This was a big step forward as it allowed computing firing elements much faster. With the continuing increase in computer memory and computational speed, more and more data of the firing table could be stored in the calculators. Even with different propelling charges selected for a single mission, calculating firing elements was no more a major factor responsible for the time delay between the fire mission request and the impact of the rounds on the battlefield.

It is important to underline the fact that the use of firing tables to compute firing elements is a technique that is less accurate than obtaining firing elements by applying a trajectory simulation model, e.g. the modified point mass trajectory model MPMM [1]. Only in standard ballistic, meteorological and topographical firing conditions, used to produce the left side of the basic table F of a firing table [2], the two techniques give exactly the same results. From the moment that perturbations have to be accounted for (i.e. differences between the actual and standard firing conditions) and corrections must be introduced, results start to deviate from those predicted by direct trajectory calculation.

Some perturbations cannot be accounted for in manual gunnery techniques. One example is the fuze mass. One should know that elevations listed in a firing table are only valid for a single weapon and ammunition combination, including the type of fuze. Using the same information for another fuze is inherently an approximation. Another example is the latitude of the gun. There are of course tables (H and I) to compensate for the Coriolis effect, but latitude also influences the value of the earth's acceleration at sea level ($g_0$). For the production of firing tables, the value of $g_0$ is normally taken to be a constant, corresponding to 45 degrees latitude.

Present computers allow to calculate trajectories using the MPMM with incredible speed and to compute firing elements within less than a second. Also, we know that the computational accuracy contributes to the overall accuracy of a fire mission. These facts have been the main reasons for the Belgian artillery community to implement the MPMM for the calculation of firing elements and break with the tradition of using polynomial approximations (compensation of firing tables) to an approximate solution (firing tables). We do emphasize, however, that the manual gunnery technique is still being used as a backup method.

The MPMM has been implemented according to STANAG 4355. A Runge-Kutta fourth order scheme is used for the numerical integration of the differential equations of motion. The integration time step is variable, and depends upon the projectile's velocity to acceleration ratio. Both range closure (stopping subsequent trajectory calculations at the target's altitude and iterating on quadrant elevation to achieve convergence in range) and height closure techniques (stopping subsequent trajectory calculations at the target's range and iterating on quadrant elevation to achieve convergence in height) have been programmed.

Verification of the correct implementation of the aerodynamic and ballistic data, and correct use of the equations of motion and iteration algorithms in different meteorological and geographical conditions, has been done by means of the (US) Fire Control Trajectories (FCT) for M109A2 155 mm (HE M107, ICM M483A1, WP M110, ILL M485).

Regarding trajectory calculations, it is worthwhile to note that the physical model, the aerodynamic and ballistic data, and the fitting factors constitute a coherent set not to be separated at any time. Problems can therefore arise in circumstances where this basic rule is violated. As an example, we mention the particular case of the recently purchased 105 mm LG1 MkII gun. The constructor of the weapon system has provided the Belgian artillery with a firing table for HE M1 ammunition. This table had been calculated with the point mass model. As the Artyfire program strictly applies STANAG 4355 for trajectory computations, implying the use of the MPMM, the fitting factors provided along with the firing table could not be used. In order to avoid expensive ballistic range firings, appropriate fitting factors have been derived directly from the contents of the firing table with the MPMM, by considering the information in standard conditions (left side of table F) as a particular set of real dynamic firing results [3]. Future use of the NATO Artillery Ballistic Kernel (NABK) [4-5] software by both developers of fire control software and people responsible for analyzing dynamic firings and deriving fitting factors will avoid this kind of problem.

## 2. FIRING APPRECIATION

Firing elements can be computed for a specific gun, ammunition (projectile, propelling charge, fuze), aiming point, and firing method (e.g. adjust fire, fire for effect with use of

registration corrections, etc.). Determining the guns to participate at the fire mission, the ammunition to be used, the aiming points, the firing method, and the number of rounds to be shot at the target in order to obtain the desired effect, are all technical problems to be dealt with by what we call the fire appreciation part of a fire control program. It concerns the analysis of a fire request. Performing this analysis logically precedes the computation of firing elements.

Contrary to computing firing elements, where only one solution is correct for each type of fire (low and high angle fire), i.e. the quadrant elevation and azimuth of fire to be used by a specific gun to hit a specific aiming point using specific ammunition in specific firing conditions, there are several solutions to the fire appreciation problem. The desired effect on the target can be obtained in multiple ways: platoon, battery or battalion fire; low or high angle fire; HE or ICM ammunition; low or high zone charges; adjust fire or immediate fire for effect firing techniques; etc.

The Artyfire program has been conceived to assist the user in quickly finding an appropriate solution to the fire appreciation problems. This feature distinguishes the program from many other existing fire control software applications used on battery or battalion level.

The fire appreciation in Artyfire is performed in two consecutive steps: a first step to choose a possible {platoon, propelling charge, firing method} combination, and a second step to select the {projectile, fuze} combination, and to compute the necessary number of rounds and the aiming points. A filtering system is used in the first step. At the top of the filters are all available platoons and propelling charges. The user of the program can interactively activate or deactivate each platoon, and manage a so-called "propelling charge politics table". This table contains the availability of each propelling charge and the minimum and maximum ranges that correspond to each charge. Based upon this information, and taking into account the platoon to target distance, the software attributes to each platoon a set of possible charges. Then, in a subsequent filter, each possible {platoon, charge} combination is automatically tested against each possible firing method, using specific artillery technical procedures. For example, the program checks whether the target is located inside the registration correction transfer zone during the examination of the registration correction firing method. Another example is for the so-called Met+MVV (Muzzle Velocity Variation) firing method, where Artyfire checks whether MVV data is available for the specific propelling charge. Although many tests are performed, going through the filtering system ultimately resulting in a set of possible {platoon, propelling charge, firing method} combinations, takes less than a second of computation time on today's commercially available computer systems. All possible combinations are presented to the user. These are all technically valid solutions among which the user can now make his choice.

Once the firing method, the platoons and the propelling charges have been selected, Artyfire automatically calculates the number of rounds and the aiming points. Depending upon the weapon system and the ammunition availability, calculations are done for HE-PD (Point Detonating), HE-Time and ICM ammunition. Again, these calculations take less than a second, and based upon the results shown to the user, one can now complete the list of data necessary for computing firing elements.

The algorithms that are used for computing the number of rounds and the distribution of the aiming points are based upon those present in the Gunfire software [6]. The latter has been developed in 1990 by the department of ballistics & weapon systems of the Belgian Royal Military Academy, and has been used as a demonstrator for a fire control program belonging

to a fully automated field artillery system. This means that a distinct aiming point can be attributed to each gun. The present Belgian artillery system does not have numerical data display devices in the guns, and the firing elements are thus to be transmitted by voice from the computing center to the howitzers. This limits the maximum number of aiming points to the number of platoons participating at the fire mission (with all howitzers in a platoon using the same firing elements). Based upon the results of numerous computer simulations, where fire missions in different circumstances were simulated and firing solutions for obtaining different fractional damages on targets were evaluated, formulas were developed to efficiently adapt the Gunfire algorithms and to cope with the particular problem of not having a fully automated system.

Before using the Artyfire program, all the checks necessary for arriving at a set of possible solutions had to be done manually. This is just a minor task if one has at its disposal a single propelling charge, a single type of projectile and fuze, and if one has decided well before performing the fire mission what firing method is to be used. However, in real circumstances, where one has a lot of different types of ammunition, where several technically valid firing methods are possible, where one has to cope with all kinds of targets, efficiently performing a fire appreciation without the assistance of a computer program can become a nightmare.

Also before using the Artyfire program, the determination of the number of rounds was done by means of a graph reflecting the number of rounds to be fired as a function of the target radius (circular targets). A look-up table was used to classify targets into different target types, depending upon their protection level. The curves in this graph were calculated with the same algorithms as those used in the Gunfire program. What is important to know, however, is the fact that these curves had been calculated in specific firing conditions (for a single gun to target range, a particular firing method, a particular ammunition, etc.). Many countries use such look-up curves or tables in their fire control process. In a certain way, one could compare them with firing tables, where the left side of table F has been calculated in a single set of firing conditions. There is, however, an important difference. A firing table contains corrections to take into account the effect of perturbations. This was not so for the manual fire appreciation approach. The same graph, calculated in specific conditions, was used for all possible firing conditions. We know that this is an approximation, since the firing conditions influence the value of the global accuracy, generally represented by ECEP (Equivalent Circular Error Probable), and that the ECEP value influences the number of rounds (as well as the position of the aiming points). Therefore, the Belgian Artillery has decided not to implement standardized graphs or tables in the Artyfire program. The Gunfire algorithms, slightly adapted as explained earlier, were implemented into the software, and techniques have been developed for obtaining the necessary entry data for these algorithms in real conditions (e.g., the values of the ECEP and the lethal area). This decision has been made after comparing the Gunfire results to those obtained by the manual approach, using computer simulations [7].

## 3. FUTURE

The Artyfire program has served the Belgian field artillery community well since July 1996, and is still in operational service today. Switching from the manual gunnery to the application of the MPMM for computing firing elements was a big step for many people. A change of ideas relative to artillery technical matters had to be introduced in the Artillery School and the operational units. Training of personnel had to be adapted, taking into account the fact that the manual gunnery techniques must still serve as a back-up.

Developing the software in-house had the big advantage of being able to keep control of the techniques that are used, which in our opinion is necessary for further improvement of the program.

It is the intention of the Belgian field artillery to develop within the Belgian Army an operational processor for the future fully automated fire control system. The current Artyfire program will serve as a prototype for this new software called Artyfire_ADA. The Artyfire software has been written in the MODULA-2 computer language, and in a DOS environment. For reasons of maintainability of the product, Artyfire_ADA will be written in a more object-oriented approach, using, among other languages, ADA 95 in a WINDOWS environment. Also, the new software will implement the standardized NABK for computing trajectories and firing elements. Consequently, it will allow for the use of a NATO standardized database format for fire control input data, which is an important advantage in view of a possible exchange of ammunition between countries on the battlefield.

Concerning the fire appreciation, the Belgian artillery is satisfied with the way the current Artyfire program is fulfilling its role as an assistant for selecting an appropriate firing solution. One must realize, however, that the current approach is still subject for further improvement. Due to time constraints, the current available technology, as programmed in Artyfire, will most likely be entirely transferred to the Artyfire_ADA program. In the meanwhile, discussions in NATO/PFP AC/225 LG/4-SG/2 have revealed that several nations are interested to start discussing and comparing technologies used for fire appreciation.

## References

[1]    STANAG 4355, the Modified Point Mass Trajectory Model (1994)
[2]    STANAG 4119, Adoption of a Standard Cannon Artillery Firing Table Format (1972)
[3]    STANAG 4144, Dynamic Firing Techniques to Determine Ballistic Data for Cannon Artillery Firing Tables and Associated Fire Control Equipment (1984)
[4]    STANAG 4537, NATO Artillery Ballistic Kernel (NABK) (1998)
[5]    O. Dullum, G. Dyckmans, R.F. Lieske, Y. Runfola, Artillery Ballistic Kernel, 16th Int Symp Bal, San Francisco, USA (1996)
[6]    G. Dyckmans, E. Celens, Automation of Fire Request Appreciations, 12th Int Symp Bal, San Antonio, Texas, USA (1990)
[7]    G. Dyckmans, Een bataljonstest op computer (in Dutch) – Aie tijdschrift 3/93 (1993)

# NATO Artillery Ballistic Kernel

## HAARSETH E., CAPPELEN D., DULLUM O.

Norwegian Defence Research Establishment, P.O. Box 25, N-2007 Kjeller, Norway

**Abstract** : The NATO Artillery Ballistic Kernel (NABK) provides a software module for external ballistic calculations, primarily for spin stabilized artillery shells. The intent has been to develop a standardized ballistic software library for NATO where sharability, reusability and portability are three main goals. The design is a four layered structure to enhance reusability and enable the user to remove top layers. Many of the implemented algorithms are already standardized technology in NATO such as the Modified Point Mass model. This paper describes the concept and rationale of the program. Further, it gives details of the design and functionality of the software, as well as the quality assurance. Finally, it touches planned usage in Norway.

## 1. INTRODUCTION

The NATO Artillery Ballistic Kernel (NABK) provides a software module which is capable of computing exterior ballistics, primarily for spin stabilized artillery shells. The intent has been to develop a standardized package of ballistic core software for NATO, where sharability, reusability and portability are three main goals.

The rational for developing a common ballistic module has mainly been two things; sharing development and maintenance costs, and standardization in the area of implementation. Traditionally, NATO countries have had their own national ballistic module. This has been both costly to develop and maintain and usually not compatible with equivalent models of other countries. The intent of the NABK project was therefore to develop a generic ballistic kernel that would satisfy requirements of all participating countries. The equations of projectile flight have been standardized in [1], so the next natural step of this process was to develop a common implementation. Another spin-off effect was that the storage format of required aerodynamic and ballistic data had to be standardized as well. This both encourage and ease interchangeability of ammunition to a large extent. The long-term goal of the effort is to continually update the software to support all artillery ammunition adopted by NATO countries.

The project was started in March 1995, and is organized as a working group under NATO Army Armament Group, AC 225, Land-group 4, Sub-group 2. Currently, eleven NATO countries participate in the effort, Belgium, Canada, Denmark, France, Germany, Italy, Netherlands, Norway, Turkey, the United Kingdom and the United States. Policy for participation of Partnership for Peace countries is currently under development.

This paper gives an overview of the capabilities and architecture of the NABK software as well as presenting the project. Further, it will touch some Norwegian applications that use the NABK as the ballistic engine. The project has earlier been presented in [2] and [3].

## 2. OVERVIEW OF SOFTWARE

The main task for the NABK is to produce gun instructions consisting of quadrant elevation, azimuth of fire and fuze setting. The NABK is a software library and does not provide any interface to interact with humans. The module therefore has to be integrated with an application providing the interface also known as the Operational Processor (Opr). The implementation is in the Ada95 language, which is fully object-oriented and is particularly design for use in safety sensitive software. The Ada95 language is also very standardized in order to minimize the need for porting.

The heart of the NABK software is the implementation of the modified point mass (MPM) model defined in [1]. The modified point mass model is a five degrees of freedom model, including the three dimensional motion of the center of gravity, spin and the vector called "yaw of repose". This vector represents the equilibrium angle of yaw, or angle between the main projectile axis and the velocity vector. The modified point mass model is therefore a compromise between the three degrees of freedom point mass model and a full six degrees of freedom model. While the first does not give the desired accuracy and the latter, at least today, require too much computation time.

Another module of the NABK contains an iteration scheme to solve the classical ballistic problem of computing a trajectory that hits a certain aiming point. The module makes an initial guess of the quadrant elevation and azimuth of fire to be applied. Then a trajectory is simulated and the quadrant elevation and azimuth of fire is adjusted based on the miss distance. The process continues until the trajectory reaches the desired aiming point.

The NABK also provides some gunnery related functionality required for trajectory calculations, computation and transfer of registration corrections and muzzle velocity management. The computation of registration corrections is supported by two methods called mean point of impact and precision. In both cases a percentage correction in range and fuze setting as well as correction in azimuth in mils are calculated. The mean point of impact method compares the mean ground or air burst location with the desired aiming point. The precision method compares the calculated firing elements (quadrant elevation, azimuth of fire and fuze setting) and actual firing elements obtained by repeated single shot firings. Computed registration corrections are stored in an internal database and transferred to later fire missions according to predefined criteria.

Muzzle velocity variation is defined as the difference between the predicted and measured muzzle velocity. The predicted muzzle velocity is based on the standard muzzle velocity with correction for non-standard propellant temperature and projectile mass. Muzzle velocity variations are postulated to consist of two components, loss due to tube wear and variation due to propellant lot. The task for the muzzle velocity management system is, based on muzzle velocity measurements, to separate and continually update estimates of the two components. The concept is taken from [4]. The muzzle velocity variation components for tube wear are normalized to the top charge, while the components for propellant lot are stored for each individual charge. The corrections are transferred to later fire missions according to predefined criteria.

The description of the firing problem is given as a gun-aiming point pair in addition to the type of ammunition. Locations can be given as UTM (Universal Transverse Mercator) or geographic coordinates. The number of rounds to be fired in order to achieve a desired

percentage of damage based of effectiveness calculations, as well as dispersion of the aiming points, must be provided by the Operational Processor.

The user can either specify the charge to be fired or the NABK can select the charge. In the latter case the NABK will select the lowest charge that reaches the specified range with a user defined margin. Further the user can specify a list of available propellant models to select from.

## 3. ARCHITECTURE

The design is based on a four layered structure to enhance reusability. The idea is that any layer only should depend on layers below. This enables the user to peel of one or more of the top layers and start the application development from there. Figure 1 illustrates the layered software architecture and gives the connection between those layers. The main frame represents the interface to the OPr when the NABK is used as a whole package.

*FCI Database Layer* provides fire control input data to all other layers in a suitable format. Fire Control Inputs (FCI) include aerodynamic coefficients, physical data (mass, moments of inertia, caliber etc.), propulsion characteristics, payload characteristics, probable error data and legality data (legal combinations of howitzer, projectile, fuze and propellant charge). The fire control inputs data are stored either as a set of ASCII-files with a predefined format or embedded in the source code. The first option can be used when the field computed provides an external storage medium (e.g. hard disk) and is more practical in a prototype version where data would need to be changed easily. The second option would be required in a fielded version when the computer does not provide an external storage medium.

*Equations of Motion Layer* implements the physical equations of motions for projectile flight and the integration scheme required to compute single trajectories. The layer has appropriate equation terms for projectiles with rocket or base burn assistance, and for computation of submunition trajectories.

The *Computation Layer* contains the iteration scheme to find the firing elements (quadrant elevation and azimuth of fire) to reach a certain predefined aiming point. The layer estimates initial values of the firing elements. The trajectory is then simulated and stopped at the desired aiming point height, and the firing elements adjusted until the desired range is achieved. Alternatively, the trajectory is stopped at the desired range, and the firing elements adjusted until the desired aiming point height is achieved. The two methods are referred to as range closure and height closure respectively.

*Fire Mission Layer* administrates computation of firing elements for a fire mission involving single or multiple guns. The layer also implements gunnery related functionality as registration corrections, muzzle velocity management, crest clearance, air corridor violation checks and charge selection. To be able to perform these tasks the layer needs a number of inputs. In figure 1, the inputs are represented boxes overlapping the main frame. Two of the inputs, map modification and unit database, are mandatory, while the other categories are optional
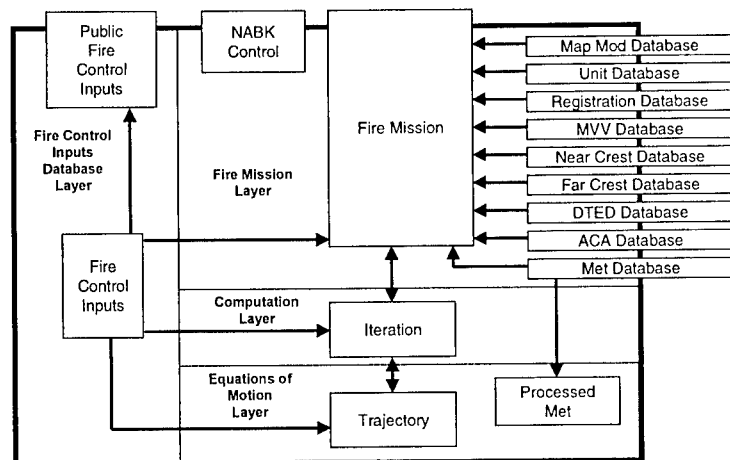
Figure 1 : software architecture

The following sections describe the required input.

- *Map Modification Database* stores information required to process UTM coordinates, and consists of the ellipsoid, the primary UTM grid zone and, when short UTM coordinates are used, a reference point defining the lower left corner the operation area.
- *Unit Database* stores information about all supported units, and includes type of howitzer and their locations.
- *Registration Database* stores registration corrections in terms of percentage for range and fuze setting and mils for azimuth or deflection. The module also provides functionality to select the best set of corrections to be applied to later fire missions.
- *MVV Database* stores corrections in muzzle velocity to compensate for two relations; loss in muzzle velocity due to tube wear and lot-to-lot variations of propellant charges. The module also provides functionality to select the best set of corrections for later fire missions.
- *Near Crest Database* stores obstacles in front of the howitzer. Near crests are normally identified by the gun crew.
- *Far Crest Database* stores hills, mountains etc. between the gun and the target locations. The format to represent a far crest is called fence. The "poles" of the fences represents coordinates of high points in the terrain that may obstruct the trajectories.
- *DTED Database* contains far crests in terms of Digital Terrain Elevation Data. The database is configurable and can process both the DTED1 and DTED2 formats. All crest databases contains functionality to check computed trajectories for crest violations. Additional clearance height is added to the crests in order to increase the probability that the crests in fact are cleared, and for safety when firing above areas with friendly troops. The far crest database and DTED database both store information about far crests, but in different format. The first uses a manual approach where crests are taken from a regular map, while the second access a database with elevation data.
- *ACA Database* stores reserved corridors for air traffic above the battle area, as well as functionality to check computed trajectories for any violation.

- *Met Database* stores meteorology data in terms of a standard NATO computer met message, as well as back up met data based on climatology. The standard NATO computer met message contains wind, air pressure and air temperature at different levels above the ground.

## 4. QUALITY ASSURANCE

The NABK is exposed to a rigorous set of tests during qualification. The NABK could potentially be used in a safety critical system, i.e. there is no human in the loop. Most other use will at least be in safety sensitive systems, even though they do not strictly satisfy the safety critical definition.

The suite of tests can be divided into three main areas, functionality test, invalid-input test and accuracy test. All tests are performed with autotest software, which read the input from script files and call appropriate services in the NABK to perform the tests. The functionality test is exposed to all layers to ensure that each individual service provide the documented functionality and gives the expected output according to the given input. The invalid-input test suite checks whether the NABK responds properly when input considered to be invalid is inserted. The appropriate response is either an exception or a status message depending on the severity. The last area, accuracy tests, is the most extensive area. A large number of trajectories are pre-calculated by some independent ballistic software, and the NABK is then checked whether it generates the same output.

In addition to the qualification tests the design and implementation are continually review and improved.

## 4. APPLICATIONS

There are different potential uses. The primary target systems are technical fire control systems. Other areas of usage are R&D (Research and Development) applications, software to compute firing tables and software for range safety.

Norway has plans to use the NABK in most of these areas. The main reason for joining this program is for use in a new fire direction system called Odin2. The implementation of the system will start in the very near future. Odin2 contains functionality for tactical fire planning and prioritizing of targets as well as technical fire control where the NABK will be a vital part. We also have an R&D application and application to generate firing tables under development.

## 5. STATUS AND FURTHER DEVELOPMENTS

The current status of the project is that a version 1.5 was released in July 1999. The next large step will be a version 2.0 planned to be released in mid 2000. The new version contains improvements both in the area of functionality and implementation. A main goal will be to improve the code quality to meet requirements for safety critical systems, which is not completely true for the current version.

Improvements in the area of functionality include support for mortars. The current version supports trajectories using point mass model in general. However, some features required by mortars will be added. The new version will also be extended to support new types of terminal guided munition.

In the area of code quality two unwelcome Ada features from a safety point of view will be removed; the use of concurrency and dynamic memory allocation. These features may increase the risk of run time failure.

An improvement beyond version 2.0 is the use of gridded meteorology data generated by a forecast model. In parallel to the NABK program, there is an effort to adopt a meteorology-forecast model, which will be run in connection with the NABK and provide this met data. The interface is a so-called 4-dimensional gridded met message where each grid location contains a separate vertical met profile. Further, several grid blocks representing different points of time may be specified. This defines the fourth dimension.

Other improvements are support for rocket artillery, and possible also tank guns and small arms.

## 7. POLICY FOR DISCLOSURE AND USE

Currently, the NABK, including source code and documentation, may only be disclosed to NATO member governments and their defense industry. However, applications with executable version of NABK may be exported to non-NATO countries as long as national export laws are satisfied. Details concerning disclosure and use of NABK can be found [5]. Policy for disclosure to Partnership for Peace countries is under development.

## 8. CONCLUSION

The NABK offers a standardized ballistic implementation in Ada95 where sharability, reusability and portability have been key words in the development. The effort represents a natural step in the standardization process in NATO. The NABK is also intended to become the standard tool for all exterior ballistic applications within NATO.

## 9. ACKNOWLEDGEMENTS

The authors wish to acknowledge Mr. Jon Miller and Mr. Robert Lieske of TACOM-ARDEC FTAB in the US for their effort in leading the project. The authors also wish to acknowledge representatives from Belgium, Canada, Denmark, France, Germany, Italy, Netherlands, Turkey, the United Kingdom and the United States who have contributed to this program.

## 10. REFERENCES

[1]  NABK STANAG 4355, "Modified Point Mass Trajectory Model", NAAG AC225 (LG/4-SG/2) D/1319, (1996)
[2]  O.Dullum, G. Dyckmans, R. Lieske, Y. Runfola, "NATO Artillery Ballistic Kernel", 16th International Symposium on Ballistics, San Francisco, California, USA, pp. 103-110, (1996)
[3]  A. Sowa, R. Lieske, J. Matts, J. Miller, "Ballistic Kernels – sharable control ballistic simulation software", Preceedings Simulation MultiConference – Military, Government and Aerospace Simulation, Atlanta, Georgia, USA, (1997)
[4]  NABK STANAG 4500, "Muzzle Velocity Management and Prediction", NAAG AC225 (LG/4-SG/2) D/1404, (1996)
[5]  NABK STANAG 4537, "NATO Artillery Ballistic Kernel", NAAG AC225 (LG/4-SG/2) D/1406, (1997)

# INTERMEDIATE BALLISTICS : SHOCK WAVE NUMERICAL SIMULATION AND SMALL SCALE MODELLING

## SENEGAS S. [(1)], BROSSARD J. [(1)], CAYZAC R [(2)], CARETTE E. [(2)]

(1) Laboratory Energetics Explosions Structures, University of Orleans, 63 Avenue de Lattre de Tassigny, 18020 Bourges, France

(2) Giat industries, Centre de Bourges, 7 route de Guerry, 18023 Bourges, France

**Abstract :** The shock wave characteristics are determined by reflected overpressure values on a plane surface. Small scale experiment studies and numerical simulation have been conducted in order to be compared. Experiments have been performed at laboratory scale with a shock wave generator tube confining detonable gaseous mixture. Calculus have been initiated by initial conditions (p, u, T) deduced from scale experimental data. An application of similarity laws allows a comparative analysis of space-time diagrams and damping curves. A discussion will be carry on the initial conditions introduced in the numerical code.

## 1. INTRODUCTION

The ballistics of projectiles needs the knowledge of the intermediate ballistics. The aim of this paper is to observe the representativeness of the small scale experiment compared with the predictive numerical modelling of the shock wave characteristics at the open end tube generator. To do that we use the reflection properties of the shock wave on a neighboring plane surface. In particular the space-time diagram and the reflected pressure decay are investigated in both the cases the calculus and the experiment.

## 2. METHODOLOGY

In this comparative study, it exists two shock wave generators which can be represented by cylindrical tubes. They have the same tube i.d. (d = 40 mm). But they have their own energy source : the one is the gaseous mixture detonation and the other is the powder combustion with projectile presence. Shock wave reflected overpressure is estimated by means of pressure gages located on a plane surface (ground). So, in order to compare the different values, an analysis method is established.

Two sources of energy $S_1(E_1)$ and $S_2(E_2)$ which are located respectively at the altitude of $H_1$ and $H_2$ lead to the same reflected overpressures $\Delta p_{r1} = \Delta p_{r2}$ when their incident wave has the same intensity $\Delta p_{i1} = \Delta p_{i2}$ and the same incident angle $\alpha_1 = \alpha_2$ (Fig. 1).

In the investigated cases the Hopkinson similarity coefficient is imposed by the ratio of energy depositions which create the shock wave at the open end of the tube. The considered expression of the energy E is $pud^3/c$ where p is the generating pressure, d is the i.d. tube and u and c are respectively the particle and the sound velocities.
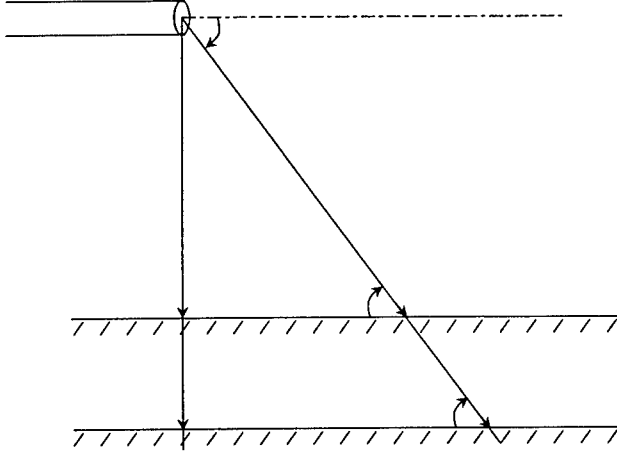
Figure 1 : Principle diagram

So, a similarity coefficient k can be defined and explained by ($d_1 = d_2$) :

$$k = \frac{R_{O2}}{R_{O1}} = \left[ \frac{p_{O2}u_2/c_2}{p_{O1}u_1/c_1} \right]^{1/3} \tag{1}$$

or by :

$$k = \frac{H_2}{H_1} = \frac{R_2}{R_1} = \frac{L_2}{L_1} \tag{2}$$

i.e.

$$\frac{L_2}{R_{O2}} = \frac{L_1}{R_{O1}} \tag{3}$$

in which L is the orthogonal projected radial distance (Fig. 1).

At this step, a case is chosen (for example experimental case) then using similarity laws a data interpolation or extrapolation is performed to determine other corresponding case values (numerical case).

## 3. NUMERICAL SIMULATION

The numerical simulation is obtained by using a second order Total Variation Diminishing scheme for solving the unsteady bidimensional Euler equations. The numerical code is the same as detailed in a previous work [1] and applied for only one tube diameter (d = 40 mm) and firing conditions (p = 510 bar, u = 1625 m.s$^{-1}$, T = 1192 K). The computational domain is a rectangular one (x, y). The parameter of the study is the parallel distance H (0.4, 0.8, 0.84 m) between the tube axis and the plane surface. The x-grid density takes into account 900 meshes for all the simulations, but density in the y-direction varies with each altitude. For example, when H is equal to 0.4 m, there are 180 y-meshes i.e. 160962 nodes, and if H = 0.84 m, there are 378 y-meshes, so 338942 nodes. A lot of measurement points have been located in the domain (x range = 0 to 1.6 m) on the plane surface. The investigated results are the

- 224 -

arrival times and the maximum overpressure of the reflected shock wave at various positions along the orthogonal projection of the tube axis on the plane surface (typical calculus Fig. 2). Results aren't distorted by the precursor presence because the altitude is sufficient so that this last one will be overtaken by shock wave and are validated in [2].
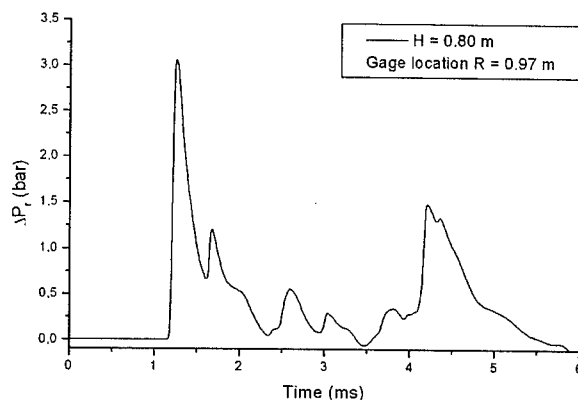


Figure 2 : Typical calculus

## 4. EXPERIMENT

The experimental set-up is similar that one used previously [3]. The shock wave is generated by the detonation of the gaseous mixture ($C_3H_8 + 5O_2$) in 40 mm i.d. tube. The parameter is the same distance H (0.2, 0.26, 0.39 m) as above and the reflected wave propagation is followed by means of pressure gages located on the plane surface at various positions (L = 0 ; 20 ; 39 ; 61 ; 124 ; 183 ; 248 and 350 mm). The pressure gages used are Kistler 603B type linked to charge amplifiers which transmit recording to computer (typical record Fig. 3).
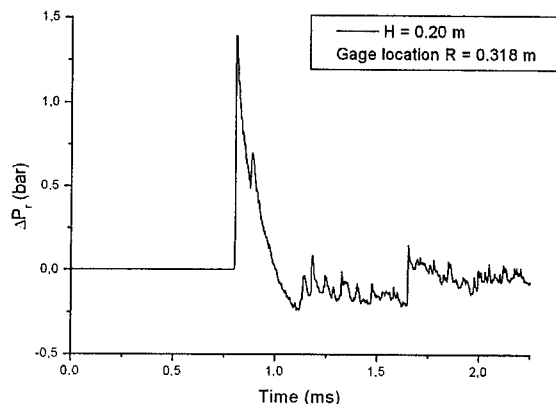


Figure 3 : Typical record

## 5. RESULTS

In previous work [2] the Hopkinson similitude of the incident overpressures is well established independently of the shock wave generating device. The correlation between calculus and small scale experimental results necessitates the use of the similarity laws. The two cases have d as a common value (40 mm), then the ratio of the nominal energies governs the similarity coefficient k ($E_{exp}$ = 180.7 J for $C_3H_8 + 5O_2$ gaseous mixture).

### 5.1 Decay diagram

We consider the simulation results for H = 840 mm and we determine the corresponding experimental case. To do that, in the numerical case we choose a point on the ground, for example, the most simple one is : L = 0, H = 840 mm (orthogonal reflection). The corresponding calculated reflected overpressure is $\Delta p_{r\_simul}$ = 5.08 bar. Then we determine its experimental associate (L = 0, H = ?) knowing that : $\Delta p_{r\_exp} = \Delta p_{r\_simul}$.

For each experimental altitude, we establish a polynomial law of $\Delta p_r$ as function of L as :

$$\Delta p_{r\_exp}(L, H) = a(H) + b(H) \times L + c(H) \times L^2 \tag{4}$$

where a(H), b(H) and c(H) are the second order polynomial coefficients.

When L = 0, (4) writes $\Delta p_{r\_exp}$ = a(H) = $\Delta p_{r\_simul}$ = 5.08 bar. By means of extrapolation the equation resolution leads to the solution : H = 99 mm. The three polynomial coefficients a, b and c and the equation (4) are clarified.

So, knowing the two altitudes we can evaluate the similarity coefficient $k = H_2/H_1 = 8.47$. Then, with the relation (1) and the classical definition of the characteristic radius $R_0$ = (E / $p_0$)$^{1/3}$, the $R_{0\_simul}$ is estimated : $R_{0\_exp}$ = 0.12 m and $R_{0\_simul}$ = 1.016 m. The pressure decay curves are plotted on the same graph $\Delta p_r(L/R_0)$ and are compared (Fig. 4).
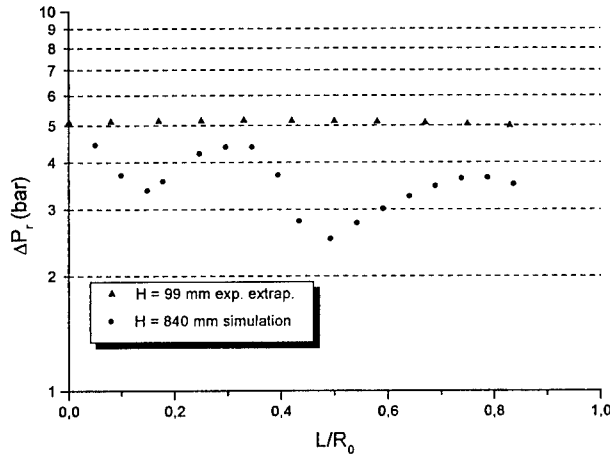


Figure 4 : Comparison of the decay curves

We can see a few difference between the two curves which seems the consequences of two effects. The first one is due to measurement uncertainties because measured values vary any test : we are not sure that the selected overpressure value is averaged exactly. The second one comes from numerical simulation. In fact, the origins of the parameters R and t (R = 0, t = 0) are considered from the interface at the open end of the tube and the surrounding air where is just created the shock wave. So, it's possible the initial conditions used in the code are overestimated, in particular p = 510 bar, and they don't correspond to the just created shock wave. Considering this pressure value, the energy $E_{simul}$ is approximately 9580 J and then the related similitude coefficient should be $k = \left(E_{simul}/E_{exp}\right)^{1/3}$ # 3.75 very different of 8.47.

## 5.2 Space-time diagram

We introduce the non-dimensional arrival times $t/t_0$ in which $t_0 = R_0/c_0$ (the sound velocity $c_0$). Then we apply the same method that used for the decay curves. The similarity coefficient is also evaluated and the equivalent experimental altitude is determined. In the same way, a polynomial equation permits to describe the shock wave arrival time as function of the distance L. Then applying the similitude we obtain a space-time curve $t/t_0(L/R_0)$ (Fig. 5).
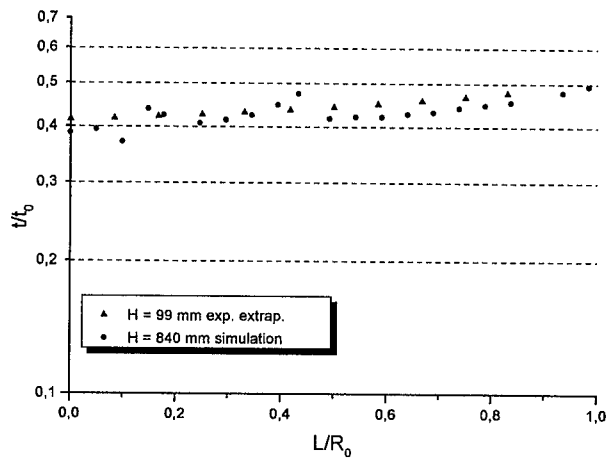


Figure 5 : Comparison of the space-time curves

We observe a very good agreement between the two curves and the relative positions are the same. In such investigated problems, always the pressure diagram appears more sensitive than the space-time diagram.

This methodology has been used with other various calculated and experimental data and the conclusions are similar to those found above.

## 6. CONCLUSION

From the numerous calculated and experimental data, we conclude that the appearance of the corresponding curves is similar. The difference of the overpressure amplitude is explained by the overestimated initial conditions introduced in the numerical code and by the fact the experimental values fluctuate. Consequently it is easy to define an equivalency energetic

coefficient which characterizes the link between the two similar curves. Now the Hopkinson similitude is clearly validated for reflected overpressure independently of the source of energy. Then is established a predictive procedure to estimate the consequence of blast wave characteristics in the intermediate ballistics.

## 7. REFERENCES

[1]    R. Cayzac, E. Carette, T. Alziary de Roquefort, C. Vaglio, J. Brossard, "Intermediate Ballistic Computations and Validations", 17th International Symposium on Ballistics, Midrand, South Africa, (1998).

[2]    S. Sénégas, R. Cayzac, J.Brossard, "Simulation numérique d'une onde de souffle : validation de la réflexion au sol", 14ème Congrès Français de Mécanique, Toulouse, France, (1999).

[3]    C. Vaglio, "Validation à l'échelle du laboratoire de modèles d'ondes de souffle. Prévision sécuritaire ", Thèse de Doctorat, Université d'Orléans, France, (1998).

# ON THE TNO-PML WARHEAD ACCELERATOR: DYNAMIC OVERFLYING TOP ATTACK WARHEAD PERFORMANCE TESTS AND ACCELERATION MEASUREMENTS

**E.J.M. VAN RIET**

TNO Prins Maurits Laboratory, P.O. Box 45, 2280 AA Rijswijk, The Netherlands

**Abstract :** The TNO-PML warhead accelerator has recently been used for overflying top attack warhead performance tests. This paper presents some details with respect to the execution of these experiments. An effort to measure the acceleration loadings at launching has also been made. VISAR measurements showed acceptable acceleration levels, that were equal or even less to the calculated acceleration loadings.

## INTRODUCTION

Shaped charges play a major role in the armour/anti-armour battle. In missile-type anti-tank weapons in particular, the shaped charge offers a superior penetration capacity. However, a defence against shaped charge warheads has been developed in the form of explosive reactive armour (ERA), reducing the shaped charge jet penetration capacity dramatically. The ERA instigated a determined search for countermeasures. These were found in the tandem warhead and in the top attack warhead.

Both tandem and top attack charges require dynamic rather than static tests for a detailed evaluation of their performance. For top attack charges, which are fired downwards, this will be readily apparent. For tandem charges, static tests may offer an indication of the charge's effectiveness, but both the timing and the effect of the front charge's detonation on the second charge are influenced by the missile motion. Moreover, obliqueness of the charge at impact can affect the penetration capacity.

Based on the need by the Netherlands MoD and the TNO Prins Maurits Laboratory (TNO-PML) for dynamic terminal ballistics tests of warheads, both in a national and in an international framework, the MoD financed a project for building a warhead accelerator. The project resulted in a 300 mm calibre gas-gun based warhead accelerator.

The warhead accelerator's design and feasibility study was presented at the 44th ARA meeting [1].A technical description of its construction, as well as some experiments with tandem charges (TOW 2A), were presented at the 45th ARA meeting [2].

This paper briefly discusses some aspects of recent experiments, which were performed for top attack charges (TOW 2B warheads). It also discusses some experiments for measuring the projectile's acceleration levels inside the launch tube. Firstly, a short summary on the warhead accelerator's construction and performance is presented.

## The TNO-PML warhead accelerator

Based on the results of the feasibility and design study [3], a warhead accelerator was constructed and installed at the Ballistics Laboratory of TNO-PML. The accelerator was completed and tested in 1994 [4]. Its major characteristics are defined in Table 1.

Table 1:     TNO-PML warhead accelerator characteristics.

| Gas-gun | |
|---|---|
| calibre | 300 mm |
| barrel/guiderail length | 30 - 40 m |
| storage tank volume | 2 m$^3$ |
| driver gas | nitrogen or helium |
| performance example: | |
| max. velocity for a 30 kg projectile package[1] | 400 m/s |
| max. warhead explosive weight | 10 kg (eq. TNT) |
| **Firing circuit** | |
| max. number of charges | 2 |
| stand-off charges to target | variable |
| 4\ | variable |
| e delay between initiation of charges | |

*1*    The projectile package consists of a launch vehicle (or carrier) and the payload (warhead)

Figure 1 gives a slhematic view of the warhead accelerator, showing its major components, as well as their placement within the large firing range of the Ballistics Laboratory.
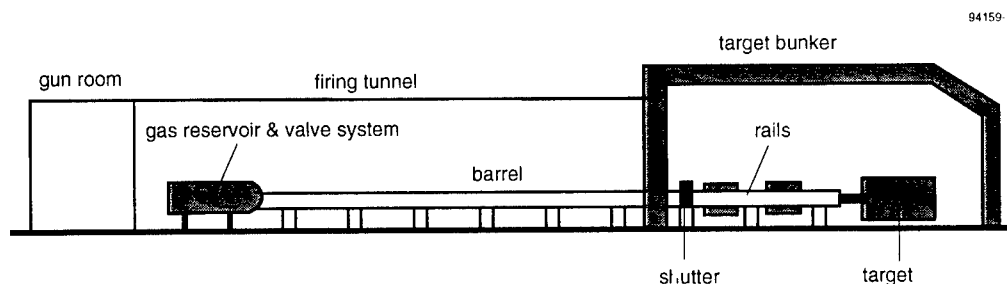


Figure 1:     Schematic view of the TNO-PML warhead accelerator.

Basically, the warhead accelerator consists of a gas storage tank, a valve mechanism and a launch tube or barrel, i.e. the gas-gun (see Figure 2). The 2 m$^3$ gas storage tank can be filled with nitrogen or helium driver gas up to 30 bar. The kind of driver gas and the pressure level inside the tank determine the muzzle velocity and the maximum acceleration level. The valve mechanism switches the gas from the reservoir (gas storage tank) to the launch tube behind the projectile package. The projectile package will thus be accelerated through the 300 mm diameter 'smooth bore' tube (total length: 22.5 metres).
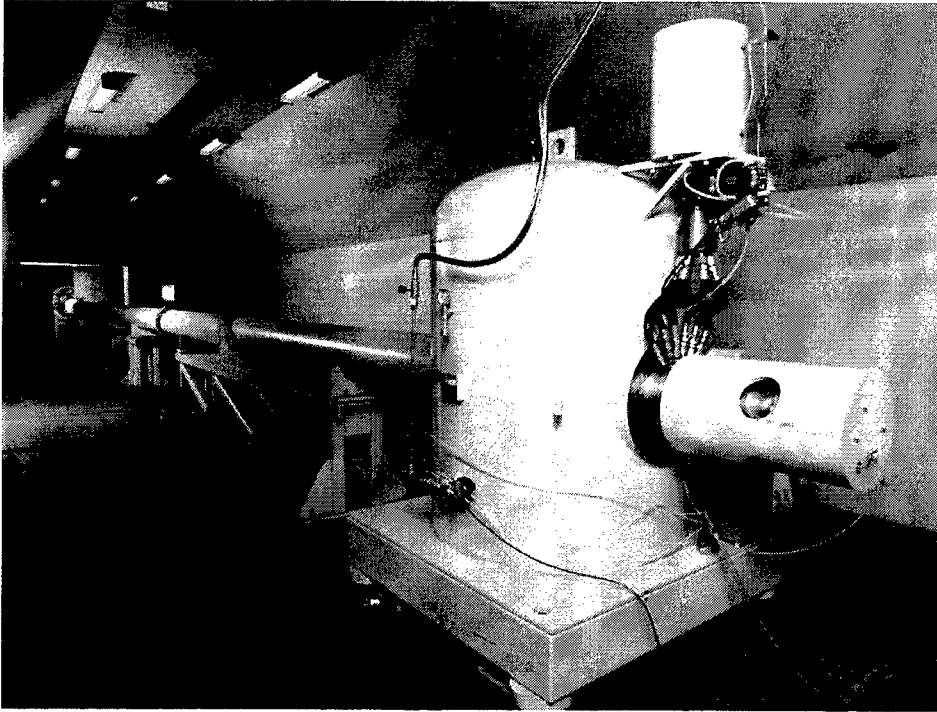
Figure 2:      TNO-PML warhead accelerator: gas storage tank, valve mechanism and launch tube
(i.e. gas-gun, located in the main firing tunnel).

For acceleration purposes, the warhead is mounted on a so-called launch vehicle or carrier (see Figure 3). Essentially, this carrier has to play the role of pusher plate and sabot. It also supplies a platform for electrical contacts to connect the warhead's detonators to the firing circuit. Finally, the carrier is used to fix the warhead in order to achieve the correct angle of incidence and warhead orientation.
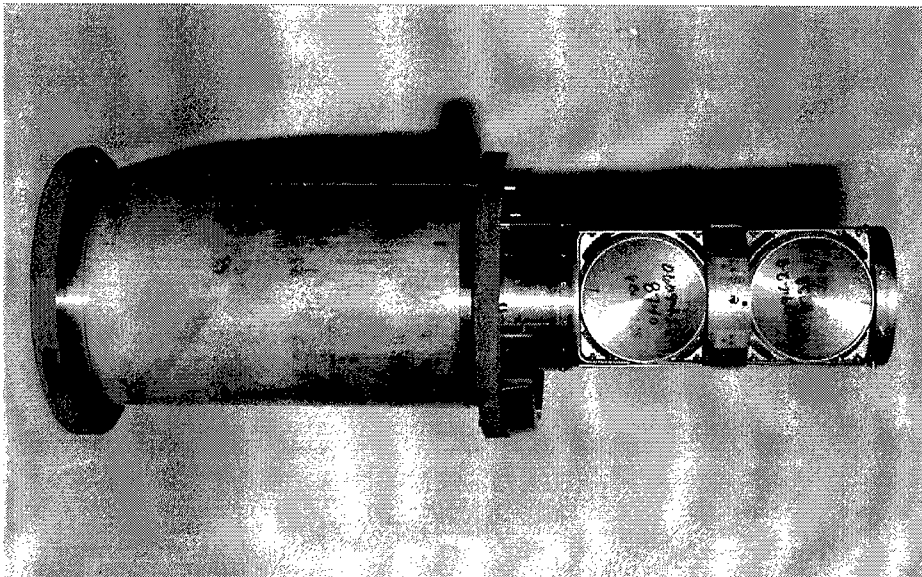


Figure 3:     The projectile package consisting of the launch vehicle and the warhead (i.e. TOW 2B warhead).

In order to prevent the forward permanent launch tube section from being destroyed or damaged, an expendable rail system takes over from the launch tube as it enters the target bunker (see Figures 5 to 7). The rail system guides the projectile onto the target. The gas-gun must also be protected from being damaged by fragments produced in the target bunker (explosion of warhead and interaction of charges with target). To that end, a fast closing shutter is placed between the launch tube and the rail system. The shutter is activated by the passage of the projectile.

Immediately before impact, the projectile passes a contact section where electrical contact is established between the projectile and the firing equipment. The contact section consists of brushes that are mounted on the rail system. The contactors on the sabot engage the brushes. As a sensor detects that the warhead has reached the target, the detonator of the charge(s) is initiated by transferring the high voltage to the brushes. If necessary (e.g. for tandem charges), a second set of brushes and a time delay generator for the initiation of a second charge can be applied.


## Dynamic overflying top attack warhead performance tests

The TOW 2 weapon system is in use with the Royal Netherlands Army for armoured warfare purposes. It is a crew-portable or vehicle mounted heavy anti-tank weapon. The TOW 2 weapon system can fire two missile configurations:
- the TOW 2A missile having a tandem warhead, thus capable of defeating targets fitted with ERA;
- the TOW 2B missile having two EFPs (Explosively Formed Projectiles) for overflying top attack (OTA).

Currently, the TOW 2A missile is in use with the armed forces.

Anticipating on current and future threats, the Royal Netherlands Army decided to perform a study in which the advantages and disadvantages of OTA weapons are examined. A part of this study concerns the terminal ballistics performance of OTA warheads. As five TOW 2B warheads were available for testing, a test programme for establishing their performance was defined.

The TOW 2B warheads were tested dynamically. The TOW 2B warhead has two EFPs which are fired downwards, almost perpendicular to the missile's trajectory. As the missile velocity is about 5 to 15% of the EFP velocity, the penetration process, thus the penetration performance, will or may be affected by the motion of the missile (the EFPs tend to 'cut' into the target instead of drilling a hole into it).

On firing OTA warheads, the warhead's velocity and position with respect to the target have to be controlled exactly. The position includes both the angle between the missile's trajectory and the longitudinal axis of the warhead ('angle of incidence'), and the orientation of the EFPs within the warhead. Other experiments using the TNO-PML warhead accelerator already demonstrated the capability of predicting and controlling the projectile's velocity within few percents. The warhead's position can be controlled accurately by fixing the warhead to the launch vehicle at the desired angle and orientation. This requires however, that the launch vehicle is prevented from rotating. In practice, the launch vehicle does not

rotate because of a wedge-like pin on the projectile package that fits into one straight groove in the launch tube (Figure 4).
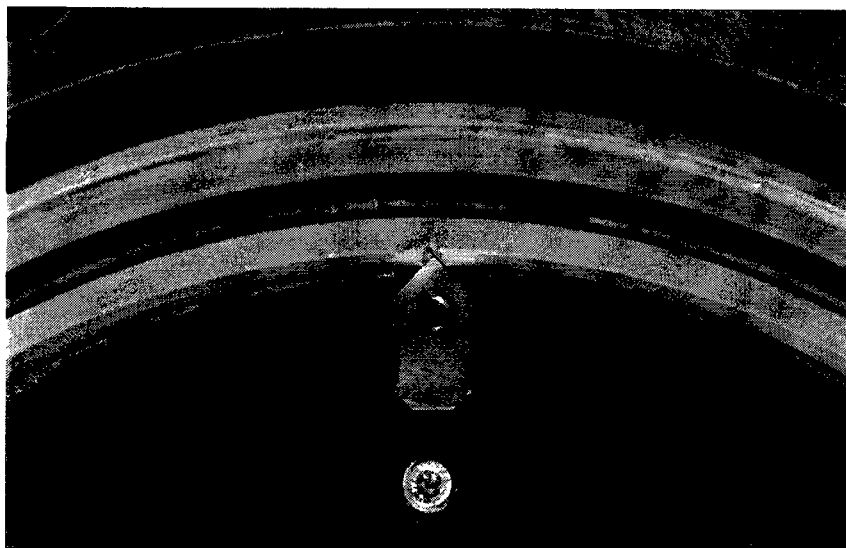


Figure 4: The wedge-like pin on the projectile package and the straight groove in the launch tube prevent the projectile package from rotating.

High-speed recordings and radiographs in order to check the warhead's condition and position were made during the TOW 2B trials. These recordings showed that the warhead reached the target intact, exactly in position and at the desired target location. The actual EFP impact positions in the targets were all very close to the aim points. The small deviations can be explained by the tolerances of the screw holes in the adaptors, which were used to mount the warheads on the launch vehicles (Figure 3).

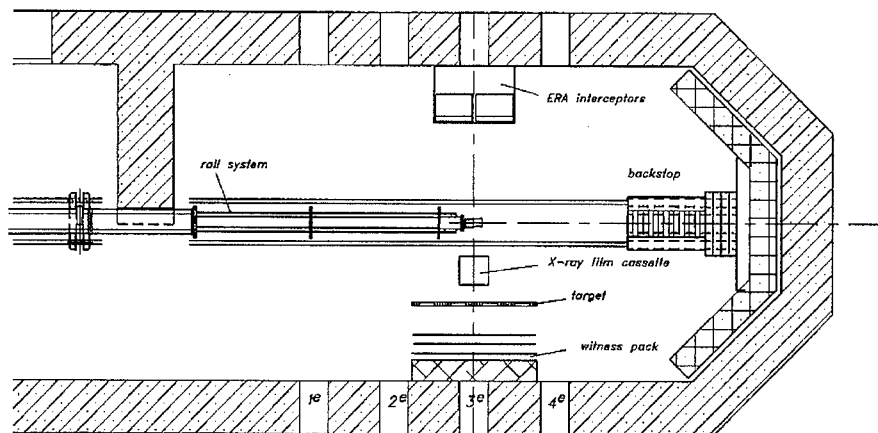A typical experimental set-up of the TOW 2B trials is shown in Figures 5 to 7.



Figure 5: Schematic view of the experimental set-up of the TOW 2B trails (main target bunker).
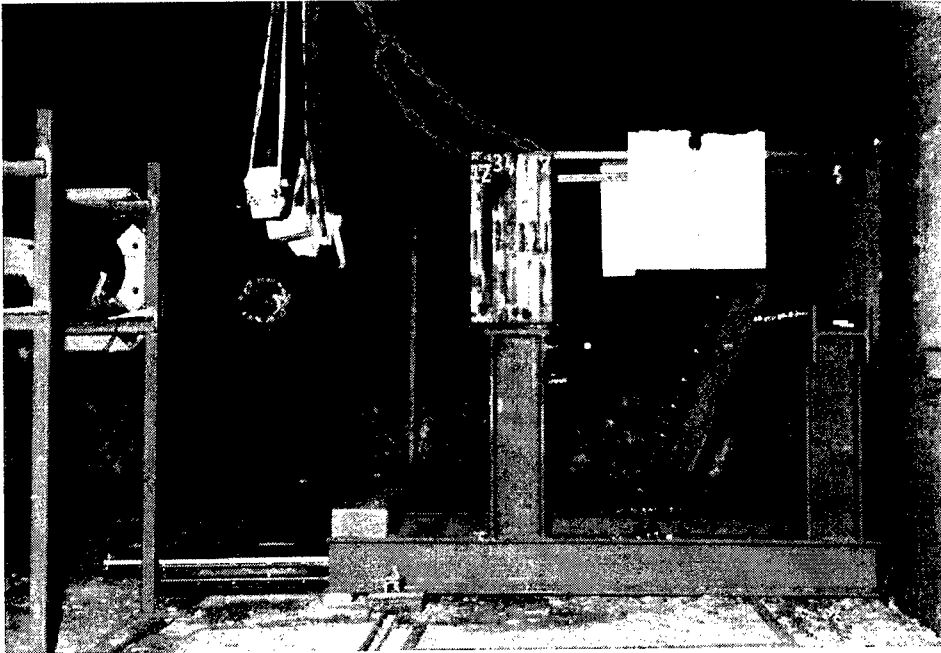
Figure 6:    Experimental set-up for penetration measurements and radiography. From left to right: guiderail system of warhead accelerator, X-ray film cassette (on the floor), semi-infinite RHA target (on top of steel table).
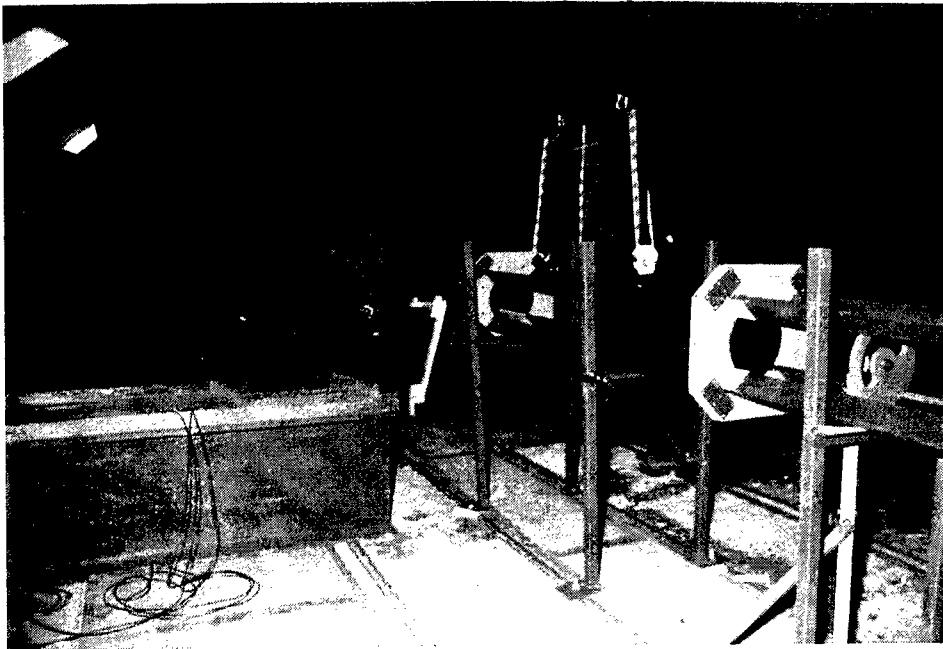


Figure 7:    Experimental set-up of TOW 2B firings against targets fitted with ERA. From left to right: steel backstops to intercept the ERA plates, guiderail system of warhead accelerator.

As can be seen from Figures 5 to 7, the complete target configuration is rotated 90° which facilitates the interception of ERA plates and the set-up of target and witness packs. The ERA plates are stopped by two massive steel backstops which are located opposite the target

- 234 -

(Figure 8). Figure 7 pictures the semi-infinite RHA target for measuring the penetration performance of the TOW 2B warhead. In other experiments, metallic witness packs to examine spall effects were placed behind the target. Figure 7 also shows the X-ray film cassette to make recordings of the EFPs in flight.

## Acceleration measurements inside the launch tube

At launching, anti-tank missiles are subjected to high acceleration loadings. Depending on the way in which the missiles are accelerated, these g-loadings may vary from few hundreds to almost 10.000 g's. In order to prevent the payload from damage, deformation or even destruction, special attention to the acceleration levels was paid at the design of the TNO-PML warhead accelerator. A computer model to predict the muzzle velocity and maximum acceleration level as a function of chamber pressure, barrel length and projectile weight was developed [3].

Before the TOW 2B trials took place, a series of test firings to check the computer calculations were performed. In these test firings, the projectile's acceleration and velocity profiles inside the launch tube were measured. To that end, a so-called VISAR (Velocity Interference System for Any Reflector) was applied.

The test firings were performed for two muzzle velocities: 160 m/s and 350 m/s. The projectiles (launch vehicle and dummy warhead) weighed about 21 kg. The results are shown in Figures 8 to 10.
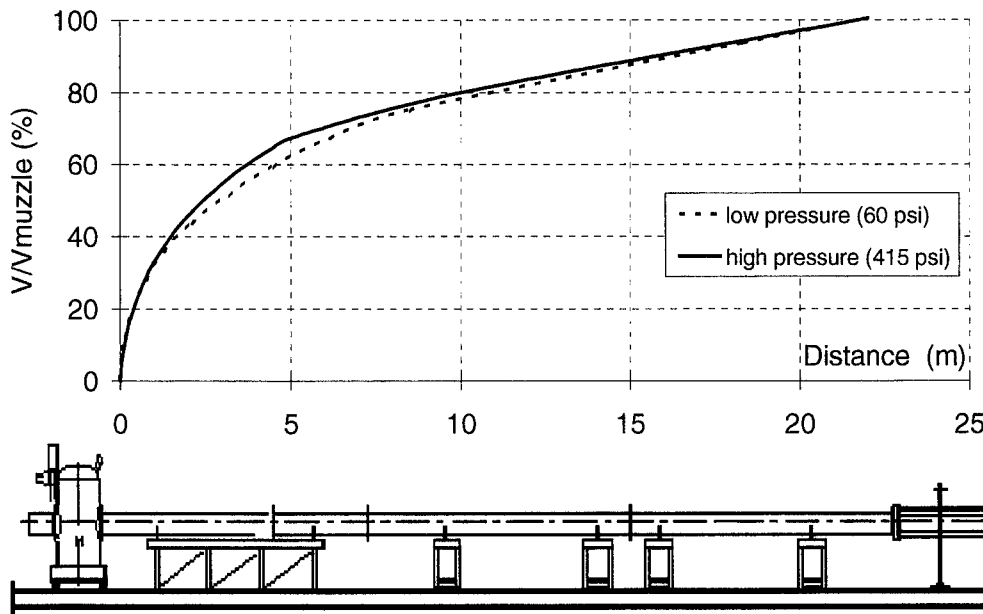


Figure 8:    Projectile velocity (normalised to the measured muzzle velocity) as a function of the position in the launch tube.

Figure 8 presents the calculated velocity profile from the VISAR data as a function of the distance travelled in the launch tube. The velocity is normalised with respect to the measured

muzzle velocity. As can be seen from this figure, the velocity profile is very similar for both low and high[1] gas pressures (i.e. low and high muzzle velocity: 160 and 350 m/s, respectively), which implicates that the acceleration profiles are also very similar (see Figures 9 and 10). In fact, the acceleration profiles are almost identical, except for the very beginning and for the maximum acceleration levels. The maximum acceleration for the low gas pressure is about 150 g; for the high gas pressure about 750 g.

The differences in the very beginning of the profiles can be explained by the pressure build up behind the projectile. The gas-gun applies a valve mechanism to switch the gas between the gas reservoir and the launch tube. At firing, a piston is pulled rearward until its forward face starts to open the reservoir/bore holes. The piston is then violently driven rearward as the valve opens completely and the gas pressure is applied to the projectile package. The projectile package is locked by two Teflon plugs in the launch tube. At a certain pressure level, these plugs will break because of shear forces. As a result, the projectile starts to move. The acceleration profile at high pressure (Figure 10) indicates that the projectile starts to move before the gas pressure can be applied to the projectile completely. At low pressures however, the pressure behind the projectile reaches its maximum before the locks break and the projectile starts to move. This phenomenon also explains the differences between the measured and calculated results. The calculated results originate from the previous mentioned computer model. This model assumes an instantaneous pressure build up behind the projectile.
Finally, both acceleration curves (Figure 9 and 10) show some oscillations. These oscillations can be explained by the gas flow and reflections.

---

[1] Low gas pressure: 60 psi
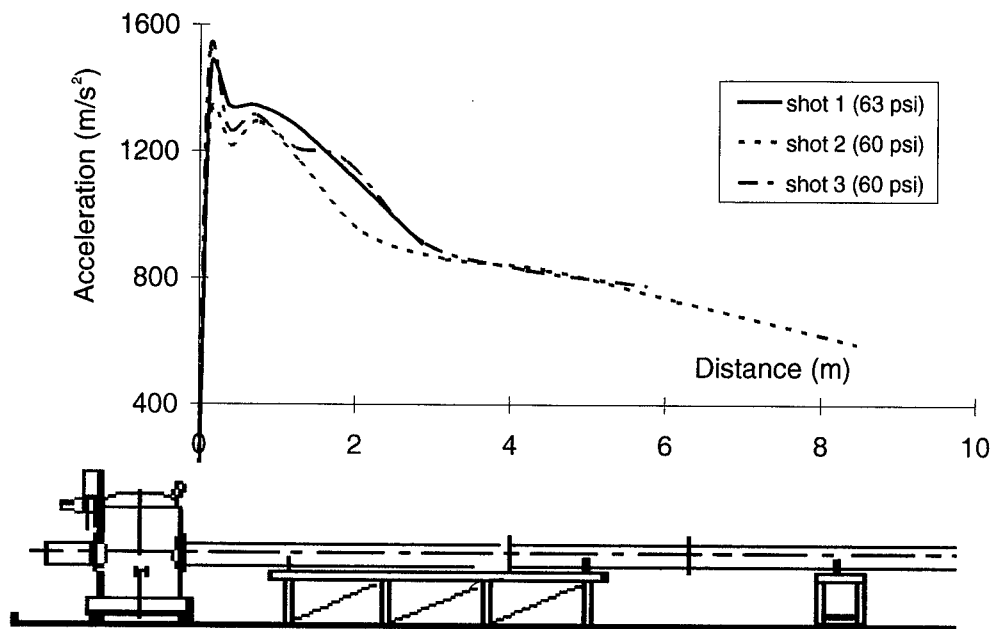High gas pressure: 415 psi, maximum allowed pressure for the gas-gun

Figure 9: Measured acceleration level as a function of the position in the launch tube (low gas pressure and muzzle velocity: 160 m/s).
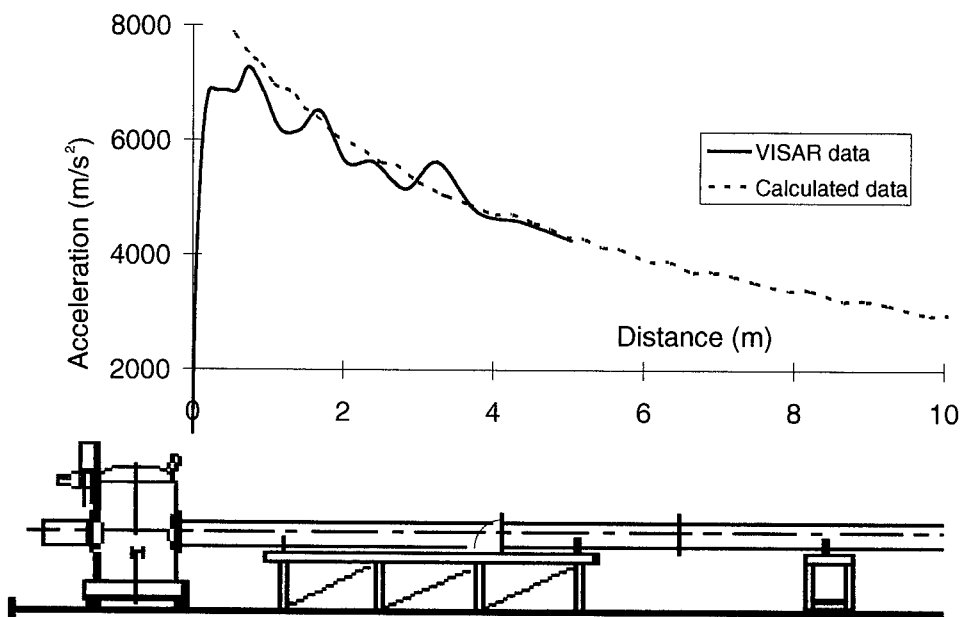


Figure 10: Measured and calculated acceleration level as a function of the position in the launch tube (high gas pressure and muzzle velocity: 350 m/s).

## CONCLUSIONS

With the successful completion of the TOW 2B test series, the TNO Prins Maurits Laboratory has proven the versatile use of its warhead accelerator. The accelerator can be used to examine the performance of both tandem charges and overflying top attack warheads.

The warhead accelerator allows 'impact' conditions to be controlled accurately. The projectile's velocity can be predicted and controlled within few percents. The position and orientation of the warhead can be controlled by fixing the warhead at the appropriate angles and in the appropriate position to the launch vehicle.

VISAR measurements showed that the acceleration loadings are acceptable for both low and high gas pressures. For a typical projectile package mass of 21 kg and muzzle velocities between 160 and 350 m/s, the maximum acceleration levels vary between 150 and 750 g, respectively.

## LITERATURE

[1]     Riet, E.J.M. van,
        'Expansion of the TNO-PML Laboratory for Ballistic Research',
        44th ARA Meeting, Munich, Germany, 1993.

[2]     Riet, E.J.M. van, and Keij, T.L.J.,
        'TNO-PML warhead accelerator',
        45th ARA Meeting, Huntsville, USA, 1994.

[3]     Manders, M.P.I. and Eggen, J.B.M.M.,
        'On the design of a gas-gun accelerator for dynamic warhead tests',
        PML 1992-64, TNO Prins Maurits Laboratory, Rijswijk, The Netherlands.

[4]     Keij, T.L.J.; Riet, E.J.M. van; Manders, M.P.I. and Eggen, J.B.M.M.,
        'The TNO-PML warhead accelerator',
        15th International Symposium on Ballistics, Jerusalem, Israel, 1995.

# Intermediate Ballistics and Aeroballistics

# MUZZLE FLOW FIELD EVOLUTION

## CROWLEY, A.B.

Cranfield University, Royal Military College of Science, Shrivenham, Swindon, Wilts., SN6 8LA, U.K.

**Abstract:** Recent experimental studies on muzzle blast overpressure histories of an 81mm mortar system have revealed a number of reproducible features following the main blast front. Some of these features are shock fronted, with pressure rises of similar magnitude to that in the main blast front. The time lapse indicates that these may be associated with the precise geometry of the projectile. A study was therefore undertaken, using our previously validated CFD code, to examine the evolution of the flowfield behind the blast front. The influence of the projectile geometry on the flowfield is also examined. The primary concern is to achieve an improved understanding of the changing flowfield, and how this determines the measured pressure history.

## 1. INTRODUCTION

Recent advances in computational fluid dynamics (CFD) techniques have led to the development of a number of codes, [1,2,3], for computation of intermediate ballistics flowfields during projectile launch. These have been applied to several different studies, to follow the flow through muzzle brakes, to clarify heat transfer and patterns of particulate damage in muzzle brakes, and to examine the separation of sabots in this flow regime. Such codes are increasingly being employed to assist the understanding of these highly transient complex flowfields, where only limited experimental data is available. In this paper such a study of a muzzle flowfield, employing both experimental measurements and CFD analysis, to provide greater insight, is discussed.

## 2. 81MM MORTAR FIRINGS.

An experimental study of overpressure histories in the muzzle flowfield of an 81mm mortar system was undertaken recently as part of an ongoing study of gun-break signatures. Twenty rounds were fired on full charge, and the pressure histories were recorded at six different positions in the resulting flowfield, at distances between 10 and 30 calibres (D) from the muzzle, on rays at angles of 5°, 30° and 60° from the forward extended barrel axis. Kistler type 603B gauges mounted side-on to the flow in a pancake configuration, connected to charge amplifiers, were used to measure the static pressure. When the recorded pressure histories were examined two features of interest were noted. The first was a number of shock fronted features behind the main blast front, see figure 1, which appeared on several traces from some, but not all the rounds. In some cases these shock-fronted features were, if
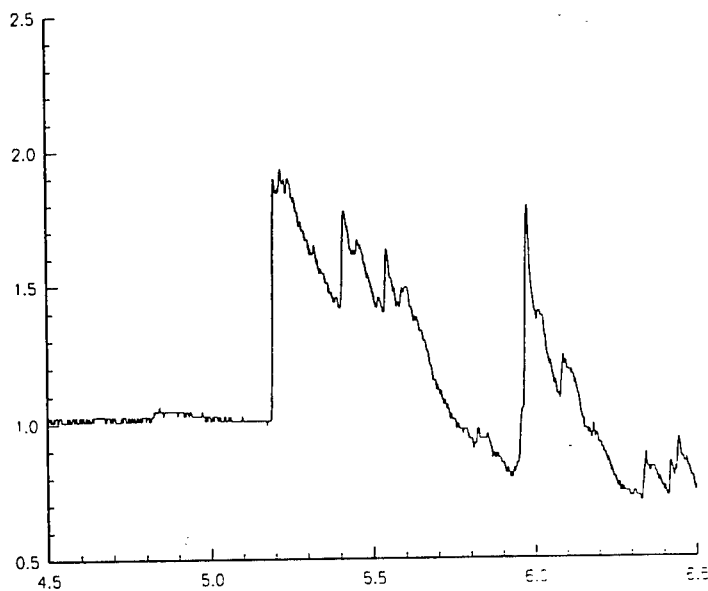
Figure 1: Experimental pressure-time history at 60°,10D gauge.

anything, more conspicuous at greater distances from the muzzle. The second feature was that when the traces recorded at the same location for different rounds were overlaid, with the blast arrival times matched, the first part of the signals showed broad agreement, but there was significant divergence of the traces a fraction of a millisecond after the blast arrival, see figure 2 for example. This was noted at several different gauge locations, but the cause was not clear. Hence this study was initiated.
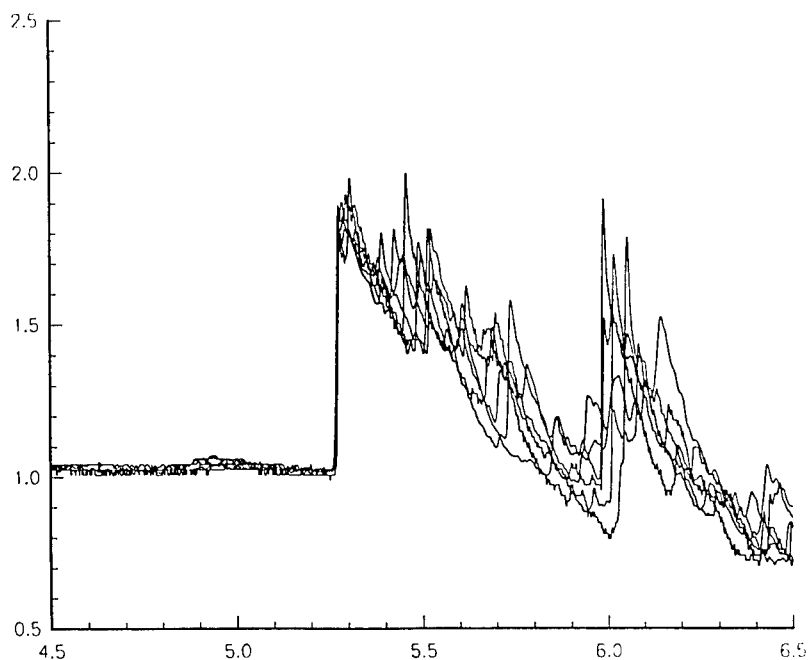


Figure 2. Overlay of pressure-time histories for six successive rounds at the same location

- 242 -

## 3. MBIB2 CODE.

The MBIB2 code [1] is a two-phase flow code developed originally for the study of particulate impact on the muzzle brake during the intermediate ballistics phase of projectile launch. It is assumed that the highly transient compressible, but inviscid, flow is symmetric about the barrel axis. Turbulence is not included in the current code. A moving projectile may be included in the simulation if required, and has been included in this study.

The code solves the finite volume form of the equations of conservation of mass, momentum and energy for the gas phase using a cell-centred Eulerian approach. If a particulate phase is present, mass and momentum equations for this phase are added. Zalesak's multi-dimensional flux corrected transport algorithm [4] is employed to limit the overshoots and undershoots commonly associated with the numerical computation of shock waves. The low order flux is calculated using a first order exact 1D Riemann solver, and the higher order flux is predicted using a second-order central difference scheme based on a predictor-corrector method.

It is assumed that both gases, that is the propellant gas efflux and air, satisfy the ideal gas law with the appropriate gas constant, and that the mixture properties are given by appropriate weighted averages.

A number of calculations have been undertaken to validate this code against published results in [3,5], and have demonstrated that the results from this code are in good agreement with experimental data.

## 4. NUMERICAL SIMULATIONS.

The general form of the intermediate ballistics flowfield has been described in a variety of texts, see for example [6]. A quasi-steady stucture exists, consisting of a main blast front, ahead of a contact surface, behind which is a highly overexpanded jet bounded to the front by the Mach disc, and to the sides by the so-called barrel shock. A vortex forms from the initial shear layer near the junction of the Mach disc and the barrel shock. Experiments with open cylindrical shock tubes have also been used to examine the structure of these fields as described in [3], where high resolution shadowgraphs of such a flowfield are shown. The questions of interest here are to what extent these structures are correctly reproduced by the current code, and how these structures interact to produce the features of the experimental pressure histories discussed in section 2. A further point of interest is to follow the collapse of the 'shock-bottle' as the venting flow weakens.

Initial simulations showed that a reasonably accurate representation of the bomb geometry, particularly to the rear of the obturating ring, is essential if the correct blast front strength is to be calculated. Figure 4 compares the pressure history calculated at the 30°, 5D and 10D, gauge locations with the bomb shapes shown in figure 3. The difference is to be expected when it is appreciated that the geometry of the rear part of the bomb determines the rate of
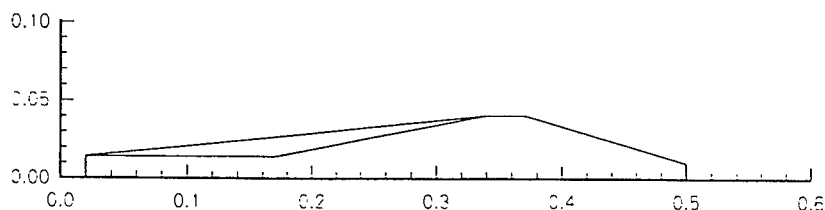


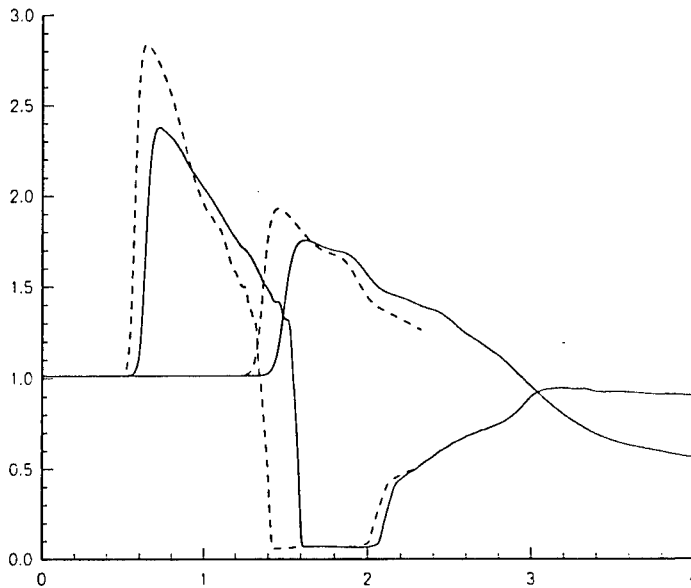Figure 3. Representations of bomb geometry.

Figure 4. Corresponding computed pressure time histories at 30°,5D and 10D gauge locations.

opening of the gun tube, and hence the supply of propellant gas to the blast wave. Moreover the inlet conditions, applied to the gas flow inside the mortar tube must be accurate. It was found that a satisfactory approach is to use an internal ballistics program to calculate the internal flow history after the shot exits the tube, and to apply this history as the inlet condition where the gun tube enters the intermediate ballistics computational domain.

The contour plots shown here correspond to the results with the more realistic bomb shape depicted in figure 3, with inlet conditions taken from the internal ballistics calculation of gun tube venting after shot exit. Pressure contour plots at several times are shown in figure 5. The time of 1.75 ms after the start of venting corresponds to the maximum extent of the shock bottle, which begins to shrink thereafter. A clear bow shock is formed around the tail of the projectile while it is enveloped in the expanding gas.

It is perhaps instructive to examine the path of some of the pressure gauges through this flowfield, in order to understand the pressure histories at these locations. Consider, for example, a gauge located on a bearing of 30° from the forward extension of the gun axis at a distance of 5 calibres from the muzzle. The computed pressure history shown in figure 6 is complex. By examining the location of the gauge in relation to the shock-bottle structure all becomes clear: first the blast wave crosses the gauge. Approximately 0.9 ms later the Mach disc passes the gauge. After a further 0.6 ms the pressure increases again, not as the Mach disc retreats, but as the barrel shock weakens and moves inward. Thus the path of the gauge through the quasi-static shock structure is as sketched below.

Hence to the original questions. Why do the pressure histories at the gauges become more variable some distance behind the blast front? The position of the gauges in question is shown in the pressure contour plot, figure 5. After the blast front passes, the location of the vortex begins to sweep forward coming near to the gauges, and increasing the round to round variability. And that second shock front? On examining the computed pressure histories it is clear that it is associated with the steep pressure rise which occurs at 0.6 ms after the passage
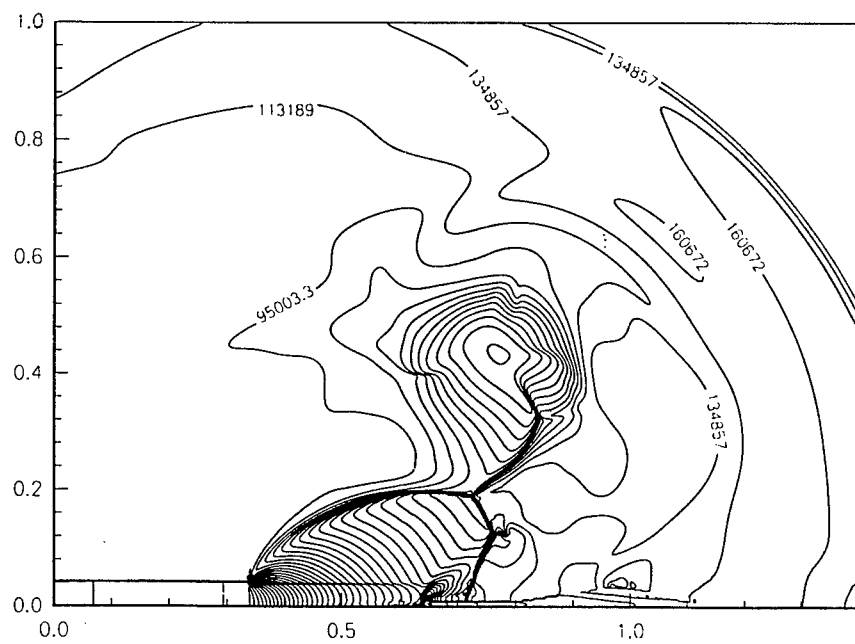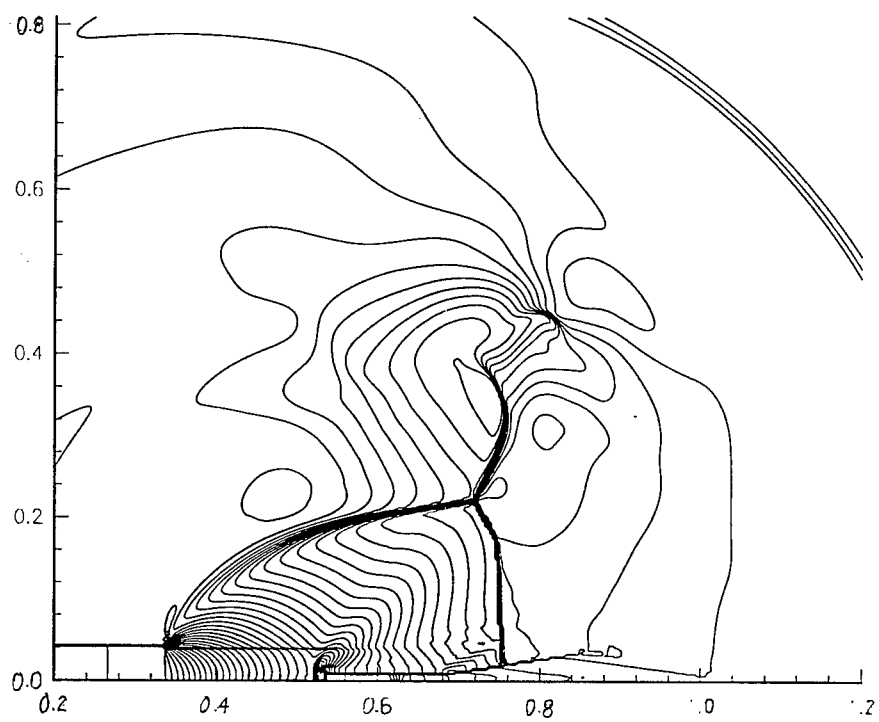
Figure 5. Pressure contour plots at 1.75 ms (upper) and 2.15 ms (lower) after shot exit.

(a)                           (b)

Figure 6. (a) Pressure history at 30°, 5D gauge, and (b) sketch of path of gauge relative to shock structure

of the blast front (see figure 7). The pressure contour plots show a pressure ridge progressing azimuthally around behind the main blast front, which arrives at the gauge location at this time.



Figure 7. Computed pressure history at 60°, 10D gauge.

## 5. CONCLUSIONS.

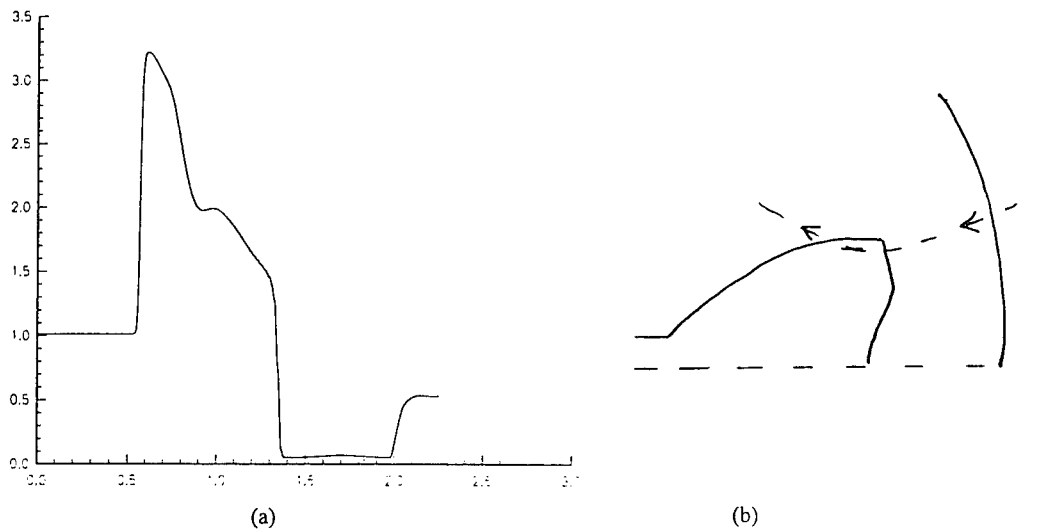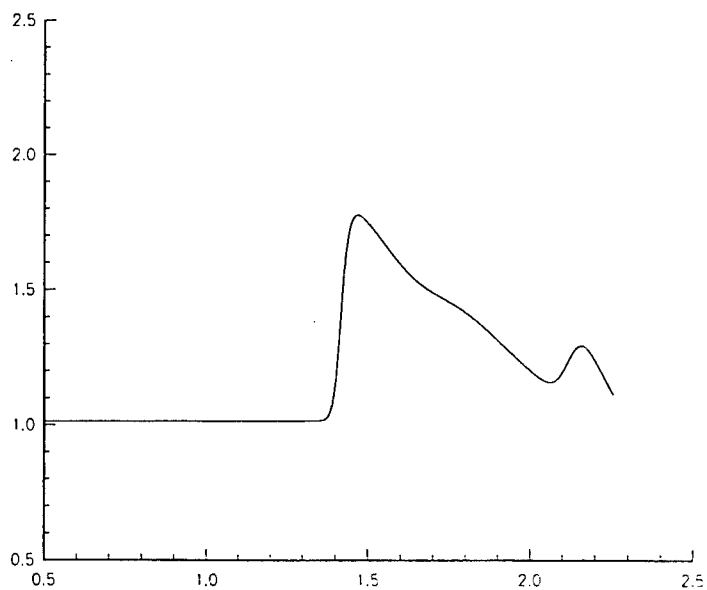The power of CFD simulations to enhance our understanding of muzzle flowfield evolution, and clarify features on experimental pressure histories has been amply demonstrated. CFD can be employed to fill in details of the flow which are beyond the reach of experimental techniques in this hostile environment, and thus improve the overall picture of complex flowfields. In addition simulations can assist the design of experiments in order to capture the data of greatest significance, and hence ensure the most cost-effective use of trials weapons and facilities.

## ACKNOWLEDGEMENT.

## REFERENCES

[1]    A. S. Dawes & A. B. Crowley, Gas-particulate flows with heat transfer into muzzle brakes, *15th International Symposium on Ballistics*, Jerusalem, (1995).

[2]    R. Cayzac , E. Carette, T. Alziary de Roquefort, C. Vaglio, J. Brossard, Intermediate ballistics computations and validations, Ballistics '98, *17th International Symposium on Ballistics*, Midrand, South Africa, (1998).

[3]    J. C. T. Wang & G. F. Widhopf, Numerical simulation of blast flowfields using a high resolution TVD finite volume scheme, *Computers & Fluids*, 18, 103-137, (1990).

[4]    S. T. Zalesak, Fully multidimensional flux corrected transport algorithms for fluids, *J. Comp. Physics* 31, 335-362, (1979).

[5]    G. F. Widhopf, J. C. Buell & E. M. Schmidt, Time-dependent near field muzzle brake flow simulations, AIAA/ASME 3rd Joint Thermophysics, Fluids, and Heat Transfer Conference, St. Louis, AIAA preprint 82-0973, (1982).

[6]    G. Klingenberg & J.M. Heimerl, *Gun Muzzle Blast and Flash*, Progress in Astronautics and Aeronautics, Vol.139, AIAA, (1992).

# SIDE FORCE PRODUCED BY LIQUID INJECTION ON A ROCKET NOZZLE

REY F.[1], JENARO G.[1], ROSAS F.[1], LÓPEZ C.[1], SALVÁ J.[2], TIZÓN J.M.[2]

(1)Laboratorio Químico Central de Armamento (LQCA)  P.O.Box 1105, 28080 Madrid, SPAIN.
(2)Escuela Técnica Sup de Ingenieros Aeronauticos (ETSIA-UPM), 28040 Madrid, SPAIN.

**Abstract:** The measure of side force produced on a rocket nozzle when injecting liquid has been determined. All the parameters that have major influence on the calculations of the total force were carefully measured using digital and analogic data recorder available in LQCA. Two theoretical approximations have been studied in parallel, the first one is an 1-D analytical and dimensional analysis, the second one is 3-D CFD analysis.

## 1. INTRODUCTION

The interest in getting smaller and cheaper actuators for projectiles, rockets or missiles has made the LQCA to study several kinds of actuators. In particular, we thought that the availability of new materials could improve the application of an old technology, the thrust vector control by secondary injection.

In order to make the rocket change attitude during flight it is necessary to reach certain level of side force in specific time intervals during the hot state. There are several ways to obtain this side control force, and the technology to get better results is continuously changing. In this paper, the selected technology is thrust vector control by high-pressure liquid injected, a method used in the 60's. This technology was mainly focused towards long burning times, in this situation the time response of the valves was not very important. When applying this control system to motors with a few seconds of burning time, the control pulses and the speed of the valve cycle must have an operation time within milliseconds to ensure that the response of attitude is correct. The improvement of the valves on performance and high time response added to the new liquids available in the industry makes this control system more affordable. In addition, liquids used in the past to obtain high performance in control systems were dangerous when handling and toxic; nowadays it is possible to find liquids yielding good specific impulse, very cheap and non-toxic commercially available.

A rocket experience a side force when high-pressure liquid is injected in the rocket nozzle exit cone. One of the purposes of this paper is to optimize parameters that have a direct impact on side force (i.e. location of the injector downstream the nozzle, pressure of liquid injection, ratio of main stream mass flow-to-liquid mass flow, injection angles).

The outline of the paper is as follows: We are going to give a brief explanation about the phenomena and theoretical prediction of side force using 1-D analysis in section 3. The experimental set-up and main results are described in Section 4. Three dimensional calculations are presented in Section 5.
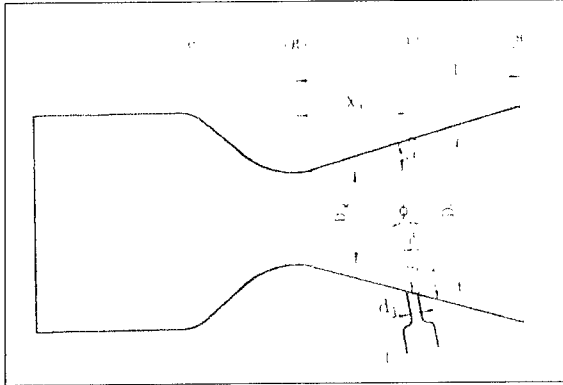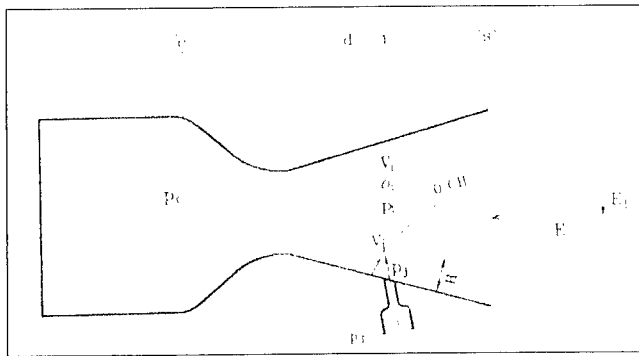
## 2. NOMENCLATURE



Figure 2.1 Nozzle geometry



Figure 2.2 Fluid variables

| | | |
|---|---|---|
| CFD | Computational Fluid Dynamics |
| $C_d$ | Discharge coefficient |
| $d_i$ | Diameter of injection |
| $V_j$ | Velocity of injection |
| n | number of injectors |
| $\rho_l$ | Density of liquid |
| $\rho_i$ | Density of main stream flow at the injection station |
| $\dot{m}_l$ | Lateral mass flow |
| $\dot{m}$ | Main mass flow |
| Mi | Mach number at nozzle station |
| $P_j$ | Injection Pressure |
| $P_i$ | Nozzle station pressure |
| $P_c$ | Chamber pressure |
| $P_d$ | Pressure upstream shock wave |
| $P_{dd}$ | Pressure downstream shock wave |

$\phi$   Injection angle (also named AOI)
$E_l$   Lateral force (also named Flat)
E   Axial thrust (also named Fax)
$\epsilon_i$   Station of injection (x/l)
x   Distance from the point of injection to the throat
l   Distance from the throat to the exit plane of the nozzle
Isp   Specific Impulse
$\gamma$   Ratio of specific heats
$D_g$   Diameter of Nozzle throat
$D_l$   Diameter of station where injection occurs
$\alpha$   Half angle of conical nozzle

## 3. PROBLEM FORMULATION AND ONE DIMENSIONAL ANALYSIS

The injection of a liquid into the supersonic exhaust of a rocket motor produces side thrust by a combination of effects that include the thrust of the injected jet itself, pressures on the nozzle wall from shock waves, and pressures on the nozzle wall resulting from the addition of mass and energy to the supersonic gas stream[1]. The efficiency of the system depends on

many parameters, for example: properties of the injected liquid, number of injection orifices, injector location, injection pressure and discharge angle.

The process is complex in nature because it involves several phenomena like liquid injection, atomization, jet penetration, evaporation, and main and secondary stream interaction. The first part of the program consisted of the study of these phenomena and a dimensional analysis. The works of Lefebvre [2] on injection and evaporation, Adelberg [3, 4], Kolpin [5] and Nejad [6] on atomization and Joshi [7], Baranousky [8], Kush [9], Schetz [10] and Thomas [11] on jet penetration were evaluated. The main-secondary stream interaction and the pressure variation in the proximity of the orifice was studied using the works of Newton [12] and Wu [13].

The experimental results are very few and they are not normalized in terms of procedure. One of the most relevant expressions is given by Green and McCullogh, reference [14]. It has been generalized in the following form:

$$\frac{E_\ell}{E} = f_G(liquid, \, \varepsilon_i, n, \phi) \left(\frac{\dot{m}_\ell}{\dot{m}}\right)^{0.5} \left(p_I - p_j\right)^{0.25}$$  [3.1]

This expression includes a function $f_g$, which takes into account geometrical parameters of injection and characteristics of the liquid used.

The experiments performed at LQCA measured all the necessary parameters to obtain the expression 3.1. If the number of injectors $n$ is 1, Then this function, $f_g$, is unique for every injection configuration. The expressions used to calculate parameters to include in expression 3.1 are:

The mass flow of the liquid is given by:

$$\dot{m}_\ell = \frac{\pi}{4} d_j^2 \rho_\ell V_j C_{Dj} n$$  [3.2]

and the velocity at which the liquid is injected follows:

$$V_j = \sqrt{\frac{2\left(p_I - p_j\right)}{\rho_\ell}}$$  [3.3]

It can be established a relation between the chamber pressures and the injection pressure. (see nomenclature and figures in section 2)

$$\frac{p_j}{p_c} = \frac{p_j}{p_i}\frac{p_i}{p_c} = \frac{p_j}{p_i}\Big/\left(1 + \frac{\gamma-1}{2}M_i^2\right)^{\frac{\gamma}{\gamma-1}}$$  [3.4]

where $\dfrac{p_j}{p_i}$ is a function of the incident Mach number (the relation between these values has been taken from reference [13]).

The application of these expressions allowed us to have an approximation for the value of the function $f_G$ for each configuration tested. Table 3.1 shows the values of $f_g$ for different configurations of injections and for the liquid used ( R-134 ):

Table 3.1 Function $f_g$ for different configuration of injection

| Configuration | $f_g$ |
|---|---|
| x/l = 0.3, di=5 mm, $\phi$ =25 ° | 1.6452E-2 |
| x/l = 0.25, di=5 mm, $\phi$ =0 ° | 1.573109E-2 |
| x/l = 0.25, di=5 mm, $\phi$ =25 ° | 1.42110 E-2 |
| x/l = 0.25, di=3.5 mm, $\phi$ =25 ° | 1.2069E-2 |

# 4. EXPERIMENTAL

The experiments carried out in the LQCA consisted of a rocket motor mounted in a vertical test bed. The test bed has a three load cells and it is able to measure axial, torsion and lateral forces. The nozzle of the rocket was prepared to introduce liquid into the main stream (downstream the throat). On one side of the test bed a tank was located containing the liquid to be injected. This tank was pressurized by an external air-compressor so that the liquid could be injected at certain level of pressure into the main stream. The tank and the injectors located at the rocket motor nozzle were connected to high pressure resistant tube and a high-response electro-valve. The electro-valve was connected to a control/acquisition computer program. The control of open/close cycle was pre-programmed so that the valve can perform the cycles automatically within the 4.5 seconds of combustion time.

The pulses programmed for the valves had mean duration of 100 ms. This train of pulses were located in the area of nearly neutral combustion of the solid rocket motor where the chamber pressure and thrust have little variation.

## 4.1 Parts of the experimental setup

Vertical Test Bed: The vertical test bed located at the LQCA facilities is capable of testing rocket motors up to 260 mm in diameter. It is able to measure axial loads up to 120000 N and lateral forces, in a single plane up to 4900 N.

Motor: The motor used for the experiments was a Duero solid propellant rocket. This motor has a 225 mm in diameter and 2 meters in length. The propellant is a HTPB/AP/Al composite and the time of combustion is nearly 4.5 seconds. The nominal chamber pressure is 12 MPa yielding a net thrust of 68000 N. The nominal mass flow is 24.83 kg/s.

Nozzle: A regular nozzle for the Duero motor was modified in order to inject the liquid at the desired station downstream the divergent section, at the desired diameter and angle of injection. The modifications performed on the nozzles involved the following: variation in the injection station (25% and 30%), variation of the angle of injection (0° normal to axial and 25° downstream the nozzle) and variation on the injection diameter (5 mm and 3.5 mm). The fixed parameters of the nozzle are, throat diameter of 68 mm and expansion ratio of 10.25. The nozzle has a parabolic configuration.

Valves: The valves allow the liquid to flow from the liquid tank to the injectors that are located at nozzle. The maximum pressure difference allowed is 10 MPa for the commercial valve used in the first tests: ASCO SCB223 A25. The use of a high response valves, such as the Circle Seal, allowed a reduction in total time at the same mass flow.
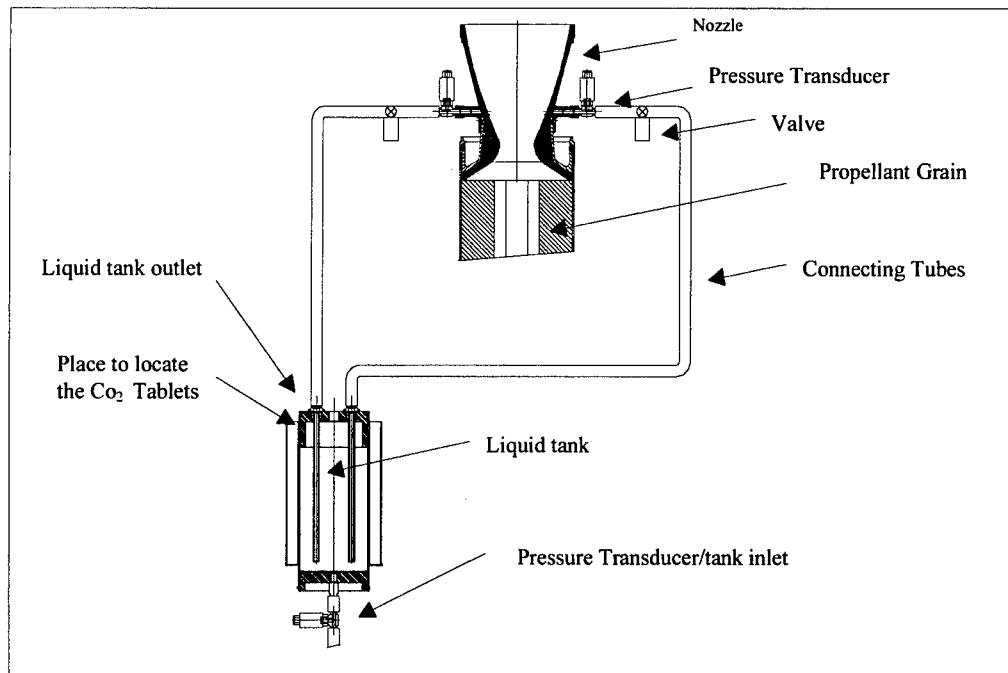
Figure 4.1 General Description of the experimental set up

**Liquid Tank:** The R134 refrigerant liquid used for the experiment was confined in a special cylinder tank composed of one inlet and two outlets. The main characteristics of liquids used for secondary injection must have high density, high specific impulse and low toxicity.

**External Compressor:** The external compressor is electrically activated from the control room in order to pressurize the liquid tank. The pressure in the liquid tank will decay at each pulse because the external compressor is not able to maintain constant pressure level within very short time.

**Measurements and Control:** A total of 12 signals were registered for the experiment. These signals provided information about: time response, mass flow and lateral forces. Specific control-acquisition software was used to control the open-close cycles of the valves, the firing signal and the acquisition parameters (scan/second, frequency, etc.). Experiments performed at LQCA involved two injectors per nozzle, and the control over the valves was studied to avoid overlapping signals.

## 4.2 Experimental Results

The following figures show some measurements taken during one of the test using a Duero motor rocket. In this particular test the nozzle was modified with two injectors at different location downstream the throat. Injector 1 had a diameter of 5 mm and was located at 30% of the divergent section of the nozzle. The angle of injection measured upstream normal to axis was 25°. Injector 2 has a diameter of 5 mm, located at 25% (closer to throat) and the angle of injection normal to longitudinal axis of the nozzle. For this particular test, a total of 7 pulses were performed. Pulses 1, 2, 4 and 6 with injector 1; pulses 3, 5, and 7 with injector 2. The

programmed pulses were 100 ms in duration, figure 4.5 shows the lateral forces (after being filtered) obtained in each pulse.
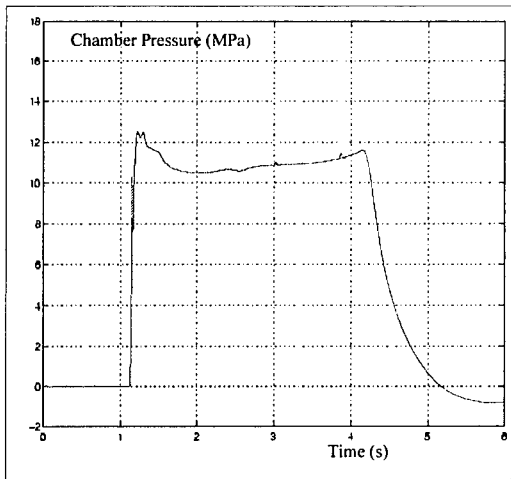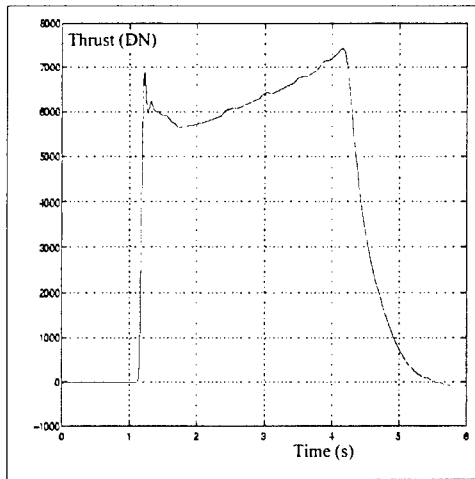


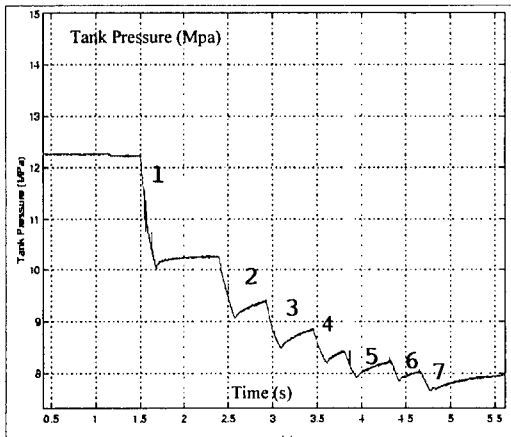Figure 4.2 Chamber Pressure



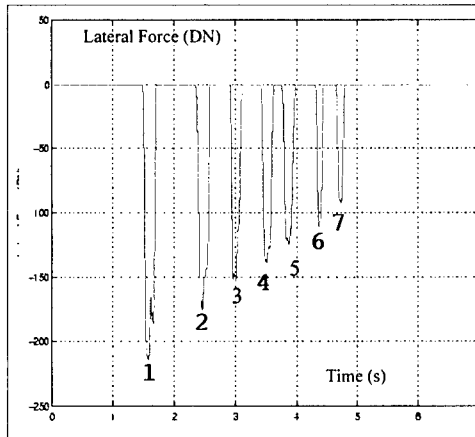Figure 4.3 Axial Thrust



Figure 4.4 Liquid Tank Pressure



Figure 4.5. Lateral Force

The influence of each pulse in the axial thrust can be observed in Figure 4.2. Since liquid was added at the nozzle, the total mass flow is increased and therefore thrust is slightly increased. Figure 4.4 shows the pressure of the liquid tank, which decreases as the pulses are taking place. These pulses generated a rebound that was registered by the pressure transducer placed in the liquid tank. Figure 4.5 show the lateral force obtained for each one of the pulses. Figure 4.6 shows the pressure after the valve, corresponded with the injector 2. This pressure is used to calculate the mass flow of liquid. The influence of the injection station, can be obtained from this test, as indicated in figure 4.7.

With the results of other tests it is possible to obtain the influence of other geometrical parameters of injection, as figure 4.8 and 4.9 shows. These results indicate how some geometrical parameters can be modified in order to obtain better side force at a constant mass flow ratio.
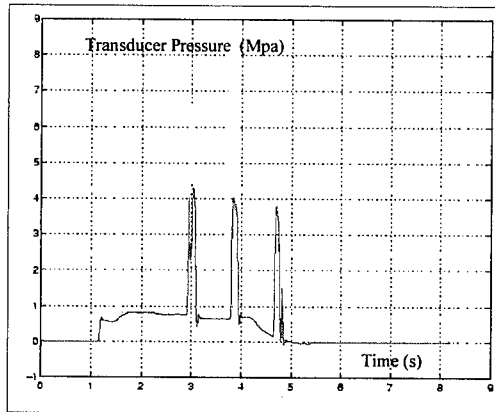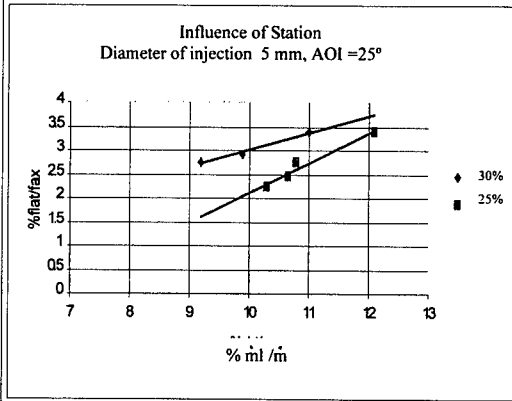
Figure 4.6 Pressure after the valve



Figure 4.7 Influence of Station
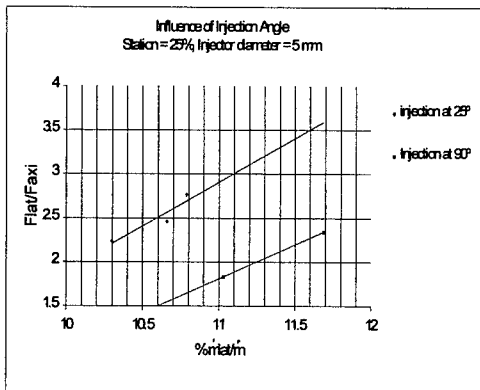


Figure 4.8 Influence of injection angle.
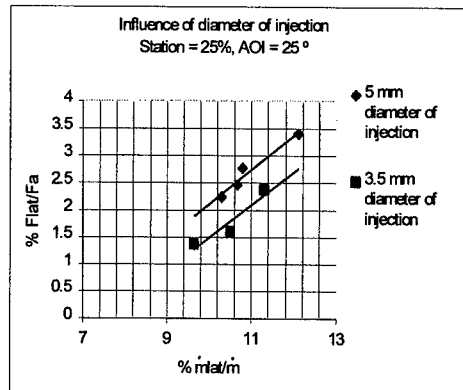


Figure 4.9 Influence of diameter of injection.

It can be observed that the liquid injection at 25° yields a higher side force, and also that the injection diameter of 5 mm worked better than the injection diameter of 3.5 mm at constant mass flow ratio. These results follow the general trends reported by other authors, for example, reference [1] has observed that a better penetration is achieved when the liquid is injected at an angle upstream the throat.

Regarding time delay, this variable depends on the time response of the valve used, the distance between the injection port and the outlet of the valve, and mainly on the pressure difference across the valve. The time delay – measured between the input signal to the valve and the first peak of lateral force - was more than 150 ms with the commercial valves, and about 25 ms with the high response valves; although the last one had a theoretical response time of about 10 ms. Therefore the time delay is higher than expected.

## 5. THREE DIMENSIONAL ANALYSIS

We have applied a finite element code in order to evaluate which is the best possible design. The first step only includes the modeling of a single non-reacting liquid jet interacting in

compressible supersonic cross-flow. The second step is trying to integrate the atomization characteristics of the liquid, and also the evaporation phenomena. In general, we have found that the most difficult task is to model the combustion phenomena.

The simulation process is done mathematically by discretizing the flow equations and then solving them. CFD solutions can pick up fluid flow and heat transfer trends that might not have been expected or predicted otherwise. The results of a simulation contain all the relevant flow variables such as velocities, pressures, temperatures and densities.

The grid of the modelling is presented in the figure 5.1. This grid has been refined in the zone around the injection. The boundary conditions are the chamber pressure, the properties of the liquid, and the conditions of the injection: the pressure of the liquid after the valve or the velocity in the injection area.
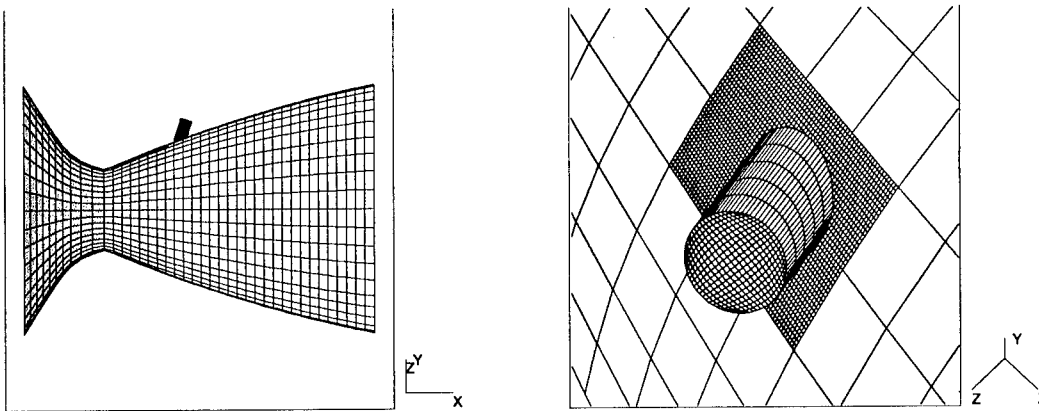


Figure 5.1 Grid of the model and detail of the injection area

Numerical results have been made for several configurations, these corresponds with those tested in the previous experimental tests.

Figure 5.2 shows that the boundary layer upstream of the jet separates, and forms a shock, which attaches itself to the main shock wave surrounding the jet. It was possible to see that the degree of jet penetration mainly depends on the jet-to-crossflow momentum flux ratio and pressure ratio, as other scientists have previously shown[5]. The simulation results show the deviation of the main stream and the penetration of the fluid injected.

As we are interested in the value of the lateral force produced, or rather, the relation between the lateral force and the axial one. On integrating the pressure on a grid which covers the contour's area of the nozzle, an asymmetry appears, related with the lateral force. Figures 5.3 and 5.4 present the results translated to terms of forces.

Figure 5.2 Case with a great deviation of the flow



Figure 5.3 Relation Flat/Fax vs Station



Figure 5.4 Relation Flat/Fax vs Diameter

It is possible to see that the solutions of the simulation are in the range of 80 to 85% of the respective experimental result. We hope to obtain better results when we have account the phenomena of evaporation and reaction of the fluid.

# 6. CONCLUSIONS

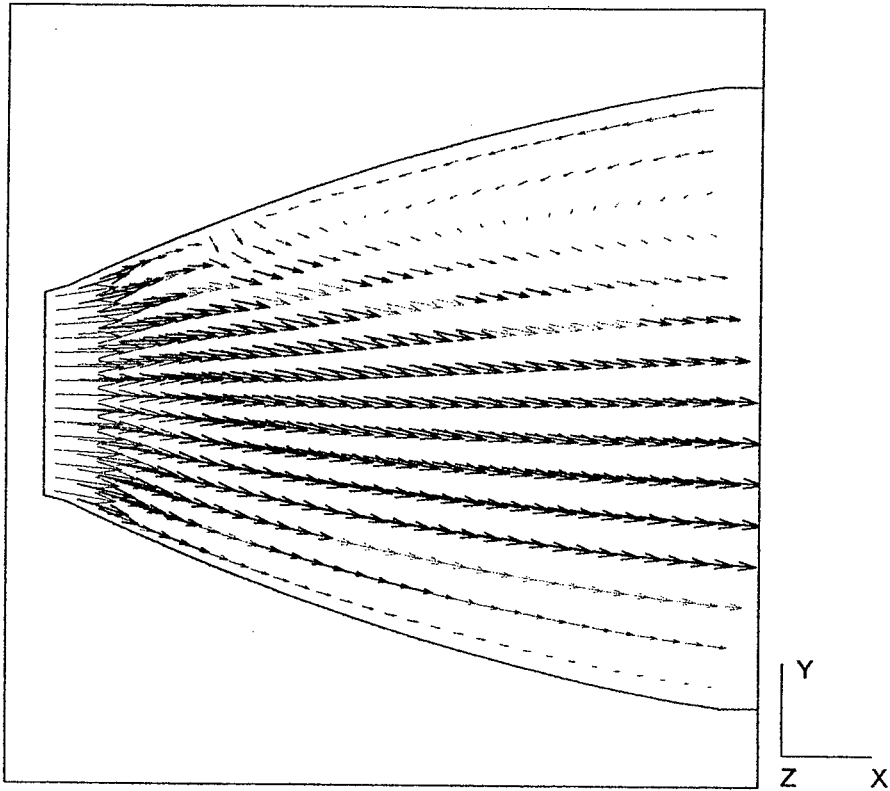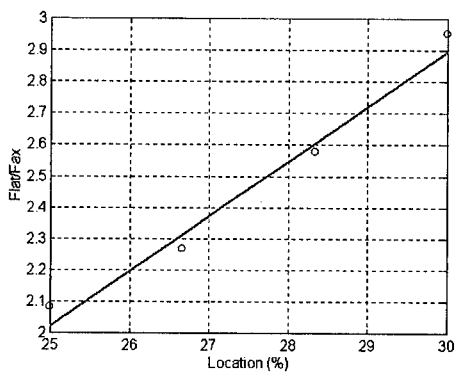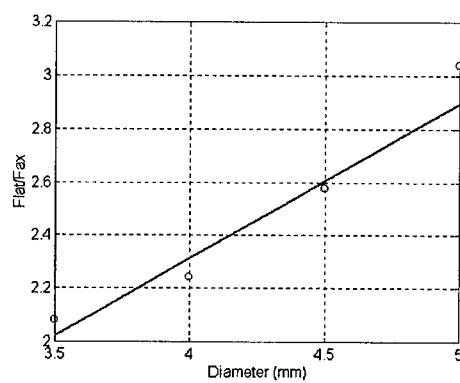The results presented show the advantages and drawbacks of the thrust vector control technology as applied to small systems: there are non-toxic and very cheap new liquids, smaller valves and new design procedures with at present CFD capabilities. However, the reaction time of the valves is low when the injection pressure is high, and the specific impulse is not as high as expected.

The three dimensional analysis has highlighted the entire process. The numerical results agree up to a point (80 to 85 % of the experimental results) with the previous tests. We hope to obtain better results when we put into account the phenomena of evaporation and atomization of the fluid. It has been found that the most difficult phenomena to model is the combustion.

# 7. REFERENCES

[1] NASA SP-8114 "Solid Rocket Thrust Vector Control", 1974.
[2] Lefebvre,A.H., "Atomization and Spray" in Combustion: An International Series, N.Chigier, De., Taylor and Francis 1989.
[3] Adelberg, M., "Mean Drop Size Resulting from the injection of a Liquid into a High-Speed Gas Stream", AIAA Journal Vol 6, No 6, pp.1143-1147, June 1968.
[4] Adelberg, M., "Breakup Rate and Penetration of a Liquid Jet in a Gas Stream" AIAA Journal Vol 5, No 8, pp.1408-1415, August 1967.
[5] Kolpin, K.P. Horn, K.P. and Reichembach, R.E.; "Study of Penetration of a Liquid Injectant into a Supersonic Flow", AIAA Journal Vol 6, No 5, pp.853-858, May 1968.
[6] Nejad A.S.and Schetz, J.A., "Effects of Properties and Location in the Plume on Droplet Diameter for injection into a Supersonic Stream", AIAA Journal Vol 21, No 7, pp.959-961, July 1983.
[7] Joshi P.B.and Schetz J.A.; "Effect of Injector Shape on Penetration and Spread of Liquid Jets", AIAA Journal Vol.13 No 9, pp. 1137-1138, September 1975.
[8] Baranousky, S.Y. and Schetz, J.A., "Effect of Injection Angle on Liquid Injection in Supersonic Flow", AIAA Journal Vol 18, No 6, pp. 625-629, June 1980.
[9] Kush, E.A. and Schetz, J.A. "Liquid Jet Injection into a Supersonic Flow", AIAA Journal Vol 11, No 9, pp.1223-1224, September 1974.
[10] Schetz, J.A. and Padhye, A., "Penetration and Breakup of Liquid in Subsonic Air Streams", AIAA Journal Vol 15, No 10, pp.1385-1390, October 1977.
[11] Thomas, R.H. and Schetz, J.A., "Distribution across the Plume of Transverse Liquid and Slurry Jets in Supersonic Airflow", AIAA Journal Vol 23, No 12, pp.1892-1901, December 1985.
[12] Newton,J. And Spaid,F.W., "Interaction of Secondary Injectants and Rocket Exhaust for Thrust Vector Control", ARS Journal August 1962, pp. 1203-1211.
[13] Wu, J.M., Chapkis, R.L. and Mager A., "Approximate Analysis of Thrust Vector Control by Fluid Injection", ARS Journal December 1961, pp.1677-1685.
[14] GreenC.J. and Mc Cullough F. Jr., "Liquid Injection Thrust Vector Control", AIAA Journal Vol 1, No 3, pp.573-578, March 1963.

# INTERMEDIATE BALLISTICS AND AEROBALLISTICS OVERVIEW AND PERSPECTIVES

## Dr. CAYZAC R. [1] and CARETTE E. [1]

(1) Giat Industries, Division des Systèmes d'Armes et de Munitions,
7 Route de Guerry, 18023 Bourges Cédex, France.

**Abstract :** The aim of this paper is to present an overview of the applied research carried out during the fifteen last years by Giat Industries in cooperation with different French research organizations like ISL, LEA, LEES, LRBA and ONERA.
Mainly, the contribution of the fluid dynamics to the field is highlighted. Experimental and numerical investigations have been carried out with the constant objectives of understanding and extensive validation. Industrial state-of-the-art and future trends are presented

# 1. INTERMEDIATE BALLISTICS

## 1.1 SABOT SEPARATION : EXPERIMENTAL APPROACHES

### 1.1.1 Firing tests [2-4]

Ammunition accuracy and dispersion is decreased by many sources of disturbance. An experimental program was designed whose aim was to quantify certain possible sources of disturbance (which is a very difficult task), and to identify and highlight certain components. For this, the launch disturbances relating to in-bore dynamics, muzzle exit conditions, and muzzle gas dynamics influences have been experimentally analyzed. Considerable apparatus and instrumentation, presented in Fig.1, were implemented in a free flight ballistics corridor. The results obtained were specific to the projectile-gun pair used. They showed that the muzzle aiming contribution is significantly small in comparison to the overall dispersion. The crossing muzzle velocity contribution is small (3% of the total dispersion in terms of standard deviation). According to X-ray and shadow visualizations, pressure ground measurements, theoretical predictions, and calculations, the sabot discard process occurs outside the different muzzle waves. In that case, external perturbations seem to be the most important source of disturbance. Examples of results are presented in Figs. 2, 3, 4, 5 and 7.

### 1.1.2 Separation processes [2-8]

An experimental study was carried out whose objective was to obtain drag, lift and rear separation processes for CFD validation purposes.

Drag separation could be obtained for a classical external sabot profile with only a forward pocket. In this case, the gas discharge generally holds the sabot components locked together, the sabot discard process occurs outside the different muzzle wave systems (Fig.7). The separation is mainly a sudden swivel round of the sabot components with contact between the projectile body and the rear part of the sabot components. In this case, the mechanical interactions are substantial. The drag separation is obtained by "pitch moment".

The lift separation process could be produced by the presence of a rear or middle pocket. The intermediate ballistic flow is employed. During the first instants, discard is guided by the gas discharge with rear separation. After that, separation is characterized by a quasi-parallel escape between the firing axis and the longitudinal axis of the sabot components. In this case, the mechanical interactions are fewer. The lift separation could be obtained by "force" or by "moment".

Rear separation, in the initial opening stage, could be obtained using a sabot with a rear pocket and with, or without, a front pocket of reduced efficiency.

Figure 6 shows that the different separation processes have been obtained. Our future aim will be to correlate the different separation processes with ballistic accuracy and dispersion.

### 1.1.3 Aerodynamic separation [3,5,7] (cooperation with ONERA)

In the case of a separation process occurring outside the different muzzle waves, purely aerodynamic separation was investigated in the ONERA blow down wind tunnel S3MA in Modane (Fig.8). Extensive unsteady surface pressure distribution measurements and shadowgraph visualizations were carried out to provide data for the calibration of CFD codes. Shock/boundary layer interactions and separated regions were clearly identified. CFD were performed using Euler and Navier-Stokes codes which incorporate the Chimera technique. An example of strioscopy is presented in Fig.9. As shown in Fig.10, a satisfactory agreement between experiments and computations was obtained.

### 1.2 CFD AND VALIDATION OF THE INTERMEDIATE BALLISTIC FLOW (cooperation with LEA)

The discharge of a propellant gas was modeled as an axisymmetric or 2D plan inviscid flow of a calorically perfect gas and computed with Harten's second order total variation diminishing scheme (code FREIN). The complex geometry, evolving in time because of the displacement of the projectile, was taken into account, within the framework of a non adapted uniform cartesian mesh, by means of a special treatment of the boundary conditions based on a generalized reflection principle. The gas behaves as a calorically perfect one, the ratio of specific heats and the perfect gas constant R of the equation of state were obtained using thermodynamic computations.

The mathematical modeling of the firing process includes the precursor flow discharge and the presence of the projectile. The boundary conditions, after projectile exit, at the barrel muzzle were computed using a 1D unsteady numerical code, based on the characteristics method, according to a pull piston analogy. The boundary conditions, before the projectile exit, at the barrel muzzle were obtained with the resolution of the 1D Euler equations according to a push piston analogy.

The main difficulties concerning the grid system are, firstly, the rather complex geometry (in particular in the case of a multi-element muzzle brake), and secondly, the fact that the computational domain evolves in time according to the displacement of the projectile.

### 1.2.1 Flow through a muzzle brake [1,5,8,12]

Experiments were performed using a 120mm gun. A single and a double-baffle muzzle brake (illustrated in Fig.11) were tested. The wall pressure was measured by means of piezoelectric transducers. Their locations are also given in Fig.11.

Figure 12 gives an example of the time history of the flow through the double-baffle muzzle brake during the first 5ms and shows that the flow involves a very complex pattern of moving shocks.

The computed wall pressures are compared with the measurements in Fig.13. Agreement is satisfactory. The measurements are often higher than the computed values. The most likely explanation for this is the fact that we have assumed an axisymmetric flow while the aperture in the baffle spans only about 180° instead of 360°.

In addition, the computed unsteady evolution of the drag force has shown a short propulsive phase just after the projectile muzzle brake exits. This is due to propellant gas thrust and local reverse flow conditions.

### 1.2.2 Blast wave interaction with a plane surface [4-6,8,9-11,13-17]

Using a 44mm smoothbore gun, the muzzle blast characteristics were investigated by visualization of the muzzle flow field by the indirect shadow system with Fresnel-Lens and also by ground piezoelectric pressure measurements (Fig.14).

The unsteady pressure fields are presented in Fig.15. The main structures of the unsteady over-expanded jet flow (Mach disk, barrel shock, and blast wave) and of the projectile aerodynamic (bow shock), are numerically well captured. The incident blast wave is reflected by its interaction with the plane surface. The transition between a regular reflection and a Mach reflection is numerically well observed.

The average pressure measurements (according to test repetitions) are compared with computations in Fig.16. This shows that the experimental overpressure, the pressure decay, and the negative pressure phase agree quite well with numerical predictions (exept in the transition region).

## 1.2.3 CFD of the separation [8]

A first attempt at the numerical prediction of the unsteady sabot separation, in the intermediate ballistic flow conditions, was carried out using the FREIN code. The sabot component trajectory was computed with the knowledge of the unsteady aerodynamic forces and of the actions of contact. The first results of the CFD lift and drag processes are presented in Fig.17.

Many theoretical and numerical difficulties are currently being encountered : breakdown of the numerical scheme in the projectile-sabot contact region, ... In the future, in the scope of more validation, we intend to carry out more complete visualizations. We also plan to solve the 3D Euler and Navier-Stokes equations.

## 1.3 SIMILITUDE LAWS [4-6,8,9-11,13-17] (cooperation with LEES)

Numerous experimental studies of the air blast due to high explosives, gaseous detonations and firing guns generators have been conducted. The positive overpressure decay versus the distance and the space-time diagrams have been analyzed. A very simple analytical quasi-universal function has been found, which correlates the two diagrams and complies the asymptotic behavior of the shock wave velocity with the sonic velocity.

This law fulfills the well-known similitude property. Figures 18 and 19 present examples of results in the case of blast waves generated from TNT and from detonation tubes.

At the moment, we are trying to show the feasibility of testing muzzle artifices with detonation tubes.

## 2. PROJECTILE AEROBALLISTICS

## 2.1 AERODYNAMICS

## 2.1.1 Yawing and spinning projectiles [30,32,33] (cooperation with ONERA-LRBA)

In order to better estimate the aerodynamics of yawing and spinning projectiles, a numerical - experimental action was set up. The attention focused mainly on the Magnus effect with the objective of understanding the essential features of the flowfield.

First, on the basis of the well-known supersonic experimental results of the spinning SOC, SOCB and TOCBT models (Fig.20). Second, the aerodynamics of a Meplat SOCBT projectile were investigated over a wide range of angles of attack, angular speeds and Mach numbers.

Extensive Navier-Stokes computations and wind tunnel tests were carried out. The computer code FLU3M was used for the predictions. This solves the time dependent form of both Euler and Navier-Stokes equations. An improvement to the Baldwin-Lomax turbulence model was performed. A "multidomain approach" was implemented in the code to deal with complex geometries and also to reduce computation memory costs. The numerical method used was Roe's approximate Riemann solver with second order TVD corrections obtained, by the MUSCL approach. The time-dependent equations were matched to a steady state using 3 ADI block implicit method.

Validation results, shown in Figs.21, and 22, demonstrate a global satisfying agreement has been obtained. Computations in the subsonic regime are in progress. In supersonic, at small incidences, the Magnus effect is due to the spin-induced distortion of the boundary layer. At higher incidences, it seems that vortex asymmetry generates an additional lateral force, which tends to invert the total Magnus force. These two sources are highlighted in Figs.23 and 24.

In order to predict dynamic instability, an ambitious program of work is actually in preparation including wind tunnel and free flight tests of instrumented projectiles and extensive CFD validation.

## 2.1.2 Kinetic projectile [18,19,22,25,28,29,31,33,34] (cooperation with ONERA-LRBA)

A first CFD computation of the Magnus effect over a spinning finned projectile was successfully undertaken and completed.

For this, an unsteady algorithm was developed to predict the unsteady flow. The 3D Reynolds-Averaged Navier-Stokes equations with the Baldwin-Lomax algebraic turbulence model were solved. The local equations were integrated over a moving control volume. For this, a general grid movement was implemented in the implicit Gear's time second order formulations of the discrete problem. A block LU factorization was used to invert the implicit system more easily.

Different flow topologies could be encountered on the lee-side part of the fins in particular an attached flow at low incidences, and a separated flow at the leading edge with a lee-side shock at higher incidences. The lee-side flow, corresponding to this second situation, on two opposite spinning fins, with respect to the plane of symmetry, is presented in Fig.25. One common characteristic is the shock, which starts from the apex to the trailing edge. It occurs when flow, rolling around the leading edges, bumps into the body boundary layer. The second characteristic is the development of a tip vortex, particularly for the right fin, whose spinning movement opposes the transversal freestream.

From a physical point of view, there are three main possible sources contributing to the Magnus effect : the interaction between the asymmetric body wake and the fins, the apex shock and tip vortex, the spin-induced modifications of the local incidences.

The first and very recent validation results are presented in Fig. 26. More detailed validation is now needed.

## 2.1.3 EFP projectiles [21,27] (cooperation with ONERA)

The hypersonic ballistic projectile HB2 was used as a benchmark configuration. This model is a standard of the sixties, and is close to EFP geometry with a low flare semi-angle (8.35°). A study was conducted whose objective was to determine a numerical strategy, which enables the static stability to be predicted.

Aerodynamics computations were performed using several methods : component build-up, local surface inclination (Newtonians, shock-expansion, mixed, ...) and CFD (3D, Euler and laminar or turbulent Navier-Stokes equations).

Local surface inclination methods using modified Newtonian law are efficient for the prediction of the normal and axial force coefficients, but are unable to estimate the pitching moment coefficient. For the HB2 model, Euler computations are accurate for the estimation of the aerodynamic coefficients CN, Cm and for prediction of the local pressure distributions for $M_\infty = 5.11$ and 8.09 and for values of $\alpha$ up to 10°. Examples of results are presented Figs.27 and 28.

## 2.1.4 Unconventional sub-munitions [20,26]

Due to large separation regions, the CFD prediction of unconventional shapes is often impossible. The main reason is the deficiency of the turbulence model (Fig.29).

Consequently, for sub-munitions, an experimental methodology, based on a wind tunnel test, was defined. Two kinds of wind tunnel tests were systematically employed. The influence of the Mach and of the Reynolds number on the static aerodynamics were evaluated with global force and moment measurements (Fig.30) in a "classical" wind tunnel. Under controlled initial conditions in angle of attack and roll rate, the Froude number influence on the dynamics free flight was investigated in a vertical subsonic wind tunnel (Figs.31 and 32).

## 2.2 AEROTHERMICS AND ABLATION

## 2.2.1 Aerothermics [23,24,27,31] (cooperation with ONERA)

In order to determine the heating loads on kinetic projectile fins, experiments were carried out in the ONERA R2Ch wind tunnel. Isolated fins fixed downstream of a long flat plate were intrumented with surface thermocouples (Fig.33). Wall heating was also measured by IR thermographie camera.

A 2D aerothermal code was developed : in the stagnation region, the heat fluxes were obtained from the formulation of Kemp-Riddell and Boison elsewhere flat plate approximations were conducted; in the material, the conduction equation was solved.

Figures 34 and 35 present validation results obtained on the wall heat flux and temperature.

## 2.2.2 Ablation (cooperation with CEA)

Arc jet tests were performed in the AEROSPATIALE JP200 tunnel. TUNGSTEN and DENAL ogives were tested in order to evaluate the survivability of projectiles subjected to high convective heat fluxes due to free flight velocity up to 2750m/s. The ablated shape histories was deduced from camera visualizations. An example of experimental results is presented in Fig.36. With an ogive radius of 3.8mm, the cold wall stagnation heat flux is about 70 MW/m$^2$. In case of TUNGSTEN, the mean ablation velocity is about 1.5mm/s.

## 2.3 AEROELASTICITY [35] (cooperation with ISL-LEES)

A recent numerical-experimental program has been defined. This program includes the development of a numerical code and the realization of wind tunnel and firings tests. The complete equations of motion, based on a Lagrangian approach, of a flexible supersonic high L/D body have been written.

Figure 37 illustrates the fact that a bending angle may be created by aerodynamics even when no initial bending is induced during the launch. In Fig.38, on the contrary, we assume an initial 3° bending angle and study its evolution during a one second flight. We can note that the projectile oscillates through a bent configuration.

In the future, we intend to carry out a complete parametric study to evaluate the influence on the body's aerodynamic behavior of key parameters like the projectile's rigidity, L/D ratio, initial conditions and roll rate. The main difficulties will probably be to obtain experimental data for validation and to well delimit the coupled aero-mechanical model.

## 3. FUTURE TRENDS

In the past, ballisticians used experimental firing tests and semi-empirical prediction methods. With increasing computer power, and memory and efficiency of the CFD codes, numerical simulation is currently invading the ballistics. As for the missile community, a standardization of the CFD codes will be necessary (turbulence models, …).

From an industrial point of view, in the field of "classical projectiles", the future realistic needs should mainly be concentrated on :

- the CFD of the sabot separation under intermediate flow conditions,
- the CFD of more aerodynamic coefficients (Magnus, pitch damping moment, …),
- the achievement of reliable data on the aeroballistics heating and ablation,
- the interdisciplinary activities (aeroelasticity, …).

## 4. ACKNOWLEDGMENTS

## 5. REFERENCES

### 5.1 INTERMEDIATE BALLISTICS

[1]  T.Alziary de Roquefort, R.Cayzac, E.Carette and P.Balbo, "Theoretical and Experimental Comparison of Unsteady Flow Through a Muzzle Brake", *13th International Symposium on Ballistics*, Stockholm, Sweden, (1992)

[2] R.Cayzac, A.Mennechet and E.Carette, "Sources of Dispersion Occuring with APFSDS Launch Dynamics", *15th International Symposium on Ballistics*, Jerusalem, Israel, (1995)

[3] R.Cayzac and E.Carette, "Kinetic Energy Projectile Launch Dynamics and Aeroballistics", *AIAA 14th Applied Aerodynamics Conference*, New Orleans, USA, (1996)

[4] C.Vaglio, R.Cayzac and J.Brossard, "Shock Wave Simulation of Firing Gun with Gaseous Detonation", *16th International Symposium on Ballistics*, San Francisco, USA, (1996)

[5] R.Cayzac, C.Vaglio, J.Brossard, E.Carettte and T.Alziary de Roquefort, "Transitional Ballistic Investigations", *47th Aeroballistic Range Association Meeting*, ISL, Saint-Louis, France, (1996)

[6] I.Sochet, T.Lamy, J.Brossard, C.Vaglio and R.Cayzac, "Critical Tube Diameter for Detonation Transmission and Critical Initiation Energy of Spherical Detonation", *16th International Colloquium on the Dynamics of Explosions and Reactive Systems*, Cracow, Poland, (1997). published in *Shock Waves 9*, pp.113-123, (1999)

[7] P.Champigny, P.d'Espiney and D.Ceroni, "Computation of Sabot Discard Using Chimera Technique", *17th International Symposium on Ballistics. Midrand*, South Affrica, (1998)

[8] R.Cayzac, C.Vaglio, J.Brossard, E.Carette and T.Alziary de Roquefort, "Intermediate Ballistic Computations and Comparison with Firing Tests", *17th International Symposium on Ballistics*, Midrand, South Affrica, (1998)

[9] S.Sénégas, C.Vaglio, J.Brossard and R.Cayzac, "Shock Wave Interaction with a Plane Surface and Indirect Method", *22th International Symposium on Shock Waves*, London, England, (1999)

[10] C.Vaglio, S.Sénégas, J.Brossard and R.Cayzac, "Quasi Universal Blast Wave Behaviour", *RAMAC 99*, Poitiers, France, (1999)

[11] S.Sénégas, R.Cayzac and J.Brossard, "Simulation Numérique d'une Onde de Souffle : Validation de la Réflexion au Sol", *14e Congrés Français de Mécanique*, Toulouse, France, (1999)

[12] D.Boisson, R.Cayzac and G.Légeret, "Study of the Heat Exchanges Occuring During the Cooling Phase in a Gun Barrel – Validation", *18th International Symposium on Ballistics*, San Antonio, USA, (1999)

[13] C.Vaglio, R.Cayzac and J.Brossard, "Shock Wave Characteristics at the Open End of a Detonation Tube", *16th International Colloquium on the Dynamics of Explosions and Reactive Systems*, Cracow, Poland, (1997). Reviewed and approved for publication in *Shock Waves*, (1999)

[14] S.Sénégas, C.Vaglio, J.Brossard and R.Cayzac, "Shock Wave Interaction With a Plane Surface and Indirect Method", reviewed and approved for publication in *Shock Waves*, (1999)

[15] D.Boisson, R.Cayzac and G.Légeret, "Study of the Gas Discharge and the Heat Exchanges Occuring in a Gun Barrel After the Projectile Leaves the Barrel – Validation for the 30 mm Gun", *European Forum on Ballistics of Projectiles*, ISL, Saint Louis, France, (2000)

[16] S.Sénégas, J.Brossard, R.Cayzac and E.Carette, "Intermediate Ballistics : Shock Wave Numerical Simulation and Small Scale Modelling", *European Forum on Ballistics of Projectiles*, ISL, Saint Louis, France, (2000)

[17] S.Sénégas, C.Vaglio, J.Brossard and R.Cayzac, "Blast Wave at the Open-End Tube : Small Scale Experiment and Prediction Characteristics", *16th International Symposium Military Aspects of Blast and Shock*, Oxford, England, September, (2000)

## 5.2 AEROBALLISTICS

[18] R.Cayzac and E.Carette, "Parametric Aerodynamic Design of Spinning Finned Projectiles using a Matrix Interpolation Method", *AIAA Journal of Spacecraft and Rockets*, Vol.29, N°.1, (1992)

[19] R.Cayzac, J.Marcillat and P.Salles, "Aerodynamic Behavior of Full-Caliber Finned Projectile", *13th International Symposium on Ballistics*, Stockholm, Sweden, (1992)

[20] R.Cayzac, "Aérodynamique et Mécanique des Fluides", *1er Colloque Scientifique et Technologique de Giat Industries*, Fascicule IV, Bourges, France, (1992)

[21] R.Cayzac, E.Carette, F.Cauchye and F.Montigny-Rannou, "Aerodynamic Behavior of Hypersonic Projectile", *4th International Symposium on Electromagnetic Launch Technology*, Celle, Germany, (1993)

[22] R.Cayzac, G.Valli, E.Carette and F.Cauchy, "AFPSDS Aerodynamic Conceptual Approach", *14th International Symposium on Ballistics*, Québec, Canada, (1993)

[23] R.Cayzac and P.Champigny, "Aerothermodynamic Design of Hypersonic Projectiles", *Axe ISL 1.3*, Saint Louis, France, (1994)

[24] R.Cayzac, A.Luc-Bouhali and E.Carette, "Aerothermodynamic Behaviour of an Hypersonic Benchmark Projectile", *7th International Symposium on Electromagnetic Launch Technology*, San Diego, USA, (1994)

[25] R.Cayzac, F.Montigny-Rannou and E.Carette, "Kinetic Energy Projectile Aerodynamics Numerical Conceptual Approach", *AIAA 12th Applied Aerodynamics Conference*, Colorado Spring, USA, (1994)

[26] R.Cayzac et P.Champigny, "Modélisation de l'Aérodynamique Externe des Projectiles", *2ème Colloque Scientifique et Technologique de Giat Industries*, Satory, France, (1994)

[27] R.Cayzac, B.Tasset, E.Carette, P.Champigny and J.M.Bernhardt, "Aerothermodynamics of Hypersonic Projectiles", *AIAA 13th Applied Aerodynamics Conference*, San Diego, USA, (1995)

[28] R.Cayzac and P.Champigny, "Aérodynamique d'un Projectile Hypervéloce", *Axe ISL 1.3*, Saint Louis, France, (1996)

[29] R.Cayzac, P.Champigny and D.Warken, "Kinetic Projectiles for Electric guns, Aeroballistic Investigations", *16th International Symposium on Ballistics*, San Francisco, USA, (1996)

[30] M.Pechier, P.Guillen and R.Cayzac, "A Combined Theoretical-Experimental Research Effort About Magnus Effects", *AIAA 16th Applied Aerodynamics Conference*, Albuquerque, USA, (1998)

[31] P.Denis, P.Champigny, F.Montigny-Rannou, R.Cayzac and E. Carette, "Kinetic Projectiles for Electric guns, Experiments and Computations", *18th International Symposium on Ballistics*, San Antonio, USA, (1999)

[32] R.Cayzac, E.Carette, M.Péchier and P.Guillen, "Navier-Stokes Computations and Validations of a Yawed Spinning Projectile", *18th International Symposium on Ballistics*, San Antonio, USA, (1999)

[33] M.Péchier, P.Guillen and R.Cayzac, "Magnus Effect Over Finned Projectiles", reviewed for publication in the *AIAA Journal of Spacecraft and Rockets*, (1999)

[34] P.Champigny, R.Cayzac and P.Denis, "Roll Producing Moment Prediction for Finned Projectiles", *European Forum on Ballistics of Projectiles*, ISL, Saint Louis, France, (2000)

[35] S.Heddadj, R.Cayzac and J.Renard, "Aeroelasticity of High L/D Supersonic Bodies : Theoretical and Numerical Approach", *AIAA 38th Aerospace Sciences Meeting and Exhibit*, Reno, USA, (2000)
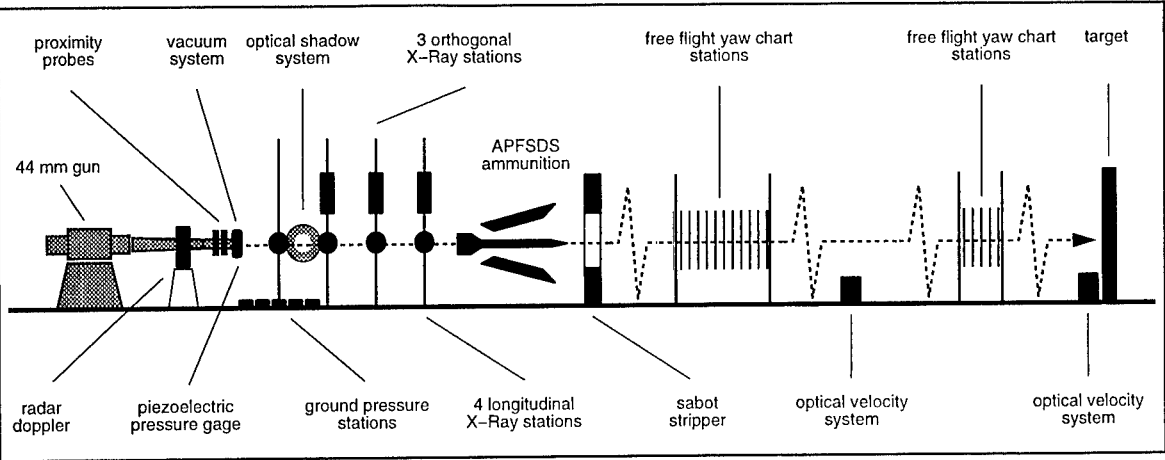
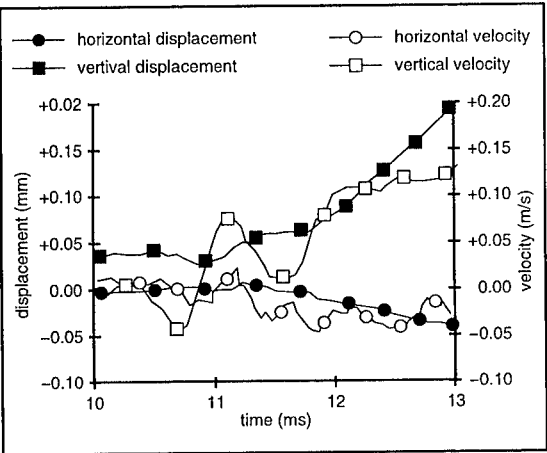Figure 1 : Diagram of the test set-up



Figure 2 : Experimental muzzle transverse displacement and velocity



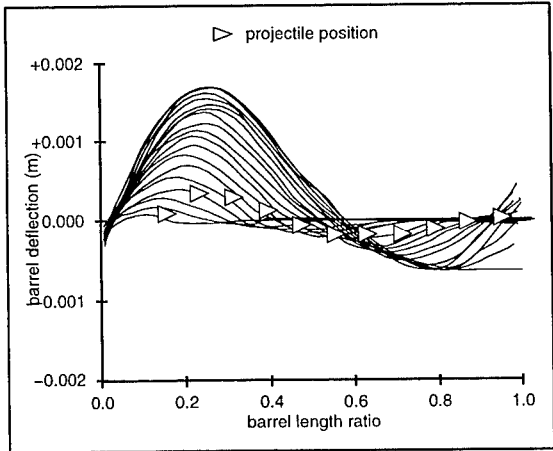Figure 3 : Shadow visualization of the discard flowfield



Figure 4 : Theoretical barrel deflected shapes in XY plane (SIMBAD code)
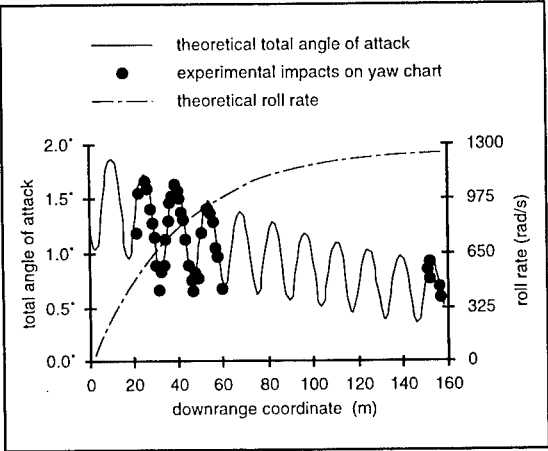


Figure 5 : Free flight motion

- 266 -

| version ❶ | version ❷ | version ❸ |
| (drag separation) | (rear separation) | (lift separation) |

0.00 m / muzzle

(0.0 cal / muzzle)

0.15 m / muzzle

(3.4 cal / muzzle)

0.60 m / muzzle

(13.6 cal / muzzle)

1.60 m / muzzle
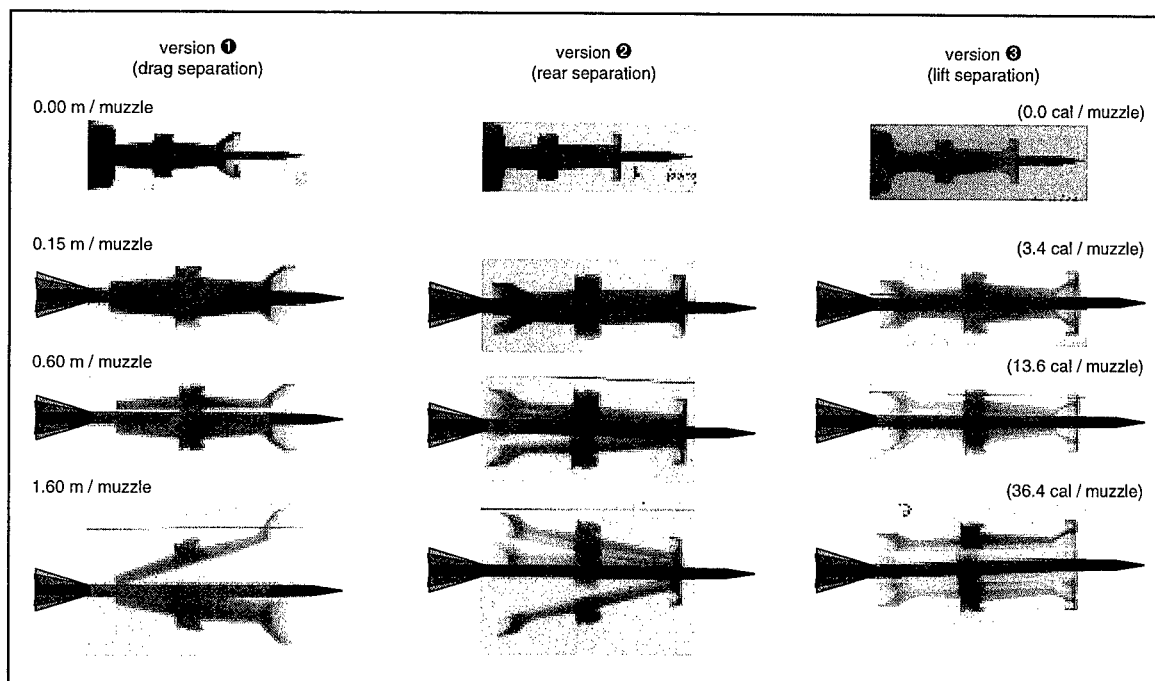
(36.4 cal / muzzle)

Figure 6 : Experimental sabot discard processes, X–Ray visualizations



— ● — boattail projectile trajectory
— ○ — nose projectile trajectory
——— theoretical propellant gas/air contact surface
— · — theoretical muzzle blast
✖ experimental muzzle blast
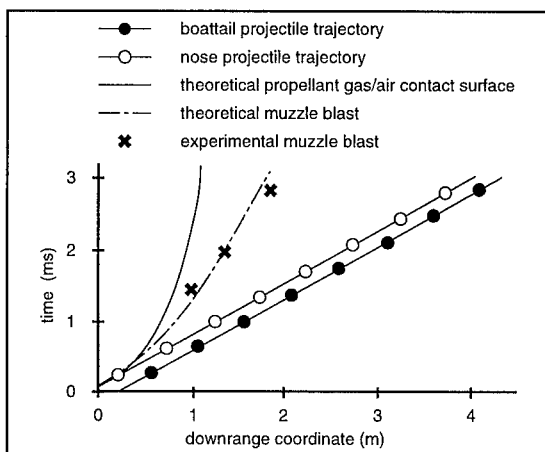
Figure 7 : Experimental and theoretical muzzle blast and propellant gas/air contact surface histories
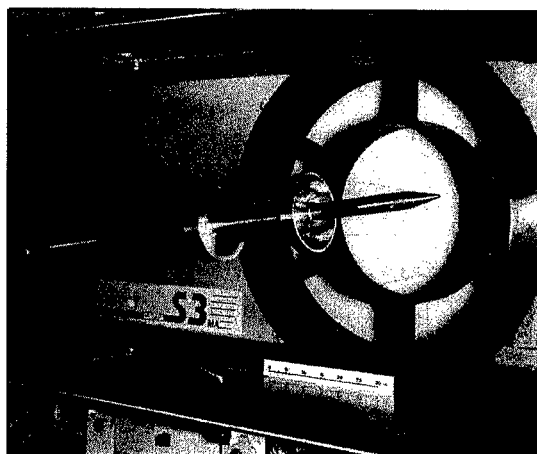


Figure 8 : APFSDS model (S3MA ONERA wind tunnel test)
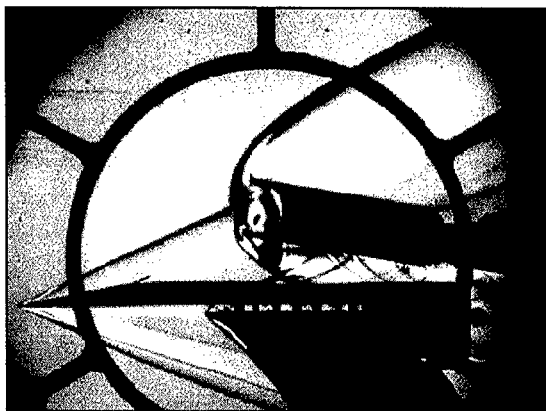


Figure 9 : Strioscopy visualization of the discard flowfield (Mach = 3.5)



○ experiment
□ Euler computation
▼ Navier–Stokes computation
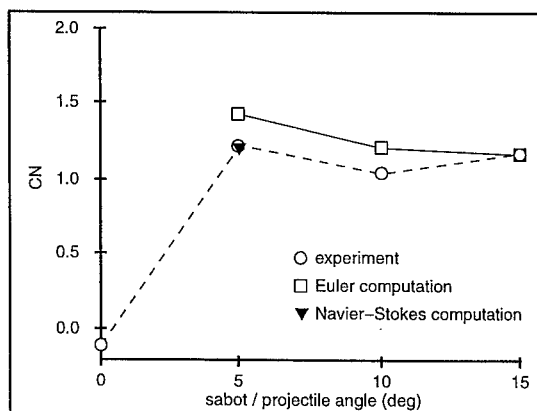
Figure 10 : Sabot normal force coefficient versus relative sabot / projectile position
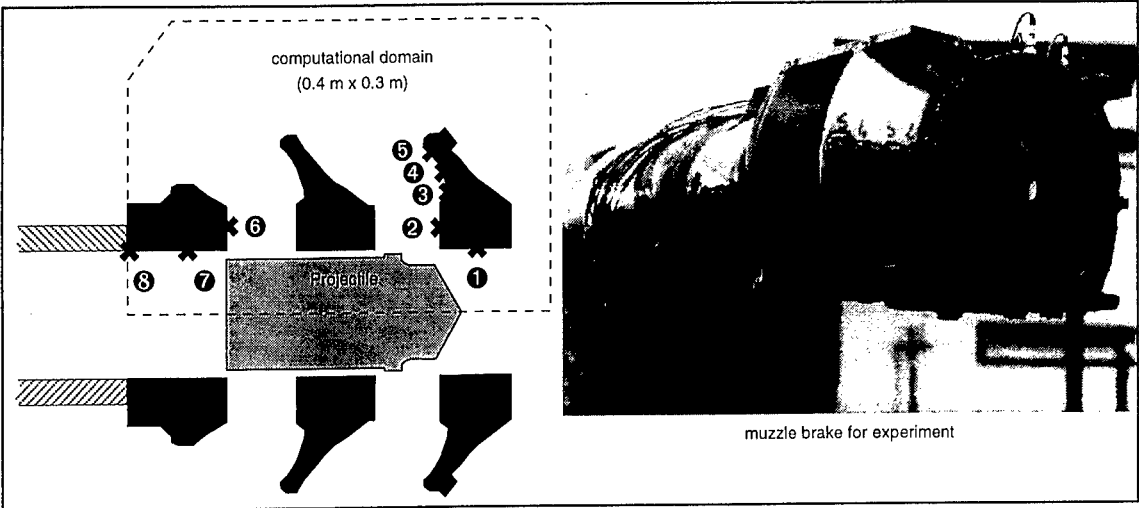
Figure 11 : Schematic diagram of the double baffle muzzle brake and pressure measurement locations
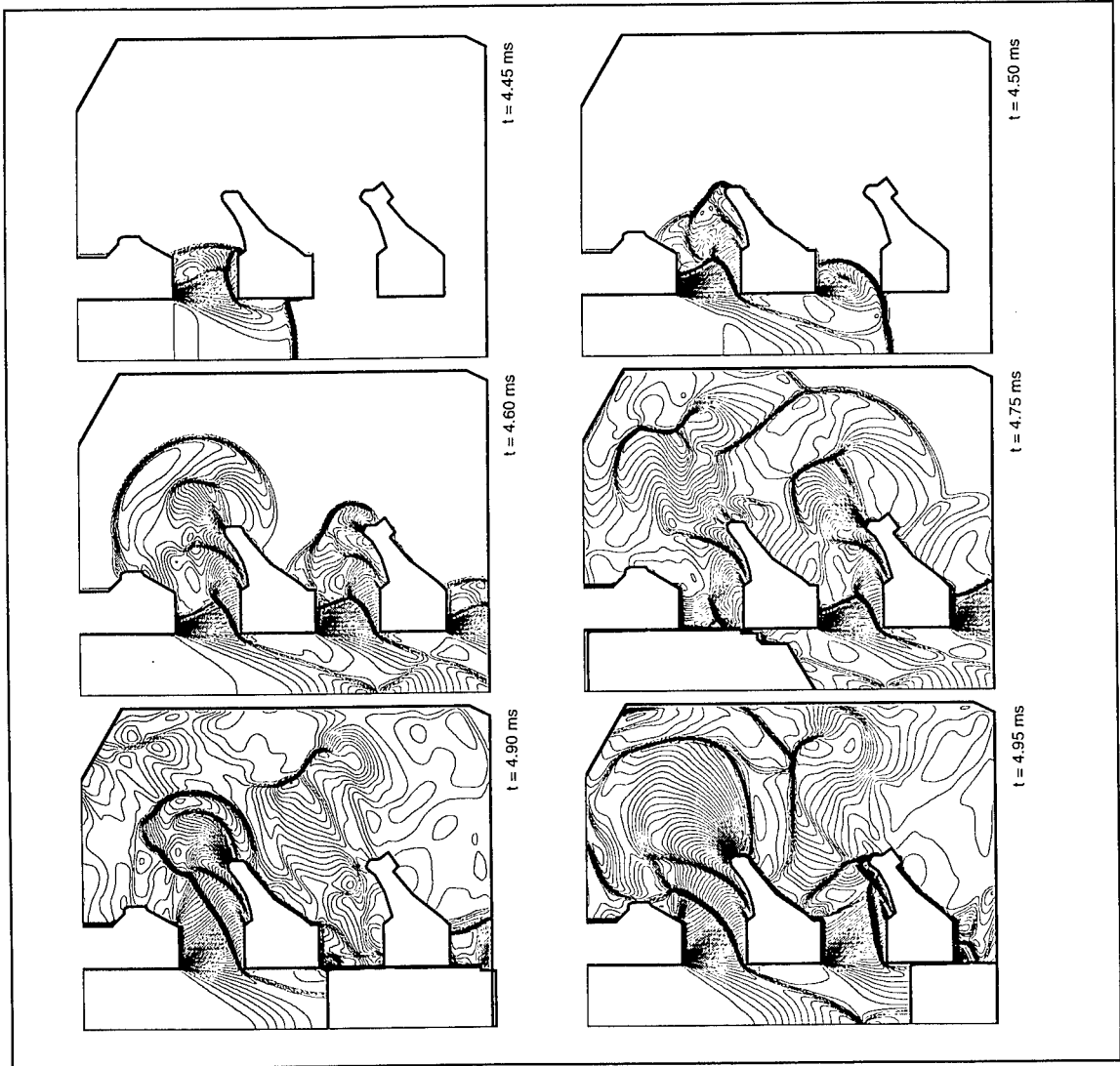


Figure 12 : Pressure fields through the double baffle muzzle brake (grid 300 x 232, 60 445 nodes used)
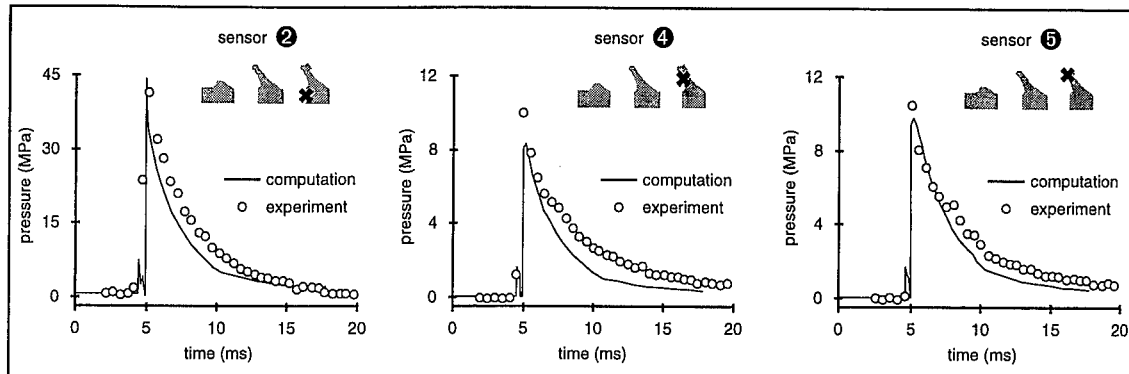
Figure 13 : Comparison between computed and measured pressures for the double baffle muzzle brake
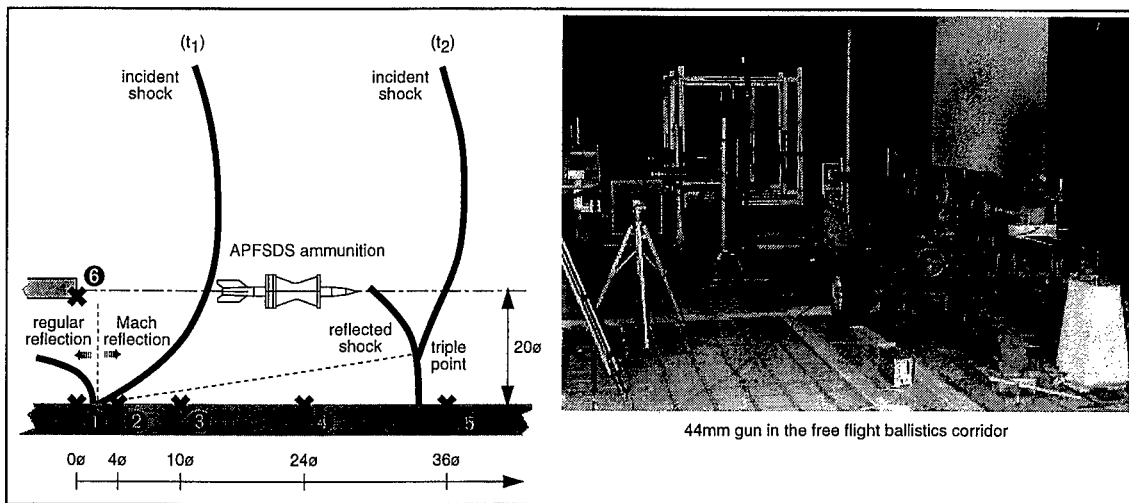


Figure 14 : Schematic diagram of the 44mm gun tests and pressure measurement locations
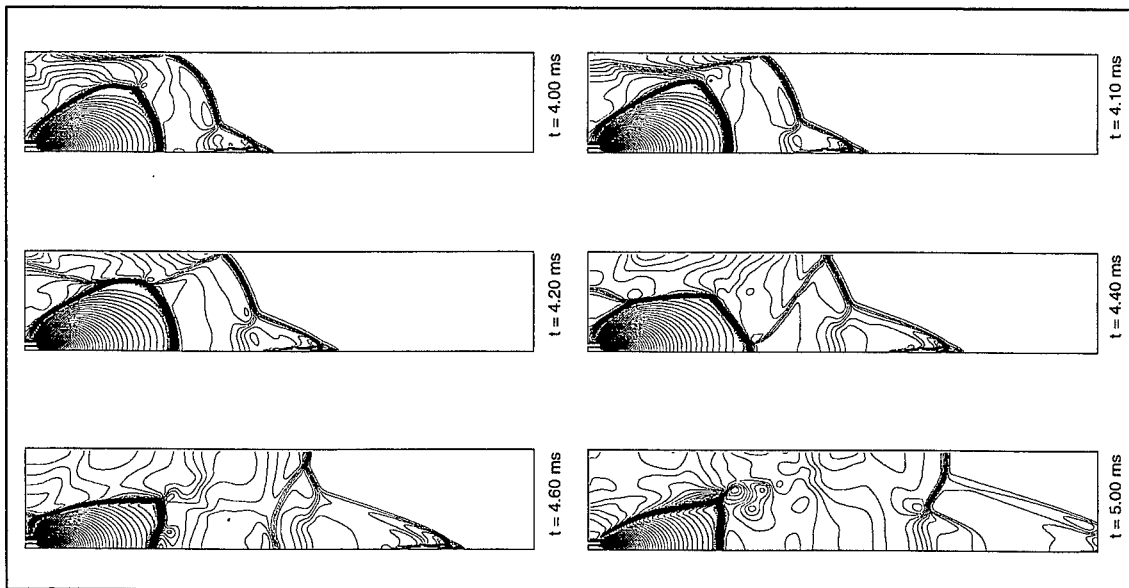


Figure 15 : Time evolution of the intermediate ballistics flow interaction with ground situated at 10ø from firing axis
Pressure fields (60 isovalues contours with logarithmic scale, grid 400 x 88, 34 770 nodes used)
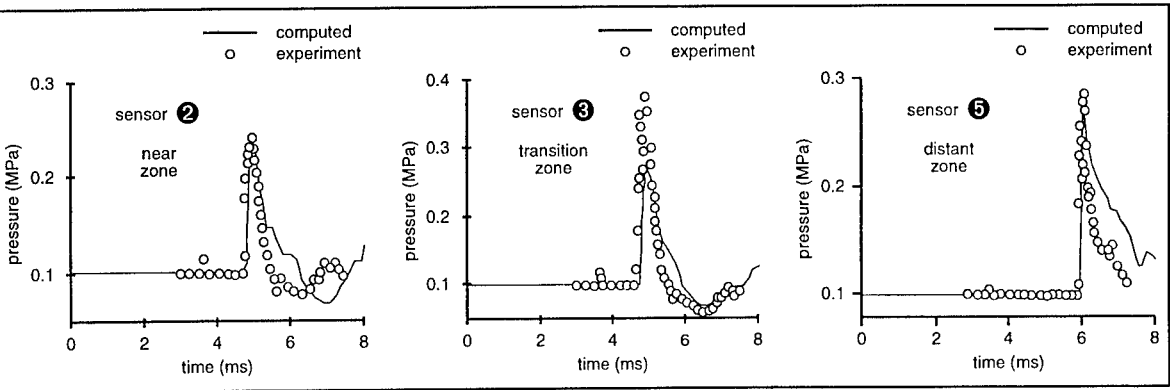
Figure 16 : Comparison between computed and measured pressures for the 44mm gun
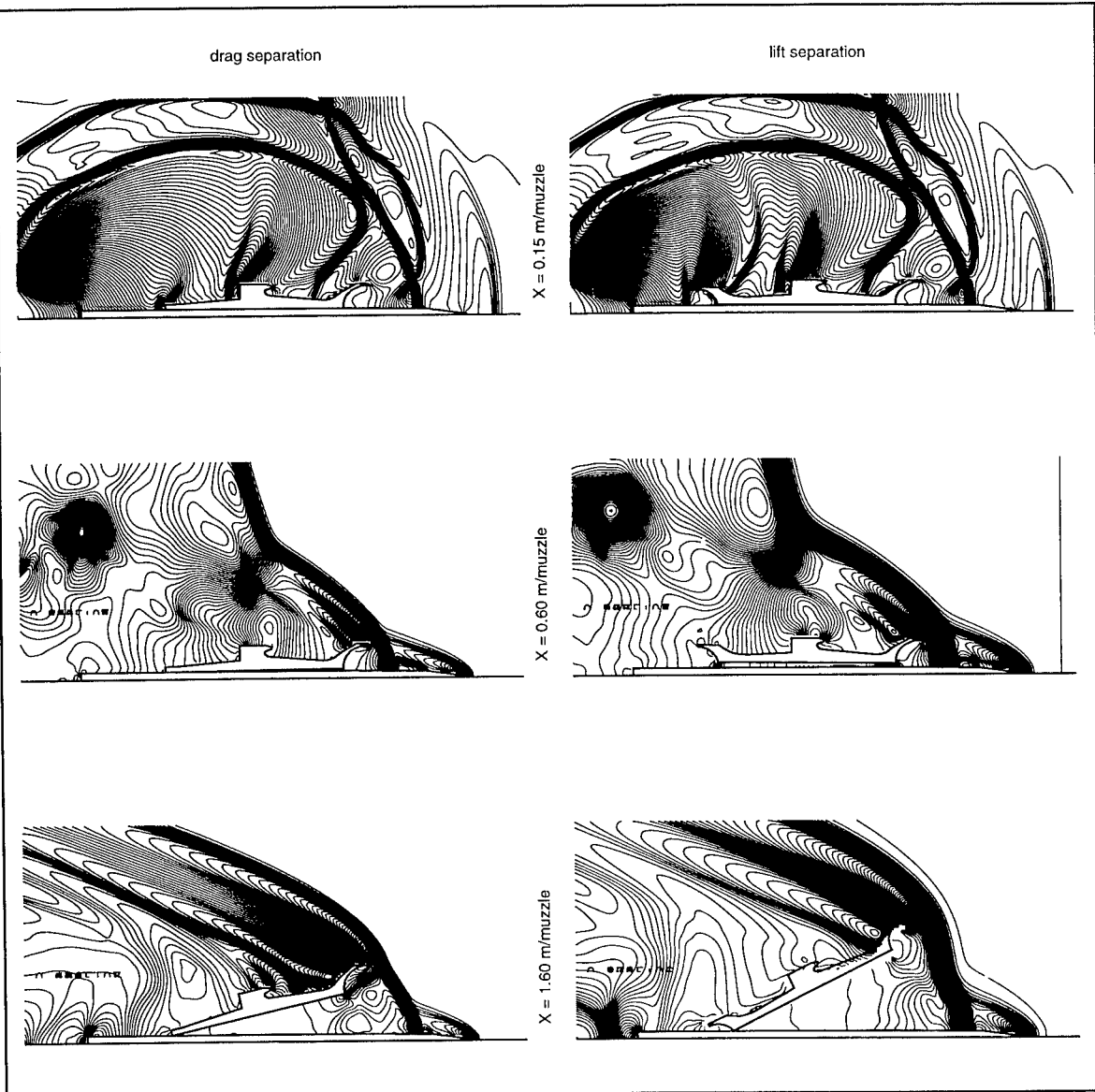


Figure 17 : Computed discard processes, pressure fields
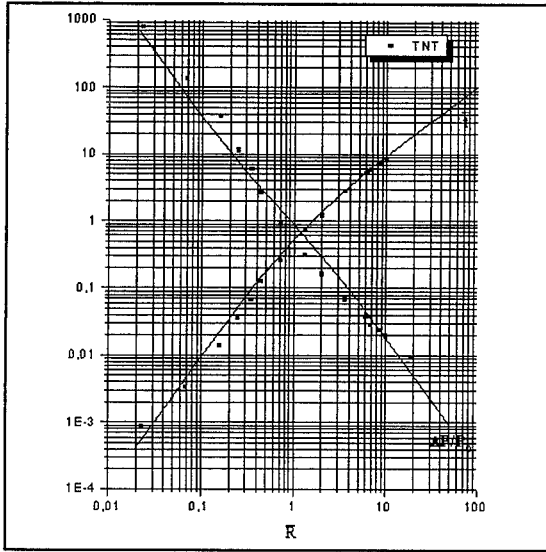
Figure 18 : Universal functions $\overline{t}(\overline{R})$, $\Delta P/P_o(\overline{R})$ and experimental blast waves from TNT
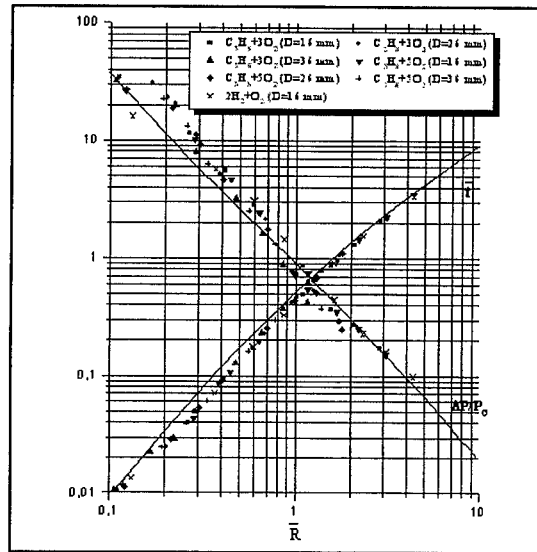


Figure 19 : Universal functions $\overline{t}(\overline{R})$, $\Delta P/P_o(\overline{R})$ and experimental blast waves from open end tubes
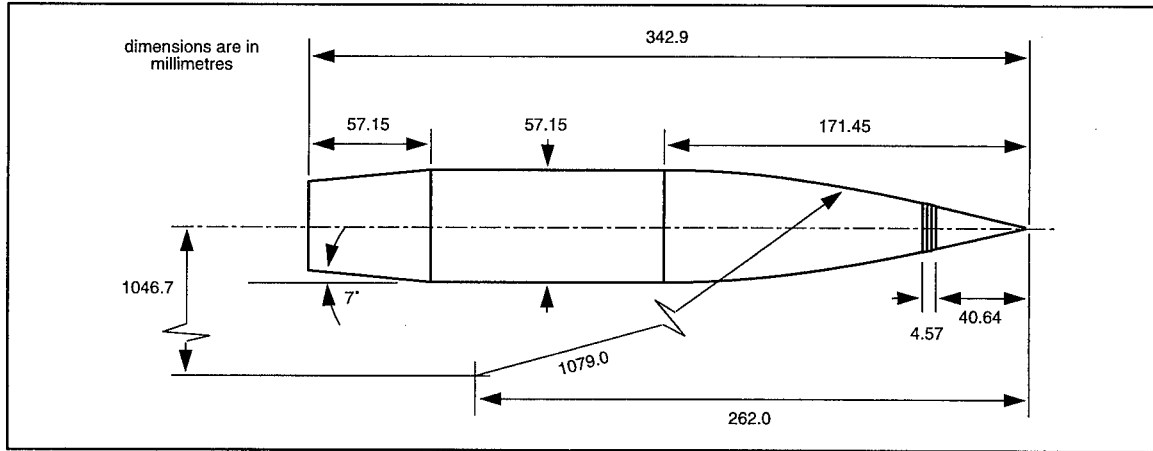


Figure 20 : SOCBT geometry
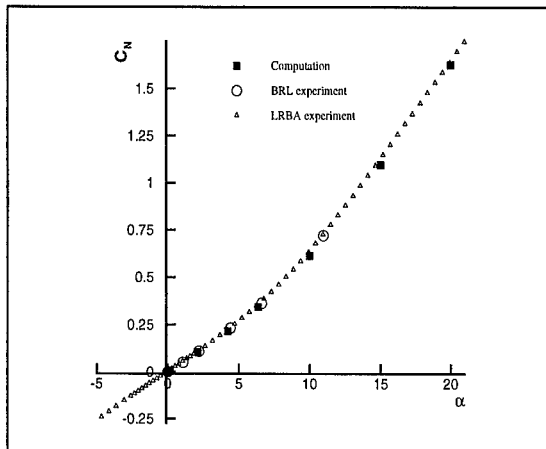


Figure 21 : Normal force coefficient versus angle of attack for SOCBT body
(Mach = 3, $Re_L = 7.3 \times 10^6$, $\Omega^* = 0.19$)
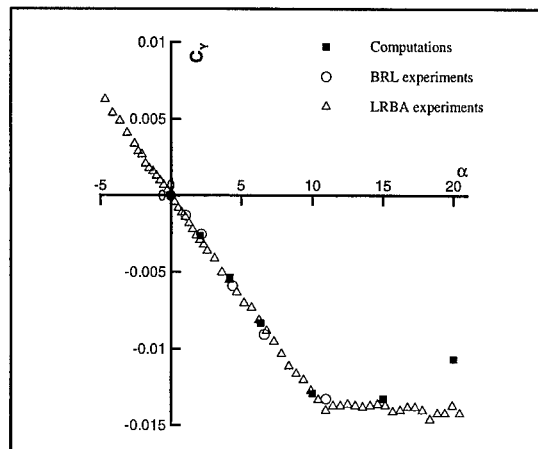


Figure 22 : Magnus force coefficient versus angle of attack for SOCBT body
(Mach = 3, $Re_L = 7.3 \times 10^6$, $\Omega^* = 0.19$)
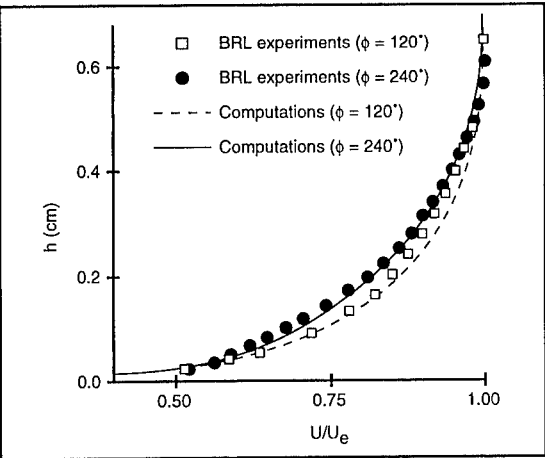
Figure 23 : Asymmetry of the boundary layer velocity profiles
(Mach = 3.0, $\alpha = 6.34°$, $\Omega^* = 0.19$)
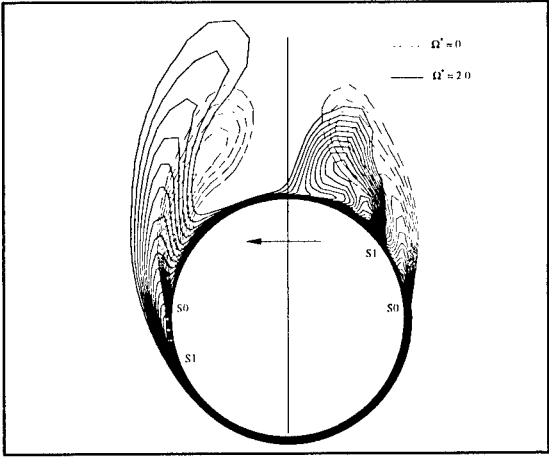


Figure 24 :          Asymmetric vortices,
numerical comparison for SOCBT model
(X/$\phi$ = 6.0, Mach = 3.0, $\alpha = 15°$, $Re_L = 7.3$ x $10^6$)
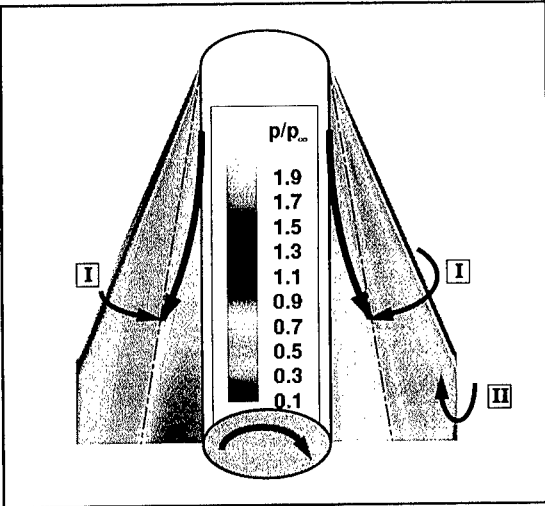


Figure 25 : Asymmetry of the lee side flow on two opposite
spinning fins, unsteady CFD
(Mach = 4.3, $\Omega^* \approx 0.041$, $\alpha = 4.22°$)
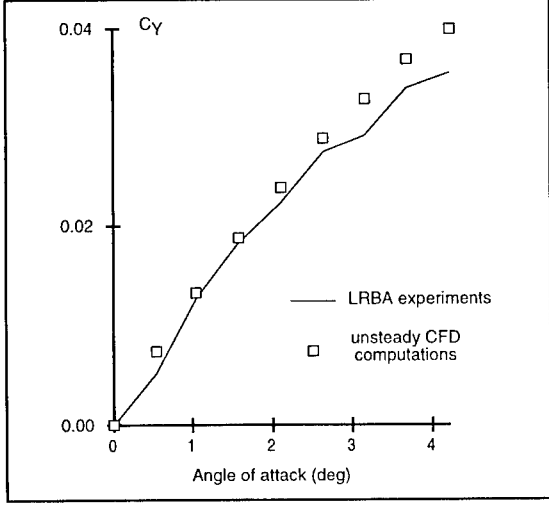


Figure 26 : Magnus force coefficient versus angle of attack
for APFSDS model (Mach = 4.3, $\Omega^* \approx 0.041$)
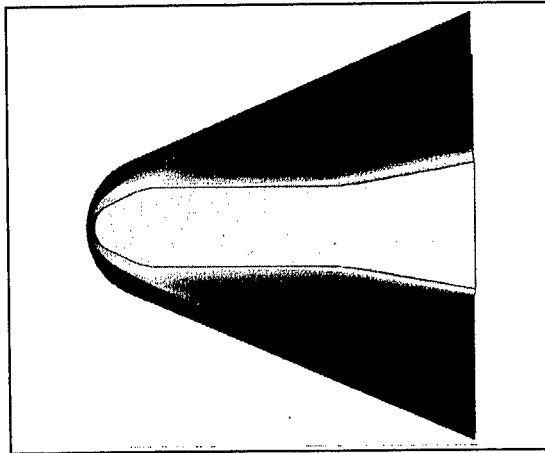


Figure 27 :          Mach fields for HB2 model,
Navier–Stokes turbulent
(Mach = 5.1, $\alpha = 2°$, $Re_L = 2.3$ x $10^6$).
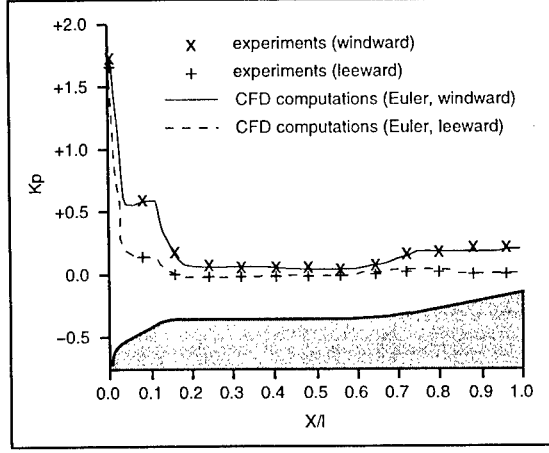


Figure 28 : Longitudinal pressure distribution for HB2 model
(Mach = 5.1, $\alpha = 10°$)
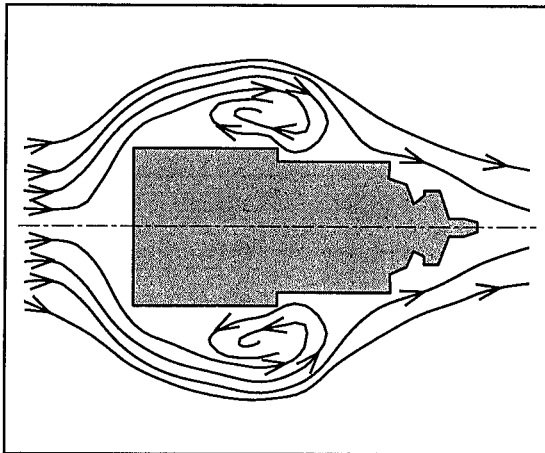
Figure 29 : Schematic representation of the flowfield around the bomblet model (Mach = 0.50)
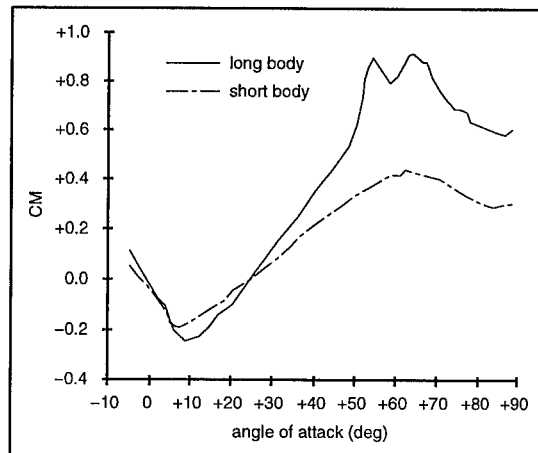


Figure 30 : Pitch moment coefficient versus angle of attack for the bomblet model (Mach = 0.50)
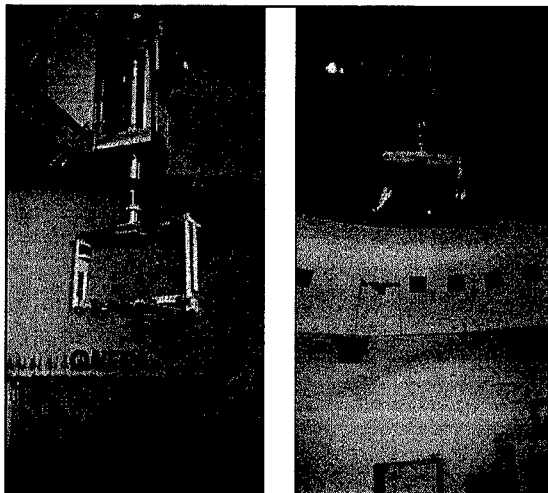


Figure 31 : Experimental vertical free flight wind tunnel, dropping device for the bomblet model
($\alpha = 90°$, p = 7 tours/s, V = 34 m/s)
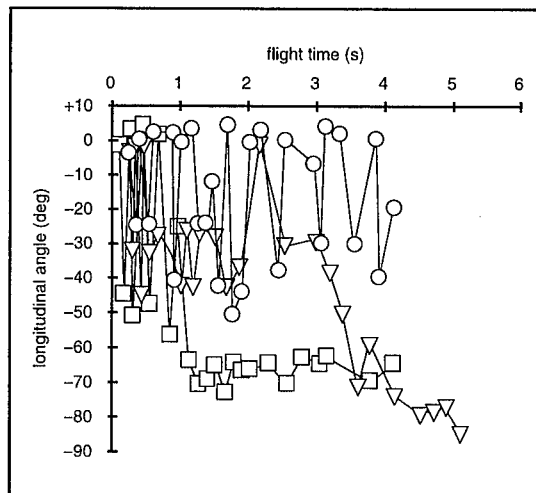


Figure 32 : Experimental longitudinal attitude of the bomblet model during the free flight
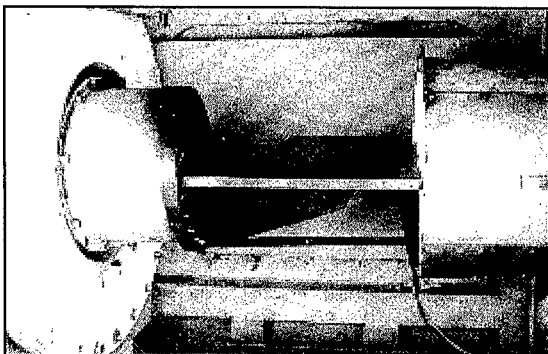


Figure 33 : Experimental measurements of the heat flux on a fin (ONERA wind tunnel R2Ch)
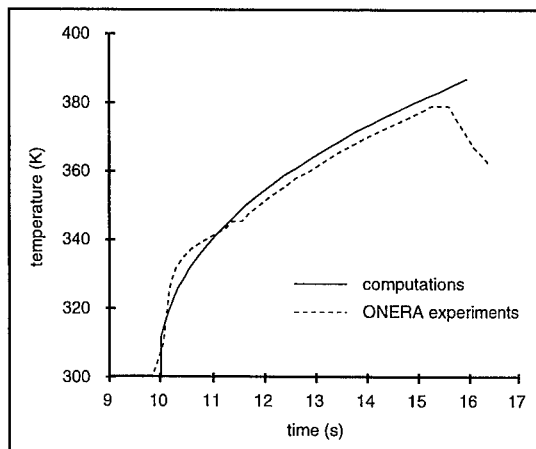


Figure 34 : Time evolution of the parietal fin leading edge temperature (Mach = 7.0)
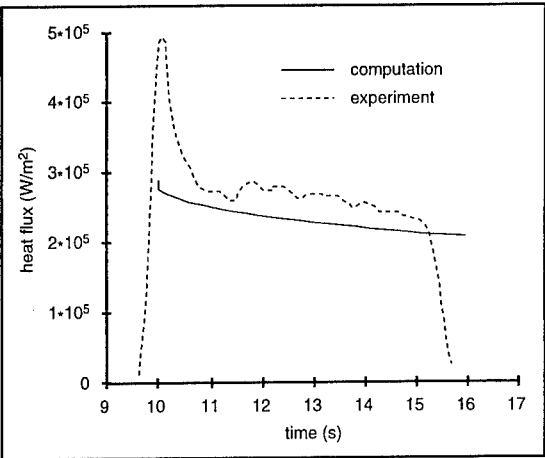
Figure 35 : Time evolution of the fin leading edge heat flux
(Mach = 7.0)
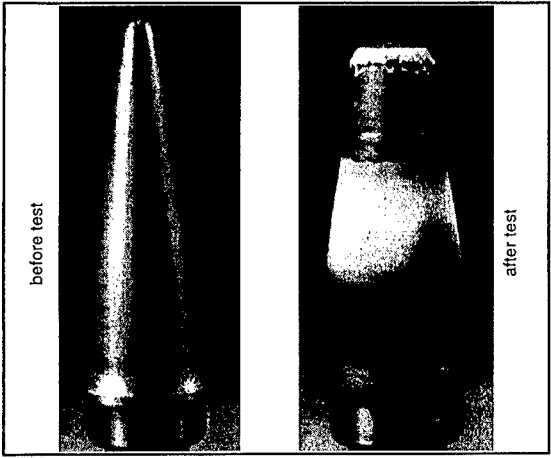


Figure 36 : Experimental evaluation of the ablation of a tungsten
nose, Aérospatiale arc wind tunnel JP200
($P_i$ = 85 bars, $T_i$ = 3500 K, $\phi_i$ = 67 MW/m$^2$)
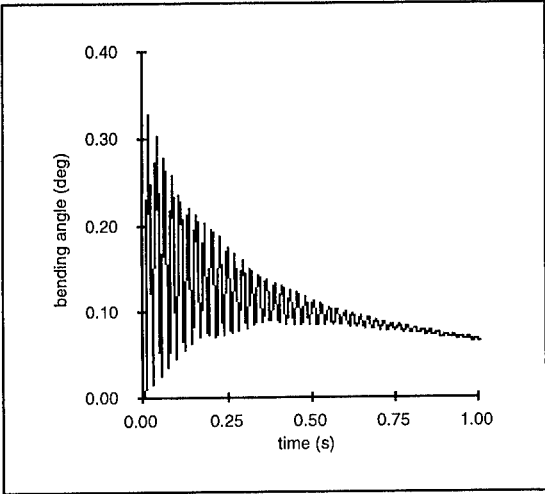


Figure 37 : Time evolution of a bending angle generated
by aerodynamics
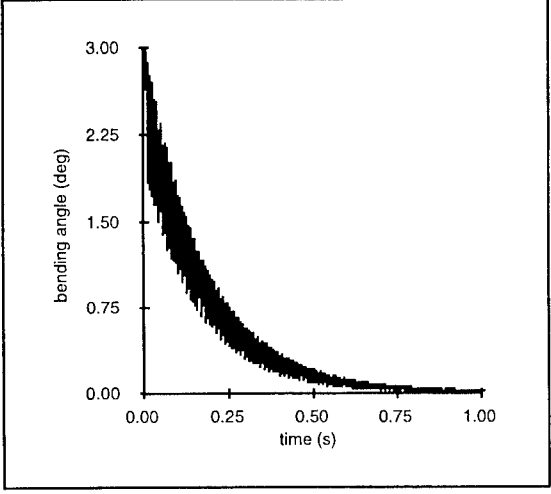


Figure 38 : Time evolution of an initial 3 degree bending angle

# THE AERODYNAMIC INTERACTION AND DISPERSION OF SHOTGUN PELLETS AT TRANSONIC VELOCITIES.

## SZMELTER J, LEEMING D W

Cranfield University, Royal Military College of Science Shrivenham,
Wiltshire, SN6 8LA, United Kingdom

**ABSTRACT:** This study was designed to determine the extent to which aerodynamic interactions affect the pellet pattern from sporting shotguns, as this has considerable influence on their lethality. After the characteristic separation of pellets was obtained from their probability densities, the detailed flowfield was obtained using Computational Fluid Dynamics (CFD) analysis. This paper presents for the first time an application of CFD to the assessment of the unsteady aerodynamics of pellet clouds. The reported initial results illustrate the influence that the wake of preceding pellets has on the trajectory of trailing pellets.

## 1. BACKGROUND

In the USA, UK, Denmark and other countries, there is current or proposed legislation against the use of lead pellets in shotgun ammunition. The principal reasons are to obviate ingestion of lead, particularly by waterfowl, and to reduce ground contamination. Soft iron pellets have been available in so-called 'steel shot' ammunition for many years. However, the rigidity of the material, combined with the need for larger and faster pellets to offset the lower ballistic efficiency due to their lesser density, can potentially damage the 'choke' muzzle constriction of the common lightweight game guns. This has prompted development of alternative non-toxic pellet materials and constructions, with concern as to ensuring 'clean kills' against gamebirds. The factors which determine the effectiveness of a shotgun include the 'pattern' — the dispersion of pellets with range. The magnitude of dispersion is controlled by the muzzle choke, but the mechanism of choke function is not fully understood. It is suspected that the close proximity of pellets immediately after launch enables aerodynamic interaction to affect the divergence and randomness of the pellet dispersion.

Experimental studies into pellet dispersion with range indicate the presence of non-linear effects. These arise mainly from combination of three factors: aerodynamic interaction between pellets, irregularities in pellet shape and their rotation during flight. Difficulties in experimental techniques prevent detailed measurements, so only generalised data is available. In contrast, CFD methods provide extensive flow field information. Recent advancements in CFD now allow pellet cloud aerodynamics to be considered in more detail.

The CFD calculations determine the relationship between lift, drag and separation. This being further analysed in order to provide a relationship between the characteristic separation of pellets within the cloud and increasing range. In this way the effects on statistical extrapolation of pellet dispersion back to the muzzle can be assessed with respect to the extent

and magnitude of longitudinal and lateral aerodynamic interaction between pellets. It should be noted that modern ammunition is further complicated by the presence of the 'cup wad' driving piston, the impact of which is not considered in this paper.

The key findings are summarised in figure 8. This was achieved by first considering the practical conditions affecting the problem then, using data on shotgun performance, determining the characteristic separation of pellets in flight so that the subsequent CFD computations are dimensioned to model the typical mutual proximities between the pellets. The graphic result illustrates a leading pellet at the origin showing, for a variety of initial starting points, the path of a trailing pellet influenced by the preceding wake.

## 2. PRACTICAL CONDITIONS AND DOMINANT FACTORS

The muzzle velocity of shotguns is typically 400m/s, corresponding to Mach 1.2, diminishing to about Mach 0.5 within a representative useful range of 40m. This paper is primarily concerned with the aerodynamic interactions between pellets within the first 10m of flight, during which the pellets are either marginally supersonic or transonic. Most shotguns possess a restriction in their diameter at the muzzle: this is referred to as a 'choke' and is used to modify the subsequent dispersion of the pellets in flight. Pellets are driven from a shotgun by a wad which acts as a piston. The wad has a low sectional density and so is soon lost from the ensemble of pellets by aerodynamic retardation. These features are illustrated in figure 1.



Comparative Effects of
CYLINDER BORE & FULL CHOKE
on
SHOT SHELL PATTERNS

4 feet from muzzle
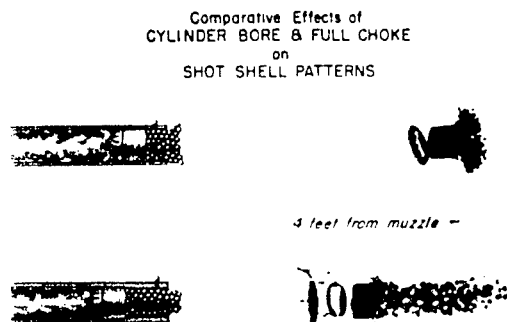
Figure 1: Cut-away sketch of the shot column exiting cylinder (upper) and choked (lower) muzzles, with superimposed flash photographs of the resultant pellet dispersions at 1.2m (4 feet) range [1].
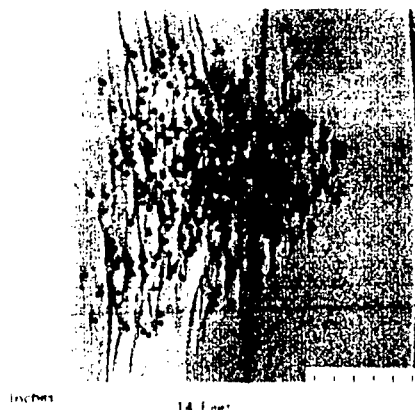


Figure 2: Flash photograph of the dispersed pellets at 4.3m (14 feet) range fired from a cylinder muzzle. Note transverse trigger wire. Also note the composite bow shock at the extreme right-hand side. [1]

Shotgun barrels are commonly choked barrels, and so the pellets will be less dispersed than that shown in figure 2 for a cylindrical 'unchoked' barrel. With increasing range the dispersion will generally increase. It has been demonstrated [2,3,4] that the lateral distribution of pellets at range generally conforms to a Rayleigh distribution (independent orthogonal Gaussian). The longitudinal dispersion of the pellets in flight was also measured, but its variability complicates the assignment of a specific distribution function.

Compton, Radmore & Giblin [5] present a stochastic model to enable prediction of the observed non-linearly increasing dispersion with range by the action of random forces. Although mechanisms for the randomising effect are discussed, these are expediently disregarded in the provision of a good fit to the observed data at useful ranges. A causative understanding requires evaluation of the three principal regions of effect: launch, pellet flight interactions and asymmetric aerodynamics, described in turn below.

It is surmised here that the initial dispersion on launch from the muzzle is caused by the residual pressure exerted upon the rearmost pellets causing these to collide with and thus disperse preceding pellets. The presence of muzzle 'choke' imparts a longitudinal velocity gradient to the column of pellets thereby reducing the potential for the rearmost pellets to disperse those preceding. This intermediate ballistic effect is part of the launch process and there is evidence [1] that it is unlikely to have any influence beyond 1 metre range. These semi-fluid processes at and just beyond the muzzle have yet to be confirmed.

Thereafter, the pellets are free from the influence of the gun, but mechanical and aerodynamic interaction are likely. This paper is concerned with estimating the subsequent characteristic separation distances between pellets and their aerodynamic interdependencies, especially at short range where pellets are in mutual close proximity. There are two issues related to pellets with near identical trajectories: one, that trailing pellets may suffer reduced aerodynamic retardation and so strike the precursors and, secondly, that the trailing pellets may establish stable positions in the wake of others. This latter possibility would undermine the ability for the ammunition to provide 'clean kills' against game, and may explain the frequent casual observation of adjacent or merged pellet strikes on test targets.

Lack of pellet sphericity and induced transverse spin are further mechanisms for disproportionate dispersion of pellets at range; these are probably the dominant causes of the effective stochastic mode of dispersion reported by Compton, Radmore & Giblin.

## 3. PROXIMITY OF PELLETS IN FLIGHT

The requirement at this level is a fair estimate of the characteristic separation of pellets in the central region of the pellet cloud, and this can be obtained from their probability densities. A range of 5m from the gun is considered representative of the region in which aerodynamic interactions of pellets may be of particular significance. The method employed here evaluates lateral and longitudinal pellet densities and uses this data to determine the average spatial void occupied by each pellet; the dimension of this void equates to the characteristic separation between pellets.

First, considering dispersion lateral to the trajectory, using right-handed orthogonal axes notation, the representative Gaussian dispersions in the lateral directions (x & z) are of similar mutual size, increasing with range. The peak probability densities at one special range can be calculated from a definition of shotgun choke [6] in terms of the percentage of pellets striking within a centralised 0.762m (30 inch) diameter target at 36.6m (40 yards). Taking a 'half-choke' gun as representative, this percentage pattern is 60%, giving a standard deviation, $\sigma_{x,z} = 0.2814m$ at 36.6m range. Taking the dispersion to grow approximately linearly with range, then at 5m range $\sigma_{x,z} = 0.0385m$. Owing to the mechanical proximity of pellets, this extrapolation clearly cannot be carried to the gun muzzle, but is reasonable at 5m range. The peak probability density occurs on-axis, being given by

$$\rho_{x,z} = \frac{1}{\sigma_{x,y}\sqrt{2\pi}},$$

which at 5m range gives a value of 10.362 m$^{-1}$.

Compton [2] presents information on the longitudinal probability density with respect to time, $dP_y/dt$ of 3.3mm diameter lead pellets over 20m to 50m range. The peak of the time-dependent probability density is approximately inversely proportional to range, and this allows extrapolation back to 5m range, giving a value of 748.5/s. Again, mechanical proximity of the pellets prevents this extrapolation from being carried to the gun muzzle.

$$\text{Since } \rho_y, \frac{dP_y}{dy} = \frac{1}{v}\frac{dP_y}{dt},$$

and the velocity v at 5m is typically 375m/s, then at 5m $\rho_y$=1.996m$^{-1}$.

Now, having established representative values for $\rho_x$, $\rho_y$ and $\rho_z$, the probable number of pellets within a small volume, $\Delta x, \Delta y, \Delta z$ is given by

$$n = N \rho_x \Delta x \, \rho_y \Delta y \, \rho_z \Delta z,$$

where N is the total number of pellets. If $a = \Delta x = \Delta y = \Delta z$ is the dimension of a characteristic volume containing only one pellet, then

$$a = \frac{1}{\sqrt[3]{N\rho_x \rho_y \rho_z}}$$

The characteristic separation, a, at 5m is thus

$$a = \frac{1}{\sqrt[3]{300 \times 10.362 \times 1.996 \times 10.362}} = 0.025m$$

which, for the 2.6mm diameter pellets being considered, is approximately 10 diameters. At around 5m range a significant minority of the pellets will be much closer than 10 diameters separation. At lesser ranges the pellets will tend to be closer together. With increasing range close proximity of some pellets (<10 diameters) will continue, but less frequently and varying with the differential motion within the pellet cloud. In this case it is therefore reasonable to consider aerodynamic interactions at separations of up to 10 diameters.

## 4. CFD MODEL

The aerodynamics involved in this problem are complex and very challenging for numerical simulation. Difficulties result from the large number of irregularly shaped objects being in relative motion and embedded in a non-uniform viscous flow in which wakes and shocks are interacting. It is expected that the detailed modelling of this problem should be achievable using the solution of the fully time dependent three dimensional Navier-Stokes equations with dynamic trajectory prediction for every pellet. The trajectory prediction could be based on integration of surface pressures on each of the pellets. Such computations, if good accuracy is maintained, are prohibitively expensive. The three dimensional numerical modelling of unsteady aerodynamics with moving bodies is rare and usually limited by simplifying assumptions - frequently those of axisymmetric flow or quasi-static approaches. It should be noted that some successful methodologies, such as for sabot discard and ejection of small segments into the wake of a flared projectile [7], have been developed.

Due to the prohibitively expensive computation times, in this study only a two dimensional, unsteady inviscid flow solver has been used. This implies the omission of viscous effects and acceptance of differences between three dimensional and two dimensional flows. Also, rotation is neglected.

Results of a detailed investigation, conducted for pellet pairs over the scope of typical longitudinal and lateral separation has been analysed and an example of a multi-pellet configuration is presented. Only spherical / cylindrical shapes are considered.

In the presented work, the 2D Euler equations are solved by an in-house code based on cell centred finite volume discretisation in space, and multistage Runge-Kutta discretisation in time. The complexity of the geometry of mutually moving bodies has been resolved using triangular meshes. The mesh generation and regeneration is based on the advancing front technique. The moderate dynamic mesh and body movement during time dependent calculation utilises spring analogy concepts. When cells become too distorted the remeshing is performed automatically. The code has been validated for oscillating aerofoils and segmented projectile applications [8].

The trajectory prediction has been implemented directly within the flow solver. At a chosen time interval, lift and drag based on pressure integration are calculated for each pellet. The equations of motion are formulated in terms of the second order differential equations and are integrated using a three-stage Runge-Kutta scheme. The code is run dynamically. The trajectory prediction is used to derive mutual motion of pellets and alteration in the flow field angle of attack. It is followed by a dynamic mesh movement and remeshing as required.


## 5. ANALYSIS SCHEME

Although the CFD model utilised can cope with multiple projectiles, to simplify the evaluation of aerodynamic interactions of a pellet cloud as a whole, the scheme chosen considers the interaction of pellet pairs alone. The pellet cloud is divergent with range, but as least divergence is exhibited between adjacent pellets within the cloud, so the analysis scheme considers the closely separated pellets in each pair to be effectively on trajectories which are initially both parallel and of identical speed (figure 3).
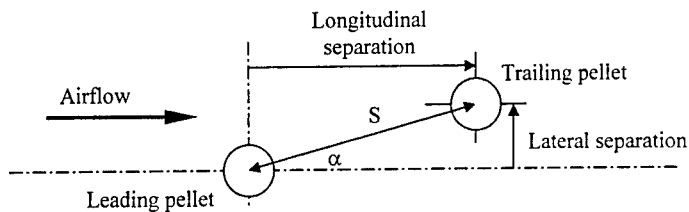
Figure 3: 'Wind axes' co-ordinates for the analysis scheme
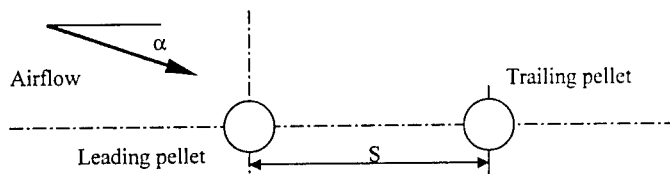


Figure 4: 'Body axes' co-ordinates for the computations

The computational reference frame is coaxial with the initial line through the pellet centres, with the airflow incident at an angle to the body axis (figure 4). The computations are scaled relative to the distance between the distal faces of the spheres, and relative to the incident airflow of Mach 1.1 at ambient sea-level conditions. The pellets are 2.6mm diameter, with mass based on the density of steel. The CFD program executes 1000 iterations to establish the steady-state conditions before the pellets are effectively released. Both pellets move relative to the reference frame under the influence of drag and lift, with corresponding distortion of the mesh. The extent of mesh distortion remained acceptable for all these computations. The CFD program continues with the unsteady-flow computations for typically 4000 further iterations. Sample illustrations of the moved mesh and pressure contours during the unsteady calculations is shown in figures 5-7; interaction between wake and shocks is clearly evident.
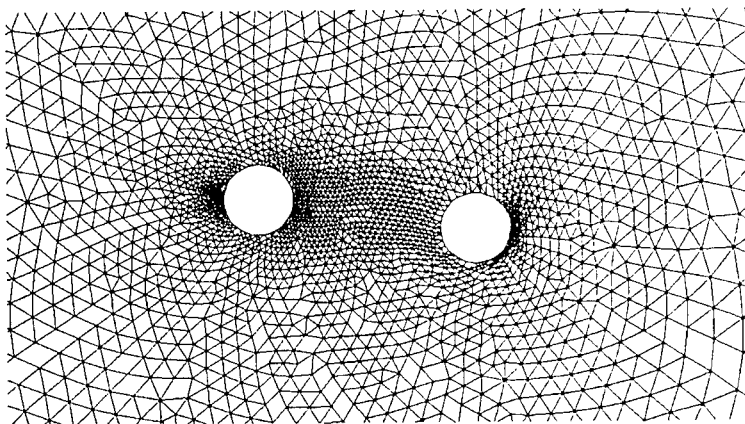


Figure 5: Sample detail from the computational mesh at completion.
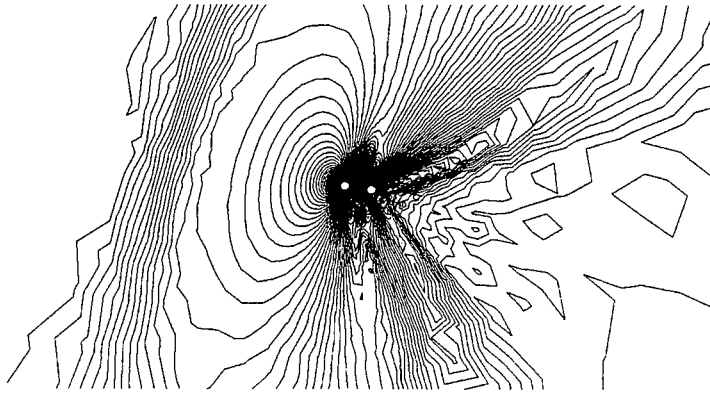
Figure 6: Example of the pressure field at the completion of computations.
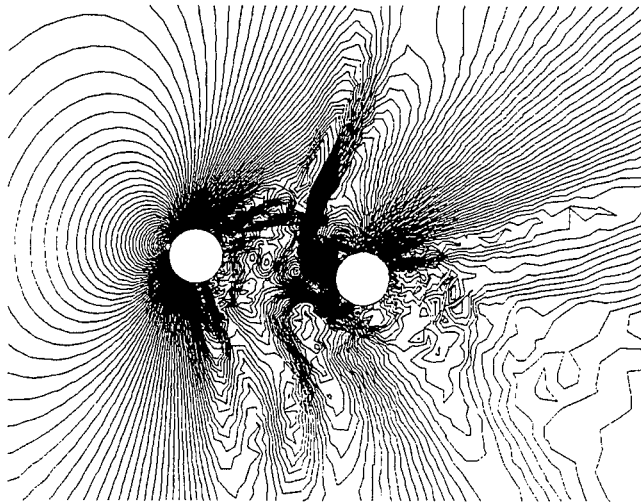

Figure 7: Detailed example of the pressure field at the completion of computations.

## 6. ANALYSIS RESULTS

The output data for the displacement of both pellets was re-mapped relative to the free field airflow, so restoring the 'wind axes' reference frame. There occurred relatively little lateral deflection of the leading pellet due to the trailing pellet, and so the deflection of the trailing pellet was referenced to the leading pellet. The arrows in the figure 8 show the computed trajectories of the trailing pellet relative to the leading pellet. The leading pellet is located at the origin of the plot (position 0,0). The origins of the arrows corresponds to each starting position of the trailing pellet, and the arrowheads show the position after a set time, illustrating the tendency for the trailing pellet to be drawn into the wake of the leading pellet, possibly inducing pellet collision.
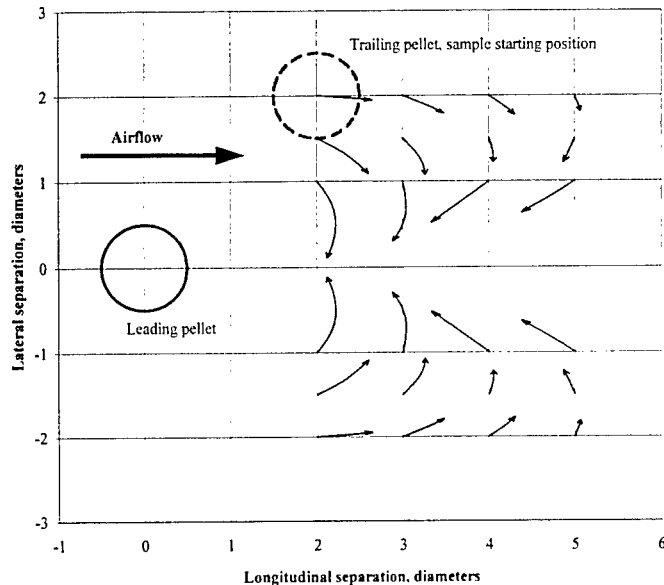
Figure 8: Plot of the trajectory of the trailing pellet relative to the leading pellet, shown for various starting positions of the trailing pellet.

Evidently the local variation in flow and pressure in the region to the side of the leading pellet enhances the retardation of the trailing pellet (see pellet starting from position 2,2). However, in the wake of the leading pellet, the lift on the trailing pellet causes it to be drawn further into the wake, and the reduction of drag enables it to close with the leading pellet. The general tendency for the trailing pellet to converge on the wake of the leading pellet suggests that the former will be laterally stable within the wake, although the pellet separation will rapidly close owing to the reduced drag acting on the trailing pellet. Although the computations were terminated before collision, it is expected that resultant collision can occur.

It is anticipated that the computed wake-effects on trailing pellet trajectories will have been over-estimated here by the use of the 2-dimensional CFD model. The wake effects with spheres rather than transverse cylinders will probably be less significant, but there is sufficient indication from this initial investigation to warrant belief that aerodynamic interactions do significantly affect pellet dispersion, either as aerodynamic cohesive effects, or leading to collision and subsequent divergence.

The timescales of the processes need to be considered further to determine whether sufficient time is available for these potential aerodynamic or consequent mechanical interactions to be significant before the pellets are mutually isolated by the range-dependent growth in dispersion.

# 7. CONCLUSIONS

The significance of the aerodynamic interaction between pellet pairs was examined to assess the potential for aerodynamic effects to influence the dispersion of shogun pellet-clouds in flight. A number of simplifications were assumed: linearity of dispersion with range was used to extrapolate back to short range so as to determine a characteristic pellet separation; and the computational model of unsteady aerodynamics was 2-, rather than 3-, dimensional for improved speed of computation. Non-sphericity and spin of the pellets remains to be assessed. Despite these simplifications a first insight into the aerodynamic interactions within a shotgun pellet cloud was made possible.

The results indicate that the trailing pellet may be drawn into the wake of a preceding pellet, and the reduced drag may then allow collision with the preceding pellet. The aerodynamic effect therefore has a cohesive effect on the pellet dispersion, but consequent collision of pellets may then promote dispersion.

The unsteady-CFD technique has been shown to be a useful tool at this introductory level, and further modelling can potentially elucidate the consequence of pellet spin and non-sphericity, and also the interactions due to multiple pellets. Relevant 3-dimensional CFD modelling is entirely possible, although the computational hardware demands are very much greater. The significance of mechanical interactions and other aerodynamic factors will require further investigation.

# 8. REFERENCES

[1]     E D Lowry, "Aerodynamic Performance of Lead and Iron Shotshell Loads", Olin Corporation, Winchester Division (1970).

[2]     D J Compton, "An experimental and theoretical investigation of shot cloud ballistics". Ph.D. thesis, University of London (1997)

[3]     D J Compton & R A Giblin, "A measurement system for the external ballistics and pattern analysis of shot clouds". In Proc. 1st Conf. on Non-toxic Shot, Royal Military College of Science (Cranfield University), 2/5/96, pp. 33-55 (1996)

[4]     D J Compton, R A Giblin, & P M Radmore, "Measurements on an ensemble of spheres in the transonic velocity regime". IEE Proc. Sci. Measurement Technol. (1997)

[5]     D J Compton, P M Radmore and R A Giblin, "A stochastic model of the dynamics of an ensemble of spheres", Proc. R. Soc. London. A 453, 1717-1731 (1997)

[6]     Eley diary (1988)

[7]     J Sahu and C J Nietubicz "Application of Chimera Technique to Projectiles in Relative Motion", J. of Spacecraft and Rockets, Vol.32, No.5, September-October. (1995)

[8]     J Szmelter, S Abdullah, "Estimation of components relative motion in segmented rods", 18th International Symposium on Ballistics, San Antonio, (1999)

# DETERMINATION OF BALLISTIC CHARACTERISTICS APPLIED TO EFP

GRIGNON C. [(1)], ZILIANI A. [(1)], RENAUD-BEZOT J.-L. [(2)]

(1) Giat Industries, 7 route de Guerry, 18023 Bourges Cédex, France

(2) Luchaire Défense S.A., B.P.13, La Chapelle Saint-Ursin, 18001 Bourges Cédex

**Abstract :** Contrary to manufactured projectile, each geometry of Explosively Formed Projectiles (EFP) can't be known before the shot. The sensitivity of the geometry to the formation conditions makes each EFP a specific projectile which has a specific flight. Nevertheless, geometries and flights can generally be classified into families depending on whether EFP are formed at high or low temperature for example. We present the methodology we followed to characterize the ballistic parameters. The two methods used are complementary and based on a minimization of the difference between 6-dof simulation results and experimental data. The first method gives a first estimation of initial condition and mean aerodynamic characteristics. The second one is a self-adapting method which gives more accurate estimations (dependence of the aerodynamic coefficients with the Mach number and with the angle of attack can be determined). Theoretical and experimental results are discussed and compared to an ideal flight in order to determine the initial jump only due to the formation conditions.

## 1. INTRODUCTION

The improvement of the simulation tools associated to a need of a better understanding of ballistic problems has finally led to a need of more accurate data. When projectile are geometrically known, some of their aerodynamic coefficients can be estimated par CFD computations [2][3]. For real flight for which projectiles are not predetermined, one of the ways to reach these data consists in performing inverse methods.

The flight is simulated with the 6-dof model developped at the ISL. The aim is to characterize the flight : initial conditions (especially the initial jump which accounts the formation conditions of the slug) and the aerodynamic coefficients. Each parameter is determined by minimizing the difference between experimental data (angular motion and/or trajectory) and calculation results.

A first estimation of the parameters is done. A more accurate characterization is then done by the iterative method elaborated at ISL [1]. As it is the case of all inverse methods, the solution is not single. It is then useful to be as accurate as possible in the identification in

order to improve the quality of the results. It is clear that the more the experimental data are numerous, the more accurate the estimation can be. Accuracy of EFP shots can be a constraint to have experimental data over a large distance. We have, for each slug, a particular shape (and specific aerodynamic coefficients), particular formation conditions, a particular flight, ... which make that each shot has often to be analysed separately.

## 2. EXPERIMENTAL SETUP

The military charge is fixed to a rotating bench in order to be in the same formation conditions of the slug in operational situation. Shots have been performed in the French experimental tunnel situated near Sauclières. The angle between the rotation axis of the bench and the axis of revolution of the charge is 30° (*figure* 1).

The experimental measurements are :

- two radiographies done close to the bench associated to time measurements in order to have some dimensional informations of the slug laterally (asymmetries, ...) and to quantify some initial conditions (initial velocity)

- yaw cards placed on the trajectory

- time measurements by optical cells placed on the trajectory to know the slug velocity

- measurement of the ambient temperature.

## 3. TREATMENT OF THE EXPERIMENTAL MEASUREMENTS

The SATTAP tool was developed at Giat Industries. This tool numerizes the holes let by the slug in the yaw cards during its flight and determines the experimental flight. It is constituated of a camera coupled to a calculation software which determines, for each yaw card, the angular motion and the trajectory of the projectile center of mass. When a particular default can be put in evidence in the rear part, its total spin can also be determined. Finally, SATTAP determines :

- the total angle of attack $\delta$ when the slug meets each yaw card

- the orientation $\psi$ respect to a vertical line of the plane containing the angle of attack and the velocity vector (resistance plane)

- the spin p of the slug

- the 3 spatial coordinates of its center of mass.

When the recovering of the slug can't be done, its inertial characteristics are missing (mass, position of the center of mass, moments of inertia). The dimensional data known laterally by X-Rays in two planes and from a rear view by the yaw cards give a very partial knowledge of its three dimensional shape. Its inertial characteristics can't be known accurately and can only be estimated by the mean of previous shots with recovering done in similar conditions.

## 4. FIRST DATA REDUCTION METHODOLOGY

### 4.1. Estimation of the mean drag coefficient Cx

Cx is estimated by using the mean velocity which has been determined by the time measurements at the distance L from the gun. Cx is the solution of :

$$Vm = -\frac{2.m.Vo}{L.\rho.S.Cx} \cdot \left( e^{-\frac{\rho.S.L.Cx}{2m}} - 1 \right) \tag{1}$$

which comes from the Fundamental Principle of Dynamics projected on the shot direction x. No dependence of Cx on the Mach number and on the angle of attack can be determined with (1). The validity of this relation is the best for small loss in deviation and altitude so that vertical and lateral velocities are negligible (no projection of the lift force on the shot direction). The situation of flat shot makes it valid for EFP flights.

### 4.2. Estimation of the roll damping coefficient Clp

Clp is determined by using the measured spin.

### 4.3. Estimation of the overturning moment coefficient Cmα

Cmα is linked to λ and, for an axisymmetrical projectile, is given by :

$$Cm\alpha = \frac{2.Iy}{\pi.\rho.D^3} \cdot \left( \left[ \frac{p}{Vo} \cdot \frac{Ix}{Iy} \right]^2 - \frac{4.\pi^2}{\lambda^2} \right) \tag{2}$$

λ is the distance separing two maxima of the angle of attack.
We note that the accuracy in the knowledge of the moments of inertia and p will directly affect the Cmα estimation. Equation (2) gives an estimation which can be improved, if necessary, with the experimental angle of attack.

## 4.4. Estimation of the lift force coefficient and the initial jump

The determination of Czα and ωo is done respect to a simultaneous good accordance with the experimental location of the center of mass on the last yaw card and with the experimental values of δ.

To perform this, a reference trajectory is calculated without initial jump (ωo=0) and for a chosen Czα. We obtain a theoretical final location of the center of mass on the last yaw card. An arbitrary initial jump is then considered and leeds to an other final point. The following steps consist in bringing successive corrections to ωo in order to reach the last experimental point. A corrected value of Czα has to be considered and determination of ωo to be done again until the two accordances are simultaneously satisfied.

## 4.5. Estimation of the yaw damping moment coefficient Cmq and the Magnus moment coefficient Cnpα

The estimation of Cmq is finally done to improve the accordance between experimental and theoretical angles of attack. The estimation of Cnpα can't be done accurately with this kind of data reduction method. We'll show that the second inverse method will improve the global estimation and can determine Cnpα.

The steps previously described give an estimation of the formation conditions of the slug through the initial jump ωo. The initial jump results from the jump due to the rotation of the bench and from the pure formation conditions. We can write :

$$\vec{\omega o}(tot) = \vec{\omega o}(id) + \vec{\omega o}(for) \qquad \text{avec } \omega o(tot) = \sqrt{q^2 + r^2} \qquad (3)$$

where :

    . $\vec{\omega o}(id)$ is the jump due to the rotating bench only (it corresponds to the total initial jump with an ideal formation of the slug)

    . $\vec{\omega o}(for)$ is the jump due to the formation of the slug

In order to quantify the contribution of the formation in the real initial jump, let's analyse the ideal flight.

## 5. THE IDEAL FLIGHT

## 5.1. Calculation of the initial jump $\vec{\omega o}(id)$ for the ideal flight

The initial state considered here is the coating fixed on the military charge.

The final state is the slug. The transformation of the coating into the slug is supposed to be perfect, that means without mass and energy loss.

The kinetic moment relation is expressed as :

$$\frac{d\bar{K}_G}{dt} = \sum \bar{M}_{Fext}$$

where

. $\bar{K}_G$ : kinetic moment at the center of mass

. $\bar{M}_{Fext}$ : moments at the center of mass due to the external forces acting on the system between the two states : aerodynamic forces, gravity, link between the coating and the military charge, thrust (which is also responsible for the coating into slug transformation).

The time needed by the transformation being short (a few μs), the action of the aerodynamic forces can be neglected. The thrust and link forces are acting symmetrically ; their moment is then zero at the center of mass.

The kinetic moment is then conservative between to coating state and the slug state. Knowing that :

$$\bar{K}_G = J\vec{\Omega}$$

we finally have :

$$(Ix.p)_{coat} = (Ix.p)_{EFP}$$
$$(Iy.q)_{coat} = (Iy.q)_{EFP}$$
$$(Iz.r)_{coat} = (Iz.r)_{EFP}$$

The ideal coating and the EFP being axisymmetrical bodies (Iy=Iz), we have :

$$p_{EFP} = p_{coat} \cdot \frac{Ix_{coat}}{Ix_{EFP}}$$

$$\omega_{0EFP}(id) = \omega_{0coat} \cdot \frac{Iy_{coat}}{Iy_{EFP}}$$

## 5.2. Ideal theoretical trajectory

Let's define θ and η as presented on *figure 2*. The slug being formed when the warhead and the rotation axis are in a vertical plane, the initial velocity vector only has x and z projections. It means that θo=0 (Vy=0). The rotating conditions of the bench lead to : Vz ~ -2.6 m/s (ηo ~ 0.075°). Consequently, the ideal trajectory is left-deviated and downwards-directed (*figures 5 and 6*). Differences between the real and this ideal trajectory will be due to the formation conditions of the EFP. The least the difference are, the best the formation conditions are.

## 6. SELF-ADAPTING DATA REDUCTION METHOD

Our first reduction method seems to be a good estimation of the ballistics of the studied EFP. But the Magnus moment coefficient was not evaluated and the adaptation of $\psi$ has to be improved (*figure* 4).

The self-adapting method used has been developped at ISL [1]. Contrary to the first data reduction method previously presented, it can determine the dependence of the aerodynamic coefficient with the Mach number and the total angle of attack.

The principle of this method is to correct successively initial values of the parameters by using a least squares method. The parameters determined by first data reduction method are the initial values used by the self-adapting method.

The results, in terms of angular motion and trajectory, are presented on the *figures* 3 to 6. The improvement in the parameters determination is clear for the $\psi$-curve. The Magnus moment coefficient has been determined and its role in the EFP behaviour can be quantified. Nevertheless, we have to be careful in our conclusion because the inertial characteristics can't be known accurately. The dimensional characterisation being done on 2D representations (X-Rays and yaw cards), the knowledge of the EFP is very partial :

- asymmetries can't be put in evidence accurately (and their consequences on the matrix of inertia have been neglected for the simulations)

- the center of mass location is approximative (only based on previous shots with recovering).

In order to improve the 3D and inertial knowledge of the EFP, a finer treatment of the 2D representations should be done by using for example shape analysis and CAD tools. Works will be done on that topic at Giat Industries.

## 7. CONCLUSION

Two complementary inverse methods have been presented to determine the ballistic parameters (initial conditions and aerodynamic coefficients). These methods are based on a 6-dof model and consist in a minimization of the differences between experimental and simulation results (angular motion and trajectory). The first estimation of the parameters obtained by the first method is then used by the second method (self-adapting) to improve the quality of the results. Contrary to manufactured projectiles, it is practically impossible to have an accurate 3D representation of the slugs without recovering. That means that the inertial properties of the slug are not known accurately. Works are going to be done at Giat Industries to improve the 3D representation using the 2D views (radiographies, holes in yaw cards) to better know the moments of inertia, the location of center of mass, asymmetries ...

**Nomenclature**

Clp    roll damping moment coefficient
$Cm\alpha$   derivative of the overturning moment coefficient
Cmq  derivative of the yaw damping moment coefficient
$Cnp\alpha$  derivative of the Magnus moment coefficient
Cx    drag coefficient
$Cz\alpha$   derivative of the lift force coefficient
D     rear diameter of the EFP
Ix    longitudinal moment of inertia
Iy, Iz  transverse moments of inertia
J     matrix of inertia
m    mass of the EFP
p     spin rate
q     yaw rate
r     pitch rate
S     rear section of the EFP
x     shot direction (line of sight)
y     ascending direction (positive when upwards)
z     lateral direction (positive when right-hand)
Vo   initial velocity
Vm  mean velocity

$\eta$     deviation angle of the velocity vector in the earth-fixed system
$\lambda$     half-length of the angular motion
$\rho$     air density
$\theta$     elevation angle of the velocity vector in the earth-fixed system
$\omega o$   initial jump
$\psi$     orientation of the resistance plane respect to the vertical plane containing the velocity vector

**REFERENCES**

[1]    V. Fleck,"Determination of the aerodynamic coefficients of an improved EFP from free-flicht tests", ISL report RT 507/98, Saint-Louis, France (1998)

[2]    Rondot F., Berner C.,"Simulations des performances de projectiles de CGN optimisés du point de vue aérodynamique", 6ème Journées Détonique, Bourges, France (1998)

[3]    Berner C., Fleck V., Warken D., "Aerodynamic predictions of explosively formed penetrators", 17th International Symposium on Ballistics, Midrand, South Africa (1998)
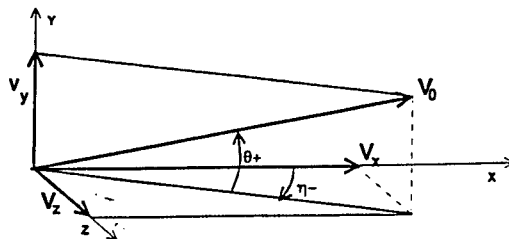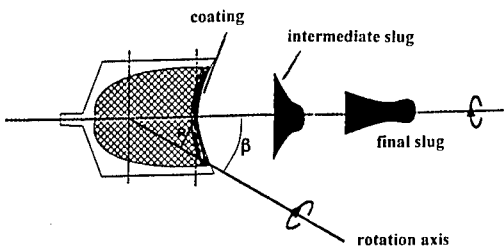
figure 1 : experimental setup

figure 2 : initial velocity projections in the earth-fixed axes
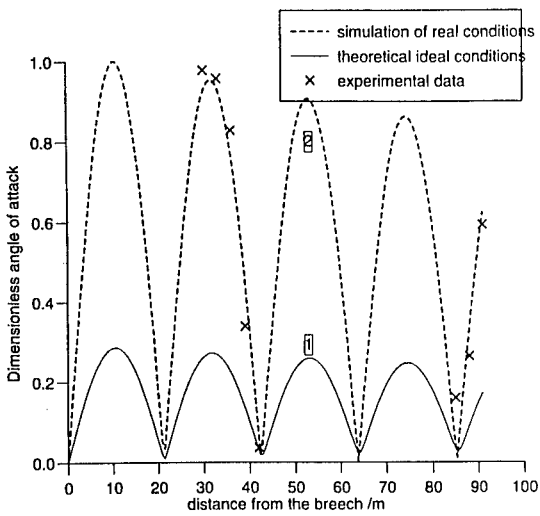


figure 3 : total angle of attack
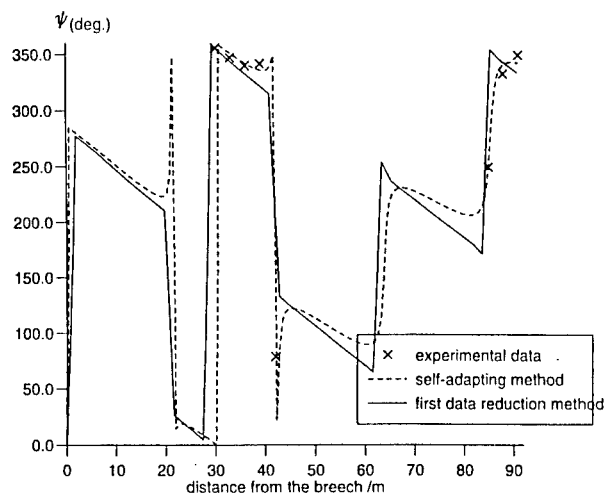
figure 4 : $\psi$-curves
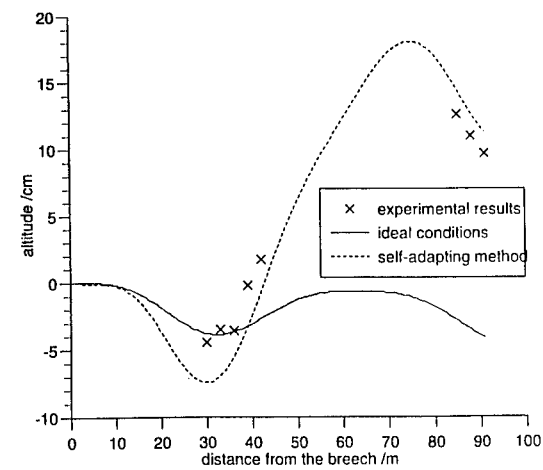


figure 5 : altitude of the center of mass
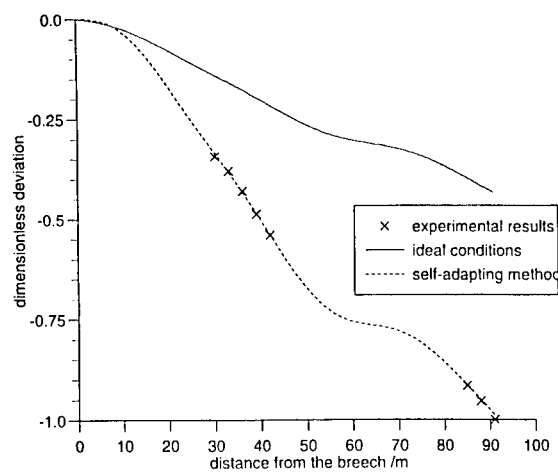
figure 6 : deviation of the center of mass

# ROLL PRODUCING MOMENT PREDICTION FOR FINNED PROJECTILES

CHAMPIGNY P. [1], DENIS P. [1], CAYZAC R. [2]

(1) ONERA, France
(2) GIAT Industries, France

*Paper not Available at the Time of Editing*

## ABSTRACT

In order to estimate the steady spin rate of finned projectiles, one needs to know the roll damping coefficient and the fin producing roll moment coefficient. The first coefficient is difficult to measure in wind tunnel, requiring specific free spinning rig. It can be also computed, but it needs high level CFD tools, solving unsteady turbulent Navier Stokes equations. On the other hand, the prediction of the roll producing moment of canted fins seems to be relatively easier, from both wind tunnel experiments or analytical methods.

This paper will show that, as a matter of fact, it is very difficult to obtain an accurate prediction of the roll producing moment for classical canted fins (partially canted or chamfered).

Tests have been carried out in the ONERA S3MA wind tunnel for different flow conditions (Mach, angle of attack), with different fins (planform, chamfer angle, sharp or blunt leading edge), and for different fin arrangements (set of 2, 4 or 6 fins). For the measurements, a specific sting has been designed with a very accurate roll balance.

The results show that the rolling moment is highly dependent on the chamfer angle, and fin planform as expected, but there is also a strong influence of the leading edge bluntness, Mach number and angle of attack. In particular, one can see that the Mach number effect is not as expected, but completely inverted, due to the interaction between adjacent fins. Moreover, a slight, but not negligible, influence of the body boundary layer has been observed.

The analysis of the results shows that semi-empirical methods are inadequate to predict with a good accuracy the roll producing moment of canted fins and that CFD codes are needed.

# SOLID FUEL RAMJETS FOR PROJECTILE PROPULSION – SUMMING UP OF A JOINT FOA – TNO RESEARCH PROJECT

KURT ANDERSSON [1], RONALD G. VERAAR [2]

(1) FOA Weapon and Protection Division, Grindsjön, SE-147 25 Tumba, Sweden
(2) TNO Prins Maurits Laboratory, P.O. Box 45, 2280 AA Rijswijk, The Netherlands

**Abstract:** A collaborative research project on Solid Fuel Ramjets for projectile propulsion was performed and was terminated in 1999 with a technology demonstration. The results and experiences are summarised and the possibilities for applications such as artillery projectiles and direct fire weapons are analysed and discussed. For artillery projectiles doubling or tripling the range may be possible with a low weight penalty, and with maintained flight times and similar or reduced dispersion. For direct fire weapons much increased hit probabilities and better terminal performances may be achieved.

## 1. INTRODUCTION

The Solid Fuel Ramjet (SFRJ) propulsion system combines relatively high propulsion performance with a very low degree of mechanical complexity, but, as all ramjets, needs to be accelerated to supersonic velocity by other means. As such, application of this propulsion system seems to be attractive to increase the flight range and/or the flight velocity of gun-launched projectiles. The functioning of the SFRJ is, however, dictated by complex physical phenomena with strong interactions. Consequently, successful design of such a projectile requires detailed knowledge of the performance both at subsystem level as well as at projectile system level.

Since mid 1995 a co-operative study programme on SFRJ propulsion for projectiles is performed by the FOA Defence Research Establishment, Weapons and Protection Division, in Sweden and the Prins Maurits Laboratory of the Netherlands Organisation for Applied Scientific Research (TNO-PML). This study programme is financed by the Swedish Defence Headquarters and the Ammunition Branch of the National Supply Agency of the Royal Netherlands Army and aims at demonstration of the technology of SFRJ propulsion for gun-launched projectiles by means of designing, manufacturing and flight testing a generic SFRJ propelled projectile.

The first 4 years of this study programme have been dedicated to technology development work on aerodynamics (FOA/TNO), combustor and nozzle (TNO), and projectile system performance (TNO). In addition, work has been performed by FOA on the gun system to launch the projectile and on the mechanical design of the projectile. To conclude the co-operation programme several series of free-flight tests have been performed (FOA/TNO). The present paper intends to give an overview of this co-operative study programme, which

formally ended at the end of 1999, and to show the benefits of using SFRJ propulsion for some possible applications.

## 2. BACKGROUND OF THE CO-OPERATION

Before the co-operative programme started, both TNO and FOA had worked on research projects concerning SFRJ-propulsion. FOA had performed both theoretical and experimental studies. Initially FOA performed fundamental studies of the combustion process and tried, like many others, to find the relation between the regression rate and the different parameters in the combustion chamber [1]. Later the work focused more on the complete system and terminated in free-flight tests of a 40-mm spin-stabilised SFRJ-propelled projectile [2].

At TNO considerable work had been done to experimentally establish the regression rate of the fuel as a function of different parameters but also on modelling of the complete system including such things as projectile external drag, air intake performance, combustor performance and the resulting thrust of the projectile [3].

Towards this background it was decided to start a joint project with TNO and FOA participating and where both parties contributed with approximately equal amounts worth of work and material. A work plan was jointly made up ending with free-flight tests of a SFRJ-propelled gun-launched projectile. To facilitate this international co-operation, it was decided not to look at one specific application but to look at a generic projectile just to demonstrate the feasibility of the propulsion concept.

## 3. TECHNOLOGY DEVELOPMENT

To successfully demonstrate the feasibility of SFRJ propulsion for gun-launched projectiles a set of requirements was defined representative for typical applications. The most important requirements are related to the desired flight performance to be demonstrated in the final flight-testing:

- Minimum propelled flight time equal to 2 seconds
- Flight Mach number equal to 4.0

To direct the technology development effort, a so-called baseline design of the generic SFRJ projectile was defined early in the study programme based on the above requirements. Throughout the study programme, the knowledge gained from the technology development work has been incorporated into the Ramjet Propelled Projectile Performance Prediction Program (RP$^5$) developed by TNO [3]. This engineering code has subsequently been used to study the projectile sensitivity to performance parameter changes and to geometric design changes in order to enable design trade-offs. In this way the baseline design of the projectile has been improved several times, thus reflecting the progress made in technology development.
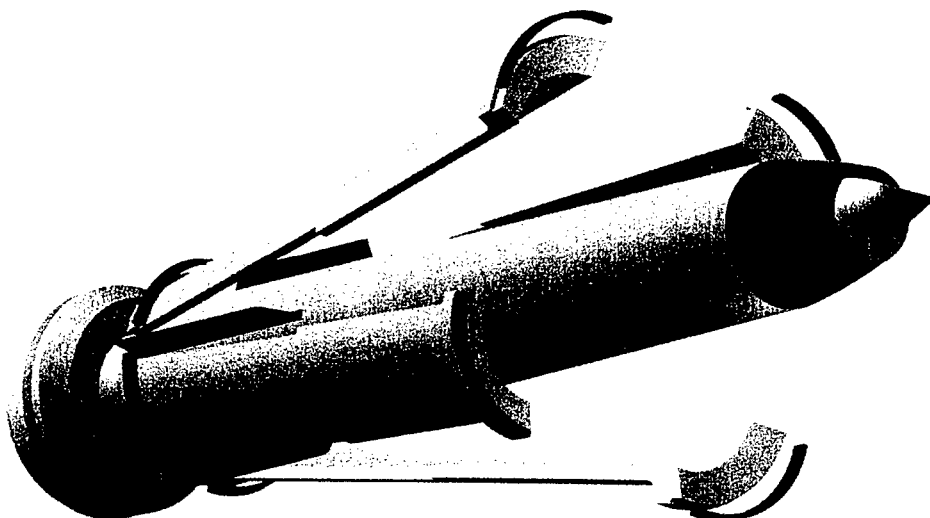
Figure 1        Baseline design of the generic SFRJ projectile

## 3.1    Description of the baseline projectile design and operation

The baseline design of the projectile is shown in Figure 1. At the nose of the projectile the axi-symmetric air intake is located. On the inner wall of the projectile body a layer of solid fuel is cast. The conical exhaust nozzle is mounted on the downstream side of the tubular projectile body as well as the 4 fixed fins to stabilise the projectile. To transfer the gas pressure of the gun propellant to the projectile during gun-launch a pusher plate is applied which fits in the exhaust nozzle of the projectile. Sabot segments are used to guide the projectile within the gun barrel.

After ignition of the gun propellant, the projectile is accelerated within the gun to the required Mach 4.0 (=1360 m/s) muzzle velocity. Directly after leaving the gun barrel the pusher plate as well as the sabot segments separate from the projectile and air starts to flow through the projectile. In the intake the air is compressed by shock waves, hereby reducing the flow velocity to subsonic speed. The hot compressed air enters the combustion chamber over a backward-facing step acting as a flame-stabiliser during combustion. The convective heat transfer causes the solid fuel to evaporate and mix with the air. Provided that the temperature of the air is high enough (roughly > 1000 K), automatic ignition of this air-fuel mixture occurs. The combustion gases leave the projectile through the exhaust nozzle in which the flow speed is increased from subsonic to supersonic speeds, thus generating a thrust.

## 3.2    Aerodynamics

Early in the co-operation programme, the external drag components of the baseline projectile design have been predicted using the projectile performance prediction code RP[5] [3] and the missile aerodynamic performance prediction code AERAM as developed by FFA [4]. These calculations included variations of all geometric parameters of the projectile in order to study the sensitivity of the aerodynamic characteristics to design changes.

The AERAM code was also used, together with Missile Datcom [5], to study such aerodynamic coefficients as the lift coefficient and the position of the centre of pressure and their dependence of fin size and position. Besides ordinary uncertainties using this type of codes there also was the uncertainty of the influence of the shape of the air intake on the stability, something that is not dealt with in the codes used.

Furthermore, the performance of the air intake in terms of external drag, captured air mass flow and total pressure recovery as predicted by RP[5] was compared to the results of the CHARISMA code as developed by FOA [6,7]. In contrast to RP[5] (see Projectile Performance Prediction), the CHARISMA code uses the method of characteristics to calculate the entire inviscid supersonic flow field in and around the air intake. From these calculations it was found that the lower order methods as implemented in RP[5] yielded the same results as the method of characteristics. Since both methods were based on inviscid flow relations, the need was identified to enable prediction of the adverse viscous effects on the air intake performance. In order satisfy this need, calculations have been performed at FOA using the general-purpose CFD code RAMPANT [8]. This code solves the Navier-Stokes equations using an adaptable unstructured meshing technique. A large number of calculations were performed on several 2D air intake configurations at a range of back pressures at flight Mach numbers varying from Mach 3.8 to 4.0 using the k-ε turbulence model and wall-functions to describe the boundary layers.

However, it was felt that the fully developed boundary layer shape assumption as implied by the use of wall functions in the RAMPANT calculations may prevent a realistic prediction of the adverse viscous effects. For this reason TNO subcontracted CFS Engineering SA in Switzerland to perform 2D as well as 3D calculations using the NSMB code on an air intake configuration selected based on the RAMPANT calculations. The NSMB code is a Multi-Block Navier-Stokes solver using block structured grids to discretize and solve the Navier-Stokes equations throughout the entire boundary layer [9] . Figure 2 shows an example of the resulting flow field in the air intake at a 2 degrees angle of attack as predicted by the NSMB code.



-8.8050E-04

0.4497

0.9002

1.351

1.801

2.252

2.702

3.153

3.604

4.054
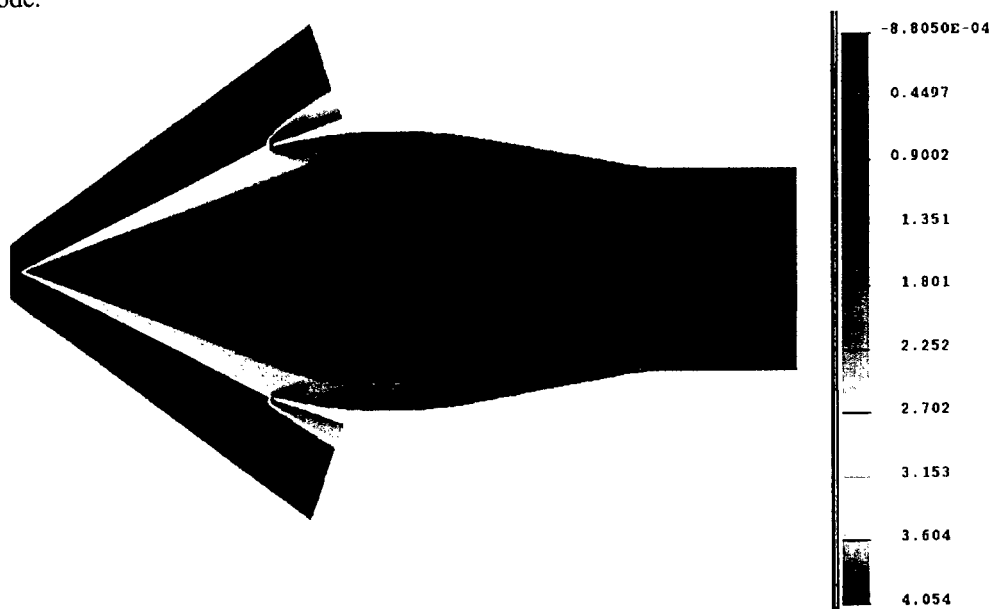
Figure 2    Mach number distribution in the air intake at 2 deg. angle of attack predicted by the NSMB code

Although the propelled flight time is only 2 seconds, the very high flight speed of the projectile results in significant aerodynamic heating. Engineering relations describing the stagnation point heating as well as the laminar boundary layer heating have been used to predict the temperature history of the most critical parts of the projectile, i.e. the intake compression cone tip, the intake cowl lip and the fin leading edges. Based on this analysis, materials have been selected for these critical parts capable of withstanding the predicted temperatures.

## 3.3 Combustor and Nozzle

One of the first activities within the framework of the combustor technology development work was to select a fuel with sufficient combustion performance to generate the required thrust and with excellent mechanical properties in order to survive the 60000 g launch load. To this end a number of promising Hydroxyl Terminated Poly-Butadiene (HTPB) based fuels have been manufactured. A large number of tensile tests at various temperatures has been performed both at FOA and TNO to derive the mechanical behaviour of these fuels at the very high deformation rates anticipated during launch.

In order to establish the combustion performance of the selected fuel, a large number of experiments has been performed using the connected pipe SFRJ test facility at TNO-PML (see Figure 3). This facility comprises a Gas Supply System (GSS) capable of supplying air, oxygen and hydrogen to the SFRJ test set-up. Furthermore, a 96-channel data-acquisition system is available to record the signals from a large number of pressure transducers and thermocouples mounted on the GSS and the test set-up. In addition, the thrust of the SFRJ test motor can be measured.
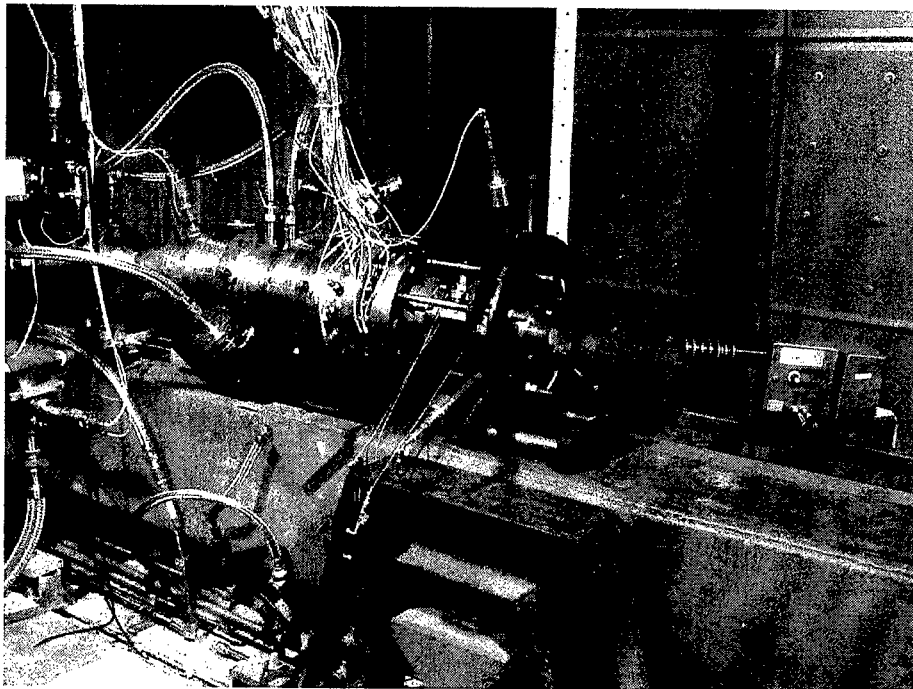


Figure 3        SFRJ test set-up during a combustor performance test

From projectile performance sensitivity analyses carried out with RP[5], it became clear that an accurate prediction of the projectile flight performance could be obtained only if the combustion efficiency as a function of the operational conditions of the SFRJ combustor is accurately known. In order to improve the temperature homogeneity of the simulated in-flight combustor entrance conditions, a new air heater was designed and built in which hydrogen is burnt to heat the air. Oxygen is added to the airflow in order to maintain the correct oxygen content of the heated air. In addition, the ultra-sonic technique [10] is applied to measure the momentary fuel regression rate during the complete SFRJ test. From the test results obtained with this improved SFRJ test set-up an empirical time dependent SFRJ combustor performance model was derived which has been implemented in the RP[5] code. In this test facility erosion of aluminium nozzles was also studied and conclusions were drawn on which steps should be taken to enable the nozzle to survive the 2 second propelled flight time.

To predict the performance of the nozzle subsystem and its sensitivity to design changes a number of calculations has been performed using the Solid Propulsion Program (SPP code) [11]. The nozzle performance module of this computer code predicts the deficiencies with respect to the ideal inviscid one-dimensional nozzle flow in chemical equilibrium. The flow divergence loss is derived from an inviscid nozzle flow field calculation using the method of characteristics. A one-dimensional finite-rate chemical kinetics module is included to account for losses caused by the nozzle exhaust gases not being in chemical equilibrium. Furthermore, a boundary layer module is applied to predict the losses due to viscosity.

## 3.4 Mechanical Design

Based on experience of previously performed work on SFRJ projectiles at FOA [2, 12] a first mechanical design was established. The aerodynamic stability characteristics of the projectile as predicted using AERAM and Missile Datcom indicated that the centre of gravity should not be located aft of 0.35 times the projectile length, seen from the nose. Since the present study is focused on demonstrating SFRJ propulsion for projectiles, no strict requirement was specified for the maximum mass of the projectile. This freedom was used to select different materials for the projectile parts in order to comply with the aerodynamic stability requirement, taking into account the aerodynamic heating as discussed in one of the previous sections.

At FOA, a large number of acceleration tests was performed on the projectile parts separately as well as on various subassemblies in order to verify the structural integrity of the mechanical design using the acceleration test facility [13]. Examples of subassemblies are the air intake with centerbody, nozzle with pusher plate and projectile body with dummy load simulating the air intake. To support these acceleration tests Finite Element calculations have been performed at FOA using the DYNA2D code [14] in order to predict the level of stress within each projectile part.

On some occasions failures occurred resulting in subsequent design changes. Figure 4a shows a projectile nose in the carrier used in the acceleration tests after a successful test. Figure 4b shows the result of an acceleration test where the struts holding the centerbody were plastically deformed resulting in damage to the whole air intake.
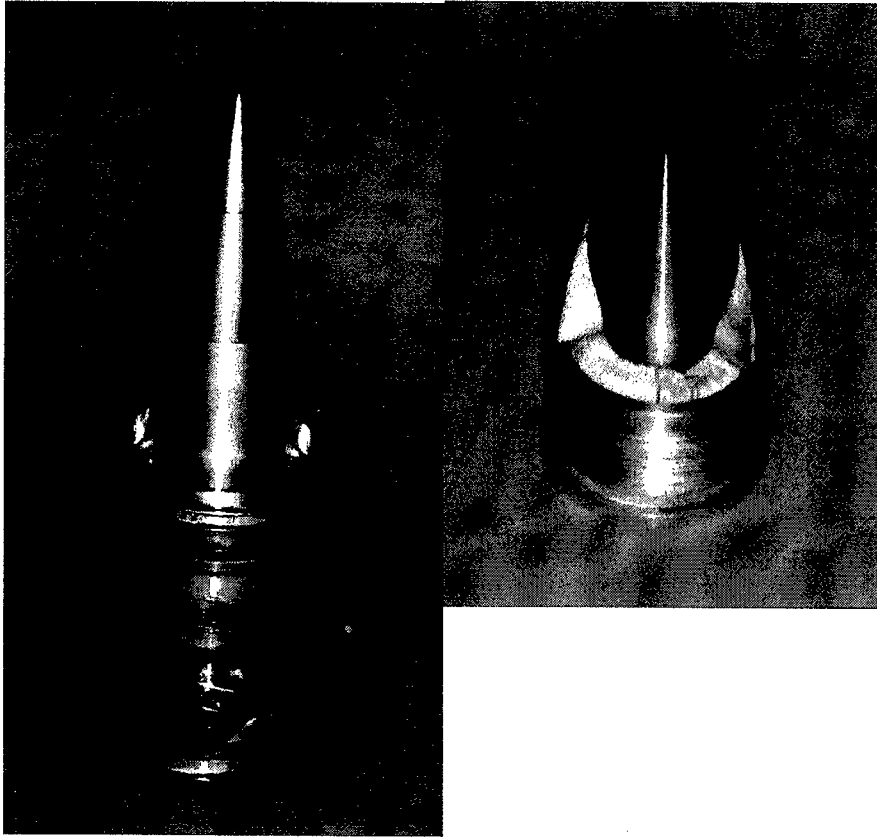
Figure 4a (left). Projectile nose that survived acceleration the carrier
Figure 4b (right). Projectile nose damaged by acceleration

## 3.5 Gun System

The gun system, partly designed for these tests, consists of a 57 mm Bofors gun barrel, smooth bored to 61 mm, and mounted in a 75 mm Bofors gun (see Figure 5 ). Interior ballistic calculations were performed using the IBKB2 code [15], developed by FOA, in order to predict the performance of the gun system. To verify these calculations a large number of gun firings was performed with dummy masses using several types and amounts of propellants. During the gun firings the pressure was measured at the rear of the cartridge using Kistler pressure transducers. Based on these gun firings a propellant has been selected which is capable to accelerate the total launch mass of the present baseline design to the required Mach 4.0 muzzle velocity [16].
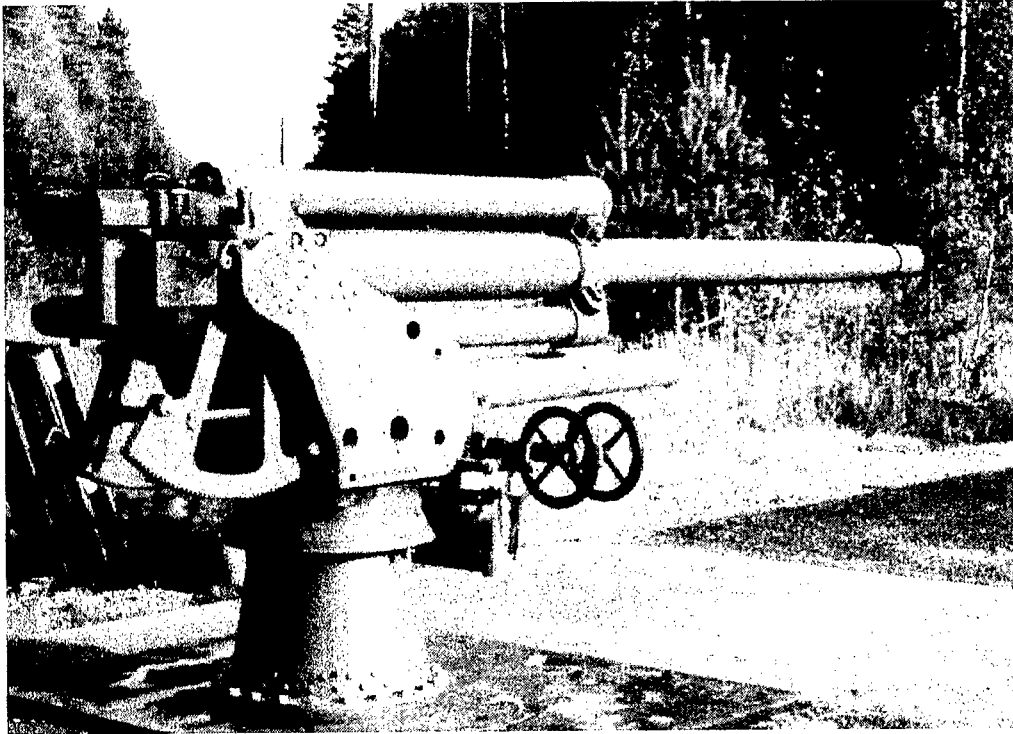
Figure 5 . The gun used in the tests

As the smooth bore 61 mm barrel is not a standard one some modifications had to be made. First of all the front end of the cartridge had a smaller diameter than the modified gun barrel. To overcome this problem a sleeve of reinforced plastic was glued to the front end of the cartridge so that the barrel wall supported it.

Furthermore it turned out to be difficult to ignite existing propellants with a projectile with less mass than ordinary 57-mm ammunition and without a resisting force similar to that a projectile experiences when it enters the rifling. This problem was solved designing the pusher plate so that it fits in the cartridge like an ordinary projectile does. Test were then done with different means like glueing and/or introducing grooves to hold the projectile back while pressure was built up in the cartridge. From these studies it appeared that it was sufficient to use one groove.

## 3.6 Projectile Flight Performance Prediction

The RP[5] code is developed by TNO to predict the flight performance of SFRJ projectiles taking off-design conditions into account [3]. By assuming the thrust, drag and projectile mass (and thus the acceleration) to be constant during a small time step of the flight, a quasi-stationary flight calculation is performed. At each time step the thermodynamic conditions and the chemical equilibrium composition of the gas flowing through the projectile are calculated at several stations throughout the system, assuming the flow to be one-dimensional. The amount of fuel that evaporates and subsequently combusts is modelled using an empirical relation derived from a large number of SFRJ experiments.

Shock wave relations in combination with the Taylor-Maccoll supersonic cone flow relations are used to predict the total pressure recovery and captured mass flow of the axi-symmetric external compression intake, while the external cowl drag is predicted using the second-order shock-expansion method. Empirical relations are included to predict the cowl lip drag, skin friction drag, base drag as well as the drag due to bluntness of the fin leading and trailing edges.
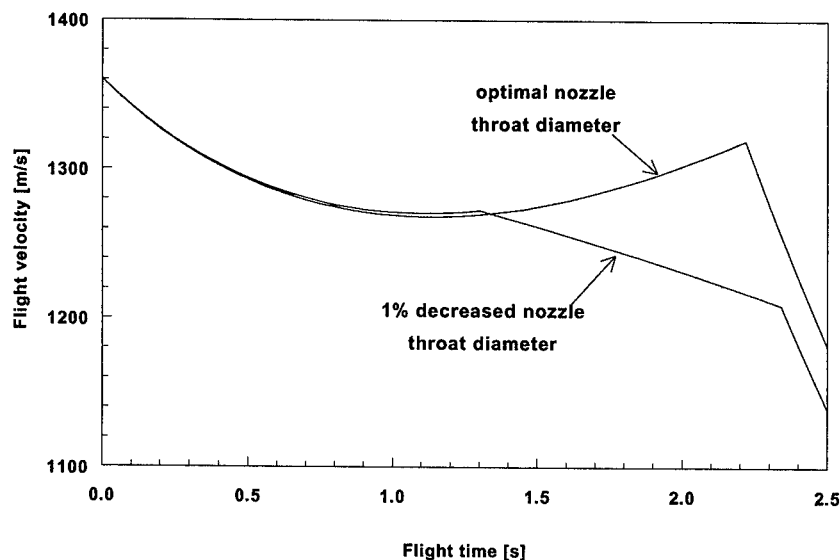


Figure 6    Predicted flight velocity for various throat diameters

Figure 6 shows an example of an RP[5] prediction of the flight velocity of the SFRJ projectile having various nozzle throat diameters. As can be seen, the nozzle throat diameter is predicted to have a significant effect on the flight performance of the SFRJ projectile, especially if the smaller nozzle throat diameter forces the air intake to operate in sub-critical condition. The latter operational condition of the air intake is accompanied by excessive spillage drag that results in a significant deceleration.

## 4    FREE-FLIGHT TESTING

### 4.1.   Free-flight Testing at FOA Grindsjön.

During late 1998 and early 1999 two series of free-flight tests were performed at FOA using a simplified projectile to verify the mechanical design and to verify clean pusher plate and sabots separation. For these test objectives it was sufficient to fire the projectile on a test range ($\approx$ 80 m) too short to obtain useful data on the propulsive performance (see Figure 7). For this reason no fuel was present in these projectiles and the actual intake was replaced by a pitot intake with a small capture diameter to ensure internal pressure build-up prior to pusher plate separation. A detailed description of these test series has been given in [17].
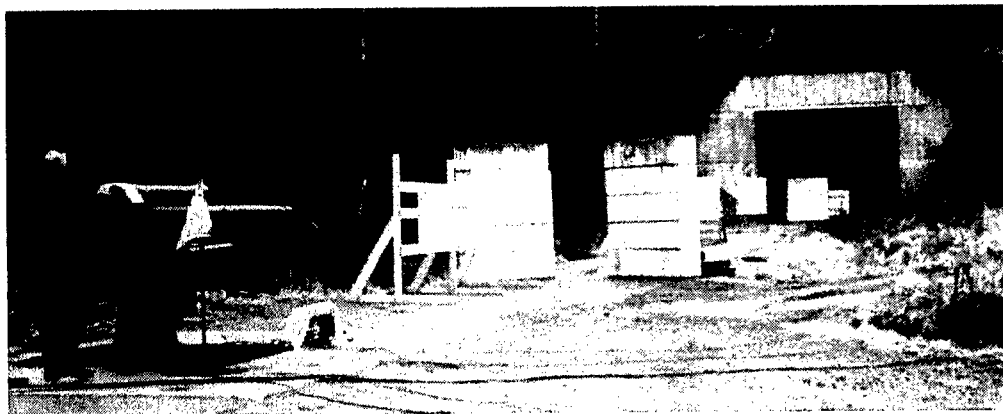
Figure 7. Photo of the complete test set up during scond test series at FOA.

The first free-flight test series was performed in October 1998. When firing the first simplified projectile at a muzzle velocity around 1400 m/s the result was that it obviously collapsed in the barrel and came out in fragments. It then was decided to reduce the muzzle velocity hoping the projectile then would survive and some opinion on sabots and pusher plate separation as well as stability in flight could be achieved. The intention was to have a muzzle velocity of 1000 m/s. When the second simplified test projectile was fired the velocity was 1025 m/s as deduced from the first high-speed video station. This projectile did withstand the acceleration in the barrel and separation of both the pusher plate and sabots seemed to function properly and stability in flight seemed to be good.

The second free-flight test series took place in April 1999. No major design changes to the simplified projectile had been made but different gun propellant was used. This propellant was more surface treated and gave a lower maximum pressure and consequently a lower acceleration in the barrel. The propellant had, of course, been tested and the propellant charge mass to achieve a muzzle velocity of 1360 m/s (M=4.0) had been determined using dummy projectiles prior to the second free-flight test series,.

Two projectiles were fired and both had a muzzle velocity close to 1300 m/s (slightly low but acceptable). Both projectiles also worked very well in all aspects that were of primary interest. Figure 8 below shows a high speed photo of the first of these projectiles at a distance of 6 – 10 m from the muzzle and figure 9 shows the second projectile at a distance of approx. 25 m.

Figure 8. High speed photos of the first of the projectiles in the second test series at a distance of 6 – 10 m from the muzzle.
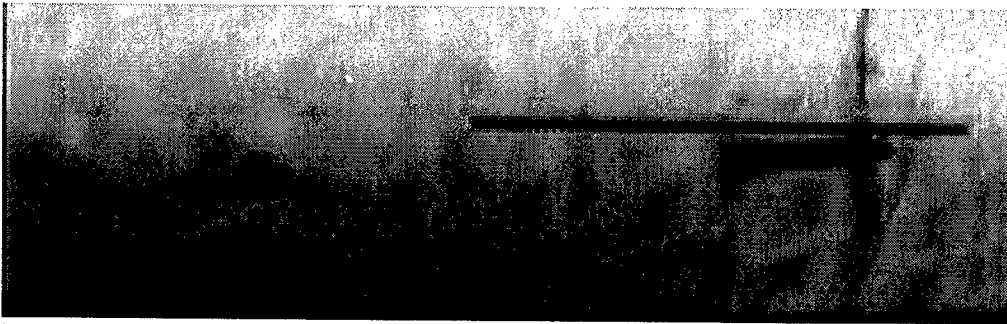


Figure 9. High speed video recording of the second of the projectiles in the second test series at a distance of 27 m from the muzzle.

The photos and video recordings together with the information obtained from witness screens indicate a clean separation of the pusher plate and sabot segments and a stable flight of the projectile.

## 4.2    Final free-flight tests at Bofors

Two final test series were done at Bofors Test Centre during the last quarter of 1999. In these tests the final design of the projectile was used with the air intake with a centre-body. The first of the two final test series was performed in October 1999 on a 600 m test range. The aim of the first test series was to verify the mechanical strength of the projectile as well as to verify the stability in flight with the final design of the air intake as it has been shown that there is an effect on the stability of the air intake shape [18]. Besides some warmers four projectiles were fired at zero degrees elevation. The muzzle velocity for these rounds as measured using a doppler radar was between 1292 m/s (M=3.87) and 1332 m/s (M=3.98). The muzzle velocity was intentionally increased during the test series.

The results showed that the final design behaved as good as the simplified projectile had done, that is to say that it did withstand the acceleration in the barrel, had quick and clean separation of pusher plate and sabots and flew stable in the trajectory (see Figure 10).
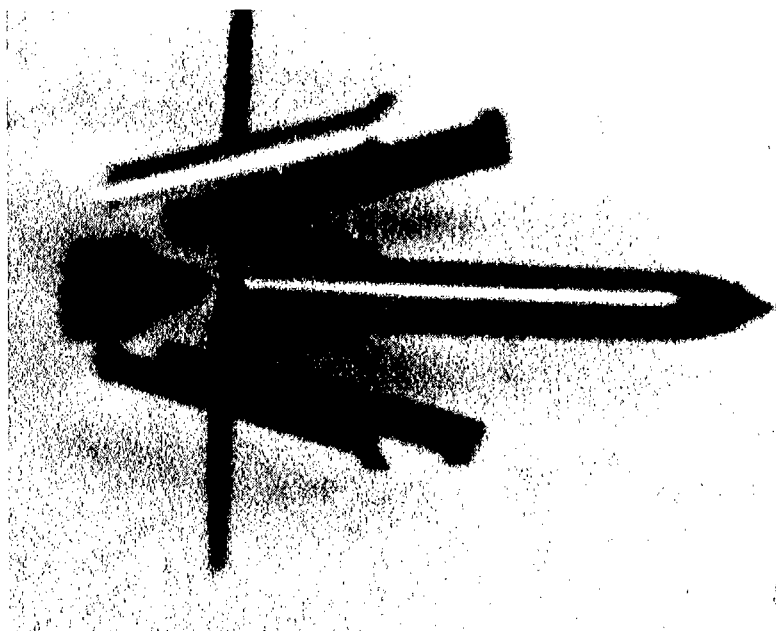


Figure 10. Projectile of the final design fired at the first of the two final test series (the vertical line indicates the distance of 5 m from the muzzle).

The second test series was performed during the first week of December and aimed at verifying the flight performance of the SFRJ projectile on a test range more than 10 km long. During this test series a Weibel Doppler radar was used to track the projectile trajectory and to measure the velocity in flight and from that deduce the resulting force on the projectile (i.e. drag minus thrust). Ten projectiles, not counting warmers, were fired at 8 degrees elevation during two days. Of these one was a reference projectile, which means that it had exactly the same design as the others but had no fuel . Subsequently the reference projectile was of slightly lower mass then the rest of the projectiles. The muzzle velocity as measured using the Weibler Doppler radar was between 1290 m/s (M=3.92) and 1382 m/s (M=4.14). The muzzle velocity was intentionally increased during the test series by elevating the temperature of the cartridge. All projectiles seemed to work very well in the sense that they had a good separation of pusher plate and sabots and stable flight after separation. The radar was able to track all projectiles except for one.

To illustrate the benefit of the SFRJ propulsion system, Figure 11 shows a Doppler radar velocity measurement zoomed in on the start-up phase of the SFRJ propulsion system. As can be seen, the initial drag of the SFRJ projectile is comparable to that of the reference projectile without fuel. But as soon as the combustor is fully ignited a thrust is generated approximately equal to the drag resulting in the flight velocity to remain essentially constant.
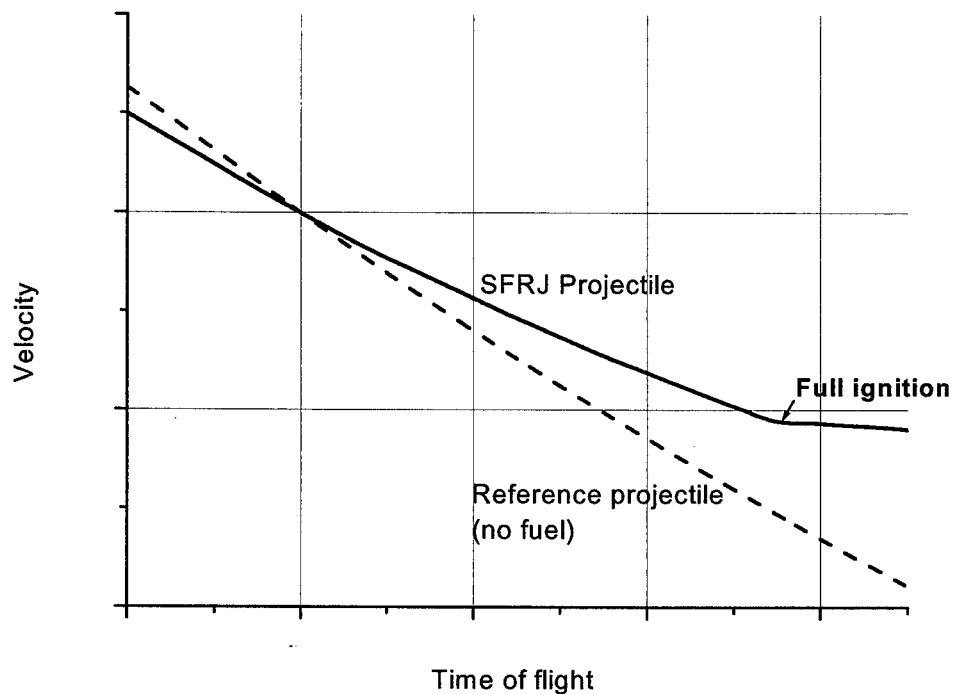
Figure 11. Velocity versus time during the initial flight phase for the reference projectile and a SFRJ projectile.

## 5    APPLICATIONS

There are many possible applications for SFRJ Propulsion. Different types of guided missiles are of course possible, but as they have to be accelerated to supersonic velocity by other means (like all ramjets) and might be sensible to manoeuvres (as there are no simple ways to compensate for changes in air influx) these applications may not be the first to think of. Gun-launched projectiles on the other hand have generally initially high velocity and even if they are terminally guided they are not subjected to large manoeuvres. As an SFRJ-motor has a very high specific impulse only comparatively small amounts of fuel are required.

Possible gun launched applications are [19]:

➤    artillery projectiles
➤    air defence projectiles
➤    KE-projectiles
➤    tank training projectile

### 5.1    Artillery projectiles

Over the years different methods to increase the range of artillery have been studied. These include, besides increasing the muzzle velocity, addition of rocket motors (RAP), addition of a base-bleed or base-burner unit (BB) or/and addition of wings to make a "fly out". The latter

method has up till now only been studied theoretically as has SFRJ-propulsion [ 20,21,22]. At FOA studies concerning the effect of SFRJ on artillery shells are performed.

There are great advantages if a SFRJ-motor can be introduced into an artillery projectile. It is very easy to theoretically show that if the drag is completely cancelled out for say 20 seconds on a modern 155-mm artillery shell the range is more than doubled. In Figure 12 the theoretical trajectories for modern 155-mm artillery shells, assuming a mass (at the muzzle) of 45 kg and a muzzle velocity of 900 m/s, are shown when different means are added to the projectile to increase the range. SFRJ propulsion is assumed to generate a thrust that equals drag so the trajectories marked D=0 10 s and 20 s corresponds to a SFRJ-projectile having propulsion during 10 respectively 20 seconds. The FOA-TNO co-operative program has theoretically shown that this is true, at least as a mean value over the propelled flight time, and the test flights have shown that the drag can be cancelled out during a certain time.
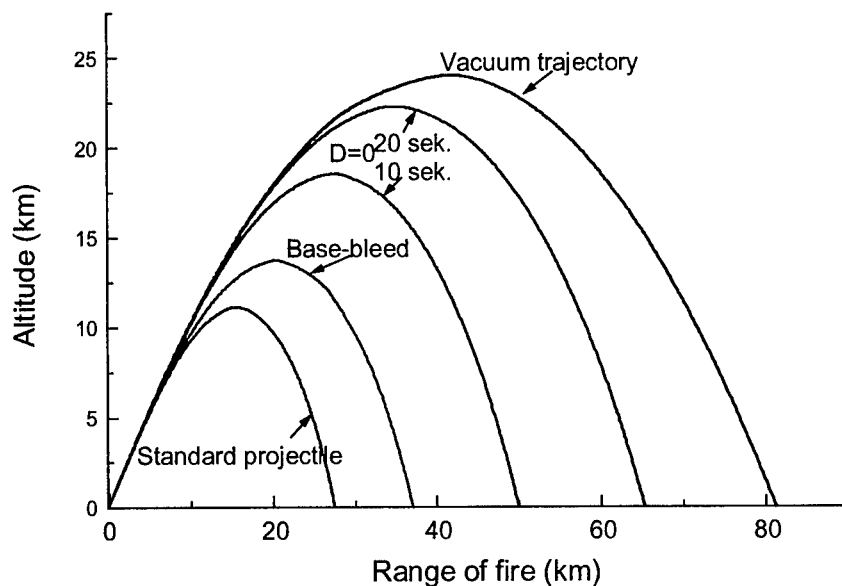


Figure 12. Trajectories (theoretically) for modern 155-mm artillery shells with different means to increase the range (D=0 equals ideal SFRJ-propulsion).

It should be noted that, as the specific impulse is much higher (4-6 times) for air breathing motors than for rockets, the fuel mass of the SFRJ-motor is of the same order as of a Base-Bleed unit.

Furthermore a very important aspect of the SFRJ-propulsion is that it considerably decreases the sensitivity to atmospheric disturbances as illustrated in Figure 13 where the sensitivity to cross wind is shown for different artillery projectiles reaching 65 km. It can also be shown, although not shown here, that an SFRJ artillery projectile at its maximum range has smaller sensitivity to e.g. wind than a standard projectile at its maximum range although the maximum range is less than half that of the SFRJ-projectile (see Figure 12).

It might seem strange to use SFRJ-propulsion for artillery ammunition as different quadrant elevations may give very different conditions in the intake. It can however be shown that, for a given muzzle velocity, the Mach number is very close to constant over a wide range of elevations and times assuming the drag is totally balanced out.
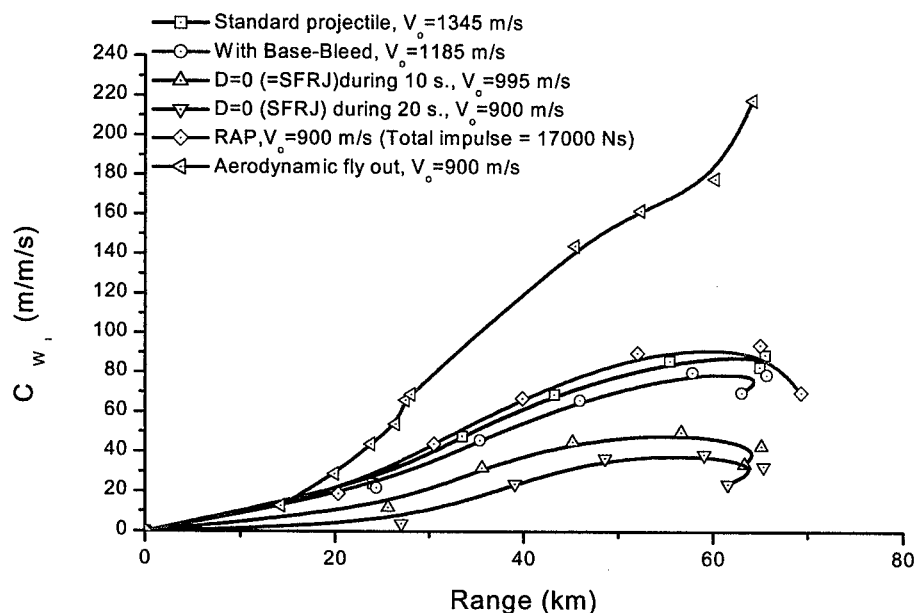


Figure 13. Sensitivity to wind for different hypothetic 155-mm projectile types reaching 65 km.

## 5.2 Air defence projectiles

The application of SFRJ propulsion to medium calibre air defence ammunition has been investigated by TNO. In this application study a spin-stabilised SFRJ-propelled projectile was considered containing a frangible penetrator similar to that of the conventional Oerlikon 35 mm FAPDS ammunition fired from the 35 mm Oerlikon KDA gun [23]. The sabot segments of the conventional ammunition were replaced by a 35 mm tubular body including an air intake and an exhaust nozzle. The results of RP[5] predictions indicated that, in spite of significantly higher flight speeds and superior kinetic energy levels at 4 km flight range, the lower muzzle velocity due to the higher projectile mass resulted in the improvements in terms of time-to-target to be marginal.

Based on these results, a new design of the 35 mm SFRJ air defence projectile was conceived in which the tubular ramjet body itself serves as the frangible penetrator. By doing so the muzzle velocity of the SFRJ projectile could be increased to values equal to that of the conventional ammunition. The time of flight as a function of flight range as predicted by RP[5] is compared to that of the conventional ammunition in Figure 14. This figure indicates that applying ramjet propulsion to air defence ammunition may result in a significant reduction in time of flight. Assuming that the hit probability of a single shot against a manoeuvring target

is inversely proportional to time of flight to the power 4 [18] results in a single shot hit probability of the SFRJ projectile normalised by the hit probability of the conventional air defence projectile as shown in Figure 15. As can be seen in this figure, a hit probability increase up to 125% at 5 km flight range is predicted for the 35 mm SFRJ propelled air defence projectile.
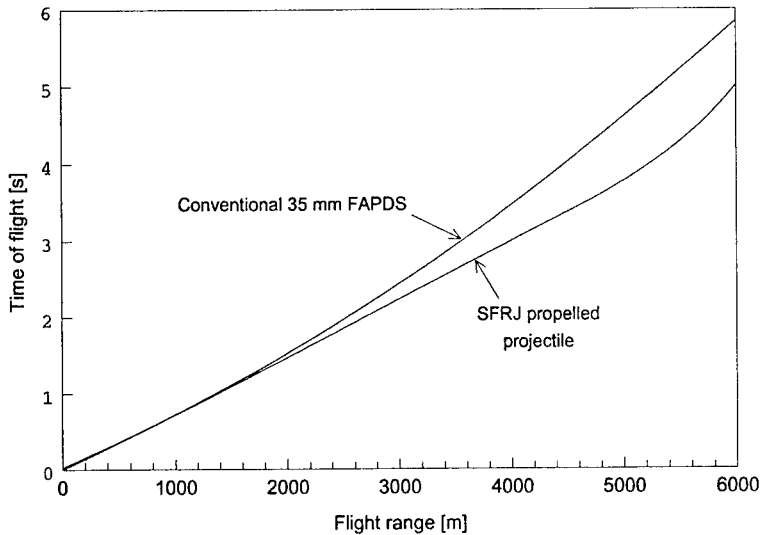


Figure 14    Predicted time of flight as a function of range of a 35 mm SFRJ air defence projectile compared to conventional ammunition
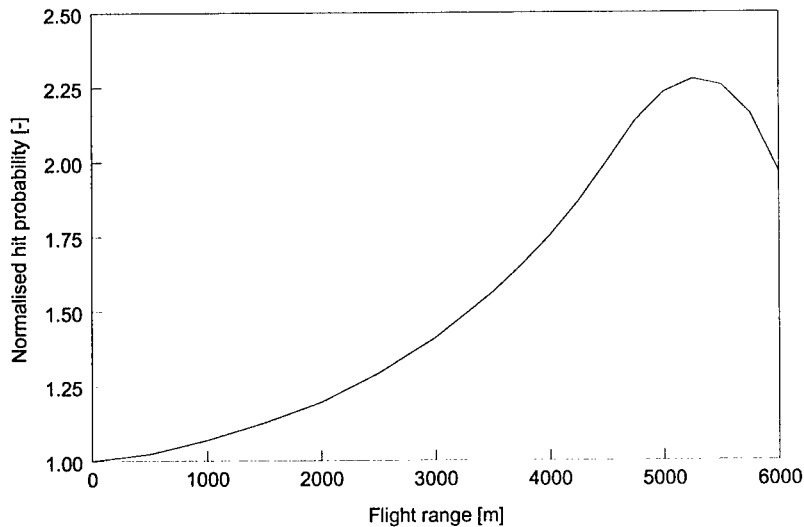


Figure 15    Predicted single shot hit probability of a 35 mm SFRJ air defence projectile normalised by the hit probability of a conventional projectile against a manoeuvring target

## 5.3    KE-projectiles

The application of an SFRJ propulsion system to 120 mm Kinetic Energy (KE) ammunition has also been investigated at TNO. The present section briefly discusses the most important results of this work of which a more extensive description was already given in [3]. Using the

TNO-PML SFRJ test facility, a large number of experiments was performed at various combustor entrance conditions in order to characterise the burning behaviour of different types of fuel. Using the experimentally obtained information, projectile flight performance predictions with RP[5] were performed to assess the performance potential of SFRJ-propelled KE projectiles. The considered fin-stabilised SFRJ projectile design (on paper) featured a 75 mm tubular body including an air intake and an exhaust nozzle build around the penetrator of the reference APFSDS-T DM33 ammunition and was assumed to be fired from the 120 mm smooth bore gun of the Leopard-2 tank. Besides the ramjet related hardware, also the required pusher plate and sabot segments caused the SFRJ projectile mass to be considerably larger than the mass of the reference KE-ammunition. Firing the SFRJ projectile from the same gun consequently would result in the muzzle velocity to be significantly lower.

The predicted flight velocity of the SFRJ projectile assuming nominal combustor performance is shown in Figure 16 (reference calculation) compared to the conventional KE-ammunition for which a velocity decrease of 75 m/s per km flight range is assumed. As can be seen, the velocity of the SFRJ projectile exceeds the flight velocity of the conventional KE-ammunition beyond a range of approximately 1400 m. Further performance improvement may for instance be obtained by fuel regression rate enhancers or by increasing the combustion efficiency. The predicted effect of a 25% increase in fuel regression rate with respect to the nominal value is also shown in Figure 16. Although the initial flight velocity is somewhat lower due to the higher launch mass (induced by the higher fuel mass required to attain a propelled flight range of approximately 2 km), the flight velocity at fuel burn-out is significantly higher. Finally, the effect of a 5% increase in combustion efficiency with respect to the reference calculation is shown in Figure 16. This results in a flight velocity of 1630 m/s at fuel burn-out, while a velocity equal to the conventional KE-ammunition is reached at a flight range of roughly 1100 m. It is important to note that, in spite of the lower muzzle velocity of the SFRJ projectile, the amount of kinetic energy at the initial flight conditions is about equal to that of the conventional ammunition. While the kinetic energy of the conventional ammunition decreases significantly with increasing flight range, the kinetic energy of the SFRJ projectile increases continuously to values 60% to 80% higher than that of the conventional ammunition at a range of 2 km.
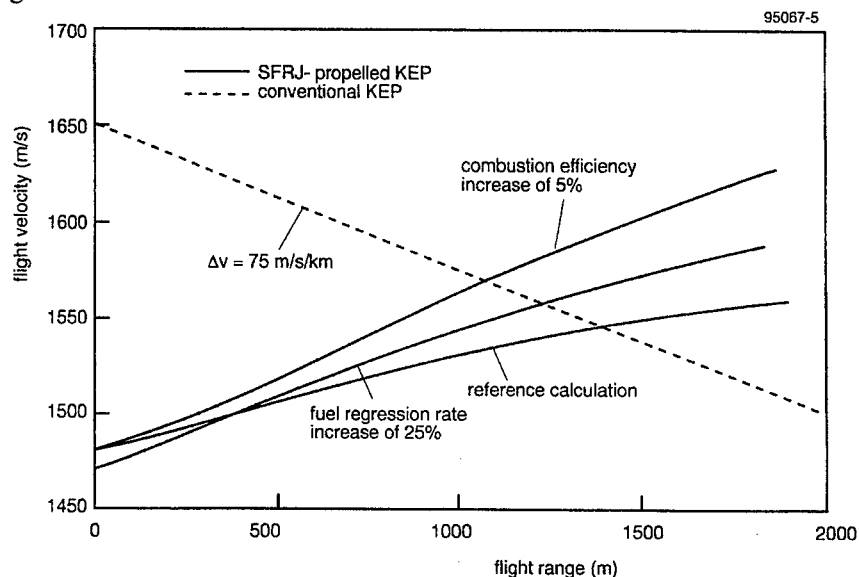


Figure 16    Predicted flight velocity of SFRJ-propelled KE projectiles compared to conventional KE-ammunition

## 5.4 Tank training projectile

Tank training projectiles were among the first possible applications of SFRJ-projectiles that were thought of, see e.g. [25]. The advantage is that during the propelled time of flight the drag can tuned to be very close to a modern KE-penetrator but as soon as propulsion ends the drag rise can be considerable which very much decreases the maximum range.

## 6.   CONCLUSIONS

From the work carried out within the framework of the Swedish/Dutch co-operation programme the following may be concluded:
- A design of a SFRJ propelled projectile has been established of which structural integrity has been verified in actual gun firings.
- The free-flight tests have demonstrated clean separation of the sabots and pusher plate and stable flight of the projectile.
- Furthermore it has been demonstrated during the free-flight tests that the SFRJ propulsion system is capable of generating a thrust approximately equal to the drag of the projectile resulting in an essentially constant flight velocity.

The demonstrated performance of SFRJ propulsion for projectiles opens the way to development of actual applications. The results of several application studies as performed separately by both FOA and TNO indicate the large performance improvement potential of SFRJ projectiles in terms of increased range, increased flight speed and reduced time of flight.

## 7.   ACKNOWLEDGEMENTS

The authors wish to thank all the people at the Swedish and the Dutch side who have contributed to the success of this co-operation programme on SFRJ propulsion for projectiles during the past 5 years.

## 8.   REFERENCES

1           Eliasson Ralf
            *Studium av HTPB-baserade bränslen för SOFRAM.*
            1984. 4:o, 52 p. FOA C 20563-D3

2           Wimmerström Peter   Nilsson Yngve   Gunners Nils-Erik
            *Initial study of a 40 mm SFRJ projectile.*
            1993, 13 p.   FOA B 20113-2.1 (14th International Symposium on Ballistics, Quebec, Canada.
            26-29 September 1993)

3           Veraar, R.G.,
            *RP5- A Computer Programme for Flight Performance Prediction of Solid Fuel Ramjet Propelled Projectiles*
            15th Int. Symposium on Ballistics, Jerusalem, May 21-24, 1995

4           Hasselrot, A.,
            *Beräkning av aerodynamiska koefficienter för rammotorrobotar*
            FFA report AU-1661, December 1980

5           Even R Vukelish, Stan L. Stoy, Marvin E. Moore
            *Missile Datcom*
            Flight Dynamics Laboratory, Wright Patterson Air Force Base Ohio, AFWAL-TR-86-3091

6        Hasselrot, S.
*CHARISMA – A Marching Code using the Method of Characteristics in Combination with the Shock Equations*
FOA unpublished work, 1992-1996

7        Zucrow, M.J. and J.D. Hoffman
*Gas Dynamics*
John Wiley & Sons, 1976

8        Anonymous
*RAMPANT User's Guide*
Release 3.1, Fluent Inc., July 1999

9        J.B. Vos, A.W. Rizzi, A. Corjon, E. Chaput and E. Soinne
*Recent Advances in Aerodynamics inside the NSMB (Navier Stokes Multi Block) Consortium*
AIAA 98-0225, 36th Aerospace Sciences Meeting, January 12-15, 1998, Reno

10      Dijkstra, F., P. Korting and R. Van den Berg,
*Ultrasonic Regression Rate Measurement in Solid Fuel Ramjets*
AIAA 90-1963, 26th Joint Prop. Conference, July 16-18, Orlando, 1990

11      Coats, D.E. G.R. Nickerson, A.L. Dang and S.S. Dunn,
*Solid Performance Program (SPP)*
AIAA-87-1701, 23rd Joint Propulsion Conference, San Diego, June 29-July 2, 1987

12      Wimmerström, P., R..Renström and Y. Nilsson
*Spinning Combustors in Projectile Applications*
15th Int. Symposium on Ballistics, Jerusalem, May 21-24, 1995

13      Andersson, K.
*A General Survey of Some Ballistic Test Facilities at FOA/Grindsjön.*
ARA 44th Meeting, Munich, September 13 – 17, 1993.

14      Hallquist, J.
*User's Manual for DYNA2D, Revision 3*
Lawrence Livermore National Library, March 1988

15      Flygar, S.E.,
*IB-KB Ett datorprogram för beräkning av det innerballistika förloppet I kanoner och bakblåsare*
FOA report C 20566-D2, January 1985

16      Lars Ström
*Solid Fuel Ramjet Projectile: Val av drivkrutladdning och patroneringsmetoder.*
FOA –R—01250-310-SE, oktober 1999. ISSN 1104-9154. Provrapport

17      K. Andersson and R.G. Veraar
*The Swedish-Dutch Co-operation Program on Solid Fuel Ramjet Propelled Projectiles – An Overview Focussing on Tests Performed*
50th Meeting of the Aeroballistic Range Association, November 8-12, San Francisco

18      Asher Sigal, James E. Danberg
*Aerodynamics Analysis of Solid Fuel Ramjet Projectile*
Memorandum Report BRL-MR-3687, May 1988.

19      R. Mönig, M. Moll
*Ramjet Propulsion for Advanced Projectiles*
AGARD Conference Proceedings 526

20          V. Fleck, C. Berner
*Increase of range for an artillery projectile by using the lift force.*
16th International Symposium on Ballistics, San Francisco,USA,
23-28 September, 1996.

21          John A Simpson
*Flight Dynamics of the Advanced Fire System (AIFS) Cannon Launched Ramjet.*
7th Symp. on Ballistics, The Hauge, The Netherlands. p455.

22          Oded Amichai
*Performance of Solid Fuel Ramjet Guided Projectile for USN 5"/54*
Naval Post Graduate School, 1982, AD A 115 108

23          R.G. Veraar
*Design Study of a Ramjet Propelled Projectile with a Frangible Penetrator*
17th Int. Symposium on Ballistics, Midrand, South Africa, 23-27 March, 1998

24          Erik Berlund
*Luftvärnskanoner mot manövrerande mål*
FOA Rapport C 20816-2.5, oktober 1990, ISSN 0347-3694.

25          William H Mermagen, Rao J. Yalamanchili
*Design and Development of a Ramjet Tank Training Round.*
8 th Symp. on Ballistics, Orlando, FL, USA, 1984. pIV-27

# AEROELASTICITY OF HIGH L/D SUPERSONIC BODIES : THEORETICAL AND NUMERICAL APPROACH, EXPERIMENTS

S. HEDDADJ [1], R. CAYZAC [1], J. RENARD [2], M. GIRAUD [3]

(1) Giat Industries, Division des Systèmes d'Armes et de Munitions,
7 route de Guerry, 18023 Bourges Cedex, France
(2) Université d'Orléans, Laboratoire Energétique-Explosions-Structures,
63 Avenue de Lattre de Tassigny, 18020 Bourges, France
(3) ISL, French-German Research Institute, BP 34, F-68301 Saint Louis, France

*Paper not Available at the Time of Editing*

## ABSTRACT

The complete equations of motion of a flexible supersonic high L/D body are written. The bending is represented by cutting the projectile into two parts, which both behave like rigid bodies. A Lagrangian approach is used, that leads to a linear set of equations, which will be exploited by two different means. The first one is a study of the first natural frequencies, that gives us information about the frequencies and associated dampings at stake. The second one is a resolution program, based on the implicit formulation of Newmark, that enables to know, at any moment of the flight, the position and orientation of the body, like for instance the angle of attack and the flexure angle of the body. A parametric study is then presented, to evaluate the influence of the initial conditions, the rigidity of the body and the steady state roll rate on bending. All the numerical results obtained will be compared with experimental results : A whole series of small scale firing tests in the 100 meter free flight ballistics corridor at ISL started last year. Initial flexure and aeroelastic free flight behaviour of the projectile is investigated by use of a multiple orthogonal shadow visualisations technique. To enhance the bending phenomenon, experiments have been conducted with very high L/D projectiles, L/D up to 70.

# Terminal Effects and Vulnerability

# FROM RESEARCH TO BONUS APPLICATION

RENAUD-BEZOT J.L. [1] ,VIVES M. [2] ,GRIGNON C. [2]

(1) GIAT Industries, Centre de La Chapelle - route de Villeneuve - BP 13
18570 LA CHAPELLE SAINT URSIN - France
(2) GIAT Industries, Centre de Bourges - 7 route de Guerry
18023 BOURGES CEDEX - France

Abstract: The EFP (Explosifvely Formed Projectile) concept was developed in the 80s. Nowadays, the concept has entered reality at GIAT Industries in the 155 BONUS ammunition. The methodology and the tools are available for future warhead development such as hybrid warhead or 3 D's EFP.

## 1.    INTRODUCTION

The development of the warhead of the BONUS 155 mm shell ended in 1999 with its qualification. This development is the logical result of the study work. But the acquired knowledge of the development is not limited to the " warhead " product, it includes tools. In addition, new concepts follow here and now from the work carried out.

## 2.    BACKGROUND

Our work on the EFP (Explosifvely Formed Projectile) concept dates back to the 80s. It is possible to classify it in two types:
* The acquisitions of know-how,
* The applications on prototypes.

As regards the acquisitions of know-how, it is necessary to mention the work carried out within GEIP-TA9 (Working party relating to EFPs). This work made it possible:
* to exchange study methodologies between the participating countries, on the characterisation of materials and on the modelling of detonation,
* to study the weight of parameters like the quality of the pure irons (Holtzer - ARMCO - REMCO), the dimensional aspect of the liners, the nature and geometry of the casings, ...

As far as the applications are concerned, one will refer to work funded by the DGA and on GIAT Industries own resources which led:
* to testing with more or less success materials for liner (Fe, Cu, Ni, Ta, U ...),
* to specifying the aeroballistic characteristics of the slugs,
* to studying the effectiveness of the projectiles formed (slugs) faced with varied targets.

All of this work saw an initial completion at the time of ACED Exploratory Development. From an experimental point of view, the feasibility and effectiveness of a EFP with Iron liner at long stand off (1000 calibres) was able to be demonstrated. From a technical point of view, it permitted the drafting of the specifications for a shell with EFP with tantalum liner type sub-munition.

## 3. ANALYSIS OF THE DEVELOPMENT OF THE BONUS WARHEAD

The development work on the warhead of the BONUS 155 mm shell led to four questions :
- What simulation tools make it possible to study the formation of a slug and its effectiveness with sufficient precision and compatible timescales of the development schedule?
- What is the effectiveness on the whole trajectory of a slug whose formation conditions and initial geometry are known?
- How to test a warhead (EFP) with the objective of demonstrating its effectiveness over the whole range?
- What structure makes it possible to guarantee the survivability of the warhead, after 15 years, in gun environments ? Is it compatible with the effectiveness required?

The answers to these various questions are developed in the following paragraphs.

### 3.1. Simulation tool

Simulation codes are both numerous and powerful : Lagrangian or Eulerian, finite elements or finite differences, integrated mesher or not, ... each code has its defenders and its detractors. The selection criteria concerned in addition the use capacity within the design department and on CPU time consumption.
Thus, the DYNA software quickly stood out. After a period of re-adjustment of the " material " and " computing " parameters, systematic studies made it possible to support and then to predict the slug shapes. The final definition was thus predicted before being tested.
By introducing the flight velocity of the slug at the characteristic stand off, it was in addition possible to predict with DYNA the expected maximum effectiveness (see fig. 1).

### 3.2. Analysis of the effectiveness over the whole trajectory

Knowledge of the effectiveness of the slug at each point on the trajectory necessitates first of all knowledge of the initial conditions. If the shape and velocity of the slug can be acquired by digital simulation and/or by experimentation, dynamic analysis alone makes it possible, on the basis of the ammunition's rotation conditions, to compute those of the slug.
The slug's initial flight conditions include, in addition to its velocity, an initial incidence and an initial rotation vector.
A flight mechanical engineering analysis of these initial conditions, combined with the geometry of the slug, makes it possible to compute, at any point on the trajectory, the velocity and incidence of the slug by a 6DDL computation. On the basis of the impact velocity and the incidence of the slug, it is then possible to compute the thickness penetrated at this point on the trajectory.
In a study of the conditions at the limits, it is also possible to introduce reduced initial conditions so as to study the weight of the initial disruptions (assembling fault, for example).

### 3.3. Test at the long stand off

In the first instance, it is necessary to reproduce the in-flight movement of the warhead in terms of orientation and rotation speed. Because of the rotation movement about the sub-munition's axis of inertia, it is necessary to create a firing window by precluding any accidental firing at another point. The firing order must then be given with compatible precision of the measurement desired.

After slug formation, double flash (X-Ray) photography makes it possible to measure its velocity and to verify its geometry in 2 planes.

On the trajectory, mosquito net panels make it possible to take a print as it passes through. Two optical barriers give fixed distance passage times and an optical cell gives the impact time on the target. An analysis of this data makes it possible to reconstruct the trajectory of the projectile at all points. The method is presented in the poster "Determination of Ballistic Characteristics applied to EFP" [1]. In addition, it is thus possible to re-compute the effectiveness at very long range (2000 calibres) on the basis of firing at a target at 1000 calibres (see fig. 2) (or vice-versa).

### 3.4 Environmental resistance

While it is usual to have equipment undergo thermo-mechanical environment cycles, it is less current to simulate its ageing by experiment. The two types of tests (environment and accelerated ageing) were carried out on the warhead. Thus it was then possible to gun-fire warheads having undergone ageing equivalent to 15 years and operational environments. The operating tests on the warhead having undergone all of the environmental stresses showed that performances were not affected by 15 years of storage.

As far as artillery shot resistance is concerned, a soft recovery system enables the warhead to be recovered after gun-firing followed by the actual expulsion sequence (ejection of the shell).

## 4. CONCLUSION AND PROSPECTS

The development of the warhead of the BONUS 155 mm shell which ended in 1999 with its qualification, was faced with a new constraint : the reduction of the development cycles. It was therefore necessary to develop the test means and tools in parallel with the development. Today, a set of tools permitting prediction, analysis and interpretation is operational, that is, they were validated at the time of the tests and their data contributed to the qualification of the warhead. The new programmes in terms of warhead will be able to benefit from these tools.

In the same way, the work carried out made it possible to demonstrate by experiment the effectiveness of the EFPs up to 2000 calibres. It also made it possible to approach the definition of the hybrid charges which will translate into an operating area up to 1000 calibres, with an effectiveness of more than 3 calibres.

It served as a basis for the definition of warheads; thus the EFP3Ds [2] permit an optimisation of the use of volumes for warheads.

## 5. REFERENCE

[1]    EFBP 2000' - Determination of Ballistic Characteristics applied to EFP

[2]    Tactical missiles seminar 1998 - CGN Tri Dimensionnelle: Etude de faisabilité et applications
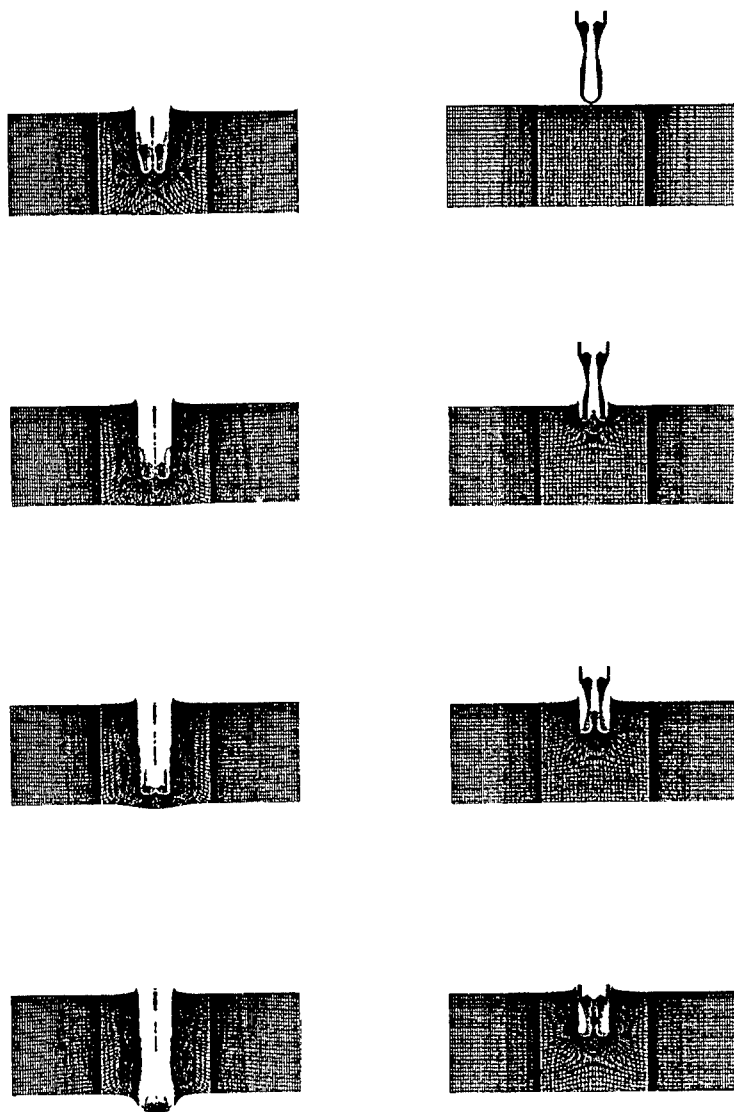
Figure 1:
Simulation of the penetration
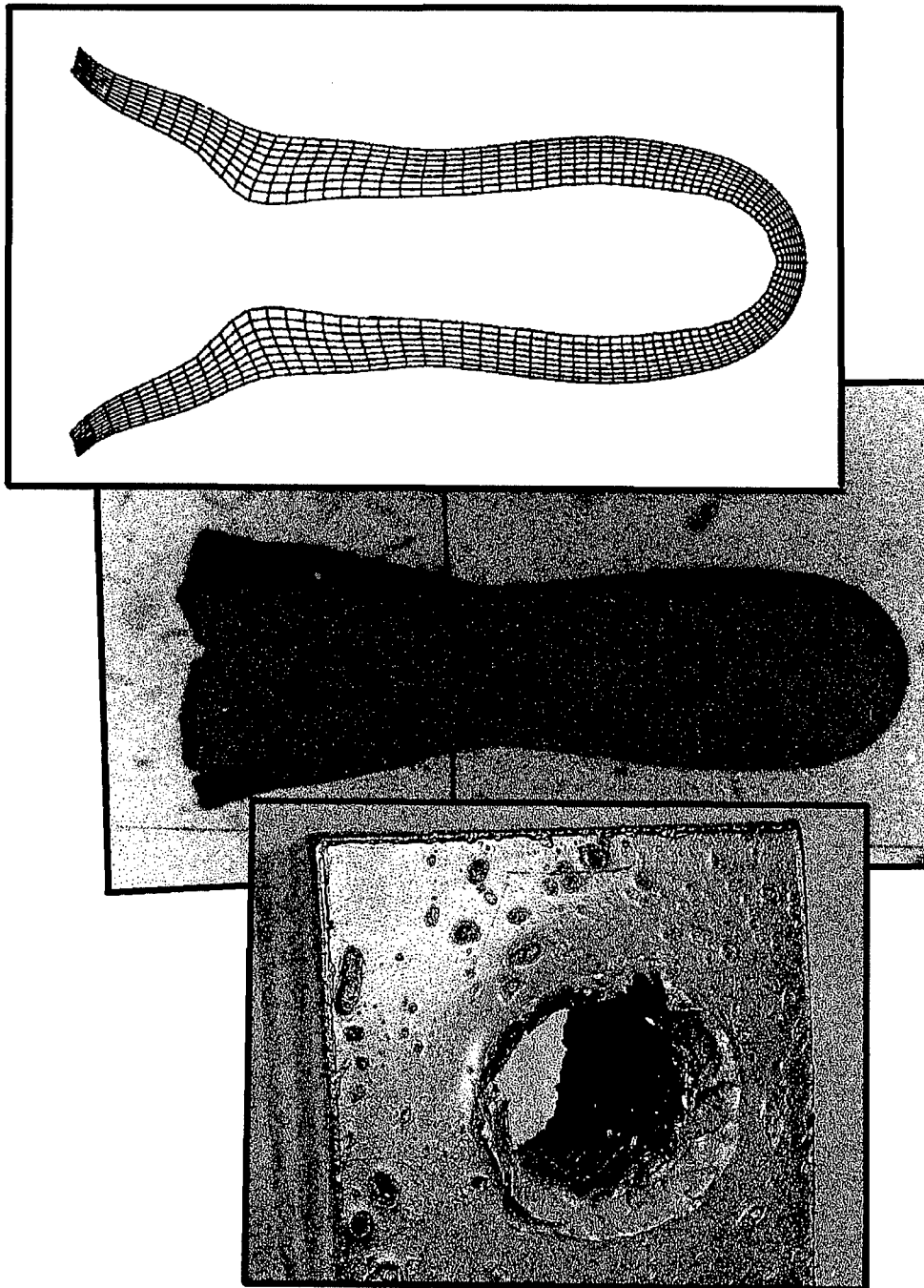
Figure 2: Comparison Simulation - Test - Effectiveness

# PERFORATION – PROTECTION : STATE OF THE ART

## CHANTERET P.Y. , WEIHRAUCH G.

ISL, French-German Research Institute of Saint Louis,
BP 34   F68301  Saint-Louis  France

**Abstract** : A review of the existing and most probable innovations in the field of armour anti-armour is presented. First, the actual potential of KE penetrators and shaped charges against homogeneous armour are analysed. The different families of protection systems are then considered with typical examples illustrating the different defeat mechanisms for advanced armour materials, spaced, laminated and reactive armours. This review is followed by a look at the most promising possibilities for increasing the performance of both KE penetrators and explosive warheads. Examples of new projectile designs with increased lethality are presented with considering the possibility to increase muzzle gun velocity and projectile length. Possible improvements in shaped charges including the use of new liner materials and special designs are also considered with the idea of achieving a better adaptation of the jet characteristics to specified targets. In the last part one address the new situation created by active protection systems and examples are given of active protection scenarios including electromagnetic acceleration of counter measures.

## 1. INTRODUCTION

An armoured combat vehicle may have to be facing a lot of threats coming from different directions. In addition to frontal threats, it may be attacked by shaped charges from overflying or diving smart missiles, explosively formed penetrators fired by sensor-fused artillery munitions or mines, blast mines and other threats. However the frontal part of the armour will have to resist the two main treats which are the large shaped charges and the kinetic energy or long rod projectiles. When interacting with homogeneous metallic targets, these two major threats get their large penetration capability rather from their length than from their kinetic energy. As it is well known, the penetration vs. velocity curve of any long projectile has a typical "S" shape with some saturation for high impact velocities. This is illustrated by the plot on figure 1 which presents such a curve for a L/D 30 tungsten rod into homogeneous 1000 MPa armour steel (RHA). It can be seen that for a standard gun velocity such as 1.75 km/s, a KE projectile will be able to penetrate its length, which means about a 600-700 mm penetration power for a 120 mm gun.
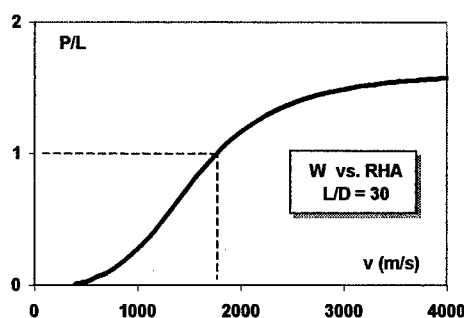


Figure 1: Penetration by unit of length of a long tungsten projectile into RHA (L/D=30).

If there may exist some benefit in increasing the impact velocity of a KE projectile at constant energy, this is different for the shaped charge which operates in a velocity regime where increasing the jet velocity does not significantly increase its P/L into homogeneous targets. Figure 2 presents a plot of the penetration vs. standoff curve for a standard precision copper lined shaped charge, together with a curve calculated with replacing the classical HMX explosive loading by a CL20 loading which has 15% more energy. The observed increase in jet performance is not due to higher jet velocities but mostly to a larger jet mass inducing larger jet break-up time. Comparing the characteristics of a 150 mm calibre shaped charge (SC)



Figure 2: Typical penetration vs. standoff curves for a copper lined shaped charge.

with those of a 120 mm KE projectile, one observes that:

- the total length of the SC jet is three times larger than the length of the KE rod;
- the kinetic energy of the SC jet is only one third of the long rod energy;
- the SC performance into RHA is nearly twice larger than that of the KE rod.

From these observations, it could be inferred that the potential of these two major tank threats is almost related to projectile length only, and that a higher energy at given length does not significantly increase performance. But this is only valid against homogeneous metallic targets and in the following, it will be shown that the higher kinetic energy of the projectile, the more difficult it will be to achieve any significant reduction in protection weight.

## 2. ARMOUR TECHNOLOGIES

Starting from RHA as amour material reference, there are two main directions for the development of lighter protections, which are first to improve the armour material resistance to penetration and secondly try disturbing or destabilizing the threat.

### 2.1 Advances in armour materials

Considering the high velocity regime of shaped charge jets, one could think that the strength of armour steel would have almost no influence on jet performance. But, if there is indeed little influence



Figure 3: Strength vs. plate thickness for different armour steel qualities.

of steel strength on the jet cratering velocity, one observes that SC performance decreases with increasing steel hardness, just because the crater diameter is smaller and the probability for jet elements to reach the bottom of the crater is reduced. There is some further protective potential to be obtained by using inclined spaced plates which induce some jet over-consumption and disturbances [1]. However, it is against KE projectiles that the larger benefit from armour steel strength is to be obtained, and figure 3 shows that it is currently possible to elaborate thick plates with high hardness armour steel.

The availability of steel plates as thick as 120 mm with a 1800 MPa strength allows to reach $E_M$ values in the order of 1.5 against KE, where the mass effectiveness $E_M$ is defined as the ratio of the reference mass of standard RHA (1000 MPa) to the armour mass. As the toughness of those new armour steels has also improved, some further mass reduction is to be expected by using special plate arrangements which can lead to $E_M$ values as high as 1.8.

The hydrodynamic penetration theory predicts that a material with density $\rho$ lower than steel density $\rho_{st}$ should provide an armour weight benefit with a mass effectiveness as $E_M = (\rho_{st}/\rho)^{1/2}$. This rule applies only for constant length projectiles and although the length of a SC jet varies during penetration, such $E_M$ theoretical values have been obtained against shaped charges, with for instance $E_M = 1.5-2$ with aluminium alloys. In the case of KE projectiles where impact velocities are much lower, high effective protections can be obtained especially if high strength alloys are used. For instance, titanium alloys have proven to be very effective with $E_M$ as high as 1.7 against both tungsten and DU rods [2].
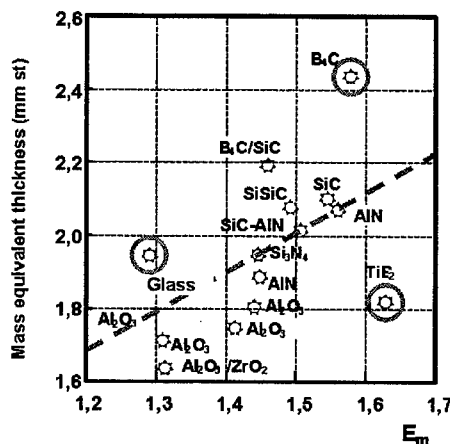


Figure 4: Mass equivalent thickness vs. mass effectiveness of unconfined ceramics against KE rods [4].

Non metallic materials, especially ceramics, possess a high protective potential due to a moderate density combined to a high compressive strength. Although ceramics are mostly used against riffle bullets, they have also been investigated against shaped charges [3] and against KE rods [4]. But as they are too brittle to be used without a steel or aluminium backing, the resulting composite armours exhibit overall mass effectiveness which are lower than that of ceramics themselves as shown on figure 4. The protective power of ceramics is also enhanced by a steel confinement and mass effectiveness of more than 2 against KE can be obtained by appropriate combination of ceramics and steel in the so-called composite armours.
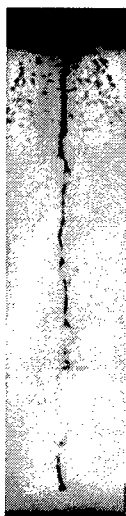


Figure 5: Residual shaped charge jet after interaction with a confined glass module.

As the armour material strength is of less influence at high impact velocities, ceramics are less attractive against shaped charges but they still have the effect of producing narrow craters and therefore reducing the penetration power of jets which in real life, are not perfectly aligned. It must be known that some ceramics may exhibit the so-called "crater collapse effect" or "rebound effect" which appears when a shaped charge jet perforates a glass target. The radiograph presented on figure 5 shows a residual shaped charge jet exiting from a steel-glass-steel module. One can see the jet perturbations created by the flow of broken glass material accelerated towards the jet, due to the dynamic dilatancy which accompanies the fracture in glass material.

## 2.2 Armours with destabilizing effects

From a simple analysis of the threat, one observes that when interacting with a target, the diameter of a shaped charge jet is about 5 to 10 times smaller than the diameter of a KE rod. Therefore, if one differentiates the armours which act by erosion from those that destabilize the projectile, the last category will be naturally more adapted to the protection against shaped charges. Historically the use of glass has been the first mechanism found in the 50's for destabilizing a jet and the explosive reactive armour (ERA) came later. Figure 6 shows a radiograph taken in the



Figure 6: Radiograph of an early ERA experiment at ISL (1972).

early 70's of a shaped charge jet destabilized by the flying front plate of a reactive sandwich, when such protections were called "active armour" at ISL.
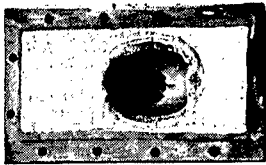


Figure 7: Interlayer of a locally reacting sandwich after shot.

If glass belongs to both the eroding and the destabilizing armour categories, the most efficient disturbing effects are obtained with reactive sandwiches, the family of which includes several types of sandwiches which differ from ERA by the nature of the interlayer. The use of a so-called self limiting explosive interlayer allows to obtain a chemical reaction which remains localized to the impact region. With this type of sandwiches the collateral effects are reduced as illustrated on figure 7, which shows a special locally reacting interlayer after perforation by a shaped charge jet. By replacing the explosive layer by a totally inert layer with specific properties, combined with an appropriate design, one can obtain protections with a very efficient jet disturbing power as illustrated on the radiograph shown on figure 8.



Figure 8 : Radiograph of a double reactive sandwich with inert interlayer.



Figure 9: Typical early experiments from reactive sandwiches against KE (1973).

Due to its significantly larger strength and mass by unit of length, a KE rod will not be affected by a light ERA designed against shaped charges. However, it was not long after the first ERA experiments against shaped charge that it was shown at ISL that a proper sandwich design could also reduce the penetration power of a KE projectile as illustrated by the radiographs on figure 9 taken in 1973 [5]. Following these first experiments, a research program was conducted at ISL which came out to a full scale demonstration program, where a reactive protection mounted on a Leopard-I was successfully tested against a 105mm KE round [6]. During more than 10 years, reactive armours against long rods were intensely studied at ISL with looking into the various mode of action of reactive armours with optimising the different sandwich elements and designing very effective sandwiches [7]. The radiographs on figure 10 presents two examples of reactive sandwiches showing that the use of thick plates allows to both destabilize and even break the rod, also under 45° and 30° incidence.

Unlike the light ERA sandwiches which have been used in additive boxes for almost 20 years, the protection against KE with heavy sandwiches must be used in the so-called integrated ERA, and it seems that until now, such heavy explosive reactive sandwiches have been implemented on Russian tanks only [8].



Figure 10: Interaction of long rods with thick plates reactive sandwiches.

If it is relatively easy to disturb the jet of a shaped charge with an inert sandwich, it is much more difficult in the case of KE rods because of the lower impact velocities -and hence lower impact pressures- and because of the need to accelerate much thicker plates. It is however possible to generate some disturbances in a KE rod with using adequately designed inert sandwiches. As illustrated by the numerical simulation shown on figure 11, the bulging plates of a steel-rubber-steel sandwich are transferring some transversal momentum to the impacting tungsten rod, generating stresses which could be large enough to destabilize and possibly fracture the projectile.

All the above described reactive sandwiches -with explosive or inert interlayer, have their maximal efficiency under an incidence of 60° or higher. Against shaped charges, the efficiency of a light ERA will linearly decrease down to zero with decreasing incidence, but the use of double sandwiches can, to some extent, reduce this loss of protective power [8].

Due to the large inertia of full scale KE projectiles fired from MBT guns, eroding the rod is the only mechanism providing some protection under normal impact. But in the case of shaped charges and as mentioned for glass armour, there exist some mechanisms for efficiently disturbing a jet at low obliquity. One of these mechanism is used in the so-called "pill armour" which is made of confined high explosive filled cells detonating under jet impact, with detonation products and confinement debris disturbing the jet in a mechanism similar to



Figure 11 : Numerical simulation of a tungsten rod interacting with a steel/rubber/steel sandwich.

glass. The radiograph on figure 12 shows a shaped charge jet after perforating such a confined explosive cell. Some jet disturbing can also be obtained if the cells are filled by some compressible inert material like water for instance [9].



Figure 12 : Jet after interaction with a "pill armour" module.

Another mechanism for defeating shaped charge jets under zero obliquity which is the "electric armour". This protection system is made of two separate plates, with one plate connected to a high voltage capacitor bank while the other plate is grounded. The attacking shaped charge jet operates as a switch between the plates, causing a large current to flow through the jet creating instabilities leading to early break-up and even radial expansion of the jet [10]. Such a system would be efficient for instant to protect a tank roof against bomblets with shaped charges functioning at extremely short standoff, but its efficiency remains questionable against fully fragmented jets from shaped charges initiated at longer standoffs.

# 3. ADVANCES IN PERFORATION CAPABILITIES

Now after reviewing the different protections systems which already exist on vehicles or are about to be fielded, it is the place to look at the possibilities which may exist for improving the penetration capability of both KE projectile and chemical energy antitank warheads.

## 3.1 Advances in KE projectiles

The penetration capability of a high density long rod penetrator is determined by its length under the condition that the impact velocity is sufficient. Considering a powder gun with a given available energy and a fixed L/D ratio, it can be shown that there exists an optimal impact velocity –usually between 1600 and 1900 m/s- for achieving a maximal penetration depth [11]. For instance, it has been demonstrated in full scale tests performed with a 140 mm gun, that a penetration of 900 mm into RHA can be achieved with a velocity lower than

Figure 13 : Tungsten KE projectile with L/D=40.

1700 m/s. In principle, the increase in the penetration depth of a long rod with increasing velocities is still significant at velocities as high as 2500 m/s. However and taking into account the fact that with increasing muzzle velocities, the interior ballistics efficiency decreases and the corresponding sabot weight increases, muzzle velocities larger than 2200-2300 m/s should be disregarded for powder guns.

Therefore all the efforts in the near future to improve the performance of projectiles should be placed in studying the possibilities to accelerate as long as possible aerodynamically stable projectiles. Figure 13 presents an experimental study performed in calibre 40 mm for designing a sabot able to accelerate a L/D=40 tungsten rod with accounting for the interior ballistics conditions. As the total accelerated mass is limited, a possibility for increasing the projectile length at constant mass is to use a jacketed penetrator like the one shown on figure 14. This projectile is made of a L/D=62 tungsten rod with a surrounding jacket made of a fibre reinforced plastic, increasing the flexural stiffness and preventing from bending deflections.

Figure 14 : Jacketed KE projectile with L/D=62 at 1960 m/s.

The concept of jacketed penetrators has been validated in 140 mm calibre [12]. An other way to improve the penetration potential of KE projectiles is to decrease the sabot weight and therefore increase the penetrator mass or velocity. A lot of work is going on in this direction and especially in the field of using plastic materials for the design of new sabots [13] and figure 15

Figure 15 : Non-metallic friction sabot.

shows a L/D=20 tungsten rod accelerated at 1700 m/s using a non-metallic friction sabot.

## 3.2 Advances in acceleration technologies

An obvious way of achieving deeper penetration consists in increasing the gun diameter and figure 16 shows the reachable muzzle velocities as a function of the accelerated mass for different gun diameters. With a given interior ballistics and projectile technologies, the penetration will be proportional to the calibre of the gun, and for a required penetration depth and a given L/d ratio, it is possible to directly determine the appropriate gun diameter. For a given class of armoured vehicles the question of the diameter of the gun is still open, and the choice for a calibre will have to account for the required penetration power but also for some other parameters like vehicle mass, number of stored ammunitions, standards compatibility, ....

In addition, there has been a tremendous amount of work on new acceleration technologies with the objective of significantly increasing the gun muzzle velocities. In particular a lot of work concerns electromagnetic launchers with the hope of achieving even more higher velocities – for instance more than 3 km/s. Such velocities might be interesting against flying targets by increasing the hit probability, but on a terminal ballistic point of view they are not realistic for

Figure 16 : Muzzle velocities vs. accelerated masses for different gun calibres.

the antitank combat. Furthermore the technical problems to be solved are still so important that such electromagnetic acceleration systems will not be fielded within a reasonable space of time. Closer to the applications are the systems which use the electrical energy to improve the efficiency of powder guns as in ETC systems. For instance the use of plasma-ignition allows to operate the gun with higher energy powder loads and to control –to some extent– the burning and hence the projectile acceleration curve. The benefit of such system has been demonstrated in a 120 mm gun. There is no reason for not thinking that the powder gun will remain the projectile launching system for tanks in the future, and there still remains much place for this conventional system to be further improved.

Figure 17 : Influence of jet tip velocity on charge performance against ERA for a given liner density.

## 3.3 Advances in antitank warheads

The penetration power of a shaped charge is mainly governed by the density and the length of its jet. Considering that modern shaped charges with copper liners have almost reached their maximal tip velocity (10 km/s) and jet ductility, one must admit that there is not much further improvement to be expected against homogeneous RHA. There still exists some benefit to be obtained from liner materials with higher density and/or higher sound speed, especially against modern targets. The maximal jet tip velocity being roughly proportional to the liner material sound speed, nickel and molybdenum liners permit to obtain jets with respectively 11.5 and 12.5 km/s tip velocities. The plot on figure 17 indicates that increasing the tip velocity of a shaped charge jet increases its residual penetration behind an explosive reactive sandwich.

- 331 -

This is due to the fact that during the ERA plate flight, the faster jet travels a longer path as illustrated by the two radiographs on figure 17 showing that despite a larger diameter, the slower (5.5 km/s) copper jet is much more disturbed than a 12 km/s molybdenum jet.
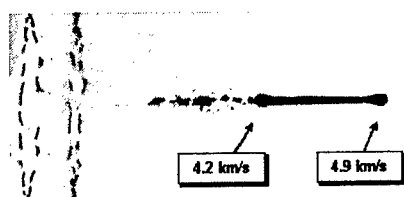


Figure 18 : Copper projectile from an hybrid charge.

There are three main candidates for high density shaped charge liners, which are depleted uranium, tungsten and tantalum. Due to an extreme ductility, depleted uranium has the largest potential against homogeneous target, but its low sound speed together with the difficulties for handling such a material make its use in shaped charges highly questionable. With the same density as uranium, tungsten has a sound speed which is as high as copper, allowing to form jets with tip velocities as fast as 10 km/s. Furthermore, the brittleness of tungsten at ambient temperatures disappears in shaped charge jets and ductile tungsten jets have been produced [14]. It remains some effort to be done for reducing the cost of manufacturing tungsten liners.

Due to a lower sound speed and a relatively high cost, tantalum will probably not replace copper in classical shaped charges, but it appears clearly to be the best material for explosively formed penetrators (EFPs) because it combines a high density with a relatively good deformability. Tantalum could also be a candidate for the so-called "hybrid charges", which produce stretching projectiles which are in between classical shaped charge jets and EFPs. With such charges, the projectiles concentrate the same kinetic energy as shaped charge jets but on a reduced velocity gradient as shown on the radiograph of figure 18 which presents a typical hybrid charge projectile. Due to their moderate velocity gradient (typically between 0.5 and 1 km/s), the projectiles eventually break-up into larger fragments, with increased stability and better performance at large standoff than classical shaped charges.

## 4. ACTIVE PROTECTION

In view of the likely coming improvements in the performances of longer and faster KE penetrators, together with the requirements of lighter vehicles with protection not only on frontal side, one is led to look at active protection systems designed to intercept, destroy or confuse the attacking threat.



Figure 19: Schematic ARENA hard kill protection against missiles and rockets.

Many countries have developed "soft kill" or countermeasure systems: once the incoming threat is detected with some sensor like laser warning receivers, infrared sensors or radars, countermeasures are triggered including obscurant, decoys and jammers which prevent the vehicle to be hit. However only Russia has already move to "hard kill" active protection which consists in launching countermeasures which effectively intercept the threat and eliminate or reduce its penetration capability. For instance, the Russian system ARENA uses a radar detection and then launches a fragmentation warhead which is aimed and detonated at the incoming missile or rocket as schematically describe on figure 19.



Figure 20: Electromagnetic active armour.

However it is against KE projectiles that active protection would bring a large breakthrough if an effective "hard kill" system would be fielded on vehicles. Fifteen years ago, ISL started studies on the electromagnetic armour concept [15] which is schematically described on figure 20. In this concept, electromagnetic repulsion is used for accelerating the intercepting element (plate, sandwich, bar....) at the incoming KE projectile, ensuring minimal time and velocity dispersions and allowing for some control in the launching direction, as patented by ISL. The radiograph on figure 21 shows a small scale



Figure 21: Interception of a tungsten rod by an electromagnetically accelerated steel plate.

experiment, where an electromagnetically accelerated steel plate intercepts a tungsten rod, breaking it and deflecting its trajectory. Numerical simulations as the one shown on figure 22, are a very effective tool for studying the influence of critical parameters such as mass and velocities of the counter elements.
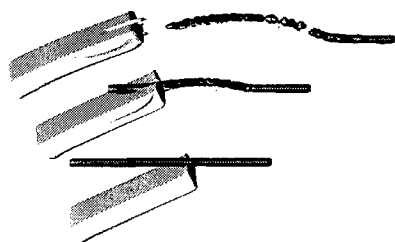


Figure 22: Numerical simulation of the interaction between a flying steel plate and a tungsten rod.

An other concept of active defence against KE projectiles called "blast effect", is schematically depicted on figure 23. In this concept, a high explosive charge is launched in order to be detonated not far from the incoming KE projectile trajectory [16]. On interfering with the pressure field generated by the detonation of the charge, the projectile may be damaged, its flight stability affected and therefore its penetration power reduced. Figure 24 presents a radiograph of a small scale experiment performed at ISL [17] and showing a L/D=20 tungsten projectile flying with a 10° incidence after interaction with a charge detonated near its trajectory. Such a yawed projectile may have lost 30 to 50% of its penetration power depending on the main armour type.
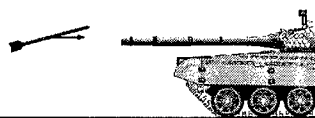


Figure 23 : Principle of protection by blast.

Active protection deals with several areas which cannot be considered independently. For instance, the requirements for sensors may vary from one hard kill system to an other and using a blast charge request an earlier detection and localisation than an interception by flying bars. Generally, the hard kill mechanism will be more effective with increasing the interaction distance because there will be more time and place for the threat to be disturbed, but in the same time, the probability to hit the incoming threat will decrease. Therefore there is a need to build simulation tools allowing to perform system analysis and optimisation like the ISL software ATHENA which was explicitly developed for active protection [18]. Using such a tool, it is possible to recognise that a given kill
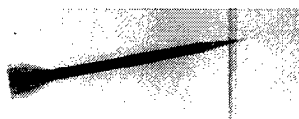


Figure 24: KE projectile destabilised by the detonation of a blast charge [17].

mechanism which is very effective in itself, cannot be used in association with a particular launching system or sensor which would not ensure a high enough overall efficiency.

Active protection is a new method which would radically reduce the effectiveness of ATGW and KE projectiles if comprehensive defence systems were to be integrated on armoured vehicles. Figure 25 presents our view of the situation concerning the positioning of active protection relatively to other protection mechanisms against KE projectiles in a mass and space efficiencies diagram.

## 5. CONCLUSIONS AND PERSPECTIVES

A presentation of the existing armour technologies against both KE projectiles and shaped charge warheads has been presented. The most promising improvements in antitank weapons and projectiles were also reviewed. Finally it has been shown that new concepts of active defence would be able in some future to significantly improve the protection level of armoured vehicles. Some questions are still not fully answered such as the availability of compact powerful electric sources, as electromagnetic armour could be a part of an "all-electric" tank which is a highly questionable concept for all reasons. Nevertheless, the arrival of active protection would not be the end of the competition between attack and protection, as new ideas are already emerging such as for instance sensor saturation, double shots and long-standoff warheads.
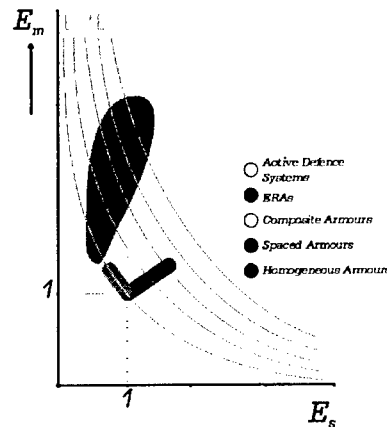


Figure 25: Situation of active protection relatively to other existing protection mechanisms against KE projectiles.

Our current estimation for the state of the art and for future times can be expressed using the following statements:

- The fundamental fighting scenario will not change in the near future;
- powder gun will remain the main acceleration system with additional equipments for increased output;
- the highest impact velocity will be lower than 2000 m/s;
- the largest improvements in KE performance will be in the medium calibre range;
- the amount of multiple charges warheads will increase;
- kinetic energy missiles with long rod penetrators will be of interest, even as tank main armament;
- improving materials will provide less than 10% increase in penetration power;
- dynamic perturbation combined with structural optimisation are the basic elements for an effective protection;
- concepts of reactive targets with some intelligence will be useful, even against existing threats;
- full protection should include neutralisation of heavy mines and EFPs;
- adapting active defence systems to middle class vehicles (20-40 t) seems to be possible;
- modular designs are necessary for a short time adaptation of new protections.

# 6. REFERENCES

[1] P.Y. Chanteret, "Blindages feuilletés contre les jets de charges creuses", ISL Report S-RT 911/77, 1977.

[2] W. A. Gooch, M.S. Burkins, H.J. Ernst, T. Wolf, "Ballistics Penetration of Titanum Alloy Ti-6Al-4V", Proceedings of the Lightweight Armour Systems Symposium '95, Shrivenham, 28-30 June 1995

[3] C.P. Woidneck, "Experimentelle Untersuchungen über Wirkungsweise und Anwendungsmöglichkeiten von Keramik gegenüber Hohlladungen", ISL Report S-RT 915/77

[4] H.J. Ernst, E. Lach, J. Bintz, T. Wolf, "Schutzwirkung von Keramiken gegen KE Geschosse. Teil 1: Unverdämmte Arnordnungen", ISL Report RT 509/92, 1992

[5] G. Weihrach, H. Müller, B. Wellige, "Untersuchung zur Minderung der Durschlagleistung von Wuchtgeschossen", ISL Report S-RT15/73, 1973

[6] "Deutsch-Französische Kommission für Angriff und Schutz", Leo-I Beschuss mit reaktivem Frontschutz mit Pfeilgeschossen im Kal. 105 mm, Lichtenau, 1977

[7] G. Weihrauch, "Recent Research Work conducted at the ISL in the fFeld of Reactive (active) Armour, BRL, Aberdeen, 30-10-1984, ISL Report S-CO 924/84

[8] M. Held, "Overview on Reactive Armour", European Armoured Fighting Vehicle Symposium, Shrivenham, UK 28-30 May 1996

[9] M. Held, "Armour", Proceedings of the 14th International Symposium on Ballistics, Quebec, 26-29 September 1993

[10] G. A. Shvetsov, A. D. Matrosov, "Influence of an Axial Electric Current on the Stability of Shaped Charge Jets", Proceedings of the 16th International Symposium on Ballistics, San Francisco, 23-27 September 1996

[11] E. Wollmann, G. Weihrauch, "Grundsätzlichen Überlegungen zum Auslegung von Wuchtgeschossen", ISL Report RT-507/96, 1996

[12] W. Lanz, H.F. Lehr, "Craters Caused by Jacketed Heavy Metal Projectiles of very High Aspect Ratios Impacting Steel Targets", Proceedings of the 16th International Symposium on Ballistics, San Francisco, 23-27 September 1996

[13] Lehr, H.F., Schirm V. "Geschoßkonzepte", Ballistische Forschung im ISL (1945-1994), G.Weihrauch Editor, Saint-Louis 1994

[14] P.Y. Chanteret, A. Kerdraon, "Studies of Tungsten Shaped Charge Jets", Proceedings of the 16th International Symposium on Ballistics, San Francisco (1996)

[15] G. Weihrauch, E. Wollmann, K. Sterzelmeier,, "Aktive Panzerung", ISL Report S-RT 915/88, 1988 and E. Wollmann, K. Sterzelmeier, G. Weihrauch, "Electromagnetic Active Armour", Proceedings of the 16th International Symposium on Ballistics, San Francisco (1996)

[16] R. Steuer, "Aktive KE-Schutzsysteme", Sitzung des Wissenschaftlichen Beirats zur Schwerpunktaufgabe 2.11 "Panzerdurschlag und Detonik, ISL, 27-29 01 1998

[17] V. Schirm, "Experimentelle Untersuchungen zur Blastwirkung gegen Pfeilgeschosse", ISL Report S-RT 914/98

[18] P. Wey, M. Salles, "Simulation and Analysis of Active Defense Systems", Proceedings of the 17th International Symposium on Ballistics, Midrand, 23-27 March 1998

# HIGH VELOCITY KE-PROJECTILE INTERACTION
# WITH MODERN ARMOURS

Mr Lars Holmberg and Ms Ewa Lidén

FOA Defence Research Establishment, Weapons and Protection Division, Grindsjön,
S-14725 Tumba, Sweden, Telephone +46 8 7064030, Fax +46 8 7064143

**Abstract:** New techniques exist that make it possible to achieve considerably higher projectile velocities than the 1500-1800 m/s that modern tank guns can achieve today. In the future velocities of the order of 2500 to 3000 m/s can be foreseen using new acceleration techniques where new energetic materials and electricity will be involved. The linear increase of the penetration depth with velocity that exists at ordnance velocities is not prevalent at hyper velocities. To make efficient use of these high velocities unconventional projectile geometries like segmented and telescopic projectiles could very well be used in the future together with high aspect-ratio long rods. The behaviour of high velocity projectiles in consuming armour like homogeneous armour steel and ceramic armour and disturbing armour like spaced oblique plates and reactive armour will be discussed. This paper presents a compilation of work carried out in this field at FOA in the 1990's.

## 1. INTRODUCTION

Modern KE-projectiles are long rods made of a high-density material. Since the penetration capability in homogenous targets increases with projectile length and velocity, longer and faster penetrators will be used in future anti-armour KE-weapons. Due to geometrical and interior ballistic limitations the aspect ratio of a long rod can not become too large. One way of avoiding this problem is to use projectiles that can be extended when they approach the target. Examples of such projectiles are segmented and telescopic rods that very well could come into use if the velocities become high enough.

There are many interesting questions associated with the terminal ballistic behaviour of high velocity projectiles but this presentation will concentrate on the following issues:

- Will increasing the strength of armour steel be efficient against high velocity rods?
- Are ceramics as efficient against high velocity rods as they are against ordnance velocity rods?
- How will armour like spaced oblique plates, reactive armour and sensor activated armour perform against high velocity rods?
- How will electromagnetic armour perform against high velocity rods?
- How can unconventional projectiles be expected to perform in modern armours?

The discussion will mainly rely on work carried out in this field at FOA in the 1990's. The experimental work was mainly done in a small scale using simple geometries to achieve a good understanding of the basic processes involved. This information has also been used as a basis for physical modelling and calibration of continuum dynamic simulations.

## 2. HIGH STRENGTH ARMOUR STEEL

A simple and effective way of increasing the protection against ordnance velocity KE-projectiles is to increase the hardness of the armour steel. Is this also valid for high velocity projectiles? To investigate this question L/D=15 tungsten rods were fired at 1500 and 2500 m/s into a quenched and tempered steel hardened to 300, 450 and 600 Vickers [1], see Fig. 1.
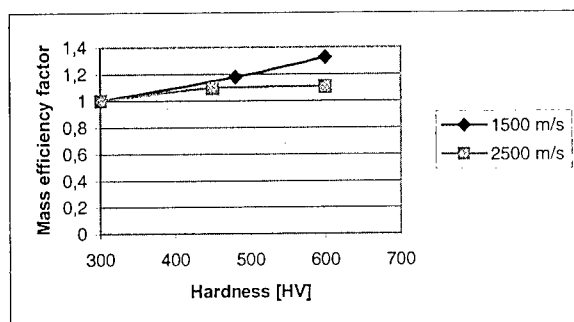


Figure 1: Mass efficiency factor for different hardness steel against tungsten rods at 1500 and 2500 m/s.

As can be seen, doubling the hardness of the steel will increase the mass efficiency factor by 30% at 1500 m/s and by 10% at 2500 m/s. The reason for this is that strength effects are more important at the lower velocity than at the higher where inertia effects dominate. To get a good benefit from increased strength at impact velocities of 2500 m/s, more extreme materials like ceramics must be used.

## 3. CERAMICS

Ceramics are brittle hard materials that have the potential to withstand very high compressive loads. When they fail they normally fail catastrophically, that is they break into a lot of small fragments. If the ceramic is confined it can still retain some of its load-carrying ability. The high protection potential of ceramics has not been exploited in the armour concepts that exist today.

In the laboratory properly confined high quality ceramic materials have been used to design ceramic armour systems capable of defeating projectiles on the surface of the ceramic. This capability, called interface defeat, signifies that the projectile material is forced to flow radially outwards on the surface of the ceramic without penetrating significantly. This behaviour can occur at normal ordnance velocities even for tungsten long rods. Is this also true for high velocity rods? A study has been undertaken to establish the transition velocity when the change from interface defeat to normal penetration occurs for the case of long rods attacking ceramic targets [2].

The pressure field on the ceramic surface under a stationary radially flowing long projectile has been modelled and the stress field in the ceramic at incipient and large-scale yield has been estimated as a function of projectile material and velocity. The incipient yield starts about 0.35 projectile diameters below the surface and by large-scale yield we mean that the ceramic material yield volume reaches the surface of the ceramic. Combining this information

with strength data for the ceramic makes it possible to estimate the transition velocity for different combinations of projectile and target materials.

In the experimental investigation two different projectile materials, tungsten and molybdenum, were used to verify the hypothesis that it is the maximum load per unit area exerted by the projectile that defines the transition velocity. 5 different ceramic materials were studied. In Table 1 and 2 data for the projectile and target materials used in the investigation are shown.

Table 1: Projectile materials

| Projectile material | Bulk modulus [GPa] | Density [kg/m$^3$] | Yield strength [GPa] |
|---|---|---|---|
| WHA | 285 | 17600 | 1.2 |
| Molybdenum | 238 | 10220 | 0.9 |

Table 2: Target materials

| Target material | Poisson's ratio | Density [kg/m$^3$] | Hardness HV [GPa] | Yield strength [GPa] |
|---|---|---|---|---|
| SiC-1 | 0.17 | 3220 | 21.6 | 10.4 |
| SiC-2 | 0.16 | 3180 | 20.3 | 9.8 |
| TiB$_2$ | 0.19 | 4400 | 20.6 | 9.9 |
| B$_4$C | 0.17 | 2500 | 33.0 | 15.8 |
| Syndie (polycrystalline diamond composite) | 0.07 | 4100 | 71.0 | 34.1 |

The target and the projectile geometries used in the (reverse impact) experiments are shown in Fig 2.
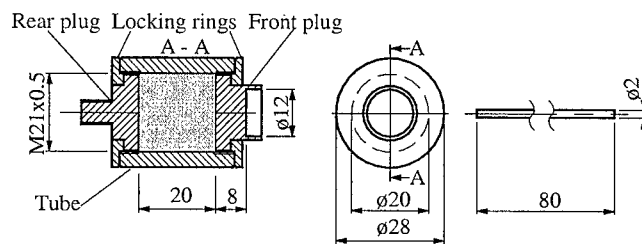


Figure 2: Target and projectile geometries

Flash X-ray technique was used to monitor the projectile-target interaction. Figure 3 shows what happens below (a) and above (b) the transition velocity.



16.6 μs    21.8 μs    26.8 μs    31.6 μs                16.6 μs    21.8 μs    27.0 μs    31.6 μs
(a)                                                      (b)
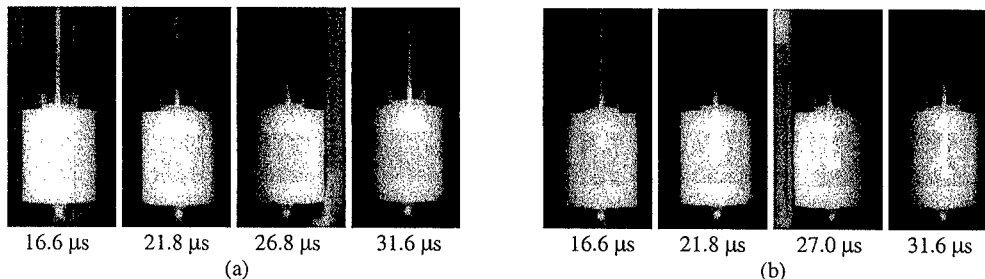
Figure 3: X-ray-pictures of projectile-target interaction in SiC-2 below (1615 m/s) the transition velocity (a) and above (1805 m/s) the transition velocity (b).

Figure 4 shows the intervals for the transition velocities obtained from the theories for incipient (lower curves) and large-scale yield (upper curve). The experimentally obtained transition velocities are plotted in the diagram and it can be seen that the B₄C and Syndie (polycrystalline diamond composite) qualities used in this investigation show a "brittle" behaviour while the TiB₂ and SiC used show a more "plastic" behaviour.
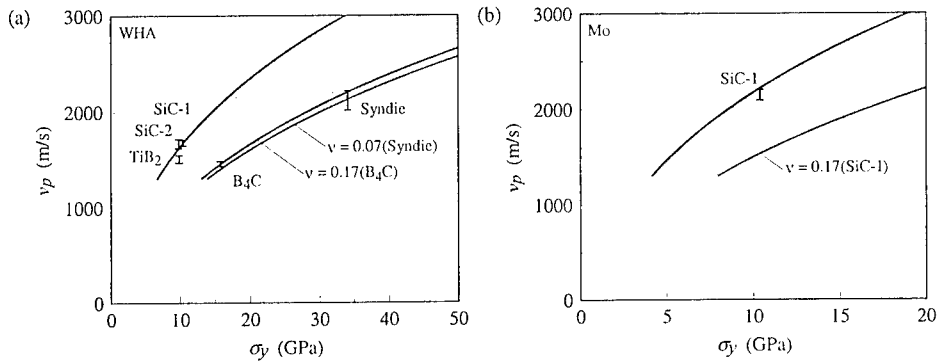


Figure 4: The intervals for the transition velocities obtained from the theories for incipient (lower curves) and large-scale yield (upper curve) and the experimentally obtained transition velocities. (a) WHA-projectile, (b) Mo-projectile.

Another conclusion that can be drawn from these results is that the transition velocity of 1700 m/s for the tungsten projectile against SiC-1 increased to 2200 m/s for the molybdenum projectile. This is the velocity that could be predicted from the theoretical estimate above.

Our studies indicate that interface defeat armours should be possible against ordnance velocity projectiles since transition velocities of 1700 m/s for SiC and 2100 m/s for Syndie were obtained. In [3] it has been shown that using a high quality TiB₂ 2000 m/s can be obtained for this ceramic as well. Against high velocity projectiles, plastic behaviour of high quality ceramic armour could mean that even these types of projectiles could be defeated.

The interface defeat experiments have been carried out as small scale experiments and the event has only been studied for about 30 μs. For large calibre projectiles the interaction time is much longer, of the order of 500 μs. It might be possible that the ceramic could break down after such a long time of loading. To investigate whether interface defeat can occur also in a large calibre situation, experiments with SiC-1 at 1500 m/s have been carried out where the ceramic target was fired against a very long projectile and the interaction monitored for 500 μs. These experiments showed that interface defeat continued for at least 280 μs and that very little penetration had taken place after 500 μs [4]. Interface defeat ceramic armour could thus be possible even as tank armour in the future.

Using normal armour ceramics with more moderate mechanical properties, will mean that penetration occurs at ordnance velocities. To investigate the difference in protection capability for ceramics of this type against high velocity projectiles, L/D=15 tungsten rods were shot at 1500 and 2500 m/s against unconfined and heavily confined cylindrical alumina targets with a diameter 10 times that of the projectile [5], see Fig. 5.
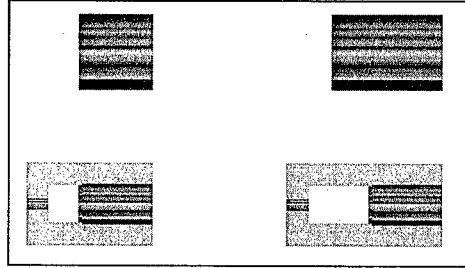
Figure 5: Unconfined (upper row) and heavily confined (lower row) alumina targets against 1500 m/s (left column) and 2500 m/s (right column) projectiles.

The thickness of the ceramic at the two velocities (8 and 16 times the projectile diameter respectively) was chosen to try to achieve a comparable residual penetration into the steel backing. The penetration into the steel backing was measured and the mass efficiency of the ceramic was evaluated, see Fig. 6.
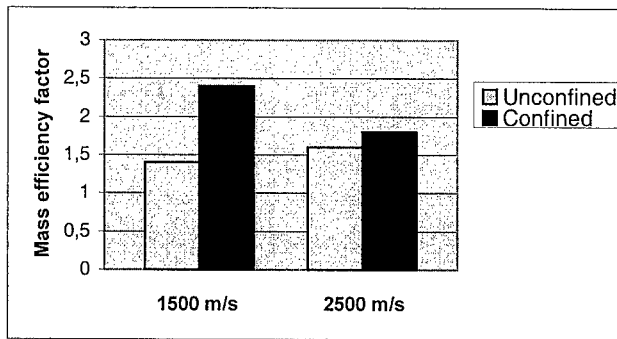


Figure 6: Mass efficiency factor of the ceramic material for confined and unconfined alumina against tungsten rods at 1500 and 2500 m/s.

As can be seen, heavily confined "normal" ceramic materials are more weight efficient against ordnance than against high velocity projectiles. For unconfined ceramics, the opposite result was obtained in this investigation. This is due to the fact that at low projectile velocity the ceramic has more time to break and get displaced, than in the case of high projectile velocity.

## 4. STATIONARY AND MOVING OBLIQUE PLATES

Most modern armours contain elements that exert transverse forces on the projectile to make it rotate, bend and/or break before hitting the basic consuming armour. This is a very weight-efficient way of reducing the penetration capability of especially long rod penetrators. Spaced oblique plates, reactive armour and sensor activated armour are examples of armour using this principle. The detailed design of this type of armour can be done in an unlimited number of ways. To get a basic understanding of the processes involved at ordnance and high velocities the elementary cases of a stationary and a moving single plate being penetrated by a long rod projectile at 1500 and 2500 m/s have been studied [6, 7].

In Fig. 7 continuum dynamic simulations and flash X-ray pictures of the residual projectile after penetrating a stationary plate are shown.
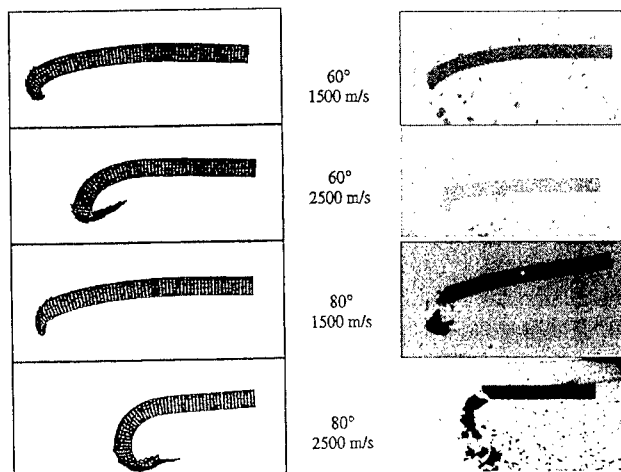
Figure 7: Continuum dynamic simulations and flash X-ray pictures of the residual tungsten projectile after penetrating a stationary plate

The projectile was a 5 mm diameter L/D=15 tungsten rod and the armour steel plate had a thickness of 5 mm at 1500 m/s and 9 mm at 2500 m/s at 60° obliquity (the thickness was chosen proportional to the penetration capability in homogeneous armour steel). The same line of sight thickness was used at 80°. No failure criterion was used for the projectile material in the simulations but the agreement with the experimental results is good. The residual projectile is shorter for the high velocity projectile, especially in the 80° obliquity case, but it is straighter and has not rotated as much as the normal velocity penetrator.

Projectiles with larger aspect ratios have larger moments of inertia that means that the rotation rates obtained in oblique plates will go down. Since future projectiles probably will be longer and more slender than today, they will be more difficult to yaw. The most relevant defeat mechanism will then be the length reduction of the projectile. This reduction will be larger for high velocity than for ordnance velocity projectiles which means that spaced thin oblique plates could be an efficient way of defeating high velocity projectiles.

Moving oblique plates, which is the basic mechanism in reactive armour, have mainly been studied by numerical simulations. Some cases have also been studied experimentally and the agreement with the simulations has been good, see for instance Fig. 8.
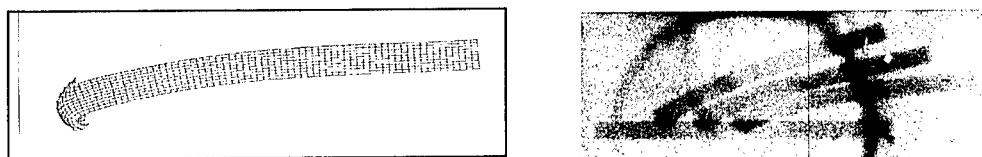


Figure 8: Continuum dynamic simulations and X-ray pictures (for three consecutive times) of the residual tungsten projectile after penetrating an oblique moving plate. Projectile velocity 2500 m/s, plate velocity 200 m/s and plate angle 60°.

- 342 -

The influence of plate angle and plate velocity of a plate thrown against the projectile has been studied numerically for L/D=15 WHA long rods with velocities of 1500 and 2500 m/s [7], see Fig. 9.
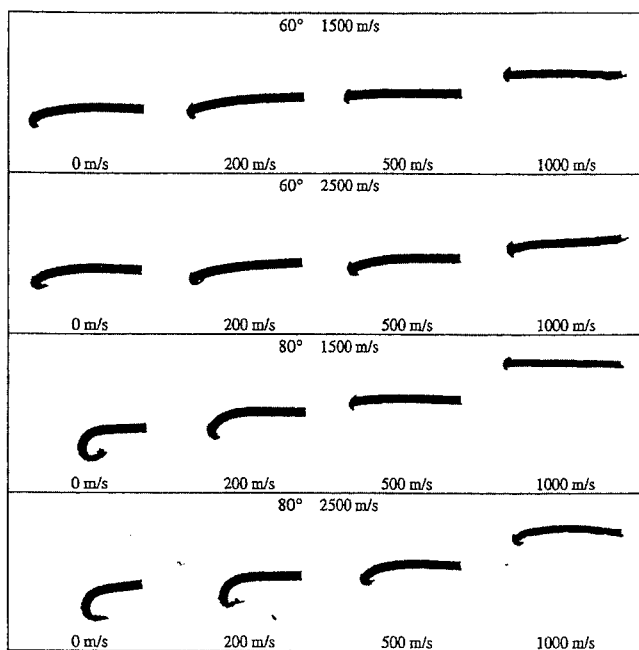


Figure 9: Continuum dynamic simulations of the residual tungsten projectile 150 μs after penetrating an oblique stationary or moving plate. 16 different cases with different projectile velocity, plate velocity and plate angle.

The plate thickness was the same as the diameter of the projectile for all the cases studied here. As can be seen from Fig. 9, increasing the velocity of the plate will not necessarily increase the disturbance on the residual projectile. High velocity penetrators seem to obtain larger disturbances than ordnance velocity penetrators do at the same time after hitting the plate (which means a longer distance behind the plate for the high velocity penetrator). It should be pointed out though, that the absence of a failure criterion could seriously affect the residual penetrator behaviour.

The discussion above concerns the front plate of a reactive armour or a plate ejected from a sensor activated armour system. The largest disturbance on the projectile from a reactive armour though will come from the back plate that flies in the same direction as the projectile [8], see Fig. 10.

(a)                              (b)                              (c)
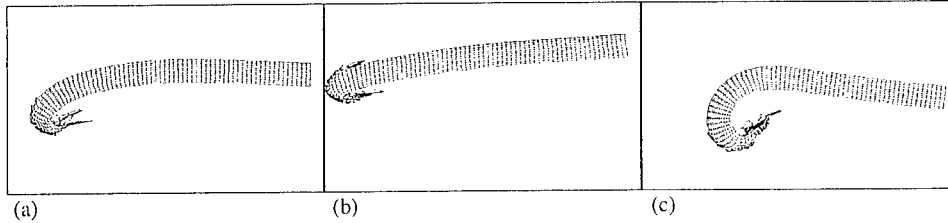
Figure 10: Continuum dynamic simulations of the residual tungsten projectile 150 μs after penetrating an oblique 60° plate. (a) stationary plate, (b) front plate with velocity 200 m/s, (c) rear plate with velocity 200 m/s. Projectile velocity 2000 m/s.

Since the rear plate flies with the projectile the interaction time is longer. This increases the length reduction of the projectile. Increasing the velocity of the rear plate will increase the interaction time and thus the disturbance of the penetrator. As can be seen from the pictures the rotation of the residual projectile received from the rear plate is in the opposite direction to that from the front plate. This can be one of the reasons why long rod projectiles normally break up in several parts when interacting with a complete reactive armour.

From these studies it can be concluded that, for the same geometry, the length reduction is larger and the disturbance on the residual projectile also larger for high velocity projectiles than for ordnance velocity projectiles. This indicates that armour containing moving plates, as reactive and sensor activated armour, could be as effective against high velocity projectiles as against ordnance velocity projectiles.

## 5. ELECTROMAGNETIC ARMOUR

If large amounts of electric power is available it could be used for armour applications. Three major principles for such an armour can be identified: ejection of protective plates, passing a strong electric current through the projectile, and using electromagnetic fields [9], see Fig. 11.



Figure 11: The major principles for electromagnetic armour.

Using electricity to eject plates is from a terminal ballistic point of view basically the same as ordinary explosive reactive armour [10]. This concept is already technically feasible. For the other two principles "the capacitor armour concept" will probably be used earlier than the "the electromagnetic field concept" since the energy requirement is much lower.

A theoretical study of the forces exerted on the projectile in a capacitor armour has been carried out [11] and the results indicate that the energy required to obtain an adequate deflection of a full scale penetrator is, even for this concept, very high (currents of the order of MA which means capacitors with energies larger than tens of MJ). These results are based on

the assumption that the projectile behaves like a rigid body. Preliminary small-scale static experiments [12] indicate though that the penetrator could disintegrate at lower currents. This is due to localised thermal effects in the matrix of the particle composite material used in the penetrator. Despite such phenomena large amounts of electric energy will be required.

Since the development in the field of more compact energy storage devices is rapid, future armoured vehicles could very well make use of capacitor armour against shaped charge warheads and KE-projectiles. Since the amount of electric energy that can be deposited in the penetrator depends on the time that the penetrator short cuts the plates, high velocity penetrators will be more difficult to defeat than ordnance velocity penetrators with this type of armour.

## 6. UNCONVENTIONAL PROJECTILE GEOMETRIES

In homogeneous armour steel, the linear increase of penetration with velocity that exists for long rods at ordnance velocities is not prevalent at high velocities. For tungsten rods, increasing the velocity above 2500 to 3000 m/s will not increase the penetration depth noticeably. The increase in kinetic energy will instead result in increasing the diameter of the penetration channel, see Fig. 12.
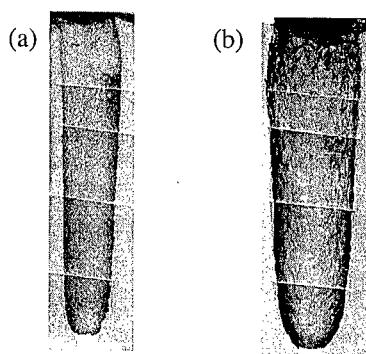


Figure 12: Penetration channels in armour steel from L/D=10 WHA rods at
(a) 2500 m/s and (b) 3000 m/s.

Another way of increasing the penetration is to use a longer projectile, as the penetration depth is proportional to the length of the projectile. Due to space constraints and interior ballistic limitations the aspect ratio can not become too large. At high velocities though, advantage can be taken of the high velocity and the large diameter of the penetration channel to design penetrators, which increase their length when approaching the target. The two most common concepts are segmented and telescopic rods, see Fig 13.



Figure 13: Segmented (left) and telescopic (right) projectiles

These projectiles give considerably better penetration than the corresponding collapsed rod in armour steel, see Fig. 14. The figure shows an increased penetration depth of about 40% for the unconventional projectiles although very simple designs where used. The conventional long rod had L/D=10, the segmented rod consisted of 10 segments with a segment distance of two diameters, and the telescopic projectile consisted of a tube and a rod where the rod diameter was half the diameter of the tube. With more optimised designs considerably better improvements can be obtained.
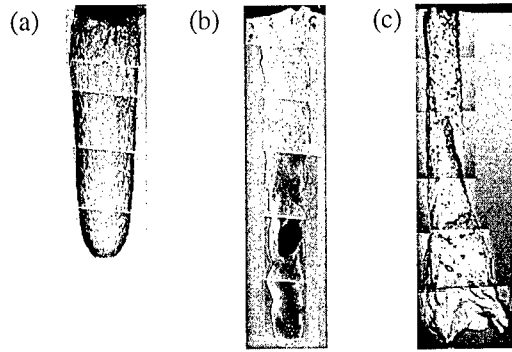


Figure 14: Penetration channels in armour steel from (a) a conventional long rod, (b) a segmented rod and (c) a telescopic projectile. All projectiles had L/D=10 as "collapsed" projectiles. Projectile velocity 3000 m/s.

In ceramic materials the penetration channels are more narrow, unsymmetrical and possibly debris-filled. How does this effect the performance of unconventional projectiles?

A study of how a segmented and a telescopic projectile performs in confined alumina has been carried out [13], see Fig 15.
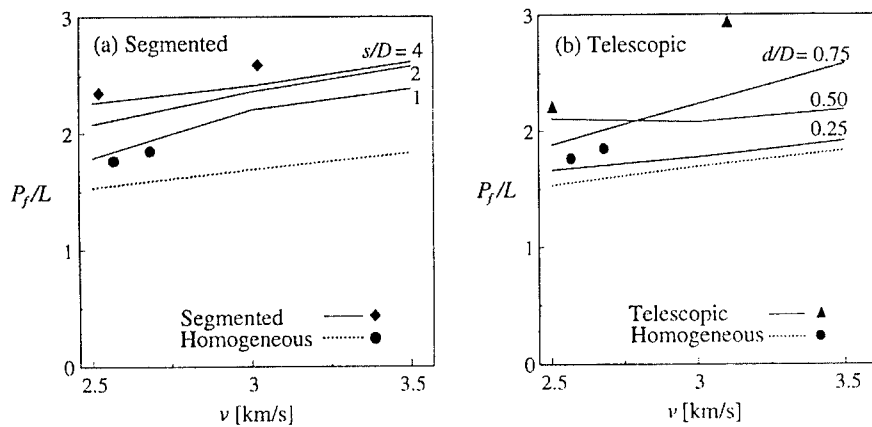


Figure 15: Normalised penetration into alumina for (a) segmented and (b) telescopic projectiles. Simulated (curves) and experimental (dots) results.

In the experimental study the segmented rod had 6 L/D=1 segments separated by a distance of 2D and the telescopic rod had a core to tube ratio of 0.5. Simulations have also been made for segment distances of D and 4D and core to tube diameters ratio of 0.25 and 0.75. The

penetration depth is compared to that of a homogeneous rod. All projectiles had L/D=6 as collapsed projectiles. The unconventional projectiles are clearly more effective than the homogeneous also in this type of ceramic target.

In oblique plates, segmented projectiles will be effective since no disturbance will be transmitted from the segments interacting with the plate to the segments coming after. Telescopic projectiles could be less effective in oblique plates as the distance between the side of the projectile and the penetration channel is small. The first part of the tube could then interact with the plate. One way of solving this problem could be to have the tube in front of the core.

Reactive armour, if the plates have a high enough velocity, will mean that every segment in a segmented projectile could make a head-on impact with the plate. This could be extremely effective against a segmented projectile and even consume it completely. Telescopic projectiles could also run into problems since, apart from the consumption mentioned above, the core and the tube could separate and not act on the same area of the main armour behind the reactive component.


## 7. CONCLUSIONS

From our studies the following conclusions can be drawn for armour against high velocity long rods:

- Increasing the strength of armour steel, and presumably the strength of other types of metallic target materials, will not be as effective as it is against ordnance velocity projectiles.
- Ceramic armour will not perform as well as it does against ordnance velocity projectiles. Interface defeat armours can not be expected in the near future.
- Spaced, large-obliquity plates should be more effective than against ordnance velocity projectiles.
- Reactive and sensor activated armour could be as effective as against ordnance velocity projectiles.
- Electromagnetic armour is probably less effective than against ordnance velocity projectiles.

Unconventional projectiles should perform well in all types of inert, consuming armour. In reactive targets their performance could be seriously degraded.

These conclusions are drawn from studies of a given projectile at different velocities. In a weapon system, the amount of energy is normally limited which means that increasing velocity will mean decreasing projectile mass.

## REFERENCES

[1]  S. Bogegård, L. Holmberg, L.-G. Olsson, "The influence of armour steel hardness on the penetration capability of long rods at 1500 and 2500 m/s", in Proceedings of the 13th International Symposium on Ballistics, Stockholm, Sweden, Vol. 3, pp. 153-160, (1992)
[2]  P. Lundberg, R. Renström, B. Lundberg, "Impact of metallic projectiles on ceramic targets: Transition between interface defeat and penetration", to be published in Int. J. Impact Engng
[3]  E.J. Rapacki, G.E. Hauver, R.F. Benck, "Ceramics for armours – a material system perspective" 7th Annual TARDEC Ground Vehicle Survivability Symposium, Monterey, CA (1996)

[4]    P. Lundberg, "Experimentell studie av "stela-väggen fenomenet" vid långa belastningstider", FOA Memo 99-5522/S (1999) (In Swedish)

[5]    P. Lundberg, "Replica modellings giltighet som skalningsmodell för pilprojektilpenetration i Al2O3 vid 1500 och 2500 m/s", FOA Dnr 94-2275/S (1994) (In Swedish)

[6]    L. Holmberg, P. Lundberg, L. Westerling, "An experimental investigation of WHA long rods penetrating oblique steel plates", in Proceedings of the 14th International Symposium on Ballistics, Quebeck, Canada, Vol. 2, pp. 515-524, (1993)

[7]    E. Lidén, J. Ottosson, L. Holmberg, "WHA long rods penetrating stationary and moving oblique steel plates", in Proceedings of the 16th International Symposium on Ballistics, San Francisco, California, Vol. 3, pp. 703-711, (1996)

[8]    J. Ottosson, "Numerisk studie av inverkan av medflygande plåt samt projektilens hållfasthet och geometri för ett reaktivt pansar", FOA Memo 99-5523/S (1999) (In Swedish)

[9]    S.E. Nyholm, "Electromagnetic Armour: An Overview", FOA-R--98-00877-310--SE (1998)

[10]   H.-J. Ernst, K. Sterzelmeier, T. Wolf, R. Nüsing, "Reactive Arour mechanisms against KE-Threat: High Explosives and Electromagnetic Forces", in Proceedings of the 17th International Symposium on Ballistics, Midrand, South Africa, Vol. 1, pp. 71-78, (1998)

[11]   A. Svensson, S. Mousavi, "Krafter och stelkroppsrörelser i ett elektromagnetiskt pansar", FOA-R--99-01341-310--SE (1999) (In Swedish)

[12]   A. Svensson, M. Skoglund "Inledande statiska försök med pilprojektiler i ett elektromagnetiskt pansar", FOA Memo 99-5502/S (1999) (In Swedish)

[13]   L. Westerling, P. Lundberg, L. Holmberg, B. Lundberg, "High velocity penetration of homogeneous, segmented and telescopic projectiles into alumina targets", in Int. J. Impact Engng, Vol. 20, pp 817-827, (1997)

# MINIMUM IMPACT ENERGY FOR KE-PENETRATORS IN RHA-TARGETS

## LANZ W. (1), ODERMATT W. (2)

(1) Swiss Ordnance Enterprise Corporation, Allmendstrasse 86, CH-3602 Thun, Switzerland
(2) Defence Procurement Agency, Feuerwerkerstrasse 39, CH-3602 Thun, Switzerland

**Abstract :** The Odermatt formula presented originally in 1992 [4] also allows to determine minimum energy impact velocities for penetrating inclined RHA plates. For plates of 800 MPa ultimate tensile strength (UTS) this velocity is around 1900 m/s.
However this velocity may considerably be reduced by tailoring the sabots for specific rods, taking into account rod length, barrel caliber and maximum acceleration. Then the optimum velocity value drops to about 1700 m/s. To compensate the velocity drop at tactical range (typically 2000 m) about 80 m/s increase has to be considered.
On the other hand the influence of the muzzle velocity dependent efficiency of solid propellant gun systems downshifts the optimum velocity to about 1540 m/s for 2000 m range.
Jacketed penetrators and sabots using new high strength light materials (e.g. FRP), allow to reach the required penetration at even lower energy levels.

## 1. PENETRATION LIMIT FORMULA

### 1.1 Penetration limit definition

In a finite target penetration limit means that the projectile reaches the rear face of the target and spalling opens the penetration channel. The penetrator residue will have a length of one to one and a half diameters. In a few of our experiments the residue stuck in the exit crater or dropped to the floor in the immediate vicinity of the target. This result is observable at the target site, whereas a semi-infinite target first has to be cut up laboriously.
The formula described below allows a quick estimation of the target inclination necessary for a penetration limit. This is then easily established with few projectiles, especially when using witness plates.

### 1.2 Governing parameters

| | | | |
|---|---|---|---|
| $D$ | penetrator diameter [mm] | $\lambda, \lambda_W$ | aspect ratio $L/D$, $L_W/D$ |
| $L$ | overall tungsten penetrator length [mm] | $v_T$ | impact velocity [km/s] |
| $L_W$ | working length of penetrator [m] | $v_0$ | muzzle velocity [m/s] |
| $\rho_P$ | penetrator density [kg/m$^3$] | $\theta$ | angle of obliquity |
| $\rho_T$ | target density [kg/m$^3$] | $m_P$ | penetrator mass [kg] |
| $d$ | target plate thickness [mm] | $m_G$ | mass of penetr. and sabot [kg] |
| UTS | target material ultimate tensile strength [MPa] | $m_L$ | propellant charge mass [kg] |
| $P$ | penetration channel length [mm] | $E_P$ | impact energy [MJ] |
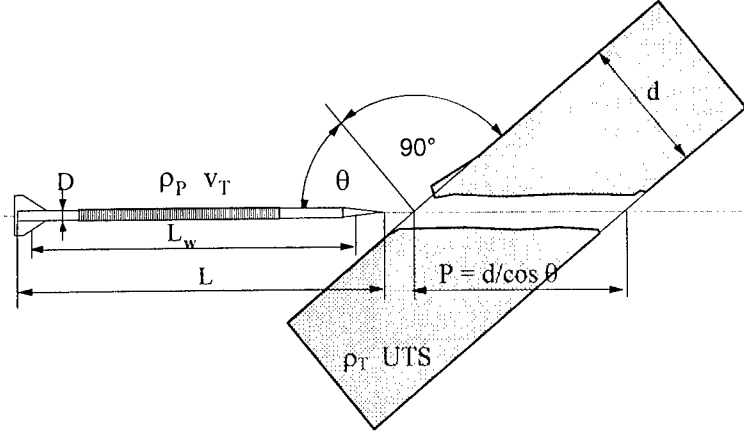
Figure 1: Definition illustration

## 1.3 Penetration limit formula

The formula has been published in [3] and [4]. Here it is presented with a slight variation, ie. P/L as the independent variable instead of d/D.

$$\frac{P}{L_w} = f(\lambda_w) \cdot \cos^m \theta \cdot \sqrt{\frac{\rho_P}{\rho_T}} \cdot e^{\frac{-c \cdot UTS}{\rho_P \cdot v_T^2}} \qquad (1)$$

$$\phantom{xxxx} A \phantom{xx} B \phantom{xx} C \phantom{xx} D$$

A   aspect ratio influence,
    a good approximation is obtained with the following equation

$$f(\lambda_w) = 1 + a_1 \cdot \frac{1}{\lambda_w} \cdot \left(1 - \tanh\frac{\lambda_w - 10}{a_2}\right) \quad \text{mit } a_1 = 3.94 \quad a_2 = 11.2 \qquad (2)$$

B   target inclination influence,
    the best fit for the exponent is $m = -.225$

C   penetrator/target density influence, this is the wellknown root $\rho$-law

D   the dimensionless exponent is derived in [1] by applying the $\pi$-theorem,
    the coefficient c depends on target material strength

$$c = 22.1 + 1.274 \cdot 10^{-2} \cdot UTS - 9.47 \cdot 10^{-6} \cdot (UTS)^2 \qquad (3)$$

## 1.4 Range of validity of the formula/results

The range of validity is defined by the bandwidth of 74 experiments with 19 different penetrators and calibers of 25 to 140 mm.

| penetrators: | | | | | targets: | | | | |
|---|---|---|---|---|---|---|---|---|---|
| L | 90 | - | 950 | mm | d | 40 | - | 500 | mm |
| D | 8 | - | 32 | mm | UTS | 800 | - | 1'600 | MPa |
| $\lambda$ | 11 | - | 37.5 | | $\rho_T$ | | | 7'850 | kg/m$^3$ |
| $m_P$ | 0.1 | - | 9 | kg | $\theta$ | 0 | - | 74 | ° |
| $\rho_P$ | 17'000 | - | 17'750 | kg/m$^3$ | | | | | |
| $v_T$ | 1'100 | - | 2'000 | m/s | | | | | |

Since the formula is also based on theoretical analyses extrapolations are permissible, yielding results with only slightly reduced accuracy. This was confirmed by several experiments.

## 2. APPLICATIONS

### 2.1 Scope

The above formula allows the comparison of results from firing tests with different target inclinations/thicknesses/material properties, penetrator geometries and impact velocities.
It also allows the evaluation of influences of penetrator aspect ratio, obliquity and other parameters.
Penetrator performance is predictable.
Reliable extrapolations from a single test result are possible.

### 2.2 Optimisations

The analytical solution permits optimisations. E.g. the **optimum impact velocity** (maximum penetration limit for a given energy) exclusively depends on target strength and penetrator density:

$$v_{opt} = \sqrt{\frac{3 \cdot c \cdot UTS}{\rho_P}} \quad (4)$$



| Tensile Strength | V optimum | |
|---|---|---|
| 800 MPa | 1.897 | km/s |
| 900 | 1.999 | |
| 1000 | 2.085 | |
| 1100 | 2.156 | |
| 1200 | 2.210 | |
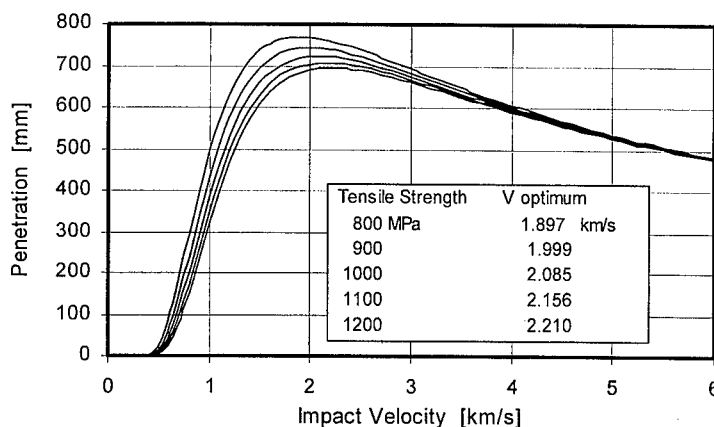
Figure 2: Optimum velocity for 10 MJ constant impact energy

For a given penetration the **optimum penetrator length** is

$$L_{opt} = e^{\frac{1}{3}} \cdot \frac{P}{f(\lambda) \cdot \cos^m \theta \cdot \sqrt{\frac{\rho_P}{\rho_T}}} \quad (5)$$

It is independent of target UTS. High penetrator aspect ratios require notably less energy. For a penetration limit of 1000 mm an aspect ratio of 30 only needs 27 % of the energy an aspect ratio of 10 requires.
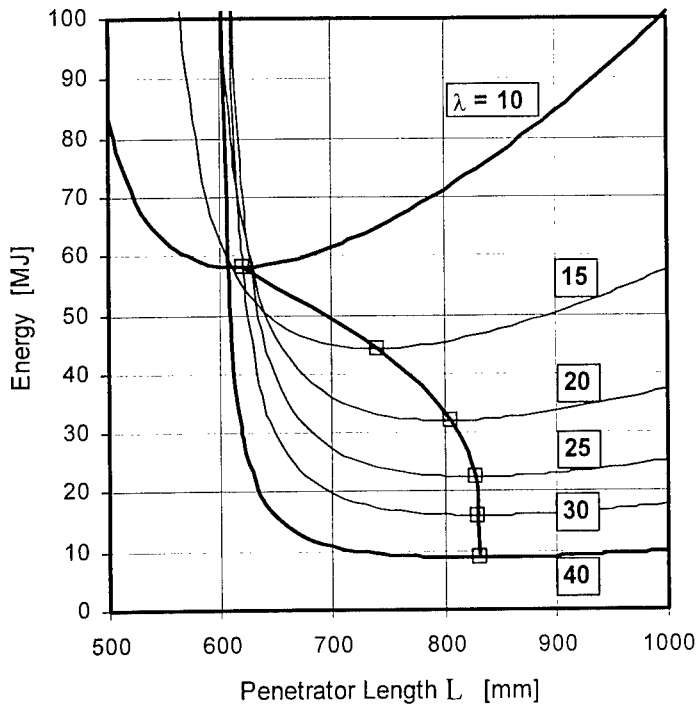


Figure 3: Optimum penetrator length vs. aspect ratio for P = 1000 mm
obliquity 60° / UTS 800 MPa / penetrator density 17500 kg/m³

It has to be noted that this optimum is purely theoretic, because neither the influence of the sabot nor the influence of the interior ballistics are considered.

## 2.3 Penetrator layouts

The graph below shows the projectile parameters for a future caliber > 120 mm with penetrator lengths between 750 and 2000 mm and diameters of 22 to 30 mm. This is a specific evaluation referring to a penetration limit of 1000 mm, 60° obliquity, 800 MPa UTS and penetrator density of 17500 kg/m$^3$.
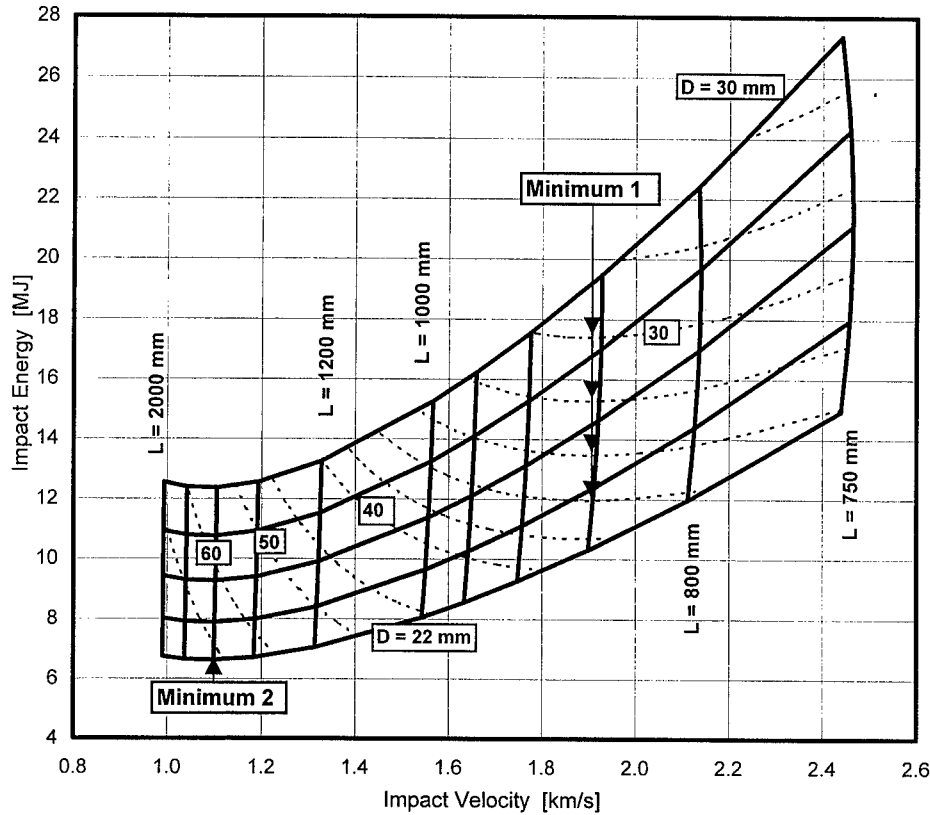


Figure 4: Penetrator parameters for 1000 mm p. limit

This graph confirms again the fact established by eq. 4 that for a given aspect ratio there exists an optimum velocity, in this case 1897 m/s. This optimum value is often cited by the experts. However this value is not necessarily an optimum.
As shown an increased aspect ratio requires less energy, eq. 4 transforms to

$$v_{opt_2} = \sqrt{\frac{c \cdot UTS}{\rho_P}} \qquad (6)$$

For the above evaluation eq. 6 yields 1095 m/s. This value is not realistic, since a rod of 24 diameter would need a length of 1600 mm. The corresponding aspect ratio of 67 is far from practicable. Fig. 4 graphically shows that for an optimisation velocity is not the only governing parameter.

# 3. APPLICATION OF THE ODERMATT FORMULA IN A SYSTEM LAYOUT

## 3.1 Length and aspect ratio (L, λ) of minimum energy KE rods for a required penetration

This is a graphic optimisation as described in item 2.3.

The Odermatt formula yields the penetration limits P for different projectile lengths L vs. projectile impact velocity $v_T$. These curves are plotted in fig. 5.

An infinite number of $L/v_T$ combinations may be found which attain a required penetration, e.g. P = 1000 mm in 800 MPa UTS RHA at 60° obliquity.

The aspect ratio (λ) influence practically disappears at values above 30. However for an assumed λ (say 36) the projectile mass $m_P$, the impact velocity $v_T$ and the impact energy $E_T$ are determined. According to the data given in fig. 7 these values are



Figure 7: Proportions of tungsten penetrators with titanium fins

| L | (mm) | 1127 | 1042 | 977 | 926 | 885 | 852 | 825 | 802 | 783 |
|---|---|---|---|---|---|---|---|---|---|---|
| $v_T$ | (m/s) | 1400 | 1500 | 1600 | 1700 | 1800 | 1900 | 2000 | 2100 | 2200 |
| $m_P$ | (kg) | 15.24 | 12.06 | 9,95 | 8.48 | 7.42 | 6.63 | 6.02 | 5.53 | 5.15 |
| $E_P$ | (MJ) | 14.94 | 13.56 | 12.74 | 12.26 | 12.02 | 11.96 | 12.03 | 12.20 | 12.46 |

These results are plotted in fig. 6.

The analytically calculated minimum energy is confirmed at $v_T$ = 1900 with $E_P$ = 12 MJ. It has to be noted that this minimum is not very pronounced: in the region of 1700 to 2100 m/s the energy variation is not more than 2.5 % or below 150 kJ respectively.

## 3.2 Sabot design influence

The 140 mm caliber with a peak pressure of 750 MPa (7.5 kbar) is taken as a reference for investigating sabot design influence. The maximum acceleration determines sabot dimensions. Fig. 8 shows a conventional aluminium sabot design.



Figure 8: Sabot proportions

Figure 5 : Penetration limit P vs impact velocity in RHA (800 N/mm$^2$ UTS / 60° obliquity) in function of length L
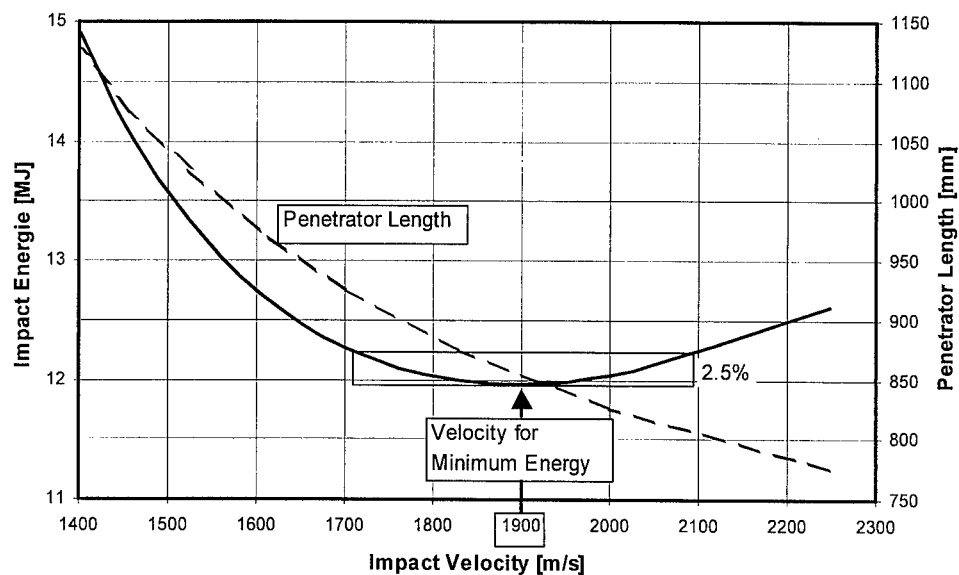


Figure 6 : Penetrators with L/D = 36 with penetration limit of 1000 RHA (800 N/mm$^2$ UTS / 60° obliquity)

For the penetrators mentioned above sabots were individually tailored, their energies $E_S$ are shown in fig. 9.
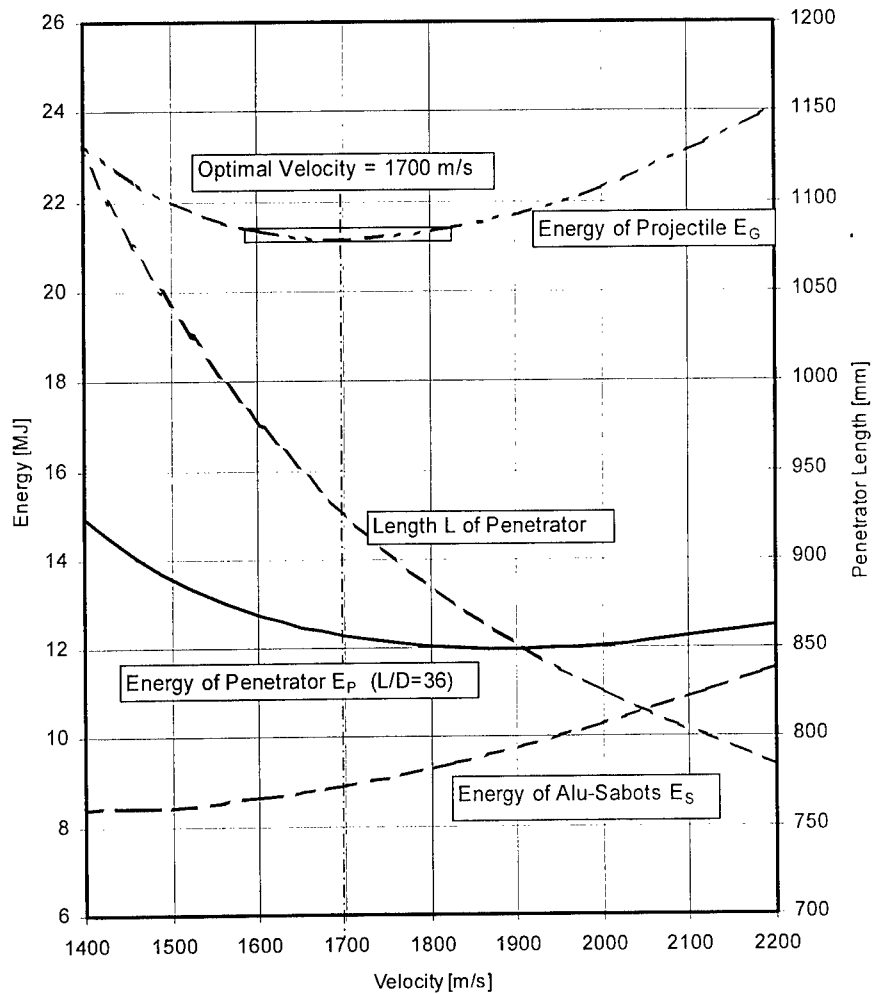


Figure 9 : Penetrators with 1000 mm RHA (800 N/mm² UTS / 60° obliquity) penetration limit
energy of projectile $E_G$ = energy of penetrator $E_P$ plus energy of sabot $E_S$
aspect ratio L/D = 36

The sum of penetrator $E_P$ and sabot energies $E_S$ is the total energy of the projectile $E_G$.
Taking sabot mass into account obviously leads to a minimum energy shift to lower velocities, not depending on $\lambda$. The new optimum velocity is at $v_T$ = 1700 m/s and again there is no distinct minimum. The total projectile energy variation is less than 2.5 % between 1580 and 1830 m/s.

## 3.3 External ballistics influence

The results presented so far refer to zero range, ie. at the muzzle. For a tactical range, typically 2000 m, the projectile velocity drop has to be considered. As shown in fig. 10 substantially more energy is required to keep a penetration limit of 1000 mm RHA.
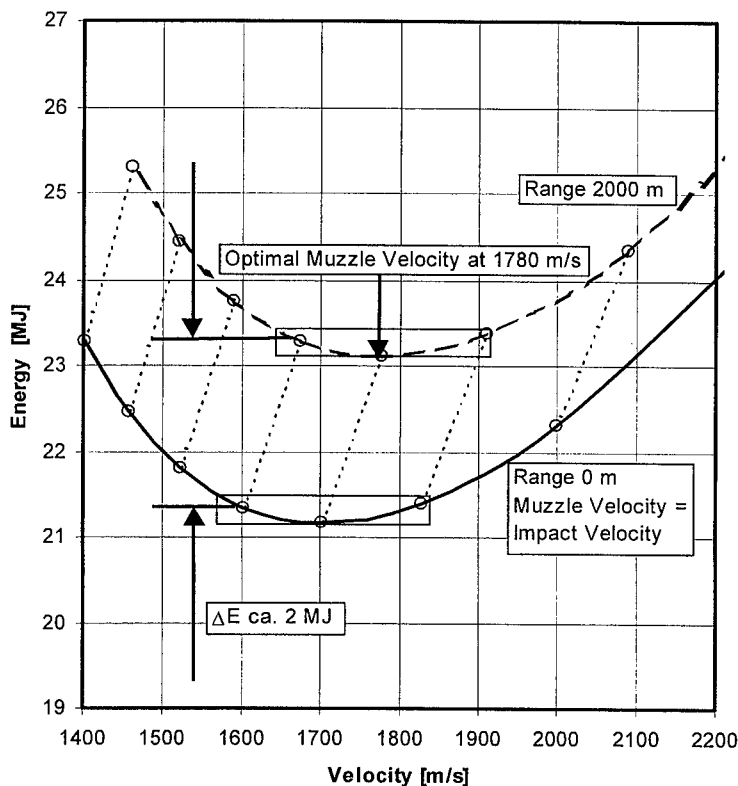


Figure 10 :   Muzzle energy for projectiles
with 1000 mm RHA (800 N/mm$^2$ UTS / 60° obliquity) penetration limit
range 0 and 2000 m

Even though light and fast projectiles loose more velocity than slower but heavier ones the terminal ballistics are still better than expected. This is due to the Odermatt curves (fig. 5) becoming flatter at the upper end and due to sabot mass influence. In fact the energy loss is nearly constant over the entire scope apart from penetrator lengths extremes below 800 and above 1050 mm. The external ballistics influence reshifts the energy minimum to higher velocitites. In RHA plates of 800 MPa UTS this shift amounts to roughly 80 m/s, the optimum velocity then being 1780 m/s for 2000 m range.

## 3.4 Integration into a 140 mm high pressure gun

Tailoring the sabots as described is one important action, however to define the entire system the energy delivered by the gun has to match the minimum energy for obtaining the required penetration.

Fig. 11 shows the internal ballistics functions for a big caliber high pressure solid propellant gun (ca. 50 cal barrel length).



The figure contains a plot with x-axis $k = m_L/m_G$ from 0.5 to 2.0, left y-axis $V_0$ [m/s] from 1000 to 2200, right y-axis $m_G$ [kg] (for $m_L = 17$ kg) from 0 to 30. Labeled curves: $V_0 = 2802 \cdot \tanh(0.3171 \cdot k + 0.3275)$ and $m_G$ (for $m_L = 17$ kg), with legend: $m_G$: Mass of Projectile, $m_L$: Mass of Charge.
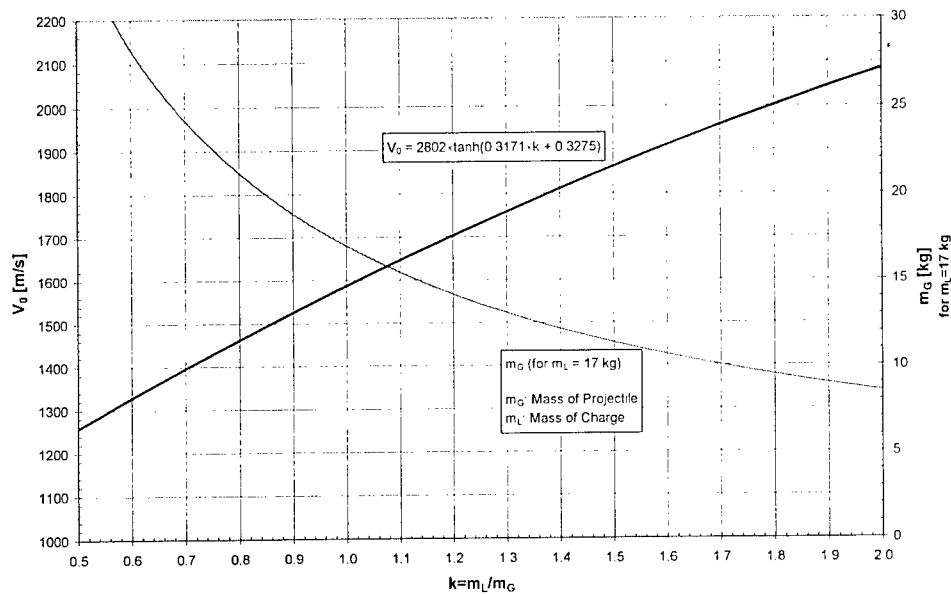
Figure 11

Depending on the propellant charge mass $m_L$ to projectile mass $m_G$ ratio the graph shows muzzle velocities and projectile mass for 17 kg charge mass corresponding to 85 MJ charge energy (combustible cartridge case included).

Transferring these curves to fig. 12 allows the selection of projectile layouts which reach 1000 mm penetration with 85 MJ energy input of a 140 mm / L50 gun at 7.5 kbar peak pressure.

Thus a rod of 1000 mm length and 36 aspect ratio penetrates 1000 mm RHA in front of the muzzle. The same penetration at 2000 m range will just be obtained by rod parameters lying on the intersection between the 85 MJ energy curve and the $\lambda = 40/2000$ m curve.

This intersection point represents a rod length of 900 mm and a muzzle velocity of 1830 m/s (lengths > 900 mm permit penetration > 1000 mm RHA).

Conclusions:

Conventional projectile technology requires very high aspect ratio rods to reach 1000 mm penetration in RHA targets even propelling them by a 140 mm gun with 85 MJ energy input. Some margin for performance increase is at hand using

• jacketed penetrators as presented in [5] and
• new sabot design technologies

both of which lead to a considerable weight reduction.
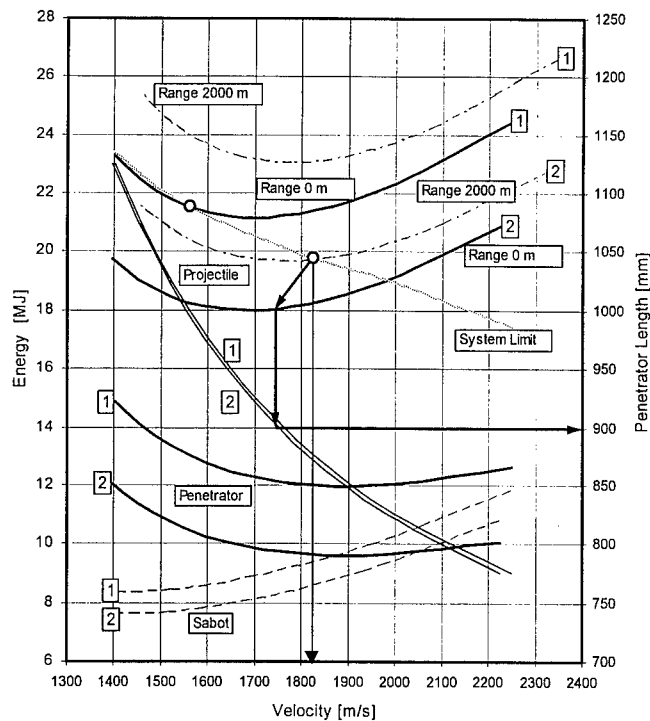
Figure 12 : Penetrators with 1000 mm RHA (800 N/mm$^2$ UTS / 60° obliquity) penetration limit aspect ratio = 36 [1] and 40 [2]

The terminal ballistics characteristics presented in [3] of solid propellant guns covering all conceivable projectile designs show a further typical optimum or maximum (see fig. 13).
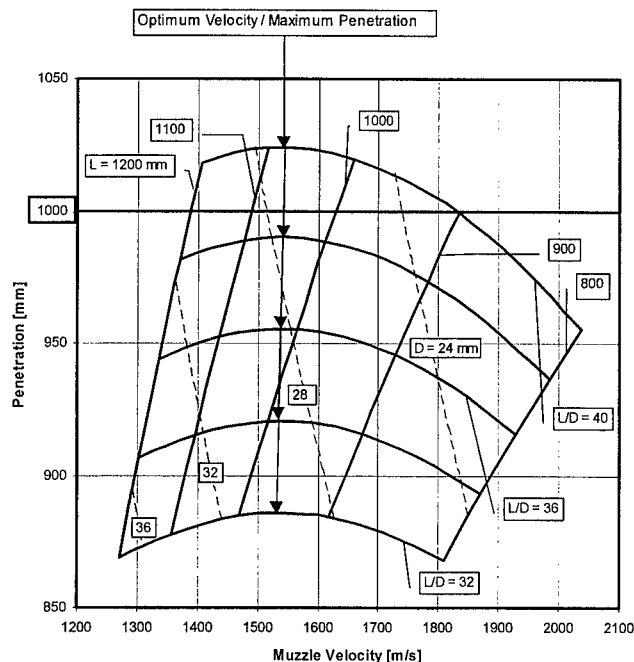


Figure 13 : Terminal ballistics characteristics for a 140 mm tank gun RHA (800 N/mm$^2$ UTS / 60° obliquity) / range 2000 m

- 359 -

For all penetrator aspect ratios there exists an impact velocity yielding maximum penetration. For 2000 m range this inherent velocity is around 1540 m/s, which can be confirmed analytically.

Referring to fig. 12 the same fact can be extracted from the common tangent of the gun energy curve and the appropriate $\lambda$-curve.

## 4. JACKETED PROJECTILES

Conventional high aspect ratio penetrators ($\lambda > 30$) have drawbacks such as pronounced elastic bending vibrations when leaving the muzzle and multiple ruptures in skirted targets leading to massive performance drops.

These drawbacks can be circumvented by jacketing a very slender heavy metal core with lighter material (preferably steel or titanium), see [ ].

Table 1 : comparison example

| Densities : | tungsten | 17.5 | [g/cm$^3$] | |
|---|---|---|---|---|
| | steel jacket | 7.85 | [g/cm$^3$] | |

| | penetrator | |
|---|---|---|
| | full core | jacketed |
| Length L | 960 | 960 |
| D | 30 | 30 |
| $\lambda = L/D$ | 32 | 32 |
| core dia $d_W$ | - | 23.4 |
| $\lambda_W = L/d_W$ | - | 41 |
| core mass $m_W$ (kg) | 11.9 | 7.5 |
| jacket mass $m_H$ (kg) | - | 1.9 |
| $m_P$ (kg) | 11.9 | 9.4 |
| $m_P$ (%) | 100 | 79 |

(inkl. Fins)

For determining the masses of jacketed penetrators see fig. 14.
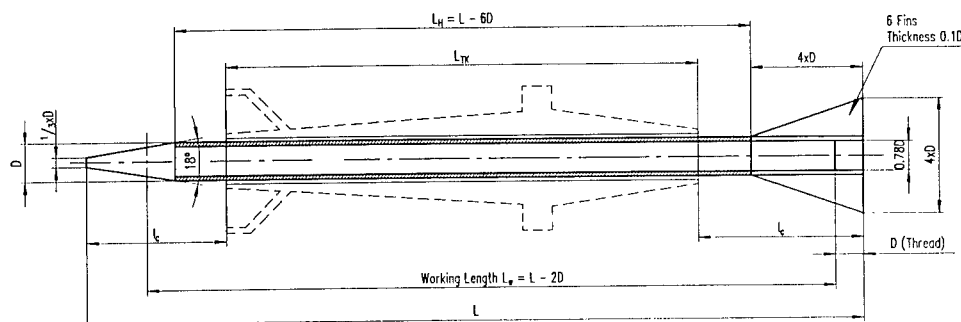


Figure 14: Proportions of steel/tungsten jacketed penetrators

Note that in the comparison both penetrator types are identical in length and outer diameter. Therefore the jacketed one is considerably lighter and contains correspondingly less kinetic energy for equal impact velocity. Despite of this fact a jacketed projectile attains practically the same penetration in thick RHA as its full core counterpart, as shown in [5].

This is due to the more favourable hydrodynamic behaviour of the tungsten/steel composite which yields a definitely smaller crater diameter, thus compensating the energy reduction, as shown in fig. 20 and [5].

Fig. 15 shows that a jacketed projectile with an overall aspect ratio of 36 reaches the 1000 mm penetration limit in RHA of 800 MPa UTS at 2000 m range.
The projectile length is (at least) 928 mm with a corresponding core aspect ratio of 46.
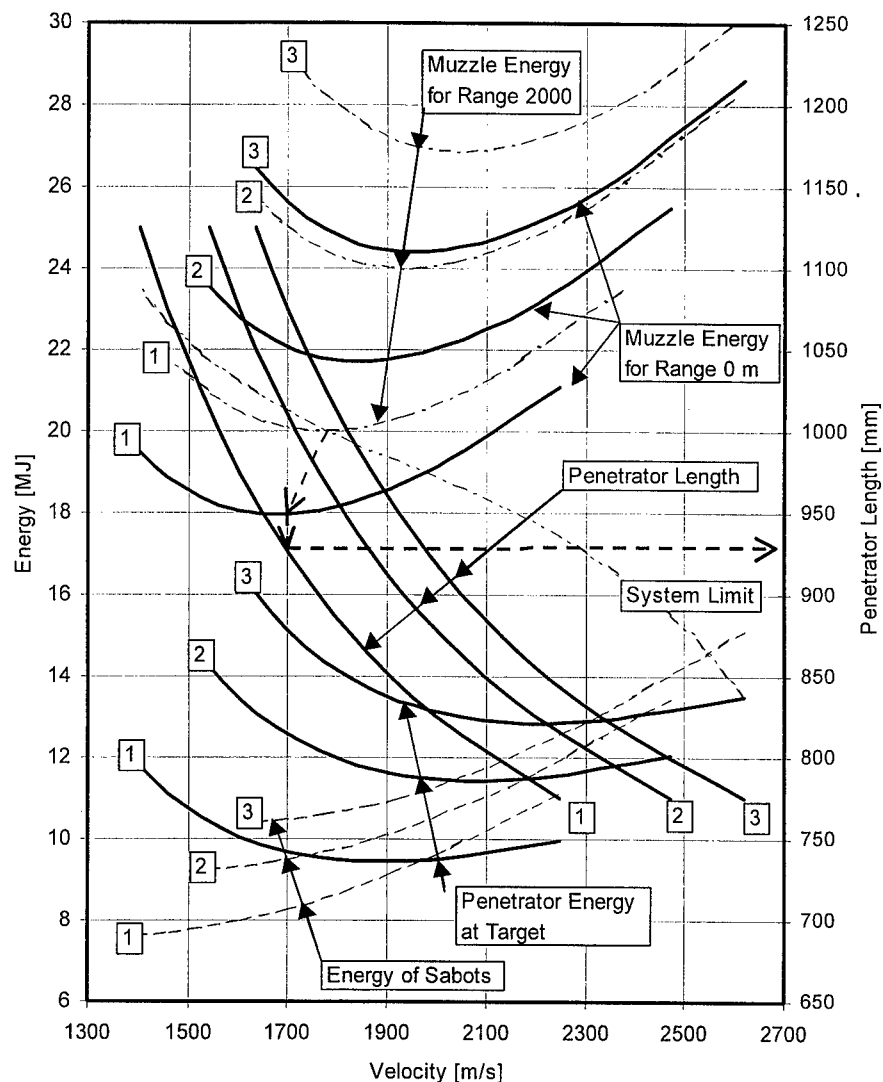


Figure 15 :   Energies for 1000 mm penetration limit in RHA , 60° obliquity
[1]  UTS of RHA    800 N/mm²
[2]  UTS of RHA  1000 N/mm²
[3]  UTS of RHA  1200 N/mm²
System limit : muzzle energy of 140 mm gun, 85 MJ propellant energy

Obviously RHA targets with 1000 MPa UTS cannot be penetrated with λ = 36 jacketed penetrators, driven by conventional alu-sabots.

## 5. NEW SABOT TECHNOLOGIES

For more than 20 years now the same sabot material has been applied. It's time for a change. Various R+D departments work on this problem, but so far no new application has materialised in the big bore business.

Obviously the sabots designed according to fig. 8 are not optimised.

For a rough estimate of the influence of fiber reinforced plastic (FRP) sabot on system performance we assume a possible weight reduction of 25 - 30 %. In the calculation this is simply accounted for by taking a density of 2.0 instead of 2.7 $g/cm^3$.

To evaluate the ultimate (theoretical) performance increase we set the density at zero. These results are presented in fig. 16
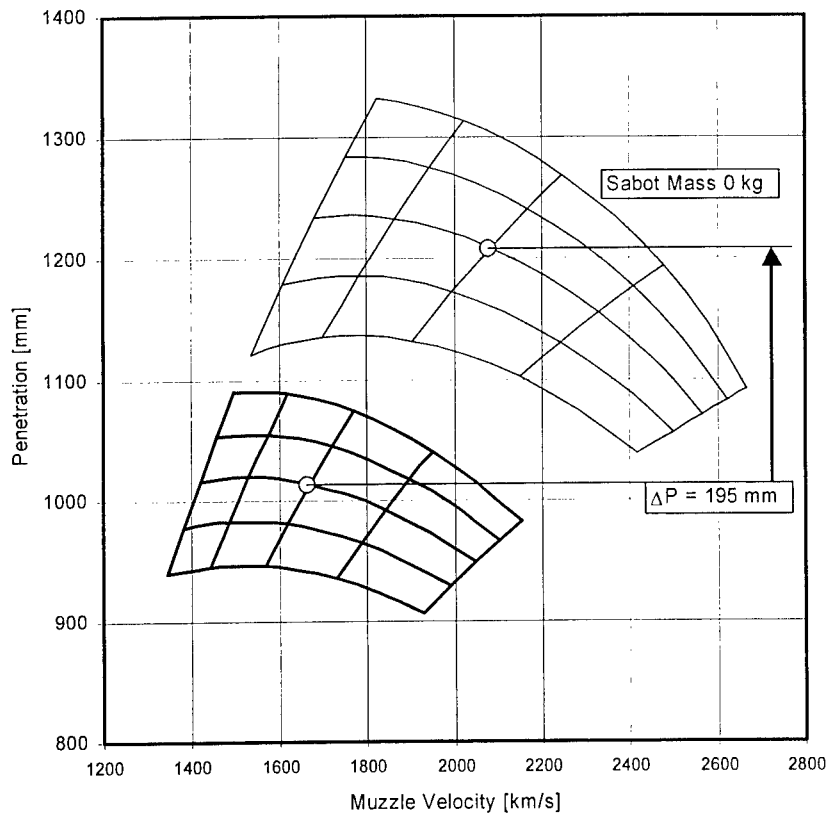


Figure 16 : Terminal ballistic characteristics for penetrators with aluminium sabots and "zero mass" sabots

The graph shows in one example an increase of 195 mm penetration for a rod (L = 1000, $\lambda = 36$) with "zero mass" sabot. In reality only about 30 % of that can be exploited, i.e. ~ 60 mm, corresponding ~ 6 %, referring to 1000 mm RHA.

# 6. ARMOR PLATE STRENGTH INFLUENCE ON OPTIMUM VELOCITY

In item 2.2 the influence of target plate strength has been derived analytically.
The higher the target UTS the higher the optimum velocity will be.
For 800 MPa UTS the optimum velocity is 1900 m/s, rising to 2200 m/s for 1200 MPa UTS.
The overall system investigation yields very similar results as shown clearly in the terminal ballistic characteristics for 2000 m range (see figs. 17 to 19).
However it has to be noted that all these system optima are situated distinctly below the generally cited level of far above 2000 m/s.
As also shown in fig. 15, the UTS influence nevertheless is quite significant (fig. 17 to 19).

- Whereas a target UTS of 800 MPa allows 1000 mm perforation at 2000 m range with L/D = 33.3 jacketed penetrators of 950 mm length and 1750 m/s muzzle velocity,
- a target UTS of 1000 MPa requires L/D = 38.5, 950 mm length and 1900 m/s muzzle velocity;
- a target UTS of 1200 MPa even requires L/D = 41.8, 1000 mm length and 1900 m/s muzzle velocity; this extreme layout is by far out of reach for todays technologies even for a 140 mm high pressure solid propellant gun system.

# 7. REFERENCES

[1]   K. Hoog, ISL, "Ableitung einer Panzerformel aus dem analytischen Modell", CCG-Lehrgang : Panzerdurchschlag und Panzerschutz, 23.-27.10.1984, Weil am Rhein

[2]   K. Frank, J.A. Zook, "Energy-Efficient Penetration of Targets", Memorandum Report BRL-MR-3885 February 1991, ARL Aberdeen Prooving Ground, Maryland US

[3]   W. Lanz, W. Odermatt
      Penetration Limits of Conventional Large Caliber Anti Tank Guns / Kinetic Energy Projectiles
      13th International Symposium on Ballistics, Stockholm 1992

[4]   R. Jeanquartier, W. Odermatt
      Post-Perforation Length and Velocity of KE Projectiles with Single Oblique Targets
      15th International Symposium on Ballistics, Jerusalem 1995

[5]   W. Lanz, H.F. Lehr
      Craters Caused by Jacketed Heavy Metal Projectiles of very high Aspect Ratio impacting Steel Targets
      16th International Symposium on Ballistics, San Francisco 1996

**140 mm Gun , 85 MJ Propellant Energy :**
Terminal Ballistic Characteristics for Jacketed Penetrators and FRP Sabots
RHA Plates , 60° Obliquity , Range 2000 m
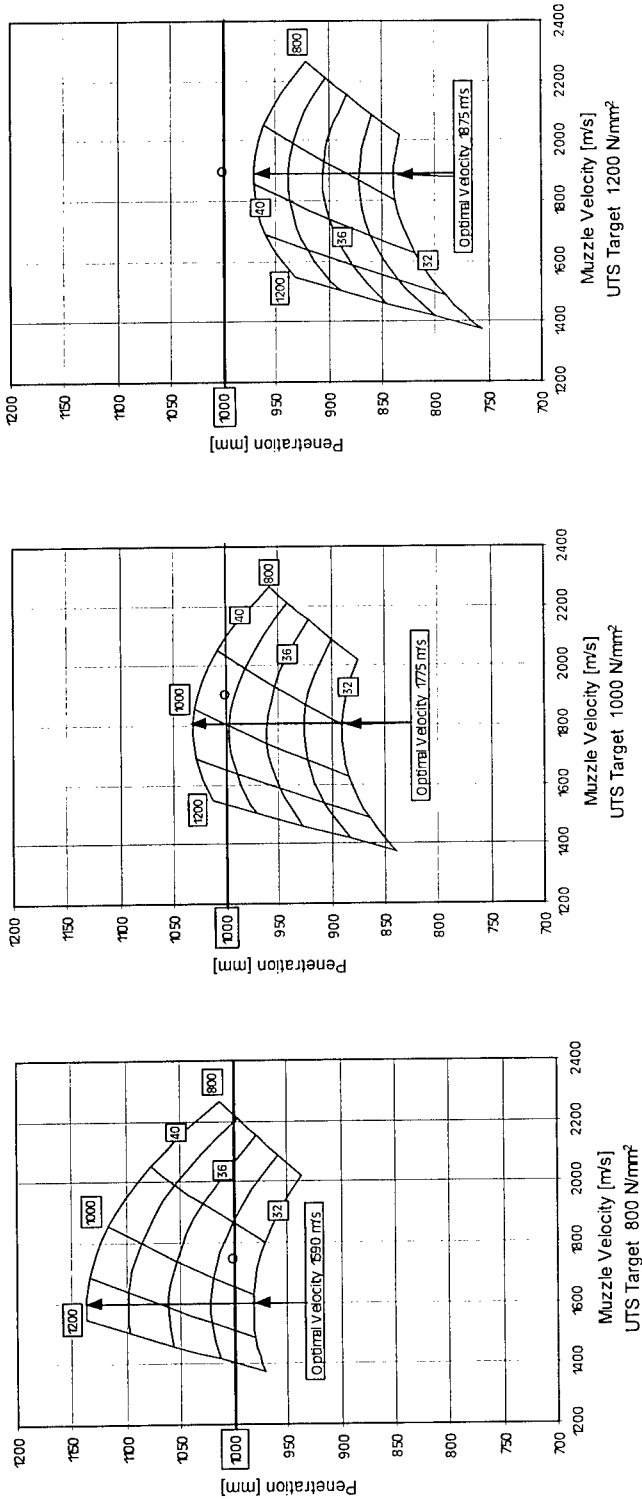


Figure 17 : 1000 mm penetration: L=950 mm, L/D=33.3

Figure 18 : 1000 mm penetration: L=950 mm, L/D=38.5

Figure 19 : 1000 mm penetration: L=1000 mm, L/D=41.8

- 364 -

**Comparison of impact craters: Full core tungsten penetrators and steel/tungsten jacketed penetrators with the same impact velocity in the same RHA plate (800 MPa UTS)**

Tungsten penetrator
Ø 22 x 680
mean crater dia = 46.1 mm

Steel/tungsten jacketed penetrator
Ø 22/17 x 680
mean crater dia = 40.75 mm

impact velocity 1850 m/s

impact velocity 1850 m/s
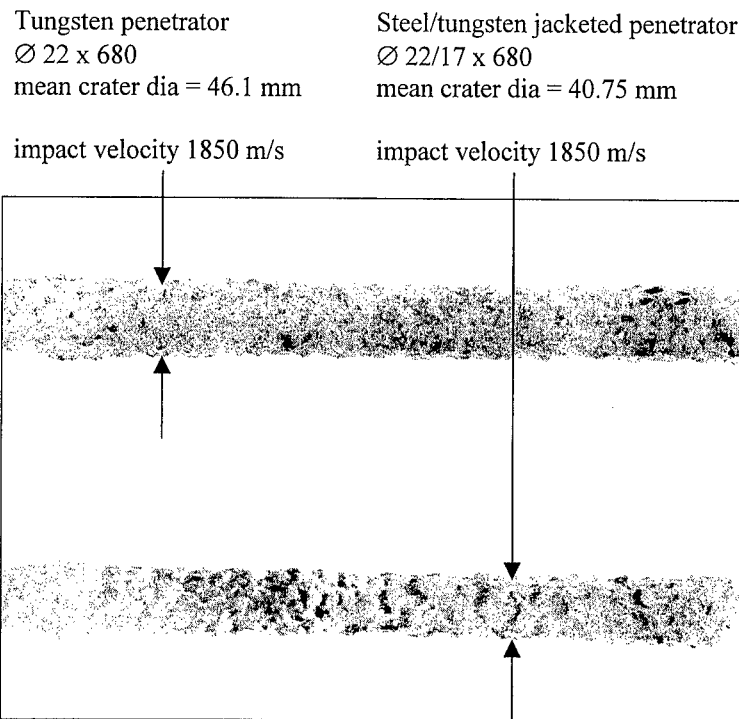


Figure 20 : Impact craters in RHA (800 MPa UTS)

# OVERVIEW ON SHAPED CHARGE

HELD M.

TDW, 86523 Schrobenhausen, Germany

*Paper not Available at the Time of Editing*

# MODELING OF SEGMENTED AND TELESCOPED ROD PROJECTILES

LAPEBIE E, CHOLLET F.

ETBS, Etablissement Technique de Bourges,
7 route de Guerry, F-18015 Bourges, France

*Paper not Available at the Time of Editing*

## ABSTRACT

The purpose of this study was to investigate the terminal ballistic performance of segmented and telescoped rods projectiles against semi-infinite targets.
Dimensional numerical simulations (code OURANOS) were performed to compare the penetration efficiency of these two types of rods projectiles with the experimental data.
The paper presents for the two concepts:
   -the description of the interaction projectiles/targets,
   -the most important parameters,
   -the performance data of different concepts,
   -the optimisation of the parameters against the semi-infinite targets,
   -the influence of the rods projectiles velocity on the terminal effects,
   -the interest for future projectiles.
The results show that the telescoped rods concept can be very interesting to improve the performance of High Velocity Projectiles.

# PENETRATION OF HIGH ASPECT RATIO PROJECTILES

MARSH A. D.[1] BESWICK M.W.[2] PROUD W. G.[3]

(1) DERA Fort Halstead, Sevenoaks, Kent TN14 7BP, UK
(2) BAE SYSTEMS, Chorley, Lancs. PR7 6AD, UK
(3) Cambridge University, Cavendish Laboratory, Cambridge, CB3 OHE, UK

**Abstract:** It is well known that for a given diameter, total penetration increases with penetrator aspect ratio, but penetration efficiency decreases. There have been several modelling but few experimental studies to date. This study aimed to correlate scale penetration results with published modelling work, and to validate the results with full calibre firings. This involved both scale and full calibre impacts at 1550 m/s. At scale, a reverse ballistic technique was used where aluminium targets impacted a static steel penetrator. Flash X-Ray was used to determine the penetrator position during penetration. A position/time graph was subsequently plotted for the penetrator nose and tail. These results were then validated by firing 120mm calibre AFSPDS projectiles at finite targets. The residual penetrator lengths were measured and compared to the scale results by putting them in non-dimensional form.

## 1   INTRODUCTION

This paper resulted from a joint DERA / BAE SYSTEMS / Cambridge University programme of experimental work undertaken to investigate the factors affecting the penetration performance of very high aspect ratio (L/D) KE penetrators. The work aimed to provide a fundamental insight into the physical processes which affect penetration performance of high L/D KE penetrators as a basis for future modelling studies.

It is well known that penetration increases with aspect ratio for a given diameter, but that efficiency, taken as penetration (P) / penetrator length (L) decreases for any given strike velocity. Several numerical modelling studies have been published on this subject, such as Anderson et al [1,2], but few experimental studies have been reported. The modelling studies have shown that the average penetration velocity decreases with increasing penetrator aspect ratio, and that this decrease in penetration velocity is the cause of the L/D effect for high aspect ratio penetrators. Other factors such as the flexure of high L/D projectiles could contribute to the L/D effect, but these effects would not be observed in two-dimensional simulations.

A series of instrumented reverse ballistic experiments were therefore carried out to obtain penetration velocity data for different L/D penetrators. The results from this work were then verified by firing full calibre (120mm ordnance) rods at finite targets. FXR was used to measure the penetrator's residual size and velocity. To align with current research work, aspect ratios of 30:1 and 40:1 were investigated at 40mm calibre and validated at full calibre using rounds of 14:1 L/D and 40:1 L/D.

## 2  EXPERIMENTAL

### 2.1  40 mm Scale Experiments

The aim of the experiment was to generate a position time curve for the front and the rear of the penetrator during the penetration process. After a review of possible measurement techniques, FXR was selected. This meant that a low-density target, aluminium, had to be used to allow radiographs of the penetration cavity to be taken. The penetrator material was chosen to match the typical Tungsten/RHA interaction in terms of strength ratio. It would have been impossible to accurately match density ratios as well using conventional alloys but it was deemed that the Steel/Aluminium ratio was close enough for the purpose of this experiment. Penetrators of constant diameter were used. The dimensions were 2.5mm diameter with lengths of 75mm and 100mm for the L/D 30:1 and L/D 40:1 respectively.

Table 1: Target and penetrator material comparison

|  | Density | Ratio | Strength | Ratio |
|---|---|---|---|---|
| Tungsten / RHA | 17.6 / 7.8 | 0.44 | 1200 / 890 | 1.35 |
| Steel /Aluminium | 7.8 / 2.8 | 0.36 | 400 / 295 | 1.35 |

To achieve consistent impacts between penetrator and target, a reverse ballistic method (RB) was selected. It was only possible to take two FXR images per shot, therefore multiple firings with differing FXR delay times were used to build up data over the entire penetration process. The trial used the DERA 40mm calibre 10m shot travel research gun. The velocity of the projectile was determined by flash radiography prior to impact; the penetrator position during penetration was measured using two FXR images taken at various times after impact. The projectile was then recovered in a soft capture unit and the final depth of penetration determined by radiography. The charge was adjusted to achieve 1550m/s strike velocity, and the barrel was evacuated to 20 millibar to minimise the blast effect ahead of the shot. This ensured the penetrator was not disturbed prior to impact.

The steel penetrator was suspended in a cradle from eight wires, four at each end. A laser and mirror system was used to accurately align the penetrator for minimum yaw conditions. Two orthogonal pairs of strain gauges were placed on the penetrator at the mid-point and towards the rear. The output from the gauges was recorded on a transient recorder. The details of the strain gauge technique and analysis can be found in the report by Proud, Flaxman and Cross [3]. The 40mm scale experimental set up is shown in figure 1.
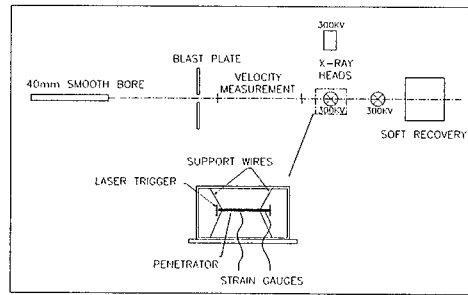
Figure 1: Reverse ballistics set up

## 2.2 120mm Firings

This trial aimed to verify the results from the reverse ballistics experiments using full calibre ammunition. Existing research rounds of L/D 14:1 and L/D 40:1 were used due to their availability. The strike velocity, measured by Doppler radar, was matched to the RB experiments at 1550 m/s. However, there were no techniques available to determine the position and velocity of the penetrators during penetration as the width of the steel targets precluded the use of FXR. A different methodology was therefore adopted.

Targets of various thickness were used to effectively 'freeze' the penetration process. The velocity, length, and condition of the residual penetrator were determined at 1.7 and 2.7m behind the target by FXR. The FXR heads were triggered from a foil on the target face with a suitable delay. The targets consisted of a combination of 600mm x 500mm RHA plates of 100 and 150 mm thickness assembled to give the required thickness. The condition and yaw of the shot prior to impact was determined using two Hadland High Speed Still Video (HSSV) cameras giving an orthogonal image of the penetrator. The 120mm experimental set up is shown in figure 2.
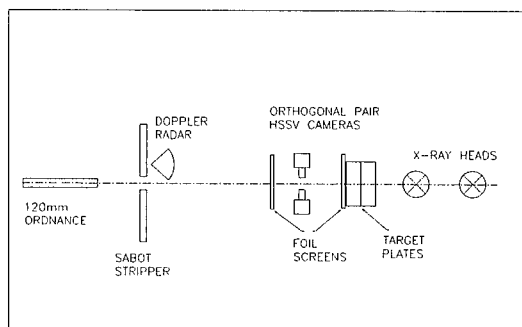


Figure 2: 120mm Experimental Set Up

# 3 RESULTS

## 3.1 40 mm Scale Experiments

24 rounds were fired in total, 12 at 30:1 L/D and 12 at 40:1 L/D. The mean penetration data is given in table 2.

Table 2: Mean Penetration Data

| Penetrator L/D | Penetration Depth mm | Efficiency P/L | Residual Length mm | Crater diameter mm |
|---|---|---|---|---|
| 30:1 | 58 | 0.77 | 5 | 6.5 |
| 40:1 | 71 | 0.71 | 8 | 6.5 |

The positions of the front and rear of the penetrators were plotted with respect to time and are shown in figures 3 and 4. The L/D 30:1 results were plotted against the modelling data published by Anderson et al [2] for comparison. The front and rear positions follow a similar trend to the modelling data, but there are some differences; i.e. the front position terminates sooner, and the rear position data is offset. These variations are due to the diameter, and therefore length difference between the penetrators used for this experiment (2.5mm diameter, 75mm long) and those for the modelling work (3mm diameter, 90mm long). The final depth of penetration is different, as would be expected, but the penetration efficiencies are markedly different; 0.77 for the experimental results compared to 0.69 for the modelling data. This difference can be attributed to the difference in density ratios for the penetrators and targets, and the difference in strike velocities which were 1550m/s for the experiment and 1500m/s for the modelling work.
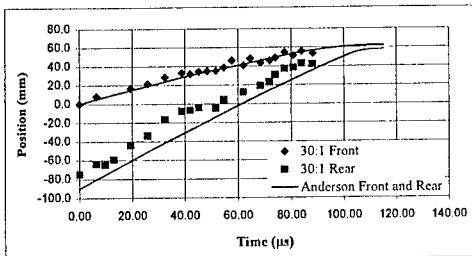


Figure 3: Position/Time graph for 30:1 penetrator
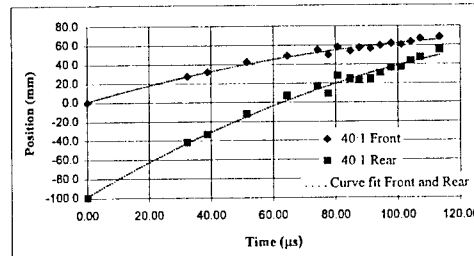


Figure 4: Position/Time graph for 40:1 penetrator

The strain gauge results gave good agreement for all firings, showing a compressive wave generated by the impact, followed by the reflected tensile wave. However, this pattern was superimposed in some cases by evidence of penetrator bending. Here, the outputs were either a difference in the measured strain between opposite gauges (indicating a semi-permanent bend), or a difference in the arrival time or phase of the wave. The latter case equated to dynamic flexure. There were 4 cases where flexure of some sort was detected by the strain gauges. These results equated to events where the penetrator was significantly bent, which was confirmed by the resultant curved shape of the penetration cavities. Figure 5 shows a radiograph of a 30:1 L/D

penetrator, 60μs after impact where the rear of the penetrator is seen to be bent. Figures 6 and 7 show penetration cavities of straight and flexed penetrators respectively.
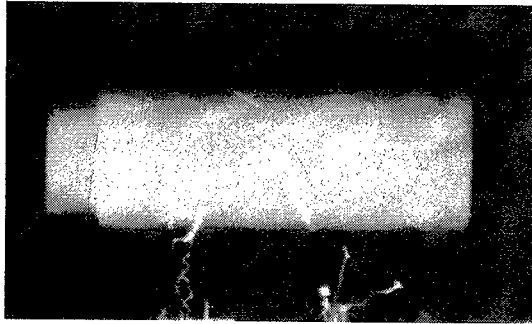


Figure 5: Radiograph of bent 30:1 L/D penetrator 60μs after impact
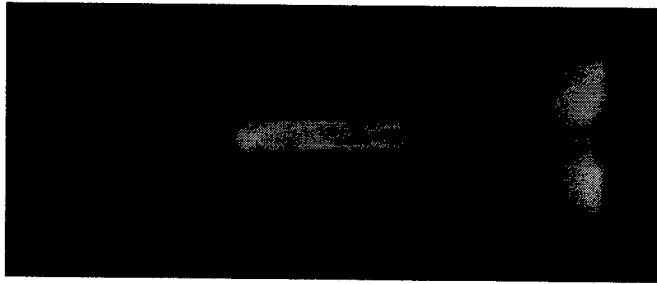


Figure 6: Radiograph of typical penetration – 40:1 L/D
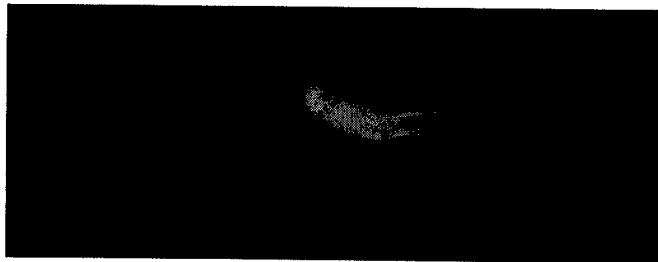


Figure 7: Radiograph of curved penetration cavity – 40:1 L/D

## 3.2    120 mm results

The four 14:1 L/D penetrators impacted the target at between 1540 and 1550m/s with less than 1° of yaw and no observed flexure. The six 40:1 L/D penetrators impacted the target at between 1530 and 1560m/s with less than 1.5° of yaw. The HSSV pictures showed flexure in all cases of between 0.3 and 1 rod diameter. This was confirmed by the multi-lobed form of the entry holes in the target front plate.
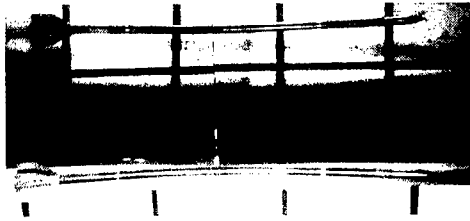
Figure 8: 40:1 L/D Penetrator highly flexed



Figure 9: Entry hole of flexed penetrator

The 14:1 penetrators produced large discrete pieces of residual penetrator, which were suitable for accurate measurement. The 40:1 penetrators however, fractured into a large number of small fragments. This precluded the measurement of a residual length except in one case. The residual fragments deviated off axis from the shot line, which considerably degraded the quality of the post penetration FXR data. In fact, due to the large number of fragments produced, only one radiograph from five rounds fired was suitable for measurement.
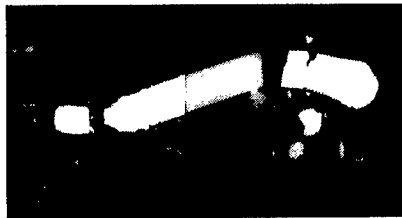


Figure 10: 14:1 L/D Post penetration radiograph
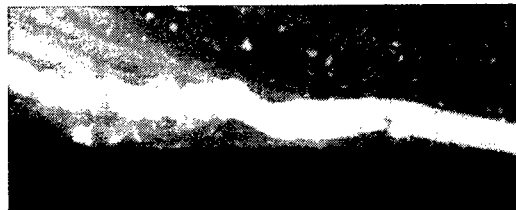


Figure 11: 40:1 L/D Post penetration radiograph

## 4 ANALYSIS

Although the data from the reverse ballistics experiment compared well with the results from Anderson et al [2], it was impossible to determine where the transition between the quasi steady state flow region and rigid body penetration occurred. Therefore, to compare the 30:1 L/D with the 40:1 L/D experiments, curve fits of the penetrator front position/time plots were differentiated to provide penetration velocity data for the quasi steady state region only. The curves of velocity against time for both aspect ratios were plotted, and were seen to overlay each other, with the 40:1 L/D curve extending further due to the increased penetrator length. The time weighted average penetration velocity was lower for the 40:1 L/D penetrators than for the 30:1 L/D penetrators which would explain the drop in penetration efficiency. However, since this was a constant diameter experiment, this effect can only be a function of penetrator length, not diameter. It must be stated that due to the inaccuracies of the experimental technique, it was not possible to determine the change in velocity caused by shock wave interactions as computed by Anderson et al [2] at the point where the elastic wave returns to the penetration interface. It is at this point where the penetration velocity curves should diverge slightly, thus leading to different decay rates in penetration for the different aspect ratio penetrators. To further investigate the L/D effect with the emphasis on D, it would have been desirable to repeat the experiment using constant length penetrators.

To compare the results from the scale and full calibre experiments, a graph showing both sets of data was plotted. The form of the graph is Lr/L against T/L, where L is the penetrator length, Lr is the residual penetrator length and T is the target thickness. The values of Lr for the scale experiment were taken as the penetrator lengths at various time intervals after impact, with the values for T being taken as the depth of penetration at these time intervals. Because the penetrators used in the 120mm calibre experiment were 'real' including noses, threads, fins etc, whereas the reverse ballistics penetrators were simple cylinders, a mass equivalence was used for accurate comparison. The methodology of Jeanquartier and Odermatt [4] was applied where the penetrator mass is equated to a cylinder of the same diameter but reduced length. The·results are plotted in figure 12 and show that the 14:1 L/D data from the 120mm experiment follows the same form as the reverse ballistics data. The decrease in efficiency with increasing L/D, is evident by the reduced residual length for a given target thickness. Unfortunately, only one result was obtained for the 40:1 L/D 120mm penetrators, but this falls on the same curve as the 40:1 L/D reverse ballistic data.
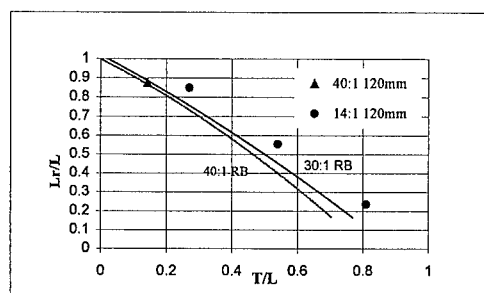


Figure 12: Reverse ballistics and 120mm calibre data non-dimensionalised

# 5 DISCUSSION

## 5.1 40 mm Reverse ballistics

The position time data from the reverse ballistics study provided a very good set of data on which to base further analysis. As can be seen from the graphs the experimental error is small and allows a curve to be fitted for the quasi steady state region of penetration. The transition from this to rigid body penetration is impossible to determine using this experimental technique. As would be expected the average total penetration of the 40:1 L/D penetrators is higher, 71mm, compared to 58mm for the 30:1 L/D penetrators. However the penetration efficiency or penetration per unit length, P/L, is lower; 0.71 compared to 0.77 for the 40:1 L/D and 30:1 L/D penetrators respectively. Similarly the residual length of the 40:1 L/D penetrator, i.e. the amount of penetrator lodged in the bottom of the cavity, is larger than that for the 30:1 L/D penetrator. The diameter of the penetration cavities is approximately the same for both penetrator types. The results from Anderson et al [2] confirm the form of the position time curves.

The strain gauge data has shown correlation between events where uneven strains were observed; i.e. compression and tension on opposite gauges. This shows that bending forces were present during some events and this was reflected in the shape of these penetration cavities. A paper by Borrmann et al [5] presented data from a modelling study on the target impact of penetrators with

L/D ratios of 15, 25 and 35:1. The study shows the deformation of the penetrator when impacting at zero yaw but with a small yaw rate. The penetrator is deformed into an 'S' shape, and produces a penetration cavity of differing diameter and a 'C' shaped curved form. In general terms this agrees with the penetration cavity profiles seen in this experimental study. Although every care was taken to ensure zero yaw impacts it cannot be assumed that this was achieved in every case. The probable maximum error when aligning the penetrator was calculated to be 0.25°. Secondly the very high L/D penetrators have comparatively low stiffness and are therefore prone to bend due to instabilities caused by the high loads being carried. Once the penetrator has deformed the resulting cavity will be similar whatever the initial reason. If angled target impacts are considered the situation is much worse as lateral forces are generated during the impact.

## 5.2 120 mm Data

The residual fragments from the 14:1 penetrators were mainly single pieces with some cracking. The residual length data followed the same trend as the reverse ballistics data as can be seen in figure 14.

The 40:1 penetrators broke up to a much greater extent, which may be due to a combination of factors, including yaw, flexure and material properties. The impact conditions contribute to penetrator break up, as a yawing or pitching penetrator will generate off-axis forces. In these experiments all impacts exhibited yaw of between 0.5° and 1.5°. The HSSV pictures showed that the rods were flexing dramatically, by up to 1 rod diameter. The residual penetrator which showed the least break-up also showed one of the smallest degrees of flexing. However there is insufficient data to establish if flexing or yaw has the greater effect. The degree of break-up is also influenced by the penetrator material, in this case a typical KE penetrator tungsten alloy which is known to be of a brittle nature.

## 5.3 Verification of 40 mm Reverse Ballistics data

The results from the 14:1 rods show the same form of curve as the reverse ballistics experiment when plotted on the non-dimensionalised graph. The expected improvement in penetration efficiency of these low L/D rods is also evident by the longer residual lengths for a given target thickness. The result of the one 120mm calibre 40:1 L/D measurement lies on the same curve as the 40:1 L/D reverse ballistics results. This also supports the accuracy of the reverse ballistics data.

The experimental results showed the expected decrease in penetration efficiency for higher aspect ratio rods. However, the results also showed that for practical shot against real targets, the higher aspect ratio penetrators may be further degraded by flexure and yaw and post impact break up. In fact, these effects may outweigh the length and diameter effects associated with high aspect ratio penetrators.

## 6 CONCLUSIONS

The reverse ballistics experiment provided detailed and high quality data which allowed the penetration process to be visualised and compared with the modelling study in the literature. The results clearly showed the increase in overall penetration along with the reduced efficiency of the

40:1 L/D penetrators, when compared to the 30:1 L/D penetrators. The reverse ballistics experiment gave clear evidence of penetrators bending and asymmetric stress wave patterns, (as indicated by the strain gauge outputs) leading to curved penetration cavities. This occurred with initially straight penetrators at normal impacts.

Post penetration measurement of the 40:1 L/D 120mm calibre penetrators proved difficult, due to the unforeseen extent of penetrator break-up. The degree of break-up of the 40:1 L/D 120mm calibre penetrators highlighted the need for further investigation into the causes of the effect. These causes include impact conditions, (flexure and yaw), and penetrator materials used for very high L/D penetrators. The limited 120mm calibre results confirmed the trends of the reverse ballistics experiment, and proved it to be suitably accurate for future use to investigate similar penetration effects.

## 7 REFERENCES

[1]     C. E. Anderson Jr, J. D. Walker, S. J. Bless, T. R. Sharron, "On the velocity dependence of the L/D effect for long rod penetrators", *Int Journal of Impact Engineering, 17, pp 13-24, (1995)*.

[2]     C. E. Anderson Jr, J. D. Walker. S. J. Bless, Y Partom, "On the L/D effect for long rod penetrators", *Int Journal of Impact Engineering, 18, pp 247-264, (1996)*.

[3]     W.G. Proud, R Flaxman, D Cross, "Strain Measurements on scaled long rod penetrators" *Draft report, Physics and Chemistry of Solids Group , Cavendish Laboratory, Cambridge University, (1999)*.

[4]     R. Jeanquartier, W. Odermatt, "Post perforation length and velocity of KE projectiles with single oblique targets", in *proceedings of the 15th International Symposium on Ballistics, Jerusalem, Israel,Vol 1, pp 245-253 , (1995)*.

[5]     M. Borrmann, I Becker, R Quidde, "Influence of small yaw rates on the penetration efficiency of long rod penetrators", in *proceedings of the 17th International Symposium on Ballistics, Midrand, South Africa, Vol. 3, pp 359-366 (1998)*.

# OPTIMAL DESIGN OF CERAMIC/METAL ADD-ON ARMOURS TO DEFEAT KINETIC ENERGY PROJECTILES

SÁNCHEZ GÁLVEZ, V.

Department of Materials Science
Polytechnic University of Madrid
Ciudad Universitaria. 28040 Madrid. Spain

**Abstract**: Ceramic/metal add-on armours are increasingly utilised for up-grading protection of Infantry Fighting Vehicles. Optimal design of ceramic/metal add-on armours can be accomplished by a clever combination of analytical, numerical and empirical methods. The paper shows the results achieved with a new analytical model developed at the Materials Science Department of the Polytechnic University of Madrid as well as results obtained with numerical simulations using the commercial AUTODYN-2D Hydrocode in which a subroutine for ceramic behaviour has been implemented. The paper shows a good agreement between analytical numerical and experimental results of both residual mass and residual velocity of kinetic energy projectiles after perforation of the add-on armour.

## 1. INTRODUCTION

The requirement for increased survivability on the battlefield will dictate that Infantry Fighting Vehicles (IFV) provide superior levels of ballistic protection [1] from 7.62 AP or 12.7 AP up to medium caliber projectiles such as the 25 APDS or kinetic energy projectiles like 25 APFSDS, with little increment of its weight.

The practice of adding plates for up-grading protection of armoured fighting lightweight vehicles started in the mid1960S by adding high hardness steel plates to the basic structure of aluminium armour. Examples include the US M2 A2 Bradley IFV and the Dardo IFV developed for the Italian Army [2].

A more radical approach to the use of a much harder material for the outer layer of vehicle armour involves the use of ceramics, which is still only about eight years old. The first example was the installation of ceramic faced add-on armour produced in Germany on the M113 and Pbv 302 carriers of the Canadian and Swedish forces in Bosnia [2]. After that, ceramic/metal add-on armours for up-grading protection of existing IFV has been increasingly utilised.

Add-on armours have many advantages. They can be transported independently to the conflict area. They can be screwed to the main skull structure very rapidly by the IFV own crew. Its repair and substitution when damaged is also very simple.

Optimal design of ceramic/metal add-on armours can be helped by a clever combination of three different approaches: analytical, numerical and empirical. Analytical modeling of the penetration process of KE projectiles into ceramic/metal armours can be used in initial stages for choice of materials and thicknesses. Numerical simulation can then be utilised for fine tuning the solution. Finally, ballistic testing is always necessary for demonstration purposes [3].

The problem for the designer of an add-on armour to protect an IFV is sketched in figure 1. Knowing the threat, the firing distance, the impact obliquity and the reduction of kinetic energy to be achieved, the design has to determine the materials and thicknesses of the armour that will give the required reduction of energy at lower weight and/or cost. At this stage, a simulation tool is called to provide results in the shortest time, inasmuch as there are numerous combinations that can solve the problem.
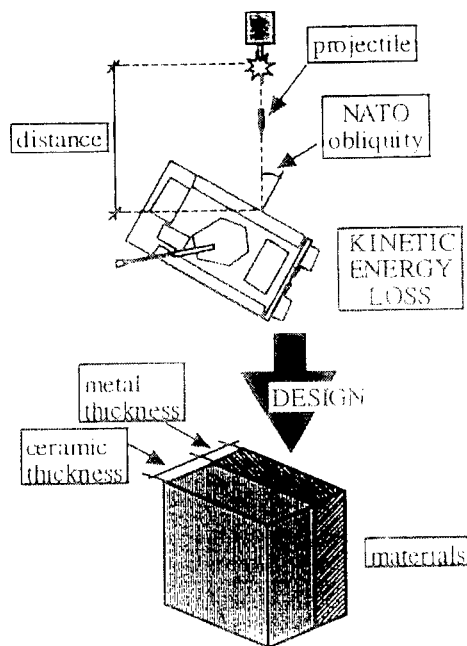


Figure 1. Factors affecting armour design

## 2. ANALYTICAL MODEL

The penetration process can be divided into three phases (see figure 2). The first one is the fragmentation stage, which occurs after the initial contact of the projectile with the armour. The penetration stage starts a few microseconds after contact, the comminuted ceramic conoid in front of the projectile distributes the load on the metal backing plate, while the projectile is being eroded by the ceramic. If the projectile perforates the ceramic, a third stage begins with the penetration into the metallic plate. If the energy of the projectile is high enough, it will perforate the add-on armour, although its residual mass and velocity being smaller than the initial ones.

A description of the process, the equations of the model and a detailed account of the physical aspects are given in a previous paper by Zaera and Sánchez Gálvez [4].
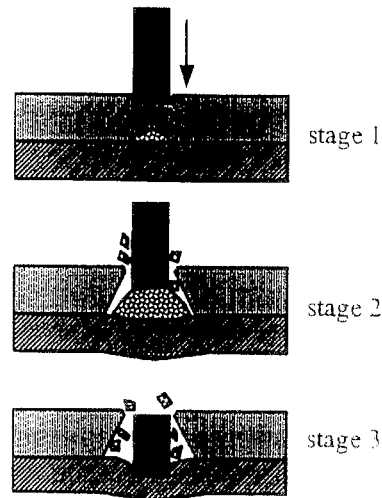
Figure 2. Stages of the penetration process

A Fortran code was programmed that allows a calculation at each time step of the eight variables that define the problem. The nucleus of the calculation was completed with a graphic user interface, programmed in Visual Basic, that simplifies data input and the interpretation of the results of the simulation.

The result is a design tool called SCARE (aSsessment of Ceramic ARmours Efficiency). In a few seconds on a personal computer, SCARE permits a simulation of the process and provides residual mass and residual velocity of the projectile after perforation of the ceramic/metal add-on armour.

With the SCARE code, graphics such as that displayed in figure 3 can be easily obtained. Knowing the threat and the materials to be used in the armour, the tool provides the combinations of ceramic/metal thicknesses that will produce the required loss of kinetic energy.
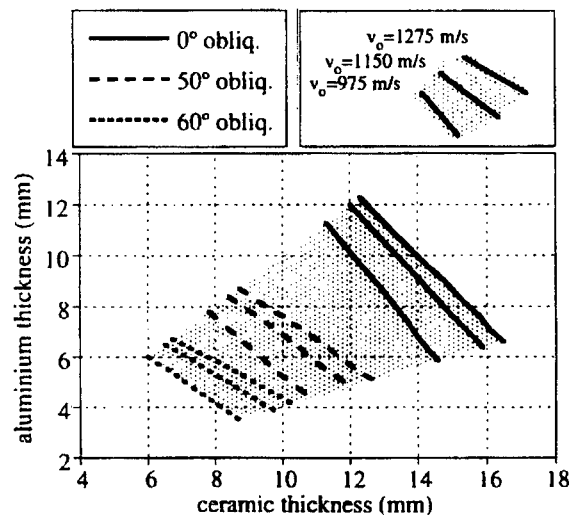
Figure 3. Design calculation of add-on protections; 25-mm APDS projectile; armour of aluminium nitride/2017-T4 aluminium alloy; kinetic energy loss, 40%

## 3. NUMERICAL SIMULATION

Numerical tools offer another approach to ballistic impact studies. Their main advantage is that they are suitable to solve a wider range of problems than any particular analytical technique. The major problem to be faced in the numerical analysis of ballistic impact on ceramic/metal add-on armour is ceramic characterisation in terms of the models that are used and the data required for then [5]. For the time being there is not yet a well settled model, valid for accurate modelling ballistic impact on ceramic armours. Damage evolution and erosion rate are parameters difficult to predict. Usually, they are simply adjusted to fit experimental data, thus loosing predictive capacity of hydrocodes.

Among the models developed to simulate the mechanical behaviour of ceramic materials subjected to impact loadings, the Johnson-Hollmquist2 model is the most widely employed [6].

At the Materials Science Department of the Polytechnic University of Madrid, a model of the behaviour of both intact and damaged ceramic has been developed. A detailed description of the model was publised before [7, 8] and its validity to simulate penetration of KE projectiles into ceramic/metal armours was demonstrated [9].

For instance, figures 4 and 5 illustrate velocity and mass histories of 20 mm APDS projectiles impacting an add-on armour with 20 mm alumina, 10 mm 5083 aluminum alloy. The figures show the results of numerical simulations using a commercial AUTODYN-2D Hydrocode [10] in which the Cortes et al. model was implemented, comparing the histories predicted by it with those predicted by J-H2 model and Mohr-Coulomb model. In all three models used, a cumulative damage parameter is included as well as an erosion strain. Experimental data of residual velocity and residual mass of 20 mm APDS projectiles after perforation of the add-on armour are also included for comparison.
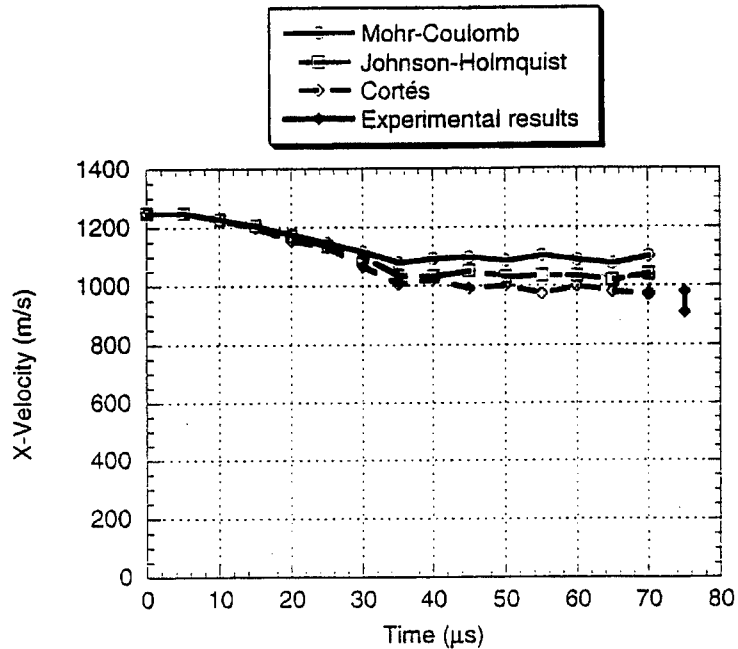
Figure 4.
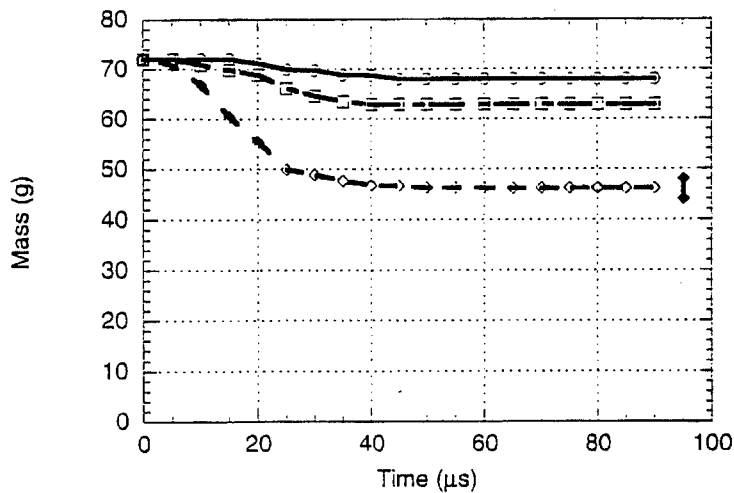


Figure 5.

## 4. EXPERIMENTS

In the framework of an EUCLID project [11] a wide ballistic test programme has been carried out. A high number of impact tests of medium caliber projectiles (20 mm, 25 mm and 30 mm APDS) against ceramic/metal add-on armours have been performed by Empresa Nacional Santa Barbara. Due to classification of fire test results only a few of then have

been published before [12] and can be shown to demonstrate the accuracy of both the analytical model and the numerical simulation.

For instance, figures 6 and 7 show some analytical results and experimental data of residual mass and residual velocity of medium caliber projectiles after perforation of ceramic metal add-on armours, whilst figures 8 and 9 summarize results obtained with the analytical programme and those obtained with the numerical hydrocode for 25 mm APDS projectile impacting ceramic/metal armours.
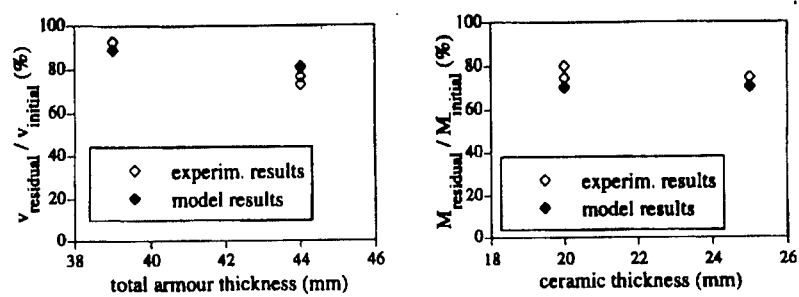


Figure 6. Analytical and experimental results of projectile residual velocities and residual masses of 25 APDS projectiles onto alumina 99.5%/aluminium alloy 6082.
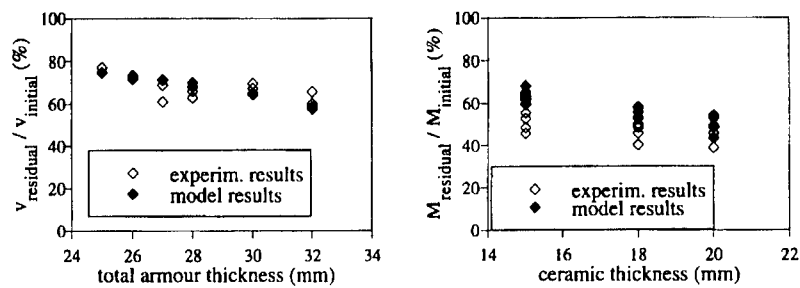


Figure 7. Analytical and experimental results of projectile residual velocities and residual masses of 20 APDS projectiles onto alumina 99.5%/aluminium alloy 6082; Impact angle: 50° NATO



**25 APDS against AlN + 7075**

-386-
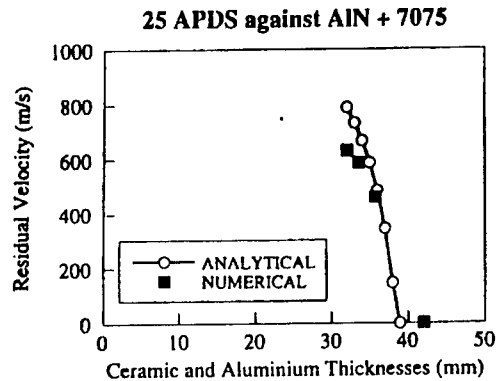
Figure 8. Residual velocity after perforation at normal impact for
AlN/Aluminium target. Ceramic thickness/Aluminium thickness = 1.



**25 APDS against AD99.5 + 7075**
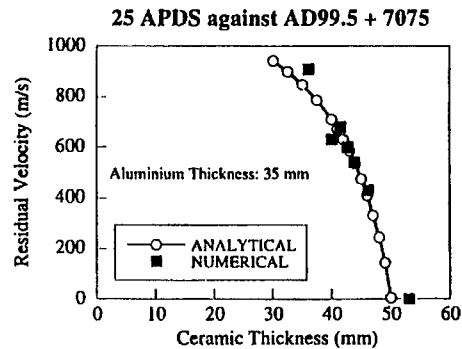
Figure 9. Residual velocity after perforation at normal impact for
AD99.5/Aluminium target. Aluminium thickness = 35 mm.

Although a few experimental data are included in this paper due to classification of
test results, both the analytical and the numerical models have been validated with hundreds
of firing tests with different projectiles, obliquity angles and ceramic/metal configurations.

## 5. CONCLUSIONS

Ceramics are widely recognised as the most effective materials to defeat modern
kinetic energy projectiles.

The practice of adding ceramic/metal plates for up-grading protection of IFV has
many advantages.

The optimal design of ceramic/metal add-on armours may be helped by the use of
analytical and numerical tools.

At the Materials Science Department of the Polytechnic University of Madrid a new
analytical model to simulate normal and oblique ballistic impact of KE projectiles into
ceramic/metal targets has been developed.

Also a new model of the behaviour of intact and damaged ceramic subjected to impact
loadings has been developed and implemented in the commercial AUTODYN 2D
Hydrocode.

A good agreement between analytical, numerical and experimental results is observed.
Therefore, the design of ceramic/metal add-on armours can be carried out by using first the
analytical tool to discriminate between different materials and thicknesses, the numerical
simulation being used after for fine tuning the solution and finally actual firing tests should
close the design by demonstrating the effectiveness of the armour.

## 6. REFERENCES

[1] T.P. Stuart, "Infantry Fighting Vehicles-Novel door concepts" in *Proc. Lightweight Armour Systems Symposium, Cranfield University*, United Kingdom (1997).

[2] R.M. Ogorkiewicz, "Lightweight armour systems. An Overview" in *Proc. Lightweight Armour Systems Symposium, Cranfield University*, United Kingdom (1997).

[3] R Zaera, V. Sánchez Gálvez, "Using an Analytical Model of Simulation in the Design of Lightweight Armours", *Simulation*, 70, 3, pp. 175-181, (1998).

[4] R Zaera, V. Sánchez Gálvez, "Analytical Modelling of Normal and Oblique Ballistic Impact on Ceramic/Metal Lightweight Armours", *Int. Journal of Impact Engineering*, 21, 3, pp. 133-148, (1998).

[5] C.J. Hayhurst, R.A. Clegg, N.J. Francis, N.K. Birnbaum, B. van den Berg, "Numerical simulation of explosive and impact loading and response using AUTODYN-3D and Auto ReaGas" in *Proc. of Asia-Pacific Conf. on Shock and Impact Loads on Structures*, Singapore, (1998).

[6] G.R. Johnson, T.J. Hollmquist, "An improved computational constitutive model for brittle materials" in *High Pressure Science and Technology*, edited by S.C. Schmidt, J.W. Shaner, G.A. Samara and M. Ross, pp. 981-984, AIP Press, Woodbury, (1994).

[7] R. Cortes, C. Navarro, M.A. Martínez, J. Rodríguez, V. Sánchez Gálvez, "Modelling of the behaviour of ceramic faced armours under impact loading" in *Proceeding of the 13 th International Symposium on Ballistics, Stockholm, Sweden*, pp. 127-134 (1992).

[8] R. Cortes, C. Navarro, M.A. Martínez, J. Rodríguez, V. Sánchez Gálvez, "Numerical modelling of normal impact on ceramic composite armours", *Int. Journal of Impact Engineering*, 12, 4, pp. 639-651, (1992).

[9] V. Sánchez Gálvez, F. Gálvez, O. Benito, "Numerical Simulation of Ballistic Impact on Ceramic/Metal add-on armours" in *Proc. 49 th ARA Meeting, Scheveningen, Netherlands*, (1998).

[10] Century Dynamics, Inc. "AUTODYN", Theory Manual (1996).

[11] C. de Benito, C. Briales, M.A. Martínez, "Ballistic Testing" EUCLID RTP 3.2 Report NMSC. 1+2, Empresa Nacional Santa Barbara, Spain, (1995).

[12] G.J. Peskes, C. Briales, M. Gualco, M. Pellegri, S. Madsen, "Optimisation of lightweight armour", *Proceedings of the 16 th International Symposium on Ballistics, San Francisco, CA*. (1996).

# TANK VULNERABILITY MODEL (PVM)
# INPUT DATA, METHODOLOGY, RESULTS AND APPLICATIONS

DORSCH H., KLUGBAUER A.                                    .

IABG, Einsteinstrasse 20, 85521 Ottobrunn, Germany

**Abstract:** The Tank Vulnerability Model (PVM = Panzer-Verwundbarkeits- Modell) was developed at IABG to simulate the vulnerability of armoured and nonarmoured army vehicles attacked by hostile weapons and to assess the weapon effectiveness against hostile army vehicles. Based on detailed target geometric descriptions on component level the penetration path of a kinetic energy penetrator, shaped charge or fragment is calculated and the damage caused is assessed with regard to kill criteria. The functional relations within the components and subsystems are represented by fault trees. Results can be provided either in a tabular or a graphical form.

## 1. INTRODUCTION

At IABG a suite of models and methodologies is available to assess the vulnerability of targets as well as the effectiveness of weapons. All models are highly sophisticated, validated where possible, and reasonably detailed to provide proper answers in the area of vulnerability and effectiveness. In case of projectiles versus armoured vehicles the IABG developed tank vulnerability model PVM (GE acronym for Panzer = Tank Verwundbarkeits- Modell) is the appropriate tool. PVM was designed to simulate the vulnerability of own armoured and nonarmoured army vehicles attacked by hostile weapons and munitions. Alternatively PVM is capable to assess the effectiveness of own weapons against hostile army vehicles like main battle tanks or personnel carriers. The main areas of application for PVM are

- assessment of protection levels and survivability of vehicles
  in service or under development

- effectiveness evaluation of anti tank weapon systems

- damage statistics to support spare part and repair part stock
  pile planning
- generation of input data for operational analyses.

The following introduction to PVM is devided in three steps

- input data
- evaluation phases
- results.

Due to the limited time the presentations will address all major issues but will not discuss technical details of methodologies and algorithms.

# 2. THE TANK VULNERABILITY MODEL PVM

## 2.1 PVM Input Data

The assessment of vulnerability and effectiveness is dependent on the interaction of a weapon delivered under certain conditions and a target. The target description (figure 1) includes the geometric model of the target combined with material information and protection levels and the functional description of the target.
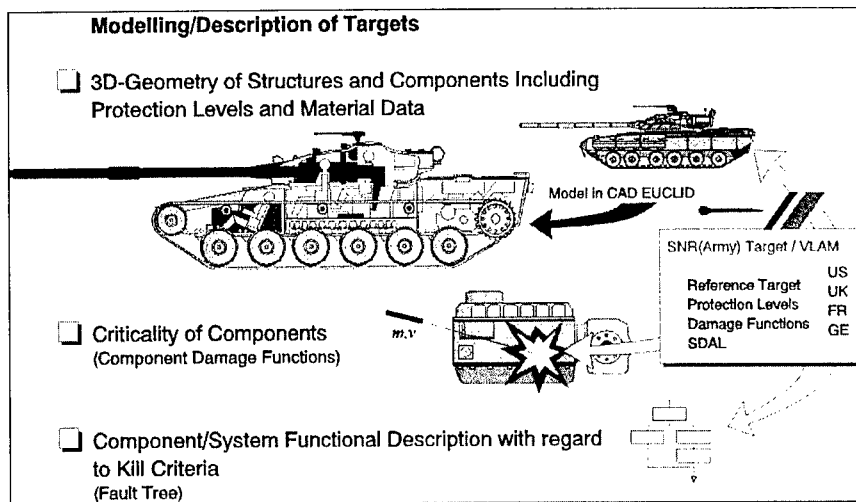


Figure 1: target description

The functional description comprises the list of critical components with regard to kill criteria and the component damage functions. Multiple vulnerabilities and redundancies on component/system level are represented by the fault tree methodology. Major target input

data are harmonized and provided by the SNR (Senior National Representatives) Target Group. Figure 2 shows a sample of the BMP2 target geometric model
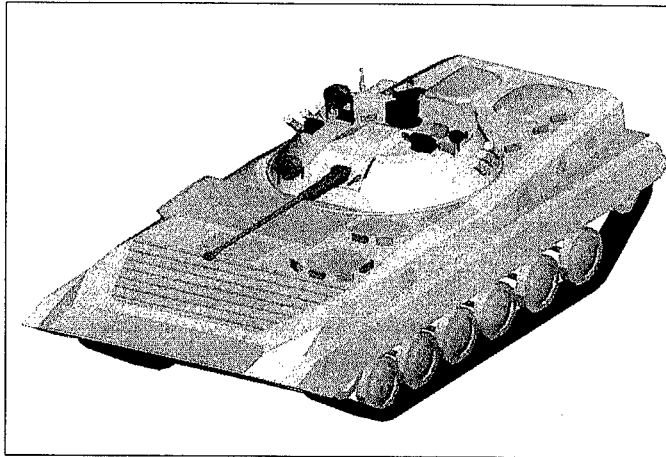


Figure 2: target sample BMP2 (Exterior)

The PVM is designed to handle three types of threats
- KE penetrators

- shaped charges

- fragments

Threats are characterized by their mass, material, dimensions and penetration performance. The delivery of the weapon is described in the scenario data as shown in figure 3



**Munitions Data :**

Kill Mechanism KE : 'Kinetic Energy'

Kill Mechanism SC : 'Shaped Charge'

Kill Mechanism HE : 'High Explosiv Fragmentation'

**Szenario Data :**

Attack Direction (Azimuth, Evelation)
Range
Exposure
Hit Accuracy
Impact Velocity
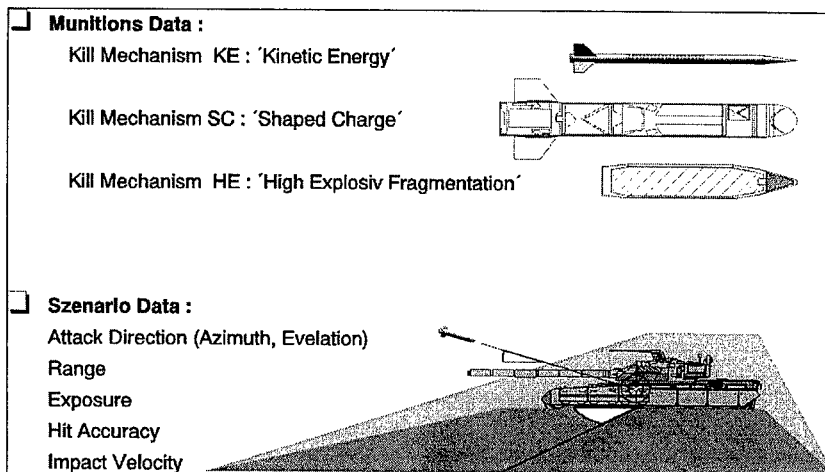
Figure 3: munitions & scenario data

Figure 4 gives an overview of the currently available target and munition combinations. Targets are split in hard targets representing main battle tanks and semi-hard targets e.g. personnel carriers and howitzers.
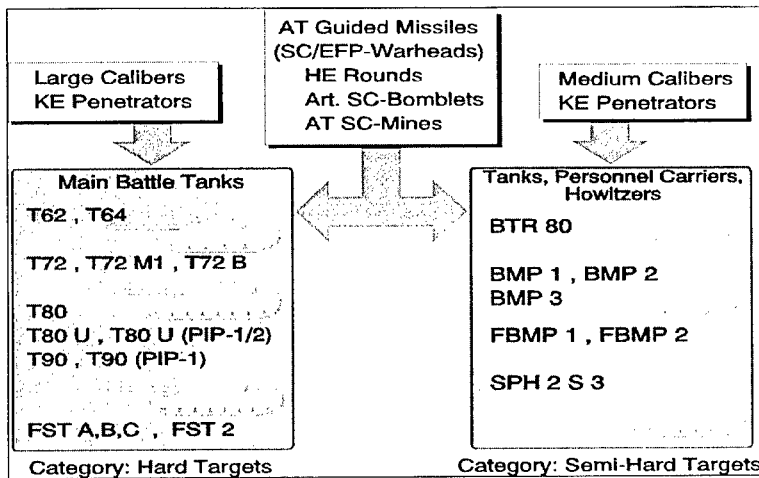


Figure 4: munition-target applications

## 2.2 Evaluation Phases

Taking the previously presented input data into account the effectiveness of a weapon is driven by its ballistic performance and its residual damage capabilities. The ballistic performance comprises the external ballistics providing the error budget with regard to aim point and CEP and the impact conditions. Based on the impact conditions the terminal ballistic behavior is simulated.
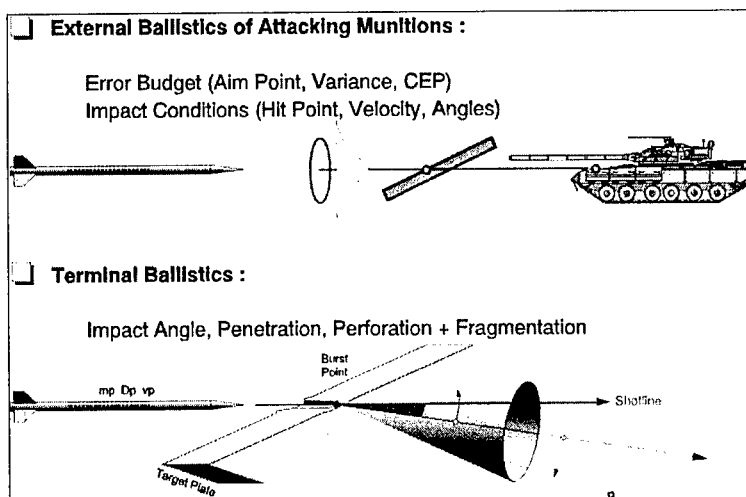


Figure 5: ballistic performance

Starting from the impact conditions the geometric shotline (line of sight) is determined in a first step. This line of sight describes the theoretical straight penetration path assuming that no mass or velocity loss would occur. Each component is then represented by its individual line of sight providing the stopping power in steel equivalent.



Figure 6: the geometric shotline (line of sight)

The penetration performance of a kinetic energy penetrator is determined by comparing the total penetration capability of the penetrator at impact to the sum of the individual line of sights expressed as stopping power of the components. If the sum of LOS gets larger than the total penetration capability the penetrator gets stuck in the last component. The sample of figure 7 shows that the penetrator cannot penetrate through component 5 the engine block. Therefore the stopping criterion is met. The penetration of a shaped charge is treated in a similar manner.



Figure 7: penetration performance
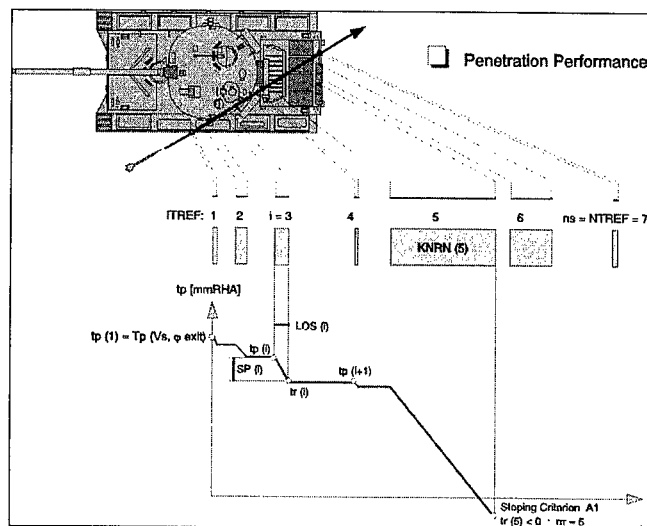
A typical phenomenon concerning the penetration of armoured vehicles by kinetic energy penetrators is the occurrence of behind armour debris often called spall (figure 8).

If suitable conditions are met

- penetrator perforated or penetrated deep enough into spall generating target structure

- there is an sufficient air gap behind armoured wall

PVM calculates the residual penetrator and the number and distribution of secondary fragments. These secondary fragments consist of broken penetrator parts, spall fragments from target material and larger but slower fragments from a circular zone at the outer edge of the perforation hole. Depending on the angle of obliquity the centerline of the cone wrapping the secondary fragments is bended towards the surface normal.
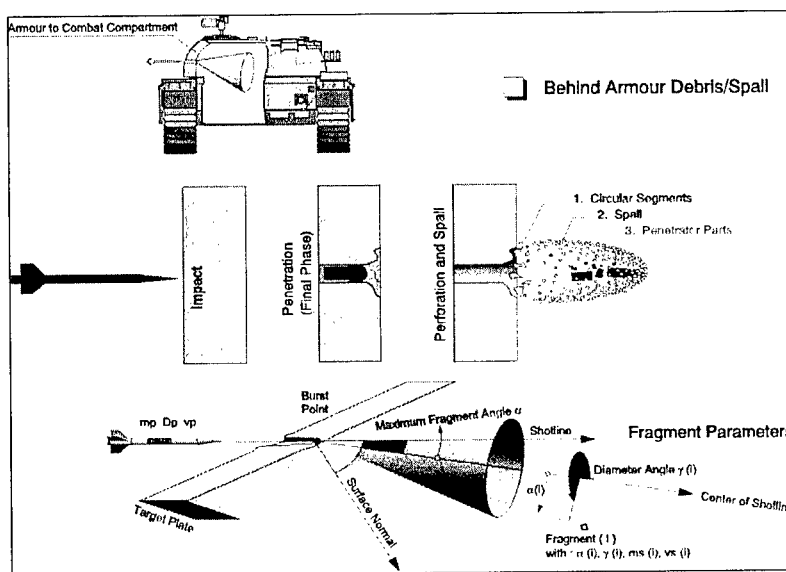


Figure 8: behind armour debris (spall)

For each critical component hit the impact mass and the current penetration capability of the primary penetrator are calculated. If applicable also the characteristics of the secondary fragments are determined. For both groups of penetrators the component kill probabilities are derived from component damage functions. The fault tree logic is then applied to calculate the component contribution to the overall target kill criterion e.g. mobility, firepower or catastrophic.

- 394 -

Figure 9: component damage assessment

The last step within the evaluation phases is the combination and contribution of the various kill criteria to the kill level to be considered. For attacking main battle tanks an appropriate kill criterion is the mission kill which is achieved by either a mobility kill or a firepower kill. Both M or F-Kill implicitly include already the K-Kill. In case of a personnel carrier the mission kill can also be achieved by a personnel kill. Figure 10 summarizes the kill logic for armoured vehicles.



Figure 10: kill logic

## 2.3 Results

The PVM analysis results represent kill probabilities for single shots, for a distribution of single shots, and for target areas. The result can be provided in graphical and/or tabular form. Figure 11 shows an illustration of single hit kill results. Each sign on the plot represents a certain kill level from hits with no damage to catastrophic kill.
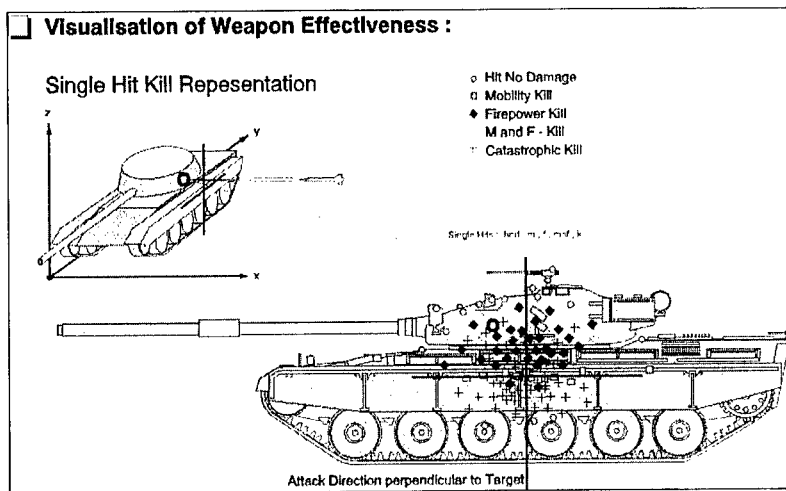


Figure 11: single impact $P_K$ values

Another possibility of graphical results are the $P_K$-plots (figure12). A grid is superimposed over the target perpendicular to the attack direction. In each grid cell a number of shots are generated and the average $P_K$-value of the cell is calculated. Different colours show the achieved mean kill probabilities ranging from 0 to 100 percent.
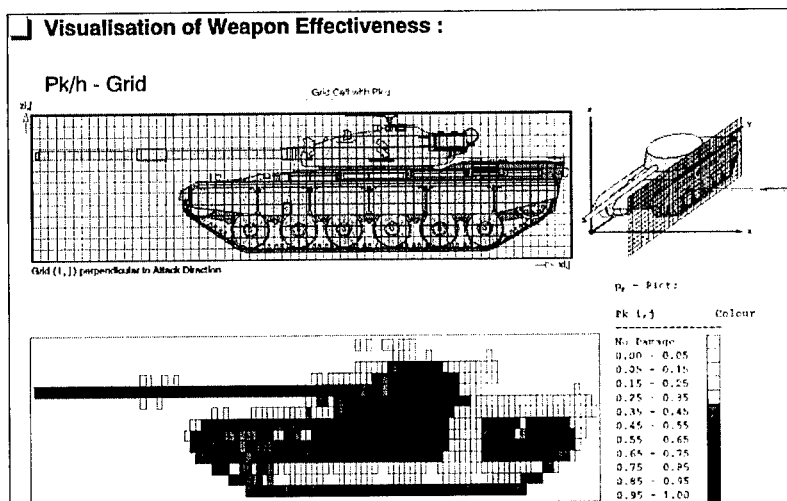


Figure 12 : $P_K$-plot

In addition to the previously demonstrated results various statistics concerning

- hit probabilities

- probabilities of perforation given a hit

- probabilities of kill given a hit

- single shot kill probabilities

- distribution of damaged components

can be provided. This information is required to support the stock pile planning with regard to spare or replacement parts.

The following figure 13 summarizes the previous statements by showing the overall structure of the tank vulnerability model PVM.
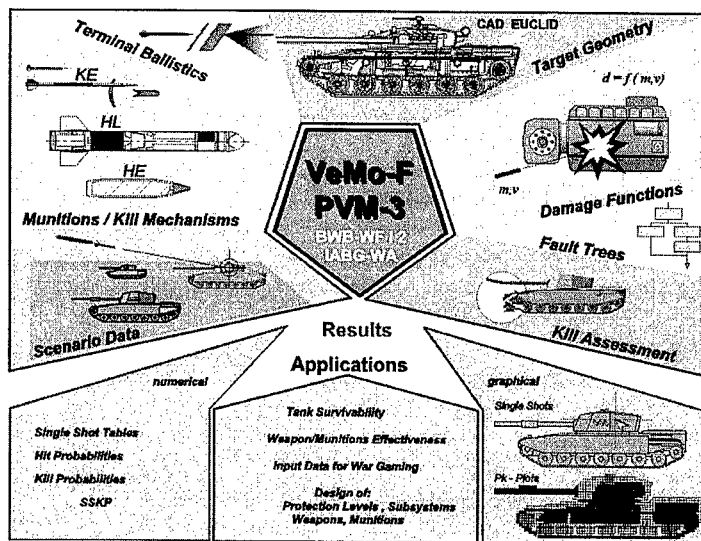


Figure 13: PVM structure

## 3. CONCLUSIONS

PVM proved over many years its applicability and efficiency concerning the evaluation of target vulnerability and weapon effectiveness. PVM passed through numerous improvement cycles and is currently available for Windows NT newly structured and programmed in FORTRAN 90 under the name VeMo-F (=Verwundbarkeitsmodell für Fahrzeuge). It fulfills the GE government requirements concerning

- level of detail for target modeling

- penetration predictions

- functional target representation

- validity of results.

Nevertheless PVM (VeMo-F) will undergo a critical design review to make the methodology part of the standardized, universal vulnerability program (UniVeMo) which is in a concept phase now under BWB WF I 2 contract.

<ISL –EFBP 2000>

# ANGLE OF ATTACK OF 7.62 MM PROJECTILES AND THEIR PERFORATION CAPABILITIES THROUGH GLASS

## HELD MANFRED

TDW, 86523 Schrobenhausen, Germany                                      .

**Abstract:** A diagnostic tool is described which allows the measurement of the angle of attack of projectiles just in front of the target. With the measurement of the angle of attack, the number of firings can be reduced respectively the target resistance can be better defined. 7.62 mm AP projectiles show mostly angles of more than 5 degrees at 10 m distance from the muzzle, which remarkably reduces the peroration performance in glass targets.

## 1. INTRODUCTION

The impact resistance of targets against hard core or AP projectiles depends, especially under zero degree arrangement, strongly from the angle of attack of the projectiles.
Just AP projectiles have the tendency that the projectile axis has an angle relative to the flight trajectory. Small inaccuracies in the geometry, respectively deviations of the mass of gravity from the symmetry axis, the vibrations of the barrel, in spite of their high spin rate introduced by the rifling in the barrel are the reason. The projectile shows a precession and nutation in connection with the air drag. To prove the target resistance against the projectile, this means no projectile perforates the target at all - even no projectiles with no angle of attack. A larger number of firings is necessary if no measuring technique is envolved. The large number of tests is necessary to be relatively sure that in the test series are also a few projectiles with no angle or at least with very small attack angles.

The requirements for a diagnostic tool are:
- defining the orthogonal angle of the projectile what means the observation of the projectile in two orthogonal plans just in front of the target
- minimum material costs per shot because the method should be used with large test series
- simple handling
- the test result of every firing should be immediately available, to be able to decide fast how the test series should go on
- simultaneously a redundant measurement of the projectile velocity
- also velocity measurements of each projectile with ripple firing
- low investment costs

## 2. TEST SET-UP

The arrangement (Fig. 1) consists of a double light barrier of the company Drello [1] with 2 m basis, a computer together with an optical display and a printer, a CCD-camera with a shutter time of 1 µs of the company PCO [2], a triggerable electronic flash unit for the illumination and finally a mirror system for the pictures of the projectiles under an orthogonal view.
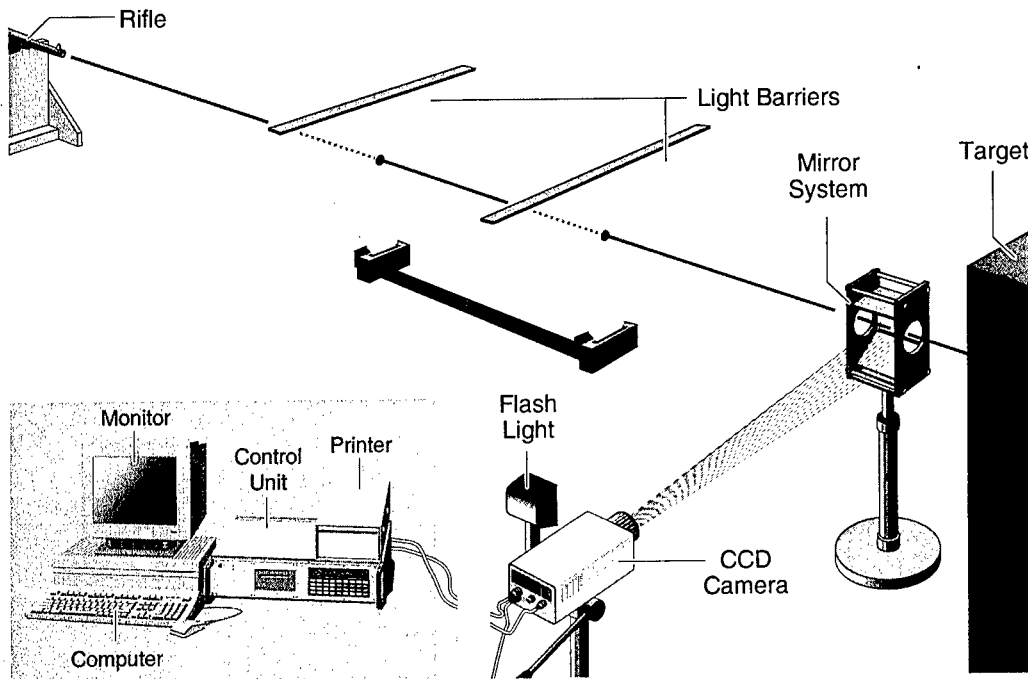


Fig. 1 : Test arrangement to define the velocity with a pair of light barriers and especially to get the angle of attack of the projectiles by orthogonal view of the projectiles with the help of a CCD-camera with a microsecond shutter time and an electronic flash, shortly before projectile impact on the target.

To get the projectile relatively large in the image field of the camera the projectile is depicted as large as possible. This means the shutter of the camera has to be triggered very exactly. This is realized by using the measured time difference between the two light barriers as a count-down equipment for triggering the flash light and the camera shutter. With this method it is achieved that the projectile is lying always in the vertical center of the picture area if the distance of the first to the second light barrier is the same as the distance from the second light barrier to the image field of the camera. The projectile is always in the center of the frame, still if the velocity of the projectile is varying remarkably.

The position of the projectiles in firing direction in the picture therefore represents a redundant velocity measurement to the one of the light barrier pair. This additional redundant and therefore very reliable velocity measurement is very useful. The block diagram of the electronic control system is shown in Fig. 2.
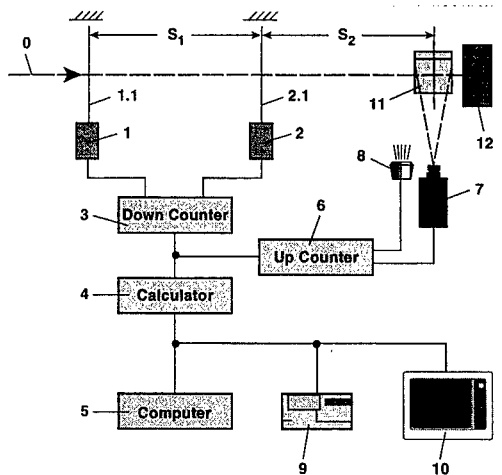


Fig. 2
Block diagram for the record of projectiles to get the angle of attack and the reduntant velocity measurement by the position of the projectile in the firing direction in the observation field of the CCD-camera.

1 and 2: pair of light barriers
3: counter to measure the time difference $\Delta t$ along the distance $s_1$
4: calculation for the velocity of the projectile ($v_p = s_1/\Delta t$)
5: computer for the data input, like test number, projectile type, target type etc.
6: up-counter for triggering the flash lamp and for opening the CCD-shutter with the exact time difference
7: CCD-camera
8: flash lamp
9: printer for the test record with the measured velocity and video printer for the achieved picture of the projectile
10: monitor to immediately view the obtained picture of the projectile
11: mirror system for the orthogonal observation of the projectile
12: target

The used CCD-camera of the company PCO <2> has "only" 756 pixels in horizontal and 580 pixels in vertical direction, not at all a great resolution. The used illumination gives also not a very high contrast. The quality in the originals is still good enough to measure the angle of attack of the projectiles with +/- 0.5 degree. This is a sufficient accuracy for this application.

## 3. TEST SERIES A

As an example an investigation with 45 firings is presented where 44 results are achieved in total. Once it was forgotten to press the reset button to distinguish the stored picture and therefore to get the reset for the camera to store a new picture. This failure was a human error.

All the presented test results are achieved with the rifle G1 caliber 7.62 mm and AP munition by FNB where the stereographic pictures of the projectiles are stored a few centimeters in front of the target but 10 m away from the muzzle of the rifle. Fig. 3 shows the first 10 investigated tests with two lines, one line gives the firing direction and the second line passes through the axis of the projectile, to analyze the angle of attack. Very noticeable is the fact that the projectiles are generally much more inclined in every upper picture, which represents the vertical observation plane, compared to each lower picture which represents the horizontal plane.
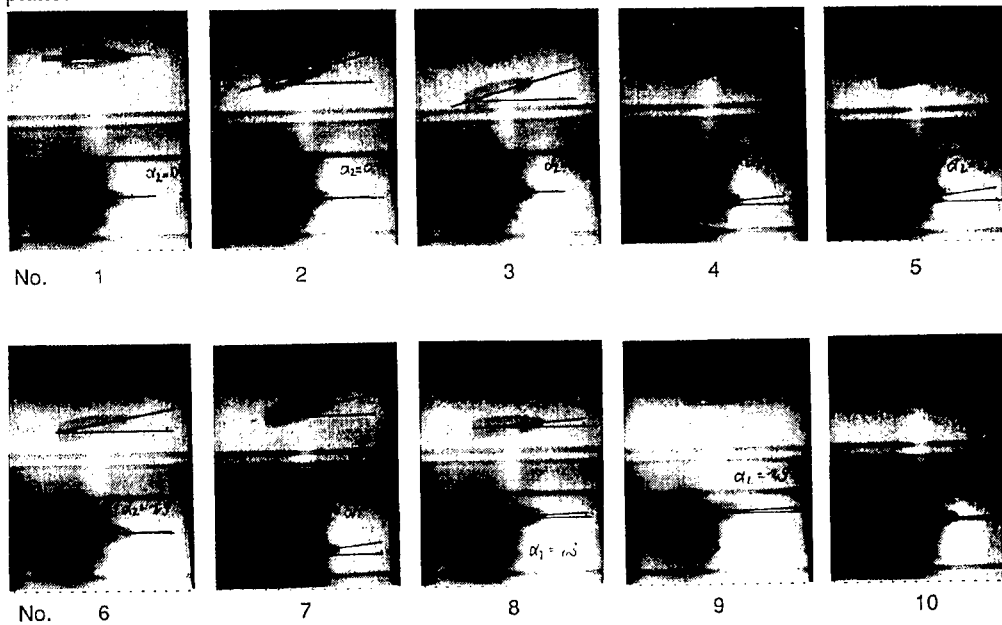


Fig. 3 : Pictures of the projectiles of the first 10 firings to define the angle of attack. The upper pictures give the vertical angles and the lower pictures the horizontal angles.

A magnified pictures of one projectile as an example is presented at Fig. 4.
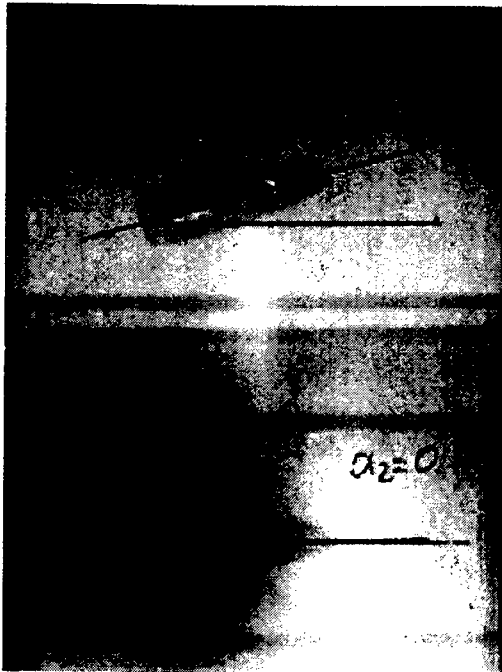
Fig. 4:
Magnification of the second picture of Fig. 3 with not very great sharpness and contrast, but the angle of the projectile can be analyzed well enough.

The following table gives the individual test numbers with the analyzed angles in vertical directions ($\alpha_V$) and horizontal plane ($\alpha_H$), and angles of attack $\varepsilon$ to the flight trajectory, calculated from the angles $\alpha_V$ and $\alpha_H$. $\varepsilon$ can be easily calculated from the two orthogonal angles $\alpha_V$ and $\alpha_H$ with the following formula (Fig. 5):
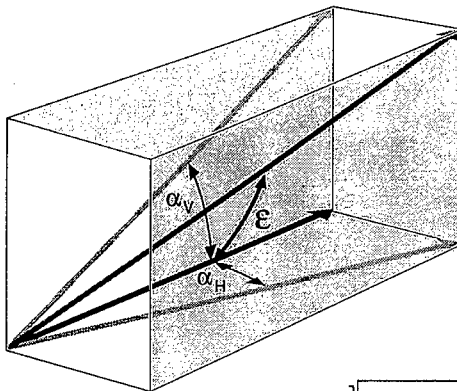


Fig. 5:
Vector diagram for defining the spatial angle or angle of attack $\varepsilon$ of the projectile with the help of the measured angles in vertical and horizontal directions, $\alpha_V$ and $\alpha_H$.

$$\varepsilon = \text{arc tan } \sqrt{\tan^2 \alpha_V + \tan^2 \alpha_H}$$

Further the table shows the measured velocities with the pair of light barriers in 6 m and 8 m distance. Also the velocities show a dispersion of around 12 m/s. The projectiles are always very well caught in the middle of the pictures. This means, the combination down-counter and up-counter is perfectly working.

Table 1 : analyzed data of 44 firings

| Firing No. | αV (Degree) | αH (Degree) | ε (Degree) | v (m/s) | Result |
|---|---|---|---|---|---|
| 1 | 1.9 | 0 | 1.9 | 831 | -- |
| 2 | 14.9 | 0 | 14.9 | 819 | -- |
| 3 | 14.0 | 0 | 14.0 | 826 | -- |
| 4 | 13.1 | 3.8 | 13.6 | 831 | -- |
| 5 | 6.1 | 6.7 | 9.0 | 832 | -- |
| 6 | 10.4 | 1.9 | 10.5 | 819 | -- |
| 7 | 10.4 | 5.7 | 11.8 | 822 | -- |
| 8 | 3.8 | 2.3 | 4.4 | 823 | ■ |
| 9 | 1.5 | 1.9 | 2.4 | 836 | -- |
| 10 | 5.7 | 1.9 | 6.0 | 833 | -- |
| 11 | 14.0 | 2.9 | 14.3 | 829 | -- |
| 12 | 7.6 | -3.8 | 8.5 | 818 | -- |
| 13 | 8.5 | 2.9 | 9.0 | 822 | -- |
| 14 | 7.6 | -2.9 | 8.1 | 834 | -- |
| 15 | 4.8 | 3.8 | 6.1 | 830 | -- |
| 16 | 14.9 | 1.5 | 15.0 | 828 | -- |
| 17 | 17.6 | 1.5 | 17.7 | 823 | -- |
| 18 | 3.8 | 3.8 | 5.4 | 828 | -- |
| 19 | 5.7 | 5.5 | 7.9 | 829 | -- |
| 20 | 2.3 | 1.0 | 2.5 | 820 | -- |
| 21 | 8.5 | 3.4 | 9.1 | 831 | -- |
| 22 | 16.7 | 5.3 | 17.4 | 826 | -- |

| Firing No. | αV (Degree) | αH (Degree) | ε (Degree) | v (m/s) | Result |
|---|---|---|---|---|---|
| 23 | 10.4 | 2.3 | 10.6 | 827 | -- |
| 24 | 9.5 | 1.0 | 9.6 | 830 | -- |
| 25 | 8.5 | 0 | 8.5 | 828 | -- |
| 26 | 9.5 | 2.3 | 9.8 | 826 | -- |
| 27 | 2.3 | 1.9 | 3.0 | 825 | ■ |
| 28 | 4.8 | 3.8 | 6.1 | 833 | -- |
| 29 | 14.0 | -9.5 | 16.7 | 829 | -- |
| 30 | 1.9 | 2.3 | 3.0 | 828 | ■ |
| 31 | 11.3 | 0 | 11.3 | 814 | -- |
| 32 | 13.1 | -6.7 | 14.6 | 829 | -- |
| 33 | 6.7 | 5.7 | 8.8 | 830 | -- |
| 34 | 14.9 | 0 | 14.9 | 815 | -- |
| 35 | 15.8 | 0 | 15.8 | 814 | -- |
| 36 | 1.0 | 1.5 | 1.8 | 832 | ■ |
| 37 | 17.0 | 1.5 | 17.1 | 814 | -- |
| 38 | 10.4 | 3.8 | 11.0 | 834 | -- |
| 39 | 13.1 | 2.3 | 13.3 | 820 | + * |
| 40 | 14.0 | 1.9 | 14.1 | 828 | -- |
| 41 | 20.1 | 0 | 20.1 | 815 | -- |
| 42 | 1.9 | 8.5 | 8.7 | 825 | -- |
| 43 | 5.7 | 5.7 | 8.0 | 819 | -- |
| 44 | 6.7 | 1.9 | 6.9 | 829 | + * |

▓ < 5°     * **Predamaged Target (Multiple Hits)**

The values $\alpha_v$ and $\alpha_H$ are graphically represented in Fig. 6 in the sequence of the test firings, whereby the $\alpha_v$ values are always higher than the $\alpha_H$ values. The projectiles are pointing only upwards in the vertical plan. Only in four of the 44 tests, this means only 10 %, the $\alpha_H$ values are in an opposite direction.
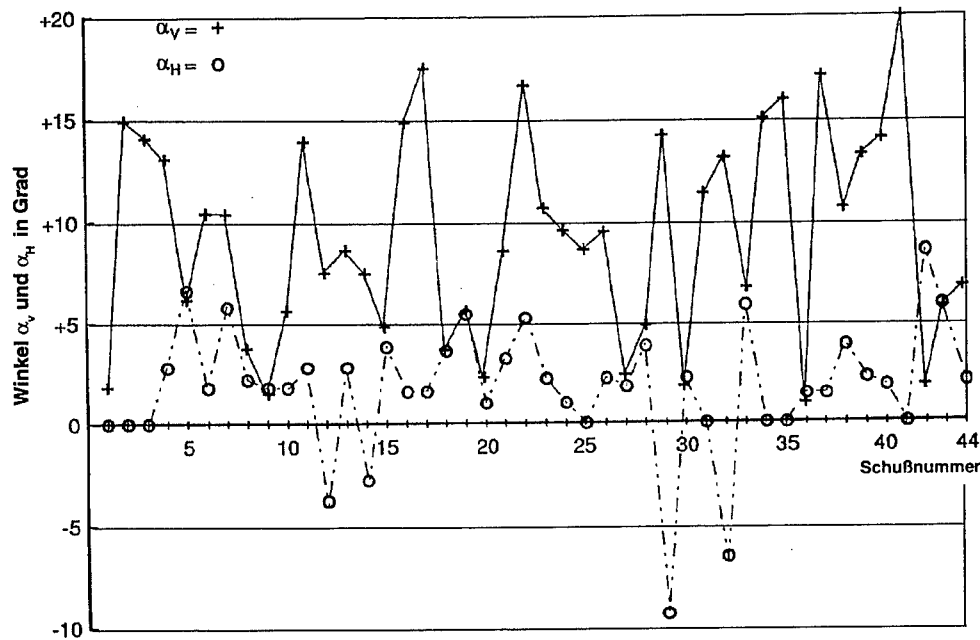


Fig. 6 : Vertical and horizontal angles $\alpha_v$ and $\alpha_H$ of a test series with 44 shots

- 404 -

The spatial angle or the angle of attack ε are presented in the sequence of the tests in Fig. 7. The figures 6 and 7 do not give any trend with the number of firings. It looks like a statistical behaviour.
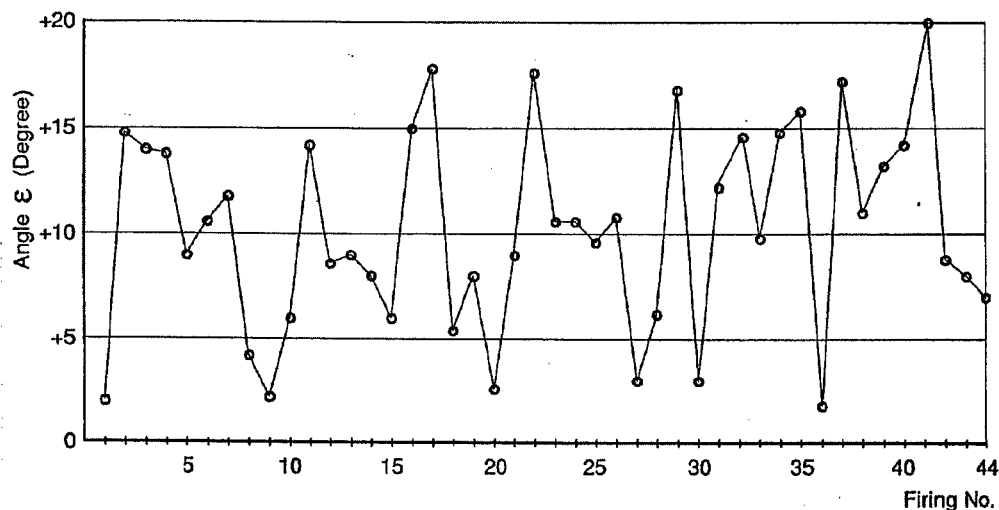


Fig. 7 : Angles of attack ε, calculated from $\alpha_V$ and $\alpha_H$, in the sequence of the 44 shots

The angles of attack ε are grouped in Fig. 8 as a function of increasing values. The angle of attack has practically a linear distribution between 1° and 18° for the 44 tests. Also from this diagram can be easily seen which percentage of the tests has an angle smaller than or equal to 3°, which is in this example 13 % respectively that the 50 % value is around 9°.
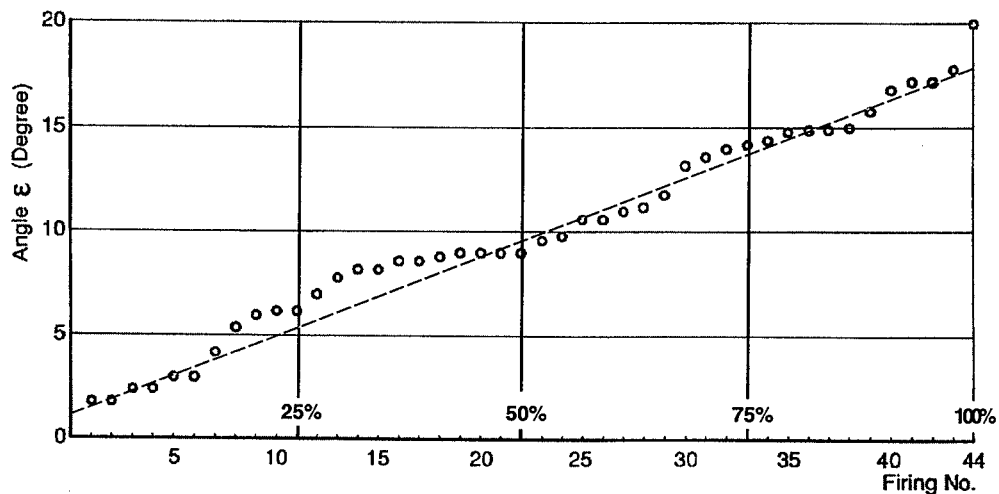


Fig. 8    The 44 shots give nearly a linear angle distribution from 1° to 18°.

This test series A against the investigated special target shows that the angle of attack has to be smaller than 5° to achieve a perforation. This seems to be a necessary but not sufficient condition for the tested target. Then, the table shows that from 7 firings against always a "new" target with an angle smaller than 5° four have perforated, although three shots have not achieved this. Projectiles with attack angles larger than 5° have always been stopped by a new or not predamaged target.

## 4. TEST SERIES B

The second test series was fired AP-projectiles against laminated glass targets of 75 mm thickness and 138,4 kg/m² area weight.

The table 2 gives the individual test results of the vertical and horizontal deviations or the space angle - angle of attack - and the Fig. 9, 10 and 11 give the achieved pictures. Only one test has given no pictures from these 18 firings.

This test series summarize again the advantage of the measurements. From 7 firings with angle of attacks equal or less than 4° have made 6 times perforations and only once not. All the other eleven firings with angles larger than 4° have given no perforations.

These results show clearly, that without detailed diagnostic of the angle of attack a firm statement cannot be made on the target resistance, especially when the tests are near the critical limit of no perforation or perforation.

Table 2 : Glass Laminated Target, 75 mm thick, 138.4 kg/m² areal weight

**Target:  Glass Laminated,  75 mm thick,  138.4 kg/m² areal weight**

| Serie | Firing No. | $\alpha_V$ [Degree] | $\alpha_H$ [Degree] | $\varepsilon$ [Degree] | v [m/s] | Result |
|---|---|---|---|---|---|---|
| 8.1 | 1 | 1 | 0 | ⊡ 1 | 817 | ⊡ - |
|  | 2 | 7 | 0 | 7 | 816 | - |
|  | 3 | 6 | 0 | 6 | 817 | - |
|  | 4 | 13 | 0 | 13 | 822 | - |
|  | 5 | 5 | 0 | 5 | 815 | - |
|  | 6 | 1 | -3 | 3.2 | 822 | + |
| 8.2 | 1 | 10 | 2 | 10.2 | 810 | - |
|  | 2 | 1 | 1 | 7.1 | 824 | - |
|  | 3 | 2 | 1 | 2.2 | 819 | + |
|  | 4 | 11 | -5 | 12.0 | 822 | - |
|  | 5 | 4 | 0 | 4.0 | 815 | + |
|  | 6 | 3 | 0 | 3.0 | 822 | + |
| 8.3 | 1 | 11 | -7 | 13.0 | 829 | - |
|  | 2 | 10 | -10 | 14.1 | 824 | - |
|  | 3 | 9 | -3 | 9.5 | 811 | - |
|  | 4 | - | - | - | 810 | + |
|  | 5 | 15 | 0 | 15.0 | 827 | - |
|  | 6 | 3 | 0 | 3.0 | 826 | + |

ε = 1°          −          ε = 7°          −          ε = 6°          ' −

ε = 13°          −          ε = 5°          —          ε = 3°          +
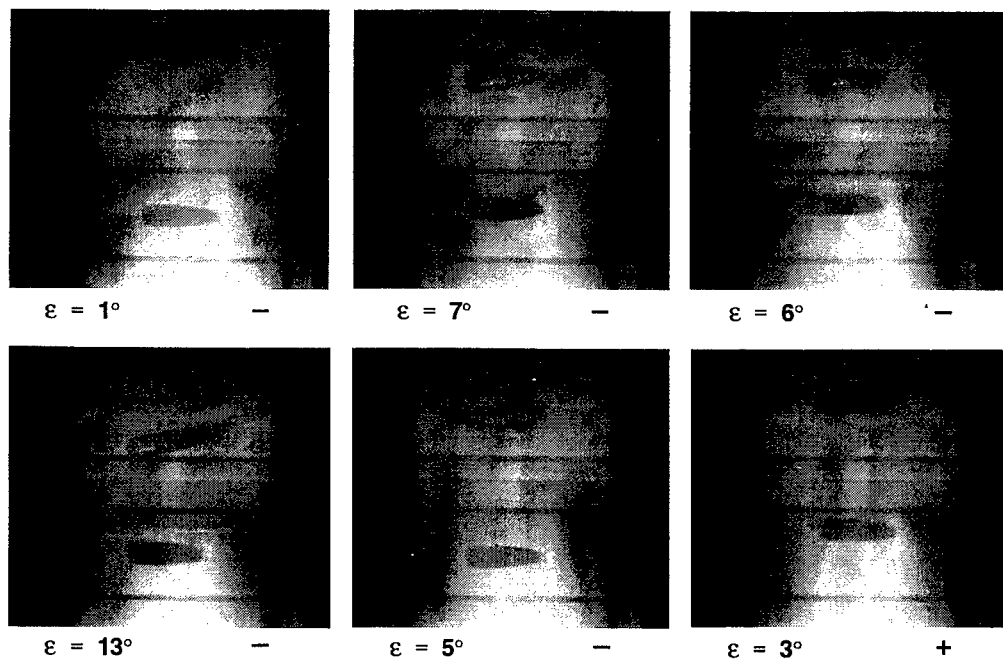
Fig. 9     Test serie B 8.1



ε = 10.2°          −          ε = 7.1°          −          ε = 2.2°          +

ε = 12°          −          ε = 4°          +          ε = 3°          +
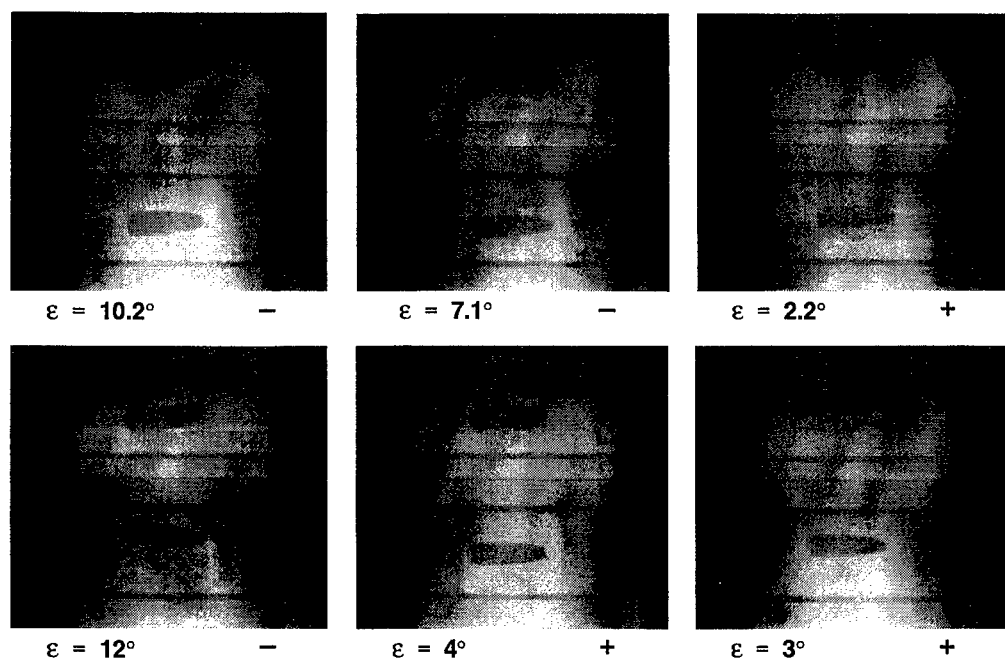
Fig. 10   Test serie B 8.2
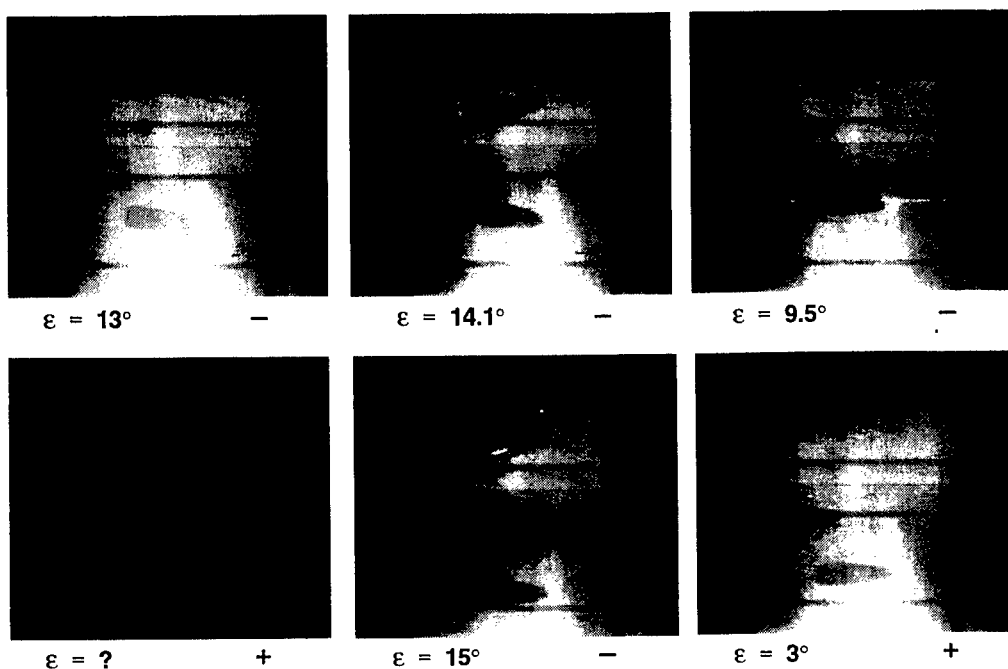
Fig. 11   Test serie C 8.3

## 5. SUMMARY

Only with the diagnostic of the angle of attack of the projectiles, especially if the weapon system together with the used projectile type leads to relatively large angles of attack, the number of firings can be reduced to achieve a well defined test result concerning to the protection capability of a target arrangement.

With the presented test equipment the material costs are very low for catching and printing the pictures. These diagnostic methods need not a special trained technician. The simple operations can be done by any working person on the test stand, from the test manager to the rifle man.

## 6. REFERENCES

[1]   Company: Drello Ing. Paul Drewell GmbH & Co KG, Max-Regerstr. 35a, 41179Mönchengladbach (Rheindahlen), Germany

[2]   Company: PCO Computer Optics GmbH. Ludwigsplatz 4, 93309 Kelheim, Germany

# AN EMPIRICAL EQUATION FOR PENETRATION DEPTH OF PRIMARY FRAGMENTS INTO CONVENTIONAL AND STEEL FIBER REINFORCED CONCRETE TARGETS, BASED ON EXPERIMENTS WITH FRAGMENTATION GENERATED BY THE HE 81 MORTAR GRENADE.

CANOVAS M.F.[1], PAMIES R.G.[2], SIMON DEL POTRO R.[3], ALMANSA E.M.[1]

[1] Department of Civil Engineering and Construction, ETSICCP, Universidad Politécnica de Madrid, Spain
[2] Department of Weapons, ESPOL-DIENADE-MADOC, Ministry of Defence, Spain
[3] Department of Fuids and Heat, LABINGE, , Ministry of Defence, Spain.

**Abstract:** In this paper we present results from seven test series of HE 81 mortar grenade against concrete targets with compressive strength up to 40 MPa. The goal of the testing program was to develop validated penetration formulas on conventional concrete and steel fibers reinforced concrete, in order to choose those that provide superior performance to withstand the penetration effects generated by the HE 81

mortar grenade with additional characteristic of a reduced cost and weight.

Several experimental penetration formulas for concrete are compared where it accounts for the parameters that characterize this material, such as the characteristic compression strength, quantity of steel fibers and for the parameters that characterize the fragmentation. Finally, the experiment data showed good agreement with known formulas for conventional concrete and permitted the adjustment of a new penetration formula for primary fragments generated by munitions about 81 mm caliber.

## 1. PRIMARY FRAGMENTS AND PENETRATION

Significant damage from accidental explosions can be caused by the impact of fragments, which were generated during the explosions and hurled against structures or other receivers at high speed.

Upon detonation of a mortar grenade, the casing breaks up into fragments with varying weights and velocities. The destructive potential of these fragments is a function of their shapes, materials, momentum and kinetic energy distributions.

The initial velocity and size of the fragments are functions of the thickness of the metal container, the shape of the explosive as a whole (spherical, cylindrical, prismatic), and

the sections of the container (ends, middle, etc.) from which the fragments will depend greatly on the metallographic history of the casing, its physical condition (such as dents, grooves, bends, or internal cracks or flaws), and the condition of joints, most notably welded joints.

Since a primary fragment can generally be categorized as a high-speed particle with a mass much smaller than the barrier or target which it strikes, the interaction between local penetration effects and any overall structural response engendered by the impact is not significant. The main effects of impact are penetration of the missile into the barrier wall and perforation wherein the missile completely penetrates the barriers and exits with a known residual velocity.

In the development of a design equation for the concrete penetration, the "massive penetration" case is considered, i.e., the following conditions are assumed: (a) the angles of obliquity and yaw are zero, i.a., both the path of the missile and the missile axis are coincident with the normal to the surface of the barrier; (b) the missile is an inert non-deforming armor piercing (AP) projectile or fragment; (c) the barrier or wall constitutes a uniform target of sufficient thickness that this finite dimension does not influence the penetration, i.a., it is assumed initially that back-face phenomena do not influence penetration; and (d) the loss of fragment mass during penetration is not considered.

Under these conditions, the penetration (Reference [1]) is obtained:

For X ≤ 2d:

$$X = 2\sqrt{kND}\, d^{1,1} V_S^{0,9} \qquad (1)$$

and for X > 2d:

$$X = kNDd^{1,2} V_S^{1,8} + d \qquad (2)$$

Where:
k concrete penetrability constant

$$k = \frac{6,53}{\sqrt{f_c'}}$$

f'c: concrete compressive strength (ksi)
N= nose shape factor
D= caliber density of the fragment

$$W_f/d^3 \quad (lb/in3)$$

Wf= fragment weight (lb)
d= diameter of the fragment (in)

Vs= striking velocity (kft/s)
X= depth of penetration (in)
f'c= concrete compressive strength (ksi)

The procedure of Reference [3] calculates the penetration depth into massive concrete by using the following two equations.

*for* $X \leq 1.4\ Wf^{1/3}$

$$X = \frac{0.95\, Wf^{\,0.37}\, V_S^{\,0.9}}{f'^{\,0.25}_C} \qquad (3)$$

*for* $X > 1.4\ Wf^{1/3}$

$$X = \frac{0.32\, Wf^{\,0.4}\, V_S^{\,01.8}}{f'^{\,0.25}_C} + 0.4 Wf^{\,0.33} \qquad (4)$$

The general expression for the maximum penetration X (Reference [2]) of an armor-piercing fragment, is derived in terms of the fragment weight $Wf$ and striking velocity Vs:

$$X = 0.162\,(10^{-5})\, Wf^{\,0.4} V_S^{\,1.8} \qquad (5)$$

Equation (5) is based on a concrete compression strength f'c equal to 5,000 psi. Maximum penetrations of fragments in concrete of other strengths may be obtained by multiplying the value of X of equation (5) by the square root of the ratio of 5,000 psi to the compressive strength of the concrete in question.

## 2. EXPERIMENTAL PROGRAM

The tests comprised a total number of seven, six of them were field tests and the other was a raw arena test.
The raw test was performed in accordance to NM-2276-EMA in order to determine the number, and size of fragments and the homogeneity of the fragmentation.
The field test was carried out with a HE 81 mm M51B mortar round surrounded by twelve concrete slabs.
The grenade was located 1.5 m above the ground and the concrete slabs were secured to the structures (Fig 1 & 2) leaving the center of each slab at 1.5 m above the ground.

Two distances from the grenade to the slabs were selected: 5 m (one test) and 2.8 m (five tests).

Sensors were located on the front face of each slab in order to measure the average velocity of the fragments on impact.

Concrete has been designed to have 40 and 25 MPa of compressive strength at 28 days, without fibers, in cylindrical $\phi$15x30 cm specimen.

Cement is an I-45 type in accordance with Spanish cement reception standard (RC-92). Siliceous sand and crushed siliceous gravel has been used throughout this work such as to have an overall aggregate size of 10 mm

Other tests performed on 40 MPa concrete grave us the following results:

-splitting tensile test: 3.18 MPa at 28 days.

-third point loading flexural test: 4.87 MPa at 28 days

-Elastic modulus: 27.72 GPa at 28 days.

From 25 MPa concrete only elastic modulus are available, being its value about 25.1 GPa.

Concrete mix proportions in weight used in this work are, for 40 MPa concrete: 1: 0.45: 2.49: 2.16, and for 25 MPa concrete: 1: 0.61: 2.89: 2.49, both expressed as weight-to-cement-weight ratios in the form: cement: water: sand: gravel. A high range superplastifier was used too.

Round steel crimped-end fibers were used in this work. Its aspect ratio, defines, as the fiber length divided by an equivalent fiber diameter, was equal to 100. To facilitate handling and mixing, fibers have been collated with water-soluble glue into bundles of 10-30 fibers.

Fibers have been added to concrete into three proportions: 0, 80 and 120 kg/m³, which imply 0, 1 and 1.5 in volume percentage. Moreover, plate thickness was varied from 8 to 16 cm. The other dimensions of plates were 100x100 cm.

## 3. EXPERIMENTAL FORMULA

By adjustment of experimental data from penetrations on conventional concrete slabs without fiber, has been obtained the following formula:

$$X = \frac{0.38 \, W_f^{0.59} V_f^{2.1}}{f_c^{0.25}} \quad (6)$$

where:

f'c: concrete compressive strength (ksi)
$W_f$= fragment weight (lb)
Vs= striking velocity (kft/s)
X= depth of penetration (in)
f'c= concrete compressive strength (ksi)

This formula expressed in units S.I. takes the following form:

$$X = \frac{1.3187 \cdot 10^{-5} W_f^{0.59} V_f^{2.1}}{f_c^{0.25}} \qquad (7)$$

where : f'c (MPa); $W_f$(g); Vs (m/s); X (mm)

## 4. TEST RESULTS

Figure 3 shows the following features found on 25 MPa characteristic compression strength concrete:
      -Experimental results are in good agreement with equations (3) and (4) (TM5-885-1 formula in Ref [3]).
      -a 50% increase in characteristic compression strength concrete reduces penetration in about 7%.
Figure 4 shows the following features found on 40 MPa characteristic compression strength concrete:
      -for small fragments, the formula in eq. (3) and (4) slightly overpredicts the depth of penetration.
      -on the other hand for fragments of weight over 2 grams gives penetration depth values below those found experimentally.

Figure 5 shows the comparison of the new formula (6) with the known formulas TM5-1300, Picatinny and TM5-855-1, as well as its degree of conformity with the experimental values.

## 5. SUMMARY AND CONCLUSIONS

Fiber dosification over 80 kg/m$^3$ does not produce substantial increase in the concrete resistance to penetration.
. For an optimal dosification it is recommended to increase the characteristic compression strength concrete yields average penetration reductions of around 10%.
Concrete with characteristic compression strength over 40 MPa do not show a substantial increase in their penetration resistance.
According to the experimental results, formula TM5-885-1 is recommended for predicting the penetration depths for primary fragmentation. This confirm the fact that, since the usual formulae consistently give larger penetration depth values than those found experimentally, the actual penetration resistance of the current conventional concrete is better than expected.
According to the experimental results, the new formula is recommended for predicting the penetration depths in concrete slabs without fibers for primary fragmentation generated by munitions about 81 mm caliber

## 6. REFERENCES

(1)   "Primary Fragment Characteristics and Penetration of Steel, Concrete
      and Other Materials". *Picatinny Arsenal, Technical Report, Draft.*

(2)   "Structures to Resist the Effects of Accidental Explosions" TM5-1300".
      *Department of the Army. (USA) (1969)*

(3)   "Fundamentals of Protective Design for Conventional Weapons".
      *TM5-855-1. Department of the Army. US Army Corps of Engineers. (1984)*

(4)   Canovas, M.F.; Pamies, R. G.; Simon del Potro, J.R.; Almansa, E.M. "Impact
      effects on the primary fragmentation generated by the HE81 mortar grenade on
      conventional concrete and steel fibers reinforced concrete". *Proc. of the Third
      International Conference "Structures Under Shock and Impact".*
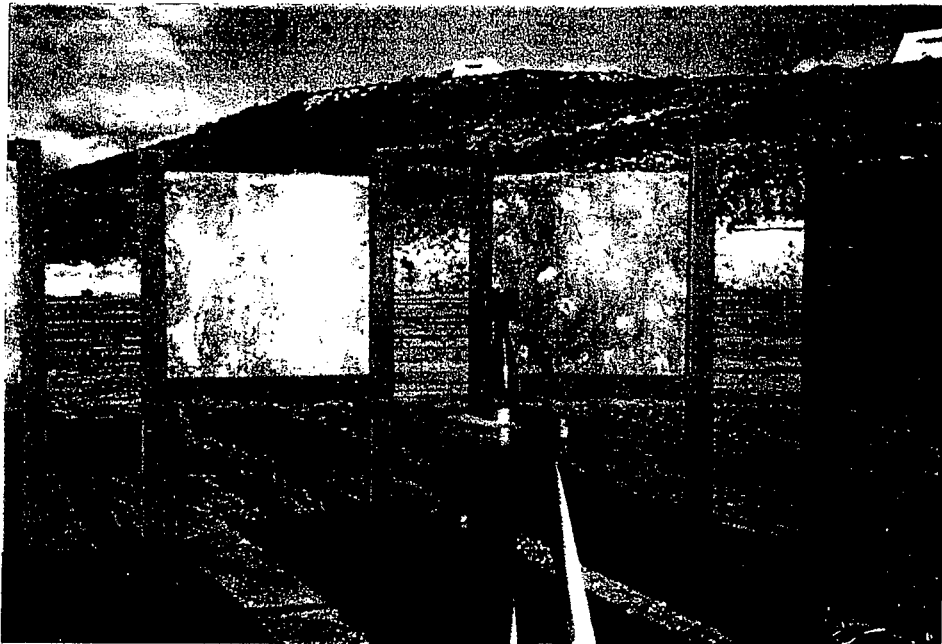
FIGURE 1
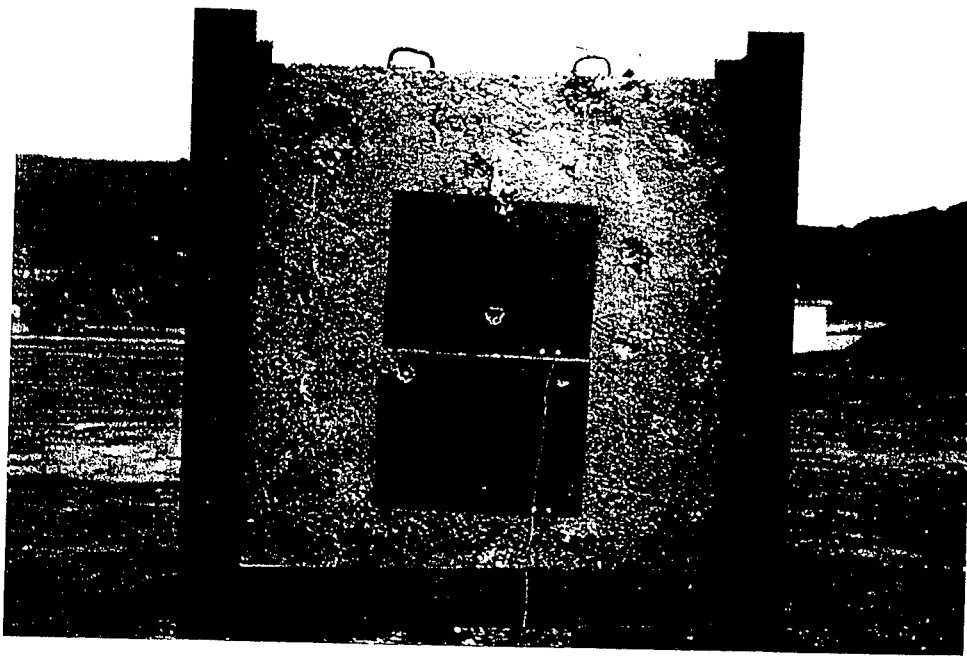
FIGURE 2

## MORTAR ROUND HE 81 mm M51B
### FRAGMENTS PENETRATION IN CONCRETE 25 MPa
#### EFFECT OF STEEL FIBER

PENETRATION (mm)



FRAGMENT WEIGHT (g)

STRIKING VELOCITY 1190,8 m/s
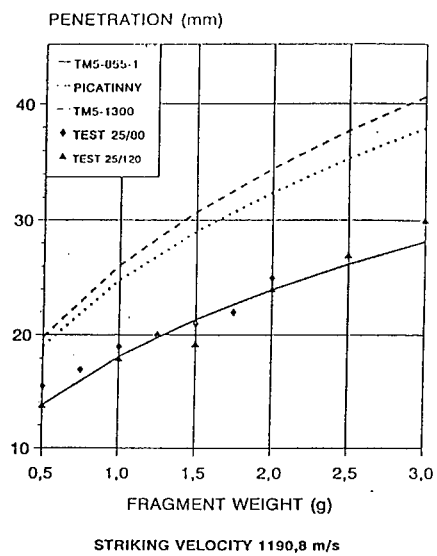
FIGURE 3


## MORTAR ROUND HE 81 mm M51B
### FRAGMENTS PENETRATION IN CONCRETE 40 MPa
#### EFFECT OF STEEL FIBER

PENETRATION (mm)



FRAGMENT WEIGHT (g)

STRIKING VELOCITY 1190,8 m/s
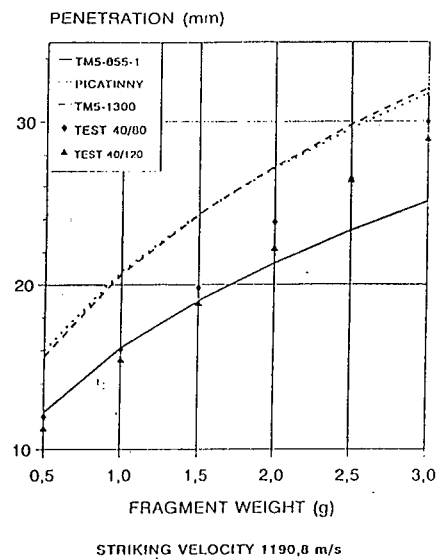
FIGURE 4

# MORTAR ROUND HE 81 mm M51B
# FRAGMENTS PENETRATION IN CONCRETE 25 MPa

PENETRATION FORMULA

PENETRATION (mm)



FRAGMENT WEIGHT (g)

◆ TM5-1300  + PICATINNY  ✿ TM5-855  ■ TEST  ✳ FORMULA
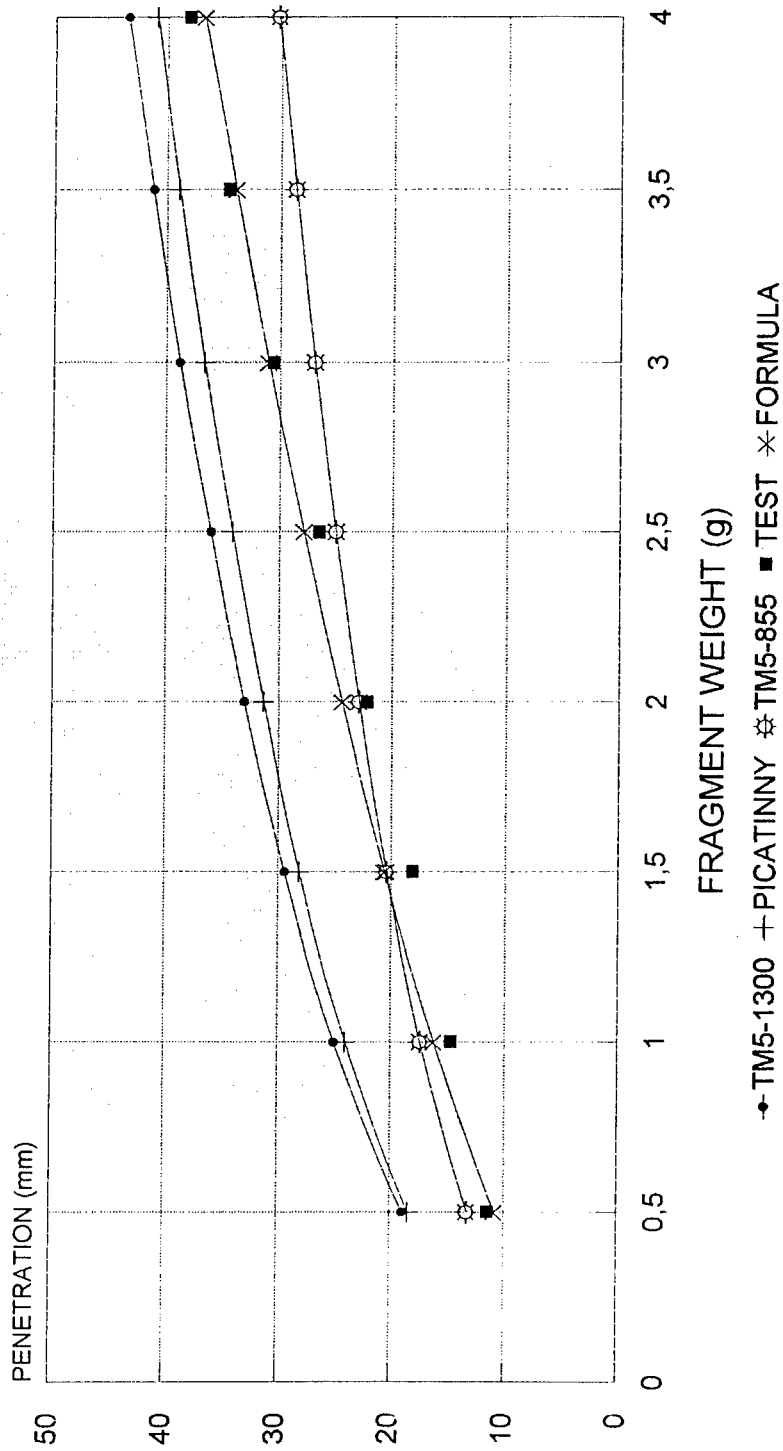
STRIKING VELOCITY 1161 m/s

Figure 5

- 418 -

# A Engineering Model For The Penetration Of Spherical Projectile Into Rubber Matrice Composite Target

SHENG YONG[(1)]      YOU ZHONG[(1)]

(1) Department of engineering scienceUniversity of Oxford Parks Road, OxfordOX1 3PJ  U.K.
Tel: 44-1865-273175Fax: 44-1865-283301email: yong.sheng@eng.ox.ac.uk

**Abstract:**By means of the combination of the spherical and cylindrical hole enlargement theories, a simplified engineering formulation is developed in this paper for predicting depth of the penetration of hypervelocity spherical projectile to the semi-infinite target. The model is simple and efficient to predict the penetration depth, and cost much fewer computer time, and the numerical tests show the same accuracy as the two-dimensional finite element method.

## INTRODUCTION

The penetration into a semi-infinite target is a two dimension symmetry problem. There were many different methods to simulate the process of penetration. Empirical models[9] were generated by fitting the experimental data, but they cost great time and money to test every particular variations. In recent years, numerical techniques[10] ( finite element method and finite difference method) were introduced to analyse the hypervelocity impact. Numerical methods have strong abilities to deal with large scale and complicated problems, and are more flexible and adjustable than empirical ways, but they are still hard to show the complete mechanical concepts in the penetration and the mechanism of the penetration. Thus, several theoretically simplified models [1-8]were developed to present simple and efficient calculations and clear physical process. In this paper by assuming that the deceleration forces are only from the ratial resistance force in expansion  of the spherical cavity, the two dimensional symmetry hypervelocity impact problem can be simplified to a quasi-one-dimension hole enlargement equivalent problem( see fig.1). then use the spherical cavity theory to derive the dynamic equations in the target and modify the kinematic solution by the cylindrical cavity expansion method.
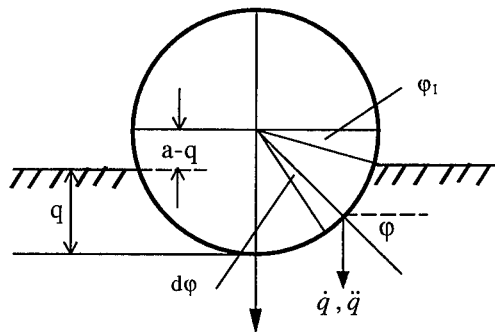


Figure.1 quasi-one dimensional penetration

## SIMPLIFICATION ASSUMPTIONS

Except the quasi-one dimensional assumption above mentioned, there are other additional assumptions to simplify the question to an engineering problem and to solve the differential equations easily.

I. The projectile is assumed to be a rigid body and has no deformation in penetration.

II. The constant velocity of compressive wave is always faster than the velocity of projectile compacts the target.

III. The volume strain in the target after the wave front increases from original value $\rho_0$ to a constant value $\rho$, which is called locked volume strain.

IV. The friction between on the interface of the projectile and the target is ignored.

V. The elastic deformation in target which is far smaller than plastic one is also neglected, the target material is always in plastic deformed and satisfy the Tresca yield criteria.

## FORMULATIONS

According to the above assumptions, the spherical cavity expansion in the target can be mathematically expressed in the a set of differential equations which generated from the conservation laws of momentum, mass, accompanied with the material state equations.
Motion equation of a spherical element:

$$\rho\ddot{u} = -\frac{\partial\sigma_r}{\partial R} - \frac{2(\sigma_r - \sigma_\theta)}{R} \qquad (1)$$

where $\rho$ is the constant density behind wave front, $\sigma_r$, $\sigma_\theta$ are the ratial and tangential stress, when time t=0, radius r increase by u(r,t) to R(r,t)

$$R(r,t)=r+u(r,t) \qquad (2)$$
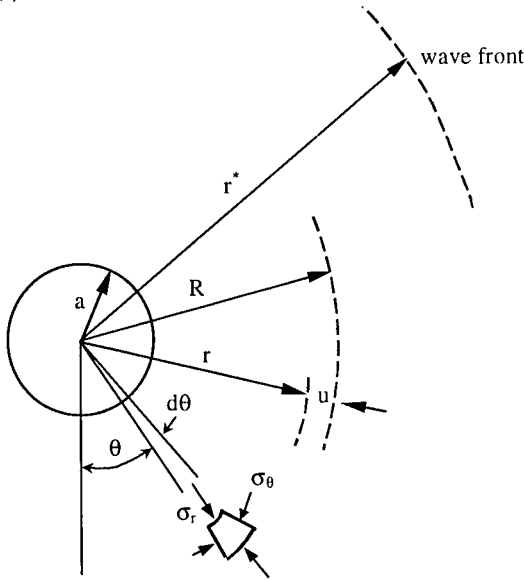


Figure.2 Nomenclature of the parameter symbols

Consistency equation:

$$\rho R^2 dR = \rho_0 r^2 dr \qquad (3)$$

By applying this equation, the eq(1) can have differentiation with respect to the lagrange coordinate r instead of the current coordinate R.
The compressibility equation

$$\eta = \frac{dV}{dV_0} \qquad \eta = 1 - \frac{\rho_0}{\rho} \tag{4}$$

Tresca yield criteria:

$$\sigma_r - \sigma_\theta = Y \tag{5}$$

Substituting (2), (3), (5) into (1) gives:

$$\rho_0 \frac{r^2}{R^2} \ddot{R} = -\frac{\partial \sigma_r}{\partial r} - \frac{2Y}{R} \cdot \frac{\partial R}{\partial r} \tag{6}$$

Spatial integration from r=0,r of (3) yields:

$$R^3 - a^3 = (1 - \eta)r^3 \tag{7}$$

in which a is the current cavity radius.

Then the velocity of the target particle can be obtained by temporal differentiation of above equation:

$$\dot{u} = \dot{R} = \frac{a^2 \dot{a}}{R^2} \tag{8}$$

and the acceleration of the target particle can be expressed as:

$$\ddot{R} = \left[ \frac{(a^2 \dot{a})^{\bullet}}{R^2} - 2 \frac{(a^2 \dot{a})^2}{R^5} \right] \tag{9}$$

In order to integrate the equation(6) , the jump condition at the wave front should be introduced to derive the relations between stress field of the particle and the cavity motion. Firstly the spatial integration of the left side of (6) gives:

$$\rho_0 \int_0^{r^*} \rho_0 \frac{r^2}{R^2} \ddot{R} dr = \rho (a^2 \dot{a})^{\bullet} \int_a^{r^*} \frac{dR}{R^2} - 2\rho (a^2 \dot{a})^2 \int_a^{r^*} \frac{dR}{R^5}$$

$$= \rho (a^2 \dot{a})^{\bullet} \left( \frac{1}{a} - \frac{1}{r^*} \right) - \frac{1}{2} \rho (a^2 \dot{a})^2 \left( \frac{1}{a^4} - \frac{1}{r^{*4}} \right) \tag{10}$$

At the wave front, u(r*,t)=0, with R=r*, from Eq.(7) the particle coordinate can be replaced by the cavity surface motion:

$$r^* = \frac{a}{\eta^{1/3}} \tag{11}$$

The jump conditions at the wave front are:

$$\eta \dot{r}^* = \dot{u}^* \qquad \sigma_r^* = \rho_0 \dot{r}^* \dot{u}^* \tag{12}$$

in which the wave propagation velocity can be written as:

$$\dot{u}^* = a^2 \dot{a} / r^{*2} \tag{13}$$

than the stress at the wave front which needed in the integration of the motion equation can be obtained from above two equations:

$$\sigma_r^* = \rho_0 (a^2 \dot{a})^2 / \eta r^{*4} \tag{14}$$

Based on the spherical cavity theory, integration of the motion equation by introducing the jump condition at the wave front, the relations between the pressure at the surface of hole element ( also assumed to be decelerate force), motion of the target and the hole surface, strength of target material and the locked density after wave front can be obtained:

$$p(t) = 2Y \ln \frac{1}{\eta^{1/3}} + \rho_0 \frac{1-\eta^{1/3}}{1-\eta} \frac{\left(a^2 \dot{a}\right)^{\bullet}}{a} + \rho_0 [\eta^{1/3} - \frac{1-\eta^{4/3}}{2(1-\eta)}] \dot{a}^2 \qquad (15)$$

Then introducing the kinematical modification of cylindrical cavity theory, which assume the velocity and the deceleration $(\dot{q}, \ddot{q})$ of the projectile have the relationship with the hole motion$(\dot{a}, \ddot{a})$:

$$\dot{a} = \dot{q} \sin \varphi \qquad (16)$$
$$\ddot{a} = \ddot{q} \sin \varphi$$

Substituting these relations to above equation of deceleration forces gives:

$$p(t) = 2Y \ln \frac{1}{\eta^{1/3}} + \rho_0 \frac{1-\eta^{1/3}}{1-\eta} a \ddot{q} \sin \phi + \rho_0 \frac{3 - 2\eta^{1/3} - \eta^{4/3}}{2(1-\eta)} (\dot{q} \sin \phi)^2 \qquad (17)$$

The whole deceleration force can be obtained by integrating above equation:

$$-p_z = -\int_{\varphi_1}^{\pi/2} 2\pi a^2 p(t) \sin \varphi \cos \varphi d\varphi \qquad (18)$$

$$\text{where:} \quad \varphi_1 = \begin{cases} \sin^{-1} \dfrac{R-q}{R} & when \quad q \le a \\ 0 & when \quad q \ge a \end{cases} \qquad (19)$$

By solving the motion equation of the projectile:

$$m\ddot{q} = p_d \qquad (20)$$

one can get the parameters of, $q(t), \dot{q}(t), \ddot{q}(t)$ at different time step, and finally obtain the penetration depth when $\dot{q}(t)$ equal 0. Some numerical tests comparing with the experimental data adopted from [7] are illustrated in table[1] and figures3,4 below.

| Missile No.& Velocity | Weight | Radius | $\sqrt{\frac{1}{2}mV^2 / \pi r^2}$ | Penetration Depth (Experiments) | Penetration Depth (Analytical) |
|---|---|---|---|---|---|
| 1-305 | 2.51 | 0.98 | 196.20 | 1.6 | 1.23 |
| 1-430 | 2.51 | 0.98 | 277.20 | 2.0 | 1.98 |
| 1-440 | 2.51 | 0.98 | 283.64 | 2.1 | 2.04 |
| 1-550 | 2.51 | 0.98 | 364.55 | 2.3 | 2.78 |
| 1-630 | 2.51 | 0.98 | 406.12 | 2.8 | 3.34 |
| 1-647 | 2.51 | 0.98 | 417.08 | 3.3 | 3.46 |
| 2-170 | 3.01 | 0.94 | 125.59 | 1.4 | 0.7 |
| 2-541 | 3.01 | 0.94 | 398.41 | 3.71 | 3.38 |
| 2-667 | 3.01 | 0.94 | 491.20 | 4.15 | 4.51 |
| 2-117 | 6.25 | 1.38 | 84.54 | 1.25 | 0.64 |
| 2-422 | 6.25 | 1.38 | 304.93 | 2.50 | 2.48 |
| 2-424 | 6.25 | 1.38 | 306.38 | 3.13 | 2.49 |

Table[1] Penetration data

In the experiments, the material data are also introduced in the analytical method, where $\rho_0$=2.5g/cm$^3$, $\eta$=0.01, Y=3500psi.

## ANALYSIS AND CONCLUSION
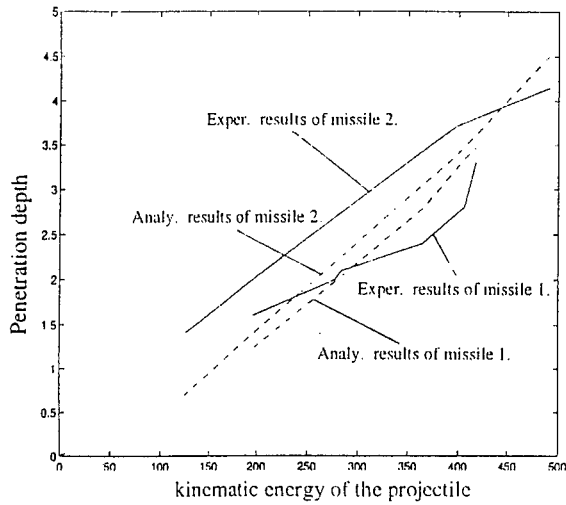


Figure.3 Analytical Results 1
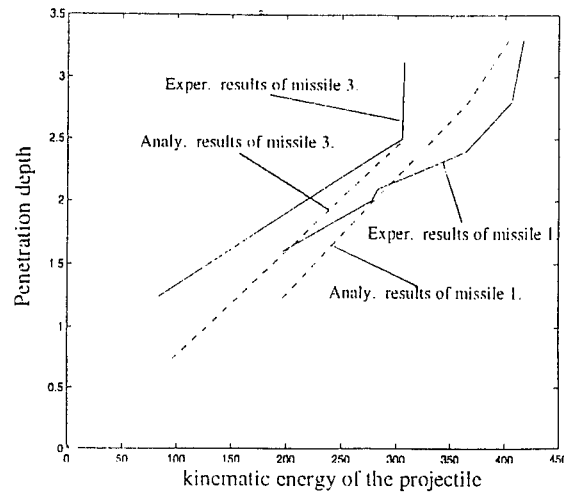


Figure.4 Analytical Results 2

Fig3. and Fig4. show that the analytical results basically agree with the test data, except with some unreasonably experimental data shown in Fig.4 that the little higher velocity causes great increase of penetration depth. All the numerical results of the current theoretical model are rational in presenting proportional relation between kinematical energy and the penetration ability. So it is confident to say that the model presented here is a simple and efficient method to predict the penetration depth, and cost much fewer computer time. It shows more rational results comparing with the experimental data. This method also can show the completely penetration process and the reaction of the target in each time step, other than some theoretical or empirical formulations which can only predict the penetration depth. Some other numerical tests will be implemented in the near future to observe the sensibility of the penetration to the compressibility of the material by adjusting $\eta$, than the model can be modified to analyze other target materials.

## ACKNOWLEDGEMENT

# REFERENCE

1) G.I.Taylor, *Q.J.Mech.Appl.Math.* 1. p.p.103, (1948).
2) S.V.Hanagud, B.Ross, *AIAA J.* 9. 905-911,(1971).
3) M.E.Backman, W.Goldsmith, *Int.J.Engng.Sci.,* 16, pp.1-99(1978).
4) R.L.woodward, *Int. J. Impact Eng.,* 6(2), p.p. 129-140(1987).
5) S.Abrate, *Appl.Mech.Rev.* 47(11), (1994).
6) V.K.Luk, M.J.Forrestal, *Int. J. Impact Eng.,* 6(4), p.p. 291-301(1987).
7) A.L.Florence, *S.J.Brown ed. Impact, Fragmentation and Blast,* ASME, (1984).
8) Goldsmith,W., et.al. *Int.J.Solids Structures* 32(1). pp. 89-103, (1995)
9) Mines, R.A.W., Roach, A.M., Jones, N. *Int. J. Impact Eng.,* 22, 561-588 (1999).
10) Mahfuz, H. et.al *International Journal of Impact Engineering,* 24, 203-217 (2000).

# EXPERIMENTAL TECHNICS TO INVESTIGATE THE
# IMPACT DAMAGE IN CERAMIC

COTTENOT C.E. [1]*, DENOUAL C. [1], THOMAS T. [1], STRAßBURGER E. [2]*

(1) DGA/CTA/MSP, 16 bis avenue Prieur de la Côte d'Or, F–94114 Arcueil Cedex, France
(2) Fraunhofer–Institut für Kurzzeitdynamik, EMI Am Klingelberg 1, D–79588 Efringen–Kirchen, Germany

**Abstract :** Ceramic materials are often used in modern lightweight armor to erode or break the projectile and to spatially spread the impact energy. In order to model armor configuration and to improve these concepts, it is necessary to understand the mechanism of damage initiation and evolution. According to these double needs, this paper presents two original test configurations, which have been developed on the basis of edge–on–impact. In both cases, the target lateral surface is filmed during impact by a high–speed camera. The first one, developed by EMI, allows a direct visualization of the fragmentation process during impact. The second one is based on high speed moiré photography and allows, througth a 2D– Fourier transform method to obtain the evolution of the strain field. These complementary methods developed respectively by EMI and CTA have been applied to ceramic during a French–German collaboration program in order to develop and validate an anisotropic damage model. This approach, which allows to obtain experimental data in real time, could be applied to study any other brittle material such as concrete

## 1. INTRODUCTION

Ceramic materials, with their capacities to erode or break the projectile and to spatially spread the impact energy, are often used in modern lightweight armor. The evaluation and optimization of the ballistic performance of composite armor require an analysis of the influence of many parameters which affect the protective strength. This is a time consuming and expensive process.
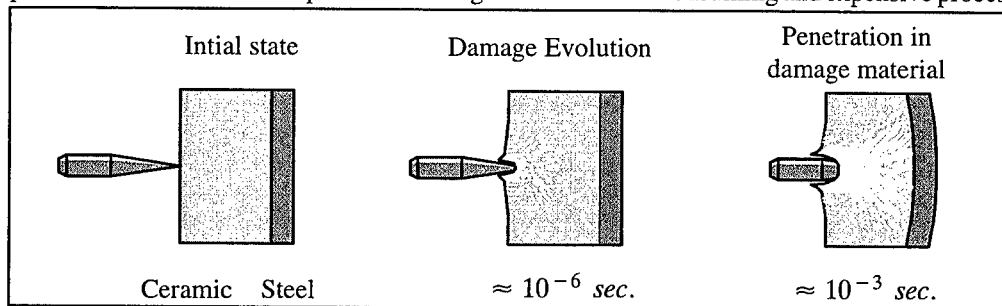


Figure 1 : Description of impact phenomenology in a ceramic–steel armour configuration

Thus, it is desirable to have a numerical tool very helpful for the design of composite armor. Two different steps can be considered by analyzing the mechanism of impact. The first one is the initiation and propagation of damage which takes place during a few micro–seconds. The second mechanism is the penetration in a damaged material and has a duration of approximately 10 milliseconds (see figure. 1). The first one is a major process prior to the second one and is induced by high stress waves which lead to a fragmentation of the material within a cone in front of the projectile [1]. A detailed knowledge of the fragmentation process is the basis for a realistic modeling of the impact damage in the ceramic. Therefore, the edge–on impact can be used to validate damage descriptions and evolution laws. A comparison between the fracture patterns in a realistic armor configuration and those observed by means of an edge–on impact configuration (see figure 2) reveals many similarities. Considering their common interest, CTA and EMI which are complementary with respect to ballistic testing, micro–structural investigations and numerical simulation, have started a collaboration on this topic.
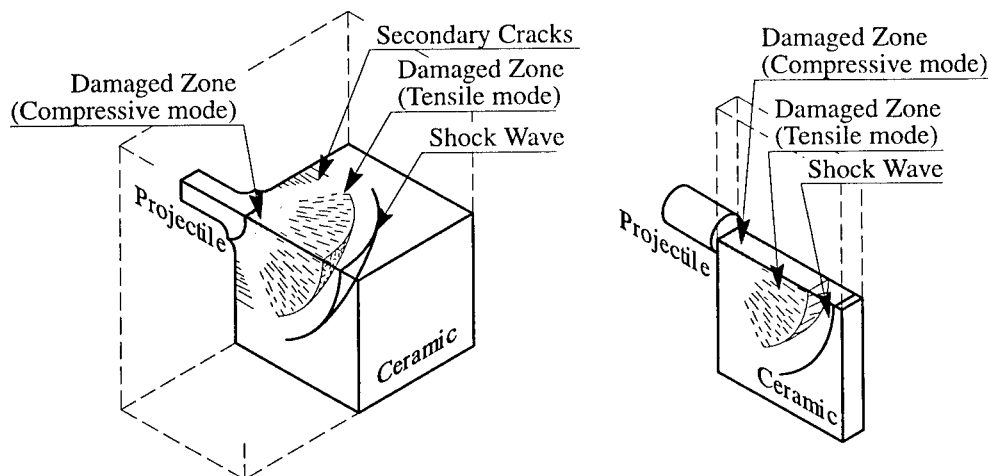


Figure 2 : Morphology of damage in a real configuration and in an edge–on impact specimen.

Thus, based on the previous needs, this paper deals with two original test configurations, which have been developed on the basis of edge–on–impact : a direct vizualisation of the fragmentation process and the evolution of the strain field by Moiré fringes. In both cases, the target lateral surface is filmed during impact by a high–speed camera.

## 2. CERAMIC PROPERTIES

In the context of this collaboration between EMI and CTA different grades of silicon carbides (SiC), which seem to be the best ceramic for ballistic applications, have been investigated. The aim is to analyze the influence of the microstructure on the ceramic behavior. In this paper two SiC grades exhibiting a crystallizes in α phase and a similar mean grain size around 5 μm are presented. The main physical properties of both grades are presented in Table 1.

- The first grade is noted SiC–B and is supplied by Cercom Company (USA). SiC–B is obtained by a pressure assisted densification process and a complete densification of material is reached. An important intergranular phase is observed and is identified as alumina.

- The second grade is denoted SSiC and is supplied by Ceramiques & Composites (France). SSiC is obtained through a pressureless sintering process with boron and carbon additives. It consists in 98% dense material. Pores can reach 30 μm, Carbon and $B_4C$ particles with respective mean diameter of 500 nm and 3 μm were also identified. The mean distance between two pores is about 33 μm and the mean distance between two carbide particles is about 2 μm. No glassy phase at grain boundary was observed by transmission electron microscopy.

Table 1. Physical properties of SiC grades.

| Grade | Density | Shear Modulus | Bulk Modulus | Weibull mod. | Mean strength | Effective vol. | $C_{longitudinal}$ |
|-------|---------|---------------|--------------|--------------|---------------|----------------|--------------------|
| SiC–B | 3.18 | 195 GPa | 223 GPa | 21 | 520 MPa | 0.4 mm$^3$ | 12250 m/s |
| SSiC | 3.15 | 175 GPa | 200 GPa | 9,3 | 370 MPa | 1.7 mm$^3$ | 11800 m/s |

## 3. DIRECT VIZUALISATION WITH E.O.I TEST

### 3.1. Test presentation

To visualize the fragmentation process during impact, an experimental method developed at the Ernst Mach Institut (EMI) [2–3] and presented in Fig. 3/a is used. In the study reported here, ceramic plates of 100 mm x 100 mm x 10 mm are impacted on the edge by a steel cylinder (φ 30 mm – length 23 mm). The impact velocity was varied in the range from 20 m/s to 1000 m/s. A Cranz–Schardin high–speed camera is used to determine the time of the onset of damage and to visualize the fracture propagation. A detailed description of the observed phenomena for different ceramics is given in [4]. Comparisons of the high–speed photographs with reassembled specimens and experiments with simultaneous high–speed photography of both sides of the specimens have demonstrated that the observed cracks are bulk cracks. This experimental technique can help to characterize ceramics by macroscopic fracture patterns, crack front velocities and single crack velocities as a function of impact velocity.
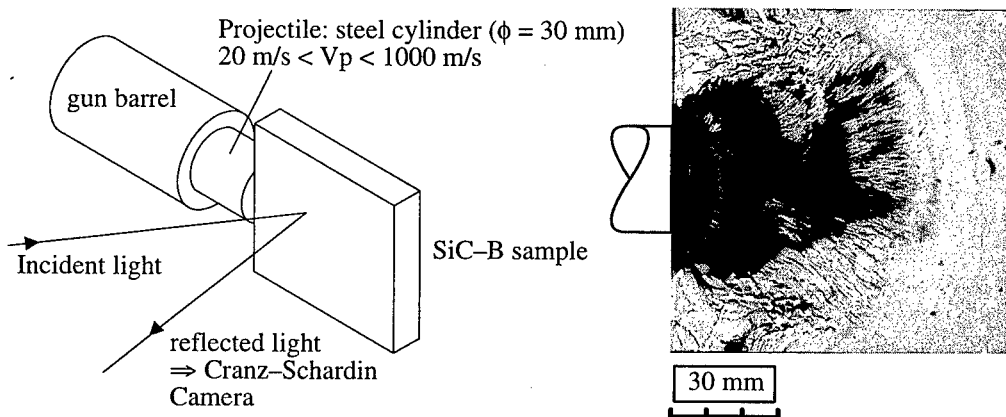


Fig. 3. The Edge–On Impact configuration (a) and a typical result of damage pattern (b) (SiC–B Vi = 513 m/s – time = 7 μs).

## 3.2. Damage phenomenology

Figure 3/b depicts one picture, taken out of a series of twenty pictures of one experiment, where a SiC–B specimen was impacted at 513 m/s. The picture shows the fracture pattern 7μs after impact. The damage front has a semi–circular shape and the whole specimen will be fragmented. Moreover, as impactor velocity decreases, it appears that below a threshold value of 370 m/s, the degradation in tension is localized in thinner and thinner corridors. However, it can be observed that the crack density in these corridors is still important. A typical result is presented for a SiC–B specimen impacted at 185 m/s. The picture (see Fig. 4/a) shows the fracture pattern 7μs after impact. Two different zones can be observed. The first one (the inner zone) appears in front of the projectile. This zone progressively widens and finally becomes localized in thin zones called corridors of varying locations. The second (outer) zone is generated at the projectile edges and can roughly be compared to a Hertz cone crack. This damaged zone then splits into a thin part that stops at the edge of the tile, and a larger one that propagates through the ceramic at a constant distance from the edge.



$-a-$     30 mm     $-b-$
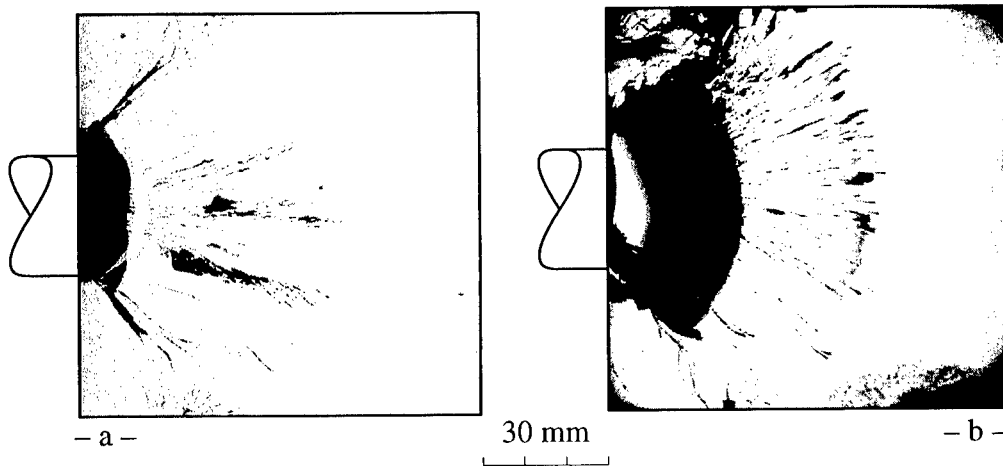
Figure 4 : Experimental damage pattern comparison between
SiC–B (Vi = 185 m/s – time = 7 μs) and SSiC (Vi = 202 m/s – time = 7 μs)

Considering the SSiC ceramic, Figure 4/b presents the crack pattern 7 μs after an impact at 200 m/s. It can be noticed that, the SSiC crack density is higher than for SiC–B. Moreover, the SSiC damage pattern is not localized. As the matter of fact, for this grade, the velocity threshold for localization is estimated to be approximately 100 m/s. Nevertheless, except when the localization occurs, damage patterns are quite similar for both materials. However, it seems that the crack density is slightly higher for SSiC than for SiC B.

## 3.3. Analysis of fracture velocities

From the complete set of frames, the crack front velocity can be measured. Thus for different damage pattern (previously presented), the crack front velocity for SiC–B is found to be equal respectively to 8270 m/s and 10090 m/s when specimens are impacted at 185 m/s and 513 m/s. Globally it has been revealed that the more the impact velocity increases, the more the crack front velocity. The evolution of the crack front velocity as a function of impact velocity for both SiC grades is presented in figure 5.
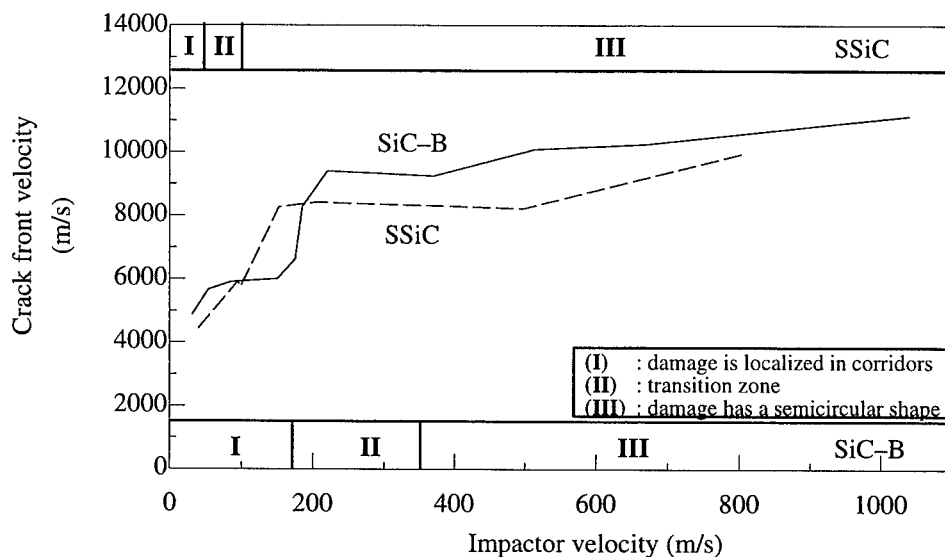
Figure 5 : Experimental damage propagation velocities for EOI between SiC–B and SSiC

Three different regimes of material response can be distinguished with respect to the projectile velocity by analyzing the damage localization. In the zone denoted **III** (see fig. 5), damage is not localized, the fragmentation process is homogeneous in the specimen for both grades. For the lower velocities, a complete localization is clearly observed in the case of SiC–B and is called zone **I**. A zone between **III** and I is a transition zone (denoted **II**) where the damage is not homogeneous but not also clearly localized. This zone is also supposed to occur with SSiC but at very low velocities. A zone between **III** and I is a transition zone (denoted **II**) where the damage is not homogeneous but not also clearly localized. This zone is not clearly observed with the SSiC materials.

### 3.3. Conclusion

This experimental technique allows to characterize during an impact sollicitation, the damage behaviour of ceramics by macroscopic fracture patterns, crack front velocities and single crack velocities. Concerning the aim of this study, experimental results has revealed an influence of material parameters on the damage behavior of SiC grades.

## 4. HIGH SPEED MOIRE VIZUALISATION WITH E.O.I TEST

### 3.1. Moiré principal

When periodic structures are superimposed, a pattern with new periods (beats) appears in addition to those of the individuals grids (figure. 6).The pattern corresponding to this new beats are the moiré fringes. The distance $f$ between two moiré fringes can be written as (see figure 6).
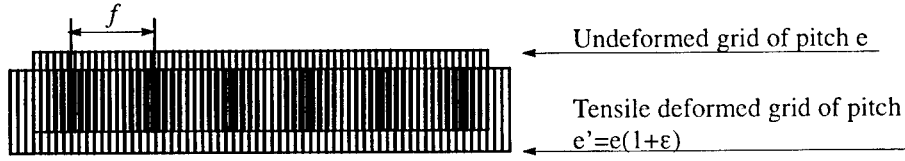
Figure 6 : Moiré pattern with a uniform tensile strain.

$$f = \left| \frac{e}{\varepsilon} \right| \qquad (1)$$

where $e$ represents the initial pitch of the grid and $\varepsilon$ the subsequent strain. Before any dynamic loading, the reference grating is slightly enlarged to generate an initial fringe pattern of $f$ spaced parallel lines (carrier fringes). If a dynamic strain $\varepsilon$ appears, $f$ is increased by $\Delta f$ and becomes $f'$. The increment $\Delta f$ is given by the definition of the acquisition set–up and defines the minimal readable strain $\varepsilon$

$$\varepsilon = e \frac{f' - f}{f f'} = e \frac{\Delta f}{f^2 - f \Delta f} \qquad (2)$$

If the minimum strain $\varepsilon$ and $\Delta f$ are known, Eqn. (2) allows to evaluate the reference grating pitch. The minimum readable strain increases when $f$ and $f'$ increase (i.e. the distance between two fringes increases) but the geometrical resolution decreases. A good compromise can be obtained with $e = 28 \ \mu m$, $f=1.7$ mm and $\Delta f=0.1$ mm so that the minimum readable strain is $\varepsilon= 7.10^{-4}$ [5].

Useful quantitative information can be easily obtained from a checked moiré pattern. For example, the strain at a few points can be calculated by measuring the local fringe spacing using Eqn. (1). The technique of partial sum extraction in the Fourier expansions are among the most powerful methods to compute strains in the whole moiré pattern. The analysis is based on a 2–D version of the Takeda Fourier method [6].

3.2. Test presentation

The grating, defined previously, has been reproduced on a 10 x50 x100mm$^3$ SSiC tile by aluminum vapor deposition, resulting in a good contrast. This checked deposit can be described as the superposition of two grid lines at ±45° and allows a 2D displacement analysis. Information on the two directions can then be simultaneously extracted, which is essential when the event is not reproducible. The optical set–up used in the experiment is shown in Figure 7.
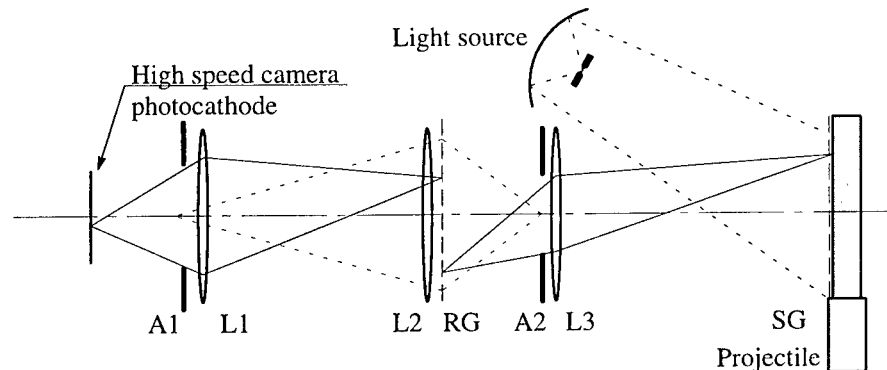


Figure 7 : Optical set–up.
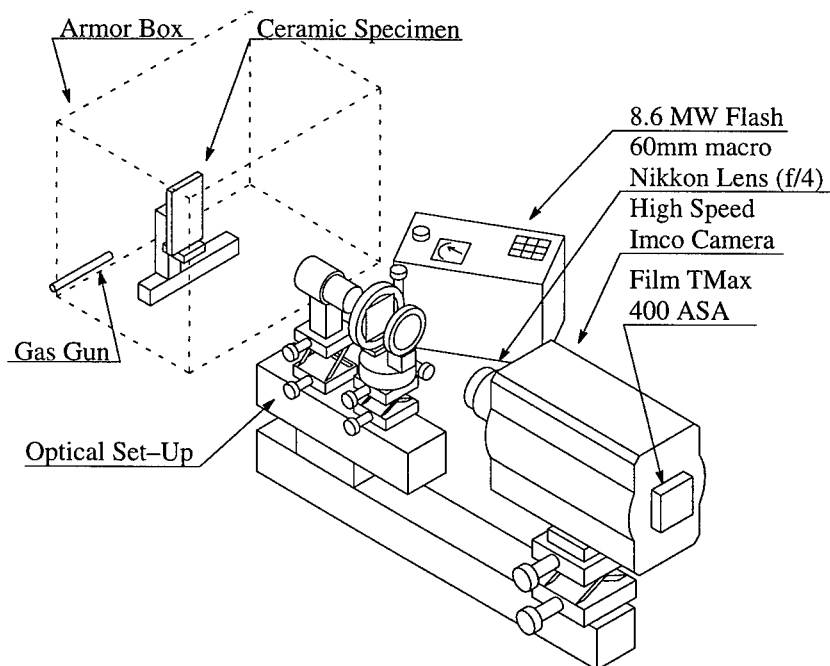
Figure 8 : Experimental Set–Up.

The specimen grating (SG) is imaged by a Nikkor ED macro f = 200 mm f/4 objective lens (L3) onto the reference grating (RG) at a magnification 1:1. The moiré pattern appears in the reference grating plane (RG) and is imaged through the camera 60 mm Nikkor macro lens (L1) onto the photocathode plane. A field lens (L2, f=125mm) is used to image the A2 iris onto the A1 iris, resulting in a uniform contrast in the film plane. The out–of–plane strain of the ceramic (several microns) is assumed not to modify the moiré pattern and has been neglected. The use of a field lens requires an objective lens aperture larger than those of the camera in order to image the entire target field. The light source is a powerful (8.6 MW) xenon flash lamp that produces a light flux during 20 $\mu$s without any orientation constraint because of the scattering power of the target surface. The checked moiré pattern resulting from the superposition of the two gratings is well contrasted but has a lens aberration which can be extracted by image processing as shown below.

All the optical bench is compact and a micrometric adjustment is applied to each bench components (including the target), resulting in a very precise and simple optical set–up (figure 8). The camera used for this study is an Ultranac FS 501 (IMCO) camera capable of providing a sequence of framing images at speeds up to twenty frames per micro–seconds with a time exposure of at least 10 nanoseconds. The camera is triggered by a short–circuit via a TTL input. The xenon flash is triggered by the TTL camera output with a delay. This short–circuit is put in front of the target edge at a distance taking into account the projectile velocity and the flash rise time (5 $\mu$s). It is composed of steel wires 63 $\mu$m in diameter disposed in a very tight grid form so that the impact surface is not disturbed. The projectile (a steel blunt cylinder 11 mm in diameter and 20 mm long) is fired by a high pressure light gas gun . The camera records sequences of 12 frames on single 127x102 mm sheets of Kodak TMAX 400 ASA film, push processed to 1600 ASA. All parameters (number of frames, time exposure, flash delay, etc.) are set by a PC.

## 3.3. Results and analysis

An application of the high speed moiré photography is presented for an impact with a hard steel blunt projectile onto a SSiC tile. The velocity of the impactor is equal to 330 m/s. A set of twelve frames has been recorded. The first frame is recorded before any physical contact, is free of constrains and constitutes the reference moiré pattern. The dynamic response of the specimen is recorded on eleven frames from 1 μs to 6.5 μs after impact with a 500 ns interframe time and a 40 ns exposure time. A typical result is presented in figure. 9.
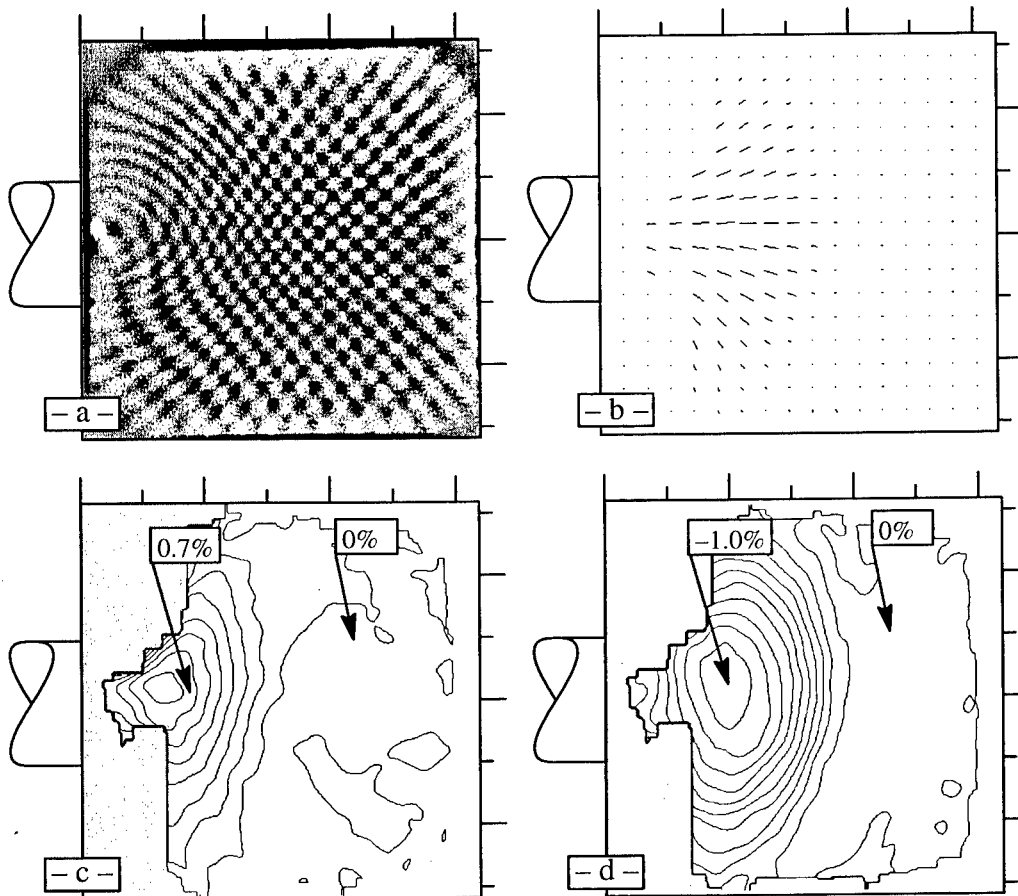


Figure 9 : A typical example of strain fields 2μs after impact. a) The initial frame. b) Second (negative) eigen strain direction. The magnitude is related to the second eigen strain amplitude. c) and d): First and second eigen strains plotted with a 0.1% step between each curve. N.B. no data available in the gray zone.

It can be noticed that the second principal strain reaches an important value before any significant evolution of the first principal strain. This is consistent with a cylindrical stress wave geometry in which the tensile strain is induced by the radial motion of the material.

The celerity of the shock wave can be evaluated from the complete set of frames and is on the order to 11 150 m/s, which is a classical value for Silicon Carbide (cf. § 2 – table 1). Those data can be used to analyze the behavior of hard materials submitted to strain rates up to $10^4 s^{-1}$.

3.4. Conclusion

A high speed moiré photography system has been developed to measure the strain states induced by impact of a hard steel projectile on a ceramic tile. The first advantage lies in a direct measure of the specimen displacements without calibration. The second one is a measurement without any interferences with the stress waves. The optical set–up and light source are compact, resulting from a fast optical configuration. Sequences of fringe patterns are analyzed by a 2–D Fourier Transform method to obtain the strain fields.

# 4. CONCLUSION

This paper has presented two experimental technics allowing to obtain experimental data in real times during a sollicitation of impact. These complementary methods developed respectively by EMI and CTA have been applied to ceramic during a French–German collaboration program in order to validate two specific models, developed respectively by Riou and by Denoual & Hild which take into account the anisotropic damage induced in brittle material submitted to a dynamic loading. A complete description of these models is given respectively in references [7] and [8–11] such has numerical results [11–13]. This approach, which allows to obtain experimental data in real time, could be applied to study any other brittle material such as concrete.

# ACKNOWLEDGMENT

# REFERENCES

[1]   Wilkins M.L., "Mechanics of Penetration and Perforation", Int. J. Engng. Sci., **16**, pp. 793–807, 1978.

[2]   Hornemann U., Rothenhäusler H., Senf H., Kalthoff J.F., Winkler S., "Experimental investigation of wave and fracture propagation in glass slabs loaded by steel cylinders at high impact velocities", Inst. Phys. Conf. Ser. No. 70, 3rd Conf. Mech. Prop. High Rates of Strain, Oxford, 1984

[3]   Winkler S., Senf H., Rothenhäusler H., "Wave and fracture phenomena in impacted ceramics", Fraunhofer–Institut für Kurzzeitdynamik, Weil am Rhein, EMI–Report V 5/89, 1989

[4]   Straßburger E., Senf H., Rothenhäusler H., "Fracture propagation during impact in three types of ceramics", Proc. of EURO DYMAT 94, Journal de Physique IV, C8, Vol. 4, pp. 653–658, 1994

[5]   T. Bertin–Mourot, C. Denoual, G. Deshors, P. F. Louvigné, T. Thomas, "High speed photography of moire fringes application to ceramics under impact", Proc. of EURO DYMAT 97, Journal de Physique IV, C3, suppl. J. de physique III, **7**, 311–316, (1997)

[6]   Takeda M., Ina H., Kobayashi S. "Fourier–Transform Method of Fringe–Pattern Analysis for Computer–Based Topography and Interferometry", *J. Opt. Soc. Am.*, **72** (1), (1982), pp. 156–160.

[7]   Riou P., Cottenot C.E., Boussuge M., "Anisotropic damage model for impacted ceramic material : Application to Silicon Carbide", *Int. J. of Impact Eng.*, (1998) **21**, (8), pp 683–693.

[8]   Denoual C., Cottenot C.E. and Hild F., "On the Identification of damage during impact of a ceramic by a hard steel Projectile", Proc. APS Conference on Shock Compression of Condensed Matter, Amherst (MA), USA, 1997.

[9]   Hild F., Denoual C., "Probabilistic Model for the Dynamic Fragmentation of Brittle Solids", Proc. APS Conference on Shock Compression of Condensed Matter, Amherst (MA), USA, 1997.

[10]  Denoual C., Barbier G. et Hild F. "A Probabilistic Approach for Fragmentation of Brittle Solids under Dynamic Loading", C. R. Acad. Sci., Série IIb, (in press), 1997.

[11]  Denoual C., Hild F. and Cottenot C.E., "A probabilistic Approach for Dynamic Fragmentation of Ceramic under Impact Loading", Presented at ICF 9, Sydney, Australia, 6, pp. 2933–2940, 1997.

[12]  Straßburger E., Senf H., Denoual C., Riou P. and Cottenot C., "An Experimental Approach to Validate Damage Evolution Laws for Brittle Materials", Proc. of EURO DYMAT 97, *J. de physique IV*, coll. C3 suppl. J. de physique III, **7**, 909–914 (1997).

[13]  Cottenot C.E., Beylat L., Denoual C. E. Straßburger, H. Senf "Experimental and numerical investigation of impact damage in different types of SiC", Proc. of the 17th Ballistic Symp., vol. 3, pp. 49 – 56 (1998).

# THE EFFECT OF LINER MECHANICAL PROPERTIES ON THE PERFORMANCE OF COPPER EXPLOSIVELY FORMED PROJECTILES

## EDWARDS M.R., MUSTEY A.J., YOUNG R.J.

Department of Materials and Medical Sciences, Cranfield University, RMCS Shrivenham, Swindon, UK

**Abstract:** Explosively formed projectiles were manufactured from both cold worked and cold worked and annealed copper. Penetrations were similar and soft captured fragments were shown to have undergone dynamic recrystallization. This indicates that for a material with a relatively low recrystallization temperature, the liner microstructure has little effect on the hole created by an explosively formed projectile. This was applicable for both thin liners that had been heavily cold worked and for thicker liners with reduced amounts of cold work. To ensure that the explosively formed projectile has maximum strength, thus aiding penetration, it is helpful to use alloys of higher melting point with correspondingly higher recrystallization temperatures.

## 1. INTRODUCTION

Explosively formed projectiles (EFPs) are characterised by a solid core travelling at a velocity of 1000-3000 ms$^{-1}$. In this velocity range the equations of Tate [1] and Alekseevskii [2] indicate that the penetration increases with increasing penetrator strength and increasing velocity, while decreasing with increasing target strength. The latter has been confirmed by Weinmann et al [3], who showed that the penetration of EFPs into steel was decreased by 30% when the target strength was increased from 700 MPa to 1400 MPa.

Soft capture experiments, where the particles of a copper shaped charge liner were captured in a non-eroding medium, by Zernow [4] indicated that the peak temperature reached was in the order of 700°C, insufficient for melting but high enough for dynamic recrystallization. Murr et al [5] showed for shaped charge liners of tantalum that dynamic recrystallization had taken place, and that there was a reduction in grain size of up to 100 times between the microstructure of the original cone and that of the jet. As there was also a difference in microstructure between the jet and the slug, the dynamic recrystallization appeared to be a function of the temperatures and strain rates seen in the various parts of the jet and slug formation process. Feng et al [6] extended this to EFPs with both copper and tantalum liners. They found that for the copper liners, the grain size had been reduced from an initial equiaxed 15-30 µm to one of 5-10 µm, indicating that dynamic recrystallization had occurred during EFP formation. Conversely, they saw no evidence of dynamic recrystallization in the tantalum liners. Work by the Royal Armament Research and Development Establishment [7] on the properties of pure iron liners as a function of explosive shock and strain rate showed that the nose of the EFP formed from the liner was shock hardened, as indicated by the presence of a large twin density and an increase of hardness from 125 Vickers to 200 Vickers. At the edges of the projectile and in the finned area at the rear, there was grain distortion and twinning. In

the centre dynamic recrystallization had occurred with the smaller grains (10 µm diameter) at the front of the recrystallized region and the larger (30 µm diameter) at the rear.

Thus it would be suggested that materials of high recrystallization temperature might well have very different projectile microstructures, depending on their initial liner microstructures. Whether this will translate into different penetrations is not so clear. Although formulae such as those of Tate [1] and Alekseevskii [2] suggest that increased penetrator strength will increase penetration, the key strengths are those at the high strain rates involved in the penetration process. Ekbom et al [8] showed for two tungsten heavy alloys of very different strengths at quasi-static strain rates, that their strengths at a strain rate of $10^4$ s$^{-1}$ were very similar. As for materials of lower recrystallization temperature, any differences in liner microstructures will be largely eliminated under the thermomechanical processing involved in liner formation.

The aim of the present work is to examine the penetration behaviour of copper EFPs, in both the cold worked and annealed conditions, in order to determine the effect of the initial liner microstructure.

## 2. EXPERIMENTAL

### 2.1 Materials

The liners were made from > 99.9% purity copper, which was initially supplied as 6 mm thick half hard plate. They were then thermomechanically processed according to four routes:

Type I: Fully cold worked (thickness reduction from 6 mm to 1.2 mm), formed into liner
Type II: Partially cold worked (thickness reduction from 6 m to 3.8 mm, annealed for 30 min at 700°C, followed by cold working to 1.2 mm and forming into liner)
Type III: Cold worked (6 mm to 1.2 mm), formed into liner, annealed at 200°C for 30 min to produce a fine-grained recrystallized microstructure
Type IV: Cold worked (6 mm to 1.2 mm), formed into liner, annealed at 700°C for 30 min to produce a coarse-grained recrystallized microstructure

A second series of firings was carried out using 4 mm thick copper liners. The thermomechanical processing was as follows:

.Type V: Fully cold worked (thickness reduction from 6 mm to 4 mm), formed into liner
Type VI: Cold worked (thickness reduction from 6 mm to 4 mm), formed into liner, annealed at 200°C to produce a recovered, but unrecrystallized microstructure
Type VII: Cold worked (thickness reduction from 6 mm to 4 mm), formed into liner, annealed at 700°C to produce a coarse-grained recrystallized microstructure

### 2.2 Explosive Configuration

The liner was cold formed in a die and machined to give a parallel-sided dish liner, the key dimensions of which are given in Figure 1.
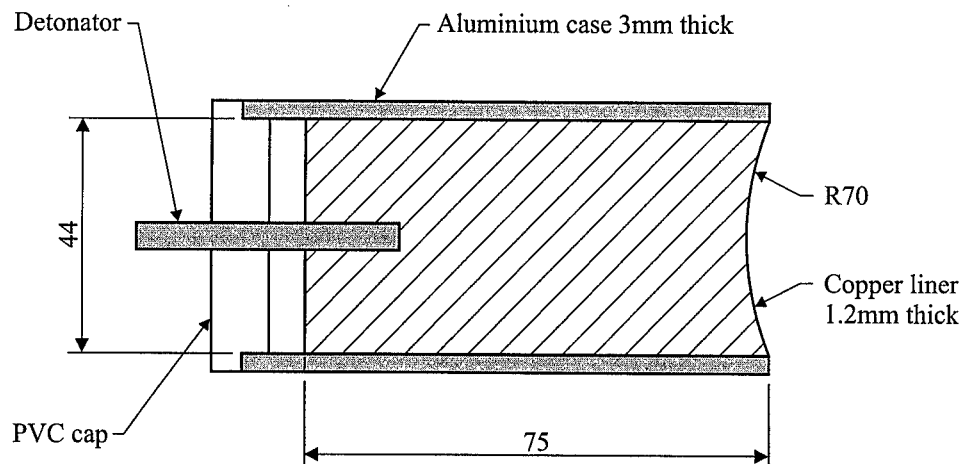
Figure 1; general arrangement of liner and charge

The explosive used was the military explosive PE4 (88% RDX – 9.6% wax – 2.4% lithium stearate, detonation velocity 8200 ms$^{-1}$) and the charge mass was 173 g. The firing arrangements were as in Figure 2, the charge being set of with a standard L2 electric detonator. The standoff distance was set at 10 cone diameters, so that the EFP would be fully formed. Steel targets were of three types:

Type A: 25 mm thick steel (hardness 123 Vickers, composition 0.18% C, normalised)
Type B: 25 mm thick steel (hardness 333 Vickers, composition 0.32% C, 1.47% Cr, 0.7% Ni, 0.39% Mo, hardened and tempered)
Type C: 10 mm thick steel (hardness 142 Vickers, composition 0.25% C, normalised)

The velocity of the projectile was measured using a timer device incorporating two aluminium trigger plates separated by tissue paper and connected to an electronic counter.

The soft capture arrangements that were used are based on capture in a horizontal 3.75 m length channel of fluoroprotein foam, followed by 1 m of vermiculite (density 81.8 kgm$^{-3}$), and a cardboard end stop. A first attempt based on vermiculite, followed by sawdust and cotton waste appeared to erode the projectiles.

The second series of firings used a 4 mm thick liner with the same mass of explosive (173 g). Otherwise the arrangements were identical.
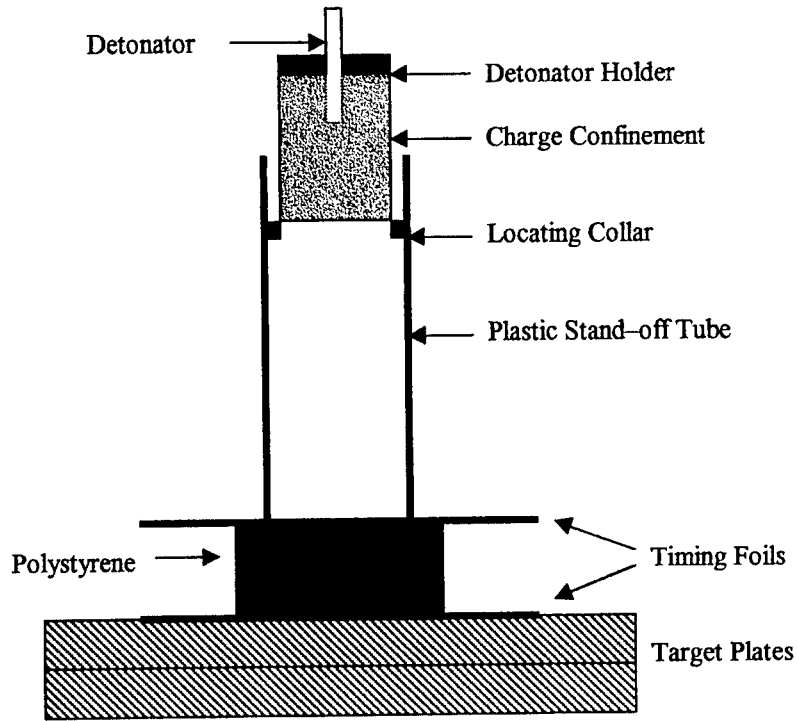
Figure 2: firing set-up in the absence of soft capture arrangements

## 3. RESULTS

### 3.1 Firings with 1.2 mm liners

Penetration results for the firings with 1.2 mm thick liners are shown in Table 1.

Table 1: penetration data for 1.2 mm thick liners

| Processing Type | Target Type | Penetration (mm) | Hole Width (mm) | Velocity (ms$^{-1}$) |
|---|---|---|---|---|
| I | A | 18.9 | 33.8 | 1750 |
| II | A | 22.8 | 32.2 | 1750 |
| III | A | 19.6 | 31.0 | 1760 |
| IV | A | 19.4 | 33.8 | 1620 |

| Processing Type | Target Type | Penetration (mm) | Hole Width (mm) | Velocity (ms$^{-1}$) |
|---|---|---|---|---|
| I | B | 16.1 | 29.4 | 1830 |
| II | B | 16.2 | 27.8 | 1740 |
| III | B | 17.4 | 27.8 | 1950 |
| IV | B | 16.1 | 27.4 | 2050 |

| Processing Type | Target Type | Penetration (mm) | Hole Width (mm) | Velocity (ms$^{-1}$) |
|---|---|---|---|---|
| I | C | 16.4 | 32.2 | 1860 |
| I | C | 18.0 | 34.8 | 1730 |
| II | C | 17.1 | 31.3 | 1890 |
| III | C | 18.0 | 32.6 | 1830 |
| III | C | 15.7 | 32.5 | 1780 |
| IV | C | 17.0 | 33.6 | 1790 |
| IV | C | 17.0 | - | 1640 |

The holes created (Fig.3) were of the characteristic wide shape of those produced by EFPs. There was some evidence for jetting ahead of the main wide hole, and this has been ignored in the measurement of penetration in Table 1.
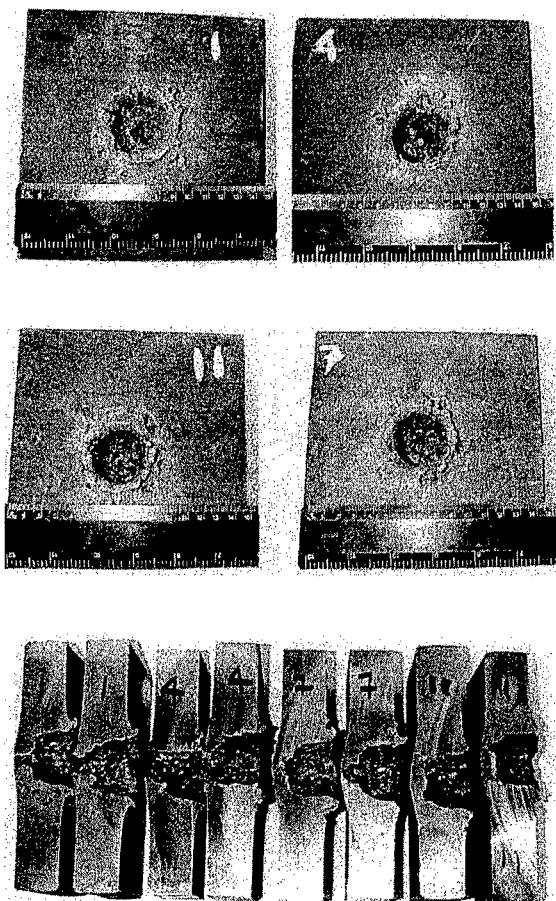


Figure 3: holes created by cold worked (1), cold worked and annealed at 200°C (4), cold worked and annealed at 700°C (7), and cold worked, annealed and cold worked (11) liners into steel of hardness 123 Vickers

The soft captured remnants of the liner appeared to be fragmented, as shown in Figure 4, which indicated that the "projectile", although producing the wide hole, was not the solid metal cylinder that EFPs were meant to be.



Figure 4: captured remnants from cold worked liner, largest fragment of 8.2 g mass and liner mass of 18.86 g

Examination of the microstructures of the recovered fragments from the 1.2 mm liners showed that the cold worked structure, as seen in the liners (Types I and II), had been converted to an equiaxed structure typical of recrystallized material. The amount of material recovered from the Type III and Type IV firings was insufficient to determine the distribution of grain sizes, and thus to compare this to the distribution in the original liners.

## 3.2 Firings with 4 mm liners

Results from the firings with the 4 mm thick liner, where the velocities are very low due to the increased mass of the liner, are shown in Table 2.

Table 2: penetration data for 4 mm thick liners

| Processing Type | Target Type | Penetration (mm) | Hole Width (mm) | Velocity (ms$^{-1}$) |
|---|---|---|---|---|
| V | A | 7.0 | 39.2 | * |
| V | A | 4.5 | 41.1 | * |
| VI | A | 5.5 | 40.1 | * |
| VI | A | 8.2 | 40.0 | * |
| VII | A | 6.7 | 40.5 | * |
| VII | A | 5.0 | 40.0 | * |

* Velocities measured were in the range 350-420 ms$^{-1}$: the width of the holes suggests that the impact velocities were similar to those listed in Table 1 for the 1.2 mm liners. Consideration of the mass of the liner would indicate somewhat lower impact velocities for the 4 mm liners. There is evidence of spreading of the projectile on impact, again suggesting lower impact velocities.

In contrast to the fragments seen in the soft capture apparatus (Figure 4), cylindrical penetrators were formed in all cases with the thicker liners, as seen in Figure 5. Hardnesses of the copper liners before firing and after soft capture are shown in Table 3. These indicate that, in a similar manner as those found for the cold worked 1.2 mm liners, both the cold worked and the recovered liners had recrystallized during projectile formation.
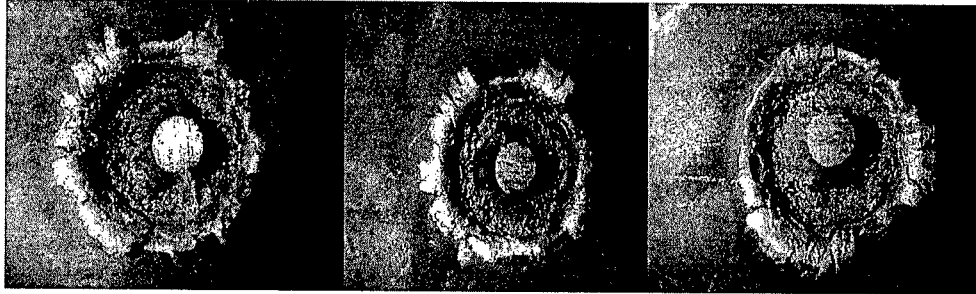
Figure 5: penetrators formed from 4 mm thick liners – cold worked (l), cold worked, annealed at 200°C (c), cold worked and annealed at 700°C (r)

Table 3: hardnesses of 4 mm liners before and after firing

| Processing Type | Liner Hardness (Vickers) | Captured Hardness (Vickers) |
|---|---|---|
| V | 104 | 58 |
| VI | 108 | 66 |
| VII | 57 | 60 |

## 4. DISCUSSION OF RESULTS

For the 1.2 mm thick liners the penetration (Table 1) did not seem to vary with type of thermomechanical processing. However, there was, as predicted by Weinmann [3], a decrease in penetration (Table 1) when the harder steel (333 Vickers) was used as the target plate. The soft capture data, which suggest that the microstructure of the penetrator just prior to impact was in all cases a recrystallized microstructure, indicate that the strength of the penetrator material will be approximately constant irrespective of the initial starting microstructure of the liner. This would suggest that the penetration, assuming that the length of the projectile is the same in all cases, would not vary with the initial liner microstructure, which appears to be the case from Table 1.

The penetration results using the thicker liners (Table 2) show the reduced penetration due to the lower impact velocities. However any effect of the initial liner microstructure on penetration performance is still absent. Examination of the penetrators formed show that the microstructure of the projectiles formed is that of recrystallized copper, which is confirmed by the reduced hardnesses seen in Table 3. Thus, since the penetrator strength is similar irrespective of any differences in initial liner microstructure, it is not unexpected that the penetration performances of the three different thermomechanically processed liners are similar.

Following Tate [1] and Alekseevski [2] penetration by explosively formed projectiles will be aided by increased strength of the projectile material in the fully formed condition. Thus it is important to reduce the extent of dynamic recrystallization during liner formation. In this way increased strength brought in, either by having a very strong initial strength for the liner through cold working and/or heat treating or by shock loading of the projectile nose as seen for iron in [7], can be retained in the fully formed projectile.

These data for copper EFPs are in contrast to the behaviour of copper liners in shaped charges. In the latter the time to break-up of the jet, which is very important when the total penetration is considered, has been shown to be affected by liner material purity [9, 10], grain size [11, 12] and surface finish [13]. This leads to the conclusion that, for maximum penetration for a shaped charge, care must be taken that the copper should be pure, of fine grain size and of good surface finish. In this way the time to jet break-up will be maximised and penetration optimised. The present data for EFPs suggest that liner mechanical properties are much less important, as in all liner material conditions a similar geometry projectile is created, and the penetration is determined by the projectile velocity and material properties. Since the latter, through the process of dynamic recrystallization, appear to be the same, irrespective of initial liner microstructure, the penetration appears to be independent of the initial copper liner microstructure.

## 5. CONCLUSIONS

a) For cold worked and cold worked and annealed copper liners there was no significant effect of initial liner microstructure on penetrator performance.

b) Capture of the projectiles formed showed that the cold worked copper had undergone dynamic recrystallization as the projectiles were explosively formed from the liner.

c) In order to ensure a strong projectile it is necessary to prevent dynamic recrystallization, something that will necessitate the use of metals of high melting point and therefore recrystallization temperature.

## 6. ACKNOWLEDGEMENTS

## 7. REFERENCES

[1] A Tate, "A theory for the deceleration of long rods after impact", *J. Mech. Phys. Solids*, 15, pp.387-399, (1967)
[2] V P Alekseevskii, "Penetration of a rod into a target at high velocity", *Fizika Goreniya i Vzryva*, 2, pp.99-106, (1966)
[3] K Weinmann, A Blache, M Cauret, R Laureson, F Gil, F Rondot, "Terminal ballistics of EFPs with high L/D ratio", in *Proceedings of the 17th International Symposium on Ballistics, Midrand, South Africa*, 3, pp.215-224, (1998)
[4] L Zernow, "An overview of the new insights into jet formation and particulation provided by examination of recovered jet particles", in *Proceedings of the 15th International Symposium on Ballistics, Jerusalem, Israel*, 2, pp. 129-141 (1995)
[5] L E Murr, H K Shih, C S Niou, "Dynamic recrystallization in detonating tantalum shaped charges – a mechanism for extreme plastic flow", *Material Characterization*, 33, pp. 65-74, (1994)
[6] C Feng, L E Murr, C S Niou, "Aspects of dynamic recrystallization in shaped charge and explosively formed projectile devices", *Metallurgical and Materials Transactions*, 27A, pp.1773-1776, (1996)
[7] Ministry of Defence IEPG Panel III, Subgroup VI, Working Party on EFP (B D Goldthorpe, convenor), "Metallurgical report of the phase I programme", Royal Armament Research and Development Establishment Report BR-309719, Sevenoaks, Kent, (1989).
[8] L Ekbom, S Bogegard, L Holmberg, S Westerling, "A comparison of the mechanical properties of KE penetrator tungsten alloys and their ballistic performance" in *Proceedings of the 9th International Symposium on Ballistics, Shrivenham, United Kingdom*, 2, pp.447-456, (1986).

[9] D H Lassila, E L Baker, D K Chan, W E King, A J Schwartz, "Effect of sulfur on the ductility of copper shaped charge jets", in *Proceedings of the 16th International Symposium on Ballistics, San Francisco, USA,* 1, pp.31-38, (1996).

[10] A J Schwartz, D H Lassila, E L Baker, "Analysis of intergranular impurity concentration and the effects on the ductility of copper shaped charge jets", in *Proceedings of the 17th International Symposium on Ballistics, Midrand, South Africa,* 2, pp.439-446, (1998).

[11] M L Duffy, S T Golaski, "Effect of liner grain size on shaped charge jet performance and characteristics", US Army Ballistics Research Laboratory, Technical Report BRL-TR-2800, Aberdeen, USA, (1987).

[12] K G Cowan, P R Greenwood, R Cornish, B Bourne, "Hydrocode and analytical code modelling of the effect of liner material grain size on shaped charge break-up parameters", in *Proceedings of the 17th International Symposium on Ballistics, Midrand, South Africa,* 2, pp.217-224, (1998).

[13] A J Schwartz, E L Baker, "Effect of interior surface finish on the break-up of copper shaped charge", in *Proceedings of the 18th International Symposium on Ballistics, San Antonio, USA,* 1, pp.559-566, (1999).

# AN ASSESSMENT OF THE PENETRATION PERFORMANCE OF FOUR TUNGSTEN ALLOYS AGAINST A TRIPLE-PLATE TARGET

N J LYNCH

DERA Fort Halstead, Sevenoaks, Kent, TN14 7BP, UK

**Abstract :** This paper reports experiments for four, L/D=20 tungsten alloys projectiles fired against an angled plate target at velocities between 1400 and 1600 m/s. It was found that the quasi-static tensile strength of the tungsten had little bearing on the projectile performance. The higher strength alloys made smaller craters in the first target plate, but this correlation was not found in the second plate. A hypothesis is suggested that the greater retardation of higher strength materials by elastic wave reflections, overcomes their initially better penetration behaviour. The best penetration results were obtained from an intermediate strength material combined with good ductility. Measurements of the crater diameters in the target plates indicate that very low pitch limits are acceptable for accurate comparison of penetration results.

## 1. INTRODUCTION

Against semi-infinite rolled homogeneous armour (RHA) the effect of changing the specification of the projectile material generally has little effect on penetration performance – the strength of the target material generally dominates. Against angled thick armour, the entry phase can cause more marked differences, but it is mostly against an array of thinner, oblique plates and ERA that material effects begin to show. Experiments reported in [1] using 65 gram, L/D=15 rods made from 93%W and 90%W (both 18% swaged), show a 3% difference in $V_{50}$ velocity against a thick RHA plate at normal incidence. Against a 1/4 scale version of the NATO triple target however there was an 11% difference. Similarly, experiments reported in [2] using rods made from sintered 95%W, and sintered and swaged 90%W, show a 5% difference in semi-infinite penetration depth. Against the NATO heavy triple target however there was a 39% difference. The aim of this work therefore was to assess the performance of a range of currently used or available tungsten alloys against an oblique plate target.

## 3. EXPERIMENTS

### 3.1 Projectiles

The projectiles used were L/D=20, their mass (without fin) averaged 154 g, and their overall length was 177 mm. The alloys used are designated A, B, C and D. Details of the material properties are given in Table 1. The materials were produced by sintering and then mechanical working/heat treatment to obtain different material properties. The main variations in the projectile materials were the quasi-static tensile strength and the ductility.

Strike velocity was increased during the experiments to obtain results at approximately 1400, 1500 and 1600 m/s.

Table 1: Material properties for the tungsten projectiles used

| Alloy | Density | 0.2% PS | UTS | Elongation | Reduction in area |
|---|---|---|---|---|---|
| | g/cm$^3$ | MPa | MPa | % | % |
| A: 91W-Ni-Co | 17.45 | 1525 | 1545 | 15 | 21 |
| B: 92.5W-Ni-Fe | 17.6 | 1190 | 1210 | 9 | 20 |
| C: 92W-Ni-Fe | 17.6 | 1071 | 1142 | 23 | 19 |
| D: 92.5W-Ni-Fe | 17.6 | 830 | 1075 | 23 | - |

## 3.2 Target

The target was a fabricated assembly of two 16 mm RHA plates and a 40 mm thick RHA back plate. The plates were separated by a normal air gap of 50 mm and inclined at 65° obliquity. The hardness of the RHA plates averaged 337 Brinell.

## 3.3 Range Layout

The shot were launched from a 40 mm calibre smooth bore cannon. An orthogonal pair of X-rays provided projectile velocity shortly before impact. Two horizontal X-rays at the target were arranged to show the projectile partly through the first plate, and between the second and third plates of the target.

## 4. RESULTS

### 4.1 General

The results of the firings are given in Table 2. The target X-rays were used to obtain projectile length before and after the second plate. The length measurement is taken from the back of the tungsten core to a line parallel with the front of the projectile, i.e. the maximum overall length. This method has been reported in other papers on this topic [3]. The fact that the nose of the projectile may be fractured in one or more places is ignored. The penetrator length after the second plate is subject to greater measurement error since the threaded rear section which carries the fin stabiliser is usually fractured by the first or second plate. Where two results are given for residual length in Table 2 these are the minimum and maximum lengths including the fractured sections. Radiographs of four typical results are shown in Figures 1 to 4. These are the lowest total yaw results at 1600 m/s approximately, providing a comparison of the fracture and erosion behaviour of the four alloys.

Although the radiographs are taken at slightly different times after impact, the disruption and fracture of the rod materials are not too dissimilar. After the second plate the two higher strength alloys show a fracture towards the rear of the rod, whereas alloys C and D appear intact.

Figure 1 : Radiograph from test 2814 (Alloy A).100μs and 265μs after impact.



Figure 2: Radiograph from test 2810 (Alloy B). 100μs and 275μs after impact.



Figure 3 : Radiograph from test 2808 (Alloy C). 108μs and 290μs after impact.



Figure 4 : Radiograph from test 2811 (Alloy D). 100μs and 275μs after impact.

## 4.2 Residual Length

Figure 5 is a plot of projectile length against impact velocity for the four alloys at the two X-ray positions. The length measurement after the first plate shows some correlation with projectile strength, i.e. alloy A is generally longest, followed by B and C with D having the

highest erosion. There is more scatter in the results after the second plate, and fewer results are available, but a similar trend can be seen.
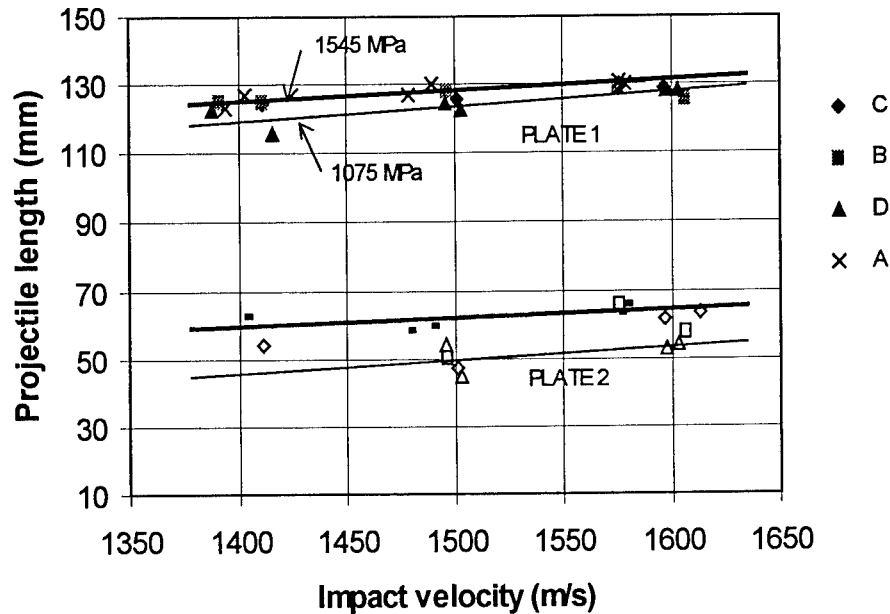


Figure 5 : Residual length of the projectiles after the first and second plate

## 4.3 Crater Size and critical yaw limits

The craters in the 16 mm plates are elliptical, with the major axis of the ellipse being along the axis of the projectile. Figure 6 shows the major and minor diameters (the length along the plate, and the width across the plate respectively) of the craters for the first and second plates. A gradual increase in crater width with velocity can be seen, and the width is slightly less than the crater diameter in semi-infinite targets according to the Bjerke crater diameter fit [4]. The crater size affects the allowable values for pitch and yaw. The critical yaw angle (i.e. the angle at which the rear of the core will strike the crater wall) using ref. [4] is 0.87° at 1400 m/s, 1° at 1500 m/s and 1.2° at 1600 m/s. A critical pitch angle is more difficult to define, but previous hydrocode simulations using this projectile against 40 mm RHA at 60° and 1550 m/s, show critical pitch values of about 0.32° to -0.64°. For assessment of penetration depths therefore, impact yaw and pitch values greater than these limits have not been included. These low values are comparable with estimates by Anderson and Littlefield of 0.16 to -0.32° for L/D 30 rods against 65° plates at 1770 m/s [5].
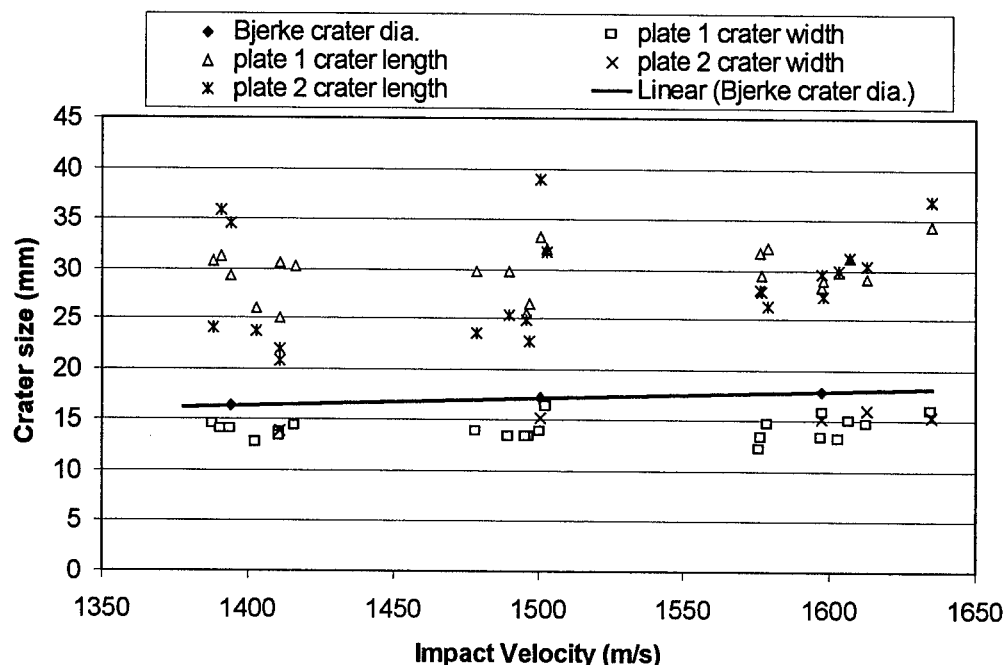
Figure 6 : Residual length of the projectiles after the first and second plate

## 4.4 Penetration Depth

Figure 7 shows a plot of penetration depth into the third plate against strike velocity. Alloy D performs relatively poorly at 1400 m/s based on the <0.1° total yaw result of test 2803. Slightly deeper craters were produced by the A material, but the deepest fair hit result was from alloy C (test 2816). At 1500 m/s, the penetration depths are ranked by pitch angle; there is little to distinguish one alloy as being better than the others. At 1600 m/s there is a wider spread of results, but alloys C and D perform as well as the high strength A alloy at similar yaw levels.

## 5. RESULTS ANALYSIS

A possible explanation why the longer residual lengths of the higher strength materials doesn't provide greater penetration lies in the projectile retardation. Physically, the rear of the projectile is slowed by reflected elastic waves according to $\Delta V= 2Y_p/\rho c$, where $Y_p$ is the projectile yield strength, $\rho$ is the density and c is the bar wave speed. Hence the stronger projectiles will retard more than the softer ones. By the time the projectile reaches the third plate from 1500 m/s there will be approximately seven wave reflections (for c = 4.22 mm/$\mu$s), and $\Delta V$ will be about 27 m/s for the 1 GPa strength of material D, and 40 m/s for the 1.5 GPa alloy A. Thus the 50 mm long residual rod of alloy D impacts the third plate at about 1500-(7 x 27)=1311 m/s and the 60 mm long A alloy rod impacts at 1220 m/s. A simple estimate of the in-line penetration of the two rods gives 37 mm and 36 mm respectively, hence the explanation appears to be feasible. This is very much an oversimplification of the shock process, and there may only be three strong reflections caused by the initial impact on the three plates. The projectile velocity between the plates

could not be measured in the air gaps available, hence there is no experimental data from these tests to confirm the above hypothesis.
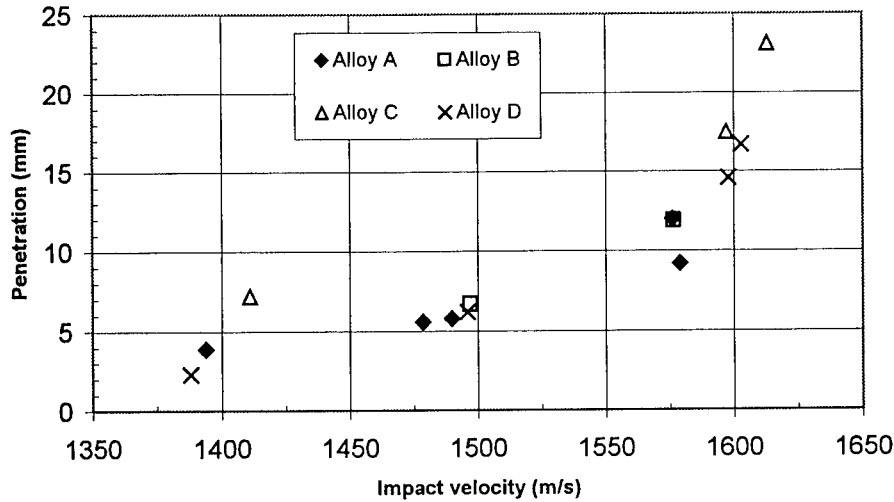


Figure 7 : Penetration depth vs Velocity for the four tungsten alloys

Referring to other work on this topic, Hohler and Stilp at the Ernst-Mach-Institute examined the effect of projectile strength on residual velocity and the results were analysed by Anderson and Walker [6]. The residual velocity of steel rods after perforation of a single 20mm RHA plate was found to increase with increasing rod hardness and tensile strength. This effect could not be reproduced with the CTH hydrocode using a ductile material model for the projectile. The speculation was that the harder steels were more brittle, leading to a smaller penetration cavity and hence a more efficient penetrator. Examining the crater widths in the first 16 mm plate shows that the narrowest craters are from the A material, and the widest for the D material. Table 4 below shows that the crater widths for the four materials increase with decreasing UTS. This supports the Hohler and Stilp results, and hence the residual velocity for the tungsten alloys should also increase with strength.

Table 3: Average crater widths in the first and second target plates

| Average crater width (mm) | A | B | C | D |
|---|---|---|---|---|
| Plate 1 | 13.5 | 13.9 | 14.32 | 14.8 |
| Plate 2 | 14.52 | 14.91 | 15.17 | 14.21 |

This relationship isn't found in the second plate however. Also, the increase in crater width between the 1st to 2nd plate is greater for the high strength alloys than the low strength ones. There is an indication then that the air-gap in the multi-plate target affects the initially small crater diameter of the high strength alloys such that they need to work harder against the 2nd plate. It appears that the higher retardation of the A alloy reduces its penetration more than the gain from its better penetration of the first plate.

The above explanation does not hold true for the experiments carried out by Magness [1] and Meyer [2] against the heavy triple target. In their experiments it was generally the higher strength alloys which performed better. This could be attributed to other material characteristics, which co-incidentally correspond with increased strength. The main difference between the NATO triple target is the larger air gaps between the plates in the NATO target, allowing more dispersion of the fractured material. For the target used, either the air gaps are too small for the debris field to disperse, or the tungsten alloys used have a better dynamic fracture behaviour than the alloys used by Magness and Meyer. It is hoped to carry out further material tests on the alloys used in this work to assess how well the penetration data against this target can be ranked with dynamic behaviour.

## 6. CONCLUSIONS

Four tungsten alloys were assessed for fracture behaviour and penetration performance against a triple-plate target. The penetration of alloys having a relatively low quasi-static strength was as good as those having a high strength but reduced ductility. The best performance came from a moderately high strength alloy with good ductility. During penetration of the first two target plates there was less erosion of the alloys having higher tensile strengths. The longer residual rod lengths however did not provide a distinct improvement in penetration. A suggested hypothesis is that this is due to the greater retardation of higher strength materials by elastic wave reflections, however this could not be confirmed with the experimental data available.

## 7. REFERENCES

[1]     L W MEYER, F-J BEHLER, K FRANK and L S MAGNESS. "Interdependencies between the dynamic mechanical properties and the ballistic behaviour of materials", Proc 12th International Symp. on Ballistics, San Antonio, (1990).

[2]     L W MEYER, L KRUEGER, I FABER et al. "About interdependencies between dynamic material behaviour and ballistic performance of full scale tungsten penetrators", Proc. 4th International conference on tungsten, refractory metals and alloys, Florida, pp 13-21, (1997)

[3]     V HOHLER, E SCHNEIDER, A J STILP, R THAM. "Length and velocity reduction of high density rods perforating mild steel and armor steel plates", Proc 4th International Symp. on Ballistics, (1978)

[4]     T BJERKE, G F SILSBY et al "High yaw penetration performance of long rod penetrators", TB28, 13th International Symposium on ballistics, Stockholm, Sweden, (1992)

[5]     C ANDERSON Jr & D LITTLEFIELD. "Pretest Predictions of Long-Rod Interactions with armour technology targets", SWRI Technical Report 06-5117/001, (1994)

[6]     C E ANDERSON, J D WALKER. "Normalized residual lengths and velocities as a function of projectile strain-to-failure", Proc 17th International Symp. on Ballistics, South Africa, TB054, Vol 3, pp 427-433, (1998)

Table 2: Experimental results

| Firing No. | Strike Velocity (m/s) | Total Yaw (°) | Penetration Depth (mm) | Length after plate 1 (mm) | Length after plate 2 (mm) | Alloy Type |
|---|---|---|---|---|---|---|
| **2802** | **1394** | **1.0@15** | **3.9** | **123** | **n/r** | A |
| 2818 | 1403 | 1.2@126 | 5.0 | 127 | 62.6 | A |
| **2822** | **1478** | **0.4@330** | **5.6** | **127** | **58.8** | A |
| **2805** | **1490** | **0.35@150** | **5.8** | **130** | **60** | A |
| **2809** | **1576** | **0.3@150** | **12** | **130.8** | **63.5-73** | A |
| **2814** | **1579** | **0.6@330** | **9.2** | **130** | **66.3-76.6** | A |
| 2817 | 1391 | 1.3@155 | 1.8 | 125 | - | B |
| 2802 | 1394 | 1.0@15 | 3.9 | 123 | - | B |
| **2807** | **1497** | **1.0@205** | **6.7** | **128** | **50.5-60.7** | B |
| **2810** | **1576** | **0.7@200** | **11.9** | **129** | **66** | B |
| 2821 | 1602 | 3.6@348 | 2.1 | - | - | B |
| 2813 | 1607 | 1.9@270 | 6.4 | 126 | 58 | B |
| **2816** | **1411** | **0.1@330** | **7.2** | **124.7** | **54** | C |
| **2808** | **1597** | **0.2@180** | **17.5** | **129** | **61.6** | C |
| 2806 | 1501 | 1.3@50 | 3.2 | 126 | 47.6 | C |
| **2820** | **1613** | **0.3@180** | **23.1** | **n/r** | **63.5-80** | C |
| 2812 | 1635 | 1.35@6 | 3.7 | - | - | C |
| **2803** | **1388** | **<0.1** | **2.3** | **122.4** | **n/r** | D |
| 2819 | 1416 | 1.9@327 | 0.3 | 116 | - | D |
| 2804 | 1503 | 1.3@330 | 2.0 | 122.4 | 44.8 | D |
| **2811** | **1598** | **0.25@355** | **14.6** | **128.5** | **53-63** | D |
| **2815** | **1603** | **0.25@240** | **16.7** | **128** | **54-64.5** | D |
| **2823** | **1496** | **0.65@150** | **6.2** | **124.7** | **54** | D |

Data in bold are below critical yaw values and are used in penetration analysis. Other results are included to illustrate yaw effects.

# ESTIMATION OF BALLISTIC LIMITS – A COMPARATIVE STUDY OF PREDICTION METHODS

## EDWARDS M.R., MAN J.H.

Department of Materials and Medical Sciences, Cranfield University, RMCS Shrivenham, Swindon, UK

**Abstract:** 7.62 mm armour piercing rounds were fired at thin (5 mm and 6 mm thickness) low alloy steel plates (hardnesses 510 and 345 Vickers) at velocities of 670-950 $ms^{-1}$ that overmatched the targets. It was shown that better estimates of the ballistic limit could be obtained by considering the momentum balance during perforation of the target, rather than the balance of energy. The assumption that the momentum change on perforation was independent of impact velocity was shown not to be the case. The momentum change increasing with increasing impact velocity. Assumptions of the energy absorbed by the target, which was independent of impact velocity, were shown to be false. Estimates of the $V_0$ ballistic limit produced from a consideration of the energy balance were higher than velocities which, in check firings, were shown to produce complete penetration. Similar estimates derived from momentum balances appeared to be much lower, and were well below the velocities of experimental firings that produced partial, rather than total, penetrations.

## 1. INTRODUCTION

Comparison of the effectiveness of materials against kinetic energy penetrators is often made by means of the ballistic limit ($V_{50}$), defined as the velocity at which there is a 50% probability of penetration occurring for a particular projectile and armour thickness. A method of measuring $V_{50}$ is described in STANAG 2920 [1] and involves the measurement of the three lowest velocity rounds that completely penetrate the target and the three highest velocity rounds that partially penetrate the target. The mean of these six velocities is taken to be the $V_{50}$ ballistic limit, provided that the range of velocities is 40 $ms^{-1}$ or less.

Although the $V_{50}$ ballistic limit is useful in comparing the ballistic behaviour of armour materials, the velocity at which the probability of complete penetration is negligible ($V_0$) is of more practical use. However, at velocities close to $V_{50}$, there is considerable scatter in the residual velocity of penetrating projectiles for small changes in impact velocity. This was noted by Tobin [2], as well as in the study of ceramic-faced glass-fibre reinforced polymer composite armour by Horsfall and Buckley [3].

Perforation can be described in terms of either an energy model or a momentum model. In the energy model the ballistic limit can be estimated by plotting the projectile impact energy as a function of the energy of the residual penetrator:

$$\tfrac{1}{2}M_pV_0^2 = \tfrac{1}{2}M_pV_i^2 - \tfrac{1}{2}M_rV_r^2 \qquad (1)$$

where $M_p$ is the projectile mass, $M_r$ the residual mass, $V_i$ the impact velocity, $V_r$ the residual velocity and $V_0$ the ballistic limit. If the energy absorbed by the target is plotted against impact velocity, the model predicts that this will be constant, as it is assumed that the energy required to perforate the target is equal to that absorbed in the "just stopped" condition. For the momentum model the ballistic limit can be estimated by plotting the projectile impact momentum as a function of the momentum of the residual penetrator:

$$M_p V_0 = M_p V_i - M_r V_r \qquad\qquad (2)$$

If the change in momentum on perforation is plotted against impact velocity, the momentum model predicts this to be constant, as it is assumed that the change in momentum required to perforate is equal to that in the "just stopped" condition.

Modelling of the perforation of a range of ceramic-faced glass fibre-reinforced composite armours by Hetherington and Rajagopalan [4] indicated that the penetration was better modelled using a momentum criterion. Correspondence between Hetherington and Shu [5] led to a discussion of energy and momentum changes in perforation by Hetherington [6] and showed that, although a momentum criterion was appropriate for an armour system where failure was by tensile stresses in the backing, the appropriate criterion (momentum or energy) was not clear for the perforation of monolithic metallic armours.

Assuming that the energy absorbed (or the change in momentum produced) by the target is a constant, and equal to that in the "just-stopped" condition, led Tobin [2] to the suggestion of using the firing results of very overmatched projectiles to estimate the $V_0$ ballistic limit. This was because the scatter in residual velocities was seen to be much less than at impact velocities close to $V_{50}$. The methods he suggested were:

a) Plot the projectile impact energy (momentum) as a function of projectile residual energy (momentum) and determine the ballistic limit from the intercept on the y-axis where the residual energy (momentum) is zero.
b) Make several estimates of the ballistic limit using equation (1) or (2). Assume that these are normally distributed, and define the ballistic limit ($V_0$) as the mean of the estimates minus 3 standard deviations.

The aim of the present work is to examine the concept of using overmatched projectiles to estimate ballistic limits for the case of rigid bullets penetrating metallic armours.

## 2. EXPERIMENTAL

Single rounds of 7.62 mm ammunition were fired from a proof barrel, which was set at a distance of 10 m from the target. All firings were carried out at zero obliquity. Velocities of the projectile were measured by optical gates (skyscreens) before and after penetration of the target. The projectile velocity was varied by downloading the propellant from the case, in order to reduce the muzzle velocity.

The projectiles used were:

7.62 mm FFV armour piercing, which contained a tungsten carbide core (composition 5.2% C, 82.6% W, 10.5% Co, 0.4% Fe, hardness 1200 Vickers), mounted in a low carbon steel jacket, coated in gilding metal, in an aluminium cup.

7.62 mm P80 armour piercing, which contained a steel core of hardness 700 Vickers, mounted in a copper jacket.

The rigid cores are shown in Figure 1. These show the differences between the projectiles, especially in regard to the included angle of the penetrator core.



Figure 1: rigid penetrator cores of 7.62 mm FFV (left) and P80 (right) rounds

The target plates, which were all mounted in a 300 mm x 300 mm steel confining frame, were:

Target plate 1 was a low alloy steel (composition 0.43% C, 0.2% Si, 0.6% Mn, 0.53% Ni, 1.43% Cr, 0.34% Mo, balance Fe) hardened and tempered to a hardness of 510 Vickers.

Target plate 2 was a low alloy steel (composition 0.37% C, 0.25% Si, 0.8% Mn, 1.1% Cr, 0.25% Mo, balance Fe) hardened and tempered to a hardness of 345 Vickers.

The experiments carried out involved firing the FFV round through the target plate 1 and the P80 round through target plate 2. In both cases, it was expected that the hard core of the bullet would act as a non-deforming projectile, since the hardness of the bullet was greater than 1.5 times the target hardness, as outlined by Tirupataiah and Sundararajan [7].

## 3. RESULTS

Table 1: 7.62 mm FFV round against steel plate (hardness 510 Vickers)

| Firing | Projectile entry mass (g) | Projectile exit mass (g) | Entry velocity (ms$^{-1}$) | Exit velocity (ms$^{-1}$) |
|--------|---------------------------|--------------------------|----------------------------|---------------------------|
| 1 | 8.274 | 5.90 | 736 | 576 |
| 2 | 8.262 | 5.90 | 783 | 640 |
| 3 | 8.278 | 5.90 | 796 | 654 |
| 4 | 8.260 | 5.90 | 820 | 681 |
| 5 | 8.264 | 5.90 | 846 | 707 |
| 6 | 8.263 | 5.90 | 869 | 734 |
| 7 | 8.264 | 5.90 | 945 | 805 |

Table 2: 7.62 mm P80 round against steel plate (hardness 345 Vickers)

| Firing | Projectile entry mass (g) | Projectile exit mass (g) | Entry velocity (ms⁻¹) | Exit velocity (ms⁻¹) |
|--------|--------------------------|--------------------------|----------------------|---------------------|
| 1 | 9.784 | 3.715 (*) | 670 | 338 |
| 2 | 9.761 | 3.739 | 679 | 342 |
| 3 | 9.747 | 3.708 | 706 | 451 |
| 4 | 9.725 | 3.716 | 729 | 475 |
| 5 | 9.731 | 3.715(*) | 760 | 523 |
| 6 | 9.708 | 3.706 | 779 | 550 |
| 7 | 9.724 | 3.708 | 818 | 609 |

(*) Projectile lost, average value of projectile exit mass assigned

Calculations can now be made using the values of mass and velocity in Tables 1 and 2 of the following:

| | |
|---|---|
| Initial momentum of projectile | Initial kinetic energy of projectile |
| Residual momentum of projectile | Residual kinetic energy of projectile |
| Momentum transferred to target | Energy absorbed by target |

Results for both experiments are shown in Tables 3 and 4.

Table 3: 7.62 mm FFV round against steel plate (hardness 510 Vickers)

| Firing | Initial momentum (kgms⁻¹) | Residual momentum (kgms⁻¹) | Momentum transferred (kgms⁻¹) | Initial kinetic energy (J) | Residual kinetic energy (J) | Energy absorbed (J) |
|--------|----------|----------|----------|----------|----------|----------|
| 1 | 6.090 | 3.402 | 2.688 | 2 241 | 980 | 1 261 |
| 2 | 6.469 | 3.780 | 2.689 | 2 533 | 1 210 | 1 323 |
| 3 | 6.589 | 3.863 | 2.727 | 2 623 | 1 263 | 1 359 |
| 4 | 6.773 | 4.022 | 2.751 | 2 777 | 1 369 | 1 408 |
| 5 | 6.991 | 4.176 | 2.816 | 2 957 | 1 476 | 1 481 |
| 6 | 7.181 | 4.335 | 2.846 | 3 120 | 1 591 | 1 529 |
| 7 | 7.809 | 4.754 | 3.055 | 3 690 | 1 914 | 1 776 |

Table 4: 7.62 mm P80 round against steel plate (hardness 345 Vickers)

| Firing | Initial momentum (kgms⁻¹) | Residual momentum (kgms⁻¹) | Momentum transferred (kgms⁻¹) | Initial kinetic energy (J) | Residual kinetic energy (J) | Energy absorbed (J) |
|--------|----------|----------|----------|----------|----------|----------|
| 1 | 6.555 | 1.256 | 5.300 | 2 196 | 212 | 1 984 |
| 2 | 6.628 | 1.279 | 5.349 | 2 250 | 219 | 2 031 |
| 3 | 6.881 | 1.672 | 5.209 | 2 429 | 377 | 2 052 |
| 4 | 7.090 | 1.765 | 5.324 | 2 584 | 419 | 2 165 |
| 5 | 7.396 | 1.943 | 5.452 | 2 810 | 508 | 2 302 |
| 6 | 7.563 | 2.038 | 5.524 | 2 946 | 561 | 2 385 |
| 7 | 7.954 | 2.258 | 5.696 | 3 253 | 688 | 2 566 |

Graphs of impact energy against residual energy and impact momentum against residual momentum are in Figures 2 and 3. The predicted ballistic limits are listed in Table 5.
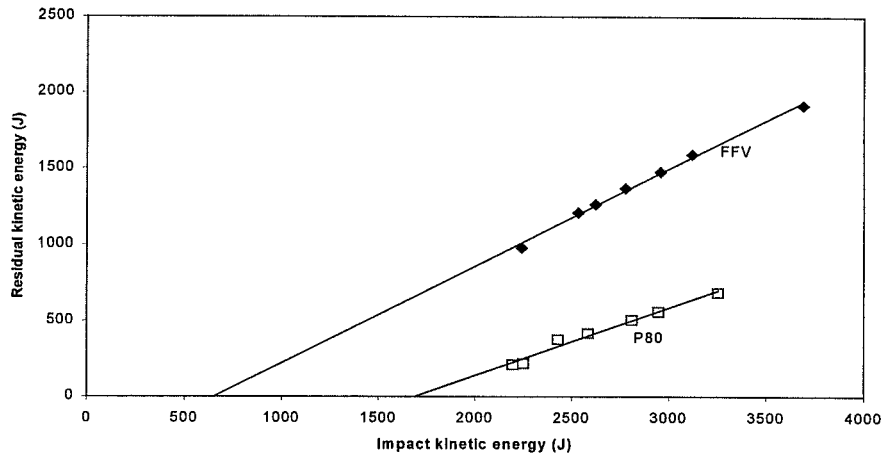
Figure 2: impact energy and residual energy for 7.62 mm armour-piercing rounds
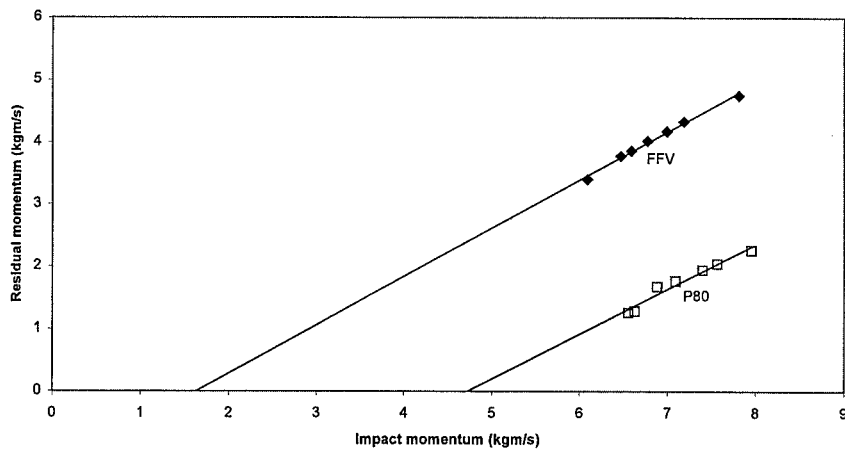


Figure 3: impact momentum and residual momentum for 7.62 mm armour-piercing rounds

Table 5: predicted ballistic limits according to energy and momentum criteria

| Experiment | Ballistic limit $(V_0)$ $(ms^{-1})$ |
|---|---|
| FFV round, energy criterion | 400 |
| FFV round, momentum criterion | 220 |
| P80 round, energy criterion | 593 |
| P80 round, momentum criterion | 482 |

Confirmatory firings were carried out in the region of the ballistic limits predicted by the two criteria. The results are shown in Table 6.

Table 6: results of confirmatory firings

| Round | Impact velocity (ms$^{-1}$) | Residual velocity (ms$^{-1}$) |
|---|---|---|
| FFV | 327 | 15 |
| FFV | 315 | Stopped |
| FFV | 305 | Stopped |
| FFV | 273 | Stopped |
| P80 | 616 | 36 |
| P80 | 533 | Perforated but no velocity recorded by optical gates |
| P80 | 510 | Stopped |
| P80 | 484 | Stopped |

The energy absorbed by the target is shown in Figure 4 as a function of impact velocity: similarly Figure 5 shows how the momentum transferred varies with impact velocity.
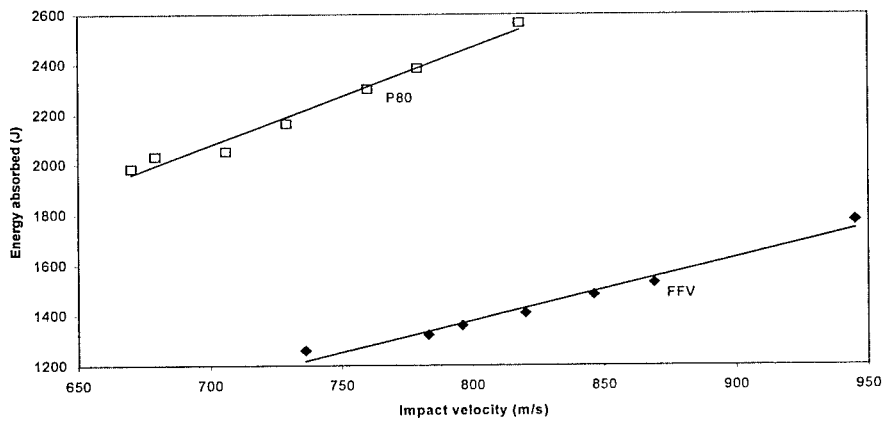


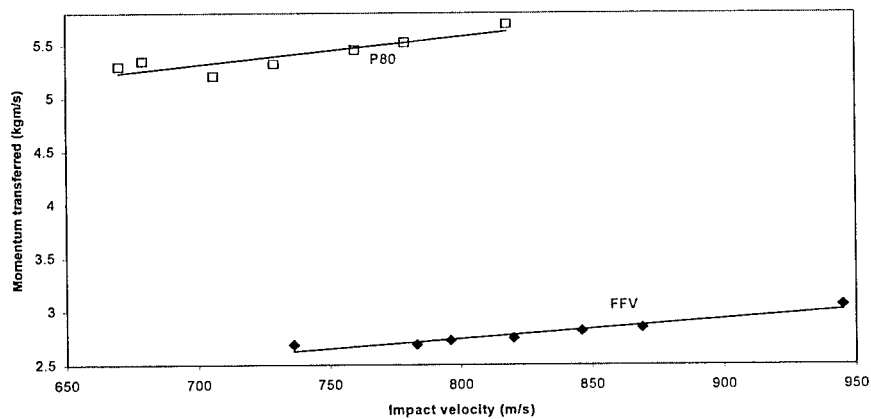Figure 4: variation of impact energy absorbed with impact velocity



Figure 5: variation of momentum transferred with impact velocity

## 4. DISCUSSION OF RESULTS

If the predictions of the energy model are taken, it is suggested that the energy required to perforate the plate should be independent of the impact velocity and that the ballistic limit ($V_0$) should be around 400 ms$^{-1}$ for the FFV round and 593 ms$^{-1}$ for the P80 round (Table 5). The results of Figure 4 and the confirmatory firings (Table 6) show that neither of these is true, with the energy absorbed rising with increasing impact velocity, and perforation occurring at impact velocities that are well below those predicted.

Considering the momentum model, it would be suggested that the change in momentum on perforation should not change as a function of impact velocity, and that the ballistic limit ($V_0$) should be approximately 220 ms$^{-1}$ for the FFV round and 482 ms$^{-1}$ for the P80 round. The results of Figure 5 show that the variation of the change in momentum with impact velocity is less than that of the kinetic energy absorbed (Figure 2), but that the assumption of a constant change in momentum is not justified. Similarly the estimation of the ballistic limit would appear to be better than that produced by the energy model, although at first glance, the estimate for the FFV round would appear low, if compared to the results of the confirmatory firings seen in Table 6.

If the results for the two rounds are compared (Figures 4 and 5), it can be seen that the P80 round has less variation of both energy and momentum as a function of impact velocity than does the FFV round. This could be due to the difference in projectile hardness, although there is little difference between the ratios of projectile and target hardness for the two cases. It may well be that the different shapes of the projectile noses (Figure 1) could explain the variation of effects.

Calculations of the ballistic limit by means of the mean and standard deviation of the estimates of ballistic limit can be made from the momentum model. These give values of the ballistic limit of 297 ms$^{-1}$ for the FFV round and 491 ms$^{-1}$ for the P80 round. If these are compared to the results of the confirmatory firings (Table 6) and the results of Table 5, they appear superficially attractive, especially in the case of the P80 round. However, the derivation of the ballistic limit through the mean and standard deviation is only appropriate for when the change in momentum on perforation is constant as impact velocity changes. Although the effect is small, especially for the P80 round, it must be stated that the change in momentum on perforation (Figure 5) appears to be a function of impact velocity, rather than a random variation due to experimental errors. Thus the assumptions made by Tobin [2] would not appear to be valid in this case, in spite of producing superficially attractive predictions.

## 5. CONCLUSIONS

a) Estimates of the ballistic limit made by means of assumptions of momentum transfer between a rigid projectile and a 5-6 mm thick armour plate are more accurate than similar estimates made by means of assumptions of energy absorption.

b) Both the energy absorbed and the momentum transferred increase with increasing impact velocity. The assumption that the energy absorbed or momentum transferred at overmatching velocities is the same as that transferred at the "just-stopped" condition is not justified.

c) Because the momentum transferred is a function of impact velocity, the derivation of ballistic limit from a series of measurements taken from overmatched projectiles is not justified however superficially attractive the resulting estimates are.

d) The increase in energy absorbed and momentum transferred seen for an increase in impact velocity appears to be a function of projectile type, with the effects being greater for the blunter nosed FFV round than the sharper nosed P80 round.

## 6. ACKNOWLEDGEMENTS

## 7. REFERENCES

[1] STANAG 2920, "Ballistic test method for personal armour and combat clothing", NATO Standardisation Agreement 2920.

[2] L Tobin, "Estimating the Probability of Ballistic Penetration", *J Defence Science,* 3, (2), pp.259-266, (1998).

[3] I Horsfall, D Buckley, "The effect of through-thickness cracks on the ballistic properties of ceramic armour systems", *Int. Journal of Impact Engineering,* 18, (3), pp.309-318, (1995).

[4] J G Hetherington, B P Rajagopalan, "An investigation into the energy absorbed during ballistic perforation of composite armours", *Int. Journal of Impact Engineering,* 11, (1), pp.33-40, (1991).

[5] D Shu, J G Hetherington, "Correspondence on "An investigation into the energy absorbed during ballistic perforation of composite armours" ", *Int. Journal of Impact Engineering,* 12, (2), pp.325-327, (1992).

[6] J G Hetherington, "Energy and momentum changes during ballistic perforation", *Int. Journal of Impact Engineering,* 18, (3), pp.319-337, (1996).

[7] Y Tirupataiah, G Sundararajan, "The volume of a crater formed by the impact of a ball against flat target materials – the effect of ball hardness and density", *Int. Journal of Impact Engineering,* 9, (2), pp.237-246, (1990).

# OURANOS : THE DGA'S HYDROCODE
# FOR IMPACT DYNAMICS STUDY

SIBEAUD J.M.

DGA / DCE / Centre d'Etudes de Gramat
46500 Gramat - France

**Abstract** : Two and three-dimensional numerical simulations are essential to economical design/testing/evaluation of advanced weapons systems and targets. Ouranos is a computer software aimed at modelling a large class of dynamic problems of interest mainly to the defense community. It is currently operated in various computational centres of DGA/DCE establishments. The paper gives some illustrations of its latest capabilities in the field of projectile/target interaction and shaped charge forming.

## 1. INTRODUCTION

Studies in the field of projectile efficiency and target protection have been rapidly expanding at CEG over the last ten years. These studies are led by the constant search for synergy between experimentation and numerical simulation. The later has experienced an ever growing activity mainly due to its high cost effectiveness when compared to full scale field experiments.

In fact, multidimensional, multi-material impact simulations are of fundamental importance in projectile / armour research and development. These simulations can help designers or analysts to explore in depth the effect of design parameters on the performance of weapons on targets.

However, computational resources needed to deal with relevant applications need now to be very powerful. Actually, real configurations are essentially three-dimensional. They require complex material algorithms and thus finer mesh resolution. Further, problem integration times often reach the millisecond regime due to requirement of late response capture of systems investigated. This means that thousands of integration cycles must be performed before obtaining the solution. The requirement for saving as much as possible the computational resources is therefore one of the key features of an efficient software as well as accurate numerics together with physically based constitutive modelling of materials.

The Ouranos hydrocode was specifically developed for this purpose by the Commissariat à l'Energie Atomique under the French Service des Programmes d'Armements Terrestres management. The major emphasis were put on :
- high quality 3D computations within engineering times on a high speed parallel computer,
- routine 2D and 3D computations on workstations.

This paper describes the techniques being developed in Ouranos to address these challenging issues for supercomputers in the years 2000.

## 2. CODE PRESENTATION

The first version of this simulation tool was described in details in [1]. The software includes a Lagrangian component and an Eulerian one closely linked to each other through space and time coupling. The Lagrangian processor is based on unstructured rectangular or hexahedral finite element material discretization. Contact surfaces are used to address the problem of sliding and friction between objects.

The Eulerian component of Ouranos uses the conventional grid-based Finite Volume method. The explicit algorithm executes a Lagrangian step followed by a second-order Van Leer limiting advection step. Ouranos has a high resolution interface tracking scheme [2] that prevents numerical break-up and distortion of material interfaces. These numerical methods reduce the dispersion and dissipation found in first order accurate Eulerian codes. The robust and cost effective Single Line Interface Calculation (SLIC) has been as well implemented.

The material behaviour is simulated by the use of two main models : an equation of state that expresses the value of hydrostatic pressure as a function of density and internal energy, and a constitutive relation between the deviatoric strain and stress, where thermal softening, work hardening and strain rate effects have been accounted for. An evolutionary damage measure can be used to handle the loss of load carrying capability of solid materials subjected to dynamic straining at elevated temperature. High explosive ideal detonation can be modelled using the so-called programmed burn logic through the knowledge of the initiation points and the detonation velocity. The response of high explosive to an unusual mechanical environment is modelled using various ignition and growth models that can handle shock to detonation transition.

## 3. LATEST DEVELOPMENTS

Since its first run on vector computers, some unique capabilities have been implemented in Ouranos such as the Euler/Euler remapping which allows any simulation to be dealt with by changing the space discretization as well as adding or removing objects from the calculation. Moreover the problem dimension can be switched from 2D to 3D when necessary. This later feature is also available in the Lagrange/Euler remapping.

Apart from the developments on numerics, a special effort was devoted on coding the Eulerian processor on a parallel machine. It was early felt that the technology of parallel computing would allow problem size to be pushed well beyond the capabilities of vector supercomputers. The technique employed is essentially based on the discretized domain distribution over sub domains, each one being treated by one processor. The structured mesh of the finite volume method is well suited for such a technique, provided that enough overlap of adjacent sub domains exists to ensure exchange of information between them.

All these features are considered now fully mature and are illustrated in the next section with test cases provided by members of the Ouranos users' club.

# 4. OURANOS CALCULATIONS OF PROJECTILE PERFORATION

Long rod kinetic energy projectiles are made of tungsten or depleted uranium alloys with densities about three times that of steel. Their effectiveness can be degraded when faced with complex armour systems using various defeat mechanisms. Capabilities for simulating the complete perforation process of high angle of attack targets, both inert and reactive, is demonstrated. The remapping technique of Ouranos/Euler is illustrated on two different impact situations involving projectile and armour interaction.

## 4.1 Oblique plate perforation

Ouranos is used to model the oblique impact of KE projectile into a thin plate and then the subsequent penetration of the residual projectile into a thick over match high hardness steel plate. The stress relaxation and yawing of the projectile in free flight was carried out within a specific discretized domain fitted to the projectile dimensions. Figure 1 shows the successive operations generated in the course of the simulation. The first and the last Eulerian simulation, involving projectile and target interaction, resulted in a total of approximately 8 million cells and ran with using 8 processors CEG's IBM SP2 parallel machine. A one piece computation would have generated as much as 28 million cells, which is beyond the current CEG's resources.
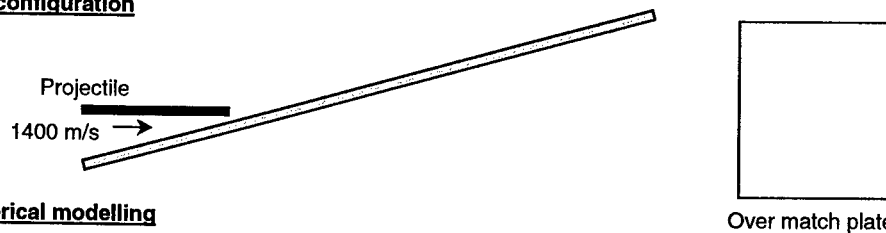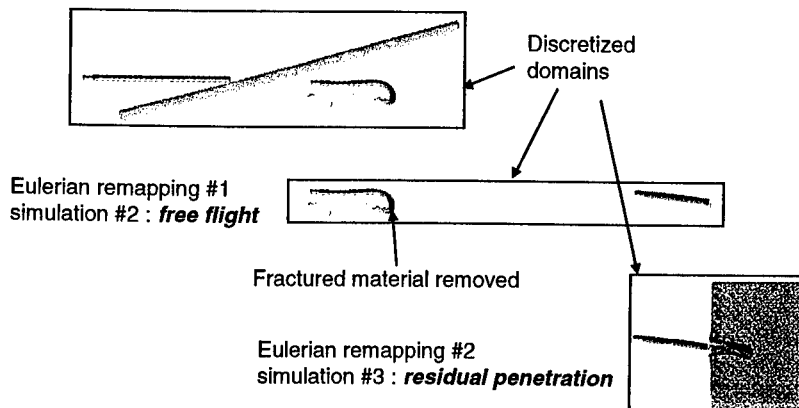


Figure 1 : computational steps generated by the simulation of a KE projectile interaction with a spaced target under obliquity.

## 4.2 Explosive reactive armour perforation

The Ouranos model for the ERA perforation scenario is shown in figures 2 at different times after impact. The quantitative accuracy needed for this simulation is dictated by the particular geometry of both projectile and target. In fact, all the experimental characteristics of the projectile and the ERA target were taken into consideration (plate dimensions, explosive geometry and projectile design) for the most reliable modelling possible. The calculation ran using 10 processors of the parallel machine and took roughly 4,5 days CPU time.

Comparison with existing experimental data were exercised. The computing performance and the simulating fidelity shown by Ouranos are very encouraging.

Future work will address a number of technical topics, including a comparison between tungsten and depleted uranium alloys as penetrator materials for KE defeat of ERA targets and an investigation in the relationship between ballistic performance and metallurgical properties.

**Step 1** : ERA perforation

**Step 2** : front plate of ERA and HE removed, over match plate added

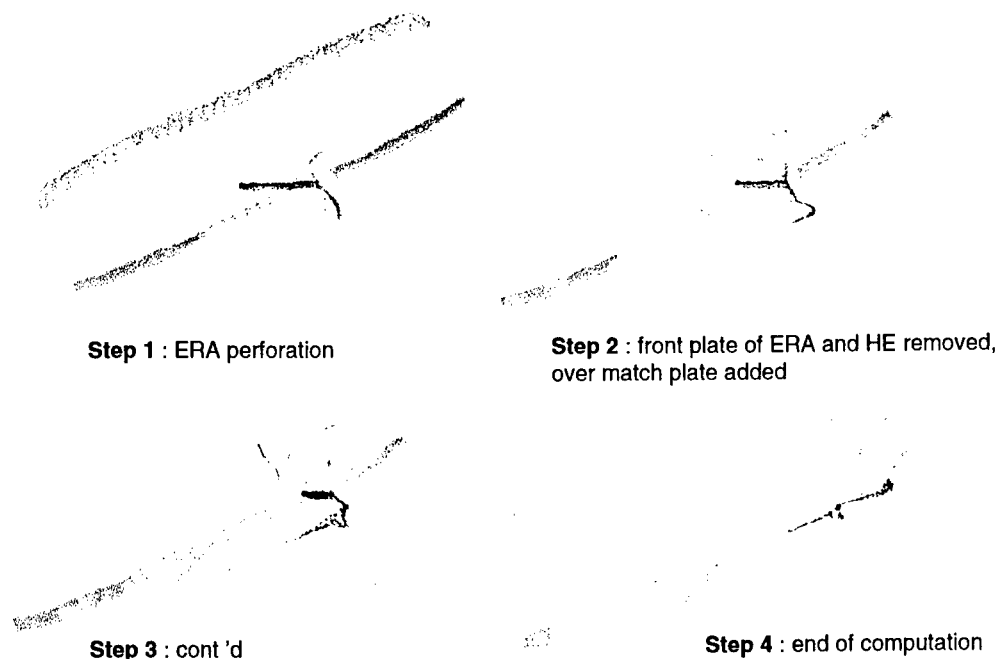**Step 3** : cont 'd

**Step 4** : end of computation

Figure 2 : perforation of a reactive armour module and subsequent residual penetration.

## 4.3 Jet and EFP interaction with armours

In order to compute the solution of the explosive detonation, the jet formation and the perforation of a non explosive reactive armour under obliquity, we used first the possibility of performing a 2D simulation because of the axial symmetry of the charge. The computation was continued until the jet was fully stretched to the correct stand-off distance from the initial position of the charge. At this stage, 2D modelling was no longer possible because of the target obliquity. The jet was then transferred into a three-dimensional domain and the NERA sandwich target could be generated. However, the plane symmetry made possible discretizing

only one half of the problem. Figures 3 and 4 present these two calculations. The 3D computation is shown just before the armour plate went in contact with the jet.

The same procedure apply for explosively formed projectiles (EFP) except that the initial 2D calculation of the projectile elongation process was performed using the Ouranos Lagrangian processor. The remapping into an Eulerian domain enables the penetration of the projectile into the baseline armour to be calculated because the Lagrangian material discretization is not well suited to the large distortions associated with the penetration mechanism. Figure 5 illustrates the different computational steps, in 2D only.
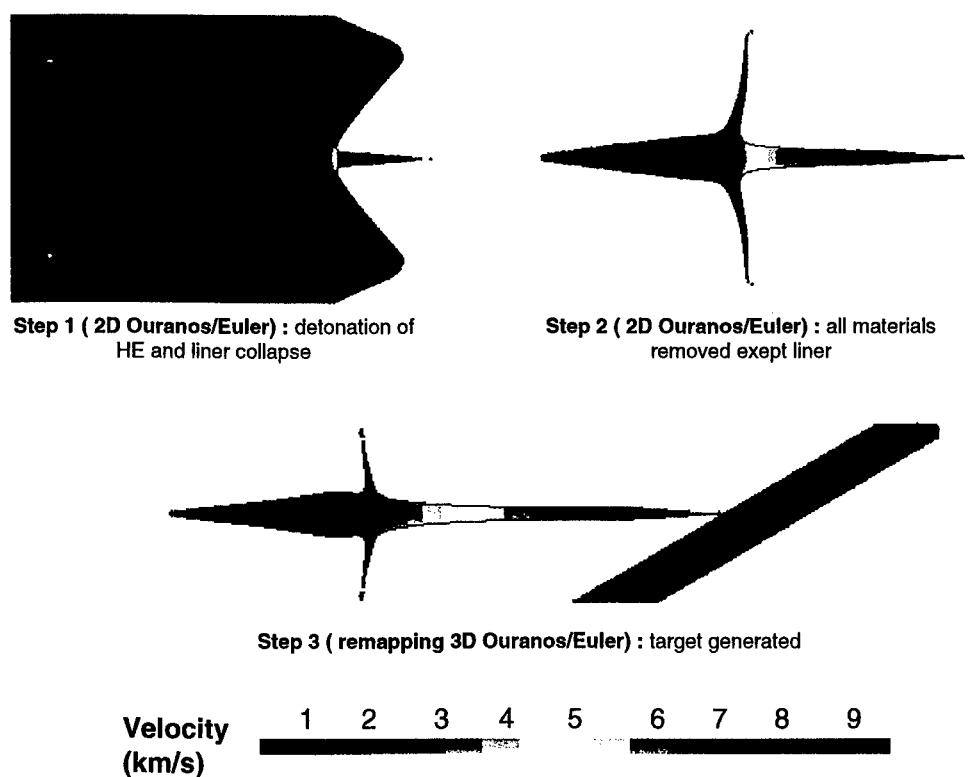


**Step 1 ( 2D Ouranos/Euler) :** detonation of HE and liner collapse

**Step 2 ( 2D Ouranos/Euler) :** all materials removed exept liner

**Step 3 ( remapping 3D Ouranos/Euler) :** target generated

**Velocity (km/s)**    1   2   3   4   5   6   7   8   9

Figure 3 : 2D computation of the shaped charge jet elongation and 3D remapping.

## 4.4 Shock to detonation transition in 3D

Simulations of the transition from shock to detonation of cased explosive were done using the Forest-Fire nucleation and growth reaction-rate model. The objective was to determine the initiation threshold of the explosive layer for various fragment impact characteristics (density, velocity, shape, obliquity...). Unfortunately, the amount of data generated by the fine mesh spacing needed for such application did not allow any 3D computation was made on classical vector supercomputers. The multidomain decomposition capability of Ouranos and the arrival of the parallel machine at CEG have enabled for the first time these configurations to be exercised routinely. Figure 6 gives an illustration of a tungsten sphere impacting at 3.5 km/s a confined explosive layer backed with polyethylene under 65° obliquity. The colour plots show the detonation build-up in the explosive layer. The last one indicates that massive detonation has occurred. This scenario was confirmed experimentally with a 2-stage light gas gun.
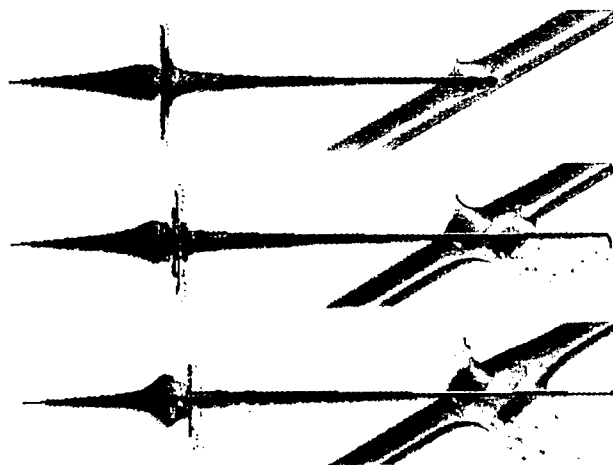
**Step 4 (3D Ouranos/Euler) :jet perforation of NERA**
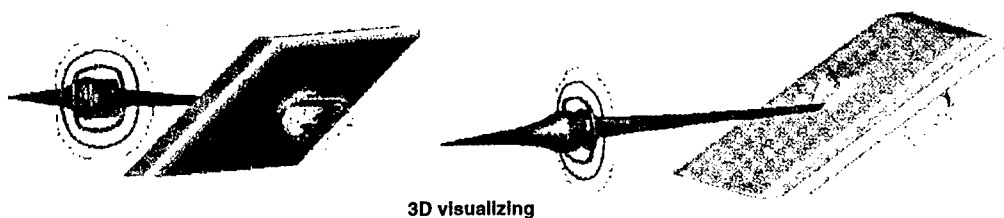
**3D visualizing**

Figure 4 : 3D remapping of the jet and computation of the jet / NERA interaction.

**2D Lagrange :** elongation process of
projectile

**Remapping and 2D Euler :**
penetration of RHA target

'X-Ray' from calculation
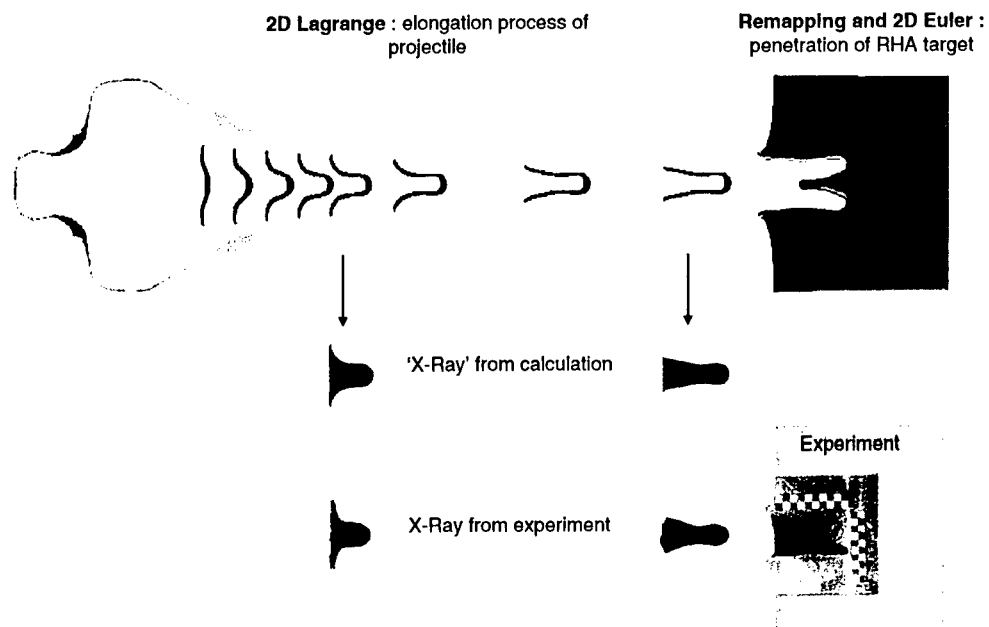
Experiment

X-Ray from experiment

Figure 5 : Lagrangian calculation of the EFP elongation process and Eulerian calculation of its penetration into
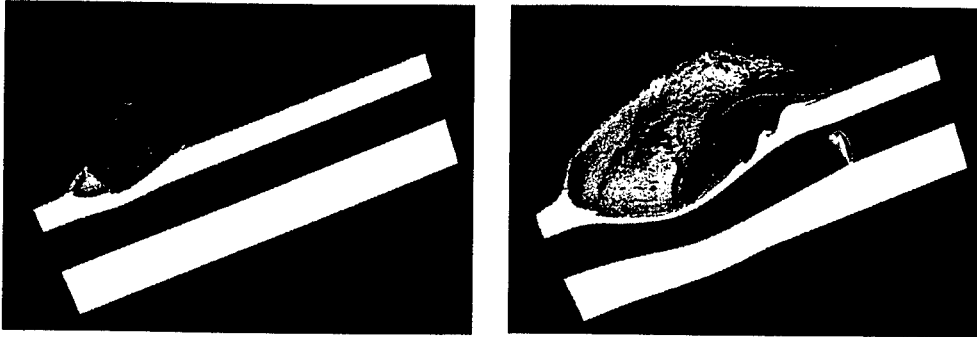the baseline armour.

Figure 6 : cased explosive shock initiation by heavy fragment hypervelocity impact at high obliquity.

## 5. CONCLUSION

This paper has summarised the progress being made in the specialisation and application of Ouranos to problems involving complex configurations. In a preliminary stage, scaled experiments have been used to guide and develop the numerical algorithms and mesh strategies and identify shortcomings in the simulation. The suitability of the code for the applications presented has been enhanced by the introduction of new data processing, namely the multi-domain decomposition on parallel computers and the remapping technique. Both techniques have made possible accurate simulations of complex 3D flows within realistic time response.

## 6. REFERENCES

[1] H. Jourdren, J.M. Sibeaud, M. Adamczewski-Cauret ; logiciel Ouranos : présentation et utilisation en détonique. Revue scientifique et technique de la défense (1995).

[2] D.L. Youngs ; Time dependent Multi-Material Flow with Large Fluid Distorsion. In Numerical Methods for Fluid Dynamics (Edited by K.W. Morton and J.H. Baines), Academic Press (1982).

# EXPERIMENTAL DETERMINATION OF WITNESS PACK CALIBRATION CURVES.

VEROLME, J.L.

TNO Prins Maurits Laboratory, P.O. Box 45, 2280 AA Rijswijk, The Netherlands

**Abstract:** For characterisation of behind armour debris, witness packs may be used. A witness pack consists of an array of metallic plates interspaced by polystyrene foam sheets. To quantify the fragment mass and velocity from the corresponding hole area and position in the individual witness plates, perforation threshold curves must be available to provide the ballistic limit velocity for each plate as a function of the fragment mass. This paper presents the results of the last phase (phase 3) of a study to determine perforation threshold curves. The first two phases of this project were focussed on developing perforation threshold curves for steel only. In addition, empirical trendlines have been developed. The work reported here consisted of extending the experimental database and calculation method to include materials other than steel. For that purpose aluminium and tungsten FSP's were fired at witness pack plates.

## 1 INTRODUCTION

Two experimental methods are commonly used to quantify behind armour (BA) debris: fragment soft recovery in combination with flash radiography and witness packs. The first method allows the direct measurement of the debris. Trajectory and velocity measurements can be obtained from the flash radiographic films of two orthogonal stations behind the armour, whereas, the mass and the distribution of the fragments is obtained from the recovery of the fragments in a soft medium such as cardboard. Such a procedure provides the maximum amount of fundamental data, but is labour intensive and thus costly.

The second method comprises of placing a witness pack behind the armour. This procedure focuses on the penetrating energy of the debris through a series of thin, equally spaced plates. Each plate is separated by an expanded polystyrene foam sheet. After a test, each individual witness pack is dismantled, and each plate is digitised. Holes are labelled and the respective centroid position and area are then computed. A disadvantage of the witness pack technique is that it does not directly quantify the fragment mass and velocity. Furthermore, perforation threshold curves for the penetration of successive plates must be available to conduct reliable data analysis. On the other hand, data reduction is much quicker, and the experimental set-up is less complex thus reducing sources of error and costs. Another advantage of the witness pack technique is that it eliminates, by its inherent nature, the very small or low energy fragments that can do little damage in practice simply because they are not capable of perforating the first witness pack plate. The latter provided that the material of the witness pack plate is suitable for this application.

The witness pack configuration selection is critical for experimental tests. For conventional ballistic tests, in which the fragments are expected to have moderate velocities, a standard metallic witness pack is used which consists of aluminium and steel plates. However, if a violent environment is expected behind the armour, for instance generated by relatively high

impact velocities or for a chemical energy (CE) threat, an all-steel witness pack would be used instead of the standard metallic array witness pack. The plate thicknesses for witness packs are selected so as to obtain an adequate signature (i.e. holes and distributions) of the BA debris. The metallic witness array packs used as examples in this investigation respect the material selection and areal density criteria defined within STANAG 4190 Edition 2 [1]. Table 1 describes the plates in an all steel (S1) witness pack, used in the U.S. and a metallic array (steel and aluminium, M1) witness pack.

*Table 1: Witness pack configurations.*

| Plate Number | Aluminium M1 | | Steel S1 | |
|---|---|---|---|---|
| | Material | Thickness (mm) | Material | Thickness (mm) |
| 1 | Al99.5 F11 (1Shh) | 1.0 | St12-3 | 0.8 |
| 2 | " | 1.0 | St37-2 | 1.5 |
| 3 | " | 3.0 | " | 1.5 |
| 4 | St37-2 | 1.5 | " | 3.0 |
| 5 | " | 1.5 | " | 3.0 |
| 6 | " | 1.5 | " | 6.0 |
| 7 | " | 1.5 | - | - |

Plates interspaced by 25.4 mm polystyrene foam sheets.

Aluminium 99.5 is commercially pure (99.5 %) aluminium, equivalent to the U.S. Aluminium Association material 1100. Steel 12-3 and 37-2 (DIN 17100 designations) are equivalent to American Iron and Steel (AISI) materials 1010 and 1020.

## 2 PREVIOUS WORK

In [2], results are presented of the efforts to calibrate witness packs S1 and M1 with steel projectiles.
A witness pack calibration curve presents critical perforation velocities as a function of the fragment mass. These curves were developed experimentally at TNO/PML's Laboratory of Ballistic Research. Standard fragment simulating projectiles (FSP's) were fired at the two witness packs described in Table 1. The perforation threshold velocity (the ballistic limit velocity $V_{50}$, equivalent to the industry standard definition) was determined for each successive plate. The FSP's are the well-known standard chisel-nose cylinders as illustrated in Figure 1. The limit velocity was calculated based on the Kneubuehl method. A family of six FSP's was tested, ranging in mass from 162 mg to 13.4 g, which is representative of the range of typical BA debris fragment masses. Tables 2 and 3 present an overview of the test results for the M1 and S1 packs respectively. Threshold velocities reported in these tables are the minimum witness pack impact velocities required for an FSP of a given mass to penetrate each plate in the witness pack. These data are for normal impact conditions (i.e. zero obliquity). It was observed that, in general, beyond the third plate, projectile yaw became significant resulting in tumbling.
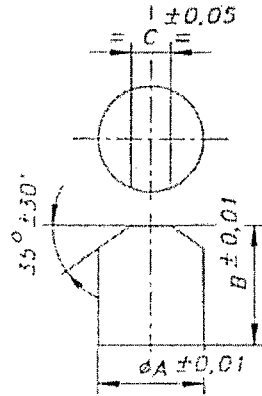
*Figure 1: Schematic drawing of typical chisel-nose FSP (dimensions in mm)*

*Table 2: Experimental threshold velocities for the M1 pack.*

| FSP mass | Experimental threshold velocity $V_{50}$ (m/s) | | | | | | |
|---|---|---|---|---|---|---|---|
| | Plate number | | | | | | |
| (g) | 1 | 2 | 3 | 4 | 5 | 6 | 7 |
| 0.162 | 187 | 314 | -† | -† | -† | -† | -† |
| 0.486 | 128 | 219 | 468 | 713 | -† | -† | -† |
| 1.1 | 111 | 174 | 348 | 511 | 716 | -† | -† |
| 2.85 | -• | 143 | 267 | 382 | 520 | 686 | -† |
| 5.3 | -• | 115 | 223 | 343 | 399 | 512 | 619 |
| 13.4 | -• | -• | -• | 235 | 287 | 419 | 474 |

• Perforation threshold value below attainable velocity, † above attainable velocity

*Table 3: Experimental threshold velocities for the S1 pack.*

| FSP mass | Experimental threshold velocity $V_{50}$ (m/s) | | | | | | |
|---|---|---|---|---|---|---|---|
| | Plate number | | | | | | |
| (g) | 1 | 2 | 3 | 4 | 5 | 6 | 7 |
| 0.486 | 200 | 554 | -† | -† | -† | -† | -† |
| 1.1 | 170 | 392 | 648 | -† | -† | -† | -† |
| 2.85 | -• | 270 | 430 | -† | -† | -† | -† |
| 5.3 | -• | 236 | 340 | 754 | -† | -† | -† |
| 13.4 | -• | -• | 273 | 509 | -† | -† | -† |

• Perforation threshold value below attainable velocity, † above attainable velocity

Once all of the threshold velocities are calculated, they can be plotted as a function of the fragment mass. A least-squares curve is then fitted to the experimental threshold velocities. The relationship between $V_{50}$ and fragment mass appears to obey the following general relation:

$$V_{50} = K_{WP,i} \left(m\right)^{-1/3} \tag{1}$$

where $\quad$ $K_{WP,i}$ $\quad$ constant for i-th plate of witness pack (m.g$^{0.3}$/sec)

$\quad\quad\quad\quad$ m $\quad\quad\quad$ fragment mass (g).

The constants for each witness pack plate combination can thus be determined based on the experimental results. The factors $K_{WP,i}$ for the witness packs M1 and S1 are listed in Table 4.

*Table 4 Factors $K_{WP,i}$ for witness packs M1 and S1.*

| Plate number | M1 | S1 |
|---|---|---|
| 1 | 103.6 | 163.9 |
| 2 | 176.3 | 416.9 |
| 3 | 369.1 | 639.0 |
| 4 | 552.5 | 1277.6 |
| 5 | 726.0 | - |
| 6 | 950.4 | - |
| 7 | 1095.6 | - |

## 3 TUNGSTEN AND ALUMINIUM FSP'S

A small number of tungsten and aluminium FSP's were fired at the two standardised witness packs. The experimental threshold values (determined exactly like before) are given in table 5. The density of the aluminium was measured 2850 kg/m$^3$ and the tungsten (alloy) was 14380 kg/m$^3$.

*Table 5A: Experimental threshold velocities for the M1 pack and tungsten fragment.*

| FSP mass (g) | Experimental threshold velocity $V_{50}$ (m/s) | | | | | | |
|---|---|---|---|---|---|---|---|
| | Plate number | | | | | | |
| | 1 | 2 | 3 | 4 | 5 | 6 | 7 |
| 2.02 | -• | 128 | 248 | 356 | -† | -† | -† |

• Perforation threshold value below attainable velocity, † projectile breaks-up

*Table 5B: Experimental threshold velocities for the S1 pack and tungsten fragment.*

| FSP mass (g) | Experimental threshold velocity $V_{50}$ (m/s) | | | | | | |
|---|---|---|---|---|---|---|---|
| | Plate number | | | | | | |
| | 1 | 2 | 3 | 4 | 5 | 6 | 7 |
| 2.02 | -• | 296 | 405 | -† | -† | -† | -† |

• Perforation threshold value below attainable velocity, † projectile breaks-up

*Table 5C: Experimental threshold velocities for the M1 pack and aluminium fragments.*

| FSP mass (g) | Experimental threshold velocity $V_{50}$ (m/s) | | | | | | |
|---|---|---|---|---|---|---|---|
| | Plate number | | | | | | |
| | 1 | 2 | 3 | 4 | 5 | 6 | 7 |
| 0.40 | -• | 328 | 822 | -† | -† | -† | -† |
| 1.94 | -• | 180 | 428 | -† | -† | -† | -† |

• Perforation threshold value below attainable velocity, † above attainable velocity

*Table 5D: Experimental threshold velocities for the S1 pack and aluminium fragments.*

| FSP mass (g) | Experimental threshold velocity $V_{50}$ (m/s) | | | | | | |
|---|---|---|---|---|---|---|---|
| | Plate number | | | | | | |
| | 1 | 2 | 3 | 4 | 5 | 6 | 7 |
| 0.40 | 372 | 702 | -† | -† | -† | -† | -† |

• Perforation threshold value below attainable velocity, † above attainable velocity

The above tables only list the succesfull experimental results. During the firing all types of problems arose:

- The tungsten fragments broke up during the perforation causing the experiments to be unuseable. In the concept the projectiles are assumed to remain rigid.
- The aluminium fragments at already moderate velocities started deforming, making almost all experimental results invalid. The only threshold velocities that can be trusted are the velocities below, say, 200 m/s.
- Some projectiles could not fit in the accelerators or damaged the barrel during acceleration.

Now comparison of the above experimental results with the methodology presented before is possible. For the 'TNO-method', the K factors need adjustment to incorporate fragment materials other than steel. The following relation may be used:

$$K_{mat} = K_{st} \left( \frac{\rho_{st}}{\rho_{mat}} \right)^{1/6} \tag{2}$$

where      mat      material other than steel (in this case tungsten and aluminium)
              st         steel.

The table below gives the comparison between the 'TNO-method' using the K factors and the experiments.

*Table 6: Comparison between predictions with the 'TNO method' and experiments (between brackets)*

| Plate | Tungsten 2.02 g | | Aluminium 0.4 g | | Aluminium 1.94 g | |
|---|---|---|---|---|---|---|
| | M1 | S1 | M1 | S1 | M1 | S1 |
| 1 | 76 | 120 | 161 | 255 (372) | 101 | 159 |
| 2 | 129 (128) | 305 (296) | 275 (328) | 649 (702) | 171 (180) | 404 |
| 3 | 270 (248) | 468 (405) | 575 (822) | 995 | 358 (428) | 620 |
| 4 | 404 (356) | 935 | 861 | 1990 | 536 | 1239 |
| 5 | 531 | - | 1131 | - | 704 | - |
| 6 | 696 | - | 1481 | - | 922 | - |
| 7 | 802 | - | 1707 | - | 1063 | - |

The correlation for the tungsten fragments is very satisfactory, with a maximum error of about 16 %. For aluminium as expected the prediction underestimates the experimental value, especially for velocities exceeding 200 m/s. This can be attributed to deformation of the projectiles which takes energy which cannot be used any more for perforation, thus increasing the threshold velocity.

## CONCLUSIONS

This work presents the development of experimental threshold curves for witness packs. Threshold curves give the threshold velocity as a function of fragment mass. These curves, together with the hole size in the first plate, essentially enable the determination of the fragment mass and velocity from the penetration depth (number of plates) into the witness pack.
It appears possible to represent a witness pack threshold curve with a formula including only the fragment mass and type of material.

## REFERENCES

[1]     "Test procedures for measuring behind armour effects of anti-armour ammunition, NATO Military Agency for Standardisation (MAS), STANAG 4190, Edition 2", AC/225_D/1375, (1996).

[2]     Verolme, J.L., M. Szymczak and J.P.F. Broos, "Metallic Witness Packs for Behind Armour Debris Characterisation", *Int. Journal of Impact Engineering*, Vol. 22, No.7, (1999).

# PLEIADES/I : THE NEW FRENCH CODE
# FOR INFRASTRUCTURE VULNERABILITY ASSESSMENT
# FOR CONVENTIONAL AIR TO SURFACE ATTACKS

## TOURNEMINE D., DARRIGADE A.

DGA, DCE, Centre d'Etudes de Gramat, 46500 Gramat, France

**Abstract :** Centre d'Etudes de Gramat is in charge of developping a code able to evaluate the lethality of air to surface conventionnal weapons against surface or buried, soft or hardened infrastructures. This software, called PLEIADES/I, is presented. It also will be an expert tool to study infrastructure vulnerability, armement behaviour or new warehead concept expected efficiency. Its frame is based on five main parts : a target database, a weapon database, an user defined attack scenario, a weapons/target interaction assessment and postprocessing tools. A Monte-Carlo approach is used to take into account any dispersions on input data, such as the aim point of each weapon, to assess the target kill probability.

## 1. INTRODUCTION

While western nations no longer have an identifiable enemy, these last years have been shown that the frequency of local crises requiring military intervention increases. This situation has led radical changes in the tasks of armed forces. Peace support operations differ from traditional military missions due to various and new constraints : not only military, but also political and humanitarian aspects must be considered. Thus, the search for optimum efficiency in the suppression of enemy defenses while minimizing collateral damage requires fast and precise tools to prepare air to surface attack missions.

The attack aims can be to neutralize, destroy, or degrade enemy defenses in a specific area. So, among other things, air forces need to evaluate conventionnal armements lethality against surface or buried, soft or hardened infrastructures.

Centre d'Etudes de Gramat is in charge of developping a code able to fit this military staff need. This software will be also an expert tool to study infrastructure vulnerability, armement behaviour or new concept expected efficiency. The paper presents this code, called PLEIADES/I.

## 2. CAPABILITIES

### 2.1 Purposes

PLEIADES/I must present two main capabilities.

This software must be able to assess the effectiveness of air to surface weapons systems against surface or buried, soft or hardened infrastructures (figure 1). The calculations must be precise, but essentially fast. This capability will be exploited by the air forces, for preparation of attacks.

Moreover PLEIADES/I must be a precise tool to help the expert in the field of ballistics and detonics : evaluation of a bomb penetration capabilities, prediction of target vulnerability to a conventionnal explosion, prediction of warehead behaviour during target penetration, evaluation of the capabilities of a new weapon design. Here, the calculations can be slower, but essentially precise.
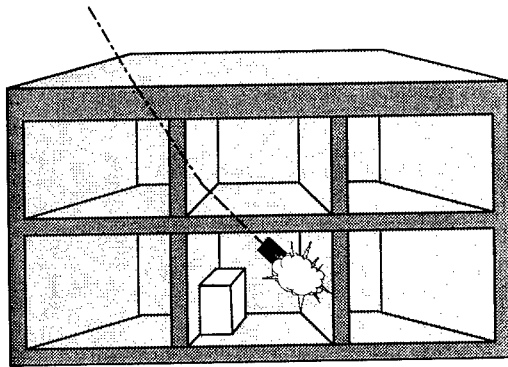


Figure 1 : PLEIADES/I : infrastructure lethality assessment

## 2.2 Operational requirement : attack effectiveness assessment

A Monte-Carlo approach is used to take into account any dispersions on input data, such as the aim point of each weapon, to assess the target kill probability. It requires the use of a large number of simulation runs to obtain a statistically valid lethality result. So, the different phenomena must be calculated by fast modules : penetration of the warhead into the target, detonation effects (structure response, damaging of equipments), probability of kill by analysing equipments and functions vulnerability. The calculation modules will use empirical formulations or tables specifically built from results from previous experiments or numerical computations. In this case, interpolations will be done from tabulated data to get the expected results.

The input data are a target model, one or several weapons models - these models are described below - and the attack scenario (figure 2). The attack scenario identifies the weapons used, kind and number, aim points and dispersions, impact conditions (velocity, angles of impact), fuzing programmation. Note at this level that only the terminal efficiency is calculated, once each weapon hits the target.

Numerous analytical computation modules can be utilized to describe the different physical processes involved such as bomb penetration, shaped charges perforation, fragments distribution, pressure loading generated by explosion, wall and equipment response to blast and fragments. Damages caused by successive weapons are cumulated.

Many informations will be stored during and at the end of a computation. The attack efficiency will be analysed thanks to different outputs. From the damage level of individual equipments, an evaluation of target global functionnal damage will be performed (figure 3). For each equipment, the probability of kill will be given versus the involved damaging process : warhead fragment hits, blast effect, damaged wall concrete, fragment hits, wall collapse, direct weapon hit, ... The kill probability of the target missions will be evaluated.



Figure 2 : scenario of attack (typical input window)
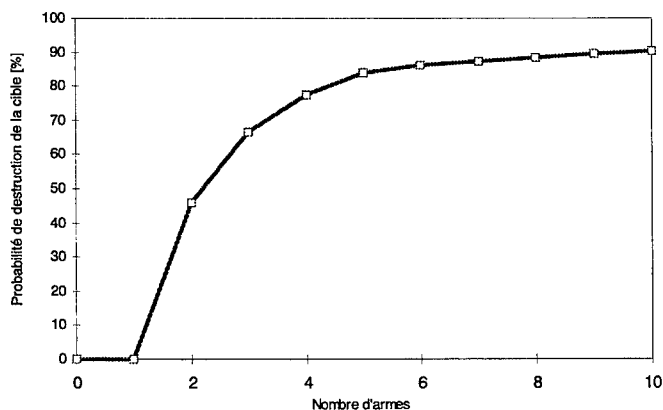


Figure 3 : cumulated efficiency

## 2.3 Expert investigation tool

PLEIADES/I will be used to investigate more precisely some specific phenomenon as warhead penetration or structure behaviour to detonation effects.

An analytical calculation module will be used to calculate penetration of kinetic penetrators through reinforced concrete slabs. The output will be characteristics of the weapon trajectory, decelerations, ... The projectile skin is discretised by surface elements. Normal and tangential forces are calculated on each element. When the projectile hits a steel reinforcement, a new force is added to the surface element. The perforating resistance near a contact surface between two material layers or near a free surface is calculated versus distances between each element and this surface. This method allow to predict the spalling effect which appears on the back face of the concrete slab. It is validated from experimental results or computational results (figure 4) [1,2].
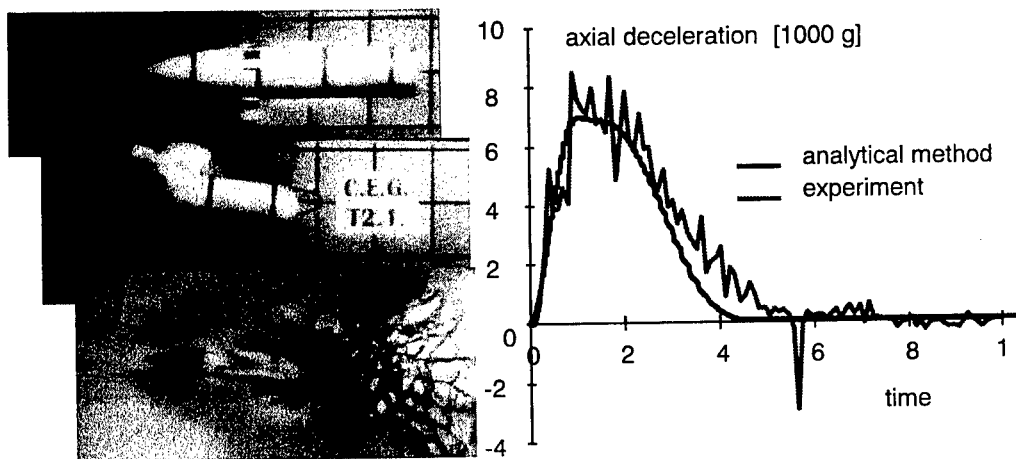


Figure 4 : validation of the penetration module

Analytical modules will also be developped to calculate concrete slab perforating by new weapon concepts as explosively formed projectile – follow through bomb tandem.

Another calculation module will be used to describe the shock wave produced by the warhead detonation, and to calculate the pressure loading of all elements submitted to the shock wave [3,4]. The module uses empirical data and analytical relations. First of all, the incident shock wave is determined by some main characteristics which are : the arrival time, the pressure amplitude, the positive phase duration and the pressure impulse. These values are calculated from data base of the litterature [5,6], or from specific experimental or computational results [7]. For each point of an exposed panels, the loading pressure depends on the incident shock wave characteristics and on the incidence angle between the incident shock wave propagation way and the normal direction to the surface, at this point. The loading overpressure amplitude is calculated by using abaqus from the litterature which give the ratio between the loading overpressure amplitude and the static overpressure amplitude of the incident shock wave,

versus the incidence angle. Multiple pressure peak process inside a room is calculated by using a source images principle (figure5).
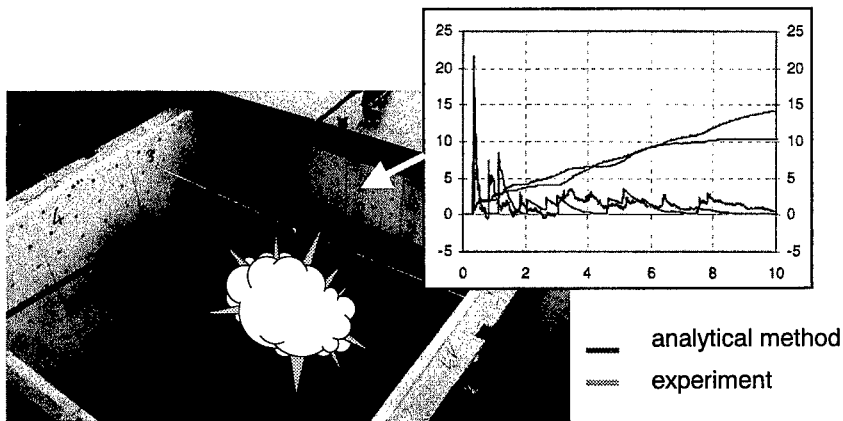


Figure 5 : pressure loading calculation

Several regimes of strutural response can occur, as the pressure loading is intense but brief, or lower but extended. A breach calculation method will be used to predict the local response to a close detonation (figure 6 [8]). Moreover, experimental results of high explosive charge detonation inside reinforced concrete panels (figure 7) will be used to developped a semi-empirical method to calculate the panel damages and the shock wave which is transfered. An analytical, semi-empirical approach to predict the behaviour of structures in a flexion mode will be used to calculate the behaviour of concrete panels when submitted to a slow dynamic pressure loading [3]. This approach is beeing validated from numerical results using a model which describes the concrete panel behaviour to dynamic pressure loadings [9].
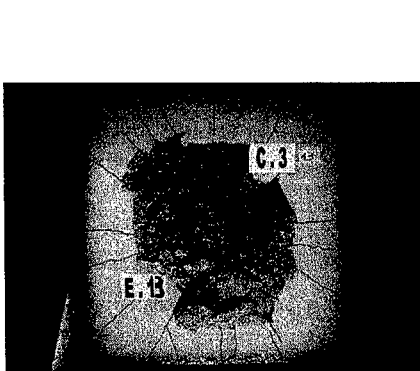


Figure 6 : structural response
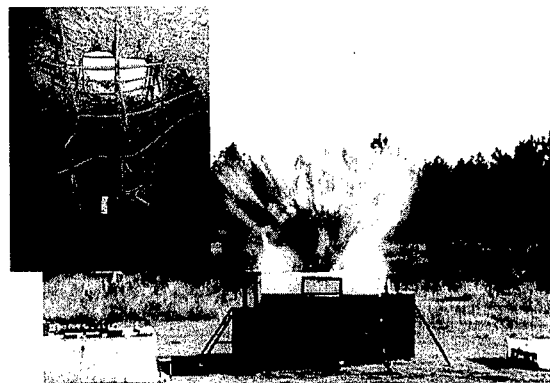


Figure 7 : detonation inside a concrete panel

## 3. CODE STRUCTURE

The software is fully modular to easily integrate any change or improvement of interaction laws. It can be also easily adapted to take into account any technological breakthrough. Its frame is based on five main parts : a target database, a weapon database, an user defined attack scenario, a numerical weapon / target interaction assessment, and postprocessing tool.(figure 8). A Monte-Carlo approach is used to take into account any dispersions on input data, such as the aim point of each weapon, to assess the target kill probability.

```
    ( weapons )  →  [ scenario ]  ←  ( targets )
         ┊                │
         └ - - - - - →  ( N )  ←─────────────┐
                          │                   │
                   [ penetration ]            │
                          │                   │
                    [ detonation ]            │
                          │                   │
                       [ blast ]              │
                          │                   │
                    [ fragments ]             │
                          │                   │
                [ structural damage ]         │
                          │                   │
            [ equipment vulnerability ]       │
                          │                   │
                  [ target damage ]           │
                          │                   │
                          └───────────────────┘
                          ↓
                [ lethality assessment ]
```
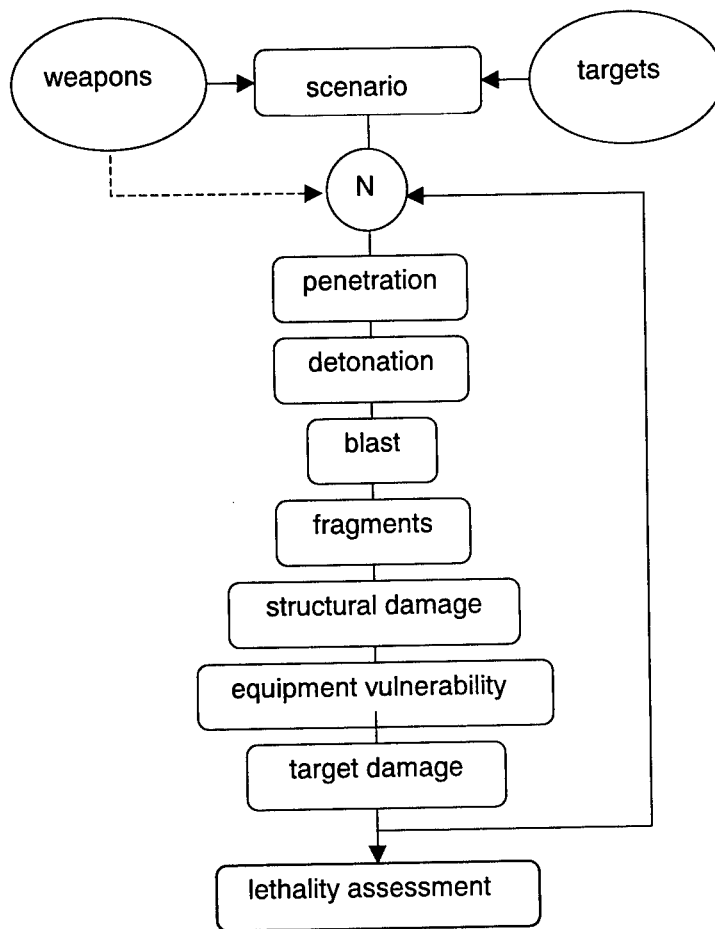
Figure 8 : code structure

To run a calculation, the user will select the calculation mode : attack effectiveness assessment or expert investigation.

Then he will select the target among the database. A target (figure 9) is described by a structural model and a functionnal model representing any target mission. The structural model is composed of rooms, reinforced concrete horizontal slabs and walls and surrounding soils. The functionnal model is composed of critical equipments. Each equipment is represented by its geometry and its vulnerability to fragments and to shock pressure levels. Fault trees describe the functionnal model.
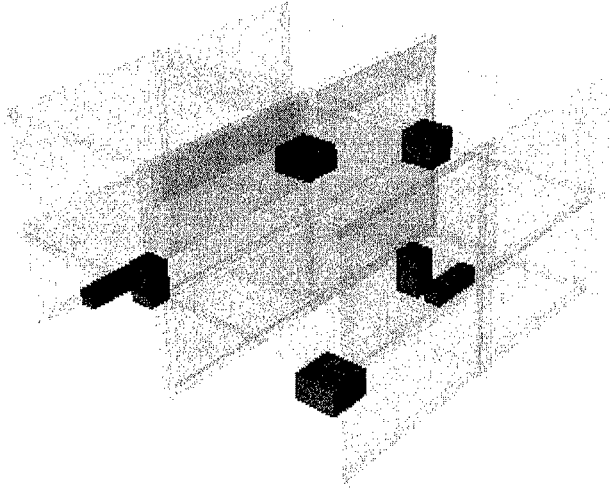
Figure 9 : target model

For attack effectiveness assessment, the input data are defined through the attack scenario : weapons kind and number - from the weapon database -, aim points, impact conditions (velocity, angles of impact), fuzing programmation. The dispersions on each value can be associated to the weapon itself or forced by the user. Then most of the calculation modules required for the weapon / target interaction assessment will be used (figure 3).

For expert investigation, the physical phenomenon to be calculated is defined by the user. So, only the required specific modules will be run.

The weapon is described by its geometry and inertial parameters : 2D axisymetrical shape, external length and diameter of each part, total mass, final dispersion, terminal effects properties : blast effects equivalent charge, fragments distribution, ...

Depending on the weapons to be used and on the calculation mode, adapted analytical or empirical computation modules are run to calculate the different physical processes involved : weapon / concrete slabs interactions to predict the weapon trajectory during the penetration inside the target, shock wave characteristics inside the room where the charge detonates, fragments distribution and pressure loading on the structural components or critical equipments which are submitted to the detonation, wall and equipment response to blast and fragments, ... Damages caused by successive weapons are cumulated.

The calculation modules will come of the litterature or specifically developped. They will be validated by experimental results or by results using numerical codes.

Then, an evaluation of global functionnal damage is performed. The kill probability of whole or part of the target missions is evaluated through fault trees. Post processing allow exploitation of global and statistical data such as target residual functionnal capacities, weapons statistical behaviour or equipment damages, as well as specific physical data such as weapons trajectories and decelerations, pressure generated by explosion or walls damages.

# 4. REFERENCES

[1]  E. Buzaud, Campagne Pénétration de Cibles Dures, Dynalis, Janvier 1999

[2]  A. Darrigade, Synthèse des Tirs de Pénétration de Cibles Dures, T2000-00014/CEG/DR, Centre d'Etudes de Gramat

[3]  D. Tournemine, A. Rouquand, A. Jaros, « An Analytical / Semi-Empirical Approach to Get Rapidly the Response of a Concrete Slab to a Detonation », 9th International Symposium on Interaction of the Effects of Munitions with Structures, Berlin-Strausberg, May 03-07, 1999

[4]  A. Jaros, « Présentation du logiciel Narcisse v2.0 », CS Communication & Systemes, CSSI/BDX/99T114, sept. 1999

[5]  M. Froböse, « Fonctions de propagation des ondes de choc aériennes sphériques » Rapport 3/68 - Institut franco-allemand de recherches de Saint-Louis - avril 1968

[6]  TM5-1300, « Structures to resist the effects of accidental explosions », Department of the Army, the Navy and the Air Force, 1987

[7]  P. Delcor, D. Tournemine, « Expérimentation EEE : étude de l'influence de la géométrie de la charge explosive sur le chargement en pression des parois internes d'une structure », NT 99-29, Centre d'Etudes de Gramat, juin 1999

[8]  L. Borny, « Vulnérabilité des Infrastructures – Essais au souffle de dalles en béton armé », RE GM 042-A/99/NP/W 120, GERBAM, dec 1999

[9]  C. Pontiroli, « Comportement au souffle des structures en béton armé - analyse expérimentale et modélisation », Thèse de doctorat, Laboratoire de Mécanique et de Technologie de l'Ecole Normale Supérieure de Cachan, Centre d'Etudes de Gramat, juillet 1995

# HUMAN BODY TISSUE SIMULANTS.

PIRLOT M.C.[1] , BASTIN I. [2]

(1)  RMA, Royal Military Academy, Av. de la Renaissance 30, B 1000 Bruxelles, Belgium
(2)  Fabrique Nationale de Herstal, Voie de Liège 33, B 4040 Herstal, Belgium

**Abstract :** The Working Group 4 of the NATO Land Group 3 is dealing with the "Assessment and Modelling of Soldier System Performance". In that context and as the successor to CRISAT (Collaborative Research Into Small Arms Technology) the group had a fresh look on the human body tissue simulants. The essential items of the adopted working method will be exposed in the paper: identification of suitable products and their description, static trials followed by dynamical ones with spherical projectiles, dynamic trials with military bullets and "way ahead". The first dynamic test with spherical projectiles was introduced to eliminate the influence of yaw angle and focus on the reproducability of the trials. The test basically consists in the registration of penetration depth versus striking velocity. More complete measurements were necessary for the characterisation of the behaviour of military bullets: length of stable track, primary and secondary permanent cavity, etc. . At our knowledge it was the first time that a comparative study of this extend was set up in the area of tissue simulants. The aim was not to compare the results on an inter-laboratory level, nevertheless some important and interesting results can be offered.

## 1. INTRODUCTION

A formal definition of the problem is described in the (New) Terms of Reference for Working Group 4 (WG/4) of LAND GROUP 3 on Assessment and Modelling of Soldier System Performance [1]: "Report on the analysis of WG/4 trials of alternative human body tissue simulants and a way ahead with respect to tissue and bone simulants".

WG/4, as the successor to CRISAT (Collaborative Research Into Small Arms Technology), has automatically and quite naturally, consulted the results of this group.

This extract from the Final Report of CRISAT Technical Area 2 (TA2) sums up the problem posed to WG/4.

The qualities of a good simulant are, in the opinion of all, as follows (in order of importance for the evaluation tests): representativity, transparency to x-rays, suitability for allowing a recording of the transitory and residual phenomena, reproducability, ease of use, slow degradation, low cost.

Comparison of the main simulants, currently in use in the countries represented in the TA2, with these criteria was proposed. Due to the elements and time, the group was not able to reach a conclusion on the relative representativeness of the various simulants. It recommends research work, if there are any test results that may help to clarify this point, but if not, to carry out the necessary comparative tests. In any case, the group recommends a simulant of elastic type (gelatine or RTV) so as to be able to record the transitory phenomena.

It was the group's opinion that it will be necessary to proceed in some cases by including bone simulants in the muscular simulant; the method of inclusion, the location and the material are to be determined.

No consideration was given to biological simulants, nor to their possibilities of realistically simulating the effect of attacks on human beings.
The table below shows the types of simulants identified by TA2.

Table 1: Suitable simulants identified by TA2 CRISAT

|  | Name | Type | Advantages | Disadvantages |
|---|---|---|---|---|
| (a) | GELATINE 10% 4°C | RUBBERY/ ELASTIC | REPRESENTATIVE + TRANSPARENT + TRANSITORY AND RESIDUAL CAVITIES SHOWN | RAPID DEGRADATION COMPLEX TO USE |
| (b) | GELATINE 20% 10°C | RUBBERY/ ELASTIC | REPRESENTATIVE - TRANSPARENT - TRANSITORY AND RESIDUAL CAVITIES SHOWN | RAPID DEGRADATION COMPLEX TO USE |
| (c) | RTV | RUBBERY/ ELASTIC | REPRESENTATIVE + NON-DEGRADABLE TRANSPARENT - TRANSITORY AND RESIDUAL CAVITIES SHOWN | COMPLEX TO USE |
| (d) | SOAP | PLASTIC | REPRESENTATIVE ? EASY TO USE | OPAQUE MAXIMUM CAVITY ONLY |
| (e) | PLASTICINE | PLASTIC | NO DEGRADATION EASY TO USE | NON-REPRESENTATIVE OPAQUE MAXIMUM CAVITY ONLY |

## 2. METHOD

We decided to adopt the working method described below:
- Identification and description of suitable products for a comparative study
- Static trials
- Dynamic trials with spherical projectiles
- Dynamic trials with bullets
- Way ahead

Each stage defined in the working method is discussed in this paper in a separate paragraph.

## 3. IDENTIFICATION OF SUITABLE HUMAN BODY SIMULANTS

On the basis of Table 1, the WG/4 chose items (a) and (b) as being the most suitable products. The gelatines were (re)named according to their origins.
The composition (a) 10% 4° is the one recommended by Dr Fackler, it will henceforward be referred to as FACKLER (gelatine) [2].
In the NATO gelatine the concentration is set at 20% and the working temperature at 10° [3]. These conditions correspond to item (b) in Table1.

These are two analogous simulants, which are distinguished mainly by their gelatine content and working temperature. Since the NATO requirements do not explicitly define the BLOOM number of the gelatine powder to be used [3], it was decided to use a powder with a BLOOM number of 250 for both the NATO and the FACKLER gelatines.

The method for producing gelatine (in dry powder form) is based on extracting collagen from bone (calibrated) or skin residues. Drying the concentrated liquid produces a specific gelatine with average values for the batch which depend upon the raw materials used and the techniques adopted. Specifications for the required gelatine are obtained by mixing gelatines from different batches; a technique which is standard procedure for powder manufacturers.

There exists a wide range of standards which describe the parameters of a specific gelatine whether it is for industrial or alimentary purposes (AFNOR, BS,...).

For the purposes of the ballistic trials, the fundamental parameters are:

- BLOOM number of the basic gelatine,

The BLOOM number is expressed in grams and corresponds to the mass needed to be added to a cylindrical piston (diameter 0.5 inches) so that it penetrates (by deformation and not by perforation) 4mm (1) into the surface of a gel contained in a vessel with defined dimensions. The gel concentration is set at 6.674% gelatine powder (105 g of water and 7.5 g of powder) and the temperature for the trial is set at 10°C. The BLOOM number is measured in a laboratory using a texture analyser which gives results to the nearest 10 BLOOM. The BLOOM number is equivalent to the gel loading measured under strictly defined operating conditions.

- Gelatine-water concentration,

- End temperature of the gelatine,

When discussing temperatures a distinction should be made firstly of the manufacturing temperature (maximum 60°C in order not to destroy - by thermal hydrolysis - the proteins in the gelatine; Fackler set a maximum temperature of 50°C). Reworking the gelatine is carried out preferably using a "Bain Marie" which ensures an optimal heat exchange. Ovens are less efficient. The relaxation time (restructuring of the complex molecule) is around 16 to 18 hours, after which a relatively stable state is achieved.
The second temperature is the working temperature, the standard value being 10°C [3] or 4°C [2] which is vital for correct performance during trials.

- Colour,

The colour of the gelatine depends on the level of extraction. Five levels of extraction are recognised, a gelatine of 250 BLOOM is obtained from the first level sometimes in conjunction with the second level of extraction. As further extractions are carried out the BLOOM number decreases and the colour intensifies. The 130 BLOOM gelatine (supplied as technical gelatine unless otherwise specified) is thus deeper in colour (brown) than the 250 BLOOM gelatine. The range of the BLOOM number of semi-finished products varies from 0 (no resistance to static penetration, cf. water) to 320. Commercial products have a BLOOM number ranging from 80 to 280. Technical gelatine (non-alimentary) is characterised by a BLOOM number of 130, and is cheaper and less transparent than the alimentary quality gelatines.
Gelatine (semi-finished product) is supplied in granular form, either fine (fine powder) or larger grains (for example 8 - 30 mesh). It is easier to dissolve the finer grain sizes. In each case the dissolution must be carried out at a "cold" temperature in order to allow the gelatine to swell.

- Other parameters,

Other parameters (acidity, viscosity(2), ash (<2%), oxidising or reducing properties, bacteriological purity, etc.) are of lesser importance. Nevertheless, mention must be made of the transparency (turbidity) as well as the colour which may play a role when examining the dynamic phenomena within a block of gelatine.

## 4. STATIC TRIALS

Static trials were carried out to determine the gel loading for the two selected temperature and concentration values (10%/4°C and 20%/10°C) for six different gelatine powders. The results are listed in Table 2.

Table 2: Gel loading for different gelatines at 10%/4°C and 20%/10°C

| Sample (BLOOM) | Gel loading at 20%/10°C (g) | Gel loading at 10%/4°C (g) |
| --- | --- | --- |
| 110 | 956 | 378 |
| 121 | 1049 | 436 |
| 133 | 1062 | 423 |
| 239 | 1667 | 714 |
| 251 | 1555 | 661 |
| 258 | 1591 | 678 |

The figures in Table 2 show that the gel loading is systematically greater for NATO gelatine compared to FACKLER gelatine. A greater BLOOM number corresponds to a greater gel loading value.

## 5. DYNAMIC TRIALS WITH SPHERICAL PROJECTILES

The procedure defined by Dr Fackler is based on a dynamic test using an air rifle. Dynamic trials using spherical projectiles are based on this concept [5]. The WG/4 group decided to measure the depth of penetration of 5.5mm diameter steel balls (ball type RB 5.5/G20) fired into blocks of gelatine (NATO and FACKLER). The advantage of using balls is that this avoids any problems caused by oblique projectile impact [6].

The procedure calls for 5 "valid" shots at three velocities (250, 400 and 600 m/s). Four countries carried out the trials: BE, FR, NL and US. The US used a different diameter of ball. The results from the other three countries are shown in the next graph [7] [8] [9] [10].
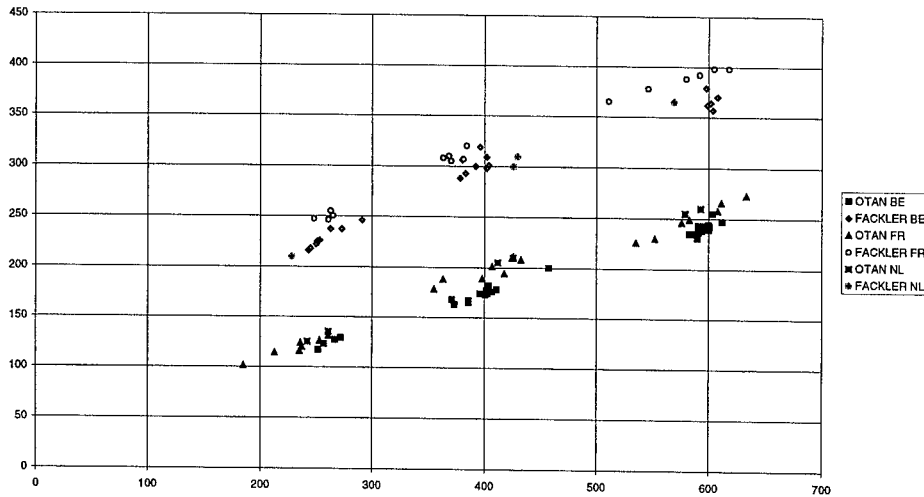


Figure 1: Penetration depth (vertical axis in mm) vs. striking velocity (horizontal axis in m/s)

The graph shows that the results from the three countries are similar; the slightly greater penetration depths obtained by FR may be explained by the use of gelatine with a lower BLOOM number (200 instead of 250) [7].

The depth of penetration is greater in the FACKLER gelatine than in the NATO gelatine. The ratio between the depth of penetration in the FACKLER gelatine and that in the NATO gelatine depends upon the impact velocity of the ball, this ratio is approximately 2 for an impact velocity of 200 m/s and 1.5 for an impact velocity of 600 m/s. It decreases as the energy of the projectile increases [11].

## 6. DYNAMIC TRIALS WITH BULLETS

For the trials using bullets (military war munitions) the WG/4 decided to employ the 5.56x45mm of type SS109. Two velocities were adopted (510 and 710 m/s) which allow easy analysis of the gelatine blocks. Analysis of the shots is, in the case of the velocities adopted, the measurement of the parameters shown in the figure below. This diagram is a schematic representation of a longitudinal section of a gelatine block. It shows an "average" result. It is probable that certain deviations from this standard situation will be observed during the trials [12].
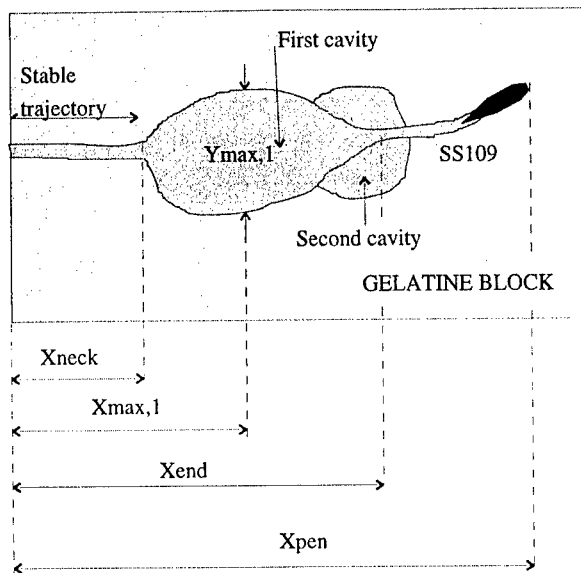
Figure 2: Schematic representation of a longitudinal section in the gelatine block

Xneck:        length of stable trajectory of the projectile in the gelatine,

Ymax,1:       maximum width of the first permanent cavity measured at right angles to the
              projectile trajectory;

Xmax,1:       abscissa of Ymax,l;

Ymax,2:       maximum width of the second permanent cavity measured at right angles to the
              projectile trajectory;

Xmax,2:       abscissa of Ymax,2;

Xend:         abscissa of the end of the first volume of the permanent cavity;

Xpen:         penetration of the projectile into the gelatine block, expressed.

The reports from the various nations are referenced [7] [8] [9] [10].

Extreme values of Xneck for each type of gelatine and each impact velocity obtained in each
of the test centres are shown on a single graph (Figure 3); similarly for the Xend values
(Figure 4).
For the Xmax and Ymax values however it was decided to represent the elliptical envelope
within there is an 80% chance that the point of the co-ordinates (Xmax1, Ymax1) would lie
(Figure 5).Normal distribution and independence are assumed for the two co-ordinates.

Despite the difficulties of measurement inherent in these tests (any measurement on a block
has a certain subjective element) and in the simulant (we procured "primary" raw materials in
order to carry out "precision" tests) the results show certain important trends.
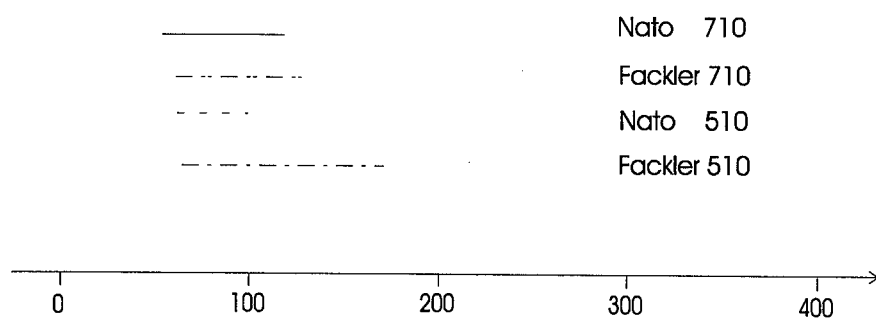
Figure 3: Extreme values for Xneck (mm)
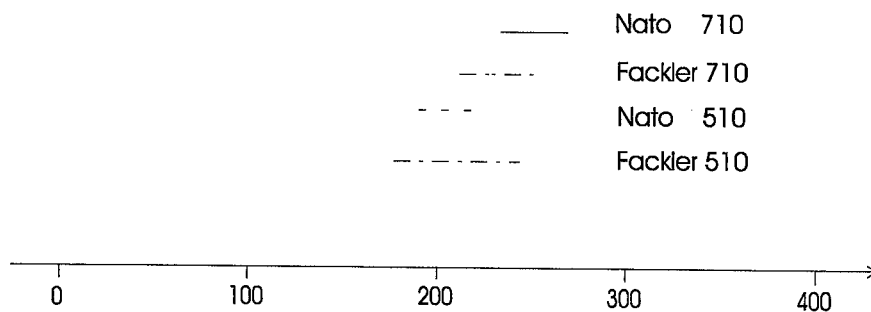


Figure 4: Extreme values for Xend (mm)
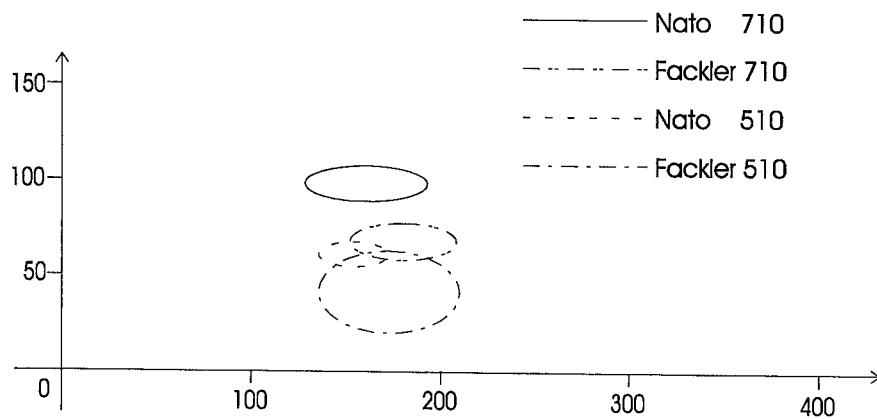


Figure 5: Elliptical distribution (p=0.80) of Xmax1 and Ymax1

Comparison of Figure 5 shows that the dispersion of the results is smaller in NATO gelatine than in FACKLER gelatine. This gives improved reproducibility in the NATO gelatine.

The neck (stable part of the trajectory in the gelatine) is longer (by some 25%) in FACKLER gelatine compared to NATO gelatine as shown in Figure 3. This gives a corresponding increase in all the X values (Figure 4).

The maximum size of the first cavity Ymax,1 is doubled in NATO gelatine compared to FACKLER gelatine (Figure 5).

The results concerning the second cavity are less obvious.

Besides the difference in volume, it can be seen that the shape of the cavity also differs considerably according to the type of gelatine used. The differences in shape can be observed in the following figures (Figure 6 and Figure 7).
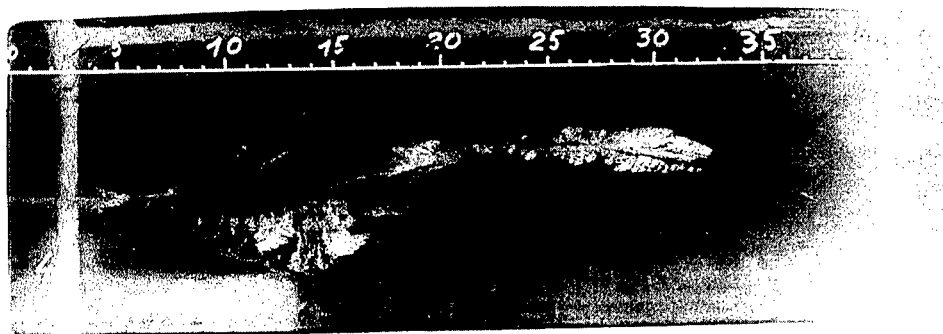


Figure 6 : Representative cavity shape in NATO gelatine blocks (~700m/s)
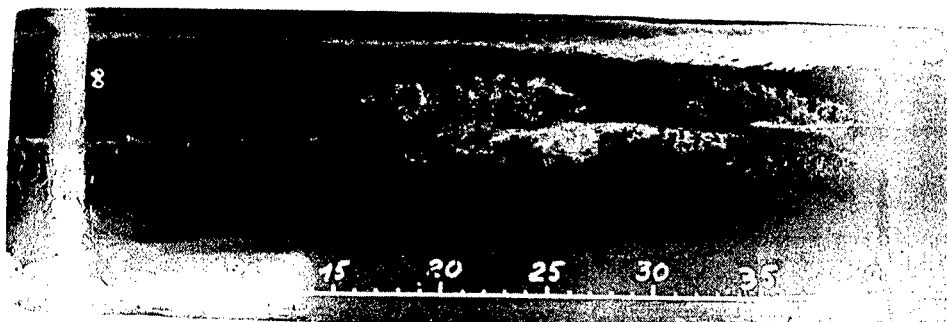


Figure 7 : Representative cavity shape in Fackler gelatine blocks (~700m/s)

## 7. WAY AHEAD

If one wishes simply to compare the effects in a bloc of simulant of two munitions, the better reproducibility of the NATO gelatine is a property which drives preference of this type of simulant.

On the other hand, if one wants to use the results to evaluate the effect of projectiles on a man, the choice must be made implicating the expertise of surgeons who have operated on personnel wounded by war projectiles and/or using data bases, possibly existing, describing this kind of wound. It will be necessary to submit to the experts the photographic evidence representative of the images gathered during the trials with the two types of simulants, and to ask them which corresponds most to lesions observed.

Two types of result can be presented as conclusion of the expert's work:

- One of the simulants is considered as representative, it can be recommended after examination of the means for improving it's reproducibility, particularly if the Fackler gelatine is indicated;

- Neither of the two simulants corresponds to actual observations and there will then be a place for research into a new representative simulant.

# 8. REFERENCES

[1]     NATO document AC225 (LG3) D/10, Paragraph 6

[2]     M.L. Fackler, J.A. Malinowski, "Ordnance gelatin for ballistic studies", in *The American Journal of Forensic Medecine and Pathology* 9(3): 218-219, 1988

[3]     NATO document AC/225 (Commission III) D/14

[4]     A.J. Corzine, G.K. Roberts, "Correlation of ordnance gelatine penetration results between 20% gelatine at 10°C and 10% gelatine at 4°C" in *AFTE Journal* Vol 25, Number 1, 1993

[5]     E. Thompson, "Ordnance gelatine testing procedures", in *AFTE Journal* Vol 25, Number 2, 1993

[6]     R.A. Poole, R.E. Cooper, L.G. Emanuel, L.A. Fletcher, I.C. Stone, "Angle effect on bullets fired into gelatine" in *AFTE Journal* Vol 26, Number 3, 1994

[7]     C. Feys, "Comparaison des gélatines OTAN et Fackler", Rapport d'essais N° RE : 13 E-SAC-000 du 15 février 1996, Etablissement Technique de BourgeS ETBS, Bourges, France, 1996.

[8]     R.N. Prather, "A comparison of 10% and 20% gelatin formulations", Test report, ARL Aberdeen Proving Ground, Maryland, USA, 1998

[9]     J. Van Bree, "Gelatine data", Onderzoeksverslag TNO Prins Maurits Laboratory, Rijswijk, The Netherlands, 1995

[10]    M.C. Pirlot, "Comparaison des gélatines OTAN et FACKLER", Rapport d'essais N° ABAL 96032 du 22 janvier 1996, Ecole Royale Militaire, Bruxelles, Belgique, 1996

[11]    L.C. Haag, "Controling variances in preparetion and a suggested method for the calibration of gelatine blocks" in *AFTE Journal* Vol 21, Number 3, 1989

[12]    M.L. Fackler, R.F. Bellamy, J.A. Malinowski, "The wound profile of the missile tissue interaction", in *The Journal of Trauma*, Vol 28, N° 1, 1988

# Sensors and Metrology

# INSTRUMENTATION OF 120mm HEAT-MP PROJECTILE

CARIS J.P.[1], SATURNIN E. [1]

(1)Giat Industries, Centre de Bourges - 7 route de Guerry 18023 BOURGES Cedex - France

**Abstract:** Within the context of ammunition/120mm barrel interaction studies, Giat Industries has designed and fired an instrumented round based on a 120mm HEAT-MP. This program has proved feasibility of round measurement equipement and data recovery under severe firing conditions.

## 1. INTRODUCTION

Within the context of ammunition/120mm barrel interaction studies, Giat Industries has designed and fired an instrumented round based on a 120mm HEAT-MP. Recovery data have been assessed after firing. This program was carried out for eight months according to the following steps.

## 2. RECORDED PARAMETERS

The aim of this experimentation was to measure the internal stresses due to HEAT-MP firing conditions. The more significant parameters have been selected:

- acceleration according to three axis at center of gravity,

- acceleration according to three axis at the top of the ogive,

- pressure levels at the obturator.

### 2.1 Firing condition analysis

Intern bibliographic research is given in table 1.

Diagram 1 gives previous sensor location.

| | Symbol | Unit | Internal Ballistic | Intermediate Ballistic |
|---|---|---|---|---|
| Time of phase | D | ms | 10 | 30 |
| Acceleration | | | | |
| axial | $\gamma x$ | g | value max. 25000 $\pm$3000 | value max. 10000 + - 5000 |
| horizontal | $\gamma y$ | g | value max. 2000 $\pm$1000 | value max. 15000 + - 5000 |
| vertical | $\gamma z$ | g | value max. 2000 $\pm$1000 | value max. 15000 + - 5000 |
| Pressure | | | | |
| Propellant: measures 1 and 2 | Pg | MPa | value max. 350 + - 100 | value max. 15+ -2 |
| Obturator: measure 3 | Pc | MPa | value max. 300 + - 250 | value max. 200+ - 50 |

Table 1: firing conditions
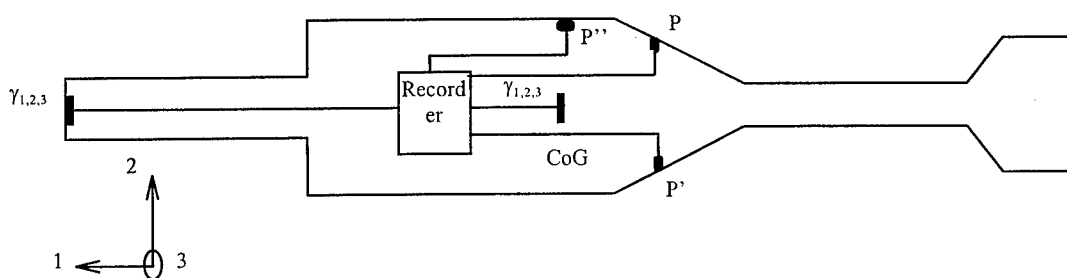


Diagram 1: sensor location

## 2.2 Sensor selection

Several sensor manufacturers have been consulted (ENTRAN, ENDEVCO, KISTLER and META MESURE). Some accelerometers have been selected but no pressure sensor meet the requirements. Pressure measurements have been cancelled for this program.

After further analysis, only one accelerometer was considered to meet the requirements with high level of confidence: Piezoresistive Accelerometer ENDEVCO model 7270A - 20K (performance characteristics given table 2).

Main characteristics taken into account in this choice are overrange limit (60000g), range 20000g (good measurement linearity since 30000g) and transverse sensivity (5% max.).

# SPECIFICATIONS—continued

| PERFORMANCE CHARACTERISTICS | Units | Model 7270A | -6K | -20K | -60K | -200K |
|---|---|---|---|---|---|---|
| ZERO SHIFT DUE TO HALF SINE ACCELERATION CAUSING 200 mV OUTPUT (or 150 000 g, whichever is smaller) | mV Max | 0.5 | 0.5 | 0.5 | 0.5 | 0.5 |
| ZERO SHIFT DUE TO MOUNTING TORQUE (0 TO 8 LBF-IN., 0 TO 0.9 NM) | mV Max | ±2 | ±2 | ±2 | ±2 | ±2 |
| THERMAL ZERO SHIFT [4] From -30°F to +150°F (-34°C to +66°C) | mV Max | ±50 | ±50 | ±50 | ±50 | ±50 |
| THERMAL SENSITIVITY SHIFT From 0°F to +150°F (-18°C to +66°C) | % Max | ±10 | +10 | ±10 | ±10 | ±10 |
| OVERRANGE LIMIT [2] | g pk | ±10 000 | ±18 000 | ±60 000 | ±180 000 | ±200 000 |
| WARM-UP TIME | Minutes Max (Seconds Typ) | 2 (15) | 2 (15) | 2 (15) | 2 (15) | 2 (15) |

**ELECTRICAL**

| | |
|---|---|
| EXCITATION | 10.0 Vdc, 12 Vdc maximum |
| INPUT RESISTANCE | 550 ±200 ohms |
| OUTPUT RESISTANCE | 550 ±200 ohms |
| INSULATION RESISTANCE | 100 megohms minimum at 100 Vdc; between sensor, cable shield and case |

**PHYSICAL**

| | |
|---|---|
| CASE, MATERIAL | Stainless Steel (17-4 PH CRES) |
| ELECTRICAL, CONNECTIONS | Integral cable, 4 conductor No. 36 AWG Teflon® insulated leads, braided shield, flourocarbon jacket |
| IDENTIFICATION | Manufacturer's logo, model number and serial number |
| MOUNTING/TORQUE [3] | Holes for two 4-40 or M3 mounting screws/8 ±2 lbf-in (0.9 Nm) |
| WEIGHT | 1.5 grams (cable weighs 3.6 grams/meter) |

**ENVIRONMENTAL**

| | |
|---|---|
| ACCELERATION LIMITS [3] [4] | ±200 000 g half sine pulse or three times the recommended range, in any direction, whichever is smaller. Pulse duration should be the greater of 20 microseconds or five periods of the resonance frequency |
| BASE STRAIN SENSITIVITY (at 250 microstrain) | Typically less than 0.5 mV |
| TEMPERATURE Operating | -30°F to +150°F (-34°C to +66°C) |
| Storage | -65°F to +250°F (-54°C to +121°C) |
| HUMIDITY | Unaffected. Unit is epoxy sealed |
| ALTITUDE | Unaffected |

**CALIBRATION DATA SUPPLIED**

| | |
|---|---|
| SENSITIVITY [5] | μV/g at recommended range or 5000 g, whichever is smaller. Time history at respective g level |

Table 2: accelerometers' performance characteristics

Signals from those accelerometers need to be amplified and translated to input digital analogic conditioner of recorder.

The accelerometer γx (top ogive and center of gravity) gain of acquisition equipment is 75 micro volts/g, means after translation:

$$Us = 2,5 + (7.5 \times 10^{-6} \times \gamma) \text{ volts} \qquad \gamma \text{ units: g}$$

30000g max. acceleration: Us=4,75V or Us=0,25V

For the others accelerometers, the gain of acquisition equipment is 100 micro volts / g, means :

$$Us = 2,5 \pm (100 \times 10^{-6} \times \gamma) \text{ volts} \qquad \gamma \text{ units:g}$$

± 5000g full scale and 250g sensitivity.

## 2.3 Choice of recorder

Giat Industries-ISL technical exchanges and knowledge of the Institute works lead to choose the transitory recorder designed and improved by ISL at high acceleration level (40000g). The main performances characteristics fit to this application: 8 analogic channels, 35 Koctets of memory (4Koctets per channel) and programmable frequency sampling.

choosen recorder data:

|  |  |
|---|---|
| MS32 | 32 Koctets Memory |
| CH8 | 8 Channels |
| ST1 FT1 | Min. time scale (between 1 et 05535) |
| TMO | Pretrigger activated |
| TO96 | Pretrigger value 10% |
| TRO | Clock trigger synchro |
| OM1 | Binary output |
| AS1 | Measurement mode activation when switch on |

Summary: Main recording characteristics:

- time between 2 sample 16µs (hightest frequency to be recorded 10kHz),
- sample 2µs,
- total record lenght: 65ms (6ms before trig and 59ms after). Trig is induced by crossing 10000g threshold on γx signal.

Signals are in memory as far as recorder is under voltage (main power supply). When main power supply fails memory is saved by backup power supply (intern recorder device). Memory read is performed by a PC: external connector is supplying by ISL. The internal connector is a specific one. This connector shall be available after recovering.

## 2.4 Synoptic and Working

Embeded electronic device synoptic is given diagram 2.

Main power supply (1) is made of three 3.6V items (eq. 10.8V), 1A/h capacity. The main power supply (13) is the same as (1).

Backup power supply (5) is made of nine 3.5V items. The 6 accelerometers are piezoresistive accelerometers ENDEVCO Model 7270A-20K.

Recorder is ISL's transitory recorder.
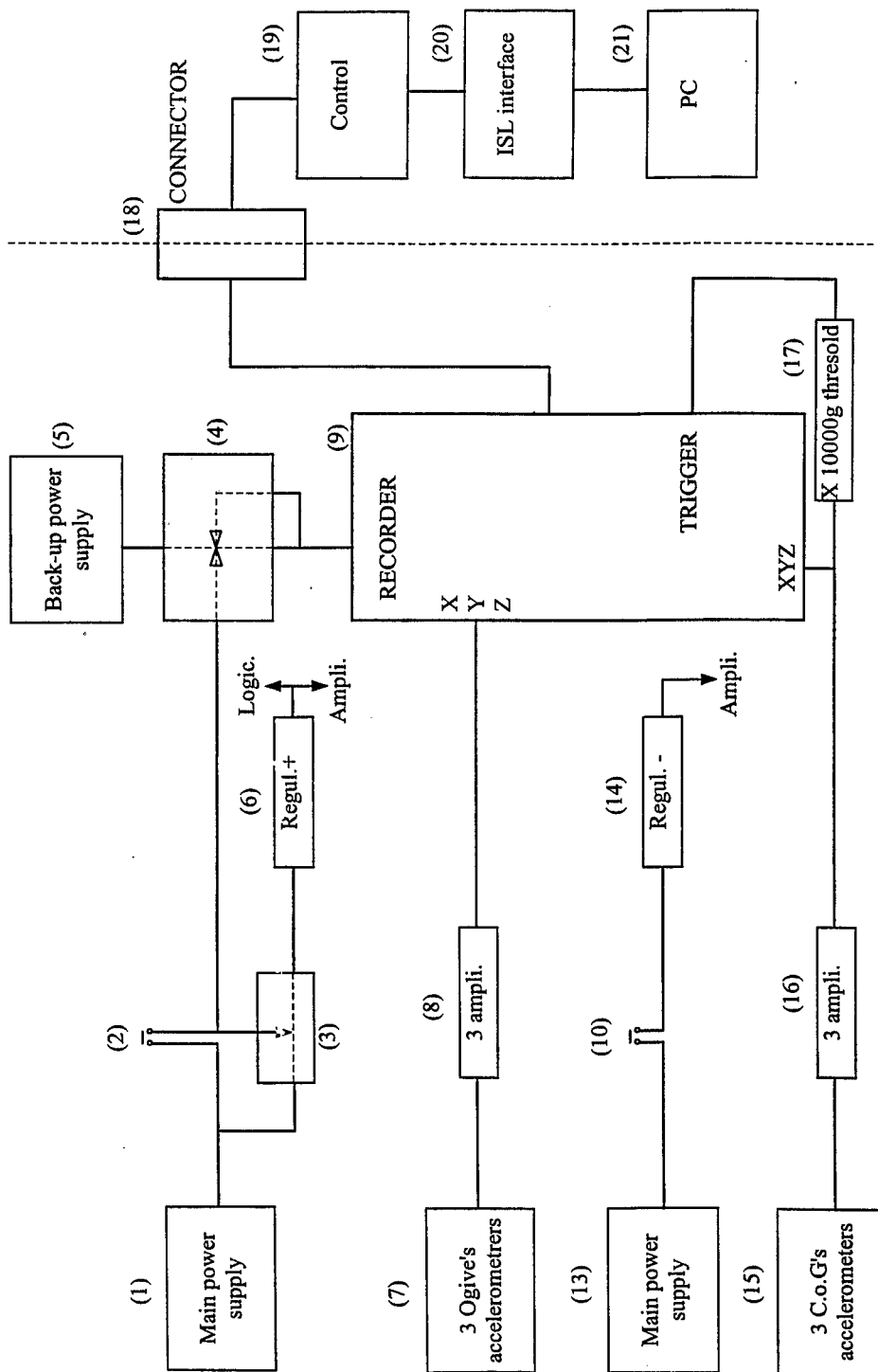
Schéma 2: Embeded electronic device synoptic

Main power supply (1) is switched on by screw-switcher (2) which is immediatly short-circuited by circuit (3). This circuit protects device from short cuts. This voltage supplies recorder (9) and positive voltage regulator (6).

This voltage supplies static relay (4) which is self connected and then supplies the recorder.

The main power supply (13) is switched on by a second screw-switcher (10). This voltage supplies the negative voltage regulator (14).

The accelerometers (7) and (15) are ±5V supplied. Output are amplified and translated by ampli. (8) and (16) and input recorder.

Center of gravity $\gamma x$  Signal is compared to  ±10000g thresold in circuit (17) which will initialize the recorder.

When main power supply (1) fails, memory is saved by backup power supply (5).

After recovery of the projectile, memory read is performed by plugging connector (18) to PC (21) by RS232 interface (20) (ISL supplyer) and control device (19).


## 3. PROJECTILE DESIGN

The specific projectile was built from the main parts of Giat Industries 120mm HEAT-MP.


### 3.1 Equipment design

A CAD assessment (body mesh diagram 3)  has given electronic case's size and confirmed body with connector hole's mechanical characteristics.

corps oecc perce
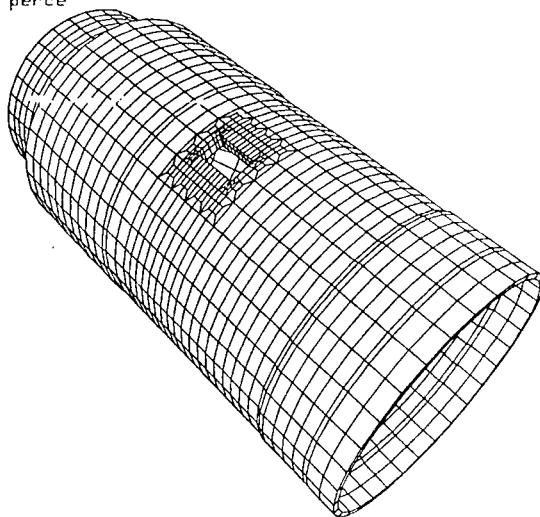


Diagram 3: body mesh

- 500 -

## 3.2 Electronic device

Mechanical assessment has been performed for electronic device like Resin's Young module for example. The RUTAPOX silica loaded resin has been chosen for its mechanical characteristics and easy implementation. A five electronic boards system with steel spacer have been designed (Diagram 4: electronique case).
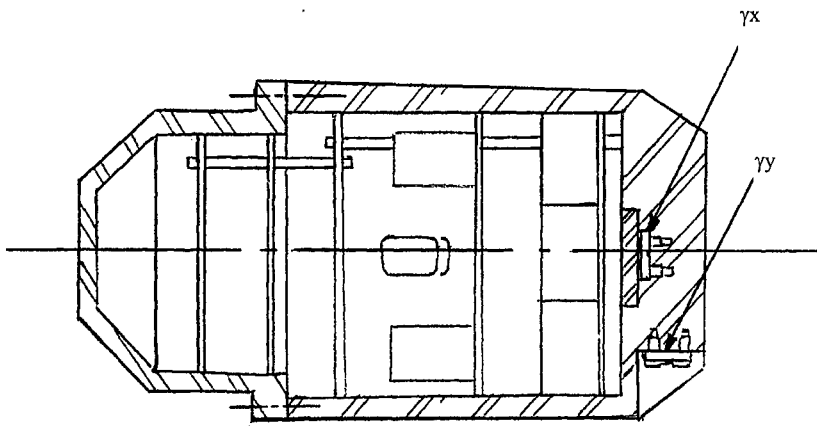


Diagram 4: electronique case

## 3.3 Ogive sensors' location

Diagram 5 gives ogive sensors' location.
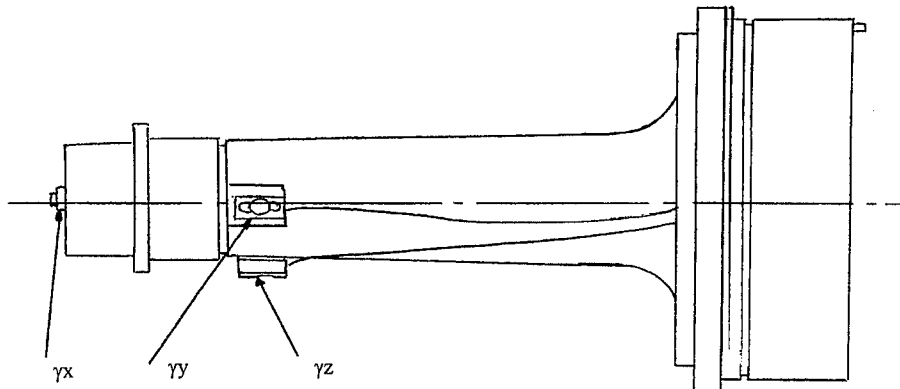


Diagram 5: ogive sensors' location

## 4. FIRING AND RECOVERY

Two instrumented rounds were assembled and fired. Recovery process is long range shoot (range > 5000m) in a plough field (decceleration < 200g) in order to keep projectile's integrity (picture 1: recovered projectiles).
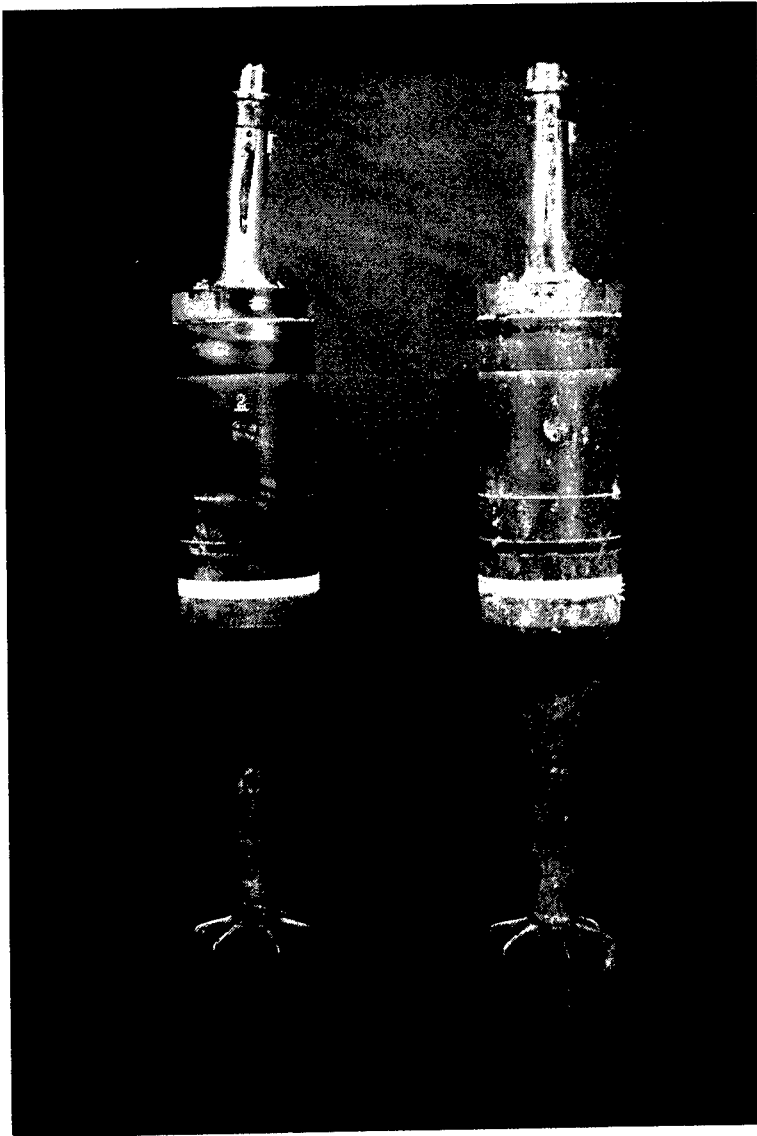


picture 1: recovered projectiles

## 5. DATA ASSESSMENT

Recovered projectiles have been connected to the PC and data have been loaded. One out of 12 channels (6 per projectile) has been lost obviously due to the cutting of sensor wire.

### 5.1 raw data and spectrogram example

Graphic 1 shows the projectile 1 γx spectrogram at the center of gravity. Graphic 2 presents raw data of the projectile 1 γx at center of gravity.
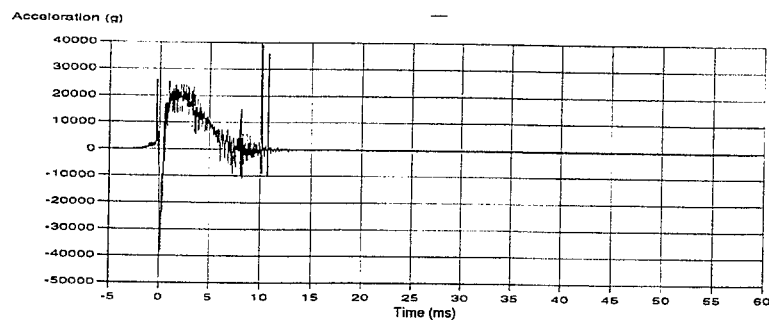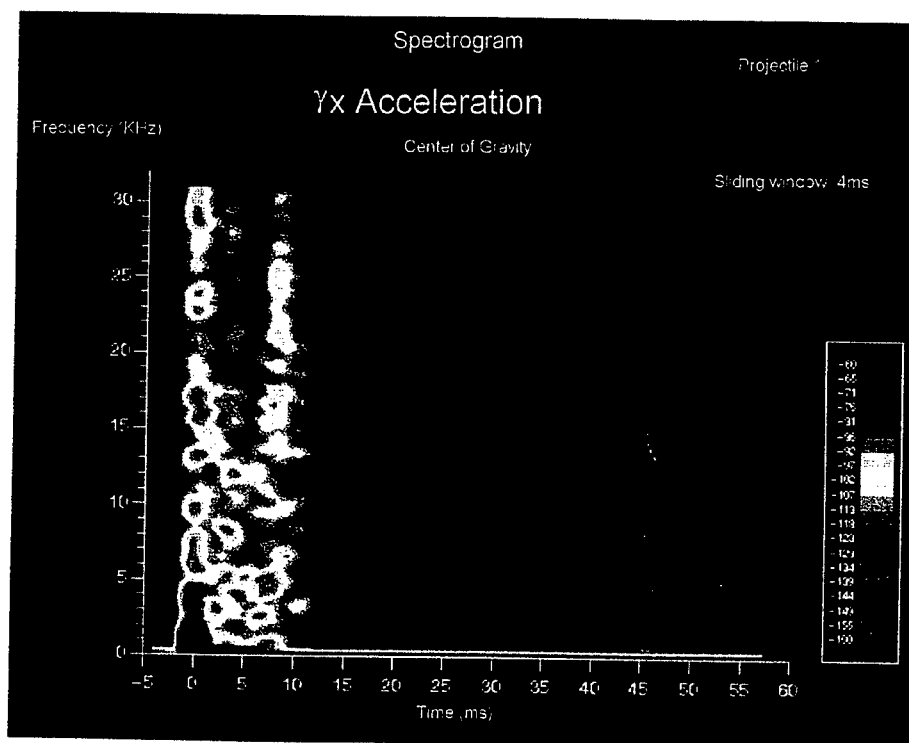


graphics 1 et 2: projectile 1 γx at center of gravity spectrogram and raw data

This kind of graphics confirms the relevance of recorded data. Then complex mathematical assessments have been performed.

## 5.2 Wigner-Ville signal processing

Graphic 3 shows Wigner-Ville signal processing of projectile 1 γy ogive's sensor. This spectral analysis shows shocks and associated resonance. Muzzle time is shown on this graphic at t=8.9ms.
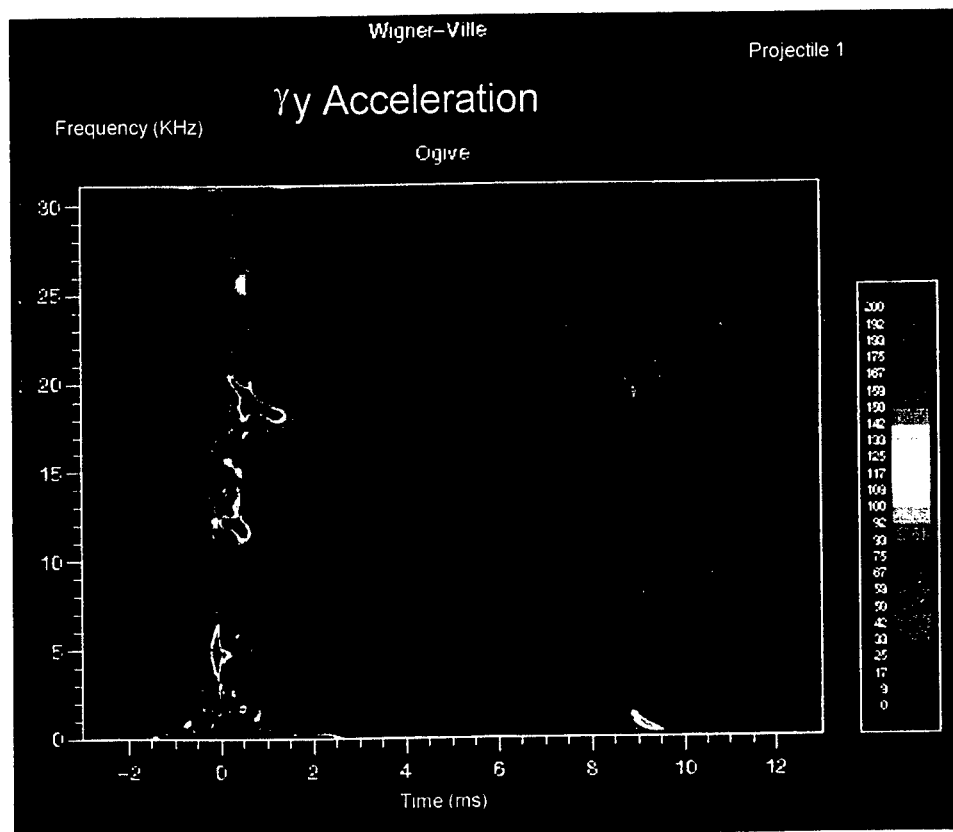


graphic 3: Wigner-Ville - projectile 1 ogive's γy

## 6. CONCLUSION

This data acquisition method, out of reach before in such severe operational conditions, is considered as an interesting developpement tool. It also opens the way to the development of rounds with high measurement and assessment capacities.

# WHAT CAN HOLOGRAPHY BRING TO BALLISTICS ?

H. ROYER
I.S.L., BP 34, F-68301 SAINT-LOUIS

**Abstract :** Since its invention, more than fourty years ago, holography has developed very slowly. However, its interest in many scientific fields is well established, in particular for the study of unsteady phenomena. The different applications to ballistics – potential or realized – are described ; the fundamental limits of the method and the main bottlenecks (technological, financial, etc.) are considered ; the possibility of future improvements is envisaged.

## 1. INTRODUCTION.

The most elementary holographic system consists in putting a recording plate close to the object in a setup where the beam emitted by a laser is separated into two parts : one illuminates the object field which reflects the light towards the plate (object beam) while the other goes directly to the plate (reference beam) where the two beams interfere. After processing, the plate becomes a hologram : when it is illuminated by the reference beam, it reconstructs a three-dimensional image of the object field.

The application of holography to ballistics became possible thanks to the invention of pulse lasers. The very short duration of their light pulses (20 ns or less) allowed the very fast movement of projectiles to be sufficiently frozen to get interesting images. The first spectacular demonstration was given by Brooks and Heflinger in a famous article showing a bullet in flight [1].

The mere observation of a phenomenon may yield interesting informations. For example, a bunch of fragments ejected from a target is typically three-dimensional and their spatial distribution can be determined by a single hologram [2,3]. However, two crossed visualizations can do about the same with classical shadowgraphy. In fact, holography is not limited to the reconstruction of nice images.

## 2. APPLICATIONS TO BALLISTICS.

When D.Gabor invented holography [4], he wished to visualize the atoms. This historical point illustrates the ability of holography to study very small objects such as micrometeorites. Crossed shadowgraphs are too fuzzy for such an application and photography can focus only in a thin slice of the reconstructed volume. The only technique which can provide comparable results, X-ray visualization, is heavy, expensive and dangerous.

The three-dimensional visualization of dangerous phenomena, which must remain at a long distance of the observer, is also an effective application of holography. Though holography is often referred to as a lensless technique, it is preferable in this case to use a lens in order to image the remote field close to the holographic plate. This increases substantially the luminosity and the resolution of the images. Fragments of a shell have been observed at more than 10 meters by this means and one cannot envisage to replace these images by crossed shadowgraphs at such a distance.

The superposition of two exposures on the same hologram has opened other possibilities of measurements :

- Holographic velocimetry. If the delay between the exposures is such that the objects have moved noticeably (which is generally the case in ballistics), the spatial separation of the twin images give the three-dimensional displacements of the objects and, knowing the delay, their 3-D velocities. This information adds to the previous ones : position, shape and size. Thus a change of orientation, of size or of shape can also be yielded by the same hologram. The combination of velocity with the size and shape can also lead to a direct determination of the kinetic energy (e.g. fragments recuperated after the shot).

- Holographic interferometry. If the studied object is modified without a substantial displacement between the two exposures, the two corresponding images are superimposed and the coherent nature of the reconstruction beam gives rise to interference fringes which are a measure of the modification (distortion, index variation, etc.). As the fringe spacing corresponds to an optical path difference equal to a wavelength (half a micrometer), this technique is very sensitive, but we will not go more into the details because it applies to relatively steady objects such as a target or the fluid environment of a projectile, but not to the projectile itself.

## 3. THE CONSTRAINTS .

To record a hologram of good quality, it is not sufficient to buy a pulse laser and to press the button. Some physical and geometrical conditions must be fulfilled :

-   As in classical photography, the total energy falling on the plate must be adjusted to its sensitivity, while the laser pulse duration must be short enough to reduce the image blur to an acceptable value.
-   The energy diffused by the object scene toward the hologram (object beam) must be slightly smaller than that carried by the reference beam.
-   The optical paths corresponding to all the light rays travelling from the laser source to the plate through the object scene, and those corresponding to the reference beam, must not differ of more than the coherence length of the laser, which is in any case limited by the duration of its light pulses.
-   The grain of the holographic emulsion must be small enough to record the fringes due to the interference of the object beam with the reference. As a consequence, the emulsion sensitivity is very low.
-   The displacement of the object must not generate a phase variation of the object beam of more than a quarter of a wavelength (about 0.1 μm) during each exposure.
-   The recording and reconstruction arrangements must be ideally identical (same wavelength, same geometry) in order to avoid optical aberrations which would spoil the images and the measures. Slight differences can be accepted according to the required quality and to the set-up geometry.

Some of these requirements can lead to contradictory limitations and it is often necessary to trade off with the object volume, distance and velocity according to the laser characteristics (energy, coherence, wavelength). Sometimes ageometrical modification can resolve the question. Let us take an example (fig.1a) : a projectile is running at 2000 m/s and we want to observe its front surface ; its displacement must be smaller than 0.05 μm ($5^{th}$ condition), thus the laser pulse must be shorter than 2.5 picoseconds ; then its coherence length is smaller than 0.7 mm, which implies that the object surface has a relief of less than 0.4 mm. A mere change
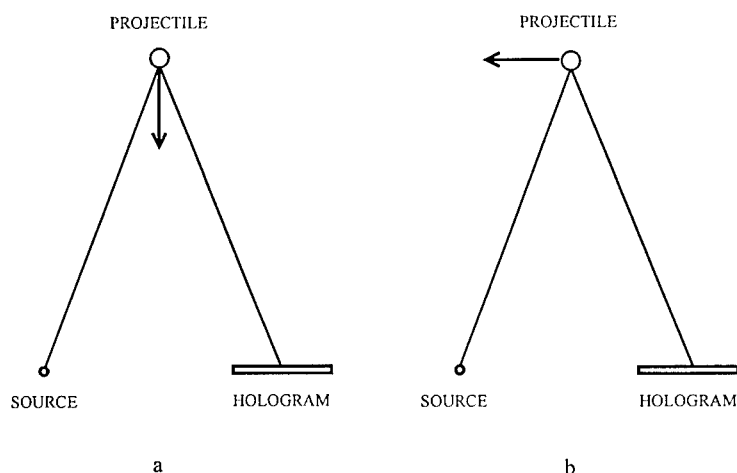
PROJECTILE

PROJECTILE

SOURCE          HOLOGRAM          SOURCE          HOLOGRAM

a                                    b

of the direction of flight (fig.1b) or of the angle of visualization can lead to a tolerance 10 000 times larger on the pulse duration and on the object relief.

## 4. DIFFERENT RECORDING ARRANGEMENTS.

For a visualization of projectile surfaces, it was first proposed to use a class of set up improperly called « elliptical »[4]. This means that the illuminating source and the recording region of the hologram are located at the two focuses of an ellipse which is tangent to the projectile trajectory. After the well known properties of the ellipse, the phase of the waves travelling from the source to the hologram through the object, varies as the second order of the object displacement during the exposure. This is of course very useful in high-speed ballistics. In fact, the ellipse is a very particular case : it can be replaced by a hyperbola, a parabola or even a straight line ; moreover, it is not necessary for the trajectory to be in the plane containing the source, the projectile and the hologram. At contrary, a good choice is to set this plane normal to the trajectory (fig.2) : the constraint is much less severe than that of an elliptical set-up and it is not less efficient.
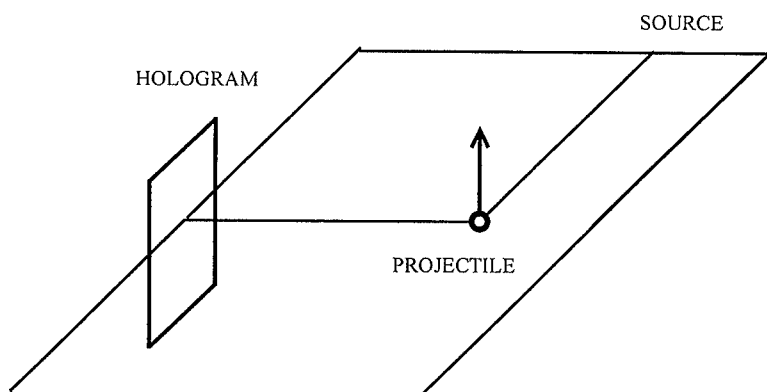


Fig.2 : A good geometry to record a high-speed projectile.

In most cases, it is enough to see the shape of the projectile. Then a back illumination is greatly preferable for two reasons : 1- the luminosity can be greatly enhanced, 2- the phases of the recording beams are not sensitive to the object motion. In fact, it is equivalent to say that a hologram of the bright, steady background is recorded, the projectile image beeing then an « absence » in the background image. For small fields at a moderate distance, the background can be a white panel or a ground glass [5]. For distant objects in a wide field, it is preferable to use a retroreflecting tape, which can bring a luminosity gain of 1000. In fig.3, the fragments coming from an exploding shell (2000 m/s) were located at about 10 and 13 meters from the hologram and the field section was of about 1 m$^2$ ; the laser energy was only 15 millijoules. Such arrangements allow accurate measurements of shapes, sizes, 3D positions and velocities to be achieved [6].

It is interesting to mention here a trick of particular interest for velocity measurements. If the two required exposures are recorded with separate reference beams, a property related to the hologram thickness (Bragg effect) allows the reconstruction of the two images at will simultaneously or separately. This gives a higher contrast ; in addition, for subsonic objects, the first and second images are clearly identified, which allows the unambiguous determination of the velocity sign.

The most simple arrangement used to record very small objects consists in a single laser beam which travels through the cloud of particles toward the hologram. In fact, if the cloud is not too dense, the incident beam is divided into two parts : the waves diffracted by the small objects constitute the object beam and the non-diffracted wave acts as a reference. This interpretation works very well, and accurate images with a resolution of a few micrometers can be obtained this way.
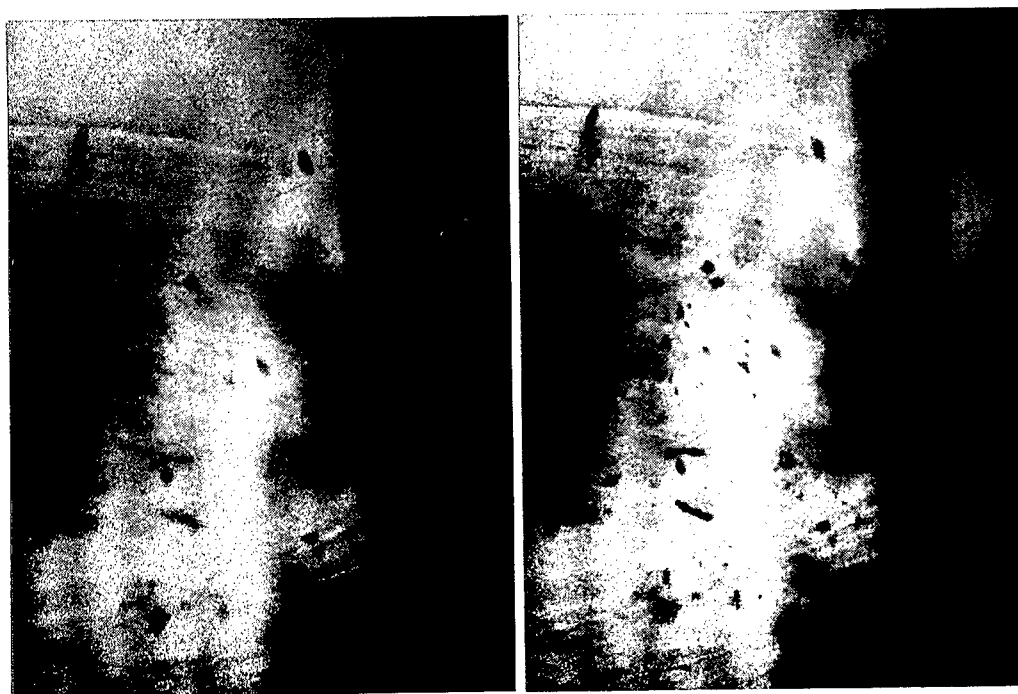
Fig.3 : Two images from a reconstructed field at 10 m and 13 m respectively.

In all the above mentioned arrangements it is advantageous to place the hologram normal to the object beam. This is not only a matter of visual comfort : as the reconstruction arrangement often differs from the recording, the resulting aberrations are minimal with this geometry and the measurements are more accurate.

For the study of very small objects ($\leq 1$ mm) such as dusts or micrometeorites, the in-line arrangement is recommended. It consists of a single laser beam which travels through the object field directly to the hologram : the waves diffracted by the small particles constitutes the object beam and the non-diffused part acts as a reference beam (fig.4). The interest of this set-up is not only its extreme simplicity ; it is also very bright (nearly all the light delivered by the laser arrives at the hologram) and the image quality is less sensitive to changes between recording and reconstruction .
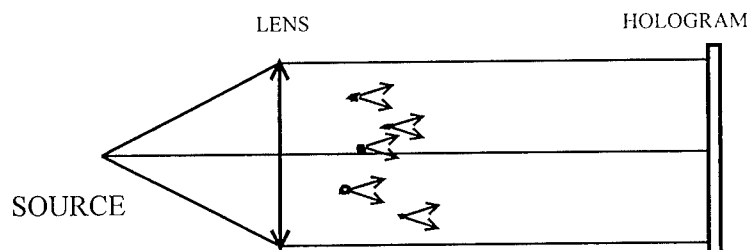


Fig .4 : The most simple arrangement to record a hologram of small objects.

## 5. LIMITS OF THE METHOD.

We have mentioned experiments where the objects were flying at 2000 m/s. In such arrangements, the velocity is just limited by the classical blur due to the object motion during each exposure. With laser pulses of 20 nanoseconds and a blur of 0.1 mm (sufficient for an object of 10 mm or more in size), the

velocity limit is 5000 m/s. Of course, for small dusts, the blur must be smaller and the velocity drops proportionally.

The limit in volume and in distance is also quite large. Our own experience has shown that a field of 100 m² located at 70 meters can be recorded with a back illumination. This requires laser pulses of 5 Joules. Such lasers are commercially available but their price is relatively high (around 200 000 euros). The richer you are, the wider the field.

The acquisition frequency of the images is one of the main bottlenecks of the method. The holographic emulsion must be changed after every recording. A holographic movie made of plates (not films) might have a frequency of one frame per second, far too small for ballistics. The thermoplastic films require still lower frequencies and the other photosensitive systems have a serious lack of resolution (CCD) or of sensitivity (photopolymeres).

Also, the delay between the recording and the final results is an important drawback. The holographic emulsion requires a half-an-hour processing before the reconstruction of the image. The delay is shorter with thermoplastic films (a few seconds). An other factor is the analysis of the image, whose tridimensional nature makes things much more complicate and much more time consuming. Some softwares have been elaborated for small particles [8] but no serious attempt has been made yet for more general objects.

## 6. FUTURE PROSPECTS.

Holography is now a well established method which offers a substantial interest for ballistic studies. However, it remains in the domain of laboratory research and it is not used at an industrial scale nor for routine experiments. The main reason is clearly identified : the holographic emulsion has not found yet an electronic equivalent with a large size, an acceptable sensitivity and an adapted resolution.. The resolution is a technological problem which should find a solution in the next few years. One may expect that future CCD wafers will have pixels of 0.3 μm with a sensitivity equivalent to 1 ISO and an acceptable noise. As to the size, it is just a matter of cost... No doubt that the birth of such sensors will give a new impulse to holography : the progress in computig capacities are such that new softwares will allow an automatic analysis of three-dimensional fields in a short enough time.

## REFERENCES ;

[1]  R.Brooks, L.Heflinger, R.Wuerker, *Appl.Phys.Letters, 7-92* (1965)
[2]  G.Hough, D.Gustafson, *33$^{rd}$ SPIE Annual Symposium*, San Diego, Cal, USA (1989)
[3]  J.Trolinger, D.Weber, *49$^{th}$ Aeroballistic Range Association Meeting*,The Hague, NL (1998)
[4]  D.Gabor, *Nature, 161-777* (1948)
[5]  A.Kurtz, H.Loh, *Appl.Optics, 9-1040* (1970)
[6]  H.Royer, M.Giraud, *Proc. of the 4$^{th}$ Congress on Ballistics, Monterey,Cal,USA* (1978)
[7]  H.Royer,J.Vermorel, *16$^{th}$ Symposium on High-Speed Photography, Strasbourg,F (1984)*
[8]  R.Bexon, J.Gibbs, G.Bishop, *Jl. Aerosol Science, 7-397* (1976)

# UTILIZATION OF SOFT X-RAYS
# IN HYPERVELOCITY IMPACT EXPERIMENTS

## LOUPIAS C., PICARD J.A.

Centre d'études de Gramat, 46500 Gramat, France

**Abstract :** Flash X-rays are very useful to observe terminal ballistics effects and they have been widely used in such experiments for many years. In the field of hypervelocity impact experiments, flash X-rays can also provide valuable information. Nevertheless, due to the specificity of hypervelocity studies (high velocities, small fragments, low density materials), X-ray systems have to present specific characteristics. The main difference with X-rays dedicated to terminal ballistics experiments at ordnance velocities lies in:
- a shorter exposure time to minimize the dynamic blur due to high velocities,
- a smaller X-ray source size to reduce the geometric blur in relation with the object size,
- soft X-rays to visualize thin objects made of low density materials.

At CEG, 150 kV soft flash X-ray systems have been in operation since 1992. The typical characteristics of these systems, especially developed by Scandiflash[1] for hypervelocity impact experiments, are 35-ns pulse width and 1-mm source diameter. The paper describes several experiments performed with the double-stage light-gas gun Persephone [1][2] which involve these soft X-ray systems for the observation of the following events:
- deformation of a stainless steel ball after impact of the launching sabot on the sabot splitter (impact velocity: 7.8 km/s) [2],
- generation of a debris cloud behind a thin aluminium (or steel) plate impacted by a steel ball at 5.5 km/s [3],
- damaging of an advanced heat shielding material penetrated (or perforated) by a steel ball thrown at 5.5 km/s [4],
- penetration of a steel ball into a 3D-CC composite target (impact velocity: 4.8 km/s).

## 1. INTRODUCTION

For many years, the flash X-ray technique has been very useful for the diagnosis of experiments in detonics and terminal ballistics. This observation technique is very attractive because it provides an inside visualization of some materials and, in addition to that, gives the opportunity to get rid of lights and smokes which usually occur in this type of experiment. For similar reasons, observing phenomena through flash X-rays in hypervelocity impact experiments is valuable. However, in this domain, the X-ray generators used must present specific characteristics which enable them to observe objects very different from those conventionally observed in detonics or terminal ballistics. These studies concern essentially the propulsion of heavy metals or the interactions of such metals, when most of the hypervelocity impact studies deal with the vulnerability of spatial targets shielded with thin walls made from low density materials. Examples involve missiles whose vulnerability has to

---

[1] Scandiflash Box 706, Seminariegatan 33F, S-75130 UPPSALA, Sweden

be studied when they are impacted in space by hypervelocity projectiles, and space structures (spatial station, orbital vehicle, satellite) whose vulnerability is analysed when they collide with orbital debris or micrometeorites. The flash X-ray radiography of a hypervelocity impact against such a target is only interesting if the generator used is able to visualize with an accurate definition the fragments generated on impact: these fragments are generally hypervelocity objects of small size and low density. The generators used for flash X-ray radiography (and then dedicated to diagnoses of hypervelocity impacts) differ from those used conventionally in detonics by:
  - a shorter exposure time to minimize the dynamic blur due to high velocity;
  - a smaller X-ray source size to reduce the geometric blur and make it compatible with the reduced size of the observed objects;
  - soft X-rays to visualize thin objects of low density materials.

The CEG has been using such generators for flash X-ray radiography since 1992. Developed by the Swedish firm Scandiflash, they are particularly fitted to diagnosis of high velocity impacts against spatial structures. Their major characteristics are:
  - operating voltage: 150 kV;
  - impulsion width: 35 ns (aluminium window) to 50 ns (mylar window);
  - source diameter: 1 mm;
  - exposure dose at 22 cm: 25 mR;
  - penetration in aluminium at 1 m: 60 mm.

This paper gives a few examples of hypervelocity impact experiments performed at CEG: the diagnoses given with these generators have proved outstandingly instructive.

## 2. APPLICATIONS

The experiments described in this paper were all performed with the laboratory launcher Persephone. This launcher presents two double-stage versions: the first one, with a pump tube and a launch tube of calibre 98 and 52 mm respectively, can propel a 150 g projectile at 4 km/s [1] ; the second, with the same pump tube and a 22 mm launch tube, can propel a 10 g projectile at 8 km/s [2]. The second version was used for the following experiments.

### 2.1 Impact configuration

The impact configuration and the target chamber are schematically presented in figure 1. In every experiment described here, the projectile is a steel ball propelled by a polycarbonate sabot made in one piece. The ball-sabot separation is produced through an impact separator installed at the muzzle of the launcher and described in [2].
To measure the ball velocity and control its state after separation, the ball is radiographed at two different instants: i) a few microseconds after the sabot impact against the separator (RXa), and ii) a few microseconds before target impact (RXb). The RXa generator is triggered by a short-circuit device (two coaxial pins) located on the separator. The RXb generator is triggered through either these short-circuit coaxial pins or a laser barrier positioned before the target. The target chamber is evacuated, then the ball velocity is constant. The double radiograph obtained on a path of about 1500 mm provides an accurate measurement of the impact velocity (accuracy ± 0.2 %) and of the target impact time (± 0.25 μs).
The cloud of fragments obtained in a perforation experiment (or the crater in the case of a penetration experiment) is also radiographed at two instants with the two X-ray generators

RX1 and RX2. To avoid any definition loss due to a double exposition of the film, these radiographs are taken in two perpendicular directions. More, lead collimators are used to limit the emission lobe of each generator and warrant that the film facing a generator is only exposed to this generator. To optimize the quality of the radiograph, the thickness of the polycarbonate windows and of the protections of the radiographic films which are also made from polycarbonate, is reduce to the minimum, *i.e.* 5 mm and 2 mm respectively. The generators RX1 and RX2 are triggered after a given delay through a short-circuit sensor pasted on the front or rear face of the target. The sensor is very thin to limit any parasitic effect induced on the observed phenomenon (thickness of insulating material: 0.038 mm, thickness of aluminium sheet: 0.015 mm).
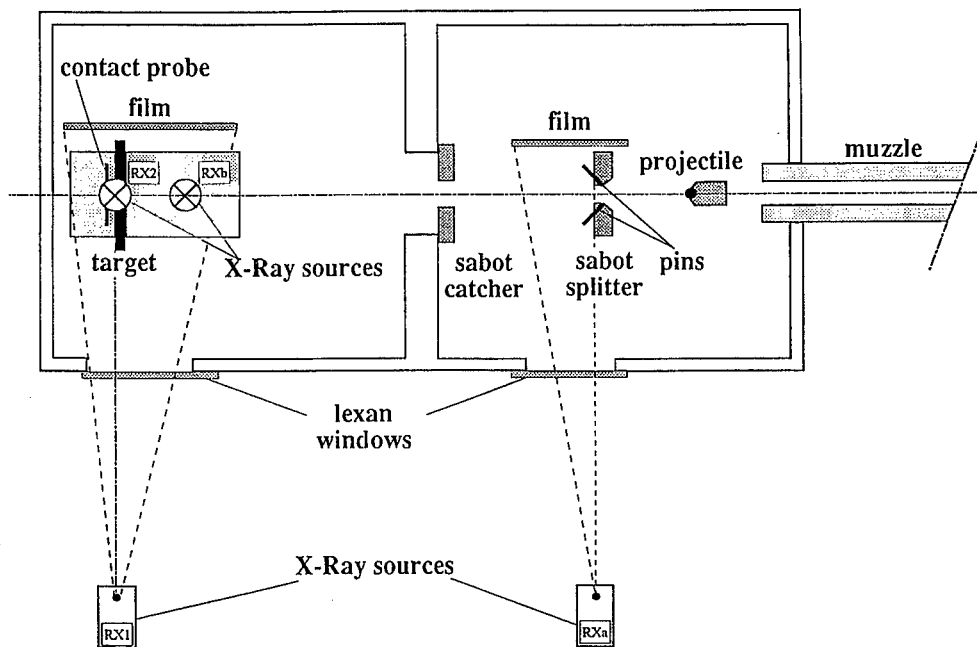


Figure 1 : Experimental configuration. Longitudinal section of the target chamber.

## 2.2 First application: a new sabot/projectile separation technique by impact [2]

In order to implement, under vacuum, hypervelocity impact experiments of balls against different targets, CEG has developed an original technique of separation through impact of a set sabot/projectile, which is based on the destruction of the sabot by impact against a foam sabot splitter. The limits of this technique concerning the propulsion of a stainless steel ball were determined by observing with flash X-rays the ball state a few microseconds after impact of the launching sabot against the sabot splitter. The radiographs presented in figure 2 show that, for a muzzle velocity of 7.6 km/s, the separation occurs without any apparent damage, while at 7.8 km/s the ball is clearly deformed after separation. In addition, owing to soft X-rays, these radiographs give the opportunity to visualize the cloud of fragments from the polycarbonate sabot and the PMMA splitter support. This type of radiographic observation, when compared to numerical simulation, proves valuable to optimize the geometry of both the launching sabot and sabot splitter.

$t = 7.8 \, \mu s$  $t = 6.3 \, \mu s$
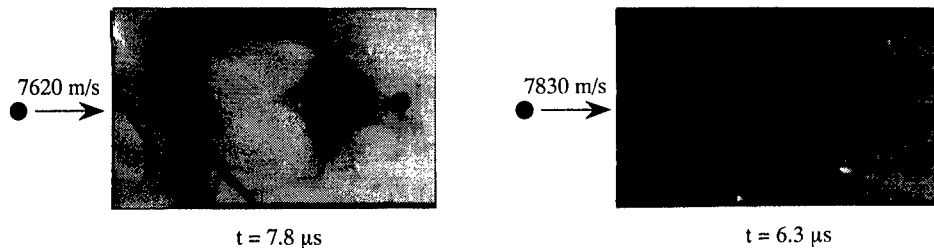
Figure 2 : Radiographs of stainless steel ball and polycarbonate sabot debris cloud after impact on the sabot breaker.

## 2.3 Second application: characterization of the fragment cloud generated behind a thin target [3]

Impact experiments of steel balls against thin plates were performed so as to explore the possibilities and limitations of the hydrocode OURANOS [5] for numerical simulations of hypervelocity impacts against thin targets. For each experiment, the cloud generated behind the target was observed with flash X-rays to determine the expansion velocity of the cloud as well as the fragment distribution inside the cloud. Figures 3a and 3b show two examples of fragment clouds radiographed behind thin targets of different materials but similar areal density. The projectile was a steel ball of 5 mm diameter propelled at about 5.5 km/s. In addition to the evolution of the clouds, the quality of the radiographs gives access to valuable data related to their constitution. It should be noticed that, for a steel/steel impact, the projectile fragments take up a space delimited by two hemispherical portions while, in the other case, the fragments are gathered inside a volume comparable to a disc centered on the firing axis. These data have been used to validate numerical simulations of such impacts. The computations used two-dimensional geometry and then the numerical/experimental comparison of the fragment size distribution was not possible. However, it was interesting to compare the different characteristic areas of each cloud to verify particularly that the computations reproduce the peculiarities of each target material.



(a) t = 9.16 μs  (b) t = 10.44 μs
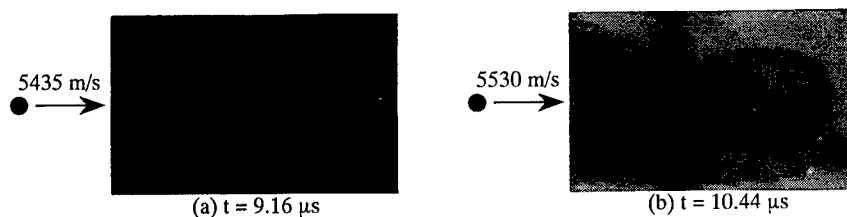
Figure 3 : Radiographs of the cloud generated after perforation of a thin plate by a 5 mm-diameter steel ball.
(a) 0.95 mm-thick steel plate.
(b) 2.85 mm-thick aluminium plate.

## 2.4 Third application : damaging a heat shielding module by hypervelocity impact [4]

On behalf of the European Space Agency, CEG had performed hypervelocity impact experiments on a thermal protection system designed for spacecraft to study its behaviour under collisions with high velocity orbital debris. The damage caused by such an impact against a module constituted of an ablative material (silica fibres embedded in a phenolic

resin matrix) on an aluminium structure was particularly investigated. For each perforation experiment, the profile of the crater obtained in the ablative material, the residual state of the ball after perforation and the fragment cloud were observed with flash X-rays. It should be noticed that the contrast of the radiography images had been increased by image processing (cf. 2.5). This set of observations exhibits typical perforation processes whose experimental confirmation proves valuable for phenomenon understanding and validity analysis of OURANOS computations. Radiography observation of typical processes brings a better understanding of phenomena. Among the processes observed we may note:

- a low expansion of the crater which is systematically observed a few microseconds after the ball crossing owing to densified areas on the crater rim (figure 4a),
- generation of a recompression wave at the interface ablative-material/aluminium-structure, which is responsible for the important damage of the thermal protection in this configuration (figure 4a),
- the unusual position of the projectile fragments in the cloud which are preceded by aluminium fragments of the structure: the aluminium fragments were accelerated before perforation owing to the compression of the layer of ablative material sandwiched between the structure and the ball (figure 4b).

Concerning the validity analysis of computations, the radiographs show clearly that the model of porous material was particularly interesting to simulate the dynamic behaviour of this ablative material.



5515 m/s

(a)                                                          (b)
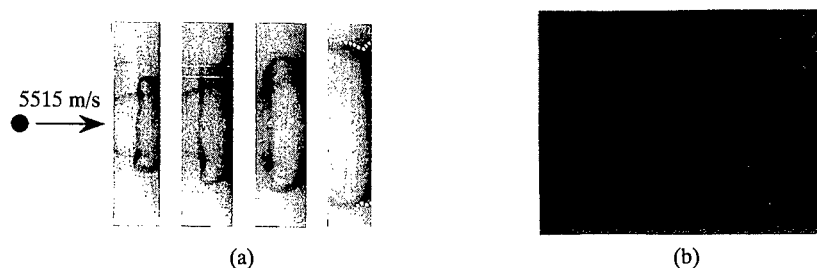
Figure 4 : Perforation of a thermal shield (ablative material + aluminium structure) by a 5 mm-diameter steel ball.
    (a) Processed radiographs of the crater created in the ablative material 12.82, 19.35, 30.73 and 74.96 µs after impact.
    (b) Radiograph of the debris cloud 19.35 µs after impact.


## 2.5 Fourth application: penetration of hypervelocity projectiles in composite material targets

The projectile penetration after hypervelocity impact were also observed with radiographs. Owing to the limited power of the generators, only the penetration of low density materials was observed. More, it appeared that the contrast of radiographs had to be increased in every case. After digitalization of shots, the standard functions of the image processing software Gipsvision (marketed by EIA[2]) were used. Figure 5 presents two radiographs of a steel ball during penetration in a composite target, after impact at 5.5 km/s. The target was a stacking of plates made from the same ablative material used in the thermal protections of 2.4. Figures 5a and 5b compare the original radiographs to the images obtained after processing. Figure 6 presents another example of radiograph: the penetration of a steel ball in a solid target made

---

[2] EIA Agence de Cestas, Z.A. de Marticot, 33610 CESTAS

from 3D carbon-carbon. For the examples presented in Figures 5 and 6, this type of observation provides, here again, significant information on the understanding of the cratering processes as well as valuable data to analyze the validity of numerical simulations. These data concern either the evolution of the crater profile, the projectile slowing down or its fragmentation.



5524 m/s

(a)                                    (b)

Figure 5 : Radiographs of a steel ball during penetration in a massive target made of an ablative material.
(a) Original radiograph taken 15.87 μs after impact.
(b) Image obtained after processing of the original radiograph.



4800 m/s

t = 11.3 μs                              t = 31.3 μs
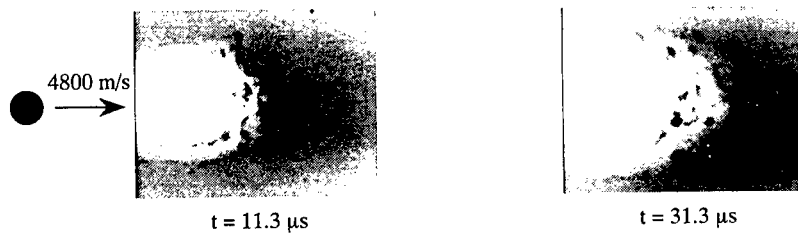
Figure 6 : Radiograph of a steel ball during penetration in a massive 3DCC target after impact at 4.8 km/s.

## 3. REFERENCES

[1]  C. Loupias, P. Chartagnac, B. Jimenez, " Description and calibration of a 50 mm caliber two-stage light gas gun ", in *Proceedings of the 40th Meeting of the Aeroballistic Range Association*, Paris, France, (1989).

[2]  C. Loupias, J.A. Picard, " Description of a 20 mm caliber double-stage light gas gun with a new sabot-projectile separation technique ", in *Proceedings of the 45th Meeting of the Aeroballistic Range Association*, Huntsville, USA, (1994).

[3]  C. Loupias, J.A. Picard, " Expertise d'impact hypervitesse (4-8 km/s) sur cibles métalliques réalisés dans le cadre d'une coopération franco-britannique ", CEG Report T96-01, Gramat, France, (1996).

[4]  C. Loupias, J.M. Sibeaud, P.L. Héreil, " Hypervelocity impacts of orbital debris on an advanced heat shielding material : comparison of Ouranos computations to experimental results ", *Int. Journal of Impact Engineering*, 20, pp. 545-556, (1997).

[5]  H. Jourdren, J.M. Sibeaud, M. Adamczewski-Cauret, " Logiciel OURANOS : présentation et utilisation en détonique ", *Revue Scientifique et Technique de la Défense*, France, (1995).

# PVDF SHOCK SENSORS: PROPERTIES AND APPLICATIONS TO POLAR MATERIALS AND HIGH EXPLOSIVES

BAUER F.

Institut Franco-Allemand de Recherches de Saint-Louis, (ISL), 68301 Saint-Louis, France

**Abstract:** Ferroelectric polymers (PVDF) with well-defined and precisely known electrical properties are now routinely available from commercial sources. Electrical processing with the Bauer cyclic poling method can produce individual films with a well-defined remanent polarization up to 9 $\mu C/cm^2$. These polymers provide an unusual opportunity to study the structure and physical properties of materials subjected to shock loading. The behavior of PVDF has been studied over a wide range of pressures using high-pressure shock loading and has yielded well-behaved reproducible data up to 25 GPa in inert materials. The application of PVDF gauges for recording shock waves induced in polar materials like Kel-F, PMMA or in reactive materials is hampered by observations of anomalous responses due to shock-induced polarization or electrical charge released inside shock compressed explosive. A solution using an appropriate electrical shielding has been identified and applied to PVDF for shock measurement studies of Kel-F, and for Hugoniot measurements of High Explosives (H.E.). Furthermore, shock pressure profiles obtained with in situ PVDF gauges in porous H.E. (Formex) in a detonation regime have been achieved. Typical results of shock pressure profile versus time show a fast superpressure of a few nanoseconds followed by a pressure release down to a plateau level and then by a pressure decay. More accurate measurements are reported with electrically improved PVDF gauges as well as with 0.25 $mm^2$ active area PVDF gauges.

## 1. INTRODUCTION

Piezoelectric materials are widely used as active elements in stress gauges used to provide nanosecond, time-resolved stress measurements of rapid impulsive stress pulses produced by impact, explosion or rapid deposition of radiation. In the earliest work the gauges used crystalline sensors made of either x-cut quartz or various cuts of lithium niobate with thicknesses of many millimeters. The wave transit times through such sensors range from many tens of nanoseconds to a few microseconds. The upper response limits of the crystalline sensors are limited by either, or both, mechanical or electrical properties: dynamic yielding of the sensors or dielectric breakdown due to the large internal fields produced by the piezoelectric effect.

Although ferroelectricity and piezoelectricity in PVDF were discovered by Kawai [1] in 1969 and subsequently confirmed by Kepler [2], the materials commercially available did not exhibit reproducible properties due to the critical importance of mechanical and electrical processing history. Early work by Bauer [3], which explored the behavior of polyvinylidene fluoride (PVDF) for high pressure applications, led to recognition of the need for such highly reproducible properties for PVDF. An international cooperative study between ISL and Sandia National Laboratories to develop the PVDF gauge, has shown that 25 $\mu m$ film PVDF can be reliably used in a wide range of precise stress and stress-rate measurements [3]. Reliable behavior under the various extreme shock conditions requires specific sample

preparations according to the Bauer process [4,5]. The 25-micron thickness of such PVDF sensors permits the gauges to be placed unobtrusively in a variety of locations within samples. Their direct stress-derivative or stress-rate signals on a few nanosecond and higher operating stress limits provide capabilities not available with any other technique. The 10 nanosecond transit time of a wave in PVDF achieves conditions in which the electrical behavior is described in the "thin mode". That is, the electrical effects as the wave propagates within the sensor are not resolved to first order.

Historically, the introduction of gauges with direct measures of stress pulse characteristics at higher derivatives such as stress, Manganin, quartz, etc or particle velocity, velocity interferometer technique (VISAR), has led to qualitative improvements to model materials behaviors under the high-pressure, short duration conditions common in shock-compression loading conditions.

The capability of PVDF to provide a direct measure of rate-of-change of stress moves experimental capability to a new sensitivity. Recognizing the need for a reproducible material for the destructive conditions of shock compression, we have developed a new poling equipment. [6] to process PVDF so that its physical properties [7] exhibit a reproducibility approaching that of piezoelectric single crystals. Thus, the combination of precise conditions concerning highly reproducible samples provides an opportunity to describe the piezoelectric response of PVDF to high-pressure shock compression and large volume compression.

The present paper summarizes the status of the experimental work. The behavior of PVDF has been studied over a wide range of pressures using high-pressure shock loading and has yielded well-behaved reproducible data for pressures up to 25 GPa in inert materials. The shock-induced polarization for 1 and 9 $mm^2$ precisely poled PVDF gauges is recalled. The analysis of their response in the " thin mode regime " using a Lagrangian hydrocode has been revisited. In situ shock measurements in polar materials or polymers are presented for PVDF gauges which use a new shielding technique. PVDF gauges shielded in such a manner have recently been utilized successfully for Hugoniot measurements of porous explosives. Furthermore, in situ shock pressure profiles obtained with PVDF gauges in porous H.E. in a detonation regime have been achieved and are described.

## 2. PROGRESS IN PVDF POLARIZATION TECHNOLOGY

In order to enhance the precision of shock gauges and to avoid some deviations in the gauge
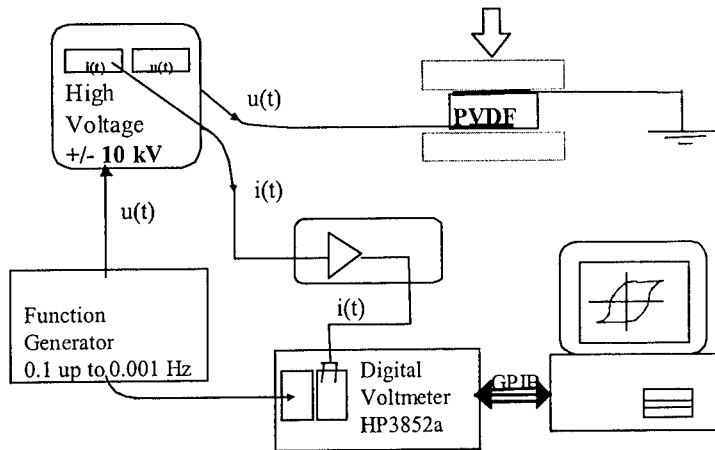


Figure 1: poling process equipment

response as reported earlier [6], we have developed new poling equipment. This equipment, as shown on Figure 1, allows us to adjust, in real time via a high voltage and data acquisition computer controlled system, the predetermined remanent polarization as well as the maximum displacement current measured at the coercive field for an individual PVDF sample, Fig. 2. Further, with appropriate attention to the electrical poling history of each sample, space charge in the samples can be eliminated [4], [5]. A higher degree of reproducibility is achieved when the maximum displacement current at the coercive field is stabilized.

With our cyclic poling process, reproducible remanent polarizations as large as 9 μC/cm² as well as identical displacement current are routinely achieved to-day. Starting at low electric fields, the sample is cycled through many "loops" until a consistent behavior is indicated. Higher applied fields are then utilized until the desired stable polarization is achieved. Because electric fields as high 5 MV/cm are utilized, inferior film is eliminated in the process. Each PVDF sample fabricated in this process is characterized with an individual poling history with well-defined remanent polarization values, better than 2 %, which can be reproduced at will.
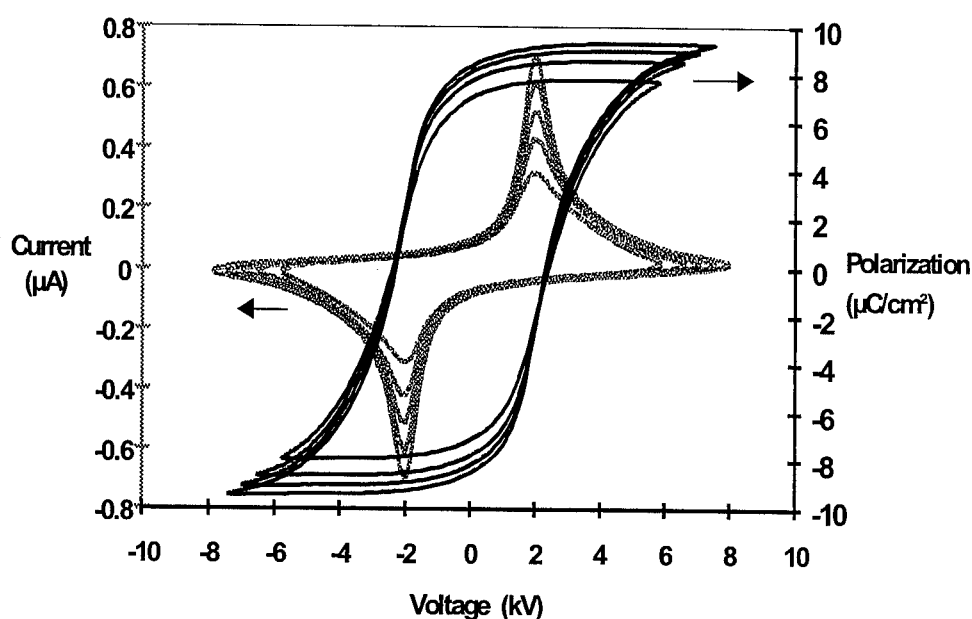


Figure 2: histories of hysteresis loops on a 25 μm thick biaxially stretched PVDF sample with a 1 mm² area. Typical displacement current and polarization versus voltage applied

## 3. PIEZOELECTRIC PVDF SHOCK RESPONSE: EXPERIMENTAL ARRANGEMENT

The impact of a precisely controlled impactor mounted on a projectile upon a test material sample provides the most accurate and well-defined pressure achievable with any technique [7]. In the impact experiment, Fig. 3, the symmetry conditions for identical impactor and sample materials require that precisely one half of the projectile velocity at impact be imparted to the sample. A range of impact velocities from 0.25 km/s to 1.8 km/s is achieved with a powder gun which accelerates the projectile to a predetermined velocity. PVDF gauges are placed on the impact surface of either z-cut quartz, sapphire crystals or selected copper which serve as standard materials to define the stress. The PVDF gauge response is determined by recording the short-circuited current during the time when the shock waves are

reverberating within the samples until mechanical equilibrium is reached, corresponding to the longitudinal stress in the standard material. In the electrical measurement circuit a carbon resistance SMD (Surface Mounted Device) resistance replaces the expensive Current Viewing Resistor or CVR. The electrical charge is determined by numerical integration of the recorded current. Typical times to achieve equilibrium in the 25 μm PVDF films are 50 to 150 nanoseconds.
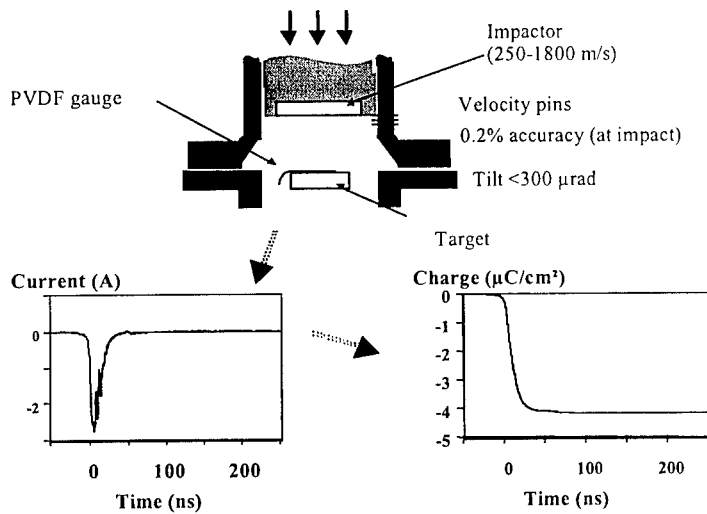


Figure 3: the piezoelectric response of PVDF film is studied with the impact of standard materials with samples placed on the impact surface of the target. This experiment achieves the most precise high pressure loading of any technique, static or shock. Other "ramp-wave" loading is achieved by placing samples behind disks of fused quartz or "pyroceram"

## 4. PIEZOELECTRIC POLARIZATION AT HIGH PRESSURE: RESULTS AND LAGRANGIAN ANALYSIS

The piezoelectric charge associated with a peak pressure is obtained upon integration of the current pulse, Fig.3. The charge data are observed to be a continuous function of the shock pressure until 25 GPa [6].
As reported in [8], it should be recalled here that the experimental electrical charge Q released by the piezoelectric PVDF film can be correlated with the global one dimensional true strain ε of PVDF. The following relationships have been found to fit well the dependence of the electrical charge Q versus true strain ε:

- for $Q < 0.8288$ μC/cm$^2$:

$$Q = 1.88 \cdot \ln (1 + 10 \cdot \varepsilon) + 0.0047; \qquad (1)$$

- for $Q > 0.8288$ μC/cm$^2$:

$$Q = 12.16 \cdot \varepsilon + 0.16. \qquad (2)$$

where $\varepsilon = \ln \left( \dfrac{e(t)}{e(t_0)} \right) = \ln \left( \dfrac{v(t)}{v(t_0)} \right)$, e = PVDF film thickness; v = PVDF specific volume and
t = time.

The piezoelectric charge released Q is a nonlinear function of the true strain, $\varepsilon$ in the true strain values region (0 - 0.03), and is a linear function of the true strain $\varepsilon$, in the range (0.03 - 0.45,), Fig. 4.
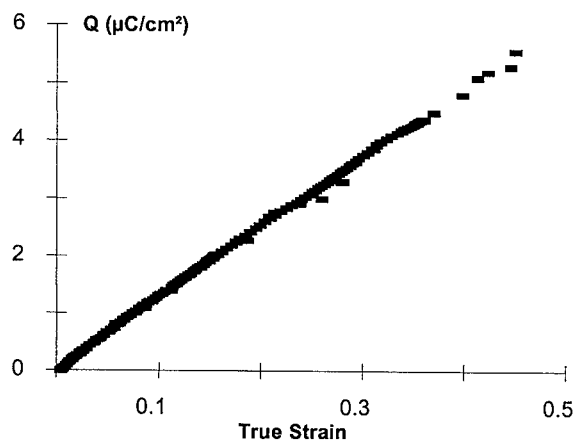


Figure 4: electrical charge versus the computed true strain $\varepsilon$

By introducing the experimental relations (1) and (2) into the hydrocode DYNA (Livermore-Software Two Dimensional Hydrodynamic Finite Element Code) [8] or SHYLAC (Hydrodynamic Lagrangian Simulation of Shocks) [11], we can compute the theoretical current or charge profile for a given test. The calculation allows us to determine the stress as well. Figure 5 shows, for both 1 mm$^2$ and 9 mm$^2$ PVDF gauges, the piezoelectric response versus stress, based on experimental and computed data.
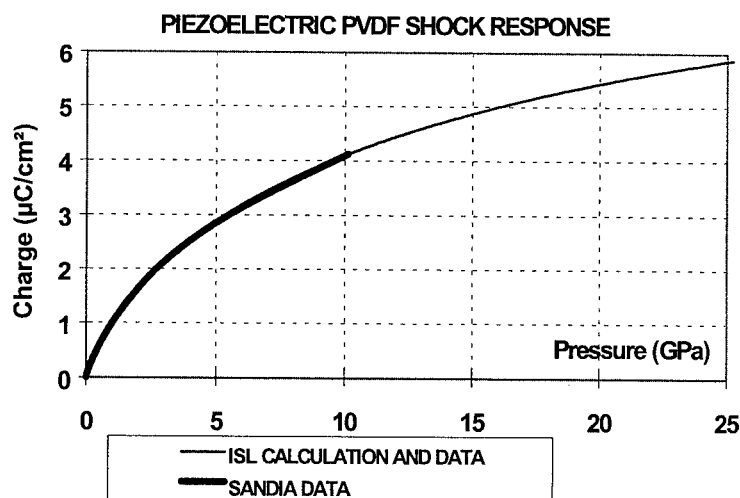


Figure 5: the electrical charge observed at various peak pressures is shown for PVDF. The experimental and computed data are on the same curve

We observe, Fig. 5, that the experimental and computed charges versus stress are in very good agreement with the published data (0 - 10 GPa) of R. A. Graham [4] on our PVDF gauges. As shown on the same Figure 5, the piezoelectric response based on experimental and computed data has been determined until 25 GPa. The behavior indicates a strongly nonlinear character.

- 521 -

## 5. IN SITU SHOCK MEASUREMENTS IN POLAR MATERIALS

Viscoelastic behaviors are strongly manifested in polymeric solids. Many Hugoniot descriptions of polymers have been tabulated, but generally ignore the consequences of viscoelasticity.
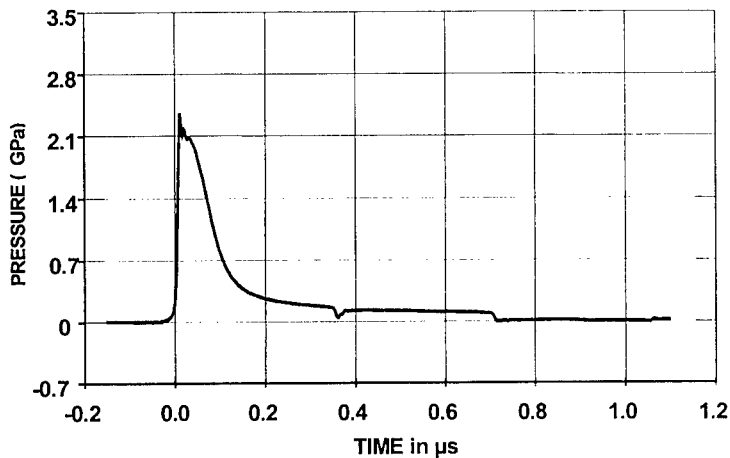


Figure 6: anomalous PVDF response on Kel-F (14mmin∅)

It should be borne in mind that shock-induced polarizations [7] are widely observed in polymeric materials, above threshold compression of about 15%. Shock measurements with PVDF placed on the impact surface of polar materials, i.e. polymers, without paying attention to the electrical environment due to the induced polarization, have led to an anomalous response, as can be seen in Fig. 6. The response should be a shock front followed by a stress plateau. The electrical coupling of the polar compressed Kel-F with the PVDF gauge is responsible for the anomalous response observed. A new electrical shielding for the gauge
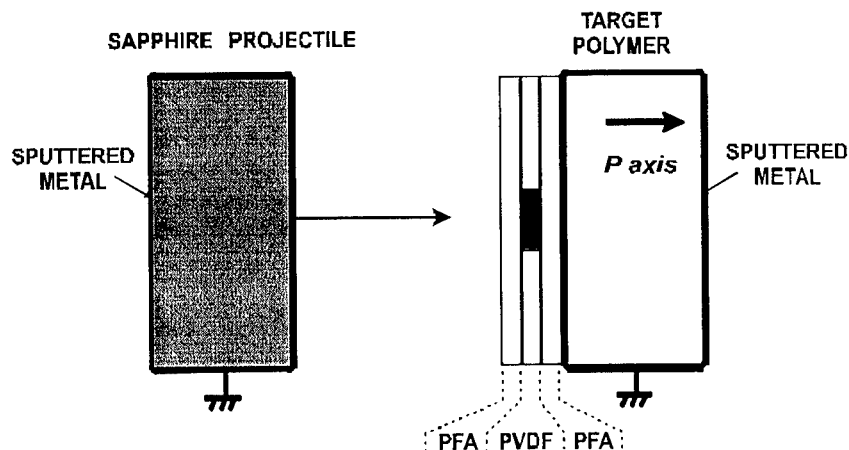


Figure 7: scheme of the experimental arrangement used for shock studies of polar materials. Typical shielding used in case of shock-compressed polar materials with PVDF is indicated

has been realized, as shown in Fig. 7. This shielding is achieved via a deposition of thin metallic layers sputtered on both projectile and sample and then connected to the ground. This leads us to avoid the capacitive coupling of PVDF with the environment. The PVDF gauge

has to be sandwiched between two 25 µm thick films of PFA-Teflon (PFA is the commercial name by DUPONT). The piezoelectric response obtained via step shock compression (Fig. 8) is similar to that observed in reference [7] using a velocity interferometer technique. The pressure profile, given on Fig. 8, is characteristic of the viscoelastic response of a polymer.

**PRESSURE (GPa)**
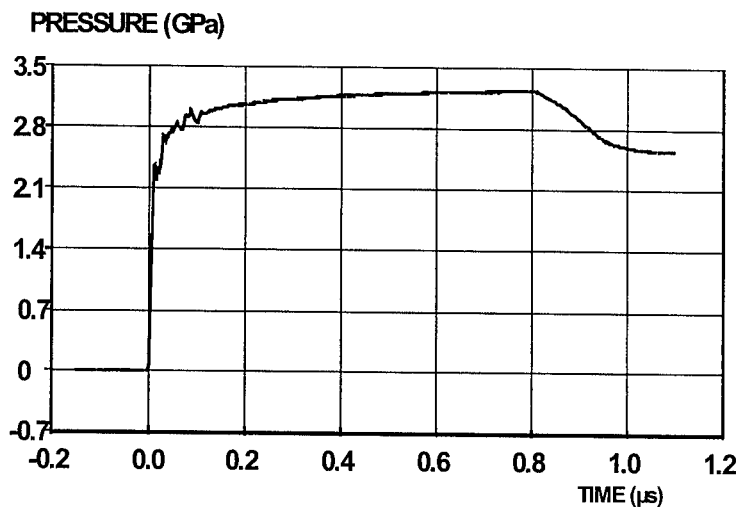


Figure 8: viscoelastic response of Kel-F (14 mm in ∅)

## 6. HUGONIOT MEASUREMENTS OF POROUS EXPLOSIVES

PVDF gauges shielded as in Fig. 7 have recently been utilized successfully for Hugoniot measurements of porous explosives. Figure 9 gives the sketch of the experimental arrangement used for Hugoniot measurements. After many trials, we have been able to shield the explosive as described in the preceding section. Sputtering of 0.01 µm thick Pt and 0.1 µm thick Au layers could be achieved on a high explosive (Formex) available at ISL.
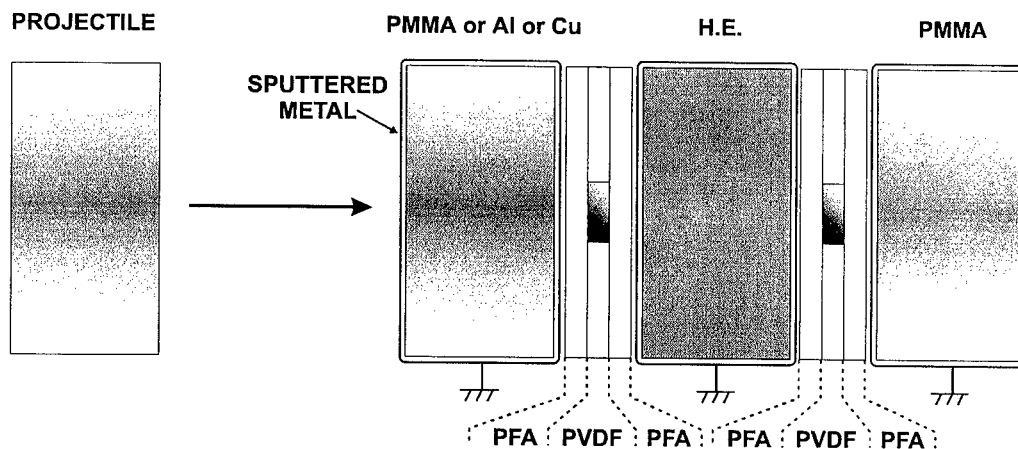


Figure 9: experimental arrangement for Hugoniot measurements of the porous H.E."Formex"

This H.E. (Formex) contains 89% Pentaerythritol Tetranitrate (PETN) and 11% rubber. The

average density of this porous explosive is equal to 1.35 $g/cm^3$. Measurements (Fig. 10) of shock pressure profiles and shock velocities (deduced) from H.E. thickness over transit time) have led to the Hugoniot determination at low input shock compression. The input wave profile, given by the PVDF gauge placed between the copper disk and the explosive (Fig. 11) seems to follow a shock profile similar to that observed by Anderson on porous materials [9]. But at the moment there is no clear explanation for the pressure collapse observed just after the first pressure jump. Nevertheless, it has been observed that the shape of the shock input
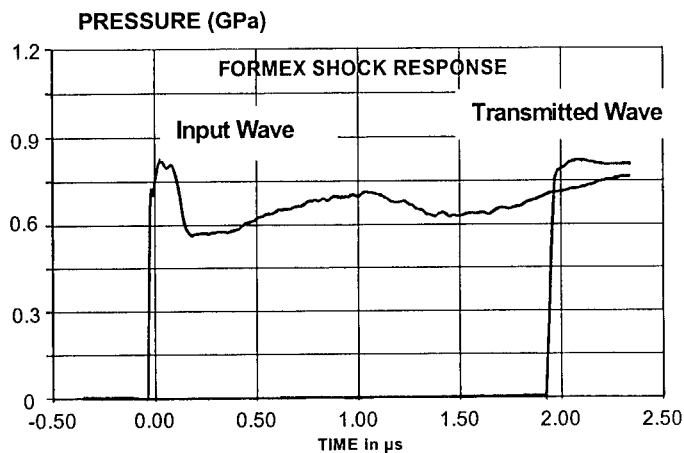
**PRESSURE (GPa)**

Figure 10: input and transmitted pressure profiles obtained on the H.E. sandwiched between two pieces of PMMA

influences the H.E. reaction.
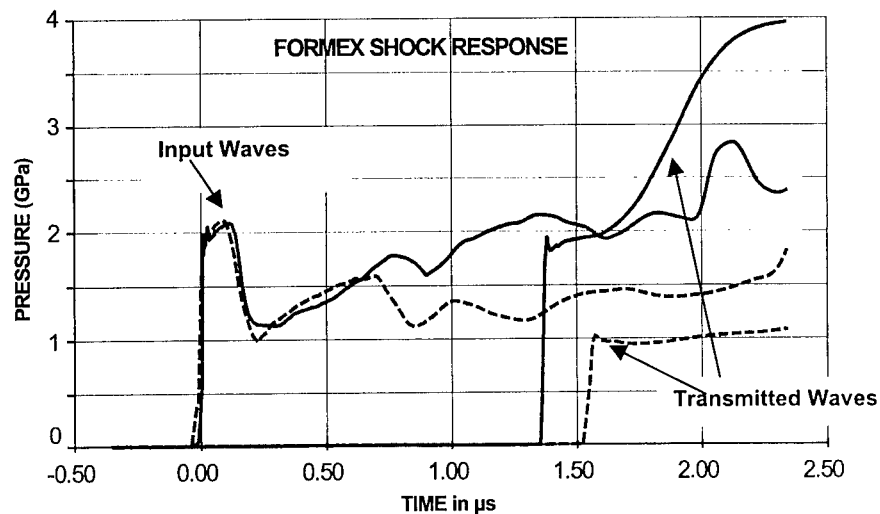
Figure 11: the dotted curves correspond to the PVDF pressure profiles obtained on H.E. sandwiched between an aluminum 2024 disk and a PMMA disk. The continuous curves correspond to the PVDF pressure profiles obtained on H.E. sandwiched between a copper disk and a PMMA disk

## 7. IN SITU SHOCK PRESSURE PROFILES OBTAINED WITH PVDF GAUGES IN POROUS H.E. IN A DETONATION REGIME

The overall features of H.E. studies under precise impact loading are shown in Figure 12. On the H.E. Formex samples, in the 12 x 12 x·5 mm³ parallelepiped form, the same shielding technique is applied. As indicated in Figure 12, a PVDF gauge of 1 mm² in active area is placed between the copper plate and the first H.E. sample, then another PVDF gauge is bonded between the two H.E. samples and finally the last PVDF gauge is mounted between the second H.E. sample and a shielded piece of Kel-F. The PVDF gauges also have to be sandwiched between two 25 μm thick films of PFA-Teflon. A range of impact velocities from 50 to 650 m/s is achieved with our powder gun system to accelerate the projectile to a
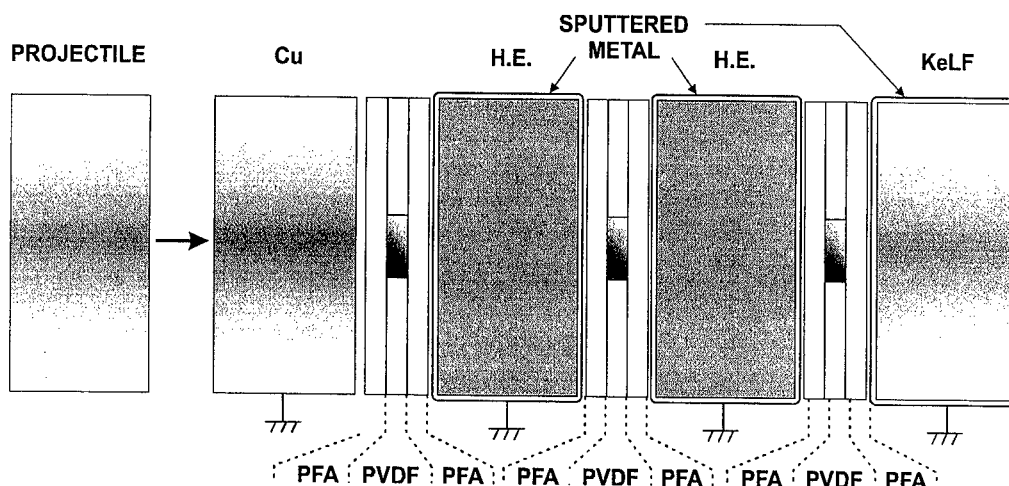
Figure 12: experimental arrangement for H.E. pressure measurements

preselected velocity. Due to the symmetric precise impact, planar loading over the surface of the 1.5 mm thick copper plate is achieved. The input shock wave is then transmitted to the explosive. The input stress loading in Formex is on the order of 2.5 GPa. The level of the induced stress is high enough to induce the detonation at a depth from about 0.5 mm up to 1 mm.
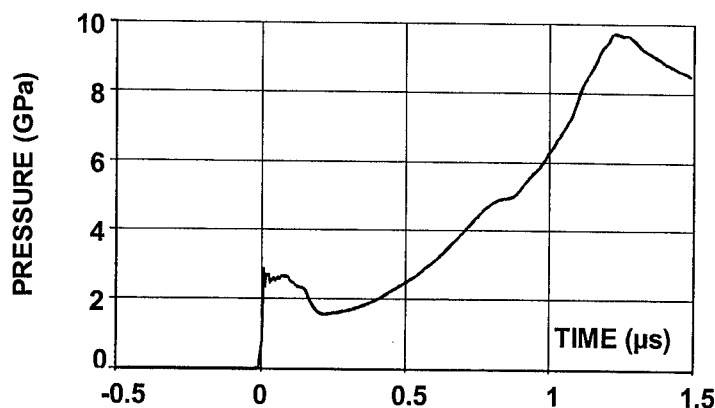
Figure 13: pressure versus time for the first PVDF gauge

The detonation wave propagates through the explosive and is transmitted to the Kel-F backing which is perfectly matched to the PVDF gauge. In order to verify in such an experiment the ability of the shielding to avoid the electrical coupling of the gauges with the electrical environment when the detonation wave occurs [12], we have placed the three gauges in the -/+ electric orientation during a test. The same experiment has been repeated
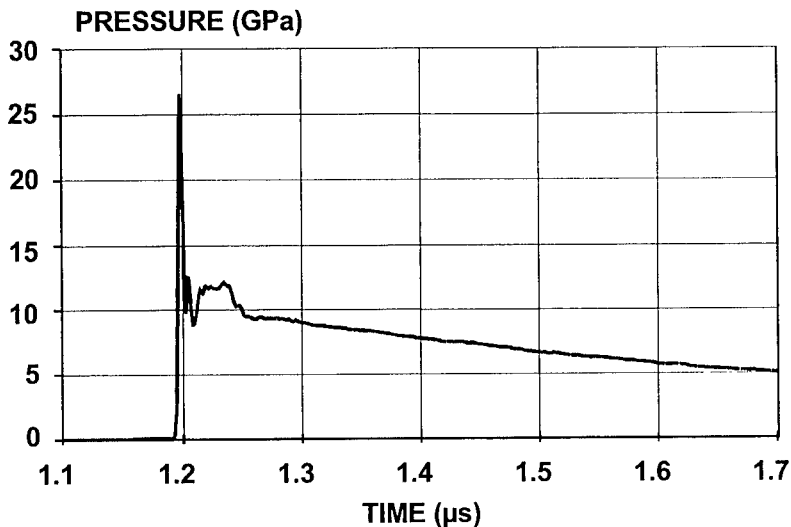


Figure 14: pressure versus time for the second PVDF gauge in situ H.E

gauges in the -/+ electric orientation during a test. The same experiment has been repeated with PVDF gauges placed in the +/- orientation, which is the usual orientation utilized [7]. The electrical signals from the PVDF gauges show the same amplitude and shape in current and in electrical charge for both experiments. A typical record of reduced data for the first PVDF gauge in shock pressure versus time is depicted in Figure 13. After a shock pressure jump and a plateau, a slight collapse is observed, then the pressure, following the reaction of the H.E., increases up to a maximum value of 9.7 GPa. Figure 14 shows the pressure versus time for the second PVDF gauge embedded in situ the H.E. The PVDF shock pressure profile
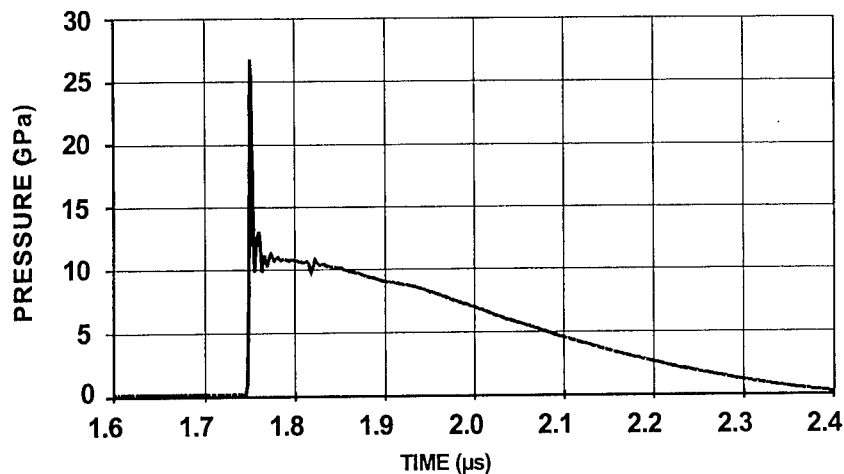


Figure 15: pressure versus time for the third PVDF gauge between H.E. and Kel-F

shows a fast superpressure of a few nanoseconds duration at a level of 24.5 GPa, followed by a pressure release down to a plateau at a pressure level of about 11 GPa and then a pressure decay. The pressure plateau (Fig. 14), measured at 11 GPa is in agreement with the Chapmann-Jouguet (C-J). detonation pressure data measured and computed for close PETN compositions and published by H.C. Hornig et al [13]. Figure 15 shows the pressure versus time for the third PVDF gauge bonded on the Kel-F backing. As can be seen, a similar profile is observed. But, on this record, the fast superpressure is not followed by a plateau level, but by a few oscillations and a pressure decay. The measured detonation velocity is equal to 6850 m/s. Other similar experiments have been carried out and similar records have been obtained.

We have compared the experimental current response corresponding to the pressure spike with the computed current response of a PVDF subjected to a 24.5 GPa single step shock compression.
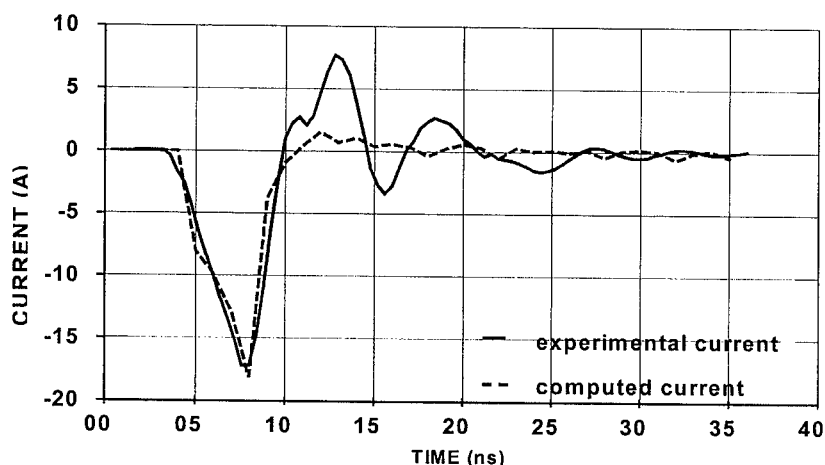


Figure 16: experimental current measured in situ H.E. and computed current for PVDF at the same shock pressure level

The configuration is a symmetric impact of Kel-F on PVDF/Kel-F. The impactor velocity was 4170 m/s which produced 24.5 GPa. The computation of the PVDF response submitted to one-step compression has been made using the SHYLAC hydrocode, taking into account the piezoelectric equations of PVDF [11]. Figure 16 gives both the experimental current measured in situ the H.E. and the computed current for PVDF at the same shock pressure level. The agreement between the two curves leads us to believe that the PVDF gauge in situ H.E. can respond to the pressure spike.

## 8. CONCLUSION

The piezoelectric response for both precisely 1 $mm^2$ and 9 $mm^2$ PVDF gauges subjected to shock loading is observed to be identical. The electrical output of the gauge is determined solely by the piezoelectric response, i.e. there is essentially no domain switching [10]. Solutions using appropriate shielding are identified and apply to shock measurements of polar materials. The shielding technique can also be applied to High Explosive Hugoniot measurements. In Situ shock pressure profiles in porous H.E. in a detonation regime have been achieved. The shock pressure profile shows a fast superpressure of a few nanoseconds followed by a pressure release down to a plateau level and then by a pressure decay. This pressure spike was predicted by Von Neumann [14] but has never before been experimentally observed in situ. Sheffield [15] has observed via a velocity interferometer technique, reaction

zone with a spike on other H.E. Our first experimental observations have to be confirmed in future studies.

## 9. REFERENCES

[1].H. Kawai, "The Piezoelectricity of Poly(vinylidene Fluoride)", Japan J. Appl. Phys., Vol.8, pp. 975-976, 1969.

[2].R.G. Kepler, "Piezoelectricity, Pyroelectricity and Ferroelectricity in Organic Materials" Ann. Rev. Phys. Chem. 29, pp. 497-518, 1978.

[3].F. Bauer, R.A. Graham, "Very High Pressure Behavior of Precisely-Poled PVDF" Ferroelectrics, Vol. 171, pp. 95-102, 1995 and references therein.

[4] F. Bauer, "Method and Device for Polarizing Ferroelectric Materials" U.S. Patent 4,611,260, 1986.

[5] F. Bauer, "Device for Polarizing Ferroelectric Materials" U.S. Patent 4,684,337, 1987.

[6].F. Bauer, "Advances in Ferroelectric Polymers for Shock Compression Sensors", *Proceedings of Shock Compression of Condensed Matter*, The American Institute of Physics, pp. 789-792, 1998.

[7] R.A. Graham, , *Solids under High Pressure Shock Compression*,: Springer Verlag New York, pp. 103-113, 1993 and references therein.

[8] H. Moulard, F. Bauer, "Lagrangian Analysis of the PVDF Shock Sensor" *Proceedings of Shock Waves in Condensed Matter*, North-Holland, pp. 1065-1069, 1995.

[9] F. Bauer (Ed), Proceedings of the 1994 PVDF Workshop, *ISL Report* 26/94,.unpublished, 1994.

[10] G.A. Samara, F. Bauer, "The Effects of Pressure on the $\beta$ Molecular Relaxation and Phase Transitions of the Ferroelectric Copolymer P(VDF0.7TrFE0.3)" Ferroelectrics, Vol. 135, pp. 385-399, 1992 and references therein.

[11] S. Couturier, "Etude de nouveaux capteurs piézoélectriques à base de PVDF. Application à la caractérisation de chocs brefs et intenses induits par impulsion laser" *Thesis*, University of Poitiers, France, June 1996.

[12] R. Schall, "Detonation Physics", *in Physics of High Energy Density*, ed. by Acad. Press Inc., New York, pp. 230-245, 1971.

[13] H.C. Hornig, E.L. Lee, and M. Finger, "Equation of State of Detonation Products", *Proceedings of the Detonation Symposium*, pp. 503-511, 1970.

[14] J. von Neumann, "Theory of Detonation Waves", (1942), *in John von Neumann Collected Works*, Vol 6 (ed. L. A .J. Taub),: Macmillan, New York, 1963.

[15] S.A. Sheffield, L.D. Lloyd, and R. Engelke, "Detonation Properties of Nitromethane, Deuterated Nitromethane and Bromonitromethane" presented at the American Physical Society Shock Wave Meeting, Snowbird, Utah, June 27, 1999.

# POTENTIALITY OF VISAR INTERFEROMETRIC TECHNIQUE IN TERMINAL BALLISTICS

## HEREIL P-L., LOUPIAS C., BERGUES D.

Centre d'Etudes de Gramat, 46500 - GRAMAT, FRANCE

**Abstract** : Potentiality of VISAR interferometer is shown in the field of terminal ballistics through four examples : 1) impact of a steel rod against a steel target plate 2) in-bore acceleration of a projectile in a two stage light gas gun 3) expansion of high explosive loaded cylinder 4) hypervelocity impact of a steel ball against an aluminum target. The informations delivered by VISAR interferometer are essential because of its 1 ns time resolution and its high accuracy.

## 1. INTRODUCTION

Since its development in 1968-1974 by SANDIA National Laboratories [1], VISAR interferometer has been widely used in the field of Shock Physics and Dynamic Behavior of materials [2]. The principle of this instrumentation is to differentiate the Doppler-shifted light coming from the target, to produce interference fringes which frequency is proportional to the specimen surface acceleration. The fringes count is related to the surface velocity by the fringe factor, a constant defined before the test and corresponding to the sensitivity of the interferometer.
VISAR has been mainly used to measure the free surface velocity history of a shocked specimen in plate impact configuration, that is in a one dimensional geometry. These studies involve determining equation of state properties of materials subject to shock loading. Nevertheless this device may be useful in others configurations to determine the velocity history of well-defined point. The main advantages of VISAR instrumentation are the risetime (~ 1 ns), the accuracy (~ 1%-2%) and the ability of monitoring either specular or diffuse reflecting surface.

This article describes the use of VISAR laser interferometer in the field of terminal ballistics. The potentiality of this instrumentation is shown through some examples :
- impact of a steel rod against a steel target plate [3],
- acceleration of a projectile in a two stage light gas gun [4],
- expansion of high explosive loaded cylinder [5],
- hypervelocity impact of a ball against an aluminum target [6].

## 2- IMPACT OF A STEEL ROD

The experimental configuration of the first example is shown in figure 1. The projectile is a rod of steel (Rolled Homogeneous Armor) and the target a plate of the same material. The dimensions of the projectile and the target are indicated in this figure. The measured velocity

profile shows the initial elastic precursor, the plastic wave and during release, the reverse polymorphic transition of steel and the spall signal. These informations are essential in testing the validity of numerical simulations realized with 2D hydrocodes.
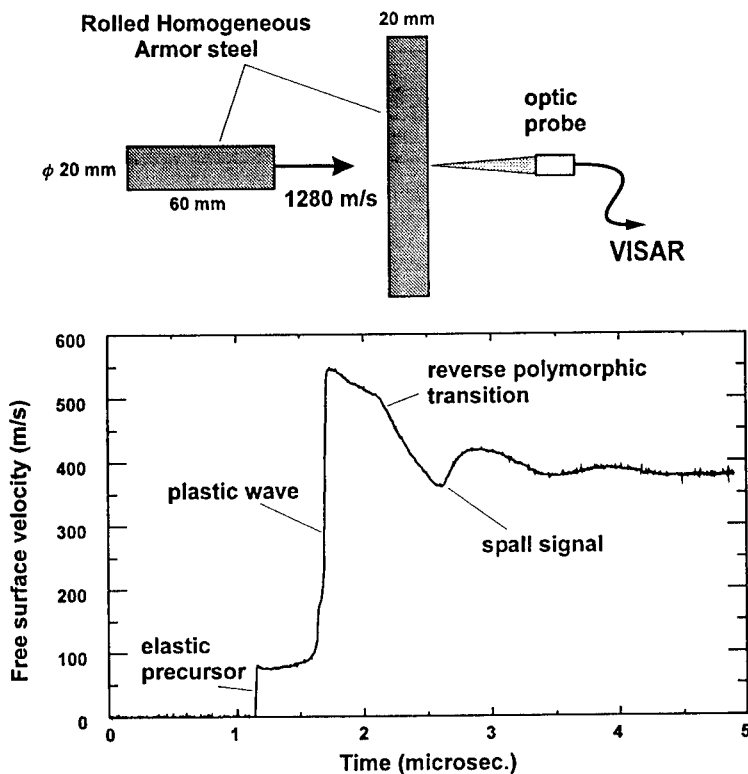


Figure 1 : Experimental configuration and free surface velocity profile for the impact of a RHA steel rod against a RHA steel target at an impact velocity of 1280 m/s

## 2- ACCELERATION OF A PROJECTILE

The second example is the measurement of the in-bore acceleration of a projectile in the two stage light gas gun PERSEPHONE. The experimental configuration and the experimental results are indicated in figure 2. In this experiment, the launch tube of PERSEPHONE has a 50 mm diameter and the mass of the projectile is 115 g.

For this measurement a special arrangement of incident and reflected laser beam has been chosen. There is no optic probe and no lens but only an expendable mirror which turns incident laser beam on the front face of the projectile inside the barrel tube and turns the reflected beam to VISAR. The front face of the projectile is specular in order to obtain enough returned intensity signal. The sensitivity of VISAR has been defined to 308 m/s/fringe.

The VISAR signals and the projectile velocity profile obtained in this experiment are represented in figure 2. Recording time is about 6 ms and the end of the VISAR signals corresponds to the impact of the projectile on the expendable mirror. VISAR signals are well-defined with the amplitude which rises when the projectile is moving into the tube. The first portion of the velocity profile gives an acceleration of 113 000 g. The singularities marked by

an arrow correspond to the reflections of shock wave between the front face of the piston and the rear side of the projectile.
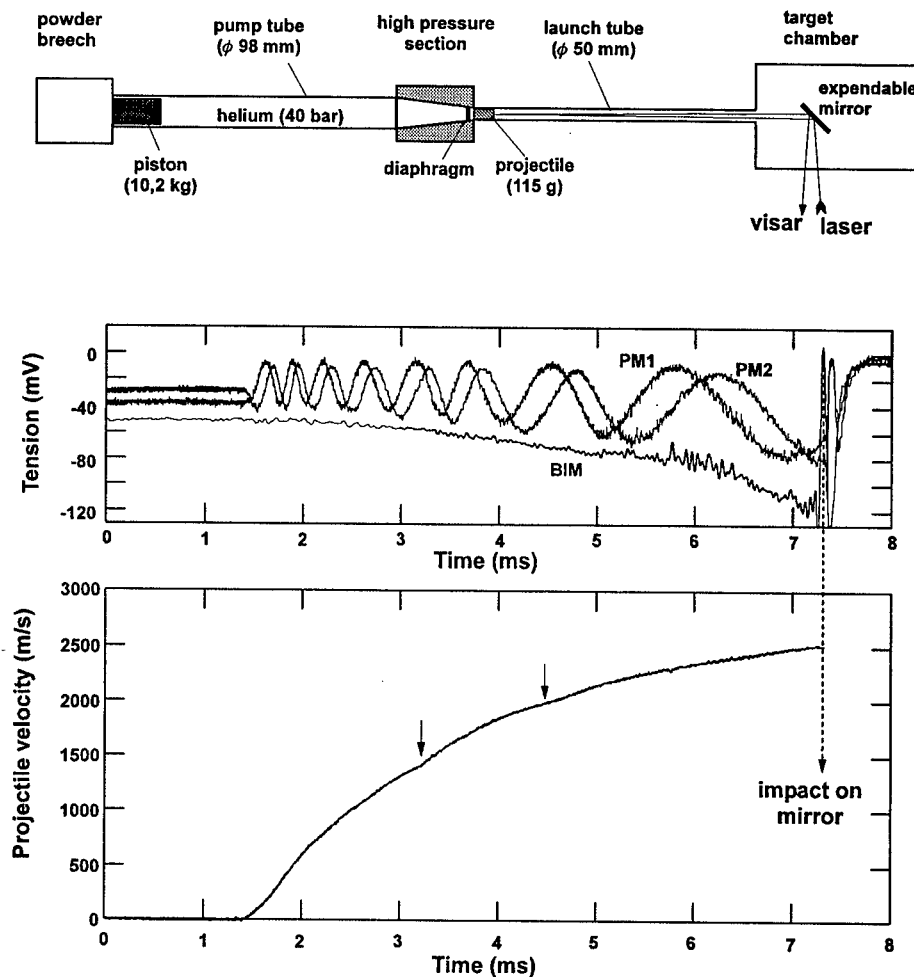


Figure 2 : Experimental set up, VISAR signals and projectile velocity profile for the in-bore acceleration measurement of a projectile in the two-stage light gas gun PERSEPHONE

## 3- EXPANSION OF A HIGH EXPLOSIVE CYLINDER

The expansion of a cylinder is used to compare the dynamic behaviors of high explosives and to calculate equations of state for their detonation products. The experimental assembly is shown in figure 3. A copper tube of 76.2 mm internal diameter, is filled with the explosive. The tube wall thickness is 7.6 mm and the tube length 400 mm. The explosive is detonating at one end of the tube and the velocity of the copper tube wall is recorded with VISAR interferometer. In order to obtain sufficient light intensity during the test, the optic probe is tilted with an angle of 5°.

The measured velocity diagram indicated in figure 3, shows a first shock followed by several recompression waves up to a maximum plateau of 1050 m/s. The recording time is about 30 µs.
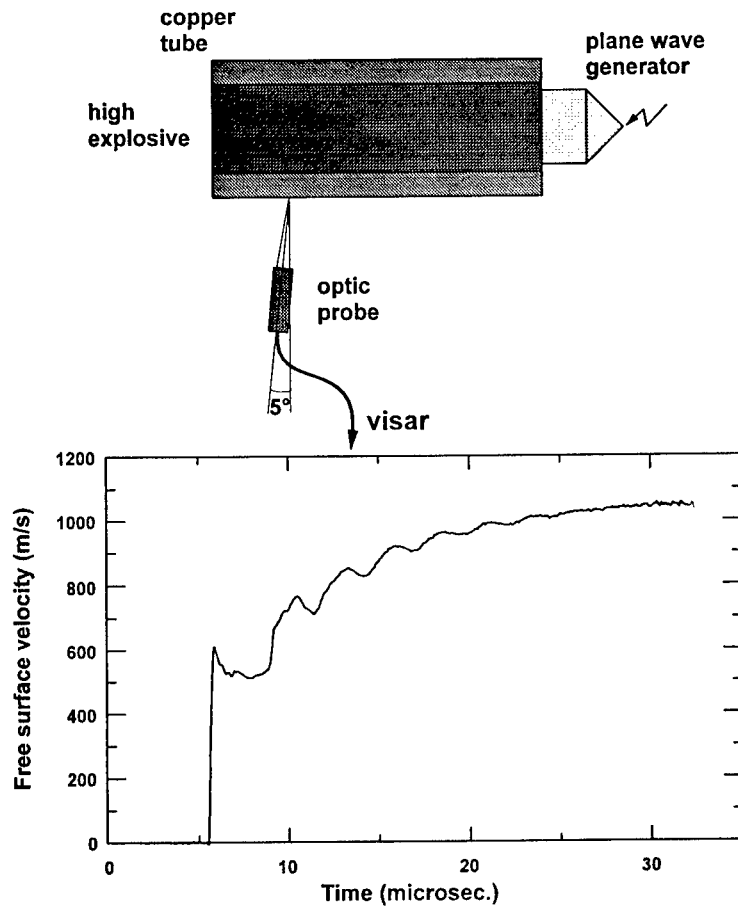


Figure 3 : Experimental configuration and free surface velocity profile for the test of expansion of a high explosive cylinder.

## 4- HYPERVELOCITY IMPACT

The fourth example of VISAR measurement concerns the high velocity impact of a steel ball against an aluminum target. The experimental configuration is shown in figure 4 a. A 5 mm diameter 304L steel ball impacts at a velocity of 5606 m/s a 30 mm thick Al6061T6 target. The measured free surface velocity of the aluminum target shows a compression wave composed of an elastic precursor and a plastic wave, then a release wave with a pullback signal (figure 4 c). This signal corresponds to the spalling of the target as it is observed on the recovered target (figure 4 b).

**Al6061T6 aluminum target (30 mm)**

**304L steel projectile ($\phi$ 5 mm)**

**5606 m/s**

**optic probe**

**visar**

*a) experimental configuration*

*b) recovered target*



*c) free surface velocity diagram*
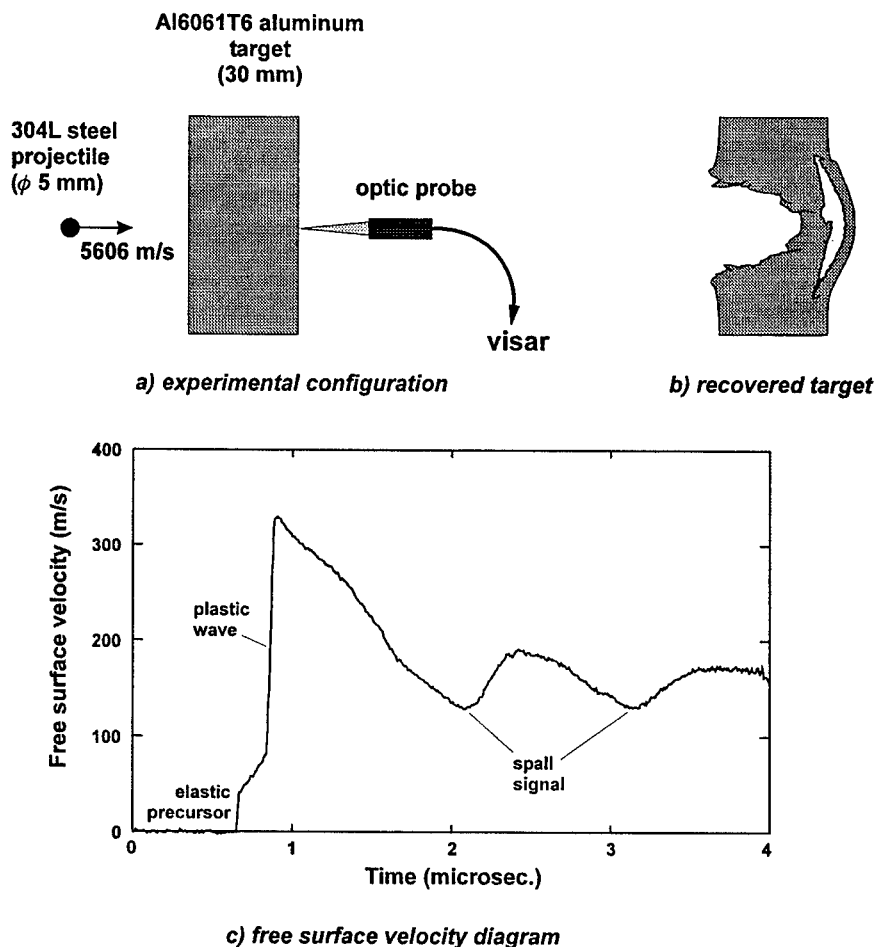
Figure 4 : Experimental configuration and free surface velocity profile for the hypervelocity impact test. The recovered target is shown on the top of the figure.

## 5. CONCLUSION

The potentiality of VISAR measurements has been shown through four examples in configurations of terminal ballistics. The informations delivered by VISAR interferometer are essential because of its 1 ns time resolution and its high accuracy. This interferometer is able to record motion of surface which deforms non uniformly and so, is an important tool in the understanding of materials dynamic behaviour in terminal ballistics.

*References :*
[1]  Barker L. M. and Hollenbach R. A., *J. Appl. Phys.*, 46, 11 (1972]
[2]  Barker L.M. and Barker V.J., *48th meeting of the Aeroballistic Range Association, Austin, Texas* (1997)
[3]  Héreil P.L. and Fanget A., *Journal de Physique IV, colloque C8, vol. 4* (1994)
[4]  Loupias C., Chartagnac P. and Jimenez B., *40th meeting of the Aeroballistic Range Association, Paris, France* (1989)
[5]  Bergues D., rapport technique CEG n° T97-048 (1997)
[6]  Loupias C., private communication

# BALLISTIC SHOCK TESTING

## LAFONT D. [1]

(1) ETBS Etablissement Technique de Bourges, Route de Guerry, BP 712, F-18015 Bourges, France

**Abstract :** This paper deals with measuring methods to evaluate ballistic shocks on armored vehicles from hostile attack. Ballistic shocks are challenging and difficult to make and interpret ; measurements from such events can produce confusing and inconsistent data because of resonant ringing of transducers, baseline shifts, and breakage of the highest range (2 Mm/s²) accelerometers that are commercially available. The Aberdeen Test Center (USA) has developed and validated a method which allows to compute a Shock Response Spectrum (SRS) from 10 Hz to 100 kHz. International tests have shown that this method was correct and that, on the contrary, the conventional European methods, based on commercial sensors or PVDF sensors, led to erroneous shock response spectra.

## 1. INTRODUCTION

Hostile attack on armored vehicles can come by any number of the following threats : mines, explosives, detonation of reactive armor, perforating projectiles, impact of non perforating projectiles on or near the vehicles. These shocks can cause malfunctions or permanent damage to mission-critical components (gun sights, electronics, etc.), even if the crew and a majority of a vehicle's systems are unharmed.

Components and sub-systems in combat vehicles can be protected from the effects of ballistic shock by taking precautions during the design stage or by making corrections after a ballistic shock weakness has been identified. In order to make informed decisions about shock vulnerability, ballistic shock must be characterized through testing that yield accurate measurements. These measurements must span the spectral range from 10 Hz to 100 kHz. Ballistic shock are challenging and difficult to make and interpret ; measurements from such events can produce confusing and inconsistent data because of resonant ringing of transducers, baseline shifts, and breakage of the highest range (2 Mm/s²) accelerometers that are commercially available.

The metrology experts of every national proving ground know the difficulty of taking shock measurements on the armor even in the far field. So they have tried to discover new methods in order to get a correct shock response spectrum : hard mount accelerometers, PVDF sensors, velocity gages, Hopkinson bar welded on the armor, vibrometers, fiber optics, "mechanical shock sensors", etc.

The experts of Aberdeen Test Center (USA) have finally standardized a method based on the use of three sensors at each measuring point. These three sensors are called "Loffi", "Bobkat" and ATC velocity gage, they allow to compute the shock response spectrum (SRS) respectively from 10 Hz to 800 Hz, from 200 Hz to 8 kHz and from 500 Hz to 100 kHz.

In spite of a few difficulties this method is now used at ETBS (France).

## 2. MEASURING PROBLEMS

### 2.1 Validation Tests

Transducer evaluation tests can be performed using a flat plate 0.5 m by 0.5 m by 0.04 m of rolled Homogeneous Armor (RHA) steel. The experimental transducers are mounted directly behind the impact point.

The shock impact can be produced either by firing small caliber projectiles on the center of the plate or by using explosives.
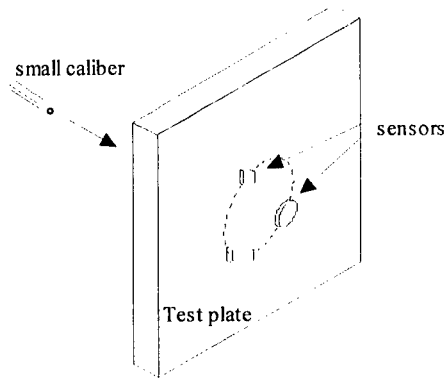


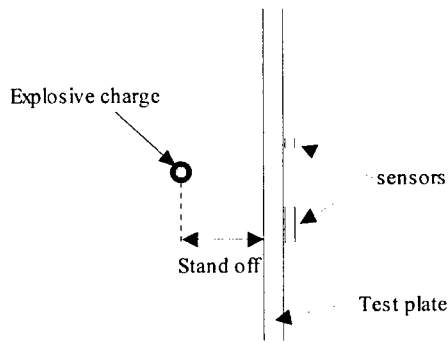Figure 1 : experimental set up used to evaluate transducer response to small caliber impact

Figure 2 : experimental set up used to evaluate transducer response to explosives

The plate is fixed to the frame by using C clamp and a laser vibrometer is used as a reference.
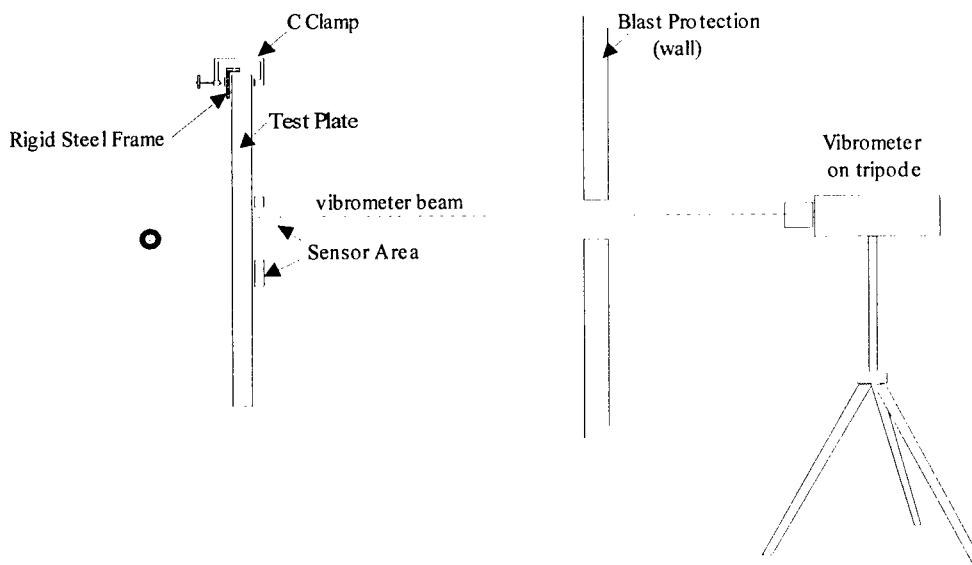


Figure 3 : experimental set up used to evaluate transducer response to explosives with a vibrometer as a reference

## 2.2 Results

The purpose of the test is to compare the shock response spectrum (SRS) for each sensor to be tested with the SRS obtained from the vibrometer signal. This comparison allows to validate (or not) the SRS ; the validation can be limited to a certain spectral range.

All the following results are transducer responses to 50 g explosive blast for a stand off of 9.5 cm.

### 2.2.1 Raw Waveforms

Before the computation of each SRS, the examination of the waveform can exhibit a transducer problem : ringing, baseline shifts, breakage... (Of course the origin of the problem can also be the setting of the acquisition system : clipping, noise, filtering or aliasing, etc.).

A few examples of problems detected on accelerometer waveforms are shown below.
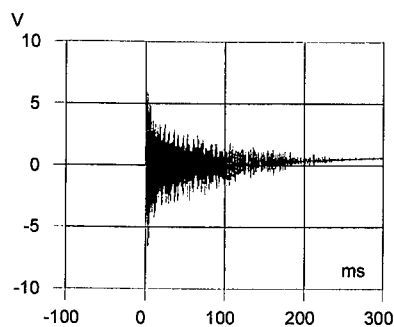


Figure 4 : Small Baseline Shift
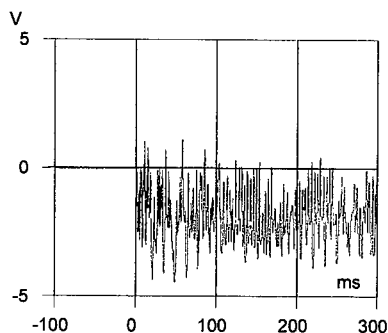


Figure 5 : Large Baseline Shift
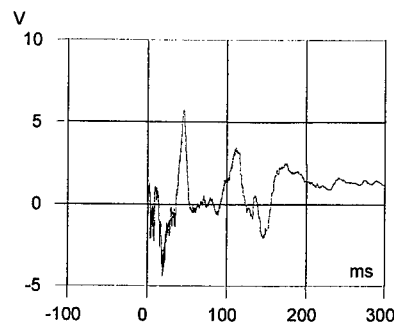


Figure 6 : Bad Looking waveform
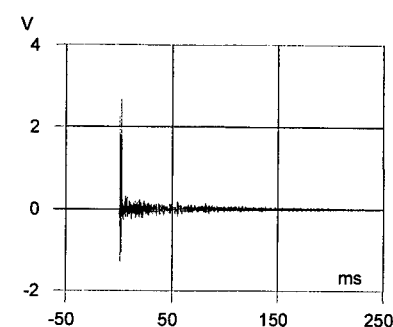


Figure 7 : Bad looking waveform
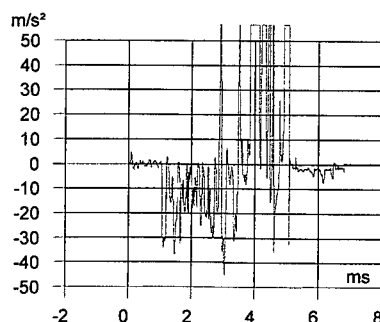


Figure 8 : Breakage of the sensor (Endevco 7270 AM4)

- 537 -

## 2.2.2 SRS Comparison

The following figures give examples of responses with different types of transducers (results from tests in Aberdeen on 23 October 1996 and in Bourges on 22 through 27 September 1995) :

A vibrometer was used as a reference in Aberdeen, it had the following response for one round of 50 g explosive with a 95 mm stand off :
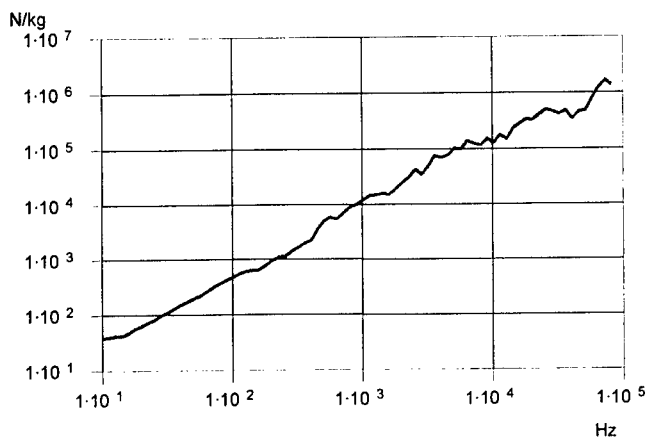


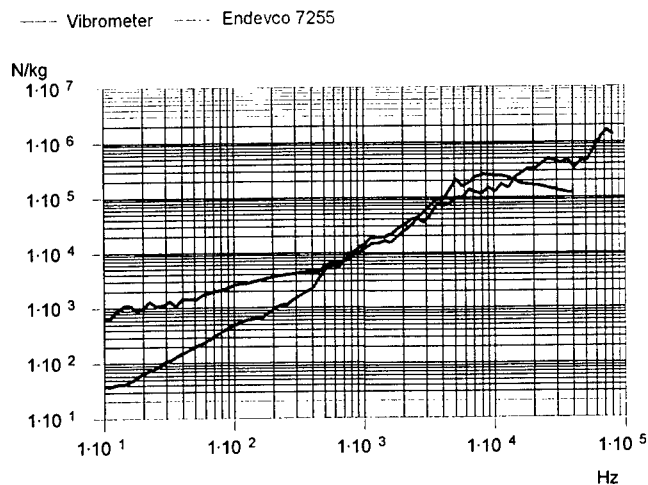Figure 9 : Vibrometer SRS (Maximum Acceleration Response, $\xi$ = 0.05)



Figure 10 : Endevco 7255

The SRS is non correct for low frequencies which is the general case with piezo-resistive and piezo-electric accelerometers. Nevertheless the response on this particular test will be considered correct from 500 Hz to about 8 kHz. The response above 8 kHz is the expected one since the sensor has an internal 10 kHz soft mount.

After more tests at this level and above, this type of transducer is not considered validated (risk of breakage, small range of frequency, not repetitive, difficulty to screw correctly the mechanical filter, etc.).

N/kg
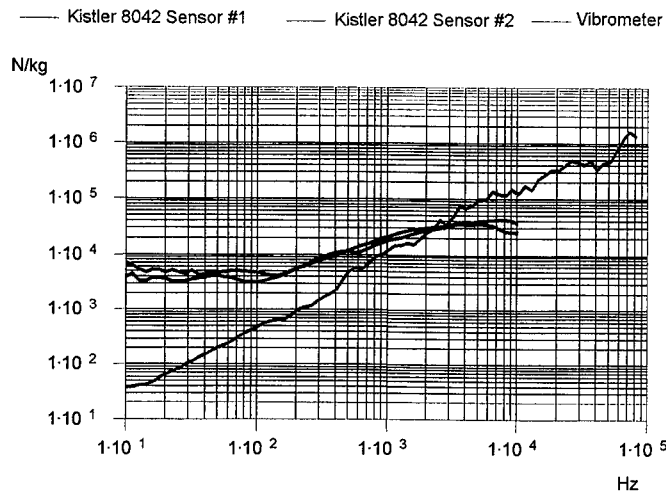


Figure 11 :  Kistler 8042 + B&K UA 0553

The SRS of both sensors Kistler 8042 mounted on mechanical filters Brüel & Kjaer UA 0553 are absolutely bad for the whole frequency range. This result was totally expected since neither the sensor nor its mounting were adapted to shock measurement. The purpose was to show how a bad response looks like.
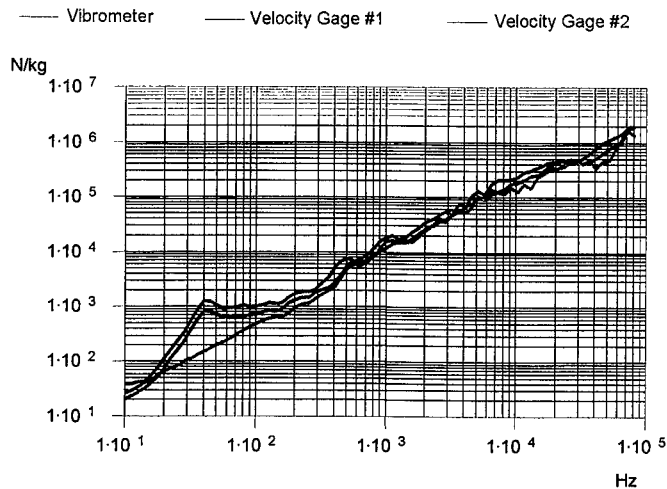
——— Vibrometer ——— Velocity Gage #1 ——— Velocity Gage #2

N/kg



Figure 12 :  CSTA Velocity Gages

The SRS of both velocity gages are correct except at low frequencies because of the resonance of the system spring-magnet (see paragraph 3). A little problem occurs in the frequency range 30 to 60 kHz especially with gage #1 but after more tests at this level and above, this type of transducer is considered validated up to 100 kHz. The lower limit depends on the type of spring which must be itself adapted to the level of the shock. To simplify, the lower limit is about 100 Hz for small caliber impacts and 500 Hz for large caliber impacts.
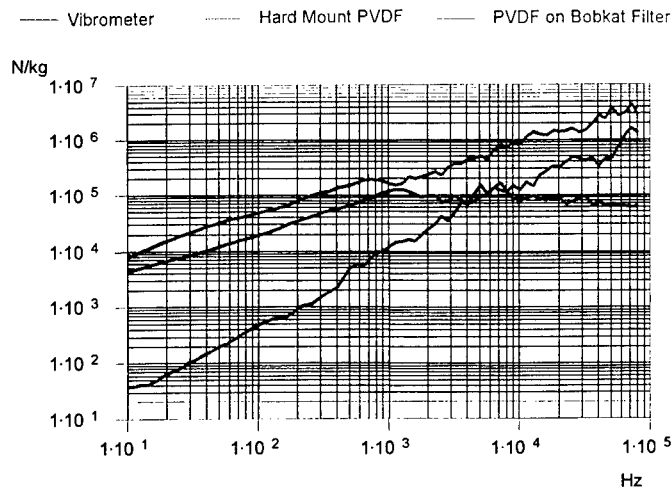
Figure 13 : Hard Mount and Soft Mount PVDF Sensors

The SRS of both PVDF sensors are very bad.

The right small range from 400 Hz to 800 Hz obtained with the Bobkat soft mount (see paragraph 3) confirms that a mechanical filter is required. It allows also to live in hopes of perfecting this technique in the future ; the challenge being to keep the so-called advantages (low cost, small size...) and to get this technique working.

For the international tests in Bourges no vibrometer was available, but the responses of different sensors can still be compared together. Two rounds were fired, the first with the three US sensors, the second with 2 types of piezo-resistive sensors usually used by ETBS at that time.
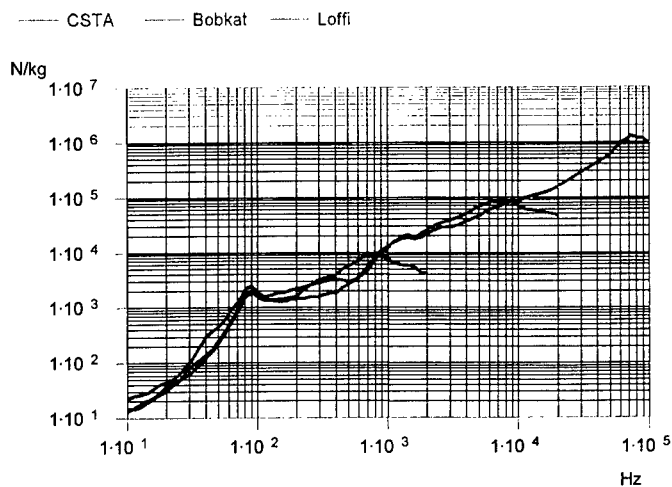


Figure 14 : First Round. Loffi, Bobkat and CSTA Velocity Gage

The resonance of the plate is more important than in Aberdeen, that may explain why the resonance of the system spring-magnet of the velocity gage is hidden. The cut off around 80 kHz seen on the CSTA velocity gage SRS comes from a limitation of the conditioning system and not from the sensor itself.

The response of the Bobkat seems correct below 100 Hz but this is not generally the case. We can observe significant discrepancies between the 3 waveforms from 200 to 800 Hz but after more tests at this level and above the Loffi is considered validated from 10 Hz to 800 Hz and the Bobkat from 200 Hz to 8 kHz.

Second Round :
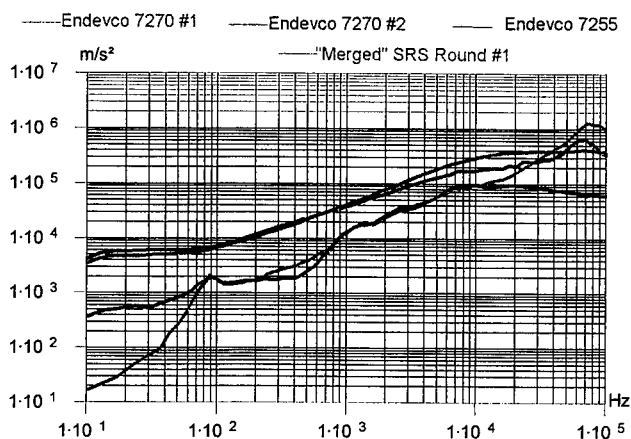


Figure 15 : Second Round. 7255 and 7270 AM4 Endevco Accelerometers.

The SRS are compared to the "merged" SRS obtained from round #1.

One of the two Endevco 7255 was destroyed. The response of the second is correct from 800 Hz to 10 kHz. The response of the other sensors (7270 Endevco AM4) are bad ; they are also very similar, reproducibility does not mean accuracy.

In the list of the sensors which are currently used, we must add the 7270 AM6 Endevco. This sensor is mounted on a mechanical filter supposed to cut around 10 kHz. As far as ballistic shocks are concerned this sensor is certainly the best commercial one at the moment.
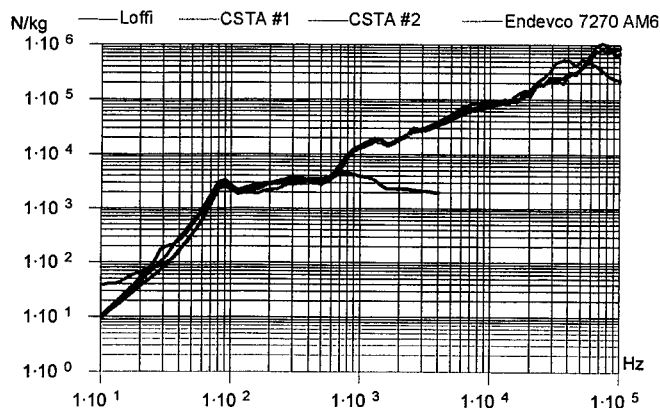


Figure 16 : Comparative Responses. 7270, Loffi, CSTA (2)

Example of response compared to Loffi, Bobkat and CSTA velocity gages during another test on a plate (Bourges, October 1998) :

The response of the 7270 AM6 is perfect from 35 Hz to 15 kHz, it even seems too perfect since the cut off mechanical frequency is supposed to be 10 kHz.

Yet the mounting of this type of screwed sensor is more fragile at higher levels than the welded Bobkat.

## 3. MEASURING METHOD

### 3.1 Transducers

Three sensors are welded at each measuring point. As far as SRS computation is concerned the frequency ranges covered by each of them are :

Loffi : 10 Hz to 800 Hz,
Bobkat : 500 Hz to 8 kHz,
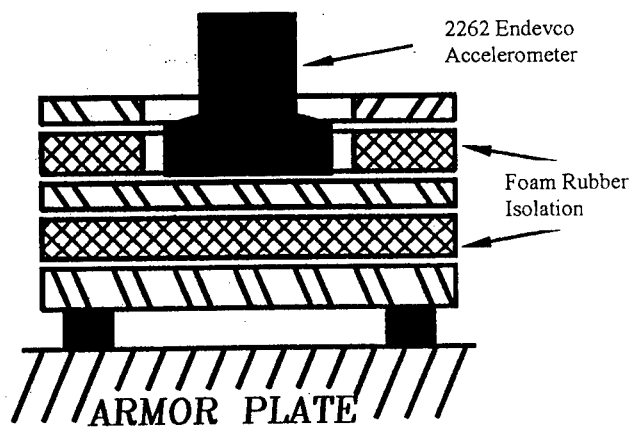CSTA velocity gage : 500 Hz to 100 kHz.

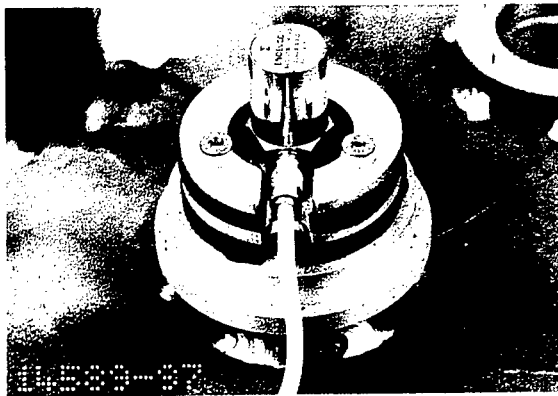Figure 17 : Loffi Accelerometer Mount

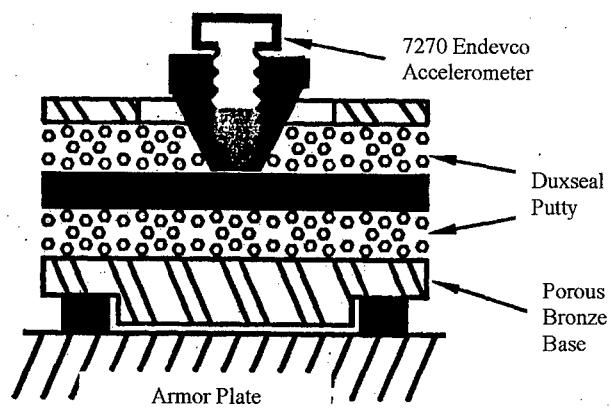Figure 18 : Loffi Welded on an Armor Plate

Figure 19 :  Bobkat Accelerometer Mount



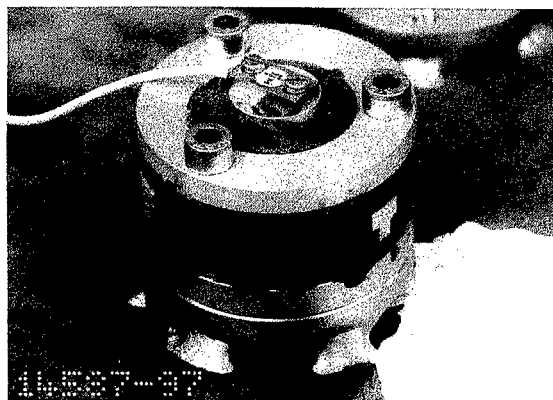Figure 20 :  Bobkat Welded on an Armor Plate



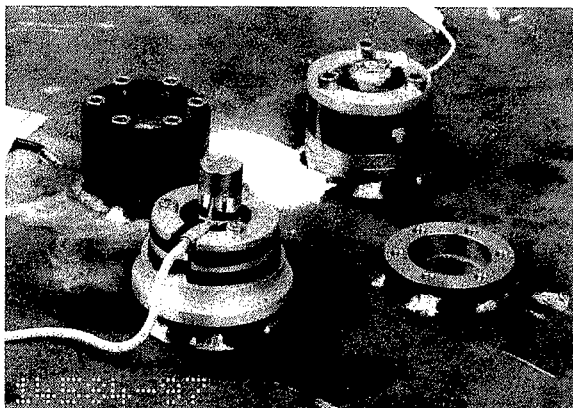Figure 21 :  One Complete Measuring Point

6 Stainless Steel
Cap Screws (10-32)

Neodymium
Magnet

Calibration
Stud

Phosphor Bronze
Spring

32 mm

13 mm

Plastic Spacer
Ring

Stainless
Steel Base

Fillet Weld
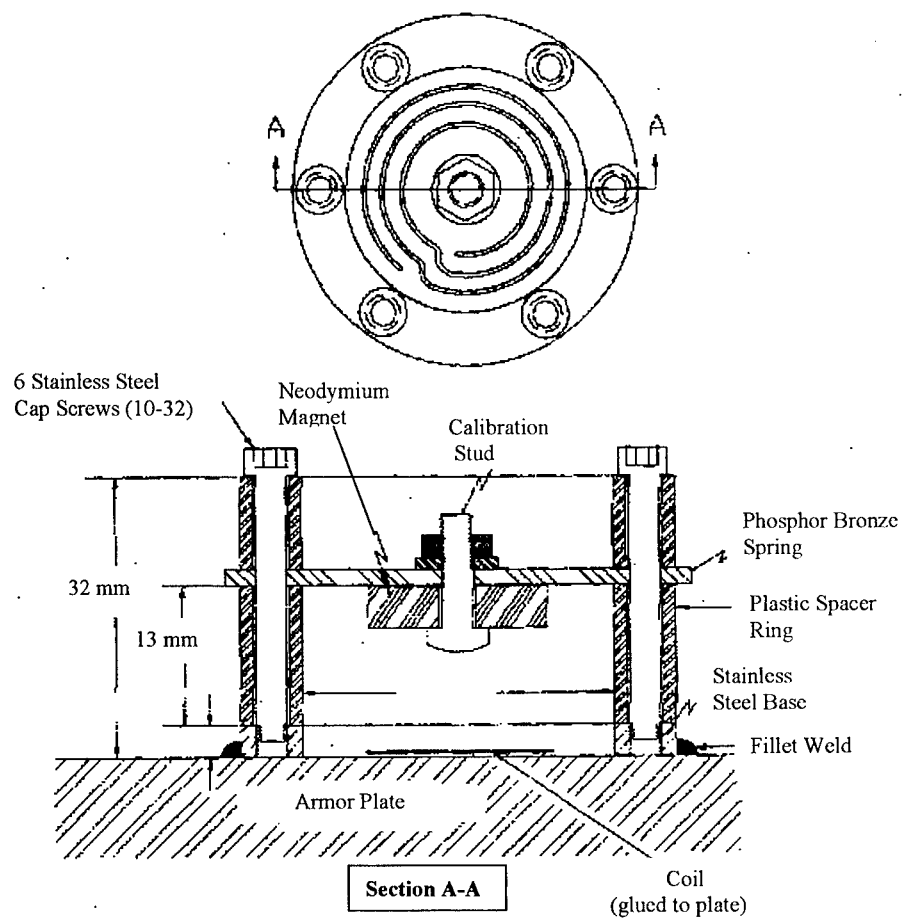
Armor Plate

Section A-A

Coil
(glued to plate)

Figure 22 : CSTA Velocity Gage Mount



Figure 23 :  CSTA Velocity Gage Welded on an Armor Plate

## 3.2. Calibration

The calibration of the 2 types of Endevco accelerometers (from Loffi and Bobkat) can be done using standard methods.

The CSTA needs to be calibrated on the field. A shock is generated by means of a "pinball calibrator", it is a pluger assembly that strikes a plastic accelerometer housing where a small accelerometer is incorporated. The accelerometer output is integrated to give a velocity record. The ratio of the voltage given by the velocity gage to that velocity record gives the sensitivity of the velocity gage. The linear range of the sensor is considered to be $\pm$ 3 dB. The sensitivity is about 10 or 20 V/(m/s).
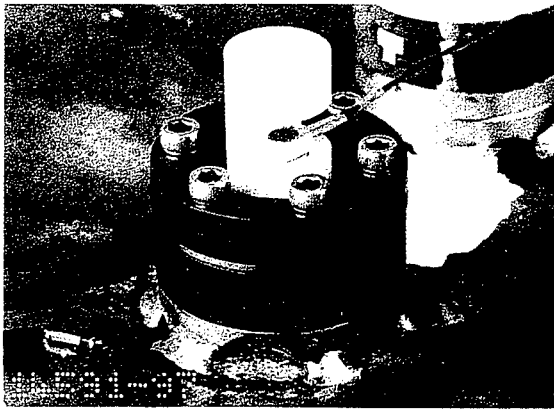


Figure 24 : 2250 Accelerometer in Plastic Housing for Calibration



Figure 25 : Pinball Calibrator

### 3.3 Final SRS result

A "merged" SRS is computed from the three responses. Two (or three) independent measurement must validate each other at medium frequencies and then give credibility to both measurements. The final response can be built taking for example the Loffi SRS from 10 Hz to 100 Hz, the CSTA velocity gage SRS from 6 kHz to 100 kHz and then the best way to build the medium part must be found by the operator "merging" the 3 SRS.
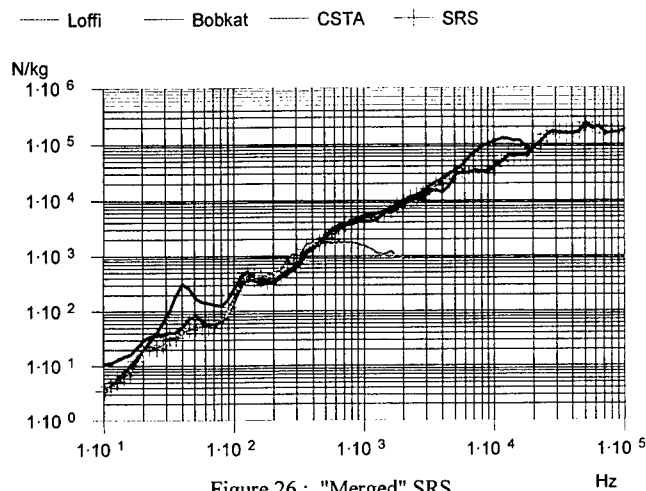


Figure 26 : "Merged" SRS

### 4. CONCLUSION

For many years many very expensive sensors have been broken during ballistic shocks (the price of Endevco sensors in France is about 2 or 3 times the price in US). For many years bad results have been produced, and sometimes no result at all. In spite of the remaining difficulties the measuring method, kindly proposed by US Army Aberdeen Test Center, allows now to be confident in the success of this kind of tests.

Improved ballistic shock instrumentation and measurement techniques are constantly being developed. The plate tests in front of projectile impact or explosives are cheap ways to try new techniques and to validate them using a non-contact sensor (laser vibrometer for example) ; they are also much more realistic and efficient than calibration tests on a Hopkinson bar.

We must also deal with other problems :
- Should we use anti-aliasing filters ? Which would change the transfer function which allows to compute each point of the SRS. So should we use filters ? We do it when we use soft mount transducers.
- Ballistic shock tests are really useful if the theory of SRS is known and if the different parameters are the same for everybody. Generally the damping factor is 0.05, but what about frequency range, resolution, maximum absolute or static equivalent acceleration, linear or logarithmic plot ?

We need also clear shock specifications, but that is an other story.

# Determination of the Angular Motion and of the Aerodynamic Coefficients from 3D Magnetic Sensor Signal.

FLECK V.

ISL, French-German Research Institute, BP 34, F-68301 Saint-Louis Cedex, France

**Abstract:** A projectile axis system consisting of three earth magnetic field sensors allows the measurement of an earth fixed reference direction. A specific data reduction code for this kind of measurements has been developed. The aerodynamic coefficients and the angular motion are directly estimated from the signals. Two applications are carried out: a shot with a 90 mm finned projectile over 1 km range and on a shot with a 155 mm rotating projectile over a range of 16 km. The results show that the angular motion derived from the recorded signals can be determined with an accuracy of 0.2°. Therefore the precision of the determination of the aerodynamic coefficients is as good, even better, as the one obtained in free flight range facilities.

## 1. INTRODUCTION

The usual method to determine the characteristic coefficients under flight conditions is the free flight range facility [1]. The projectile shadow is recorded during the flight on orthogonal photographs and the angular motion is determined from the pictures. A data reduction code is used for deriving the aerodynamic coefficients from the observed motion. The method is accurate but limited in range. For the study of the motion over longer range "yawsonde" tests are used. In this case the angular motion of the projectile is determined with respect to a fixed point, the sun position [2]. In this paper the proposed method is similar, but the reference direction is given by the earth magnetic field [3].

## 2. THE METHOD

The earth magnetic field vector $\mathbf{H} = H_i\,\mathbf{i} + H_j\,\mathbf{j} + H_k\,\mathbf{k}$ is recorded in the projectile as $\mathbf{H} = H_c\,\mathbf{c} + H_a\,\mathbf{a} + H_b\,\mathbf{b}$ by 3 orthogonal magnetic sensors. The following matrix gives the transformation of the reference direction as a function of the angles $(\theta,\eta)$ of the trajectory of the center of gravity and of the angles $(\delta,\psi,\varphi)$ of the angular motion around of the center of gravity [4].

|   | c | a | b |
|---|---|---|---|
| **i** | + cosδ cosη cosθ<br>− cosψ sinδ cosη sinθ<br>+ sinψ sinδ sinη | − cosφ sinδ cosη cosθ<br>− cosφ cosψ cosδ cosη sinθ<br>+ sinφ sinψ cosη sinθ<br>+ cosφ sinψ cosδ sinη<br>+ sinφ cosψ sinη | + sinφ sinδ cosη cosθ<br>+ sinφ cosψ cosδ cosη sinθ<br>+ cosφ sinψ cosη sinθ<br>− sinφ sinψ cosδ sinη<br>+ cosφ cosψ sinη |
| **j** | + cosδ sinθ<br>+ cosψ sinδ cosθ | − cosφ sinδ sinθ<br>+ cosφ cosψ cosδ cosθ<br>− sinφ sinψ cosθ | + sinφ sinδ sinθ<br>− sinφ cosψ cosδ cosθ<br>− cosφ sinψ cosθ |
| **k** | − cosδ sinη cosθ<br>+ cosψ sinδ sinη sinθ<br>+ sinψ sinδ cosη | + cosφ sinδ sinη cosθ<br>+ cosφ cosψ cosδ sinη sinθ<br>− sinφ sinψ sinη sinθ<br>+ cosφ sinψ cosδ cosη<br>+ sinφ cosψ cosη | − sinφ sinδ sinη cosθ<br>− sinφ cosψ cosδ sinη sinθ<br>− cosφ sinψ sinη sinθ<br>− sinφ sinψ cosδ cosη<br>+ cosφ cosψ cosη |

Table 1: Transformation matrix from earth fixed system to projectile axis system

Note that all the angles have an influence on the radial **a** and **b** axis signals. The rotation ($\varphi$) has no effect on the axial **c**-axis signal. If the trajectory of the center of gravity is known (angles $\theta,\eta$) it is theoretically possible to solve the 3 equations given by the 3 signals in **c,a,b**, directions and so to determine the 3 angles ($\delta,\psi,\varphi$).
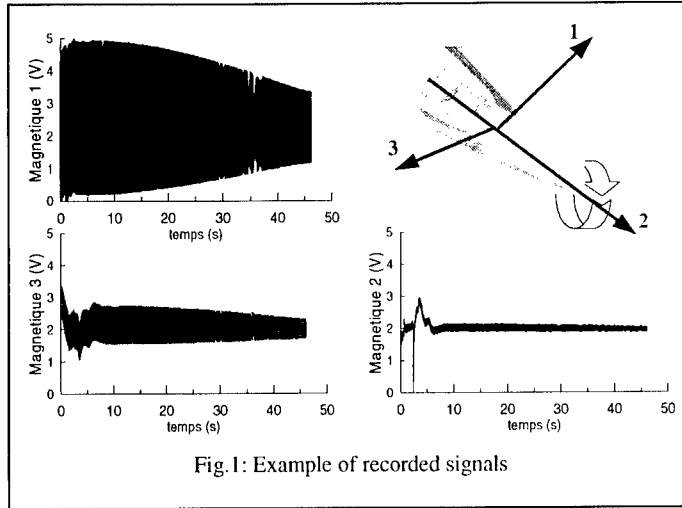


Fig.1: Example of recorded signals

But the analysis of recorded signals (Fig. 1) shows that each sensor has a different sensitivity and the orientation of the measure is not corresponding to the theoretical value. For instance the 2 radial channels (1 and 3) should have the same magnitude and no rotation should appear on the axial channel (2). For these reasons it is necessary to preprocess the data. In this case it is easier, in order to use directly the recorded data, to carry out a classical data reduction by a simulation method. This method is described in Table 2.
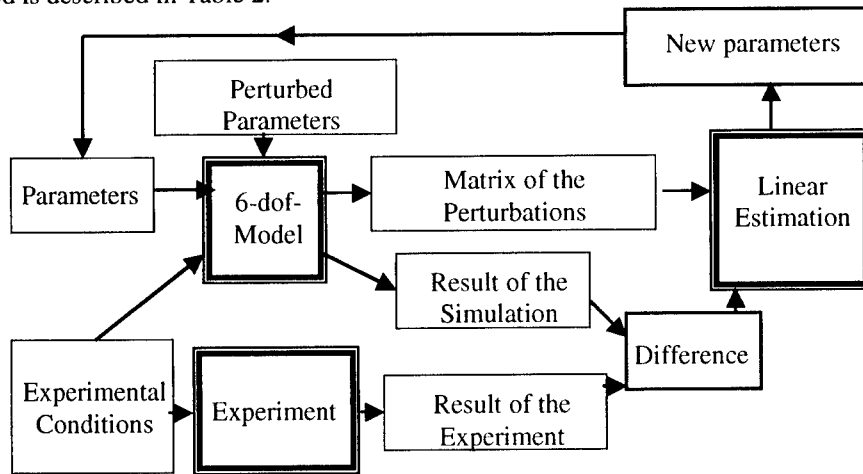


Table 2: Iterative model based-method for parameter estimation

A 6-dof model is used for the simulation of the recorded data. The comparison with the measure and the determination with the same model of the influence of each parameter on the results allows a correction of the parameters. The estimation of the corrections is achieved by a maximum likelihood method. The process is repeated until convergence. The problem linked to this method is the convergence to a relative minimum of the difference between simulation and measure. In order to eliminate false solutions, because the problem has no one-to-one solution, it is necessary to control the results by using different sets of initial parameters.

## 3. THE RESULTS

The capabilities of use of this method are tested on two types of projectile:
- a 90 mm slow rotating finned projectile over a range of 1 km,
- a 155 mm gyroscopic stabilized projectile over a range of 16 km.

In the two cases the same strategy is used for the determination of the motion and of the aerodynamic coefficients.

At first, by using the radar and the meteorological data the model describing the trajectory of the center of gravity is determined. This is a classical step in exterior ballistic, but in this case a high accuracy is required in order to determine accurately the elevation angle $\theta$ and the side angle $\eta$. In a second step the roll motion is determined and the difference between simulation and the measured data is computed. The difference signal is analyzed, and if periodic signals appear on these difference signals a pitching and yawing motion is estimated in order to minimize the difference signals. Note that in this last process a new evaluation of the rotation is performed simultaneously.
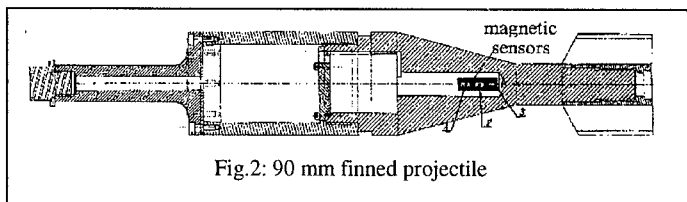
### 3.1    90 mm finned projectile



Fig.2: 90 mm finned projectile

Fig.2 shows a sketch of the projectile. The sensors are placed in the rear part made of Dural.

The trajectory of the projectile is flat and easy to fit over 1000 m. The drag coefficient is determined for 3 values of the Mach number (1.8, 2.2, 2.6) in order to cover the whole range of velocity. Under these conditions the accuracy of the simulated trajectory is satisfactory in time and space.

The analysis of the measured and simulated signals shows that the radial channel contains, as expected, the information of the rotation (fig. 3). In order to have a better view, only the signal over the last part of the trajectory is represented. The simulation fits the measure very well. The
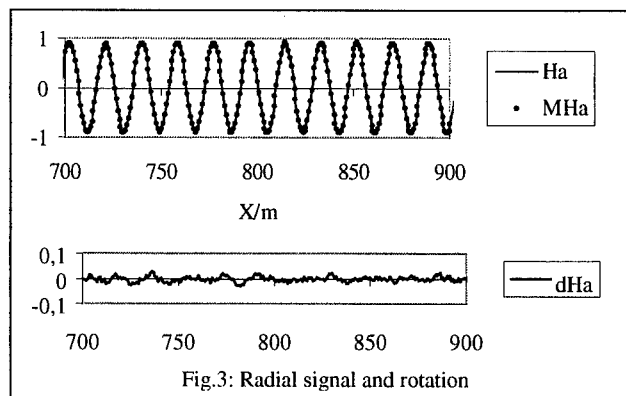


Fig.3: Radial signal and rotation

difference between measure and simulation is represented in an amplified form in the second diagram of the fig. 3. After the elimination of the rotation on the axial channel, fig. 4 shows that the measure is precise enough for the determination of the pitching and yawing motion



Fig.4: Axial signal and pitching, yawing motion

from this signal. dHc_rot is the difference between simulation and measure after the elimination of the rotation, and dHc is the difference after inducing the estimated
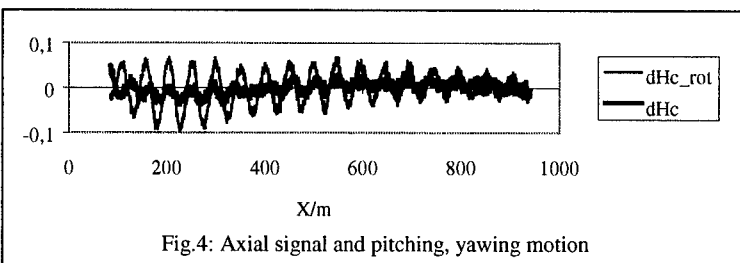
pitching and yawing motion. Note that all three angles, rotation, pitching, yawing are estimated with a mean standard deviation of 0.2° over all the trajectory.

The iterative adaptation process of the simulation to the measure allows the determination of the aerodynamic coefficients that must be changed in order to have a good fit. Only the derivative of the pitching moment (Cmα) and of roll moment (Clp) can be estimated. The pitch damping moment (Cmq) and the Magnus moment (Cnpα) have a too small influence on the signal (or the measure is not accurate enough) in order to be correctly estimated. The results are shown in table 3. For this case 1000 points of measure are used for each channel.

|  | Mach Number | Value | Standard Deviation |
|---|---|---|---|
| Rotation Clp | 1.8 | -0.08251 | 0.00008 |
|  | 2.2 | -0.06160 | 0.00003 |
|  | 2.6 | -0.06120 | 0.00002 |
| Pitching Cmα | 1.8 | -3.33 | 0.03 |
|  | 2.2 | -4.02 | 0.01 |
|  | 2.6 | -4.02 | 0.01 |

Table 3: Estimated aerodynamic coefficients for the 90 mm projectile

## 3.2    155 mm gyroscopic projectile

As shown in fig. 1 the sensors are placed in the nose of the projectile.



Fig.5: Radar data of the trajectory
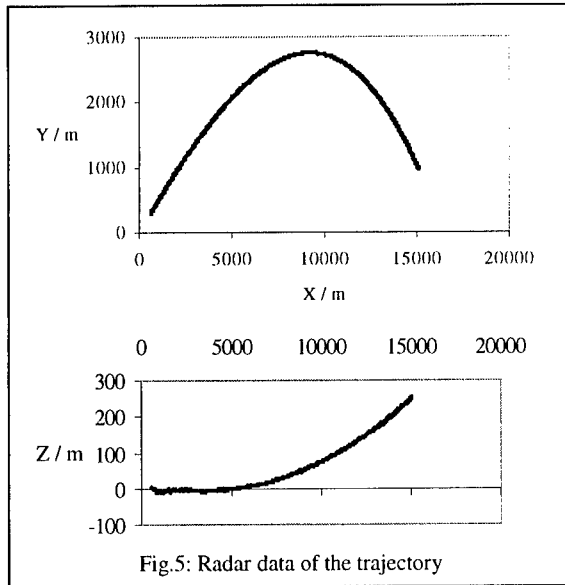
In a first step it is necessary to fit with the model the radar data of the trajectory. The meteorological data must be taken into account. Note that the wind is varying in space and time specially in the low altitudes less then 1000 m. Therefore the fit is stopped at 16 km in order to have a good matching of the 3 space coordinates over the time with a mean standard deviation of 2 m. This quality of fit is obtained by using a description of the drag coefficient Cx for 6 Mach numbers. A linear interpolation is assumed between the different values. The model used for the fit is a 6 dof model computing the angular motion in body fixed coordinates. This is necessary for the further fit of the magnetic signals. The results are shown in table 4.

|  | Mach Number | Value | Standard Deviation |
|---|---|---|---|
| Drag Cx | 0.90 | 0.141 | 0.001 |
|  | 0.975 | 0.183 | 0.001 |
|  | 1.05 | 0.377 | 0.003 |
|  | 1.25 | 0.278 | 0.002 |
|  | 1.60 | 0.283 | 0.003 |
|  | 2.00 | 0.240 | 0.009 |

Table 4: Estimated drag coefficient for the 155 mm projectile

The results are obtained by using approximately 800 points of radar measure.

For the fit of the magnetic signals the developed code doesn't allow the simultaneous processing of all the 32000 points of measure for each channel. For this reason only small parts of the trajectory are fitted.

For the first part of the trajectory, fig. 6 shows for the axial (c) and for a radial channel (b) the differences between the measure and the simulation. dHc_rot and dHb_rot are the differences if the projectile is only rotating and dHc and dHb is the final result; the projectile is rotating, pitching and yawing. Note that the precision is better than before. A small pitching and yawing motion can be observed on the axial channel, but more
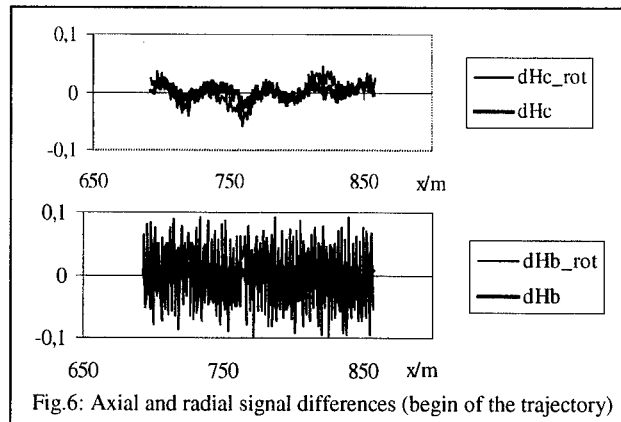


Fig.6: Axial and radial signal differences (begin of the trajectory)

information on this motion can be extracted from the radial signal. Naturally, as shown later, the radial signal gives a good measure of the rotation. The corresponding motion of the angle of attack is shown in fig. 7. The precision of the determination of the angle of attack is 0.2°.
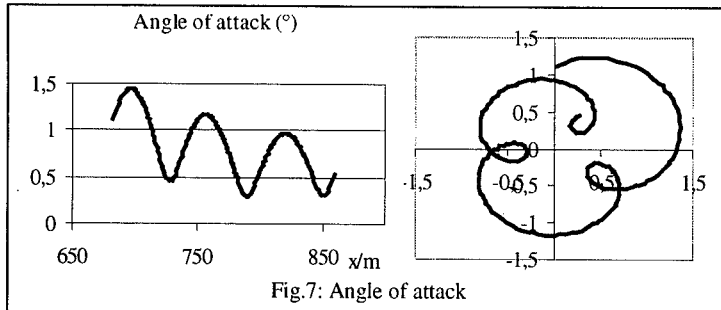


Fig.7: Angle of attack

The matching of the magnetic signals are based on the aerodynamic coefficients given in table 5. In this case an evaluation of the derivative of the Magnus moment coefficient is possible if the value of the pitching damping moment is assumed known. If both coefficients are estimated no one-to-one solution is possible.

|  | Mach Number | Value | Standard Deviation |
|---|---|---|---|
| Rotation Clp | 1.6 | -0.00892 | 0.00003 |
|  | 2.0 | -0.00829 | 0.00001 |
| Pitching Cmα | 1.6 | 4.64 | 0.003 |
|  | 2.0 | 4.38 | 0.008 |
| Magnus Cnpα | 1.6 | 0.8 | 0.1 |
|  | 2.0 | 0.9 | 0.1 |

Table 5: Estimated aerodynamic coefficient for the 155 mm projectile

The results are obtained by using approximately 300 points of magnetic measure for each channel.

For the end part of the trajectory an other data reduction of the magnetic signals is carried out. It is only necessary to induce the right rolling motion in order to match the recorded data. As shown in fig. 8 the difference between simulation and measurement is very small. For instance for the radial b channel the difference is in the magnitude of the 8 bit resolution of

the recording system. In this case the measure of the roll position is very accurate (0.1°). Fig. 9 shows a part of the fitting. There are only 5 measurements for each period of rotation.



Fig.8: Axial and radial signal differences (end of the trajectory)



Fig.9: Radial signal and rotation
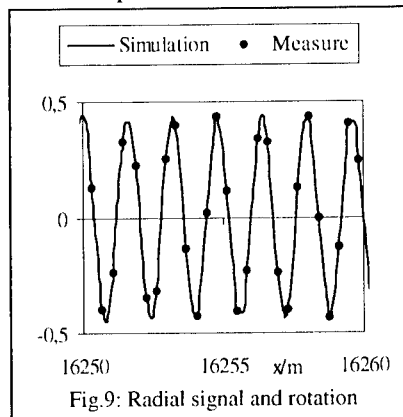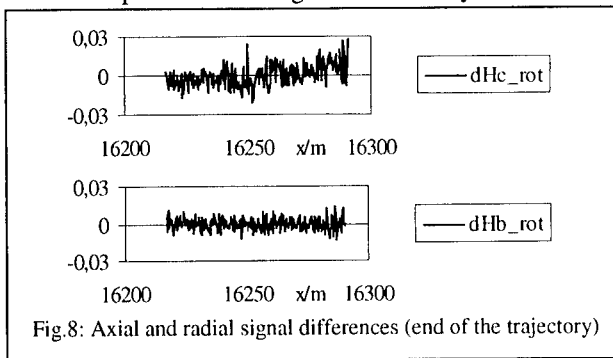
The last point of interest is the determination of the yaw of repose. Due to the unknown sensitivity of the magnetic sensors under flight conditions, it is necessary to have an information on the yawing motion an at least one radial channel in order to correct the amplitude of the axial channel. On a short flight path the orientation of the yaw of repose remains almost constant and the magnitude varies slowly. Therefore it is necessary for the determination of the yaw of repose to analyze a great part of the trajectory (4-5 km). In the actual state of development of the data reduction code it is not possible to solve such a problem. An analysis of a short part of the trajectory in this domain of maximum of curvature only shows that a nutation motion with an amplitude less than 0.2° occurs. So it is obvious, if an instability occurs, the variations of the angle are larger and faster and a detection is already possible on a short flight path.

## 4. CONCLUSION

The data reduction of signals, recorded during the flight, of earth magnetic sensors shows that is possible to extract from the measurements the angular motion and the aerodynamic coefficients of the projectile. The described method may be in the future an new way for the study of the projectile behavior. Combined with radar data for the determination of the trajectory of the center of gravity, this kind of sensor may be a useful tool for the definition of the model needed for the computing of firing tables.

## 5. REFERENCES

[1] Winchenbach G.L., "Aerodynamic Testing in a Free Flight Spark Range", *WL-TR-1997-7006, Wright Laboratory, Armament Directorate, Eglin AFB, FL, March 97*
[2] Haden H.G., "Yaw Measurement Analysis", *RARDE Memorandum 54/64, Fort Halstead, Kent, December 64*
[3] Rateau Ph., Wernert Ph., Junod E., "Détermination de la position en roulis d'un projectile en tir tendu ou courbe, *ISL Report /00, Saint-Louis, France*
[4] Fleck V., "Introduction au mouvement à 6 degrés de liberté", *SAE, Stage D10, Paris, 99*

# KINETIC STUDIES IN THE FLAME OF GUN PROPELLANT COMPOSITIONS

## C. BONNET, C. REYNAUD, D. ROLLER

*SNPE*

Interior Ballistics Laboratory

Centre de Recherches du Bouchet - 91710 VERT LE PETIT – France

**Abstract :** Rotationally resolved emission and absorption spectroscopy in the $A^2\Sigma$ - $X^2\Pi$ (0-0) band system of OH around 309 nm has been performed to determine respectively the OH temperature and concentration in solid propellant flames, in order to modelise thermochemical calculations. This technique has been applied to SNPE propellants burning under atmospheric pressure. The detector was a spectrometer equipped with an intensified photodiode array. In the case of absorption spectroscopy, the light source was an arc lamp. Experimental OH spectra have been compared to synthetic spectra and have been least squares fitted. The OH temperature and concentration values are consistent with thermochemical equilibrium values.

## 1. INTRODUCTION

The detailed chemical steps involved in solid propellant combustion are not well understood. In order to develop a detailed chemistry model, it is necessary to study the gas-phase region close to the burning surface (the reaction zone). In this reaction zone chemically active transient species are created and will provide information about the detailed chemical pathways from reactants to final products. That is why it is important to determine in this zone which are the combustion diatomic radicals created and to find out their temperature and concentration in terms of their height in the flame.

Both emission and absorption spectroscopy are non intrusive probing techniques that can be used to identify and profile intermediate combustion products.

In this article, we will present the results of the temperature and concentration profiles of the OH radical, as well as the experimental and data analysis procedures.

## 2. EXPERIMENTAL

The propellant is incorporated in the center of an open combustion chamber. This setup is equipped with a servomechanism that raises the propellant as it burns. The quantitative study of solid propellant flame chemistry requires that spatially and temporally resolved species temperature and concentration measurements be made at known positions above the solid

propellant surface. This implies that the propellant burn rate must be well known in order to locate the measured point in the flame.

For emission spectroscopy, the radiant emission from the open combustion chamber is collected, collimated and focused on the entrance slit of a spectrometer by a lens. A 0,5 mm pinhole defines the spatial resolution. A Chromex 500IS grating spectrometer (0,5 m of focal length) disperses and projects the flame image into an intensified Princeton silicon photodiode array detector (1024 pixels), controlled by a Princeton ST121 detector controller and data acquisition system.

The detector controller allows data collection in several modes. A variable number of scans of the detector can be recorded, with the amount of signal integration time also a variable. The spectrometer is used to collect data over a fixed spectra region (which depends on the species studied: OH, CN, CH...), with the spectra range and resolution determined by the selection of a grating. We have the choice between three gratings: 150 grooves/mm, 2 400 grooves/mm and 3 600 grooves/mm which permit us to study different wavelength.

For absorption spectroscopy, a high intensity mercury-xenon arc lamp light is incorporated to the previous arrangement. This light delivers 1 kW and it is focused on the upper surface of the propellant thanks to a lens.

In order to increase absorption artificially, the setup is equipped with a multi-crossing cell which by a play of mirror obliges the beam of the xenon lamp to cross six times the flame before being analysed by the spectrograph.

The beginning of the data acquisition is given by a He-Ne laser beam which strikes a photodiode when the surface of the propellant burns. When illuminated, the photodiode triggers the data acquisition system.

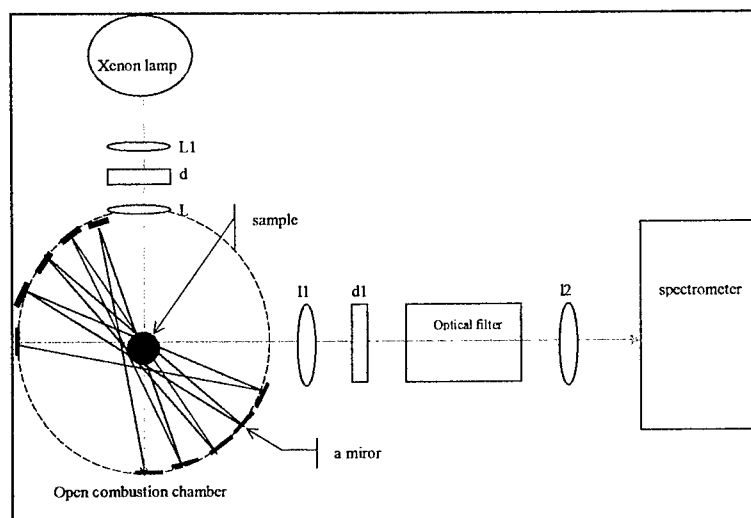A schematic of the setup and optical system is shown in Figure 1.



Figure 1 : Top view of open combustion chamber and associated optics
for absorption experiments.

## 3. THEORETICAL APPROACH

During the combustion of a propellant, the temperature of the produced molecules is high enough to make them emit a spectra and luminous signal. The spectroscopic analysis of the propellant flame is powerful means of determining which chemical radicals are present in that flame. The knowledge of the energy levels involved in the chemical reactions enables to find out the temperature of these radicals. Indeed, when local thermodynamical equilibrium is reached, energy levels are linked by the temperature function Boltzmann law:

$$\frac{N_m}{N_n} = \frac{g_m}{g_n} \times \exp\left(-\frac{h\nu_{nm}}{kT}\right) \tag{1}$$

where T is the temperature,

$N_m$ and $N_n$ are the populations of the energy levels $E_m$ and $E_n$, $g_n$ and $g_m$ their statistical weights,

and $h\nu_{nm} = E_m - E_n$ is the radiative energy of the transition.

Each radical emits a radiation when it goes from a rovibrational excited level to an inferior electronic transition. Each of the energy levels depends on the electronic (n), vibrational (v), rotational (K) and under-rotational (J) states of the molecule.

When the emitting system (flame) is optically thin, the intensity of an emission line resulting from a particular transition is given by :

$$I_{n',v',K',J'}^{n'',v'',K'',J''} = \frac{A_{n',v',K',J'}^{n'',v'',K'',J''} \, hc\sigma_{n',v',K',J'}^{n'',v'',K'',J''}}{4\pi} N_{n',v',K',J'} l \tag{2}$$

where $A_{n',v',K',J'}^{n'',v'',K'',j''}$ is the transition probability,

$hc\sigma_{n',v',K',J'}^{n'',v'',K'',J''}$ is the radiative energy,

$N_{n',v',K',J'}$ is the superior level population,

$l$ is the flame thickness.

The Einstein coefficient $A_{n',v',K',J'}^{n'',v'',K'',J''}$ can be written as below :

$$A_{n',v',K',J'}^{n'',v'',K'',J''} = A_{n',v'}^{n'',v''} \frac{HL_{K',J'}^{K'',J''}}{2J'+1} \tag{3}$$

where $HL_{K',J'}^{K'',J''}$ is the Holn-London coefficient.

The vibrational transition probability can be written as below :

$$A_{n',v'}^{n'',v''} = \frac{64\pi^4}{3h} p_{n',v'}^{n'',v''} \left[ \sigma_{n',v',K',J'}^{n'',v'',K'',J''} \right]^3 \tag{4}$$

The mathematical expression giving the emission intensity of a transition is:

$$I_{n',v',K',J'}^{n'',v'',K'',J''} = C(n') A_{n',v',K',J'}^{n'',v'',K'',J''} \sigma_{n',v',K',J'}^{n'',v'',K'',J''} e^{-\frac{hc}{k}\left\{ \frac{F_{v'}(K')}{T_{rot}} + \frac{G(v')}{T_{vib}} \right\}} \tag{5}$$

where $F_{v'}(K')$ and $G(v')$ are the energy level rotational and vibrational contributions.

Identically, we can introduce the optical thickness l in the middle of the ($k_0$) line :

$$k_0 l = \left[ \frac{m}{2\pi k T_{cin}} \right]^{1/2} \frac{2J'+1}{8\pi \left[ \sigma_{n'',v'',K'',J''}^{n',v',K',J'} \right]^3} \frac{A_{n'',v'',K'',J''}^{n',v',K',J'}}{Z_{rot} Z_{vib}} e^{-\frac{hc}{k}\left\{ \frac{F_{v''}(K'')}{T_{rot}} + \frac{G(v'')}{T_{vib}} \right\}} N_{n''} l \tag{6}$$

where $Z_{rot}$ and $Z_{vib}$ are the partition functions.

The spectral transmission of the l width system is then :

$$\tau_v = e^{-k_v l} \tag{7}$$

The entire spectra response of a radical is obtained by sorting out the wavelength and the emission intensity (or the absorption intensity) of each feasible transition and by convoluting this spectrum with a line profile depending on temperature, pressure and on the apparatus resolution.

## 4. DATA ANALYSIS

The previous equations are the bases of molecular spectroscopy [1]. They were computed in a software thus enabling us to sort out synthetic spectra. Rotational and vibrational temperatures as well as the species concentration and the spectral resolution are used as parameters.

In the aim of finding out the temperature profile in the flame, a series of emission spectra is recorded at regular time period. These raw spectra are processed in order to take into account the optical attenuation of the system, the spectral response of the photodiode array and the line basis correction. Each processed spectrum is then compared to a synthetic one: for each experimental spectrum, the best parameters set (rotational and vibrational temperatures) is determined by iteration and by minimising the mean quadratic difference between the experimental spectrum and the synthetic one computed with the above parameters.

Each of the successive spectra matches a spatial region in the flame which depends on the dimension of the pinhole set between the spectrometer and the open combustion chamber. The position of the radical in the flame is known thanks to the burn rate of the propellant and the recorded time of the spectrum.

A OH (or CN, CH...) rotational temperatures profile can be drawn, giving the radical temperature as a function of its height in the flame.

The concentration of a species in a flame is estimated by the absorption it creates when crossed by the light of a continuum spectrum arc lamp. This method presents two main advantages:

⇨ it is independent of the detector spectral response and the system optical acceptance cone, since both of these factors are eliminated when the transmitted spectrum is divided by the direct one.

⇨ the absorption mechanism implies the molecules are coming from the fundamental level, the most crowded one at usual flame temperatures.

The concentration profile of a radical is found out as previously described, that is to say by searching the best parameters set (rotational temperature, vibrational temperature and concentration), or by using the temperatures measured thanks to emission spectroscopy and proceeding to an iterative calculation only on the concentration parameter.

## 5. TYPICAL RESULTS

The Figure 2 shows different species (OH, CH, NH and CN) of double base propellant. The spectrum is obtained with 150 grooves/mm grating and a pinhole giving 0,5 mm spatial resolution.
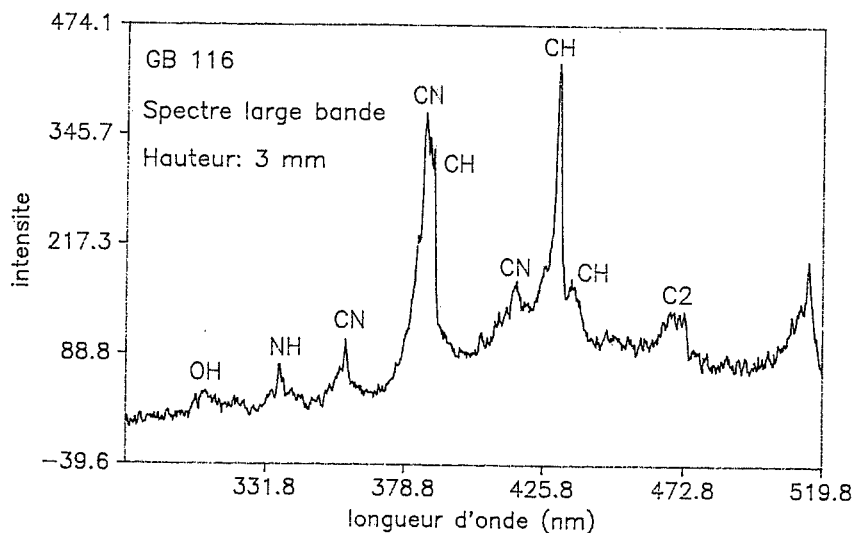


Figure 2 : Main radical species of double base propellant (at 3 mm in the flame).

The Figure 3 shows profiles of OH concentration for three different propellants: double base, multi base and LOVA propellants. The concentration level depends of: height in the flame and propellant composition.
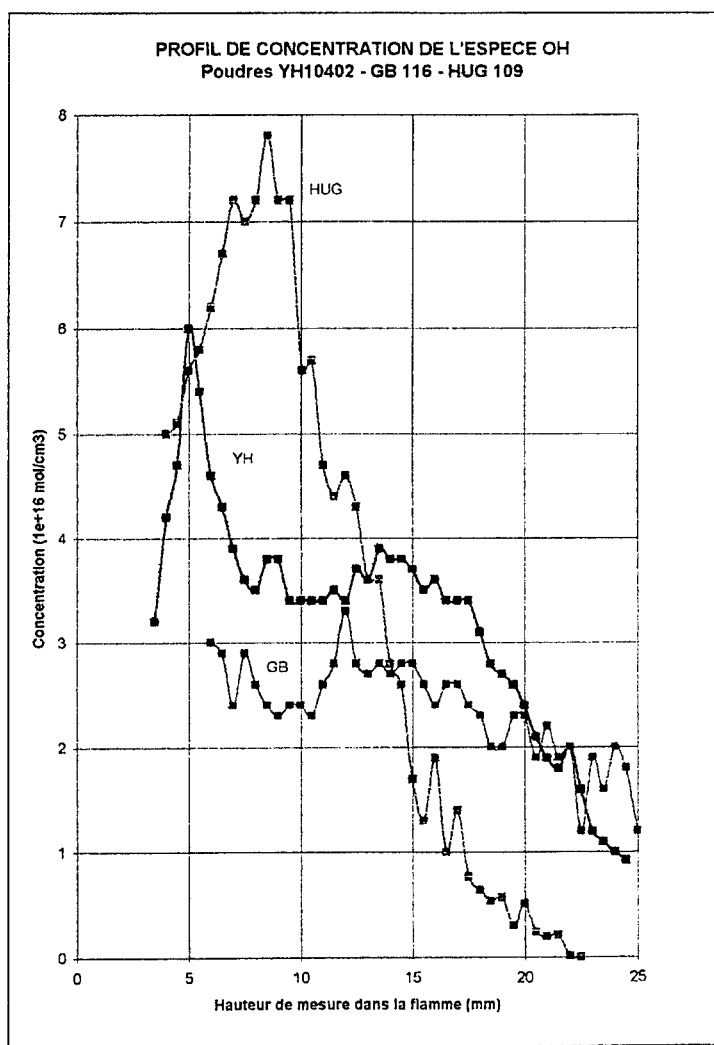


Figure 3 : OH concentration profiles of different propellants.

All the OH spectra, whether emission or absorption, are obtained with a 3 600 grooves/mm grating and a pinhole giving a 0,5 mm spatial resolution. The search of temperature and concentration is computed from the combustion of 15 propellant strands.

In order to know the species which appear during the ignition phase, two compositions of propellant are studied: double base propellant and double base propellant + igniter powder. Examples of emission and absorption OH spectra are given on Figures 4 and 5. These two figures show a good matching between experimental and synthetic spectra.
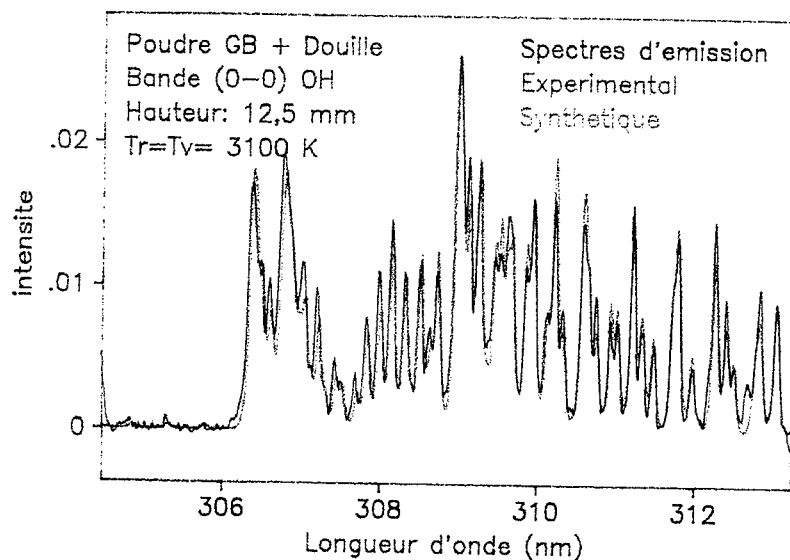
Figure 4 : Emission OH spectra at 12,5 mm in the flame (double base propellant + igniter powder).
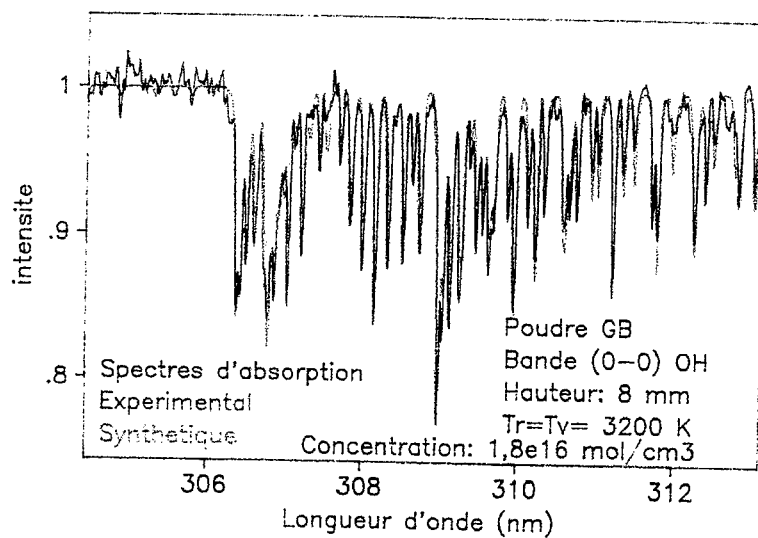


Figure 5 : Absorption OH spectra at 8 mm in the flame (double base propellant).

Those emission spectra are normalised in relation to the most intensive line at 309 nm (for OH). This implies that the rotational temperature is found out thanks to the relative intensity of the different lines.

The measured flame temperature of the double base propellant increases from 3 000 K up to 3 300 K between 0,5 mm and 5 mm above the solid surface of the propellant. This temperature stays steady up to 25 mm in the flame.

The average temperature of the double base propellant + igniter powder propellant is less about 200 K. The combustion of the double base propellant + igniter powder is not complete, so the temperatures and the concentrations are measured between 0 mm and 15 mm starting from the surface of the combustion.

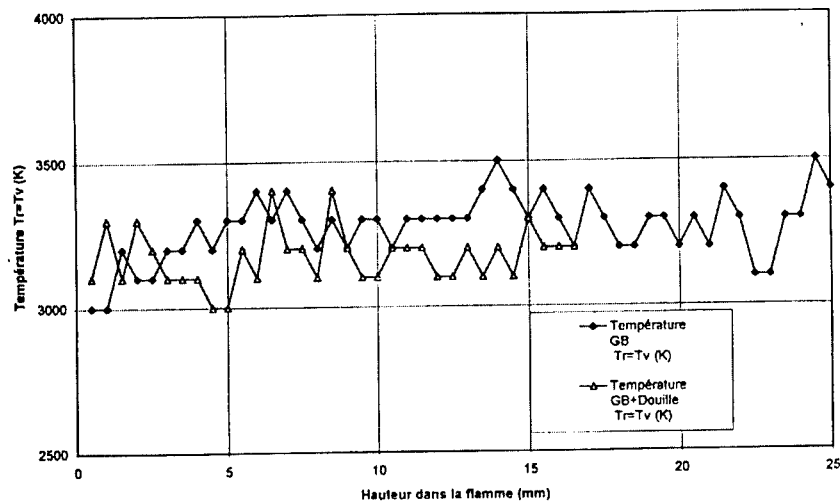The profile temperature is given on Figure 6.



Figure 6 : Temperature profiles.

By studying the OH concentration spectra of the double base propellant, it is noticeable that the OH concentration increases from $3,4 \ 10^{15}$ mol/cm$^3$, close to the combustion surface, up to $2,7 \ 10^{16}$ mol/cm$^3$ at 12 mm in the flame. This concentration stays steady up to 22 mm in the flame. Above 22 mm, the concentration starts a slow decrease.

The OH concentration of base propellant + igniter powder was measured on 15 mm in the flame, but the measurements on the 3 or 4 first mm are very disturbed by the presence of a "carbonaceous carrot" in the flame center.

Between 5 mm and 15 mm, the OH concentration profile follows that of double base propellant, but it is lower by a quantity of approximately $0,5 \ 10^{16}$ mol/cm$^3$.

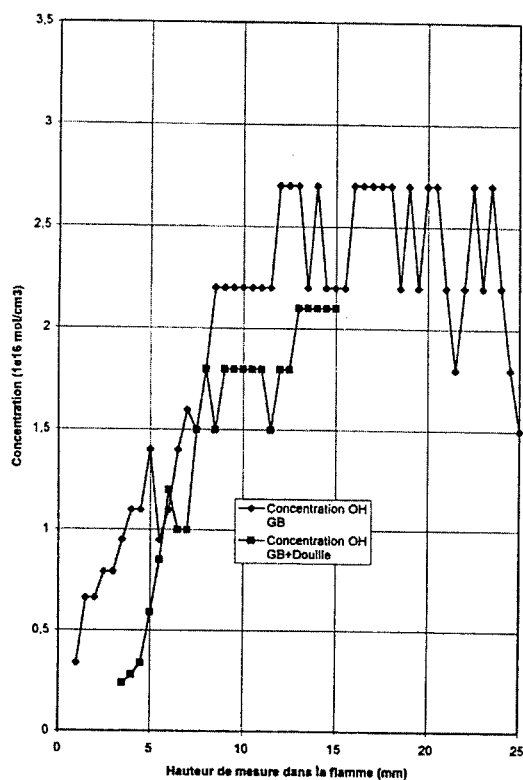The OH concentration profiles are given on Figure 7.



Figure 7 : Temperature profiles.

## 6. SUMMARY

OH temperature and concentration profiles have been obtained for solid propellants burning at atmospheric pressure, using a sensitive emission and absorption technique together with least squares fitting of a number of rotationally resolved lines.

OH varied slowly in comparison to many other radical species (CN for example, which is studies too), it is believed that the rest of the profile is adequately represented.

Finally, both the temperature and the concentration obtained are constituent with the solid propellant flame burning at its adiabatic temperature, and OH concentration in thermochemical equilibrium.

# REFERENCES

[1]     B.G. Cheron, "Molecular Spectroscopy", *private communication, LE CORIA, URA230,* Faculté des Sciences et Techniques de Rouen

[2]     J.A. Vanderhoff, "Species profiles in solid propellant flames using absorption and emission spectroscopy", in *Combustion and Flame* 84:73-92, (1991)

[3]     J.A. Vanderhoff, A.J. Kotlar, "Simultaneous determination of temperature and OH concentration in a solid propellant flame", *23<sup>rd</sup> Symposium on Combustion/ The combustion Institute*, 1990 / pp-1339-1344

[4]     J.A. Vanderhoff, M.W. Teague, A.J. Kotlar, "Absorption spectroscopy through the dark zone of solid propellant flames", *Technical report BRL-TR-3334*, (1992)

[5]     D. Roller, S. Untereiner, "Determination of OH temperature and concentration in a nitramine solid propellant flame", to be published (1997)

Perspectives towards the 21st Century

# BALLISTIC RESEARCH: QUO VADIS?

DirBWB Dr. SCHMOLTZI, W

BWB, Unterabteilung WF IV, Postfach 7360, D-56057 Koblenz, Germany

**Abstract:** The whole of ballistics has to be reviewed for promising research themes. Sometimes, the individual scientist should make a stop, postpone his particular interests and watch what is going on around him. The paper is intended to give a stimulus preventing the formation of blind spots in the field of ballistics. It also proposes to bring scientists with related objectives together.
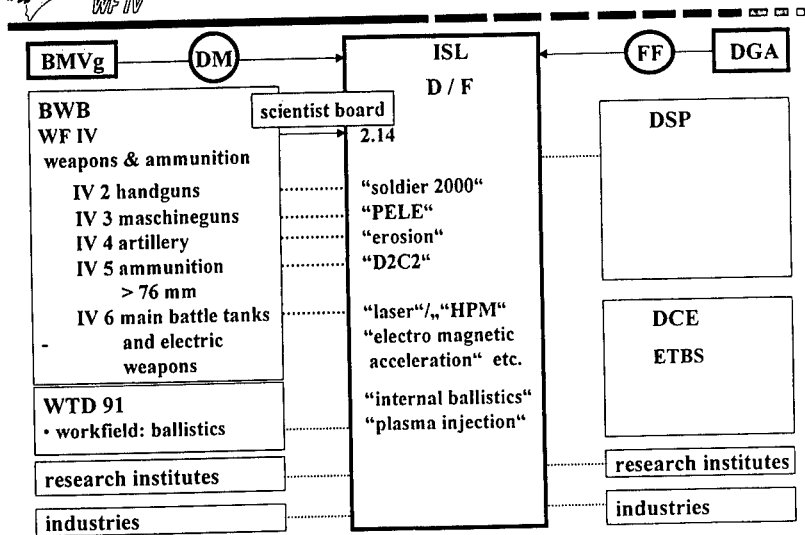
**European Forum on Ballistics of Projectiles**

**Research on Ballistics**

**Quo vadis ?**

**Common Interest**

BWB WF IV

| BMVg | — DM — | ISL D / F | — FF — | DGA |

BWB
WF IV
weapons & ammunition

scientist board

IV 2 handguns ........... "soldier 2000"
IV 3 maschineguns ........... "PELE"
IV 4 artillery ........... "erosion"
IV 5 ammunition ........... "D2C2"
 > 76 mm
IV 6 main battle tanks ........... "laser"/„"HPM"
 and electric "electro magnetic
 weapons acceleration" etc.

2.14

DSP

WTD 91
• workfield: ballistics ........... "internal ballistics"
"plasma injection"

DCE
ETBS

research institutes

industries
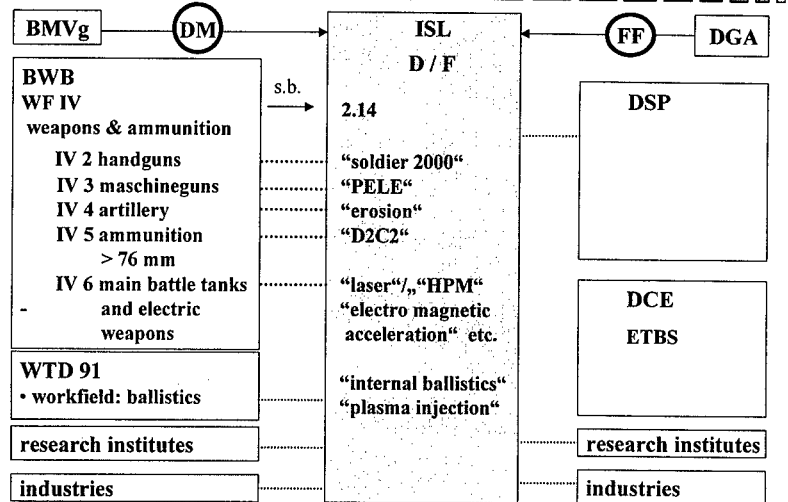
research institutes

industries

May I introduce myself:

- My name is Walter Schmoltzi. I am leader of the subdivision Weapons + Munitions in the German office for procurement and development.

-

* As a member of the scientific board I support the activities on the ballistic sector (activities 2.14)

* The illustration shows the simplified structure of the Franco-German research cooperation.

* Each country finances the half of the ISL budget. At the moment the ISL is analysing the possibility of obtaining industrial orders as well.

* Research-work which has a relation to systems and is matured, can lead to cooperation with both countries.

* Some exemplary themes of interest for the departments of the <u>WF IV</u> are listed in the illustration.

## Common Interest

**BWB WF IV**

| BMVg | DM | → | ISL D / F | ← | FF | DGA |

BWB
WF IV
weapons & ammunition

s.b. →

2.14

IV 2 handguns ............ "soldier 2000"
IV 3 maschineguns ............ "PELE"
IV 4 artillery ............ "erosion"
IV 5 ammunition ............ "D2C2"
    > 76 mm
IV 6 main battle tanks ............ "laser"/„"HPM"
-      and electric        "electro magnetic
       weapons             acceleration" etc.

WTD 91
• workfield: ballistics ............ "internal ballistics"
                                    "plasma injection"

research institutes ............
industries ............

DSP

DCE
ETBS

research institutes
industries

---

\* The research work, concerning internal ballistics, lead to cooperation with WTD 91, which participates in this symposium and will surely report its own main points.

\* The contact of scientists to other research institutes is necessary for the exchange of ideas and the complementary support. Only by this way it is possible to participate in the front row of research.

The institutes on the German side are the FGAN, FhG and DLR.

This symposium also should intensify the contacts with all the european institutes.

\*Last but not least - the contacts with the industries! I am sure that the priority of industrialization is growing because the knowledge should come to realisation.

As the degree of transition is an important measure for the research efficiency and for success, all institutes should be interested in this domain.

Even the companies have realized the benefits of cooperation with the research institutes. In the age of shareholder value they can not afford longlasting research-work or studies.

I am interested in supporting the exchange of knowledge and cooperation with the goal of raising success in our field.
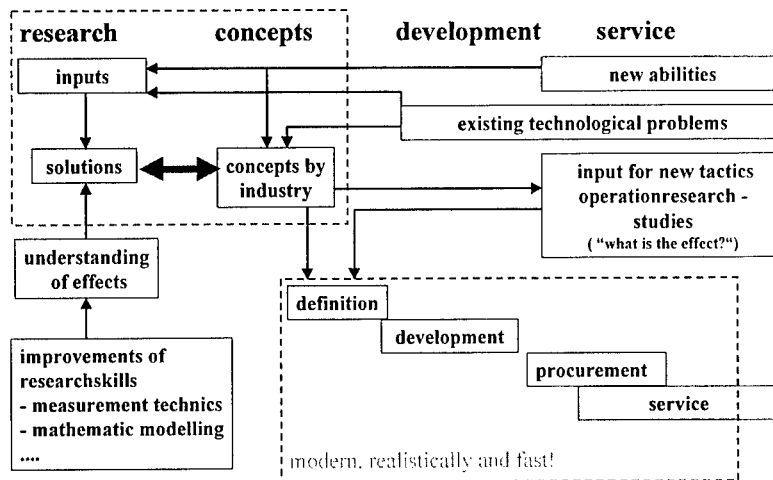
The result at the end has always been important, but since the change of threat and the shrinking budged we have to pay more attention to this aspect.

It is necessary that the research does not remain the cause in itself. In the applied research the scientist has to look for orientation on the "market". He has to find the problems that ought to be solved.

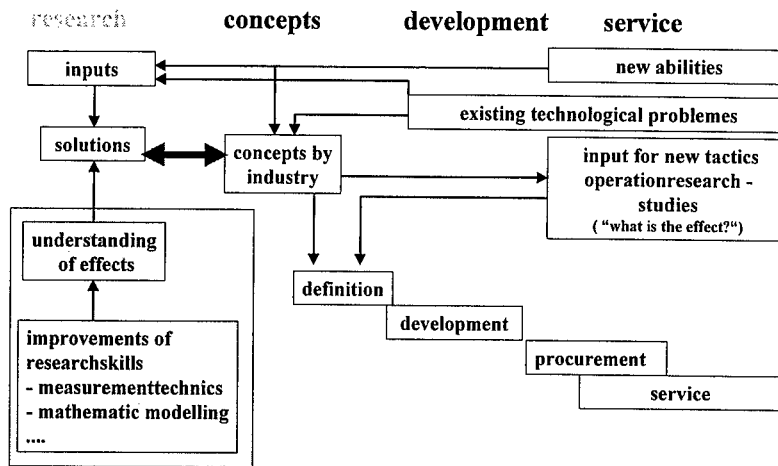- „What to do with the greatest invention if nobody needs it?" -

All the participants who are concerned with the defense technology have to explain their views to the scientists. The scientists need this information to inspire their work.

* favourable new abilities for the user,

*   technological problems known of the development and in service

research          concepts          development          service

| inputs |

new abilities

existing technological problemes

| solutions | ⟷ | concepts by industry |

| input for new tactics operationresearch - studies ( "what is the effect?") |

| understanding of effects |

| definition |

| development |

| improvements of researchskills - measurementtechnics - mathematic modelling .... |

| procurement |

| service |

While we are trying to improve the efficiency we must pay attention, <u>not neglect the basic research work</u>.

Even if there is no specific use in sight yet, the scientists have to take care of new effects.

Furthermore they have to develop the necessary measurement techniques and calculation models.

Good research is impossible without the adequate means of measuring and the mathematical support.

If you would reduce your research-work into marketable products, there would be no more innovation.

After this general discussion of the actual situation, let us come to the themes which I think are profitable objects of research.

### electromagnetic acceleration

- as missile - defence
- as "silent" acceleration
- electro-magnetic-interference, localisation

### plasma-ignition

- denser packed charge (more muzzle energy)
- ignition of lowvulnerability energetic material ("lova")
- reproductible ignition of small charges in big loadingchambers
  (unimodul without basismodule)
- electro-magnetic-interference

### barrel-erosion

- neue materials for charges, binder and additives
- erosion / wear and tear

### external ballistik

- directly definition of ballistic calculation factors by measuring the magnetic field in the 3-axle during flight of a rotating shell

- flow of energy in the turbulence-layer and heating-effect to projectiles with high speed in dense air

### target approach

- destination of position of projectiles during flight (GPS, Radar, Laser ...... )

- different methods to create forces to steer (body-lift, aerodynamic wings, impulse-motors, fluidic-elements)

- communication with the projectile (pictures, position-datas, commands to steer ....)

- directing of the effect of amunition (expell and sail, directed explosion)

**mecanically**

- affordable penetrators with lateraleffekt ("PELE")

- lightweight-sabots with optimised penetratordesigne (stiffness)

**elektrically**

- active protection (electromagnetic- / explosive-driven)

- interaction LASER / materials

- high-power-microwave - munition

# ENERGETIC MATERIALS AND BALLISTICS RESEARCH AT FOA FACING THE 21st CENTURY

## JANZON B., ÖSTMARK H.

FOA Defence Research Establishment, Weapons and Protection Division,
Grindsjön, SE-147 25 Tumba, Sweden

**Abstract:** During the 20th Century few real breakthroughs have occurred in energetic materials. During WW 2 HMX was synthesised. Later new materials as TATB and HNIW (CL-20) were synthetised. In 1995 a new effective synthesis process for Ammonium Dinitramide (ADN) was found at FOA. ADN is primarily a rocket propellant oxidiser with high performance, low signature and low environmental impact. Other explosives for which FOA has found synthesis processes are FOX-7 (Diamino-dinitro-ethylene), a high-performance, low vulnerability explosive, and FOX-12 (guanylureadinitramide), which is a highly thermally stable potential replacement for nitrocellulose. A high risk project at FOA with a very high yield potential is to try to synthesise tetrahedral $N_4$. This High Energy Density Material (HEDM) promises to have 3-4 times the energy of HMX, with a detonation velocity exceeding 15000 m/s and a detonation pressure of around 1.4 GPa (1400 MBar). Synthesis must occur by unconventional means. Assessments of the potentials resulting from use of HEDMs for weapons and protection applications and improvement are presented, relating to:
- interior ballistics
- exterior ballistics
- warheads, including electromagnetic warheads
- armours
- terminal ballistics

## 1. INTRODUCTION

During the 20th Century few real breakthroughs have occurred in the field of energetic materials. Most of the explosive substances in current use, such as TNT, RDX and PETN were synthetized already in the 19th century, and still prevail. During WW 2 HMX (octogen) was synthetized. Later synthesis processes were found for such new materials as TATB, a highly insensitive high explosive, HNB (hexanitrobensene), judged only ten years ago to be the theoretically best explosive conceivable, and HNIW (CL-20) which later proved to be about 20 % better than HMX and 6 % better than HNB.

ADN (ammonium dinitramide), primarily to be applied as an oxidiser for rocket propellants and underwater warheads, was synthetised in the US early in the 1990's, by a very complex process, and it was indeed one of the most costly materials ever at about USD 560,000 per lb. However, already as early as in the 1970's ADN had been synthetised in the Soviet Union and also used for propulsion of ballistic missiles. ADN contains no chlorine and thus gives a much lower signature in rockets than the common Ammonium Perchlorate (AP), and the new propellants could, in fact, have resulted in a first strike capability for the Soviets, since the satellite-carried launch detectors might not have interpreted the launch of an ICBM as such, but rather as a tactical missile launch, when using this type of propellant. In addition

ADN is much less environmentally damaging than AP, and enables creation of higher performance propellants than the traditional ones.

## 1.1 Explosives synthesis and research at FOA

In 1995 a new effective synthesis process for ADN was found at FOA. The new process was very efficient and cost-effective, gave a very pure product and was patented. The Bofors Explosives Co., now part of NEXPLO Industries, bought an exclusive license for exploitation of ADN, which is now produced in ton quantities and sold world-wide for experimental and testing purposes. Eventually ADN may become the standard oxidiser for rocket propellants, replacing the harmful AP. Since ADN has an excess of oxygen it can also be used to enhance the performance of many traditional explosives, and for other applications, such as underwater explosives.

ADN was soon followed by several other interesting substances. Here only two shall be mentioned, namely FOX-7 (FOX = FOA explosive, Diamino-dinitro-ethylene), a low vulnerability explosive with lower sensitivity than TNT and about similar performance to that of RDX, and FOX-12 (guanylureadinitramide), which is a highly thermally stable potential replacement for nitrocellulose. Both these are also being licensed to the NEXPLO Industries for exploitation, the latter one having its first potential application for gas generators for automotive airbags.

A high risk project at FOA with a very high yield potential is to try to synthetise tetrahedral $N_4$. This substance, which does not exist in nature, was modelled at FOA by numerical quantum mechanics, using the methods that were awarded the 1998 Nobel Prize for Chemistry. This substance promises to have 3-4 times the energy of HMX, with a detonation velocity exceeding 15000 m/s and a detonation pressure of around 1.4 GPa (1400 MBar). Synthesis must occur by unconventional means, and one of the routes followed is that of laser synthesis. The greater part of financing for this project [1] comes from a 3-year contract, 1999-2001, with DARPA, US; the project is also in part supported by the Swedish Armed Forces.

## 1.2 Further possibilities in High Energy Density Materials

Other nitrogen clusters than $N_4$, such as $N_8$ or polymeric $N_x$ promise even higher yields than the former one, up to 10-20 times that of HMX. Even this does not seem to be a limit for the power of new explosives. Potential candidates might be nuclear isomers, characterised by the following

- Nuclear isomers are "chemical", not "nuclear".
- They have a potential specific energy of $1000-10^6$ x HMX, i e 1 kg may yield up to 1 kton of HMX equivalent effects.
- Nuclear isomer ouput is mainly produced in the form of hard $\gamma$-radiation.
- However, so far there is no known way of initiating an explosive event in a nuclear isomer.

## 2. INTERIOR BALLISTICS

## 2.1. Interior ballistic modelling

FOA is working to develop new, fully 3-dimensional, fluid-mechanical, reactive, multiphase tensor-based object-oriented models (FOAM) [2] for interior ballistic flows. Modern modelling techniques, such as LES (Large Eddy Simulations) [3] will be used to enable time-resolved computation of unsteady turbulent and boundary-layer flows.

## 2.2. Electrothermal-Chemical Propulsion

For its studies of interior ballistics FOA has chosen ETC as a model system [4]. One of the reasons for this is that it requires also a build-up of conventional interior ballistics knowledge, sought after by the Swedish Armed Forces. FOA is not primarily studying plasma ignition of conventional or consolidated charges, done at many other research institutes, but instead looking at ways of directly steering or influencing the propellant combustion by various ways of using electricity and plasmas, especially with the aim of being able to use higher density and impulse charges. Some examples are shown in fig 1.
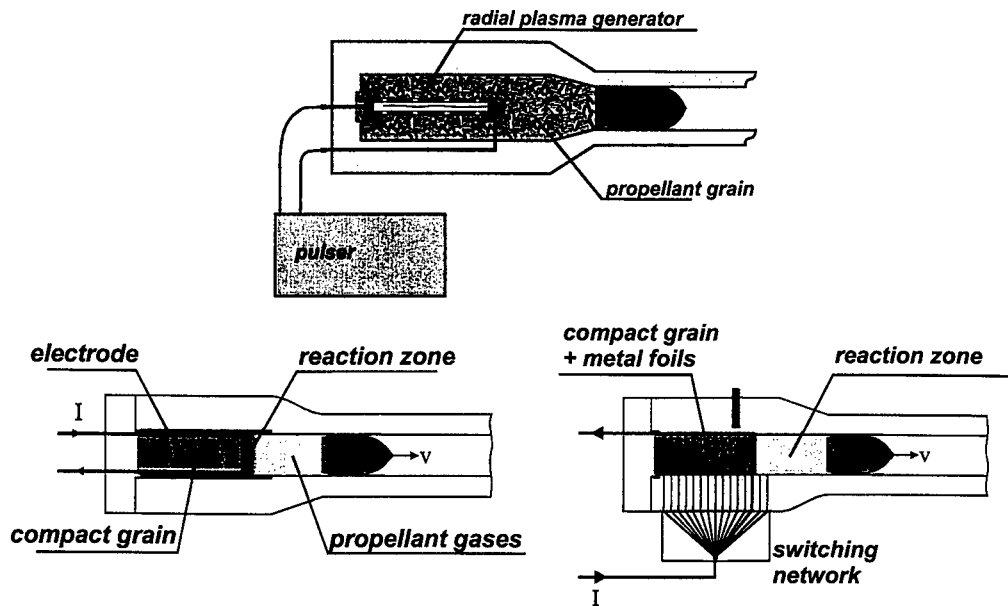


Figure 1: Electro-thermal-chemical concepts studied at FOA

## 2.2 New propellants

One way of reaching higher velocities within the limitations of current guns can be to seek propellants which produce gases of a lower molecular weight than those current. In the light gas guns, use of helium or hydrogen make it possible to get a much higher part of the propulsion energy available transferred to the projectile. Some composite propellants (fig 2) were theoretically studied and results indicated that they might be interesting for use as gun propellants. Their higher force is partly due to a lower average meolecular density of their combustion products. It can be noted that for some the maximum burn temperature is not higher than for a conventional tank gun propellant such as the M5, indicating that wear can be controlled.

For LOVA propellants based on RDX, the new explosive FOX-7 has shown to be a potent burn modifier, able to increase the burn rate by a factor of 2-3.

The ultimate propellant may be metallic hydrogen, which was synthetised at the Lawrence Livermore National Lab. a few years ago. Its theoretically computed force is of the order of 10000 J/g, compared with about 1100 for the currently best conventional propellants, i e an improvement exceeding 800 %.
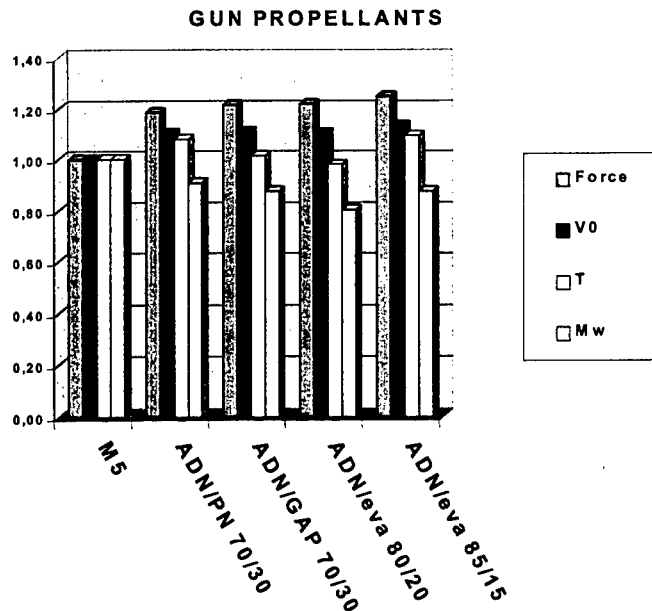
**GUN PROPELLANTS**

Figure 2: Relative performance of composite gun propellants (computed, Cheetah 1.40)

## 3. EXTERIOR BALLISTICS

FOA currently carries out appreciably little research in exterior ballistics and aerodynamics. Since a lot of focus is put on both longer ranges for artillery, higher velocities for tank guns and other direct-fire weapons, and higher velocities and longer ranges of missiles, the priorities could be questioned. However FOA has good competence in flow modelling and also some experimental facilities useful for exterior ballistic research.

### 3.1. Modelling of ballistic flow

The same model family (FOAM) as mentioned under 2.1 is also well adapted for exterior ballistic modelling, especially looking at transient and unsteady flows with turbulence, such as for yawing projectiles, separation of sabots etc.. It can easily be adapted to include base-bleed or propulsion. One example of a computation of a simplified base-bleed projectile is shown in fig 3 [3].



Figure 3: FOAM LES computation of flow around base-bleed projectile

## 3.2. Base-bleed and propulsion in trajectory

As known by most experts in ballistics base-bleed was invented at FOA about 30 years ago [5]. The patents have now expired and base-bleed is used for artillery ammunition in many countries around the world. Among its advantages are simple add-on designs, low additional weight, range increase of up to about 40 % and substantial increses of precision and lower sensitivity to disturbances such as wind. When higher range increases are needed propulsion in the trajectory will be needed. The simple add-on rocket propulsion (RAP) long ago proved inferior to the base-bleed, both in efficiency and very much in precision.

New concepts may be possible, one type was experimentally studied at Bofors and FOA, involving a high-velocity rocket with a KE integral warhead, launched from a counter-mass-weapon mounted on a lightly armoured vehicle [6]. The launch velocity is moderate, of the order of 600 m/s, but the rocket will then accelerate the penetrator up to more than 2000 m/s in just a few tenths of a second. It will then fly like a normal fin-stabilised long rod penetra-tor. To reach the accuracy required, one concept idea is to have inertial steering effective only during the propulsion period, and assuring that the accelerated projectile's trajectory vector has the same direction as on exit from the muzzle of the launcher. Another concept will of course be to have some terminal guidance included in the penetrator.

A theoretical study of the possibility to enhance the range of an artillery shell by adding a solid fuel ram-jet propulsor was performed at FOA [7]. It shows that with a very moderate weight penalty - addition of less than 5 % of propellant - ranges can be increased to over 65 km for a 155 mm shell (fig 4). The flight time remains about the same as for the normal maximum range, meaning among other things reduced dispersion and less sensitivity to cross-wind (fig 5). The solid-fuel ramjet concept was jointly demonstrated as viable by FOA and the Prins Maurits Laboratory/TNO of the Netherlands [8].
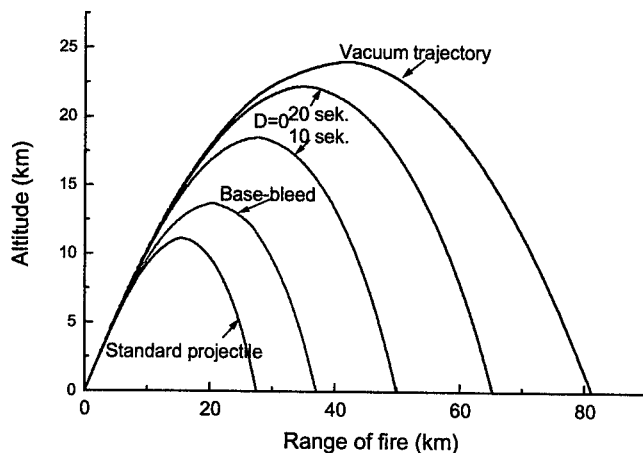


Figure 4: Trajectory plots for SOFRAM propelled projectiles

Another type of air-breathing motor which might become suitable for propulsion in the trajectory of ballistic projectiles is the Pulse Detonation Engine [9]. It is highly fuel efficient, and might be adapted also to external combustion.
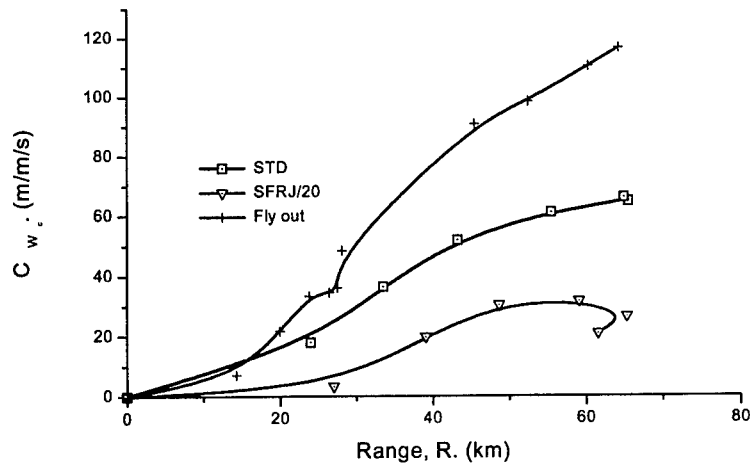
Figure 5: Cross-wind sensitivity of various long-range projectile concepts

## 4. WARHEADS

For warheads it is evident that new much more energetic explosives will have a profound impact on their opportunities, see fig 6 [10]. Going to for instance $N_4$ the changes will be so great as to probably necessitate totally new designs and principles.
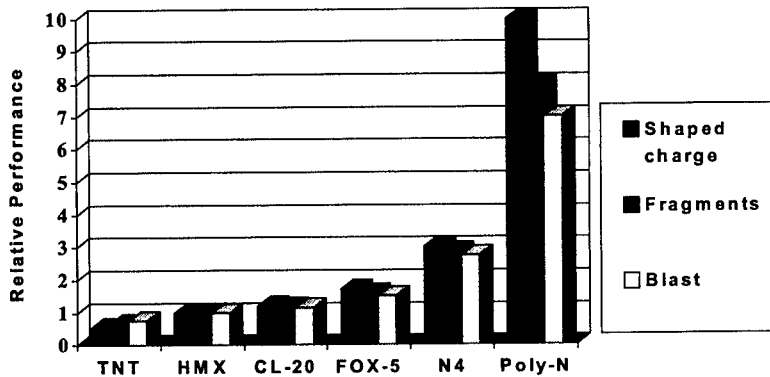


Figure 6: Estimated relative performance potential of new explosives for different applications

### 4.1. Shaped charges

The potential for increase in penetration by shaped charges is believed by FOA to be quite considerable. Already by exploiting known technologies, such as CL-20 as the explosive and molybdenum or sintered tungsten as liner material (fig 7), increases of the order of more than 40-50 % seem feasible relative to the currently best-performing charges [10]. If more exotic HEDMs, such as $N_4$ are exploited potential increases of the order of 200 % seem possible. It however remains very unclear how a shaped charge based on such an explosive could be designed.
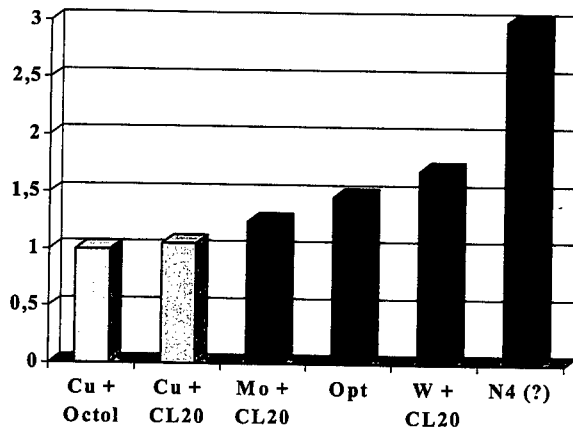
Figure 7: Estimated relative penetration performance of various explosive-liner combinations

## 4.2. Fragmentation warheads

More energetic explosives give the potential to increase fragment velocities and/or to decrease their sizes. Especially in combination with prefragmented, heavy material fragments, efficiency can increase much. Multiple warheads and adaptable designs that concentrate the fragments in the direction of the target can, in addition, yield extremely large increases of efficiency. The HEDM's will give more freedom for efficient designs in warheads limited by calibre or size.

## 4.3. Blast warheads

The most important category here is the warheads designed for penetrating and detonating inside a structural target. HEDMs will directly yield an increase in efficiency proportionate to the increase in energy. They will also give more freedom to design charges that withstand the penetration loads. Air-consuming explosives can add to the advantages. Use of advanced initiation systems can give directional effects.

Deep penetrating warheads against qualified fortifications need very insensitive, high-performance explosives. Design limits will be less restrictive with the use of HEDMs.

## 4.4. Electromagnetic warheads
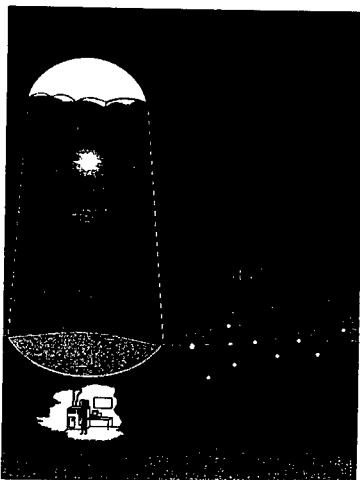


If the new high energy density materials (HEDM's), such as $N_4$, mentioned can be realised they may create a need for completely new warhead and propulsion technologies. Traditional warheads convert the chemical energy of the explosive into mechanical energy in the form of blast, kinetic energy of fragments, EFP's or shaped charge jets, which in turn convert part of their energy to damage to the targets. Depending on the behaviour of materials under these extremely high loads these kinds of mechanical conversion processes may no longer be efficient. Another type of energy that may then be considered is electromagnetic energy, in the form of high power microwaves (HPM), non-nuclear electromagnetic pulse (NNEMP) (fig 8), laser radiation, x-ray or $\gamma$ radiation. FOA does research on

HPM, NNEMP and other radio-frequency (RF) weapons, and also on explosively driven lasers, fig 9 [11].
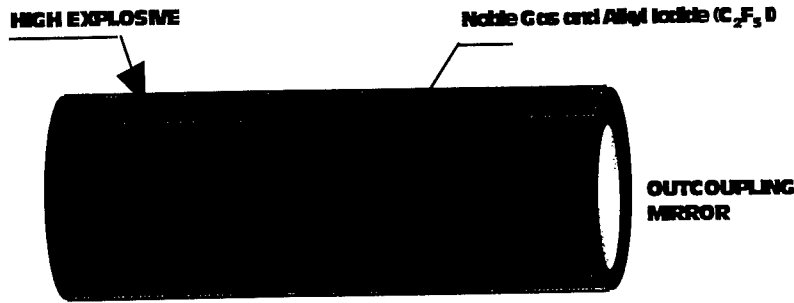


Figure 9: Principle sketch of an explosively driven laser

## 5. ARMOURS

For tank applications the armours now seem superior to the weapons and warheads, both for KE where there is a close balance, and for CE (shaped charges) where the armour is over-qualified due, especially, to the advent of reactive armours. All available protective techno-logies will be applied to the future tank armours.

### 5.1. Conventional Armours

In the future light alloys, such as aluminium or titanium will permit weight reductions or protection increases. Metal matrix composites may become interesting for armour applica-tions. Ceramics have a great deal of unused potential, among others current applications utilise their very high compressive strength in an inefficient way. FOA and others have shown that if heavily confined and pre-compressed a high quality ceramic may act as a rigid wall to sintered tungsten long rod penetrators up to about 1500 m/s and even up to 2000 m/s, see fig 10 and [12]. All current fielded APFSDS penetrators for tank guns have muzzle velocities lower than this.

Spaced armours and external protection devices can be highly efficient.



PENETRATION

TUNGSTEN LONG ROD PENETRATOR VS. CONFINED BORON CARBIDE
CERAMIC AT 1400 M/S, FLASH RADIOGRAPHED AT SAME TIME

HEAVIER CONFINEMENT,
PRESTRESSED
NO PENETRATION
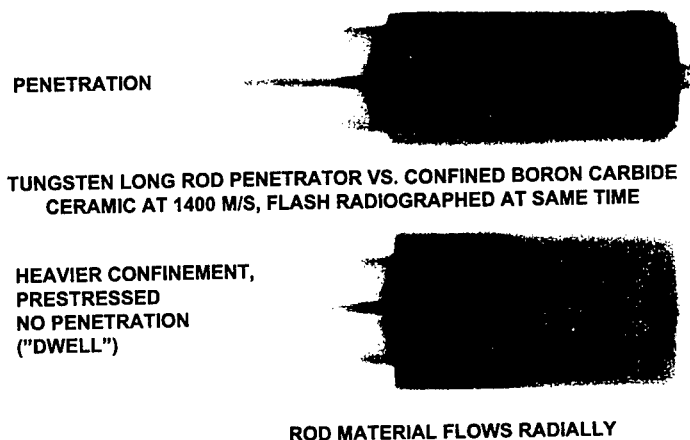("DWELL")

ROD MATERIAL FLOWS RADIALLY

Figure 10: Rigid wall behaviour ("dwell") of pre-compressed boron carbide

## 5.2. Reactive Armours

For reactive armours, the new HEDMs can prove very important, both by increasing the energy available to accelerate armour components, and by enabling very low sensitivity high performance explosives. Especially for anti-KE reactive armours, this may prove very important. Such armours may pose a very severe threat to the penetrators. In the future reactive armours will be likely to become an integral part of the armour design, rather than, as now, being add-on elements.

## 5.3. Electric Armours

Some varieties of electric and electromagnetic armours are shown in fig 11 [13]. Depending on the ability to store or generate large amounts of pulsed power (see [11]), they may become quite important in the future.



Electric energy destroys the projectile

Electric energy to accelerate objects against the projectile. (Reactive and sensoractivated armour)
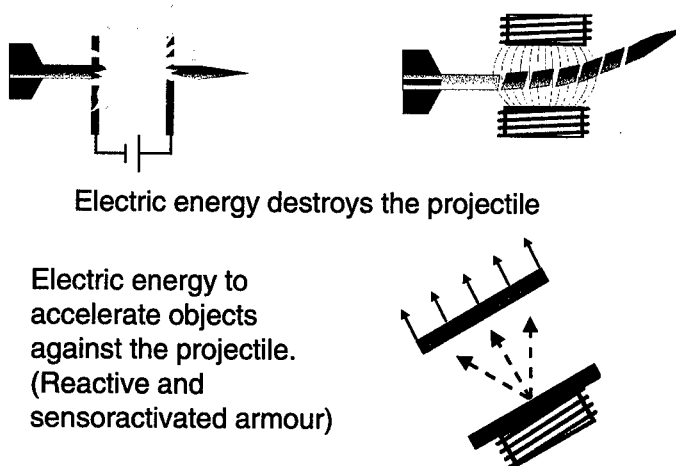
Figure 11: Sketches of some types of electric/electromagnetic armour principles

## 5.4. Sensor-Activated Armours (DAS)

A sensor-activated armour senses the incoming threat at some distance from the target by microwave optical or infrared sensors, decides a suitable counter-action and throws out one or more plates, rods or special warheads to kill or affect the threat while still at some distance from the target. To be able to design very compact such warheads by use of HEDMs should prove extremely valuable, and should greatly improve the efficiency of such systems. Better and more discriminating sensors add to make this technology a very severe threat against all weapons. Sensor-activated armours or similar may be used in the future for both heavily and lightly armoured vehicles, for fixed installations, possibly also for ships and aircraft. The less the built-in protection of the target, the longer range is required of the system.

## 6. TERMINAL BALLISTICS

### 6.1. Shaped charges

Better use of existing technologies and better liner materials such as Mo or W, and optimisation will enable considerable improvement in penetration against RHA, of at least of 40-50 % [10]. As mentioned above HEDMs could theoretically lead to a 200 % increase of penetration. It may be more likely that the energy available will be used to give better possibilities

to optimise and adapt the jet to the target. It may also be used to give a single-charge capability of combating reactive armours, for instance by creating very high velocity long coherent projectiles, intermediate between shaped charge and EFP, at over 5000 m/s, rather than a traditional fragmenting jet.

## 6.2. Long Rod Penetrators

Long rod penetrators currently become longer and longer (35-45 calibres), calibres increase (trend towards 140 mm) and there is a strive to increase muzzle velocities, yielding both higher hit probabilities and better penetration. The optimum velocities for most heavy alloy long rod penetrators seem to be between 2000 and 3000 m/s, i e considerably higher than today's. Ways of achieving this can be by ETC or EM launchers, or by propulsion in the trajectory. Most of the additional energy, though, will be spent in enlarging the size of the hole in the armour, rather than the penetration depth. Ways of solving this may be by using telescoping or segmenting projectiles, see fig 12.
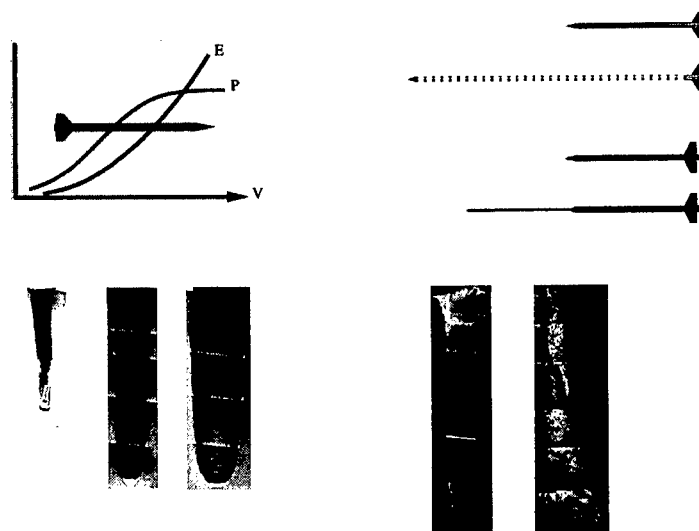


Figure 12: Ways of increasing penetration at high impact velocities
Left: Solid long rod penetration in semi-infinite target at 1500, 2500 and 3000 m/s
Right: left picture: segmented projectile, right picture: telescoped projectile, both at 3000 m/s

## 6.3. Medium And Small Calibre Penetrators

In medium and small calibres many new designs have appeared, some using tungsten carbide or other heavy and high-performing alloys as a core material, others designed as fin-stabilised long rods approaching the design of tank KE penetrators. As a result there now exists an increasing imbalance between the protection level of armoured personnel carriers and infantry fighting vehicles and the performance of their own weapons. In fact, an APC or an IFV can now be vulnerable even to the single soldier with a 5.56 or 7.62 mm weapon. There is also an increasing number of heavier calibres, such as .50", 14.7 and 20 mm, which will appear on a battlefield.

This necessitates new protection concepts. Better use of ceramics, as mentioned under 5.1, or sensor activated protective measures may provide a solution.

## 7. CONCLUSIONS

Already the step in energy density from HMX to $N_4$ is greater than the change from black powder to modern high explosives, like Picric Acid or TNT, which occurred in the 1870's. That change most certainly caused a complete revolution in warfare methods and weapons technology.

For some weapon-target combinations, the balance is presently quite even, meaning that also small changes can mean great differences to the weapons' efficiency. One such example is anti-tank weapons vs. main battle tank armour, where currently the armour seems to have the upper edge. However, improvements in weapons effects can be countered by increased protection levels, utilising new materials such as ceramics, reactive components, active, or sensor-activated close-in defence systems (DAS).

Electricity and electromagnetics have now permanently entered the ballistics sphere. Examples are electromagnetic launchers, electrothermal and hybrid guns, and electric/ electromagnetic armour designs. Combustion, detonation and many ballistic processes can interact with electrical and electromagnetic energy for much increased performance and safety. A demand for large amounts of pulsed electric energy to be stored or generated will be created by EM, ET and ETC guns, electric armours and vehicle propulsion. New explosive technology may assist in producing this. For instance new explosive dinitramide salts such as potassium or cesium dinitramide were created, which might prove highly suitable for use in high-yield pulsed magnetohydrodynamic (MHD) generators [11].

Entirely electronic fuzes constitute another important change, permitting in-line detonator designs. EBW and laser inititiation are other innovations increasing munitions safety.

In addition the reduced weight, volume and cost for computer processing power makes it increasingly feasible and likely that all weapons will, in the future, have some degree of intelligence. Applications can be guidance, trajectory, flight path and propulsion control, target seekers and terminal guidance, proximity fuzes, controllable and adaptable warheads and many other possibilities. Such weapons will, however, become more susceptible to electronic countermeasures and electromagnetic weapons, meaning that the duel between weapons and protection will continue.

### 7.1. The future war in 20-30 years ?

It is quite possible that new explosives with up to 10 times higher energy than the best current types will be ready for use 20-30 years from now. They may indeed exist in labs within a year! This will have profound consequences for all weapons technologies, such as:

- A 40 mm shell can get 3-4 times better effects than a current 155 mm shell
- Penetration of KE may more than double, of CE may triple
- Armour protection against KE may more than double, against CE less than double
- An aircraft may carry up to 5 times the current "weapons load"
- Artillery ranges may triple to quadruple for "ordinary" shell loads, increase to up to 10 times higher for special ammunition

Another important consequence may be that a terrorist could carry explosives the size of a cigarrette pack, able to bring down a jumbo jetliner

### 8. REFERENCES

[1] Östmark H, Launila O, Tryman R: Summary of activities and achievements within the $N_4$ project during the first three-quarter of 1999. FOA-R--99-01256-310--SE, ISSN 1104-9154, 1999

[2] Weller H G, Tabor G, Jasak H, Fureby C: A tensorial approach to CFD using object oriented techniques. Computers in Physics, 12(1998)6, p 620 ff, 1998

[3] Fureby C, Nilsson Y, Andersson K: Large eddy simulation of supersonic base flow. FOA-R--99-01043-310—SE, ISSN 1104-9154, 1999

[4] Nyholm S E: Elektrotermisk-kemisk utskjutning . En översikt samt preliminär bedömning av prestanda och realiserbarhet. FOA-R--99-01355-310--SE (in Swedish), ISSN 1104-9154, 1999

[5] Hellgren R: Basflödesprojektiler (Base Bleed Projectiles). Banberäkningsprogram och effektivitetsjämförelser. FOA C 20516-D2 (in Swedish), ISSN 0347-3694, 1983

[6] Eiderfors B, Renström R: PVS 2000 dynamisk mätrigg. FOA-R—98-00906-310—SE (in Swedish), ISSN 1104-9154, 1998

[7] Andersson K: Different means to reach long range, $\geq$ 65 km, for future 155 mm artillery systems. Possibilities and limitations. Proceedings, 17th Int. Symposium on Ballistics, Midrand, South Africa, p. 1-149 ff, ISBN 0-620-22077-5, 1998

[8] Veraar R, Elands P J M, Andersson K Nilsson Y: Overview of the Swedish-Dutch co-operation programme on solid fuel ramjet propelled projectiles. Proceedings, 18th Int. Symposium on Ballistics, San Antonio, Tx., USA, p. 409 ff, ISBN 1-56676-901-9, Technomic, Lancaster, Pa., USA, 1999

[9] Tegnér J K: Initial studies of the pulse detonation engine. FOA-R--98-00795-310—SE, ISSN 1104-9154, 1999

[10] Berglund E (ed.): Teknisk hotbild 2015-2025 (Technical Threat Description 2015-2025) . Delrapport 1 – Teknikutveckling. FOA-R--98-00890-201--SE (in Swedish), ISSN 1104-9154, 1998

[11] Östmark H, Pettersson A, Pettersson J: Projektförslag för "Energiomvandling". FOA-R--97-00449-310—SE (in Swedish), ISSN 1104-9154, 1997

[12] Lundberg P, Holmberg L, Janzon B: An experimental study of long rod penetration into boron carbide at ordnance and hyper velocities. Proceedings, 17th Int. Symposium on Ballistics, Midrand, South Africa, p. 3-251 ff, ISBN 0-620-22079-1, 1998

[13] Nyholm S E: Electromagnetic armour: An overview. FOA-R--98-00877-310--SE, ISSN 1104-9154, 1998

# ARTILLERY SYSTEMS – THE FUTURE OF GUNS AND ROCKETS

ASHLIN S.; CLAY R.; COOPER P.; McCLAGGAN D.; SHAND W.; STROUD-TURP J.; SMITH G.

Defence Evaluation and Research Agency, Fort Halstead, Sevenoaks, Kent TN14 7BP, United Kingdom

Abstract : A paper supporting the European Forum on Ballistics of Projectiles (April 11-14 2000) is presented on the topic of 'Artillery Systems – The future of Guns and Rockets'.

## 1. INTRODUCTION

### The future role for artillery

In common with all other combat arms the artillery is faced with an ever increasing range of tasks and roles, from attack of armour at extreme range during high intensity operations to force projection and patrolling during wider peace keeping operations.

The wide diversity of roles and tasks creates a dilemma in terms of future requirements; as a platform/ammunition mix tailored for high intensity armoured operations may be unsuitable for operations other than war (OOTW) and vice versa. The challenge is, therefore, to ensure the artillery is capable of meeting a wide spectrum of tasks under diverse operational scenarios in any climatic region, against a background of financial and political reality.

This will require technology to be exploited to its full in order to offer the user the best and most flexible mix of platforms and munitions linked to a capable surveillance and target acquisition (STA) suite via responsive and flexible command, control, communications, computation and information (C4I) system.

### Overview of future artillery requirements

Requirements placed on future artillery are diverse and are likely to become more varied. The relative emphasis on high intensity war fighting as opposed to OOTW is likely to change as the political pressures become more acute. To adapt to this continuing change, the key characteristic of future artillery will be flexibility in both firepower and mobility.

Potential capabilities are being stretched with the introduction of novel materials, designs and munitions in order to enhance firepower and mobility. This applies equally to the gun and rocket artillery system elements.

Recent studies have shown that the gun, far from being made redundant by the rocket as predicted in the late 50's, now forms an integrated and complementary system to that of the rocket. Together they give the enhanced capability both for precision and area munition delivery for long and short range against a range of targets.

## 2. GUN PLATFORMS

### General

The principal gun system platforms in UK service will be the 155mm Self-Propelled (SP) AS90 and the Lightweight Mobile Artillery Weapon System (LIMAWS) (155mm Gun). The performance, cost and reliability of these weapon platforms will improve with the insertion of key technologies within this decade and just beyond.

**Electro-thermal chemical (ETC) propulsion:** ETC technology and conventional charge technology would bring extended range, improved dispersion of fire, survivability and sustainability. The ETC 'smart gun', utilises a closed loop ballistic control using ETC technology to improve the precision; this may include the ability to predict muzzle velocity during in-bore projectile travel.

**Gun Fire Control System data:** MV variability is currently a large part of the error within the indirect fire system. First round fire for effectiveness will increase in importance and this will require accurate estimates of MV. The employment of prediction techniques for muzzle velocity and management of charge temperature will improve the accuracy of predicted fire, thus enhancing performance, operational flexibility and survivability.

Charge temperature measurement: Charge temperature measurement will make a significant contribution to reducing MV variability. Automatic ammunition identification will be used to improve fall of shot accuracy and safety.

**New navigation technologies:** GPS orientation will be available for light force operations and low cost pointing systems will lead to improved deployability and increased levels of survivability.

**Thermal Management:** Due to improvements in reliability and power ramming, the rate of fire of SP and towed guns will increase to the point where both safety in gun and operational availability will be affected. Mid-wall cooled, thermally managed barrels will become available for SP artillery which will improve system availability.

**Novel Gun Structures:** Mainly focussed at towed guns, lightweight structure technologies for platforms and gun barrels based on composite structures could be used in conjunction with soft recoil systems; this will open the way for improved performance, lighter systems giving improved mobility at the strategic operational and tactical level.

**Recoil & Muzzle Brake Systems:** Developments of new charge systems and ETC will lead to increased levels of muzzle energy giving greater levels of muzzle blast and increased recoil forces. The management of the recoiling mass by improved muzzle brake and recoil technology will reduce platform mass without loss of accuracy and stability. Risk to the detachment emanating from blast will also reduce.

**Meteorology studies:** A meteorological forecasting model and its interface will be included in the future fire control computer system to ensure the smooth provision of spatially and temporally enhanced meteorological messages for fire control.

**Insensitive Munitions:** The vulnerability of platforms will be improved by the introduction of Insensitive Munition technology for future charge and projectile systems.

## 3. GUN DELIVERED MUNITIONS

### General

Future munitions will comprise two groups: general purpose short range munitions (30 to 35 km) and guided munitions with longer ranges (60 to 100 km). General purpose munitions will be used for suppression, destruction and control of the battlefield. Guided munitions will be for the precision strike of armoured and soft skinned vehicles and control of choke points.

The benefits of generic carriers, modularity and common warhead technology between gun and rocket delivered munitions will be exploited.

General-purpose payloads will include obscurants, illuminating, RF, blast/fragmentation, and possibly bomblet. Those for guided munitions will comprise of Sensor Fuzed Munition (SFM), Terminally Guided Sub-Munition (TGSM) and possibly RF, HE or bomblet.

## Key technologies

**Fin stabilised munitions:** To meet the requirement for increased range and precision, fin stabilised munitions will mature within the next decade. Fin stabilised projectiles will be capable of operational ranges from 60 km, to in excess of 100 km with airframes built of lightweight materials. Forward control section will provide guidance by using a GPS/INS navigation system and control canards. These systems are likely to be modular with the ability to deliver a range of sub-munitions.

**Navigation:** Gun hardened global positioning systems and emerging low cost inertial sensors (micro-electromechanical systems (MEMs)) will improve precision from hundreds of meters at extended ranges, to an order of tens of metres. The inertial measurements will aid guidance by permitting attitude control giving glide capability to produce extreme ranges.

**Composites:** Lightweight airframe structures will permit the reduction of parasitic mass to be replaced by lethal mechanisms.

**Course corrected and future fuzes:** A Future Fuze (FF) will replace the existing multi-role fuze and a single dimensional Course Correcting Fuze (CCF) is also likely to be available. In both cases it is anticipated that these will be resistant to counter measures. Inductive fuze setters will be integrated into gun platforms, the ability to set friendly nations' fuzes, and smart munitions will remain a key requirement for interoperability.

## 4. MULTIPLE LAUNCH ROCKET SYSTEM PLATFORMS

**The M270 vehicle:** The M270 vehicle is the current MLRS launcher in service with UK and other MLRS nations. Key enhancements are aimed at improving performance, sustainability and reducing vulnerability.

**Future Fire Control System (FFCS).** FFCS will enter service in the near future and this will permit the M270 launcher to fire GMLRS and other future munitions, and fibre optic missiles (FOM). It will also integrate the launcher into the future digitized battlefield.

**M270 Capability Enhancement Programme (CEP):** It is planned to undertake a Capability Enhancement Programme for M270 in the future. It is unknown what form this will take, but areas likely to be addressed are the launcher mechanical system; defensive aid suites; signature reduction and manpower efficiency.

**LIMAWS (R):** LIMAWS (R) is a lightweight rocket launcher planned to enter service in the next 10 years. It is intended to be able to launch GMLRS and FOM. LIMAWS (R)'s driving requirement is its ability to be transported by aircraft, both fixed and rotary wing, and be deployed with rapid reaction forces.

## 5. ROCKET MUNITIONS

**Guided Multiple Launch Rocket System (GMLRS):** The GMLRS rocket is a major upgrade to the capability of the MLRS Family of Munitions (MFOM). The integration of the a guidance and control package and a new rocket motor to achieve a range in excess of 60 km with precision using inertial guidance only. Significantly greater accuracies are being achieved with GPS updates to the inertial measurement unit (IMU).

The baseline GMLRS rocket will carry an increased number of bomblets as its payload, and Area Denial Mine variant could be deployed within the next 10 years, political judgement permitting.

**GMLRS pre-planned product improvement (P3I):** Plans for a GMLRS P3I in the 10 to 20 year timeframe will give improved range of greater than 100 km and improved payloads. Methods for range extension include glide range extension with wings or an improved rocket motor. Improved payloads may include RF munitions, novel explosives and a unitary warhead.

Mid and long term improvements may include a GMLRS with a SFM payload as a possible mid term anti-armour solution, while GMLRS with a TGSM payload may be a longer term solution.

**FOMS:** The Fibre Optic Missile System will give the Artillery a precision strike capability. Once the FOM is launched, an air-breathing motor provides the cruise propulsion, giving it a loiter capability. The view of the IR seeker is passed down Fibre Optic cable to the operator, who selects targets from thermal cues and ultimately chooses the target the missile will attack. Ranges are anticipated to be around 60 km with the potential to extend up to 100 km. An operational capability is expected with the next 10 years.

## 6. SURVEILLANCE AND TARGET ACQUISITION

The Indirect Battlefield Engagement (IBE) system will comprise various elements of the Counter-Battery loop; ISTAR, communications to the weaponry, the weaponry, and Battle Damage Assessment (BDA). The intelligence, surveillance, target acquisition and reconnaissance (ISTAR) assets (Phoenix, counter battery radar (COBRA), MAMBA, advanced sound ranging project (ASP)) and their future counterparts form a complex system of systems, when their outputs are considered in concert.

Civil sector developments in communication and processor hardware have provided the potential for substantial improvements using commercial off the shelf (COTS) solutions. In the future ISTAR systems will work more closely together requiring data fusion technology and computer aided man machine interfaces (MMI) to provide the necessary battlefield coverage.

Increases in range and mobility of future weapons and advances in material technology are likely to lead to significant reductions in the projectile's radar cross section (RCS) and the launcher's acoustic and IR signature. Therefore, the Future ISTAR Sensor suite will require matching the range and mobility of the current and future indirect fire system.

### Radar concepts

**Improved Traditional Approach:** Depending on the effect and impact of Low RCS projectiles or the increase in range requirement. The first option will be to develop a more advanced version of the current COTS solutions, with better more powerful radar systems and increased mobility but in essentially the same arrangement, i.e. transmit/receive in a single location and ground based. However, should future weapon systems include both longer ranges and low RCS projectiles it is unlikely that the advances in signal to noise ratio received by the weapon locating radar (WLR) could keep pace.

**Bistatic operation:** Bistatic operation could improve the performance of WLR. Firstly, the separation of the transmit and receive components allowing the receive elements to be closer to the front line of own troops (FLOT) since receive only elements are less vulnerable. Secondly, by using bistatic radar it may be possible to obtain stronger return from the shell at less favourable angles.

**Uninhabited Airborne Vehicles (UAV):** Once fully developed the gain obtained from positioning the UAV within the target area would far outweigh the disadvantages in loss of transmitted power. The extra elevation coverage would enable the target to be tracked from its source, significantly increasing the accuracy of the system.

**Acoustic sensors:** The main thrust for acoustic sensors will be to deploy the sensors closer to the area of interest. Small disposable sensors could be fired or dropped into the target area, or vehicle mounted sensors on reconnaissance vehicles or UAV's could provide a forward reach into hostile territory.

## 7. C4I

### Forces for Change

The three major factors that are driving change to C4I are digitization, Joint Operations and munition natures.

**Digitization:** This will be a seamless supply of information to provide commanders and their staffs with the information they need in a timely fashion. Much of that system should be in place within 10 years, offering a range of tools (known as BISAs, battlefield information systems applications) such as decision aids, route planning, targeting and enemy picture. The system will be installed progressively and its software will need to be flexible enough to accommodate new doctrine and equipment.

**Joint Operations:** C4I will embrace all doctrine and procedures particular to maritime, land and air operations. There should be no restriction in where, during Joint Operation, command is exercised from and how that command is passed.

**Muntion Natures:** With the evolution of smart munitions, there is the prospect of weapons with discrete dwell/loiter times awaiting a target or perhaps for a forward observer to acquire an incoming munition and then guide it onto a target. The C4I system must have the speed and agility to control such changes.

### The Future

Artillery C4I is to be enhanced in the future as part of the digitisation initiative. The artillery currently use the Battlefield Artillery Target Engagement System (BATES), one of the first digital communication systems in the British Army.

Current equipment used by forward observation officers (FOOs) and battery command posts (BCPs) is limited. In the near future an improved computational facility is to be provided for artillery ballistic calculation. It is anticipated that this system will be a springboard for the development of the Fire Control BISA and the subsequent Fire Support BISA. The FS BISA will bring together the control of all aspects of indirect weapon delivery, including artillery, mortars, naval and air support. Target locating equipment (TLE), currently being introduced for mortars, is expected to be integrated with the emerging Fire Control BISA to enhance capability in terms of accuracy and speed of response.

The ballistic computers which are being developed will be available via the first implementation of the FC BISA.

Inaccuracy in Meteorological Data makes up a significant proportion of the error budget. A better means of sampling and collecting battlefield MET (possibly by equipment fitted on a projectile) than the current Battlefield MetS of radiosondes, will be available in the future to supply ambient data to the Computerised MET System for localised prediction. The resultant

Future MET System will be made available through the Fire Support BISA and should cover issues over a range of MET requirements.

**Technical Issues**

**Change of command responsibility:** With the development of the concepts of sensor to shooter links, there is the probability of more (pictorial) information being sent to the shooter and commander, this will require doctrinal and procedural changes to be developed in order to re-target in a timely fashion.

**Ballistic data:** There is going to be a mismatch between weapons available (especially in joint, combined or host nation support operations) and those included and validated in fire control computers. Rules may need to be established to cover when each weapon can be used bearing in mind the local safety rules and the type of firing (training, peace support, and offensive support).

**Data Management:** The future artillery system will have information exchange requirements both internally and externally. It is necessary to identify how data is distributed and to ensure it is circulated at the appropriate command levels.

## 8. CONCLUSION

When considering all of the above opportunities that technology offers the future indirect fire system, it should be clear that the key word is system. If developments are created in isolation, there is the real danger that the full potential of the system will not be maximised. Therefore, it is essential to have the right platform delivering the right munition at the right time, to the appropriate target.

# SOME TRENDS IN BALLISTICS OF FUTURE WEAPON SYSTEMS IN THE NETHERLANDS.

HOFFMANS, D.W.

TNO Prins Maurits Laboratory, P.O. Box 45, 2280 AA Rijswijk, The Netherlands

**Abstract:** A Defence whitepaper has been published recently in the Netherlands. From this a number of trends can be deduced for research on ballistics of future weapon systems. Major trends are being discussed in the areas of urban warfare, non lethal weapons, personal protection, more mobile/electric vehicles, precision weapons and tactical missile defence. These form challenges for ballistic research to cope with and are part of the TNO PML work programme in the coming years. More and more this research is being done in close collaboration with Canada, Denmark, Germany, Italy, Norway, Portugal, Spain, Sweden, Switzerland, UK and under Data Exchange Agreements with the US.

## 1 INTRODUCTION

Recently a defence whitepaper was published by the Netherlands Ministry of Defence. As I write this it is still under discussion in the Netherlands Parliament.

In my opinion some of the major drivers from the white paper for research in the coming years are:

-   The increasing threat and proliferation of ballistic and cruise missiles with chemical/biological warheads are a major source of concern
-   In "operations other than war" there is a strong tendency towards more protection on the one hand (less victims on own side) and non-lethal or more precise ("surgical attack") weapons on the other hand (less victims on hostile faction's side). Also tactical mobility plays a major role especially with regard to (air) transportability and countering the mine threat. Operations will also take place more often in urban terrain.

From a technology viewpoint an important trend is that weapons and weapon carriers will become smarter, more electric and more stealthy.

Furthermore diminishing defence budgets mean that it is imperative to come to closer collaboration in order to keep up one's expertise.

These issues represent major challenges with regard to the ballistics of future weapon systems.

## 2 MAJOR TRENDS IN BALLISTIC RESEARCH IN THE NETHERLANDS

### Urban warfare

Urban warfare still is a difficult operation, as has been shown in Grozny, Chechenia. Special weapons will be necessary in such an environment, e.g. bunker busters, controlled penetration and smart fuzing of dedicated small arms for infantry.

### Non lethal weapons

Preferably one would like an incapacitation mechanism which functions immediately but which is totally reversible and thus harmless. In practice however occasional permanent damage is practically unavoidable.
The challenge now is to prove that there is a large margin between effective use and possible lethal effects (see fig. 1).
Research is carried out among others:
- on flash bang grenades, where especially tympanum rupture is the critical mechanism
- on soft knock out projectiles, where blunt trauma is the dominant mechanism
- on others like blast and infrasound.

### Personal protection

Threats which now may more frequently occur are:
- stab weapons, whereby for adequate protection we may have to go back to a coat of mail
- flechettes, whereby the hardness of the material of the flechettes may make all the difference of the world in penetration capability (see fig.2). This is a difficult threat to counter
- a big challenge is to study the mechanism involved in the effects of stepping on an AP mine and to find adequate foot protection (see fig.3)

### Vehicle protection

The threat is in general considered to be not so much heavier but focussed on more areas of the vehicle, i.e. front, side, back, top and bottom. We have calculated that if all these areas are protected against the heaviest realistic threat using conventional armour the vehicle would weigh up to 360 tons. Clearly this is not realistic, so we have focussed on selective protection, i.e. add-on armour for certain vulnerable spots and mine protection (see fig.4), whereby crew survival plays an important role. Besides these active protection is becoming more and more a feasible solution. We have studied the Russian ARENA system (see fig.5) in detail and are right now studying the Canadian SAPROS system.

### More mobile/electric vehicles

This was one of the weapon systems which proved to be a very attractive option in the NATO study on Land Operations 2020 [1].
Important issues are:
- the use of ceramic armour (or cermets) is becoming more and more attractive due to the light weight. As an example LIBA™ armour (see fig.6) will be widely used in the advanced amphibious assault vehicle for the US marines and is a viable option for RNLA vehicles.
- the use of titanium, although still somewhat expensive, becomes more and more attractive as a light armour material.

-more frequent use of composites is to be expected, also with regard to stealth properties. This is important because other damage mechanisms will occur, e.g. delamination.
-the electrification of a vehicle will have an impact on armour and armament. Electromagnetic armour is right now being widely studied and seems promising [2, 3]. For electric armament the most feasible option right now is the electrothermal chemical solution, whereby it is expected that the muzzlevelocity of a 120 mm tankgun can be increased from 1750 to about 2000 m/s [5], which will probably be the practical limit of a powder gun.
Another more long term option is the use of an electromagnetic gun, whereby velocities much larger than 2000 m/s can be reached. This option may be very attractive because one may have the firepower of a tank for much smaller calibres, which means potentially a substantial saving in weight. Especially the US have recently started a programme with this goal. In order to exploit the higher velocity new penetrator design will be necessary.

**Precision weapons**

There is a strong tendency towards more precise "surgical" weapons, which attack targets with great precision at large ranges in order to avoid collateral damage. For long range missiles smart propellants and ramjet propulsion become more and more the preferred options. A very interesting ramjet application is also for mid calibre air defence munition [4]. The control mechanism is more and more application tailored, e.g. side thruster control is used for ballistic missile defence, but also for hypervelocity missile control. The smartness of a weapon is in general not a hardware problem (besides hardening the electronics against setback forces), but smart algorithms need to be developed. Fuzing becomes more and more intelligent especially in combination with a multiple initiated aimable warhead.

**Tactical Missile Defence**

Where tactical missile defence is concerned only biological and chemical warheads are considered. With defence against ballistic missiles one of the first issues is whether to counter the threat in an early phase or in a late phase. If one can score a hit in an early phase a structural/control kill may be sufficient so that the missile will not reach its target. A structural/control kill may be easier to attain provided that detection and timing is adequate. If a kill is attained in a late phase a warhead kill seems necessary, because if biological or chemical warheads are only partly destroyed the residual effect may still be considerable.
If a warhead kill has to be attained this will be a great challenge. It means that the warhead (unitary as well as submunition warhead) has to be penetrated and then the chemical or biological agent has to be defeated by some mechanism, probably heat.
To defeat a cruise missile is even more difficult, because the trajectory is almost unpredictable.

## 3 CONCLUSIONS

I have tried to give you a flavour of the planned and ongoing research in the Netherlands in the field of ballistics, where new trends will provide new challenges. Diminishing defence budgets mean that it is imperative to come to closer collaboration in order to keep up one's expertise. At TNO PML more than 1/3 of the projects in ballistics are being executed in the form of collaborative projects with Canada, Denmark, France, Germany, Italy, Norway, Portugal, Spain, Sweden, Switzerland, Turkey, UK and US, bilaterally, trilaterally or under EUCLID or NATO programmes. Each year the number of collaborative projects grows larger.

## 4 REFERENCES

[1]    Land Operations in the year 2020 (LO 2020), NATO RTO-TR-8 AC/323 (SAS) TP/5, (1999)

[2]    H.-J. Ernst, K. Sterzelmeier, "Reactive electromagnetic armour against medium calibre KE-projectiles" in IIIrd European Armoured Fighting Vehicle Symposium at RMCS, Shrivenham UK, April 28-30, (1998)

[3]    H.-J. Ernst, T. Wolf, R. Nüsing, "Experimental medium calibre studies with electromagnetic armour against KE and SC threat" at 18th International Symposium on Ballistics", San Antonio US, 15-19 November, (1999)

[4]    K. Anderson, R. Veraar, N. M. S. Roman, "Solid fuel ramjet for projectile propulsion-summing-up of a joint FOA-TNO research project" poster presentation 16 at European Forum on Ballistics of Projectiles, ISL, April 11-14, (2000)

[5]    H. Hilgendorf, "The benefits of AECV technologies for future military combat and support vehicles", 3rd International AECV conference, Königswinter Germany, September 21-23, (1999)

# Figure 1: NLW: Seeking a margin
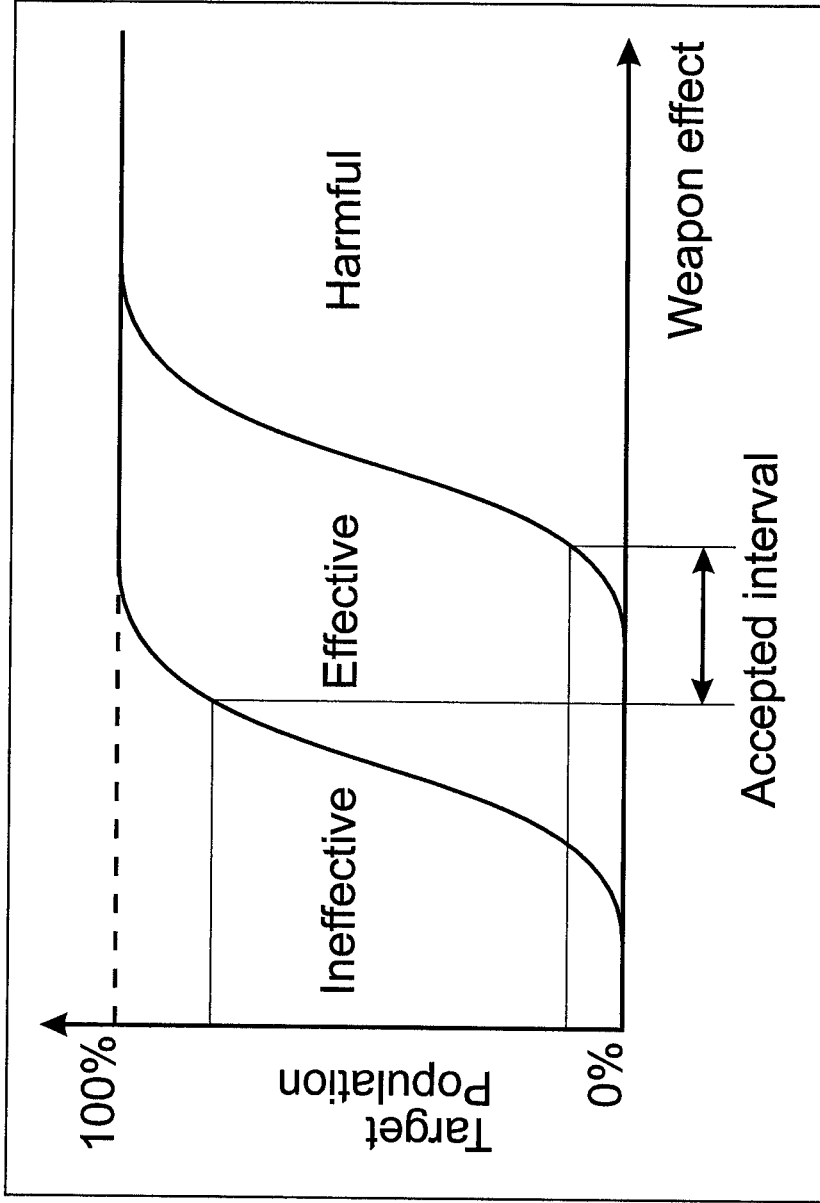
# Figure 2: Flechette impact on 3 mm Al. target
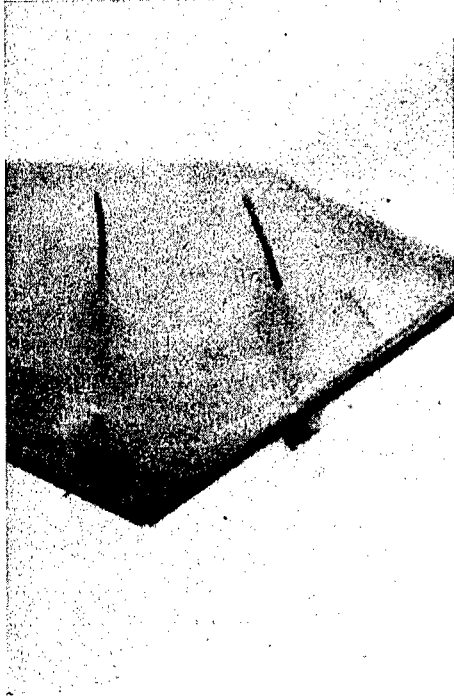


- US (335 HB)
  Velocity: 295 m/s
  Obliquity: 35 degr.
  240 μs
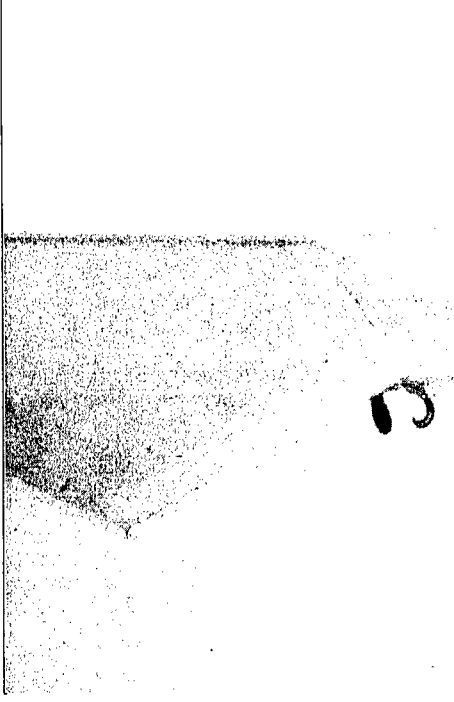
- Russian (147 HB)
  Velocity: 290 m/s
  Obliquity: 30 degr.
  130 μs

98-000 1
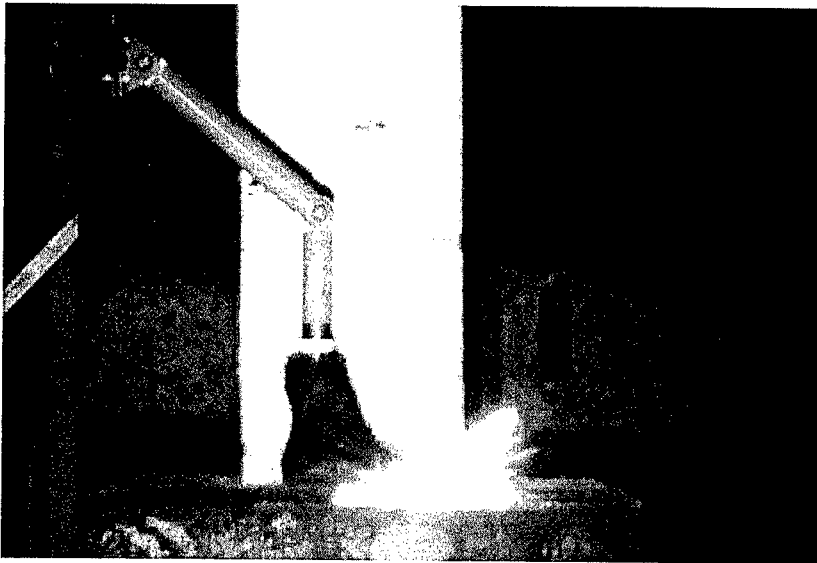
*Figure 3: Testing of protective shoe against AP mine*

# Figure 4: Vehicle Mine Protection

## Balanced approach
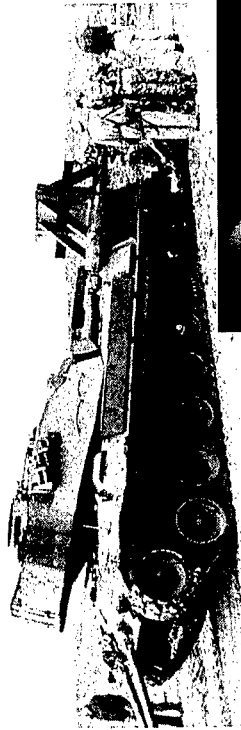


Madymo simulation

Leopard blast mine trials

Hybrid III crash dummy

DEA1182 / 99 -10  1
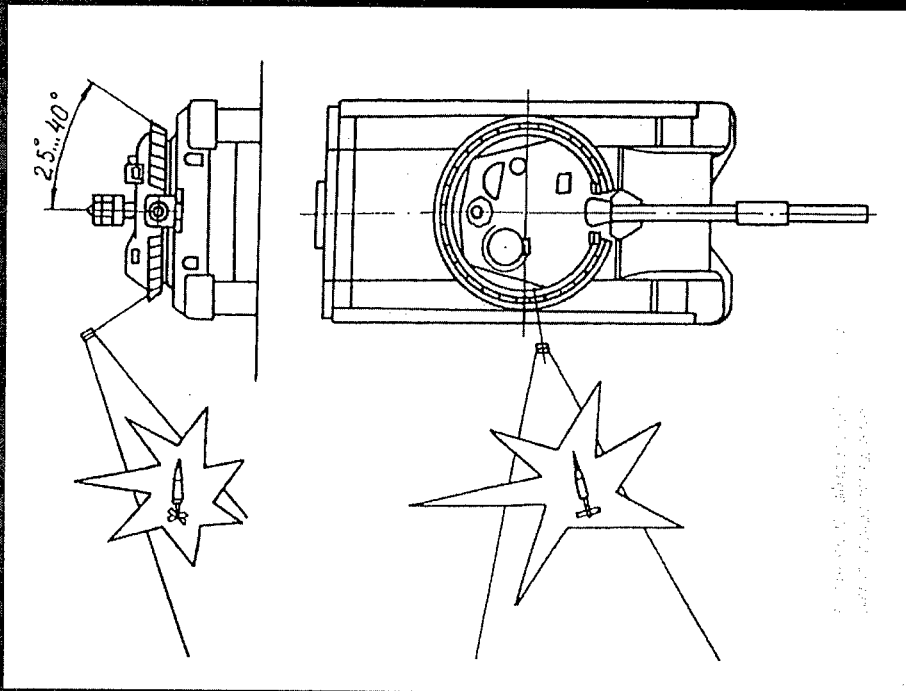
98-259 20

*Figure 6: View on LIBA™ ceramic armour*

# BALLISTICS AND FUTURE MILITARY OPERATIONS
# THE CASE OF THE AIR-LAND ENVIRONMENT

## J.-B. PENE (1), B. CHATENET (1), C. JURCZAK (2)

(1) DGA/DSA/SPART, BP 19, 10 place Georges Clemenceau, F-92211 Saint-Cloud cedex
(2) DGA/DSP/SASF, 26 boulevard Victor, F-00457 Armées, France

**Abstract** : the role of ballistics in the technical and operational thought process should be analysed taking into account to the environment in which it is placed. In order to meet the challenges set by future military operations, the technical and operational innovation potential of ballistics should not be considered at the level of single weapon systems but at a higher level of system architecture. The main lines requiring future studies in the area of ballistics are the protection of deployed units, of transport and infantry vehicles, the graduation of weapon effects and the increase in the size of controlled areas.

## 1. INTRODUCTION

Weapon systems based on ballistics have always played an important role, giving air-land forces the capability to accomplish their missions. The scope of military operations, ranging from war to violence control, combined with technology improvements, provides ballistics with new challenges at the threshold of the 21th century. The purpose of this article is on one hand to present the changing environment in which ballistics can contribute and on the other hand to mention the main lines addressed by research in France to prepare changes in the use of weapons.

## 2. PLACE OF BALLISTICS IN FUTURE OPERATIONS

### 2.1 A vision of future combat

Future capabilities of air-land forces can be qualified by two key factors : reactivity and adaptability.

The first point is already stressed in present studies, which emphasise not so much platforms but overall architecture of systems (for example, associating sensors and weapons) and battlefield digitisation. By making the best of communication and data processing technologies, it is possible to impose on the enemy, in a decisive action phase, a rhythm that is greater than his own action capabilities and to generate surprise tactics by concentrating in the right place and at the right moment the systems' different effects.

Moreover, the effects which are traditionally associated with ballistic weapons will have to be included in a wider range of effects intended to provide new capabilities ranging from warning to destruction. The variety of situations encountered will not call for a single answer,

thus it will be necessary to have a whole set of equipments tailored to the various situations. In areas where forces will be present, they will carry out combat actions making a great use of vehicles. When required by terrain or enemy conditions, troops will dismount and, if they are not fighting, they may carry out inspection missions using crisis management weapons. Such weapons should have graduated effects adaptable to any tension increase. There will also be large areas where forces will not be physically present but which will have to be controlled with weapons deployed either within the area or outside it. In all cases, precision strikes with no collateral damages will be preferred.

## 2.2 Ballistics in operational functions

This vision of future combats leads to an architecture of air-land combat systems taking into account the two key factors previously identified, while integrating existing systems to the best of their capabilities.

Let us now analyse the place of ballistics, in the short or medium term, with respect to the main operational functions associated with future equipments ; these can be grouped in six categories : C3I (communication, command, control and intelligence), mounted close combat, dismounted close combat, fire support, area control, protection and mobility. Ballistics encompass weapon action modes and effectiveness through the identification of new targets to be engaged and through the analysis of changes in the protection of existing targets against ballistic threats.

In the approach presented here, operational aspects clearly drive the emphasis placed on ballistics but, conversely, this emphasis is a source of technology innovations which eventually lead to operational innovations. For instance, considerable progress could be achieved in the medium term through new explosive molecules with radically greater performances than presently known molecules. This would have a major operational impact which would naturally have to be capitalised as quickly as possible. Therefore, there must always be a dialog between the operational and technological aspects as illustrated in the second part of this article.

### C3I

Improvements of the enemy's intelligence capabilities, especially through the rapid proliferation of information technologies and the increasing availability of high-performance sensors, no longer lets us hide our intentions from the enemy. Counterintelligence may be based on countermeasures or, more simply, on the deployment of decoys. But a ballistic component should also be envisaged, particularly against intelligence drones and counter-battery radars, both of which are becoming widespread. In both cases, we must be able to develop an attack mode suited to a threat that is discreet and very mobile.

### Mounted close combat

Weapons on armoured vehicles will evolve in the short term in an incremental way without any changes in their employment concept. However, there are now new protection concepts against the ballistic threat which are not solely based on armour, but on its synergy with stealth technology and countermeasures. Furthermore, this balanced protection of armoured vehicles should be omnidirectional in order to take new threats into account : top-attack anti-tank missiles, new field artillery sensor-fuzed shells, new direct fire sensor-fuzed munitions,

area defence mines, etc. A balanced protection goes hand in hand with the search for increasingly lighter army vehicles, a constraint imposed by air transportability. From a ballistics viewpoint, on one side the effectiveness of ballistic protection will have to be reassessed and armour will have to be considered only as a part of a global architecture ; on the other side, the effectiveness of ballistic weapons will have to be reassessed so as to defeat armoured vehicles protected by innovative concepts.

In combats between armoured vehicles, the advantage often goes to the one who engages its target first. Firing on the move, which is one of the characteristics of the Leclerc tank, participates in this concern for anticipation. Taking the same perspective even further, the next generation of armoured vehicles for close combat could have the capability to acquire and destroy targets which are beyond direct sight. This extension of close combat could be achieved with weapons such as guns or missiles.

Looking further into the future, there could be a radical change in vehicle propulsion systems, such as the introduction of all-electric vehicles. Given this perspective combined with the goal of achieving very compact armoured vehicles, the benefit of weapons such as electric thermo-chemical guns can be questioned.

Finally, as regards helicopters, the versatility necessary to satisfy operational requirements goes together with a greater variety of armaments. Each of them will take advantage of the improvements in ballistics with no substantial change in combat modes.

<u>Dismounted close combat operations</u>

The dismounted soldier will remain in the future, the same way as yesterday and today, the foremost element in the engagement of army forces. The priority given to a strategy of preventing crisis and keeping violence at the lowest possible level, makes contact forces necessary. They can be called into action in an environment of civil populations or in an urban environment against increasingly diversified enemies, using new action modes. Although the dismounted soldier's current missions (close combat, long-term control of terrain and environment) are not expected to change much, the spectrum of engagement circumstances will become wider and will place him in a new tactical context. This, reinforced by the media impact of any human losses and the fact that current equipments have certain weaknesses, makes it necessary to considerably improve his operational capabilities.

The FELIN soldier system, which will come into service in 2005, will take advantage of the integration of many advanced technologies. The main innovation will be the implementation of a new integrated system, at the service of man, enabling the soldier to perform all his missions under the best possible conditions from the human factors, protection and operational effectiveness viewpoints.

The dismounted soldier will be exposed to ballistic aggressions, bullets and shell splinters. His protection will be based on a modular concept which can be tailored to all situations while meeting the constraint of a carried load limited to 23 kg. As such, full protection will be provided for the combatant's head by a helmet, an eyeshade, a chin strap and a lower flap ; protection against bullets and shell splinters will also be provided for the bust and the pelvic zone and, finally, for his hands, elbows and knees.

Once dismounted from his vehicle, the soldier will be able perform either combat or control operations, depending on his equipment. Initially, short-term developments will concern the

possibility of firing without being seen by using of an offset sight. Eventually, a new individual weapon will be developed. Ongoing work concerns twin-calibre weapons or explosive ammunition for engaging undercovered enemy. The main difficulty is to maintain a high degree in the weapon's ease of use despite the variety of its functions. As regards inspection operations, crisis management equipments should be non-lethal weapons. Of course, there are such weapons in the arsenal of police forces but, amongst the new one, very few of them have demonstrated their effectiveness in service. A major field of investigation for ballistics is open in this area.

For the infantry combat vehicle, work carried out on protection against the ballistic threat only provides a partial answer given the great constraint on weight imposed by air transportability. Innovations in armour are expected to follow the progress of the whole medium calibre projectile threat or even anticipate it.

Finally, in the field of anti-tank missiles, future developments in active protections will represent over time a real challenge : equipment such as ARENA, new active armour. Neither short term incremental performance improvements of warheads nor progress in terminal ballistics will likely be sufficient. New methods of attack will have to be imagined.

Fire support and area control

For field artillery, recent technological developments will make precision munitions an operational reality. Sensor-fuzed munitions have reached maturity and only incremental improvements are expected. Trajectory correction munitions will soon be operational and will no doubt renew the scope of studies in external ballistics. In particular, there could be a renewed interest in concepts such as Multiple Round Simultaneous Impact (MRSI).

The city is a new, privileged environment which requires equipment adaptations in all areas (command, intelligence, fire support) for all sorts of operations, including combat. An initial theme of investigation for ballistics is the penetration of hard concrete targets which are treated in the first place by deep attack strikes with air-to-surface weapons and specific warheads but also by surface-to-surface fire support. Trajectories will also have to be examined closely in environments such as streets lined with buildings where maybe purely ballistic solutions would not be the most effective. A weapon using image transmission technology by optical fibre (POLYPHEME concept) could satisfy this requirement.

Finally, a new concept is the integration into a man controlled system, of accurate long range weapons (approximately 50 km range), sensors and miniature armaments spread in an area so as to enable the effective control of such an extended area. Here again, this is a field open for investigation in new ballistic studies, especially for abandoned armaments.

Protection

The major development in the field of surface-to-air defence is the use of a theater air defence system. This would need specific developments for warheads. Also, ballistics of hypervelocity missiles is a subject which interests surface-to-air defence in a more general sense.

In order to ensure in the short term the protection of army deployments against incursions, the SPECTRE programme aims to implement a man-controlled network of sensors and other

equipments to enable the graduation of effects from warning to destruction. Here again, armament technologies need to improve so as to have the widest range of means available.

Finally, future logistic transport vehicles will be based on civil technologies, but specific technologies derived from armoured vehicles will have to be adapted in order to ensure cabin protection against any threat, even behind the line of contact.

## 3. MAIN BALLISTIC STUDY THEMES ADDRESSED IN FRANCE

Ballistics are at the heart of weapon systems intended to produce destructive effects on the enemy, if offensive electronic warfare is put aside. Changes in warfare and new operational orientations mentioned earlier generate new requirements in terms of weapon systems' performances. The various fields of ballistics are solicited to provide these improvements or these technology breakthroughs which are sources of enhanced performances. Also, with these technology improvements, new levels of operational performances can be imagined and original answers can be found to new requirements.

### 3.1 Internal ballistics

Most of the performance in terminal ballistics are derived from what happens during the first tens of milliseconds of the projectile's active life. That is why considerable efforts are made in internal ballistics. New formulations are sought for gunpowder in order to obtain higher levels of initial kinetic energy. The integration of these materials into new propellant charges requires work on the ignition and architecture of propellant charges. For example, one way of improving the performance levels is to use agglomerated charges, but it is difficult to control the ignition for large calibre ammunition. One solution could consist of plasma ignition as long as the required electric energy is minimised in order to allow the integration of such an ignition system on board a tank.

Seeking high muzzle velocities raises new problems for the weapon designer. In particular, the wear of barrels must remain compatible with a realistic lifetime in both wartime and training. Processes for surface deposits on the inside of barrels and the development of effective anti-erosion additives in gunpowder are essential research paths.

With the decrease in the dead weights of projectiles, in particular the sabots of Armour Piercing Fin Stabilised Discarding Sabot (APFSDS) ammunition, more of the projectile's kinetic energy can be dedicated to its terminal effect.

Finally, in the long term, mention should be made of the new possibilities brought by electric guns. In the medium term, the most promising path is the electro-thermal chemical gun and in the long run, the rail gun. But considerable reductions in weight and volume still have to be achieved for the generation and storage of energy. Today, gunpowder represents the most effective way of storing large amounts of energy which can be easily released.

### 3.2 External ballistics

Higher muzzle velocities raise new problems concerning the mechanical resistance of projectiles. In the case of APFSDS projectiles, hypervelocity projectiles and even artillery projectiles, new phenomena now appear which do not exist with the current generation of projectiles or only marginally. Barrel erosion disturbs the projectile's geometry and,

consequently, its external ballistics. In the same way, increasing the length of the projectile, in the search of better penetration performance, requires better control of its flight stability.

The constant search for greater artillery ranges requires two types of actions :

- the development of shell trajectory correction devices so as to maintain or even improve accuracy at the new maximum ranges ;
- the search for new ballistic formulas for howitzers such as fin stabilised shells in order to achieve ranges well above the 40 km limit of gyro-stabilised shells fired in 155mm diameter and 52 calibre length barrels ; these new formulas, in which the projectile has to be equipped with guidance and control devices, opens the debate on the possible switch from rifled barrels to smooth barrels for field artillery, in the same way as what took place with tank armaments.

Although the Global Positioning System (GPS) is a technically credible solution, the fact that Europe has no control over this system constitutes a great handicap. Low-cost inertial sensors, compatible with the severe environment of an artillery shell, could constitute an alternative.

In the past, many efforts have been made in terms of smart munitions. But the cost of these new munitions was considered prohibitive and developments have been abandoned. The current challenge is to find solutions which combine low cost and accuracy. Laser designation could constitute a first answer.

## 3.3 Terminal ballistics

The improvement of enemy armour, even though it is not happening as fast as in the past, causes an increase in the length of projectiles and in their kinetic energy. Therefore, one of the permanent research goals is to improve the mechanical characteristics of penetrators.

As for shaped charges, work is being carried out on hybrid charges which are effective at action distances of 10 to 100 calibres and on multi-point ignition which would reduce the weight of Explosive Formed Penetrators. The use of nanocrystalline materials is also being considered for liners.

For fragmentation charges, studies address concepts designed to focus the flight direction of fragments.

To maintain the performance level of anti infrastructure penetrators, studies are carried out on both the penetrators themselves and on intelligent fuzes for these munitions.

## 3.4 Protection

Terminal ballistics of munition being a dual domain (combining sword and shield aspects), protection cannot be separated from it.

For heavy tanks, the protection level will no longer be based solely on armour. The need to protect them from all angles and the increase in the threat would lead to a tank with an unacceptable weight. From now on, protection must be based on new reactive or active concepts. Therefore, studies are more directed towards the balanced protection architectures of tanks rather than simply improving armour materials.

On the other hand, in the case of lighter vehicles, research for light armour, adapted reactive armour and transparent armour is particularly active.

Protection of the dismounted soldier raises a particular problem : the threat is developing towards the use of increasingly larger ammunition calibres (5.56, 7.62, 12.7 then 14.5 and even 20mm) with ever better penetration performances ; however, the desired protection level, which should be the best possible, must remain compatible with an acceptable level of mobility. This is one of the challenges of the FELIN programme.

## 4. CONCLUSION

The use of weapons is evolving, and so are technologies, breakthroughs are appearing in certain fields. Ballistics, which is at the heart of air-land military operations, must provide a suitable answer to the new operational requirements.

DGA, the French government organisation for weapon procurement, is adequately structured to identify new trends in combat practices and technology developments. When contracting for technology studies, advanced concept demonstrators and weapon system programmes, DGA ensures that not only the various technology aspects are addressed but also the system integration and overall consistency aspects, taking into account stringent life-cycle cost constraints. For this purpose, DGA has a comprehensive range of experts and assets which can adequately address all areas of ballistics, from threat assessment, specification preparation and continuous evaluation through simulation and testing.

# IMPENETRABLE INFRASTRUCTURES :
# A NEW CHALLENGE FOR THE NEW MILLENIUM

## A. DARRIGADE[1], E. BUZAUD[2]

[1] : DGA/DCE/CEG 46500 GRAMAT
[2] : DYNALIS - Rue Lavoisier - BP 24 - 91710 Vert-Le-Petit

**Abstract** : The work presented here concerns characterization of some High Performance Concretes ( HPCs ) with unconfined compressive strengths between 140 and 600 MPa. Penetration and perforation tests have also been performed with a 1000 lbs bomb like projectile and with a plain steel projectile. Experimental results are compared with numerical simulations, using Krieg and MCWS models, and with Penco2D analytical simulations. This analytical tool is used to evaluate some emerging concepts in penetrators field.
This work contributes to improve understanding of models definition and HPC behaviour in terminal ballistic. Results indicate the high protection capacities of this kind of materials and the technological gap needed to go through.

## 1. INTRODUCTION

The Centre d'Etudes de Gramat ( CEG ) is at the meeting point of different national defense requirements in the field of concrete infrastructures and has to perform assessments of weapon efficiency and structure vulnerability.

CEG has been involved for a few years in the evaluation of different High Performance Concretes face to shaped charges and perforating bombs for the benefits of French MoD or armement companies. STBFT, the army technical office involved in hardened infrastructures, is our partner to manage this work. The studies contain full and reduced scale testings as numerical computations and bring informations on numerical technics, concrete models, penetration mechanisms and capacities of HPC to protect infrastructures.

HPCs constitute a large material group in constant evolution which has, for instance, quite a few applications in military field. Nevertheless, their mechanical, static and moreover dynamic properties could be interestingly used to improve the protection of strategic infrastructures.

Materials tested till now at CEG and presented in this paper are :

**Table 1 : Materials definition**

| Material | Supplier | $f'_c$ (MPa) | $\rho_o$ (kg/m$^3$) |
|----------|----------|--------------|---------------------|
| BPR 200  | Bouygues | 220          | 2500                |
| BPR 300  | Bouygues | 297          | 2545                |
| BPR 600  | Bouygues | 580          | 2951                |
| CRE 140  | Lafarge  | 145          | 3300                |

## 2. HPC MECHANICAL CHARACTERISTICS [1,2,3]

Unconfined compressive strength $f'_c$ is the main characteristic used in civil engineering for concretes. Whereas the $f'_c$ value for common concrete is about 40 MPa for a density of 2200 kg/m³, it is in the 140 to 600 MPa range for HPCs tested here. But this gap in unconfined compressive strength, even if very noticeable, is not enough to explain HPC mechanical and ballistic performances. Isotropic compression curves and failure envelops give an other consideration of their capabilities.

### 2.1 Isotropic compression

Isotropic compression curves ( Figure 1 ) represent the compaction influence and the "cold" part of the equation of state. HPC exhibit a higher resistance to isotropic compression than common concrete but without direct connection with unconfined compressive strength.
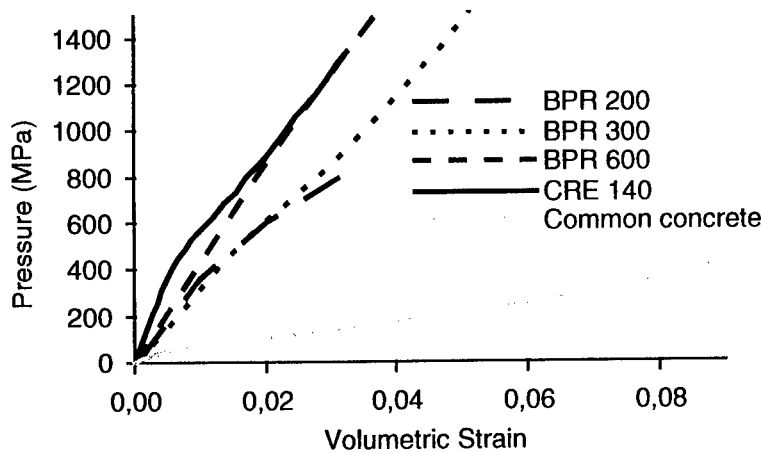


**Figure 1 : Isotropic compression**

### 2.2 Failure envelop

These curves ( Figure 2 ) represent the influence of isostatic compression on the resistance to shear rupture. But, once again, there is no evidence of the influence of the concrete unconfined compressive strength.
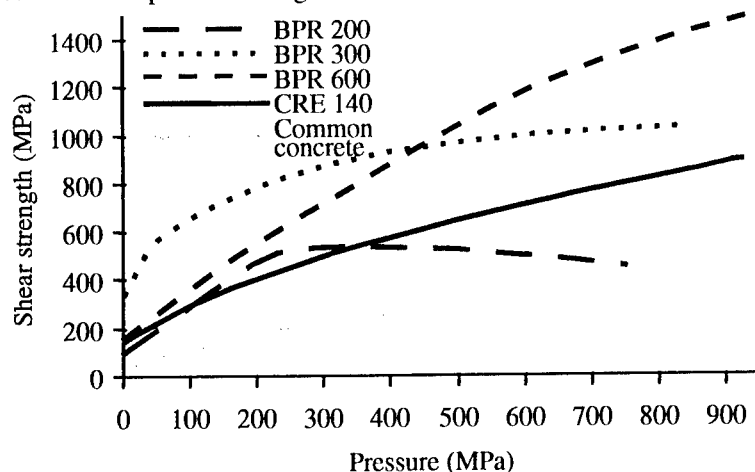


**Figure 2 : Shear strength at failure vs pressure**

## 3. TERMINAL BALLISTIC PERFORMANCES

Two different terminal ballistic studies have been performed, both experimentally and numerically, with different concretes. One study, managed by STBFT, was related to the penetration of semi-infinite targets, the other, managed by CEG, was related to perforation of concrete slabs.

### 3.1 Semi-infinite targets penetration

CRE 140, BPR 300 and a common concrete have been used to study the penetration of thick target by a projectile similar to the 1000 pounds bomb.

7 tests have been performed, at scale 1/2 [4] and 1/5 [5] , with CRE 140 and common concrete and 9 numerical computations have been performed, at scale 1/1 [6], 1/2 [6] and 1/5 [7], with CRE 140, BPR 300 and common concrete.

#### 3.1.1 Projectile definition

Projectile :    1000 pounds bomb type at scale 1:1, 1:2 et 1:5
Casing :    35NC6
Nose :    Ogive CRH = 6
Filling :    Nylon type elastomer

| Scale | 1/1 | 1/2 | 1/5 |
|-------|------|------|-----|
| L | 2270 | 1135 | 440 |
| D | 300 | 150 | 60 |
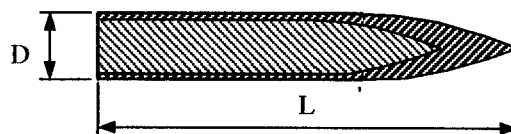
**Table 2 et Figure 3 : Projectile definition**

#### 3.1.2 Target definition

For cost reasons, HPC targets have been built with a layer of HPC and a layer of common concrete for background confinement to avoid spalling ( Figure 4 ). Striking configurations are presented in Table 3.
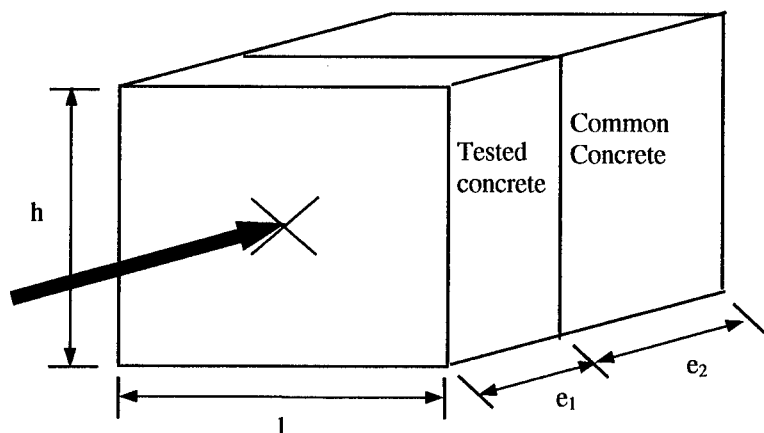
**Figure 4 : Target description**

**Table 3 : Experimental and numerical configurations**

| Concrete | Scale | l | h | $e_1$ | $e_2$ | Type |
|---|---|---|---|---|---|---|
| Standard | 1:1 | 6.0 | 6.0 | 5.0 | 0.0 | S |
| CRE 140 | 1:1 | 6.0 | 6.0 | 5.0 | 0.0 | S |
| BPR 300 | 1:1 | 6.0 | 6.0 | 5.0 | 0.0 | S |
| Standard | 1:2 | 2.0 | 2.0 | 1.5 | 0.0 | X/S |
| CRE 140 | 1:2 | 2.0 | 2.0 | 0.5 | 0.7 | X/S |
| BPR 300 | 1:2 | 2.0 | 2.0 | 0.5 | 0.7 | S |
| Standard | 1:5 | 1.0 | 1.0 | 1.0 | 0.0 | X/S |
| CRE 140 | 1:5 | 1.0 | 1.0 | 0.2 | 0.8 | X/S |
| BPR 300 | 1:5 | 1.0 | 1.0 | 0.2 | 0.8 | S |
| S : Simulation | | | | | | |
| X : Experimentation | | | | | | |

Impacts are on the target center, without incidence at 300 m/s.

### 3.1.3 Computation definition

Computations have been performed with LS-DYNA2D. Models are elastoplastic with linear hardening for bomb's casing, hydrodynamic for filling and Krieg's model [8] for concrete. Krieg's model, initially defined for soils and crushable foams, already exhibits good capacities to represent concrete penetration.

### 3.1.4 Launcher

The launcher used here is the Ø300 gaz gun based at CEA/CESTA facilities. Sabots have been used for 1/2 scale testings and calibre reduction for 1/5 scale testings.

### 3.1.5 Results

For common concrete, experimental and numerical results, at all scales, are in good agreement ( Figure 5 ). Scale factor apply correctly and computations are close to testings.
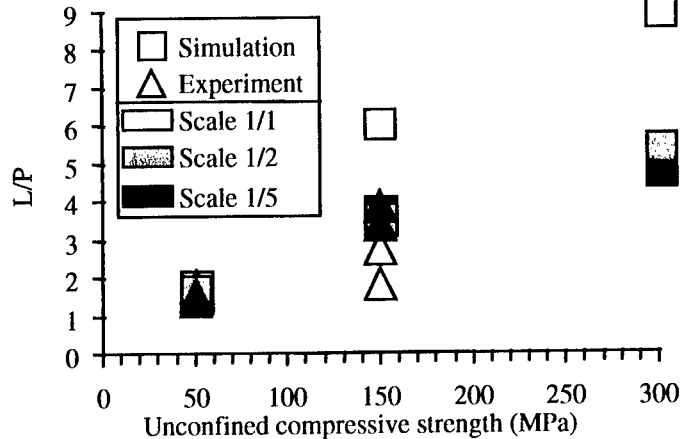


**Figure 5 : Experimental and numerical results**

On the other hand, CRE 140 and BPR 300 experimental and numerical results are much more scattered. This does not necessarily imply that HPC behaviour depends on strain rate or that models are not adapted to. In fact, face to HPC, the projectile, instead of having a nearly rigid behaviour, is subjected to much more strain and damage than it is supposed to do ( Figure 6 ).
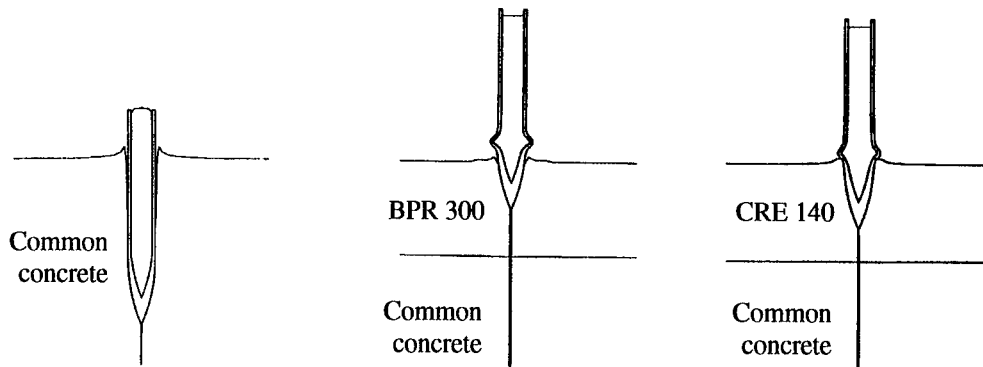


**Figure 6 : 1/2 scale numerical results**

CRE 140 1/2 scale experiments confirm these very large strains.

### 3.2 Slab perforation [3]

CRE 140, BPR 200 and BPR 600 concretes have been used to study perforation of thin slabs by a plain projectile.

Scale used for these testings is much lower than the one usually allowed with concrete. But these HPC have a quite good homogeneity that give us the opportunity to perform valid small scale experiments.

### 3.2.1 Projectile definition



Material : 35NCD16
Mass : 500 g
Nose : Ogive CRH = 3
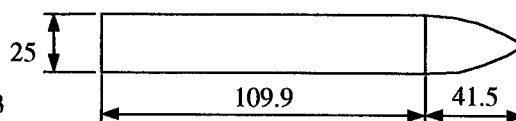
A CEG ∅32 powder gun have been adapted to launch this projectile.

### 3.2.2 Target definition

Target is a ∅500 mm circular slab with a 50, 100 or 150 mm thickness.
Impacts are on the target center, without incidence.

### 3.2.3 Computation definition

Computations are performed with LS-DYNA2D. Model used for the projectile is elastoplastic with linear hardening. Concretes are modeled with Krieg [8] or Malvar - Crawford - Wesevich - Simons ( MCWS ) [9] models.

### 3.2.4 Results

Results of the 13 testings are presented in Table 4.

**Table 4 : Experimental configurations and results**

| Target type | Target thickness | Initial velocity | Experimental residual velocity |
|---|---|---|---|
| | (mm) | (m/s) | (m/s) |
| BPR 200 | 110 | 550 | 425 |
| BPR 200 | 107 | 445 | 305 |
| BPR 200 | 56 | 335 | 278 |
| BPR 200 | 55 | 250 | 168 |
| BPR 200 | 50 | 135 | 10 |
| BPR 600 | 105 | 560 | 351 |
| BPR 600 | 104 | 440 | 255 |
| BPR 600 | 50 | 352 | 249 |
| BPR 600 | 52 | 250 | 151 |
| BPR 600 | 53 | 140 | 0 |
| CRE 140 | 156 | 547 | 20 |
| CRE 140 | 105 | 545 | 350 |
| CRE 140 | 103 | 445 | 234 |
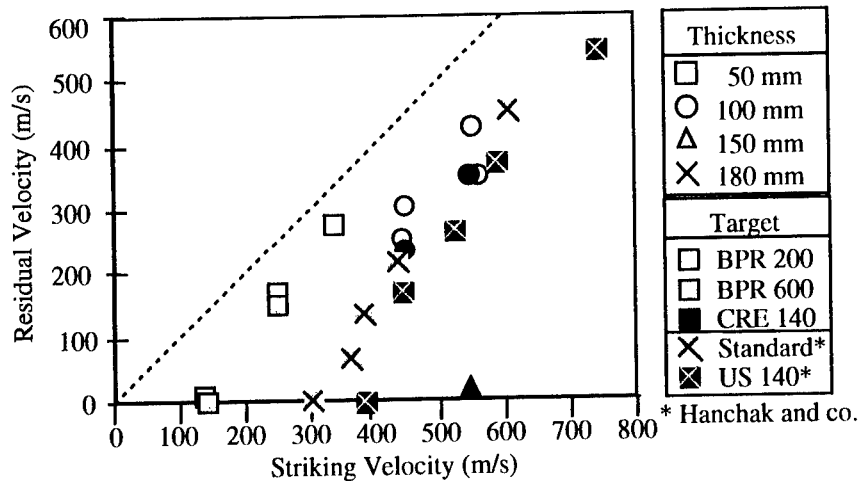


**Figure 7 : Experimental results**

CEG results can be compared with these published by Hanchack and co. [10] ( Figure 7 ). Projectile is similar. Square 178 mm thick 610 mm large targets are made of a common concrete or a high performance concrete noted here US 140. Unconfined compressive strengths are, respectively, 48 MPa and 140 MPa.

CRE 140 and BPR 600, with a thickness of 100 mm, are as efficient for ballistic protection as a common concrete with a thickness of 180 mm. On the other hand, US 140 is just slightly better than the common concrete, with the same thickness, in spite of an unconfined compressive strength similar to CRE 140.

### 3.2.5 Computation - experiment comparison

Numerical and experimental residual velocities are in a good agreement ( Figure 8 ).

Krieg model [8], which takes into account only compaction and shear pressure sensibility, is less efficient than MCWS model [9], which, in addition, takes into account damage and

- 610 -

strain rate effects. Scattering of results is still important and other works are needed to obtain new more predictive models.

The analytical code Penco [11] is designed to assess projectile trajectory in soil or concrete using spherical cavity expansion. The code, based on concrete density and unconfined compressive strength, has a precision similar to hydrocodes models.
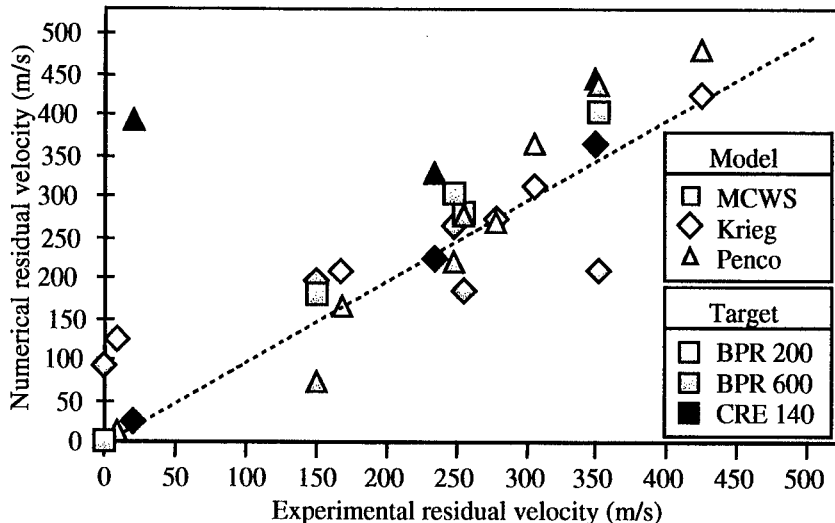


**Figure 8 : Numerical vs Experimental residual velocity**

### 3.3 New technologies to go through

#### 3.3.1 High Striking Velocity Concept

Recent publications mention new penetrators with high striking velocities up to 1000 m/s or 1500 m/s. We never evaluate Penco 2D at such high velocity. Nevertheless, as long as rigidity hypothesis is acceptable, and a penetrator have to remain undeformed to preserve the payload efficiency, Penco 2D is thought to be able to give first order results. On the other hand, HPCs have not been experimentally tested above 800 m/s ( with small caliber projectiles ), but as those materials exhibit no highly brittle behaviour, they are supposed to keep, at least, their ballistic capacities.

With those precautionary hypothesis, we can compare deceleration level and penetration depth for the 1000 pounds like bomb, from conventionnal to high striking velocity, face to common concrete and HPC targets ( Figure 9 ).
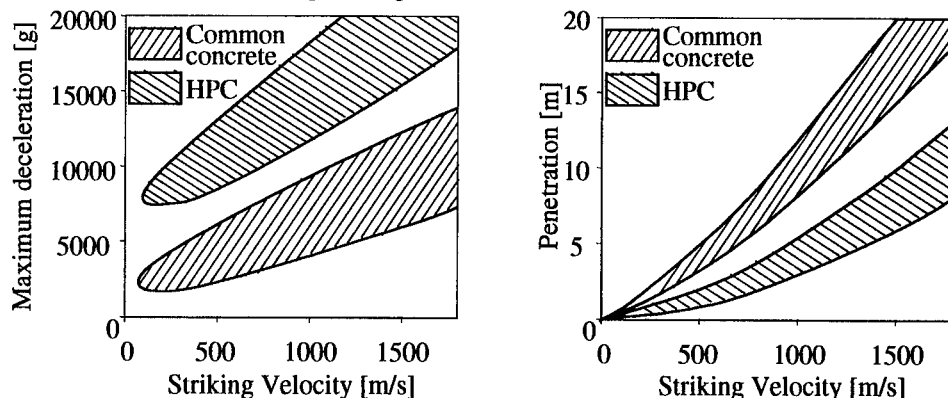


**Figure 9 : High striking velocity**

- 611 -

The maximum deceleration level on HPC have a 2 to 4 ratio over the one on common concrete. The maximum deceleration levels at high velocity on common concrete and at conventionnal velocity on HPC are similar, and we have seen what it means in terms of structural effects for current weapons.

Maximum penetration depth reachable at high striking velocity on common concrete is in the 15 m to 20 m range. But this penetration depth is reduced by half on HPC.

### 3.3.2 Front Shaped Charge Concept

The front shaped charge concept is describe in Figure 10.
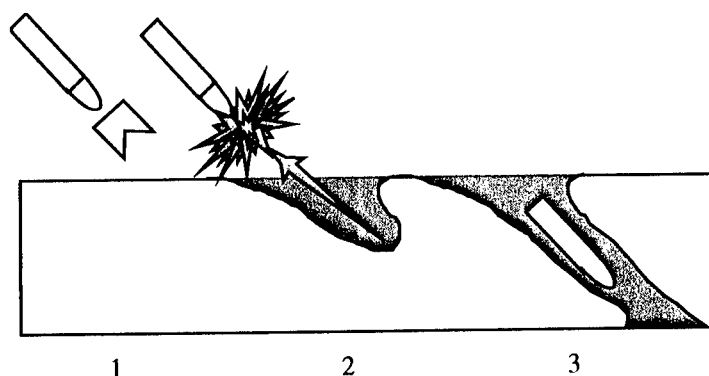


**Figure 10 : The Front Shaped Charge Concept**

A front shaped charge is fired just before impact on the target surface. The shaped charge jet generate a hole, allowing the following penetrator to go through the target with limited contacts with the hole sides.

If the shaped charge have been designed for a common concrete target, the jet hole sizes may vary in an HPC target, essentially due to the HPC higher density. HPC density is about 50% higher than common concrete's one. This lead to a 20% reduction of jet hole depth, but a 12% increase of jet hole diameter, with the hypothesis of a constant volume hole.

The increase of hole diameter allows an easier passing through of the following penetrator. On the other hand, the decrease of the hole depth, or the increase of the target residual thickness, is not necessarily a huge obstacle as the remaining material, supposed to be not to far from the rear free surface, have been subjected to an intense tensile stress which could have cause its failure.

This concept seems to be efficient against HPC targets.

### 4. CONCLUSIONS

Works on HPC show that a new kind of infrastructure protection is raising which can not be defeated by current and even some new penetrator concepts.

Numerical computation is already an efficient tool to perform studies on new penetrators design or efficiency. However, better models could improve phenomena understanding and simulation capabilities.

## REFERENCES

[1] : J. Cagnoux, D. Don, "Etude de pénétration des bétons : caractérisation triaxiale d'un béton haute résistance de la société Bouygues", Note Technique T93-43 n° 356/CEG/DM/CI

[2] : E. Buzaud, D. Don, "Etude de pénétration des bétons : caractérisation triaxiale d'un béton haute résistance de la société Lafarge", Rapport Technique T96-11 n° 150/CEG/DM/CI

[3] : A. Darrigade, E. Buzaud, "Performances mécaniques et balistiques de bétons à hautes performances", Note technique T99-014 n° 046/CEG/DT/EA/CD/CI

[4] : Compte rendu d'expérimentation du STBFT, "Durcissement des installations de l'Armée de l'Air", 08/89

[5] : Compte rendu d'expérimentation du STBFT, "Durcissement des installations de l'Armée de l'Air", 06/90

[6] : J. Cagnoux, E. Buzaud, "Simulations numériques de pénétration de différents bétons par la bombe de 1000 livres", Note Technique T95-06 n° 067/CEG/DM/CI

[7] : J. Cagnoux, E. Buzaud, "Simulations numériques de la pénétration de deux bétons haute résistance et d'un béton standard par la bombe de 1000 livres à l'échelle 1/5", Note Technique T95-22 n° 209/CEG/DM/CI

[8] : Krieg R. D., "A simple constitutive description for soils and crushable foams", Sandia National Laboratory, report n° SC-DR-72-0883, 1978

[9] : Malvar L. J., Crawford J. E., Wesewich J. W., Simons D., "A plasticity concrete material model for DYNA3D", International Journal of Impact Engineering, Vol. 19 N° 9-10, pp 847-873, 1997

[10] : S.J. Hanchak, M.J. Forrestal, E.R. Young, J.Q. Ehrgott, "Perforation of concrete slabs with 48 MPa and 140 MPa unconfined compressive strengths", Int. J. Impact Engng Vol 12, N0 1, pp 1-7, 1992

[11] : D.C. Creighton, "Non-normal projectile penetration in soil and rock : User's guide for computer code Penco2D", Waterways Experiment Station, Technical Report SL-82-7, 1982

# INSTRUMENTATION FOR BALLISTIC METROLOGY AT ISL: RECENT APPLICATIONS AND FUTURE DEVELOPMENTS

SOMMER E., KREITZ J., RATEAU PH.

ISL, French-German Research Institute, BP-34, F-68301 Saint-Louis, France

**Abstract :** ISL's department for Optronics and Telemetry for Ballistics (OTB) covers a wide range of applications with its onboard instrumentation techniques, ranging from measurements in 30 mm projectiles up to 155 mm artillery shells. Data acquisition and data transmission devices have been developed and successfully applied to different measurement tasks. Various sensors of the commercial market have been adapted to the requirements of ballistic applications. This includes electro-optical devices for imaging tasks, temperature sensors for heat flux measurements, magnetic transducers for roll or attitude determination and a C/A-code GPS receiver. Extensive testing as well as numerical simulations have been performed to certify that the applied modifications for g-hardening are successful.

This paper summarizes the available techniques, shows some of the recent applications and will mention future developments.

## 1. INTRODUCTION

Since more than 20 years instrumentation of projectiles is a basic tool for testing the design and supporting the development of new weapon systems. Nowadays it becomes more and more a must in future smart munitions for guidance or fuse enhancement, for sophisticated sub-munitions or battle damage assessment devices. Reduction in size and weight of electronic components, increased integration level of different technologies and the ability to simulate complex systems have enabled a wide spread of instrumentation possibilities. This paper will show some progress on a research level, supporting as well basic studies as commercial product development.

## 2. COMPONENT TESTING

Instrumentation of projectiles essentially depends on the components that can survive the harsh conditions of a gun launch. G-loads from 15 000g up to 100 000g are the common range in this area. As most of the components available on the market do not resist from the first these g-levels, g-hardening is mandatory. Depending on the specific task, the components intended for use have to be certified for the expected acceleration levels.

ISL uses different techniques for pre-/post-launch comparative tests or in-flight characterization. For the lower g-levels the vertical launch is often used. As the required facilities are not close to ISL (available at the WTD91 in Germany and the ETBS in France) they are only used if a certain quantity of different com-
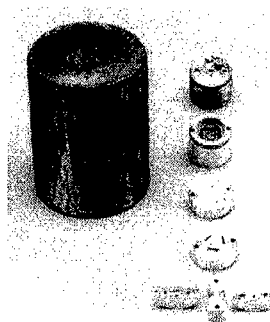


Figure 1: Test container

ponents can be tested together. An instrument available at ISL is the RAM-accelerator which is used in deceleration mode as soft recovery tool [1]. Figure 1 shows a cargo cylinder with some samples after test. For the high acceleration levels where soft recovery is a problem, in-flight testing with either direct wire transmission or onboard telemetry is performed.

## 3. TELEMETRY TRANSMITTER

This miniaturised S-Band telemetry transmitter (s. Fig. 2), developed at the ISL [2], offers versatility for ballistic metrology. With a power consumption of 2.5Watt, the transmitter provides an RF output power of 0.5Watt with an overall DC to RF efficiency of about 20%. The carrier frequency is software programmable between 2200 and 2300MHz by means of a three wire interface. Carrier frequency stability is established by a quartz oscillator that provides a stable reference for the PLL. The transmitter is capable to send standard monochrome video signals. The large modulation bandwidth also allows the transmission of FDM or TDM data with reasonable data rates in multi channel environments. Because of its locking and tracking behaviour transmission in short range applications, lasting one or several seconds after firing, are possible. The RF output power of 0.5Watt also allows long range applications, when the projectile remains in line of sight of the ground station antenna.



Figure 2: S-band telemetry transmitter

The transmitter has been used successfully under various g-loads in different projectiles (from 15000g in 155mm calibre up to 35000g in 90mm calibre) and distances from 1km up to 17.5km. Some results from these applications will be shown later.

Future telemetry development will focus on two topics: onboard transponder systems and pure digital modulation techniques. Transponders can either serve as a tool for projectile guidance with the ability of a two way communication or as relay stations in unfavourable long range telemetry applications (no line of sight transmission path). Digital modulation will offer an enhanced signal-to-noise behaviour and higher data rates compared to analogue techniques. It will be applied in a new telemetry transmitter and in a relay transponder system as well.

## 4. ANTENNAS

Microstrip antennas were invented for application as conformal antennas on missiles and air-craft. They can be fabricated using lithographic techniques in printed circuits. Different types can be formed with simple geometric structures like discs, annular rings, rectangles... Planar arrays and wrap-around antennas can be built using strong coupled or quasi non-coupled elements. Depending on geometry, placement, orientation and feed-network design nearly every radiation diagram can be realised. If an antenna consists of only one radiating patch, this will allow integration into small projectiles or in a small part of an artillery fuse. Different types of



Figure 3: Microstrip antenna mounted on nose

-616-

microstrip antennas have been studied at the ISL [3]. The mechanical stability was found to be sufficient to resist high g-loads when using suitable materials and proper mounting. Some antennas were successfully tested up to 40 000g. One of these designs, a stacked circular-disc antenna, is shown in Fig. 3 . At 2.25GHz the gain is about 8dB and the half-power beamwidth 70°. The input is sufficiently matched over the whole telemetry S-band (2.2 ... 2.3GHz). Antennas of the same type, mounted at the projectiles bottom, also survived tests without an additional protection.

## 5. DATA ACQUISITION DEVICES

For various in flight measurements radio transmission of acquired data is not useable or not recommended. Typical applications are in-bore measurements or terminal ballistics studies. For these tasks we have developed an autonomous data acquisition system which serves as transient recorder for high speed data capturing and storage [4]. This recorder is micro controller based which allows the acquisition parameters to be chosen depending on the requirements. The device can handle up to 4 or 8 analog input channels and acquires 32Kbytes of data with a maximum rate of 500kHz (see Figure 4).

Acquired data are either read back after recovery of the projectile or can be transmitted by telemetry in a free flight phase by means of the included PCM-encoder. The device has also been used as a flight recorder for system monitoring in differently instrumented projectiles. The non-volatile data retention capability without backup battery assures that error analysis is still possible even on total failure of the other systems.



Figure 4: Transient recorders for ballistics

The PCM-encoder alone is also used as a channel multiplexer which digitizes multiples analog signals and feeds the time multiplexed data into the modulation path of the above mentioned transmitter. This approach avoids the necessity of multiple sub carriers in the transmitter and the corresponding frequency discriminators in the receiver signal chain.

The achieved raw data rate is about 1Mbit/s which corresponds to a 90Kbytes/s throughput. Future enhancements will improve ADC resolution to 12Bit and increase the available data memory. Single channel devices with higher data rates are also under development.

## 6. APPLICATIONS

### 6.1 Fuse temperature measurements

An investigation for image acquisition in a 155mm artillery projectile is underway (Project D2C) which requires knowledge of the expected heating of the projectile nose during flight. This is as well important to protect the optical and electronic components from damage as to predict the thermal radiation onto an IR sensor housed in the nose. A registration fuse was equipped with thermal sensors to measure the temperature variation during flight. The coaxial transducers, build at ISL, are placed close to the surface and inside the nose to allow comparisons to theoretical heat flux calculations [5]. Data were transmitted to a ground station with ISL's S-band telemetry over a range of 17km.

A different temperature measurement was performed on a fiber glass reinforced nose. In this application data were not transmitted by telemetry but stored in the transient recorder men-

tioned above. This approach requires less effort because all the electronics are integrated in the registration fuse and the body of the original projectile does not have to be modified. The measurement results from a 155mm artillery shell are shown in Figure 5. Initial launch velocity was 640m/s. The upper trace represents the temperature close to the tip, the lower trace corresponds to the temperature of the internal reference point.
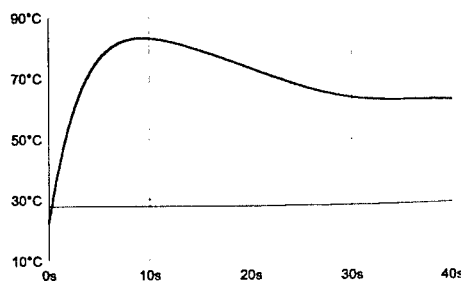


Figure 5: Fuse temperature

## 6.2 Magnetic roll angle sensors

The use of the earth's magnetic field can serve for different purposes in spinning projectiles: to support or even replace the inertial system for guidance and navigation [6], and to synchronize roll angle dependent sensors or actuators like imaging devices or trajectory correcting forces. A 3-axis magnetic sensor based on magneto-resistive transducers has been developed



Figure 6: 3-axis magnetic field sensor
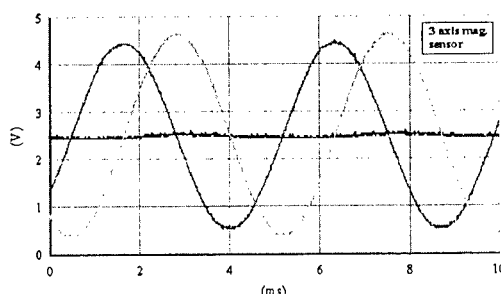


Figure 7: 3-D magnetic roll signals

which allows to measure the 3-D movement of a projectile (s. Fig.6). The attainable accuracy is measured to be better than of 1.5 degrees [7]. An example of transmitted roll data from a 155 mm projectile is shown in Fig. 7.

## 6.3 Terminal ballistics

Penetrator design and testing is very expensive, so down scaled modes were fired instead. The behavior of these models is different to the full scale penetrator, which requires additional numerical simulation. Onboard acceleration measurements can support the theoretical models by in-flight data. Accelerometers and ISL's non-volatile data acquisition system were integrated into a 1" model [8]. This device will allow for 1- to 3-dimensional acceleration measurements. Data were read back from the transient recorder after recovery of the model.



Figure 8: Penetrator instrumentation packages

Figure 8 shows the instrumentation package: the left part includes the transducers and the data acquisition system, the right one contains the batteries. These packages are connected by a miniaturized 9-pin shock tested connector. Evaluation of the system is going on.

## 6.4 Image acquisition

Image acquisition has been demonstrated successfully with a CCD area sensor in a 90 mm non-spinning projectile [9]. A look into an equipped model shows Fig. 9. Spinning of the projectile introduces smear on the image if the exposure time is not very short. An other approach uses the spin to scan the area in the line-of-sight. A low cost linear photo diode array was mounted in the tip of a spinning projectile to build a circular scanning device (s. Fig. 10). Individual line scans are synchronized by roll angle information from the magnetic sensors mentioned above. This allows to reconstruct the observed scene by properly combining the transmitted scans afterwards in an inverse scanning algorithm [10].
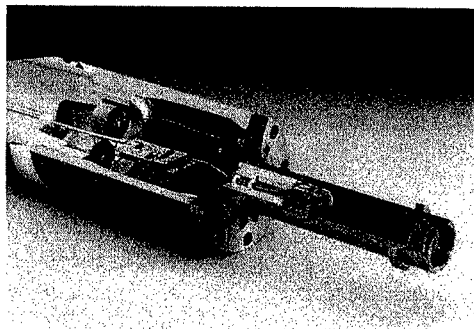


Figure 9: Image acquisition projectile
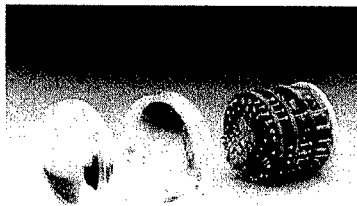


Fig. 10: Image scanning device
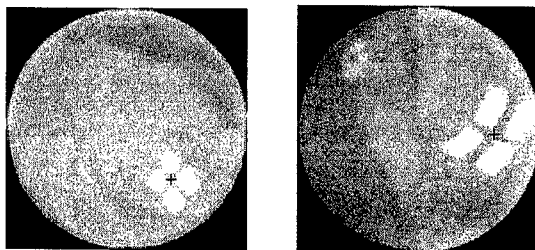


Fig. 11 : Reconstructed images

Figure 11 shows the obtained images of a simple black cross on a white background, acquired over a range of 200m (left) and 50m (right). The spinning rate of the projectile was about 30/sec. The projectile's nutation is clearly visible in these images.

## 7. ONBOARD GPS SYSTEM

GPS (Global Positioning System) has become a reliable tool in guidance and navigation for rockets and missiles. Applying this technique to projectiles is quite attractive especially for
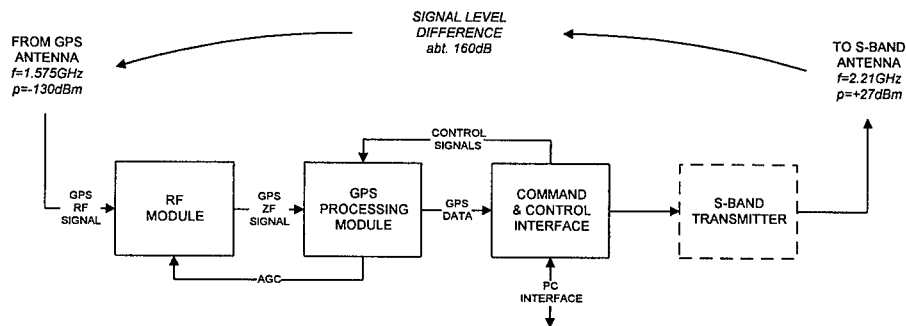


Figure 12: Block diagram of onboard GPS-system

future long range munitions, but it is more difficult to implement because launch loads and dynamics are much higher. An C/A-code system was designed at ISL and successfully fired in a 155mm shell [11]. The block diagram is shown in Fig. 12.

A passive non-ideal mono-pole antenna mounted in the projectile nose feeds the GPS-signal into the RF module which consists of a two stage low noise amplifier, a GPS-RF band filter, a RF front-end IC and a quartz reference. Special attention has to be paid for the reference clock which should have low phase noise and must be shock resistant. As navigation data are transmitted to a ground station the design of the amplifier section has to take into account the great signal difference between the high S-band transmitter power and the low received GPS signal (about 160 dB). This was achieved by a high dynamic range and narrow band adaptation of the RF input. Additionally all modules are realized with proper shielding and decoupling as demonstrated in the RF-module (s. Fig. 13).
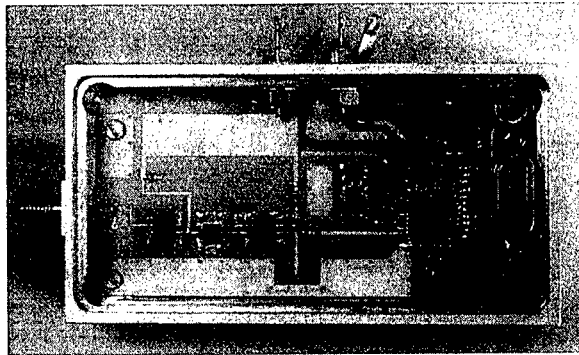
A control unit performs the link to a computer for system setup and monitoring. It also schedules the different tasks during the experiment (pre-flight, launch, post-launch phases) and does the data encoding for the radio transmis-



Figure 13: GPS RF-module

sion. First tests have shown the feasibility of this concept, the achieved accuracy was found to be within the expected limits. Future work will focus on an enhanced antenna design and the investigation of component and subsystem behavior to improve the overall system performance.

## 8. CONCLUSION

The examples described above have demonstrated that a variety of measurement tasks can be solved successfully with the available instrumentation tools and techniques. The continuing progress in projectile development however involves a permanent adaptation to future measurement requirements. The fast innovation steps in micro electronics and in transducer design will lead to new measurement techniques in the near future. With these techniques and the ongoing enhancements mentioned above we try to satisfy the rising new demands.

## 9. REFERENCES

[1] J-F. Legendre, M. Giraud, E. Sommer, "RAMAC 90 facility used as projectile recovery system - SIBREF 90-", in *49th Meeting of the Aeroballistic Range Association*, The Hague, Netherlands, (1998)
[2] J. Kreitz, "S-Band Telemetriesender für die ballistische Meßtechnik", ISL-Report to be published
[3] Ph. Rateau, P. Hirzlin, "Antennes microrubans á large bande passante pour télémesure balistique en bande L ou S", ISL-Report RT-516/1995, Saint Louis, France, (1995)
[4] E. Sommer, A. Lentz, "Transientenrekorder für die ballistische Meßtechnik", ISL-Report to be published
[5] P. Gnemmi, E. Sommer, K.W. Naumann, V. Fleck, "Aerothermal Study of a Projectile in Flight: Experiment-Computation Comparison", in *18th International Symposium & Exhibition on Ballistics*, San Antonio, TX USA, pp.94-101, (1999)
[6] V. Fleck, "Determination of the Angular motion and of the Aerodynamic Coefficients from 3D Magnetic Sensor Signal", in *European Forum on Ballistics of Projectiles*, Saint Louis, France, (2000)
[7] Ph. Rateau, Ph. Wernert, E. Junod, "Détermination de la position en roulis d'un projectile en tir tendu ou courbe", ISL-Report to be published

[8] E. Sommer, A. Lentz, "Instrumentierung von kleinkalibrigen Penetratormodellen zur Messung des Eindringvorganges ", ISL-Report to be published

[9] Ph. Rateau, P. Raymond, F. Christnacher, "Formation et transmission temps réell d'images à bord d'un projectile soumis à de fortes accélérations", ISL-Report RT-501/98, Saint Louis, France, (1998)

[10] E. Sommer, J. Kreitz, A. Lentz, "Drallsynchronisierte Bildabtastung mittels linearer Diodenzeile im Projektil", ISL-Report to be published

[11] J. Kreitz, E. Sommer, "Untersuchungen zum Einsatz von GPS in rohrverschossenen Projektilen", ISL-Report to be published

# UNDERWATER BALLISTICS IN THE TRANSONIC DOMAIN: FIRST COMPUTATIONAL RESULTS WITH THE CODE OTiHULL AND FIRST EXPERIMENTAL RESULTS IN A MODEL BASIN

SCHAFFAR M., PFEIFER H.J.


ISL, French-German Research Institute, BP 34, F-68301 Saint-Louis, France

**Abstract:** This paper presents our first two-dimensional calculations with the commercial code OTiHULL for the cavities created in water by high speed projectiles. The velocity domain from 1000 to 2500m/s was studied with cylindrical and conical projectiles. The results show : - the cavities are predicted to be not larger in diameter than 3D ( D is the projectile diameter) - the drag coefficient increases with the velocity, - the drag coefficient decreases with the ratio (cavitator diameter/D)$^2$. However for cavitators smaller than 0.2D the computation does not converge anymore. These results have to be confirmed with 3D computations and the stability of the projectiles has to be controlled.

## 1. INTRODUCTION

The interest in studies and experiments on high speed projectiles in water became more important in the last years [1].
At ISL recently a bibliographic research began on the underwater ballistics in the transonic domain (speeds from 1000m/s to 1800m/s). Underwater projectiles may be used from submarines to attack other submarines or some torpedos in the near vicinity of the defender.
It is a well known phenomenon that high speed underwater projectiles undergo dramatical velocity drops because of the drag in water; nevertheless above a certain speed limit the projectile will travel in the supercavitation regime, that means only the nose (cavitator) of the projectile will produce drag and the rest of the body will travel in a gaz-vapor bubble, and so the total drag may be similar to that in air!
If the cavitator is well designed and if the initial speed is high enough the final speed at the target may be high enough to cause severe damages on a submarine or on a torpedo for a range of distance of 400m for example.

The bibliographic research shows rapidly that there are not too much computational methods available for a direct computation of a cavitating projectile travelling at speeds near the sonic speed in water. The only method we can use was an hydrocode of continuum mechanics named OTiHULL.

We will describe briefly the code and the first results obtained for cylindrical and conical projectiles. At the end we will give some news about our experiments.

## 2. PRESENTATION OF THE CODE OTiHULL

### 2.1 Generalities

The code OTiHULL [2] is an Euler and/or Lagrange code, with finite differences, which is able to compute the entry of a projectile into material like water or steel, etc.
The preprocessor creates a rectangular grid, and the projectile is cut in this grid and so the conical form is divided into a step (this can be avoided if we use the coupled Euler/Lagrange calculation). The code solves the equations of the continuum mechanics and uses equations of state to take into account the materials and the high pressures generated by high speed projectiles. We use the Mie-Gruneisen equation of state, with the following equation:

$$P = P_H(1-0.5\Gamma\mu) + \Gamma\rho(I - I_0) + P_0 \quad (1)$$

where $P_H$ is the pressure on the Hugoniot curve, P is the pressure, $\Gamma$ is the Gruneisen coefficient for water (0.28), $\mu$ is the compression coefficient $(\rho/\rho_0-1)$, I is the internal energy, $\rho$ is the density (0 is the index for the free flow). The validity of the Mie-Gruneisen equation of state for water is not easy to verify, but in the transonic regime we can compare the results with the Tait equation for water (used for underwater explosions) given below :

$$P - P_0 = B ( (\rho/\rho_0)^n - 1) , \quad (2)$$

where $B = \rho_0 a_0^2/n$ , $a_0$ is the sound velocity in water, n is an experimental value here equal to 7.15 ; we found a reasonable agreement for velocities near the sonic speed in water.

In our computations the initial pressure is the atmospheric pressure ( $1.01325.10^6$ dynes/cm$^2$ ) and the ambient temperature is 288K. The gravity is not taken into account for the first calculations, but it may play a role for horizontal underwater shots. The hydrostatic pressure is also an important parameter and for some tests, we set this pressure at 11,51 and 101 bars.

With the code we can compute two types of projectile: the first named "island" which is not deformed during the test and the second which may be deformed. In the "island" case, we compute after every 5 cycles the forces acting on the projectile and the velocity loss of the projectile; with these quantities, we can compute the drag of the projectile.

### 2.2 Type of projectiles tested

The first projectile tested (see Figure 1) is a cylinder of diameter 1cm and of length 10cm.
The computation is two-dimensional, that means axisymmetrical, and the reservoir is also a cylindrical tube of a diameter of 40cm.
The second projectile (see Figure 1) is a truncated cone with a cylindrical rear body; the front part is the cavitator whose diameter is varied from 1cm to 0.1cm, the total length being always 10cm. With the rectangular grid, the cone is changed into a stair.
The computation can be started either with the projectile in the reservoir which is suddenly moved from the rest to the chosen velocity or the projectile enters into the reservoir through a membrane.

The crater created by the projectile looks like a cavity bubble. Figure 2 gives an example of the cavity development for a cylindrical projectile: in the first picture, we see 2 cavities, the first starts

from the nose of the projectile and the second from the base of the projectile, but the real cavity in which we are interested in is the first one; we see also that after 90μs this cavity reaches the base and extends far away progressively.

In all cases, we have controlled the development of the cavity with the contour plot of the following variables: density, pressure, velocity and temperature. Sometimes, we place eulerian or lagrangian stations near the limits of the cavity or on a line perpendicular to the projectile to obtain a time evolution of the same quantities. From the "island" calculations, we compute the drag coefficient $C_X$.

## 3. RESULTS OF THE COMPUTATIONS

### 3.1 Some interesting features about the cavity

Figure 3 shows the cavity and the velocity vectors after 160μs and 480μs respectively near the base of the projectile. The limits of the cavity are not smooth just behind the projectile but these limits become more and more smoother downstream; the velocity vectors shows above and around the projectile the positive sense of propagation, but in the cavity we find some velocities that indicate the opposite sense towards the base; there are some vortices, but the density is very small.

On average, we find a low pressure in the cavity, typically between 0.03 and 0.01 bar and the density varies between $1.10^{-7}$ and $1.10^{-8}$ g/cm$^3$.

For one particular case, we have computed a cavity over more than 30 projectile lengths (8 days of computation); the projectile is located between 0 and −10cm on the X axis. Figure 4 shows the cavity between −140 and −340cm behind the projectile after 3.2ms : we find that the cavity is always existing after this time, there are no interrupts, only some small areas on the axis are lighter indicating that perhaps the cavity may be interrupted in the next ms.

We see also that the diameter of the cavity varies between 2.5 to 3 times the projectile diameter; this value is small in comparison with the approximated formulas [1] used in this case, these formulas give for the cavity a diameter of near 60 projectile diameter; this difference coms probably from the OTiHULL code, where the vaporization conditions are not clearly defined.

### 3.2 Effect of the velocity for the cylindrical projectile

For the velocity domain from 1000 to 2500m/s, we have tested the cylindrical projectile. Figure 5 shows the unsteady drag coefficient evolution with the time: in all cases, the curves reach a limit after near 50μs, and this limit increases with Mach Number.

Figure 6 shows the drag coefficient as a function of the Mach Number. Our results can be compared with the compressible formula published by Vasin [3]: the trends are the same, the drag coefficient increases with the Mach Number, but the results obtained with the code OTiHULL are near 20% above the values obtained by Vasin.

### 3.3 Effect of the cavitator diameter

From the diameter of the cylinder (1cm) we have progressively reduced the diameter of the front part of the projectile to 0.1cm, the projectile becoming tronconical. Down to a cavitator diameter of 3mm the computation seems correct and the unsteady drag coefficient converges towards an expected value. From the diameter of 2mm, the computation is correct only for 20 to 25μs, and

then the computation diverges!; the check of the pressure contour plot after 50μs shows some pressure artefacts on the conical part of the projectile, which becomes a step with the griding as we wrote early.

These artefacts are normal from the code designer point of view and are only avoidable with an coupled Eulerian/Lagrangian calculation; a test we made works for the diameter of 2mm but the time step is too small and the computation takes several days.

Figure 7 shows the variation of the drag coefficient with the diameter; for the 3 curves (black, blue and pink) the normalization factor is the cylinder diameter; for the red curve where the normalization factor is the cavitator diameter, we find approximately a constant value. The 3 other curves shows the same trend: the drag coefficient becomes very small when the diameter is decreasing, but the HULL results are above the approximate law $C_x=C_x(0)*(d/D)^2$, with $C_x(0)$ equal to the incompressible drag coefficient for a plate. Anyway the drag coefficient is approximately reduced by a factor of 100 when the diameter of the cavitator is reduced by a factor of 10, this is an interesting feature for the water penetration of projectiles.

**Remark**

We have also tested the influence of the depth, but only some qualitative effects appear, like interrupts of the cavity with a depth of 1000m, but the drag coefficient seems to be unchanged. The effect of the gravity was also tested, but the results are not very different from those without gravity. These computations will be made again in 3D case. The stability of the projectile is also one important parameter in this case and can only be controlled with 3D computations.

All the results presented here will be published soon in an ISL-Report [4].

## 4. EXPERIMENTS

Experiments in a water tank (see Figure 8) have been started recently, and up to now two shots were made with spheres at a velocity near 1600m/s. A test series is planned next with spheres of 1cm in diameter where we want to measure the pressure on the wall first before we built windows in the tank and before we define the parameters for the subsequent studies.

## 5. CONCLUSION

The results described in this paper confirm the high potential of high speed underwater bodies. This is especially true with respect to military applications. It turned out that substantial efforts will be needed in particular to extend the 2D model to the 3D one.

It is also obvious that the computational results call for experimental validation.

## 6. REFERENCES

[1]  Workshop AGARD, "High speed body motion in water", Kiev , Ukraine, 1-3 Sept 1997
[2]  D.A. MATUSKA, J.J. OSBORN, E.W. PIBURN, "HULL Documentation, Users Manual" Orlando Technology, Incorporated, Shalimar, Florida, 1991
[3]  A. VASIN, "Calculations of axisymmetric cavities dowstream of a disk in supersonic flow", Fluid Dynamics, Vol.32, n°4,1997.
[4]  M. SCHAFFAR, "Balistique sous-marine et projectiles supercavitants: méthodes de calcul et premiers résultats avec le code OTiHULL" , ISL-Report  to be published
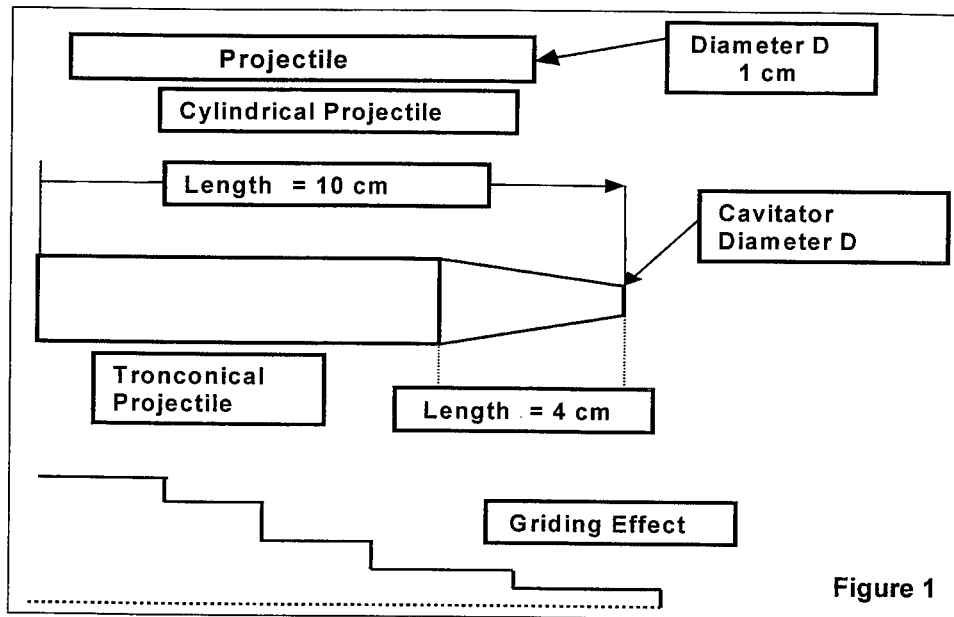
Figure 1

## Contour Plot of the Density – Cylindrical Projectile – Velocity 1300 cm/s



65cm

40cm

-12,5        0        12,5

30 µs

60 µs

90 µs

**Velocity = 1300 cm/s**
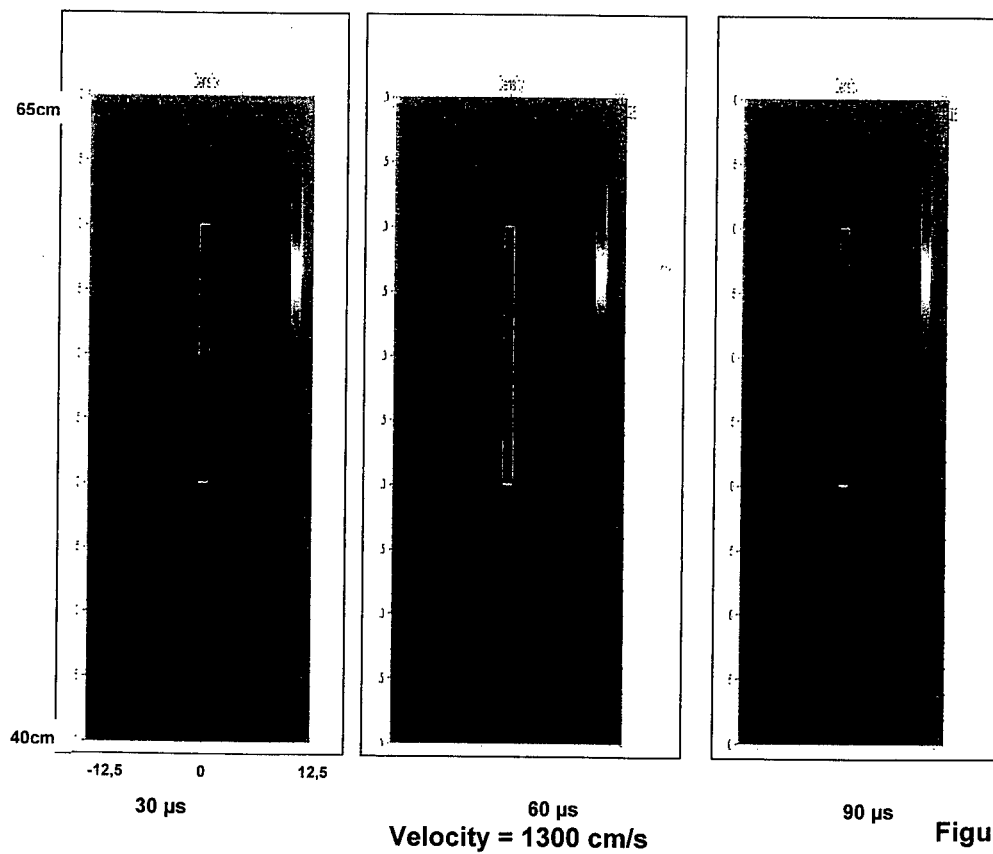
Figure 2

## Tronconical Projectile with Cavitator Diameter 4mm - Velocity 1300cm/s



160 μs

160 μs

480 μs
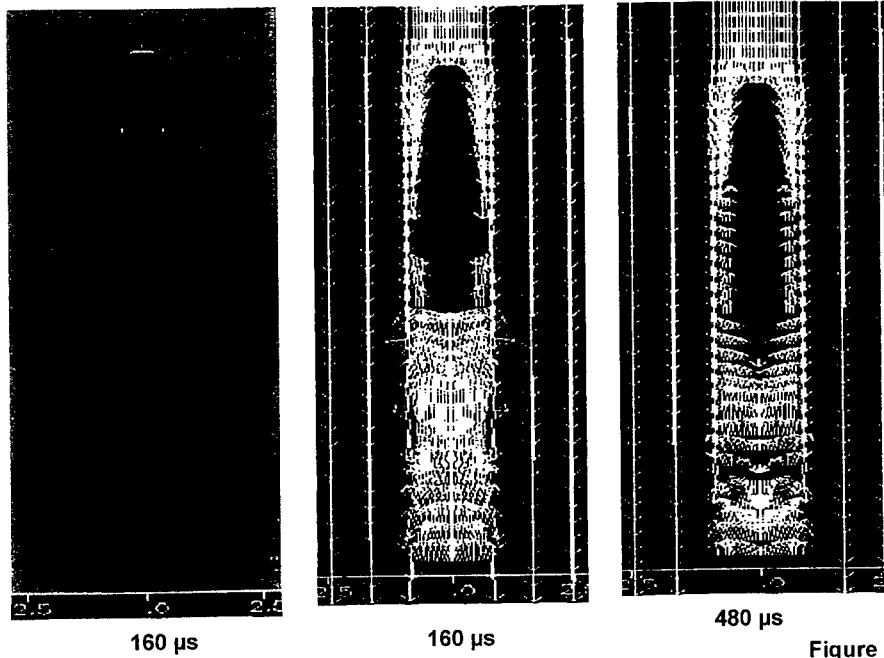
Figure 3

## Computation of a long Cavity Contour Plot of the Density



Time = 3,200ms
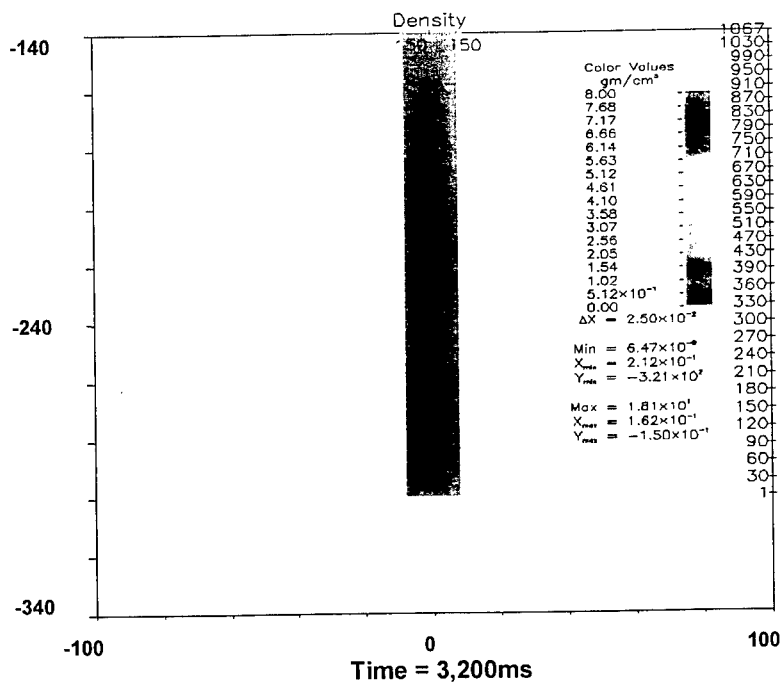
Figure 4
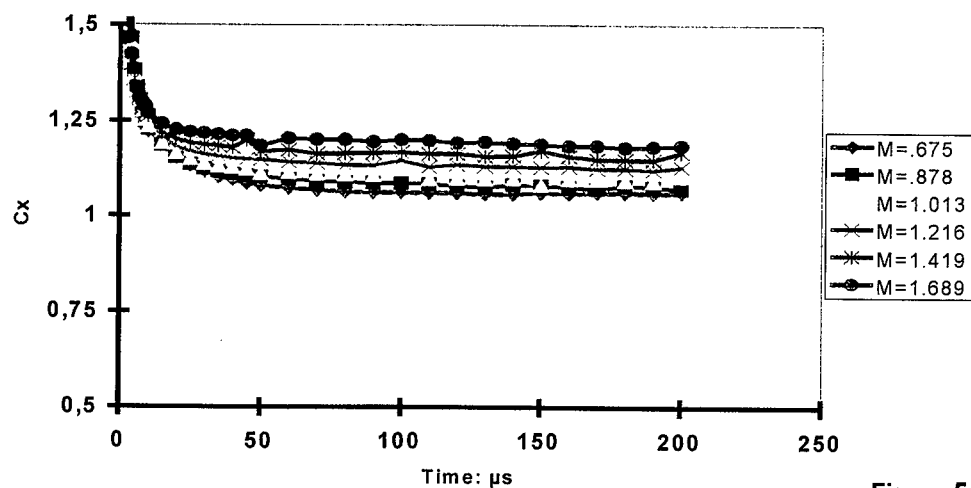
**Cylindrical Projectile: Velocity Effect on the Drag Coefficient**

Figure 5



**Comparison between the OTiHULL results and the compressible formula of Vasin: cylindrical projectile**
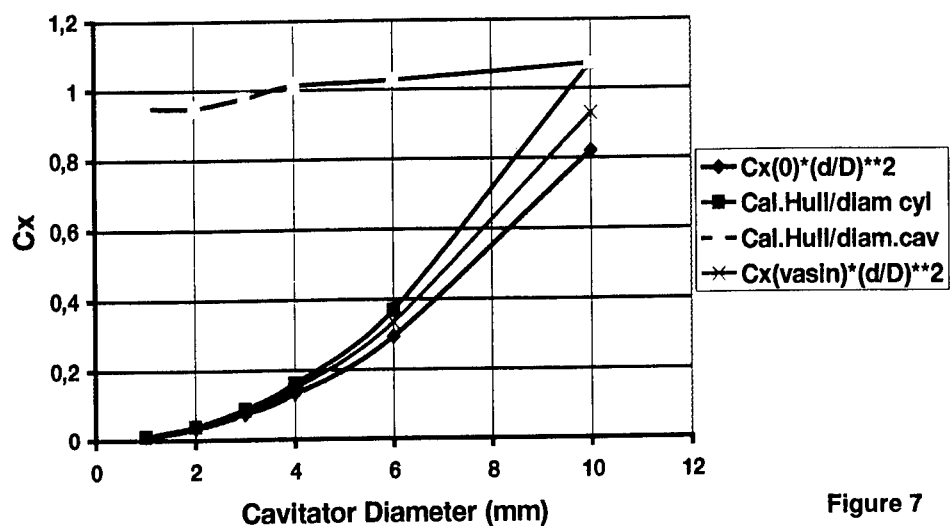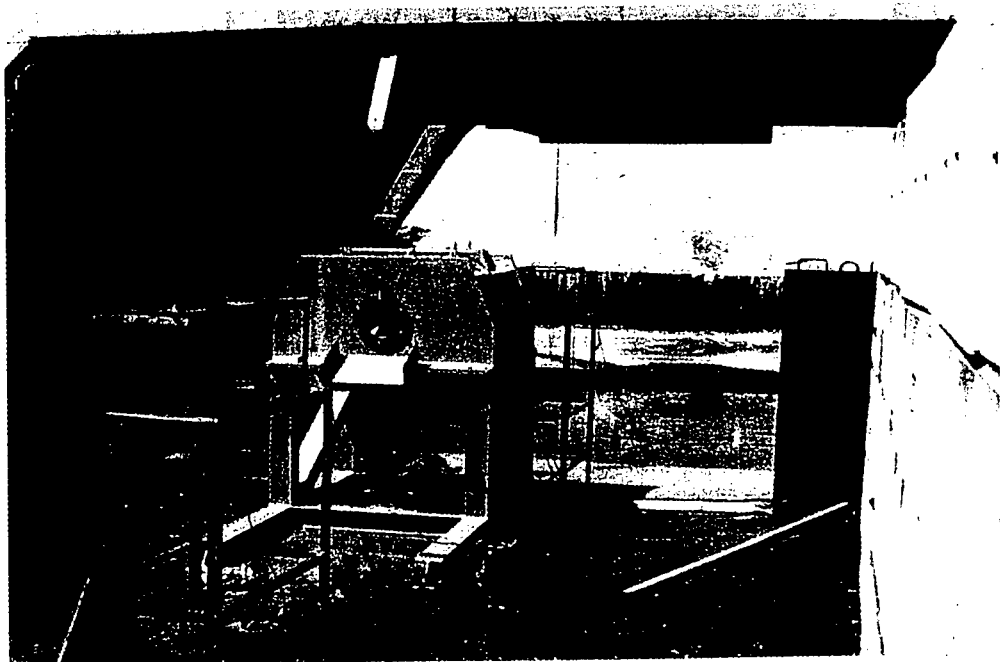
Figure 6

Figure 7



Figure 8

# NEW FIREWORK AMMUNITION : CHALLENGE 2000

## VILLEDIEU N.[1], SIEGLER J-P.[1], GENDRE P.[1]

(1) E. LACROIX Tous Artifices, BP 213, F-31607 Muret Cedex, France

**Abstract :** The LACROIX company has been designing, manufacturing and marketing fireworks for over 150 years. To keep our position in the face of foreign competitors, we are trying to excel through innovative and high quality research. We aim at drawing figures, letters and logos in the sky, using pyrotechnical effects.

On the occasion of the Year 2000 celebrations, we are putting on the market a first firework that permits writing 2000. It consists of a salvo of four ammunition – each generating a figure. To provide for a proper orientation of the « 2 », we cannot use any remote control device. We had to face the roll stability problem of a ammunition. During our study, we have noticed that a cylinder is longitudinally stable and do not interfere with his rolling motion. we designed a firework that is a cylinder without any stabilisation device.

## 1 INTRODUCTION

It seems that the various components used in fireworks have not evolved for several decades. Thus, it is the setting rather than the products themselves that make each firework original. We will not be wrong if we state that the visual effects are reached through bombs, bombettes and candles. As for the ground effects, they consist of fountains, cascades, pole-fireworks and Bengal illuminations.

We should bear in mind that fireworks are first and foremost designed to appeal to and be appreciated by the general public ; therefore their magic is directly associated with their perception. In such highly subjective and artistic context, the concept of « beauty » in technological progress is difficult to quantify.

However, it is widely held that being able to write and draw figures in the sky constitutes a major technological and artistic breakthrough. Besides, the passage to year 2000 celebrations have given us the perfect opportunity to take up this challenge. In this respect, for the past few years, we have worked on « Challenge 2000 » to write the fire letters 2000 in the sky. This project is to be regarded as the gateway to a new generation of pyrotechnical effects.

## 2 FIRST ANALYSIS

A bomb usually consists of a spherical structure from which a delay and a ring with the ignition fuse through protrudes. When bursting, the bomb generates a roughly spherical visual effect (see figure 1). On this type of product, the position and the orientation of the bomb when it bursts have no influence whatsoever on the quality of the visual effect.
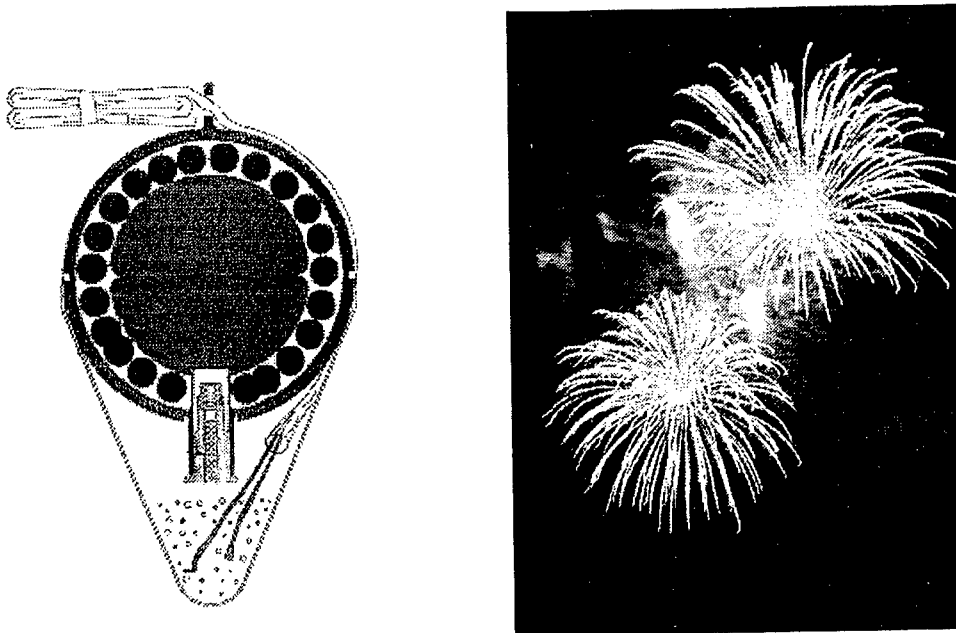
Figure 1 : a spherical bomb and its visual effect

On the contrary, in the case of Challenge 2000, to produce an impressive effect that is as clear as possible, the following criteria have to be mastered :

- drawing of each figure : each figure must be plane as well as well formed;

- simultaneity : all the characters must be displayed (and disappear) at the same time;

- reliability : the non-appearance of one figure out of four makes the drawing impossible to read;

- co-localisation : all four figures must be properly positioned;

- orientation of the « 2 » : contrary to the « 0 », this figure must have a specific orientation vertical-up.

Considering the accuracy to be expected from the operating means (use of mortars and pyrotechnical delays), the solution that meets best the above-mentioned requirements consists in producing each figure from a single firework ammunition. Thus, this operation covers two quasi-independent sub-operations :

- the ballistics : to position and orientate the four fireworks properly during bursting;

- the production of a figure : a figure that is plane and large enough is to be produced from a firework.

Both interact only as a pyrotechnical delay making the ammunition burst is used. We intend here to deal with them separately.
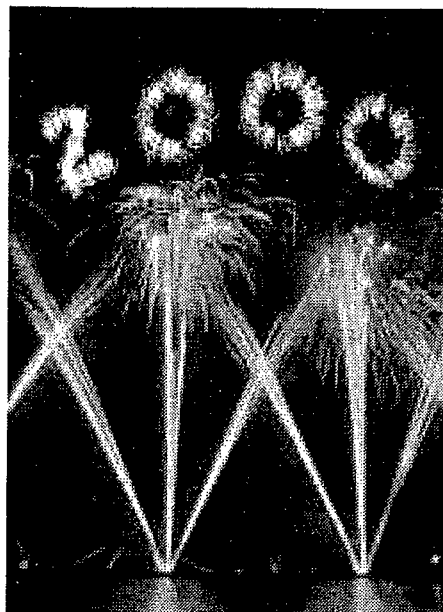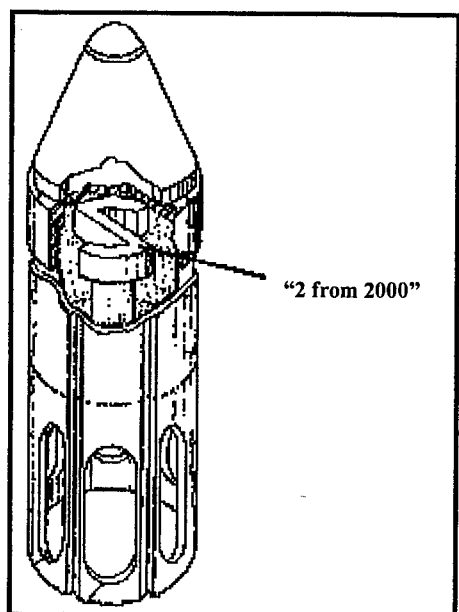
Figure 2 : "2" bomb and the "2000" visual effect.

## 3   PRODUCTION OF A FIGURE

As this operation is not meant to be the topic of this article, we will not go into all its details. However, this project represents a challenge as important as that of the ballistics mastery which is to be explained in the following paragraphs.

As a matter of fact, a plane and continuous pyrotechnic effect (see figure 2) is to be generated. A continuous drawing permits slightly improving the quality of the drawing while effectively striking spirits. As all our products use the method of stars or particles ejection so far, we obtain effects with or without luminous trail (see figure 1). Thus the pyrotechnical effect as well as its generation has to be re-thought.

Having experimented various potential solutions, the solution as shown in the above-figure has been chosen. The payload consists of two elements :

> - the bursting charge : it is used to make the bomb structure burst, generate the drawing and ignite it. It is to be symmetrical about the perpendicular plan to the firework axis, thus generating a plane effect;

> - the drawing : it consists of titanium grains. Following the structure bursting, they are radially ejected and the visual effect that results from their burning will be an similarity of the initial shape. When burning, the high grain density will give the visual impression of a continuous drawing.

One of the greatest difficulties consists in obtaining a drawing that is large enough while keeping a high grain density during burning and providing for their proper burning.

## 4　VEHICULE DESIGN

Having dealt with the ammunition pyrotechnical composition, we now intend to design the ammunition external shape that would make the figure 2000 clear. As previously stated, all four figures should be on the same plane, well positioned close to one another. The « 2 » should also be properly set vertically.

Besides, as our product is to be fired as part of fireworks, we must make sure no blunt fallouts occur for safety purpose. Thus, apart from these specific reasons, we have had to discard any solution using any inertial power unit or any remote control unit for cost reasons.

Therefore, we must design a device, mortar-propelled, with a proper longitudinal stability and that ensure a reliable orientation. As a consequence, we intend to perform wind tunnel tests, numerical simulations and firings in real conditions.

### 4.1　Internal ballistics

A first set of tests, which is performed in real firing conditions and uses the device shown on figure 2, permits controlling and validating the pyrotechnic charge. In the course of this firing session, rolling output speeds that are apparently random and could be superior to 10 rotations per seconds are recorded. Although these results may seem surprising, these speeds are measured during several tests. They cannot possibly be considered as marginal phenomenon and be ignored in the rest of our study.
As the in-air duration time before the ammunition burst is roughly 1 second we cannot properly orientate the figure 2 in case of very strong initial rolling.
As a result, to successfully carry out this project, we must not only design a ammunition with good flying capabilities but also, we must reduce the initial perturbations. The internal ballistics is to be studied with a view of limiting the ammunition rotations when fitted in the mortar and when fired.

The changes brought to the system are then to be controlled and validated accordingly. The mortar is horizontally installed on a frame. Therefore we can collect the ammunition when it falls in a rags-box, and film the mortar firing and the first meters of flight with a 1000 images/second camera. We can measure the translation speed, the rolling speed and study the behaviour of the mortar-ammunition set. The following amendments are made :

> - a <u>more vivace propelling powder</u> is to be chosen to reduce the volume of generated gas while keeping the same output speed;
>
> - an <u>ammunition pin</u> is to be fitted on puller to improve the powder ignition and ejection reliability;
>
> - <u>gas vents</u> are to be machined near the mortar mouth to evacuate gas easily and reduce the extremity perturbations;
>
> - a <u>cylindrical structure</u> is to be fitted in the mortar to improve the ammunition guiding;
>
> - a <u>sealing lip or a thrust disk</u> is to be added to provide for the ammunition tightness.

All these modifications permit reducing the perturbations during the internal ballistics as well as the transition phase to the external ballistics. Thus the firings can be better reproduced.

Finally, for safety reasons, we use cardboard mortars during fireworks. They consist of paper foils around cylinder. There is a spiral groove on their inner face. This spiral makes the ammunition roll. However, we get an output rolling speed, which is constant – approximately ½ rotation per second - and always in the same direction since we take great care of the internal ballistics and the mortar manufacturing. The adjunction of a sealing lip also reduces the effects provoked by some defects.

## 4.2 External ballistics

Once the internal ballistics has been set, we can now go on designing a structure while taking into account the previously mentioned constraints so that the ammunition is correctly orientated and positioned when the payload is ignited.
When developing the internal ballistics, we abandoned a 10 rotations/second-rolling in favour of a ½ rotation/second one during the mortar firing. It results in constraints on the ammunition geometry but opens up the way to new potential solutions. We may :

> - either design a structure with a single point of stability when rolling. The ammunition will go back to its pre-defined angular position all alone;

> - or design a structure with no damped rolling or point of stability during rolling. In such case, its initial rolling speed is kept throughout firing.

The first set of solutions permits constantly orientating the figure no matter the initial rolling speed of the ammunition, provided it is maintained in a determined plane. Besides, if a point of stability is to be reached, the ammunition must not be cylindrical. Such dissymmetry may alter the results that are obtained in internal ballistics. Furthermore, defective stabilisation components (winglets or others) may generate a rolling motion rather than prevent it.

The second set of shapes cannot not modify the rolling as it cannot counter the initial rolling. However, a cylindrical ammunition fired under constant initial rolling speed will keep the same angular position when bursting. Besides, a cylindrical structure without any removable part or fins to be precisely positioned offers the best level of cost and reliability.

During our study, we notice that a right cylinder with no stabilisation device remains longitudinally stable. Thanks to this stability and to the internal ballistic results, a pure right cylindrical shape is a answer to the rolling motion problem. As a result, we have to study the longitudinal cylinder stability in order to be able to determine the structure dimensions and to position the payload properly. In this respect, tests are performed in wind tunnel. Numerical simulations enable us to extrapolate the results to right Mach and Reynolds numbers. We can then carry out firings in real conditions to validate this definition.

### _Wind tunnel tests :_

These tests aimed at studying the evolution of the stability incidence of a cylinder according to the centre of gravity position. We use real scale models and a 30m/s wind. As we intend to study the influence of the criteria of length and diameter, we define 3 lengths and 3 diameters i.e. 9 ammunition all together. They are numbered from 1 to 9.

- **1** : $\Phi$ = 22.5 mm et L = 60 mm ;
- **2** : $\Phi$ = 22.5 mm et L = 120 mm ;
- **3** : $\Phi$ = 22.5 mm et L = 240 mm ;
- **4** : $\Phi$ = 45 mm et L = 60 mm ;
- **5** : $\Phi$ = 45 mm et L = 120 mm ;
- **6** : $\Phi$ = 45 mm et L = 240 mm ;
- **7** : $\Phi$ = 90 mm et L = 60 mm ;
- **8** : $\Phi$ = 90 mm et L = 120 mm ;
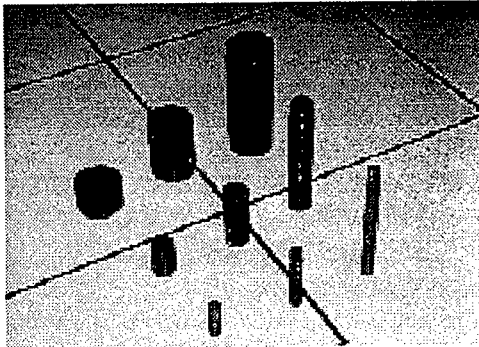- **9** : $\Phi$ = 90 mm et L = 240 mm.

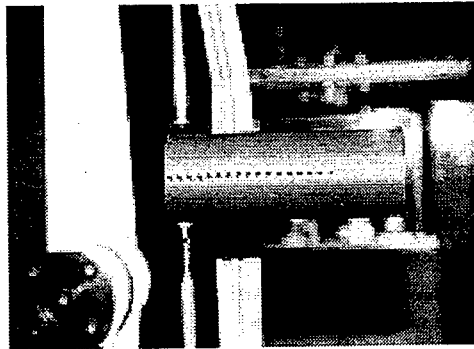Figure 3 : Wind tunnel models.



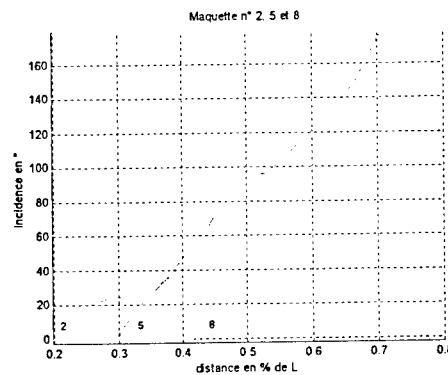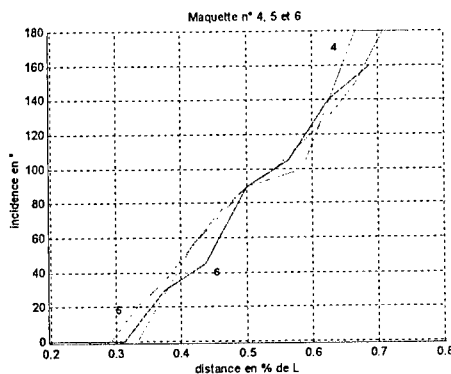Figure 4 : Model n° 5 in the wind tunnel.



Figure 5 : Evolution of incidence of stability according to the centre of gravity position.

On the curves in figure 5, we can see that each ammunition can be divided into 3 parts. Let us take ammunition 5 for example. If the centre of gravity is situated between 0 and 30 % of the length, the ammunition is stable at incidence, $\alpha = 0$ °. If the centre of gravity is at over 70 % of the length, the ammunition is stable at incidence, $\alpha = 180$ ° Between both values, the larger the distance between the nose and the centre of gravity is, the higher the stability incidence is. The same applies to each ammunition with slightly different percentages.

We can note that, for the same diameter (ammunition 4, 5 and 6 ) the three above defined areas are roughly identical. However, for a single length (ammunition 2, 5 and 9) the lower the diameter is, the greater the intermediate area is. Therefore it seems that the ammunition diameter has the greatest effect over the longitudinal stability.
As a matter of fact, a recirculation area starting from the leading edge can be clearly seen. We get confirmation of this fact if we look at the parietal current lines. The size of the area seems to be proportional to the ammunition diameter and independent of its length.

Although these results seem promising enough, they have to be taken carefully. These tests suffer from the limitations inherent to the wind tunnel tests : the ammunition is in static position, the assembly can affect the results (see figure 4) and we are not under the right Mach and Reynolds numbers conditions. Our results have to be confirmed by means numerical simulations before performing firings in real conditions.
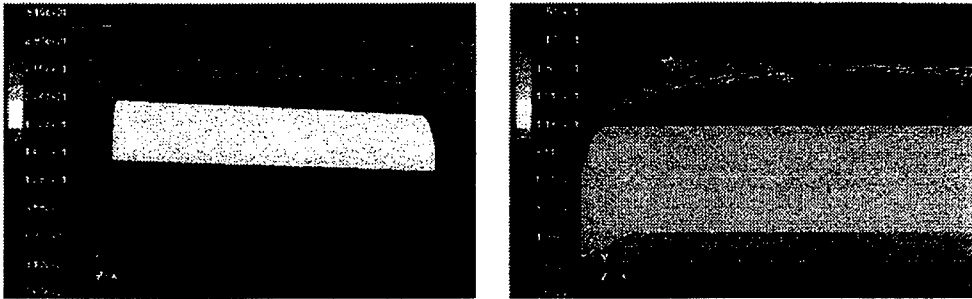
Figure 6 : Visualisation of the steam lines and the speed arrays at the leading edge.

| Length (mm) Diameter (mm) | 120 | | 240 | |
|---|---|---|---|---|
| | Wind tunnel | Simulation | Wind tunnel | Simulation |
| 22.5 | 35 | 30 | 35 | 32 |
| 45 | 70 | 65 | 70 | 60 |
| 90 | > 120 | > 120 | 140 | 145 |

Tableau 1 : Size of the separation area, comparison between wind tunnel and simulations.

## *Numerical simulations:*

These simulations are carried out using the FLUENT 5 software. We are using the coupled explicit solver with cylindrical and tri-dimensional geometries. The numerical study consists of two sets of operations. First, we reproduce the same conditions (Mach, Reynolds, turbulence ...) as those in the wind tunnel tests. It enables us to directly compare the results that are thus obtained. Then, we simulate the right Mach and Reynolds number flow and we try to deduce some firing information. During both operations, our study more specifically focuses on the separation generated by the leading edge and the evolution of the pitching coefficient according to the incidence.

Figure 6 shows that, with a nil incidence, the simulated flow has the same structure as the one observed in the wind tunnel. There is an area of recirculation starting from the leading edge, and if the ammunition is long enough, the flow is brought back onto the ammunition surface before the trailing edge.
Table 1 shows, with a nil incidence, the comparative size of the recirculation on different ammunition. This size is expressed in millimetres from the leading edge.

Figure 7 shows the evolution of the pitching moment coefficient according to the incidence, and for different positions of the centre of gravity for ammunition 5. Due to the adopted conventions, when the cylinder is in positive incidence, a positive moment tends to diminish the incidence. Thus, for these three positions of the centre of gravity, we record a stability with a nil incidence and with an incidence situated between 60 and 90 °.

Although the values of relief angles are different, we notice the same phenomena as in the wind tunnel. For ammunition 5, if the centre of gravity is close to the nose, 0° is the only point of stability. If the centre of gravity is beyond 40 mm there is another point of stability. The greater the distance between the nose and the centre of gravity is, the less stable the ammunition will be.
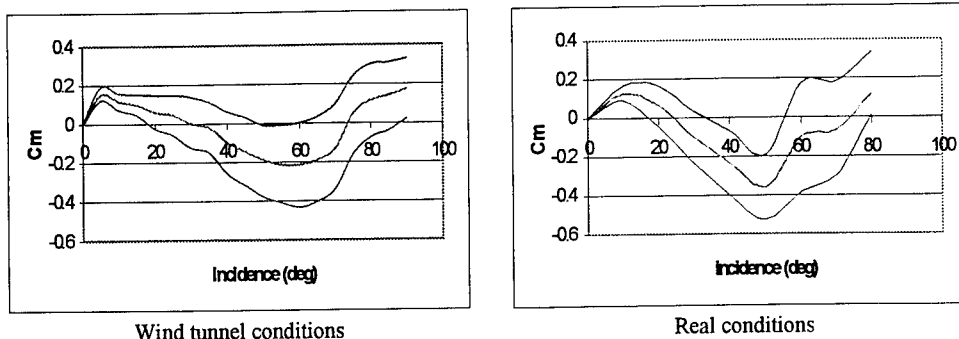
Figure 7 : Evolution of the pitching moment coefficient according to the incidence.
(blue : $X_G$ = 40 mm, green : $X_G$ = 50 mm and red : $X_G$ = 60 mm)

The simulations performed in real conditions give results which are similar to previous simulations. However, we can notice that the recirculation area has grown by 10 mm on ammunition 5, and as shown on figure 7, for a single ammunition and with a similar position of centre of gravity, stability at 0° is less marked.

All the results exposed until now were obtained under static conditions. In wind tunnel, the model has one degree of freedom: it can only rotate around axis that is perpendicular to model main axis. During the simulations, we compute the flow around a static ammunition. So, it's a little bit hazardous to directly extrapolate this results to dynamic flight.

## 4.3    Real firings

The aim of this firings is to study the dynamic motion of the ammunition and to validate its shape. However, we have to keep in mind that we cannot clearly distinguish undamped oscillating stability at nil incidence from a damped stability at few degree of incidence. To do a complete interpretation of this tests, we have to take into account all the results from wind tunnel tests and numerical simulations.

Following the wind tunnel tests and the simulations, we have chosen this geometry :

  - $\Phi$ = 45 mm diameter L = 112 mm and length;

  - the payload is loaded at the ammunition extremity, with a length of 50 mm;

  - the ammunition rear part is left void.

Thus the centre of gravity is 30 mm from the nose. The nose can be weighted with iron powder to move the centre of gravity forward. We are performing flat firings to film the ammunition as properly as possible with a 1000 images/s-camera and video cameras placed almost in the firing axis. Firings using an active payload also take place at night to visualise the effect quality.

We notice that the pitching and yawing oscillations interact. Such phenomenon has not been recorded during the wind tunnel tests or the simulations as the ammunition was in static position. However, the closer we get to the ammunition centre of gravity, the lower the oscillations are. In view of the potential positions of the centre of gravity, they will not disappear.

# 5   CONCLUSION

Our challenge has been met at 90 % : a good quality visual effect has been obtained, the four figures appear at the same time and are well positioned. The consequences on the visual effect of the ammunition "imperfect" longitudinal stability are minor. The public can see the four figures appearing in the same plane.

Two points remained to be improved :

- the effect duration : the effect can be seen for a little less than 1 second;

- the "2" orientation : in view of choices made, all the imprecisions and the uncertainties, the 2 is not always perfectly vertical.

However, the drawing quality, due among other reasons to the continuous drawing and the brain capability of adaptation, permits us obtaining that can be easily read and understood.

Significantly increasing the effect duration without altering the figure seems difficult. As for the "2" orientation, we are currently working on the design of a stable ammunition rolling and with an internal ballistics as good as that of the actual ammunition.

Once all the question of the drawing orientation will be mastered, we will be able to draw other figures, letters or symbols using the same ammunition structure. We will have just to modify the payload according to the wanted drawing. This product should be regarded as the first step towards a pyrotechnical writing or at least new pyrotechnical effects.

# Author index